Cerebral damage following ischaemic stroke: The role of Angiotensin-(1-7)

Mariana Moreira Arroja

B.Sc (Hons) Pharmacology
King's College London, UK

Submitted in fulfilment of the requirements for the

Degree of Doctor of Philosophy (Ph.D)

Institute of Neuroscience & Psychology
College of Medical, Veterinary & Life Sciences
University of Glasgow

April 2018

Abstract

The renin angiotensin system (RAS), a homeostatic system involved in blood pressure and volume control, is implicated in the pathology of several risk factors for ischaemic stroke. Mounting evidence now suggests that the RAS may play a role in the pathophysiology of ischaemic stroke. This is thought to be due to an imbalance between the classical RAS axis, Angiotensin converting enzyme/Angiotensin II/Angiotensin II receptor type I (ACE/Ang II/AT_1R), and the counter-regulatory RAS axis, Angiotensin converting enzyme 2/Angiotensin-(1-7)/Mas receptor [ACE2/Ang-(1-7)/MasR]. The counter-regulatory axis has been shown to provide neuroprotection in ischaemic stroke animal models. Therefore, the studies conducted in this thesis aimed to test the neuroprotective potential of Ang-(1-7) as a post-stroke therapy following transient focal cerebral ischaemia. Furthermore, experiments were conducted to test a potential synergistic effect between MasR and alternative Ang II receptor, Angiotensin II receptor type II (AT_2R), agonism following stroke.

Aim 1: To optimise the experimental model of stroke and carry out exploratory therapeutic studies with an ACE2 activator following stroke.

The intraluminal filament model of transient middle cerebral artery occlusion (MCAO) allows for investigation of reperfusion following stroke; however, the model leads to considerable variability in lesion size thereby limiting data interpretation particularly in therapeutic studies. Therefore, there is a need to address confounding variables and determine methods to predict final infarct outcome. Additionally, counter-regulatory RAS targeting therapies have been primarily studied in ischaemic stroke through intracerebroventricular (ICV) administration, which is not a recommended route of administration for clinical use. Consequently, we aimed to optimise the animal model used and RAS targeting therapies. We show that following permanent MCAO, Wistar rats display significantly larger lesion volumes with less variability than Sprague Dawley animals. Importantly, the use of Laser Doppler Flowmetry did not successfully predict final infarct volume. Finally, systemic administration of diminazene aceturate (DIZE; ACE2 activator) did not reduce final infarct volume following transient MCAO. For future studies, we decided to use Wistar rats, ICV route of administration and acute magnetic resonance imaging (MRI) to confirm successful occlusion of the MCA.

Aim 2: To determine the effects of Ang-(1-7) and/or Compound 21 (C21) on the extent of tissue salvage following transient focal cerebral ischaemia.

We investigated the impact of Ang-(1-7) and/or C21 (AT_2R agonist) on the extent of tissue salvage following reperfusion. Acute MRI angiography was carried out during MCAO to confirm successful MCAO and to assess baseline lesion volume. At day 7 following reperfusion, MRI-T_2 was carried out to determine final infarct volume thereby allowing us to longitudinally assess the change in lesion volume. We demonstrate that prior to therapy there was substantial variability in baseline lesion volume across the treatment groups. When normalising the data to initial lesion for each animal, Ang-(1-7) along with reperfusion significantly increased tissue salvage compared to vehicle animals with no effect on blood pressure. C21 and combination group [Ang-(1-7) +C21] however, did not induce a therapeutic effect. Additionally, neurological score was comparable amongst groups. Gene expression experiments confirmed that there is an imbalance of the RAS following stroke as *AT_2R* was upregulated and *MasR* downregulated at day 7 following MCAO. Ang-(1-7) did not influence inflammatory gene expression markers; however, it significantly attenuated the increase of *NADPH oxidase type 1* (*NOX1*) seen in the control animals, possibly promoting a neurogenesis effect at the time point assessed.

Aim 3: To determine the impact of Ang-(1-7) on blood brain barrier (BBB) breakdown and microglia activation following transient focal cerebral ischaemia.

Evidence from the literature suggests that Ang-(1-7) induces an anti-inflammatory effect particularly at acute stages of injury (24 hrs and 72 hrs) following transient MCAO. Accordingly, we hypothesised that post-stroke Ang-(1-7) therapy exerts a therapeutic effect by attenuating BBB breakdown and microglia activation and inflammatory profile at 24 hrs following MCAO. Using T_1 contrast enhanced MRI we demonstrated that Ang-(1-7) did not alter BBB breakdown at 24 hrs and that BBB disruption was highly variable amongst animals. Ang-(1-7) treatment did not alter infarct volume at 24 hrs post MCAO compared to control and there were no differences in neurological outcome. There was no influence of Ang-(1-7) treatment on microglia number and activation within the peri-infarct and homotopic contralateral regions. Moreover, gene expression showed that pro-inflammatory markers were upregulated following MCAO with no effect of Ang-(1-7) on these markers. Interestingly, RAS receptor components were comparable to Sham animals, indicating that the RAS follows a biphasic pattern and does not promote injury at 24 hrs following transient MCAO in the filament model.

Aim 4: To determine whether Ang-(1-7) acts on the cerebrovasculature to improve CBF following transient focal cerebral ischaemia.

Results from the previous studies raised the question whether Ang-(1-7) post stroke therapy enhances cerebral blood flow (CBF) at hyper-acute stages of injury after 90 min MCAO. The effects of Ang-(1-7) intravenous infusion at start of reperfusion and for a period of 90 min on cortical CBF were studied with Laser Speckle Contrast Imaging (LSCI). LSCI allowed changes in cortical perfusion to be assessed with a high temporal resolution across the entire cortical surface of the brain. Regions of interest were determined based on perfusion thresholds during MCAO and post-reperfusion treatment was assessed. Ang-(1-7) significantly attenuated the increase in CBF within the contralateral hemisphere compared to control animals. However, therapy did not alter CBF within the ischaemic hemisphere. Furthermore, Ang-(1-7) did not alter mean arterial blood pressure (MABP), which was maintained within normal ranges for both treatment groups, nor did it influence the occurrence of peri-infarct depolarisations. The Ang-(1-7) effect observed in this study could be the outcome of “steal phenomena” reversal, therefore, preventing CBF shift towards the non-ischaemic side.

Conclusion

This thesis conducted novel studies that demonstrate that central administration of Ang-(1-7) following transient MCAO induces a mild to moderate neuroprotective effect where it increases tissue salvage. Conversely, Ang-(1-7) did not prevent BBB breakdown or exert an anti-inflammatory effect at the microglia level. These experiments highlight the neuroprotective potential of selective MasR agonists in the ischaemic stroke context.

Table of Contents

List of Tables

List of Figures

Acknowledgement

Firstly, I would like to express my gratitude to the Medical Research Council for funding this research and for all the opportunities given to me. Importantly, this PhD would not have been possible without the incredible support of my primary supervisor Chris McCabe. I am extremely grateful for your help and knowledge, for always keeping me motivated and for making the difficult times a bit more enjoyable with your sense of humour! To my secondary supervisors, Stuart Nicklin and Lorraine Work, thank you so much for your invaluable knowledge and for your patience and encouragement. Words cannot thank you enough.

I would like to thank Mhairi Macrae and Debbie Dewar for their constant guidance throughout this PhD. You are an amazing role model for young women and I have learnt immensely with you. A special thank you to Vicore Pharma® for providing Compound 21, Lisa Roy for performing the histology in this thesis, Linda Carberry for cutting all the brain tissue, John McClure for helping with statistics, Lindsay Gallagher for sharing her surgical knowledge and Emma Reid for performing the neurological score in Chapter 4. I would also like to thank the staff at the Wellcome Surgical Institute, the Glasgow Experimental MRI Centre and the British Heart Foundation. In particular, Ann Marie, Lisa, Lindsay, Linda, Jim, Michael, William, Antoine, Graeme, Rob, Emma and Mass: thank you for your all your help and for making this PhD so enjoyable! I will miss the afternoon chats.

An eternal thank you to my parents Lina and Pedro, my sister Sofia, my brothers Bruno and Ricardo and my partner Argyris. Thank you for your never-ending love and encouragement. This thesis would not have been possible without you. To my friends Katelyn, Marie, Estrella, Chike, Becca, Sofia, Isabel, Miguel: thank you for always being around and for all the laughs.

I would also like to thank my mentors Christoph Thiemermann, Lawrence Moon, Hélder Mota-Filipe for helping me grow as a professional and to Bernardo Ratilal for teaching me the animal model. I would like to express a special acknowledgement to my undergraduate degree mentor and friend Domenico Spina, who passed away last year. Thank you for always believing in my abilities and for your unconditional support and advice for 8 years. I am forever grateful to you.

To my parents & to Dom

Author's Declaration

I declare that, except where explicit reference is made to the contribution of others, this dissertation is the result of my own work and has not been submitted for any other degree at the University of Glasgow or any other institution.

Mariana M. Arroja

Published Manuscripts

Arroja, M.M., Reid, E., McCabe, C. (2016) Therapeutic potential of the renin angiotensin system in ischaemic stroke. *ExpTransl Stroke Med*, 8:8.

McCabe, C., **Arroja**, M.M, Reid, E., Macrae, I.M (2017) Animal models of ischaemic stroke and characterisation of the ischaemic penumbra. Neuropharmacology (doi:10.1016/j.neuropharm.2017.09.022) (PMID:28923277).

Abstracts

Arroja, M.M., Reid, E., Holmes, W.M., Nicklin, S.A., Work L.M., McCabe, C (2015). Angiotensin-(1-7) increases tissue salvage following focal cerebral ischaemia with reperfusion. MRC postgraduate day, University of Glasgow, UK [Poster Presentation]

Arroja, M.M., Reid, E., Holmes, W.M., Nicklin, S.A., Work L.M., McCabe, C (2015). Angiotensin-(1-7) increases tissue salvage following focal cerebral ischaemia with reperfusion. Pre-clinical Stroke Symposium, Glasgow, UK [Oral Presentation]

Arroja, M.M., Reid, E., Holmes, W.M., Nicklin, S.A., Work L.M., McCabe, C (2015). Angiotensin-(1-7) increases tissue salvage following focal cerebral ischaemia with reperfusion. XXVIIth International Symposium on Cerebral Blood Flow, Metabolism and Function and the XIIth International Conference on Quantification of Brain Function with PET, Vancouver, Canada [Poster Presentation]

Arroja, M.M., Reid, E., Holmes, W.M., Nicklin, S.A., Work L.M., McCabe, C (2016). Angiotensin-(1-7) increases tissue salvage following focal cerebral ischaemia. 9th Symposium on Neuroprotection and Neurorepair, Leipzig, Germany [Poster Presentation]

Arroja, M.M., Reid, E., Holmes, W.M., Nicklin, S.A., Work L.M., McCabe, C (2016). Angiotensin-(1-7) increases tissue salvage following focal cerebral ischaemia. Scottish Neuroscience Conference, St. Andrews, UK [Oral Presentation]

Prizes

Best oral presentation at the UK preclinical stroke Symposium (June, 2015)

Best poster presentation at the MRC postgraduate day (June, 2015)

Best poster presentation at Glasgow Neuroscience Day (January, 2016)

Awards

MVLS Travel Grant – University of Glasgow, 2015

Guarantors of Brain Travel Grant – Cambridge, 2015

MRC funded Science Policy internship at the Academy of Medical Sciences, London, UK – April to June 2017

Definitions/Abbreviations

ACA	Anterior cerebral artery
ACE	Angiotensin converting enzyme
ACE2	Angiotensin converting enzyme 2
aCSF	Artificial cerebrospinal fluid
ACTB	Beta-actin
ADC	Apparent diffusion coefficient
AMPA	α-amino-3-hydroxy-5-methyl-4-isoxazolepropionic acid
Ang I	Angiotensin I
Ang II	Angiotensin II
Ang-(1-7)	Angiotensin-(1-7)
Ang-(1-9)	Angiotensin-(1-9)
AP-1	Activator protein 1
ARB	Angiotensin type 1 receptor blocker
Arg1	Arginase 1
AT_1R	Angiotensin II receptor type I
AT_2R	Angiotensin II receptor type II
AT_4R	Angiotensin type IV receptor
ATP	Adenine triphosphate
AU	Arbitrary unit
AUC	Area under the curve
B2M	Beta-2-microglobulin
B_2R	Bradykinin receptor type 2
BBB	Blood brain barrier
BDNF	Brain derived neurotrophic factor
BP	Blood pressure
BSA	Bovine serum albumin
C21	Compound 21
CBF	Cerebral blood flow
CCA	Common carotid artery
CCD	Charged-coupled device
CCL22	C-C motif chemokine 22
CCR2	C-C motif chemokine receptor 2
CCR5	C-C motif chemokine receptor 5
CCR7	C-C motif chemokine receptor 7
CD11b	Cluster differentiation 11 b
CD32	Cluster differentiation 32
CD86	Cluster differentiation 86
CD163	Cluster differentiation 163
CD206	Cluster differentiation 206
cDNA	Complementary DNA
cGMP	Cyclic guanosine monophosphate
$CMRO_2$	Oxygen consumption
CNS	Central nervous system
COX	Cyclooxygenase
COX-2	Cyclooxygenase 2
CPP	Cerebral perfusion pressure
CSD	Cortical spreading depolarisations
CT	Computed tomography

Ct	Cyclic threshold
CVD	Cardiovascular disease
CVO	Circumventricular organs
CXCR2	C-X-C motif chemokine receptor 2
DAG	Diacylglycerol
DAPI	4’,6-diamidino-2-phenylindole
DCE-MRI	Dynamic contrast enhanced MRI
DIZE	Diminazene aceturate
dH_2O	Distilled water
dNTP	Deoxyribonucleotide triphosphate
DWI	Diffusion weighted imaging
EB	Evans Blue
ECA	External carotid artery
EGFR	Endothelial growth factor receptor
eNOS	Endothelial nitric oxide synthase
ERK1/2	Extracellular-signal-related kinase ½
ET-1	Endothelin-1
FAK	Focal adhesion kinase
FOV	Field of view
FRET	Fluorescence resonance energy transfer
GAPDH	Glyceraldehyde 3-phosphate dehydrogenase
Gd-DTPA	Gadolinium-diethylenetriamine penta-acetic acid
GPCR	G protein coupled receptor
H&E	Haematoxylin and Eosin
HARM	Hyperintense acute reperfusion marker
HRPT1	Hypoxanyhine-guanine phosphoribosyltransferase
HT	Haemorrhagic transformation
IBA1	Ionized calcium-binding adapter molecule 1
ICA	Internal carotid artery
ICH	Intracranial haemorrhage
ICP	Intracranial pressure
ICV	Intracerebroventricular
IL-1β	Interleukin 1 beta
IL-6	Interleukin 6
IL-8	Interleukin 8
IL-10	Interleukin 10
IMPROVE	Ischaemia Models: Procedural Refinements of in Vivo Experiments
iNOS	Inducible nitric oxide synthase
IP_3	inositol-1,4,5-triphosphate
IQR	Interquartile range
IV	Intravenous
ITGAM	Integrin Subunit Alpha M
JAK/STAT	Janus kinase/signal transducer and activator of transcription
JNK	c-Jun NH_2-terminal kinase
Kdr	Kinase insert domain receptor
KO	Knockout
LDF	Laser Doppler Flowmetry
LSCI	Laser Speckle Contrast Imaging
LT	Leukotriene
MABP	Mean arterial blood pressure
MAPK	Mitogen-activated protein kinase

MasR	Mas receptor
MCA	Middle cerebral artery
MCAO	Middle cerebral artery occlusion
MCP-1	Monocyte chemoattractant protein-1
MKP-1	MAP kinase phosphatase
MMP	Matrix metalloproteinase
MMP2	Matrix metalloproteinase 2
MMP9	Matrix metalloproteinase 9
MRA	Magnetic Resonance Angiography
MRI	Magnetic resonance imaging
NC3R's	National Centre for the Replacement, Refinement and Reduction of Animals in Research
NEP	Neprilysin
NF-κB	Nuclear factor kappa beta
NIHSS	National Institutes of Health Stroke Scale
NMDA	N-methyl-D-aspartate
nNOS	Neuronal nitric oxide synthase
NO	Nitric oxide
NOS	Nitric oxide synthase
NOX	NADPH oxidases
NRTK	Non receptor tyrosine kinase
NS	Neurological score
NVO	Named Veterinary Officer
NVU	Neurovascular unit
OA	Occipital artery
OEF	Fraction of oxygen extracted from arterial blood
OGD	Oxygen glucose deprivation
PA	Pterygopalatine artery
$PaCO_2$	Partial pressure of carbon dioxide
PAM	Paraformaldehyde
PaO_2	Partial pressure of oxygen
PDGF	Platelet derived growth factor
PEP	Prolyl endopeptidases
PG	Prostaglandin
PID	Peri-infarct depolarisation
PKB	Protein kinase B
PKC	Protein kinase C
PLA_2	Phospholipase A_2
PLC	Phospholipase C
PLD	Phospholipase D
PP2A	Protein phosphatase 2
PRR	Pro-renin receptor
PU	Perfusion unit
PTGS2	Prostaglandin-endoperoxide synthase 2
PWI	Perfusion weighted imaging
qRT-PCR	Quantitative real-time polymerase chain reaction
RANTES	Regulated on Activation Normal T cell Expressed and Secreted
RARE	Rapid acquisition with refocused echoes
RAS	Renin angiotensin system
rCBF	Relative cerebral blood flow
RNA	Ribonucleic acid
ROI	Region of interest

ROS	Reactive oxygen species
RTK	Receptor tyrosine kinase
rt-PA	Recombinant tissue plasminogen activator
RT-PCR	Reverse transcription polymerase chain reaction
RVLM	Rostral ventrolateral medulla
SAH	Subarachnoid haemorrhage
SC	Subcutaneous
S.D.	Standard deviation
SHP-1	SHR2 domain-containing tyrosine phosphatase
SHR	Spontaneously hypertensive rats
SHRSP	Stroke prone spontaneously hypertensive rats
SNR	Signal to noise ratio
STAIR	Stroke Therapy Academic Industry Roundtable
TBS	Tris Buffered Saline
TE	Echo time
TGF-β1	Transforming growth factor beta 1
TIMP1	Metallopeptidase inhibitor 1
TJP	Tight junction protein
TOAST	Trial of Org10172 in Acute Stroke Treatment
TOP	Thimet oligopeptidase
TR	Repetition time
Treg	Regulatory T cell
TTC	2,3,5-Triphenyl-2H-tetrazolium chloride
UBC	Ubiquitin C
VEGF	Vascular endothelial growth factor
VEGFR-2	Vascular endothelial growth factor receptor 2
VRF	Veterinary Research Facility
ZO	Zona occludens

Chapter 1: General Introduction

Chapter 1

1.1 Stroke

Stroke is a complex and devastating neurological disorder characterised by a vascular induced injury to the central nervous system arising from more than 150 known aetiologies (Chen et al., 2012). The World Health Organisation describes stroke as a vascular condition that quickly leads to clinical signs of cerebral dysfunction due to focal or global injury and with symptoms lasting for at least 24 hrs or death. Conversely, cerebrovascular accidents in which the symptoms are prevalent for less than 24 hrs are deemed as transient ischaemic attacks (Saver et al. 2008; Sacco et al. 2013). The exact definition of stroke is under extensive debate as it encompasses a wide range of cerebrovascular disorders. For this reason, the American Heart Association/American Stroke Association published a report on updated stroke definitions where these are categorised depending on stroke type, location and duration (Sacco et al., 2013).

There are two types of stroke, haemorrhagic and ischaemic (Chen et al., 2012). Haemorrhagic stroke constitutes up to 15% of all strokes and is subdivided into subarachnoid haemorrhage (SAH) and intracranial haemorrhage (ICH) (Chen et al., 2012). SAH occurs due to the rupture of a cerebral vessel causing haemorrhage within the subarachnoid space whereas ICH is associated with brain parenchyma bleeding (Dupont et al., 2010; Elliott and Smith, 2010). Ischaemic stroke accounts for 85% of all strokes and is classified as an occlusion of a cerebral blood vessel, resulting in the blockage of cerebral blood flow (CBF). The condition occurs suddenly and is characterised by the rapid onset of symptoms such as aphasia, hemiparesis, ataxia, visual field deficit, hemisensory impairment and facial droop.

1.1.1 Epidemiology

Currently, stroke is the second leading cause of death in the world and fourth in the UK (Stroke Association, 2017). It is estimated that in the UK alone, more than 152,000 people will suffer from the condition and stroke accounts forapproximately 40,000 deaths a year (Stroke Association, 2017). Although the mortality rates in the UK have decreased by 46% in 20 years (1990-2010), there has been a steep increase in stroke survivor numbers, now consisting of a 1.2 million population (Stroke Association 2017). In terms of disability, stroke is the leading condition in the UK. Over 50% of survivors are left permanently disabled whereas two thirds of all surviving patients display visual and speech, limb

movement, swallowing as well as bladder and bowel control complications (Adamson et al., 2004; Stroke Association, 2017). Additionally, recent reports indicate that stroke survivors are at higher risk of developing dementia in the longer term, particularly the younger patient population (Corraini et al., 2017). Consequently, stroke outcome management accounts for approximately £8.9 billion of tax payer costs and 5% of total NHS expenditure, a concerning health and socio-economic burden (Adamson et al., 2004; Saka et al., 2009).

1.1.2 Risk factors

Stroke is a multifactorial condition and can arise from several risk factors that are classified as non-modifiable, modifiable and potentially modifiable (Khare, 2016). Table 1-1 provides an overview of the most common risk factors within these categories.

Table 1-1 Stroke risk factors. Adapted from (Go et al., 2014; Khare, 2016)

Non-Modifiable	Potentially Modifiable/Modifiable	
Age	Hypertension	Psychological stress
Sex	Cardiac disease	Diet
Race	Diabetes Mellitus	Physical inactivity
Family history	Obesity	Drug abuse
Genetics	Dyslipidaemia	Current smoking

Non-modifiable risk factors comprise age, sex, race and family history/genetics. Of all these, age is the most well documented factor, with risk for a stroke doubling every 10 years after the age of 55 (Sacco et al., 1997). Although stroke may be considered a condition primarily occurring in elderly individuals, the number of strokes in people aged between 20 and 64 has increased by 25% worldwide in a decade (Feigin et al., 2014). In terms of sex differences, males have a higher incidence; however, after menopause, the incidence in females increases drastically due to a decline in oestrogen levels (Appelros et al., 2009). Furthermore, black people are twice as likely to have a stroke at a younger age

and black men over the age of 85 are mostly affected when compared to Mexican and non-Hispanic whites (Khare 2016).

A study carried out across 22 countries identified that there are ten crucial risk potentially modifiable/modifiable factors associated with 90% of stroke risk (O'Donnell et al., 2010). These risk factors include hypertension, current smoking, waist to hip ratio, diet risk score, lack of regular physical activity, diabetes mellitus, alcohol intake, psychosocial stress and depression, cardiac causes and ratio of apolipoproteins B and A1 (O'Donnell et al., 2010). Of all these conditions, hypertension is the single most important risk factor for ischaemic stroke, inducing a relative risk of approximately 4-fold when systolic blood pressure is over 160 mmHg and/or diastolic blood pressure above 95 mmHg (Khare 2016; Sacco et al. 1997). In addition, the relationship between high blood pressure and stroke is considered linear and independent of other risk factors (Goldstein et al., 2006). Currently, hypertension is responsible for 54% of all stroke cases and treating the condition is an effective strategy to prevent stroke occurrence (Chalmers et al., 2003; Stroke Association, 2017).

1.2 Ischaemic stroke

Ischaemic stroke results from an occlusion of a cerebral blood vessel, typically arteries, due to the presence of a thrombus or embolus, resulting in the blockage of blood flow to the brain (Figure 1-1) (Deb et al., 2010). There are several ways in which ischaemic stroke may occur; therefore, subclassification methods were developed with Trial of Org10172 in Acute Stroke Treatment (TOAST) being the most widely used method. TOAST divides strokes into large artery, cardioembolic, small-vessel occlusion, stroke of other determined causes and stroke of undetermined aetiology (Adams and Biller, 2015).

Large artery occlusions are usually characterised by the formation of lipid laden atherosclerotic plaques in the inner vessel wall due to pre-existent conditions such as hypercholesterolaemia, hypertension or diabetes (Luitse et al., 2012). These co-morbidities cause endothelial cell damage and predispose the vessel to the generation of atherosclerotic plaques that may diminish or completely obstruct blood flow (Figure 1-1). It often occurs in the bifurcations of the common carotid arteries, along the middle cerebral artery (MCA) and at the origin of the vertebral arteries (Derdeyn, 2007; Rovira et al., 2005) and represents approximately 50% of all ischaemic strokes (Staals et al., 2014). This type of

stroke may also occur due to the rupture of the atherosclerotic plaques, forming a thrombus that may travel through the circulation reaching a cerebral vessel (Rapp et al., 2003).

Cardioembolic stroke is characterised by cerebral vessel occlusion due to blood clots. The blood clots, or emboli, are typically formed in the heart as a result of atrial fibrillation. In turn, these will travel in the circulation leading to cerebral vessel occlusion, accounting for 18-25% of all stroke cases (Olsson and Halperin, 2005). This type of stroke usually occurs in multiple arteries and has the worst clinical prognosis (Arboix, 2015). In addition, small vessel or lacunar strokes account for one quarter of all ischaemic strokes. These take place in the microcirculation due to lipohyalinotic alterations in the vessel wall or microatheromas (Arboix and Martí-Vilalta, 2009). Lacunar occlusions are typically located deeply in cerebral vessels such as the corona radiata, internal capsule and MCA supplied branches. Patients with this type of stroke are identified by the classical lacunar syndrome, which consists of motor symptoms, sensory, sensorimotor, ataxic hemiparesis or dysarthria-clumsy hand and display lower functional disability when compared to the other types (Arboix et al., 2005). Other less common causes of stroke include vasospasms due to SAH, cerebral vasculitis and coagulopathies (Ferro, Massaro and Mas, 2010).

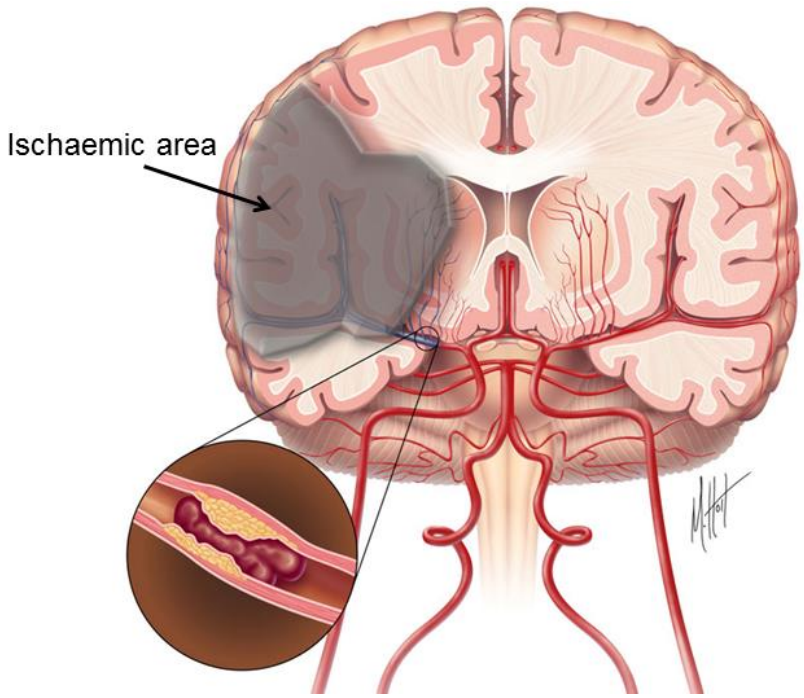

Figure 1-1 Ischaemic stroke illustration. Coronal brain section displaying the cerebral vasculature. The left middle cerebral artery is occluded due to the presence of an atherosclerotic plaque and blood clot obstructing blood flow. Grey area illustrates ischaemic damage due to cessation of blood supply and subsequent cell death. Figure adapted from strokecenter.org.

1.2.1 Cerebral blood flow and ischaemic stroke

Although the brain represents 2% of overall body weight, it is estimated that it receives 15-20% of total cardiac output (Heiss et al., 2011). As a result of an intense metabolic demand, the brain relies on CBF being maintained at critical levels despite variations in mean arterial blood pressures (MABP). Normal CBF in humans is approximately 50-60 mL/100g/min (Ellenbogen et al., 2012; Hossmann and Traystman, 2008). The effective cerebral perfusion pressure (CPP) is the difference between the systemic MABP and intracranial pressure (ICP) and is regulated by a number of factors. The arterial blood partial pressure of carbon dioxide ($PaCO_2$) is a critical regulator of cerebral vessels where it is a potent vasodilator (Shardlow and Jackson, 2008). Cerebral blood vessels possess a unique property where they have the ability to autoregulate (passively dilate or constrict) in response to fluctuations in systemic blood pressure and CPP thereby maintaining CBF within normal levels. If CPP fluctuates within a range of 60-150 mmHg, the brain has the capacity to maintain a relatively constant CBF. However, if CPP drops below this critical threshold then autoregulatory capacity is lost and CBF will then become linearly dependent on changes in MABP (Figure 1-2). Consequently, when CPP is below the autoregulation limit, cerebral ischaemia occurs (Hossmann and Traystman, 2008). In addition, following cerebral ischaemia the cerebral vessels lose their ability to autoregulate and therefore CBF follows a linear relationship with CPP (Figure 1-2) (Dirnagl and Pulsinelli, 1990).

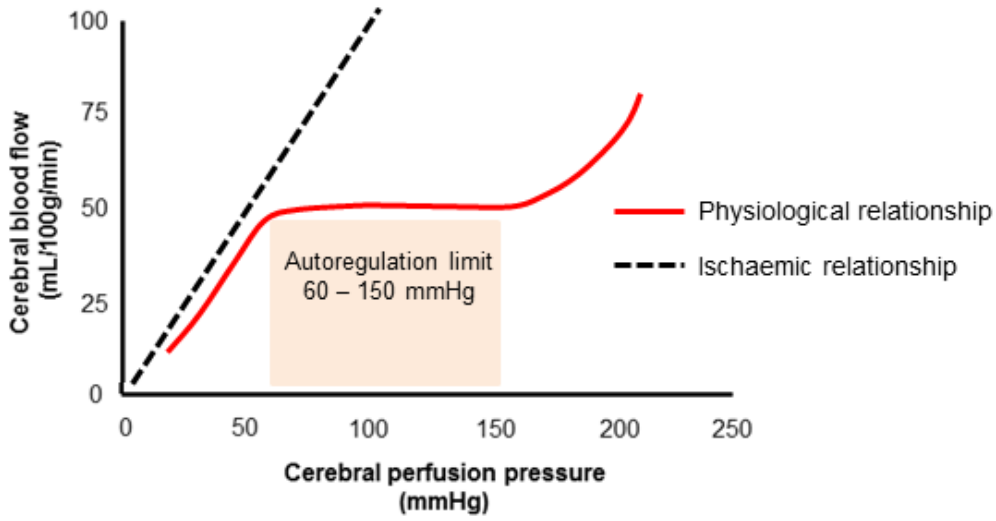

Figure 1-2 Relationship between CBF and CPP. When CPP fluctuates between 60-150 mmHg, CBF is maintaned at normal levels through autoregulation. If CPP is below or above that limit, it will become linearly dependent on mean arterial blood pressure. During ischaemia, autoregulation is lost and therefore CBF is linearly dependent on CPP.

During ischaemic stroke, CBF reduces across the vascular territory of the occluded vessel at differing levels. In the early 70s, Symon and colleagues identified that following cerebral ischaemia in baboons, CBF progressively decreased among three separate brain compartments that were later defined as irreversibly damaged (ischaemic core), tissue at risk of infarction (ischaemic penumbra) and hypoperfused tissue not at risk (benign oligaemia) (Symon et al., 1974).

1.2.1.1 The ischaemic penumbra: the therapeutic target

Critical CBF thresholds were first identified in non-human primates where it was observed that the area directly affected by the occluded vessels comprises the ischaemic core of irreversibly damaged tissue. In the ischaemic core, CBF is less than 6 mL/100g/min (Astrup et al., 1981); therefore, this area undergoes energy failure and irreversible cellular necrosis within minutes of stroke onset. In humans, position emission tomography studies identify the ischaemic core as tissue with a flow less than 12 mL/100g/min (Heiss, 2000).

Surrounding the ischaemic core is an area of brain tissue referred to as the ischaemic penumbra. The ischaemic penumbra was first identified in 1981 by Astrup and colleagues and described as:

“areas with less severe ischaemia with electrical failure but sustained energy metabolism (…) with the possible potential for recovery”, (Astrup et al., 1981).

Therefore, the ischaemic penumbra is a region of non-functioning but viable tissue. This concept was then expanded with the aid of imaging techniques where it was seen that the penumbral tissue consists of metabolically active tissue with reduced CBF yet increased oxygen extraction fraction (OEF, the fraction of oxygen extracted from arterial blood) and maintained oxygen consumption ($CMRO_2$) (Baron et al., 2008). CBF within the ischaemic penumbra ranges between 8-22 mL/100g/min in non-human primates and 12-22 mL/100g/min in humans (Astrup et al., 1977; Ford et al., 2012; Heiss, 1983, 2000). There are varying functional thresholds within the penumbra region, which means that there are different levels of possible neuronal recovery. For instance, in non-human primates, mild paresis is observed at 22 mL/100g/min whereas complete paralysis is seen at 8 mL/100g/min (Jones et al., 1981). Plus, spontaneous neuronal activity is abolished at 18 mL/100g/min and evoked potentials are prevented between 15-20 mL/100g/min CBF

(Branston et al., 1974; Heiss and Rosner, 1983). Therefore, at certain levels of CBF deficit, neurons are functionally inactive; however, structurally viable and possibly salvageable.

Perfusion within the penumbra is maintained by collateral blood supply. These include primary collaterals that form the arterial segments of the circle of Willis and secondary collaterals that include the ophthalmic artery and leptomeningeal vessels (Liebeskind 2003). Still, these cells have limited energy supply and if adequate blood supply is not provided, in time, the tissue becomes part of the core (Dirnagl et al., 1999). The characteristics of the penumbra led to the conclusion that this area provides a potential therapeutic opportunity to limit infarct size and progression (Figure 1-3). Consequently, the scientific community has been committed to the development of adjuvant neuroprotective drugs that could prevent penumbral cell death prior to and following reperfusion.

Benign oligaemia is characterised by CBF thresholds of above 22 mL/100g/min in both non-human primates and humans (Heiss, 2000). Here, tissue is characterised by reduced CBF but increased OEF and normal $CMRO_2$, therefore, CPP is fairly maintained due to autoregulatory compensation mechanisms (Lee et al., 2005). Oligaemic tissue is not usually at risk of infarction; however, if hypoxia persists and secondary events such as hypotension or hyperglycaemia take place, it may force this area to become at risk (Lee et al., 2005).

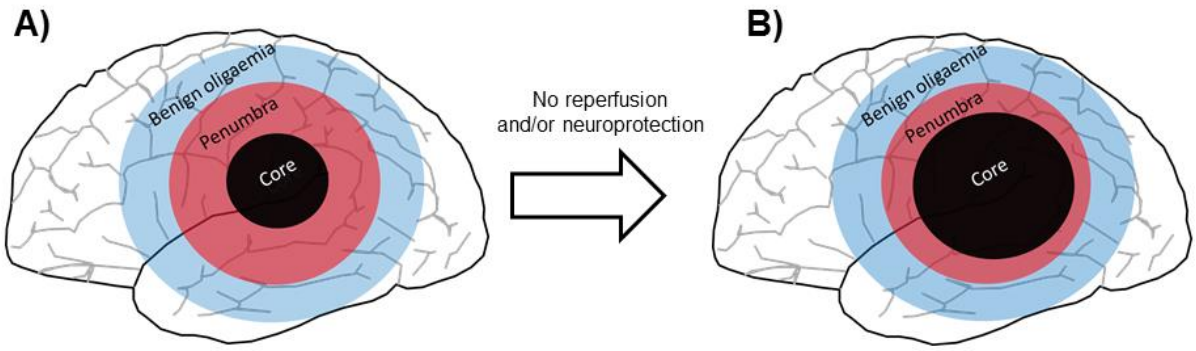

Figure 1-3 Cerebral blood flow compartments following cerebral ischaemia. A) CBF compartments after stroke onset. Irreversibly damaged (ischaemic core; black), tissue at risk of infarction (ischaemic penumbra; red) and hypoperfused tissue not at risk (benign oligaemia; blue). **B) Ischaemic core evolution.** If reperfusion is not established or a neuroprotective agent administered, penumbral tissue eventually becomes part of the infarct, increasing neuronal damage.

1.2.2 Pathobiology overview: from hypoxia to infarct

Ischaemic stroke is characterised by a substantial loss of glucose and oxygen delivery to the highly metabolic brain. Lack of adequate CBF delivery quickly triggers a pathophysiological cascade involving multiple mechanisms: bioenergetic failure, excitotoxicity, peri-infarct depolarisations, oxidative stress, blood brain barrier (BBB) breakdown, inflammatory responses and apoptosis (Brouns and De Deyn, 2009). Collectively these events are known as the "ischaemic cascade", a process that starts minutes after stroke onset and that lasts for several days, even when reperfusion is established. In fact, reperfusion alone results in secondary damages characterised by enhanced oxidative stress, inflammation and BBB disruption (Brouns and De Deyn, 2009). The components of the ischaemic cascade occur at different time points following the initiation of ischaemia with the collective end point resulting in cell death (Figure 1-4).

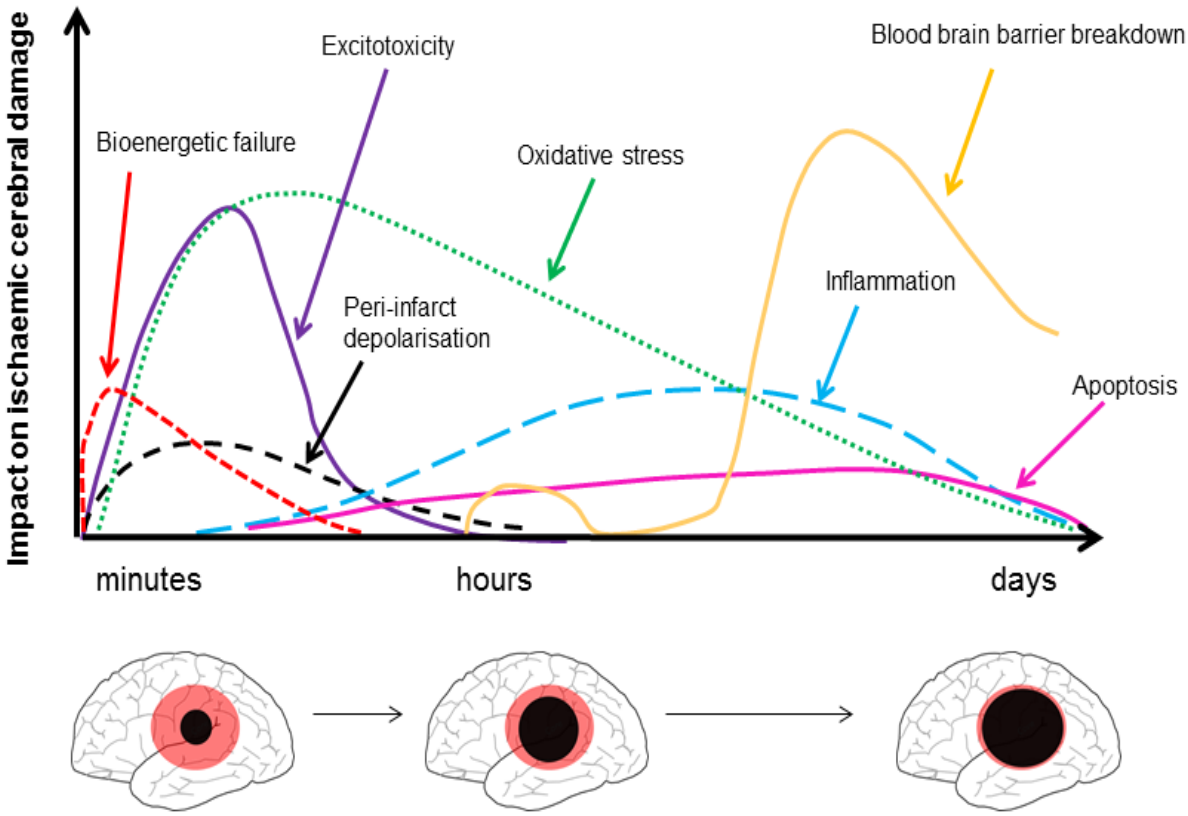

Figure 1-4 The ischaemic cascade. Injury starts with bioenergetic failure followed by excitotoxicity, oxidative stress and peri-infarct depolarisations. At later stages, inflammation and apoptosis take places with subsequent BBB breakdown. Figure adapted from Brouns & De Deyn 2009.

1.2.2.1 Energy failure and excitotoxicity

A normally functional brain is dependent on energy in the form of adenine triphosphate (ATP) primarily produced in the mitochondria (Sanderson et al., 2013). During ischaemia, glucose and oxygen cessation results in mitochondria failure and ATP production depletion, impairing ion transport pump maintenance. This results in depolarisation and excitatory amino acid release into the pre-synaptic space, particularly glutamate (Dirnagl et al. 1999). Glutamate extracellular accumulation is then further exacerbated by loss of energy dependent reuptake within astrocytes, triggering excitotoxicity (Dirnagl et al. 1999). Excessive glutamate overwhelmingly activates N-methyl-D-aspartate (NMDA) and α-amino-3-hydroxy-5-methyl-4-isoxazolepropionic acid (AMPA) receptors. In turn, intracellular Ca^{2+} and Na^{+} disproportionately accumulate in brain cells, triggering oxidative stress, cytotoxic oedema and necrosis (Dirnagl et al., 1999; Lipton, 1999).

1.2.2.2 Peri-infarct depolarisations

In healthy brain tissue, slowly propagating depolarisations take place across the cerebral cortex, a phenomena termed cortical spreading depolarisations (CSD) (Leão, 1944). These are triggered when a strong stimulus depolarises a certain volume of brain tissue, approximately 1 mm^3 in rats (Ayata and Lauritzen, 2015; Matsuura and Bureš, 1971). CSD are characterised by an intense depolarisation of both neurons and glial cells and subsequent rise in metabolic demand to restore ionic gradients (Ayata and Lauritzen, 2015). In a healthy brain, CSDs do not induce cell death and are well tolerated (Matsuura and Bureš, 1971; Nedergaard and Hansen, 1988). However, during cerebral ischaemia, CSD like depolarisations occur in the penumbral cells and are termed peri-infarct depolarisations (PIDs) (Hossmann, 1996).

PIDs are characterised by repetitive propagating depolarisations across the whole hemisphere, typically travelling at 3 mm/min and are associated with accelerated cerebral infarction (Hossmann, 1996). PIDs arise spontaneously within the ischaemic penumbra and are triggered by cells within the ischaemic core (Ayata and Lauritzen, 2015). In the latter, neuronal cells are undergoing permanent anoxic depolarisation, resulting in exacerbated extracellular release of glutamate and K^{+}. This ionic imbalance propagates to surrounding penumbral cells inducing depolarisation (Ayata and Lauritzen, 2015). On the contrary to cells within the ischaemic core, penumbral cells can repolarise; however, the mismatch between metabolic demands to support repolarisation and CBF delivery, further exhausts the limited ATP supply and potentiates cell death (Back et al., 1996). PIDs are crucial

elements of ischaemic stroke pathology as these exacerbate hypoperfusion. Plus, the PID number and duration correlate with infarct progression in several animal models and in humans (Dohmen et al., 2007; Fabricius et al., 2006; Mies et al., 1993; Shin et al., 2006).

1.2.2.3 Oxidative and nitrosative stress

Oxidative and nitrosative stress is characterised by the overwhelming generation of free radicals that surpass endogenous scavenger actions, resulting in cellular damage. There are several sources of free radical formation including Ca^{2+} overload, inflammation and reperfusion injury (Lakhan et al., 2009). Intracellular Ca^{2+} overload, triggers the activation of endonucleases, proteases and lipases (Crack and Taylor, 2005), which degrade cellular integrity components such as actin and laminin (Ankarcrona et al., 1995; Furukawa et al., 1997). In addition, Ca^{2+} overload activates phospholipase A_2 (PLA_2) and cyclooxygenase (COX), which generate reactive oxygen species (ROS) leading to lipid peroxidation and cellular damage (Jovin et al., 2008; Mattson et al., 2000). As a result of ROS formation, mitochondria become disrupted and leaky resulting in free radical burst, accentuating oxidative stress (Kristián and Siesjö, 1998). ROS are a main source of tissue damage by directly inducing cell death and their main source are NADPH oxidases (NOX), membrane-bound enzyme complex composed of membrane and cytosolic subunits (Girouard et al., 2009). In the brain, there are 3 main types: NOX1, NOX2 and NOX4. NOX1 is expressed in human brain tissue and in microglia (Cheret et al., 2008; Infanger et al., 2006), NOX2, or phagocytic NOX, is an inducible isoform localised in intracellular phagosomes and microglia (Cheret et al., 2008) whereas NOX4 is expressed in cortical neurons and capillaries after ischaemia (Vallet et al., 2005). NOX2 is the most crucial ROS generator during cerebral ischaemic injury (Girouard et al., 2009).

Another crucial player in free radical generation is nitric oxide (NO), a water soluble radical produced by nitric oxide synthase (NOS) on L-arginine (Iadecola, 1997). There are three types of NOS: neuronal NOS (nNOS), inducible NOS (iNOS) and endothelial NOS (eNOS) (Iadecola, 1997). During ischaemia, Ca^{2+} overload activates NOS generating NO which then reacts with superoxide to form a potent reactive nitrogen species, peroxynitrite (Iadecola, 1997). During ischaemia, nNOS and eNOS become quickly upregulated whereas the increased iNOS expression is delayed by 6-12 hrs after stroke onset and primarily associated with reperfusion injury (Iadecola, 1997; Lakhan et al., 2009).

1.2.2.4 Post-ischaemic inflammatory response

Inflammatory responses are triggered within hours of ischaemia onset and are part of a secondary phase of injury. During hypoxia, intracellular Ca^{2+} and free radicals activate a series of pro-inflammatory transcription factors such as nuclear factor kappa beta (NF-κB), which in turn stimulate the production of cytokines, chemokines and adhesion molecules that stimulate leukocyte infiltration (Moskowitz et al., 2010). Following the initiation of reperfusion, a robust inflammatory response takes place by permitting inflammatory cells to flow into the injury site. In turn, these inflammatory mediators contribute to cell death, BBB disruption and leukocyte infiltration in a temporal manner (Figure 1-5) (Benakis et al., 2015). Microglia and infiltrating leukocytes play a crucial role in exacerbating cell damage by releasing ROS, pro-inflammatory cytokines [i.e interleukin 1 beta (IL-1β)& interleukin 6 (IL-6)], iNOS and matrix metalloproteinase 9 (MMP9) as well as enhancing cyclooxygenase 2 (COX-2) expression and NF-κB activation (Lakhan et al., 2009; Liu et al., 1994; Schilling et al., 2009; Suzuki et al., 1999).

Resident microglial cells are the first cells to respond to ischaemic insult by changing from a ramified (resting) phenotype to an active amoeboid shape (Kettenmann et al., 2011). Activated microglia in the brain can be identified by ionised calcium binding adapter molecules (IBA1) and it has been shown that they are present within the peri-infarct region from as early as 3.5 hrs post-stroke whereas in the ischaemic core they typically appear from around 24 hrs post injury (Ito et al., 2001). In addition to microglia activation, inflammatory cells such as neutrophils, macrophages and lymphocytes accumulate within the injured site. Several chemokines and receptors are involved in leukocyte recruitment with interleukin 8 (IL-8), monocyte chemoattractant protein-1 (MCP-1) and regulated on activation normal T cell expressed and secreted (RANTES) receiving particular focus (Deb et al., 2010). IL-8 activates C-X-C motif chemokine receptor 2 (CXCR2) stimulating neutrophil chemotaxis (Jickling et al., 2015; Kostulas et al., 1999). MCP-1 activates C-C motif chemokine receptor 2 (CCR2) leading to macrophage infiltration (Dimitrijevic et al., 2007) whereas RANTES mediates its effects through C-C motif chemokine receptor 5 (CCR5) acting as a powerful leukocyte activator, particularly T cells (Deb et al., 2010; Terao et al., 2008).

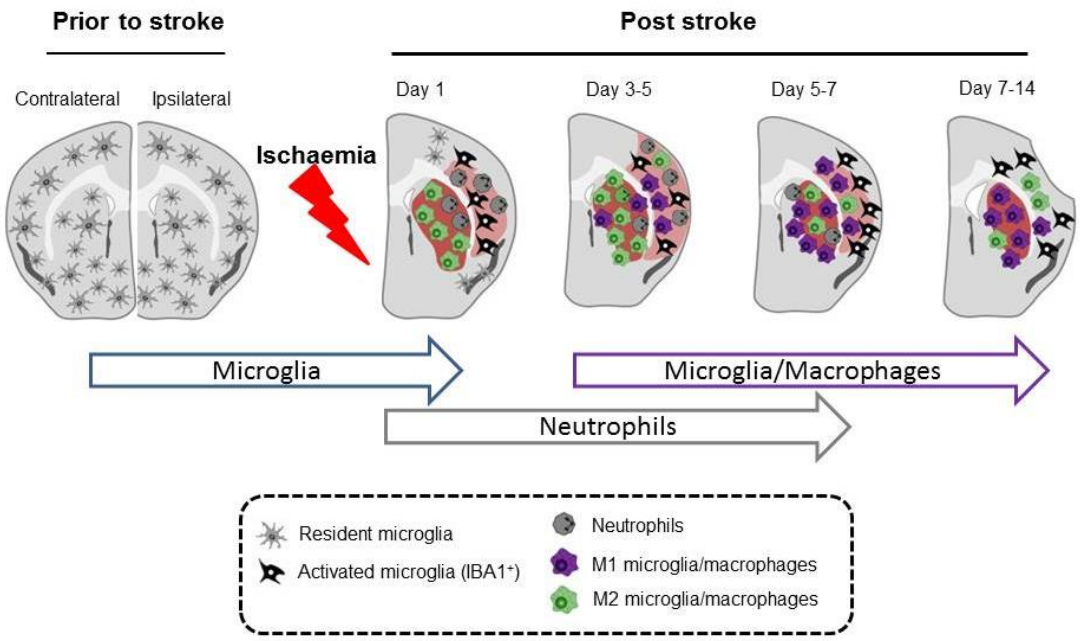

Figure 1-5 Spatio-temporal profile of microglia and leukocytes in infarct and peri infarct regions following transient middle cerebral artery occlusion (MCAO). In the infarct area (outlined in red), neutrophils are the first leukocytes to arrive to injury site with subsequent infiltration of M2 microglia/macrophages. In peri-infarct regions (outlined in pink), microglia are the first cells to become activated followed by neutrophil and macrophage infiltration. M2 type microglia/macrophage are concentrated within the infarct from 1-5 days post MCAO and then shift towards a M1 phenotype from 5-14 days post injury. In the peri-infarct, M1 phenotype is primarily present at 3-7 days and then becoming M2 type at 7-14 days. Figure adapted from Benakis et al., 2015.

Neutrophils are the first leukocytes to reach the ischaemic area and are detected from 1 to 7 days post stroke (Figure 1-5) (Huang et al., 2006). These are followed by macrophage infiltration, which are highly present across injured areas between 3-7 days after insult. As dying neurons activate macrophages, these become morphologically undistinguishable from microglia, and are referred to as microglia/macrophage. Microglia/macrophages are suggested to exert a dual role in ischaemic stroke (Benakis et al., 2015). Initially these cells induce neurotoxic effects through the production of ROS, IL-1β and IL-6 cytokine release (Rothwell et al., 1997) whereas at later stages microglia/macrophages are neuroprotective by phagocytosing excitotoxins and releasing neurotropic factors including transforming growth factor β1 (TGF-β1) and interleukin 10 (IL-10) (Iadecola and Anrather, 2011). These two alternating states are defined as M1 profile for pro-inflammatory and M2 for an anti-inflammatory and exhibit a specific gene expression profile (Table 1-2) (Hu et al., 2012). M1 phenotype is first observed in the peri-infarct region from day 3 whereas from day 5 onwards it is widely expressed in the infarct core. On the other hand, M2 type is highly expressed within the core between 1-5 days (Figure 1-5) (Benakis et al., 2015). Finally, lymphocytes can enter the infarcted brain in the later phases of cerebral ischaemia

between 3 to 7 days post strokeand peak no earlier than 5 days post stroke (Grønberg et al., 2013).

Table 1-2 Simplified list of microglia/macrophage M1 and M2 type specific genes

M1 type genes	M2 type genes	References
• Cluster differentiation 86 (CD86) • Cluster differentiation 32 (CD32) • Cluster differentiation 11b (CD11b) • C-C chemokine receptor 7 (CCR7) • IL-1β • IL-6 • iNOS	• Ym1/2 • TGF-β1 • C-C motif chemokine 22 (CCL22) • IL-10 • Arginase 1 (Arg1) • Cluster differentiation 163 (CD163) • Cluster differentiation 206 (CD206)	Hu et al. 2012; Cherry et al. 2014; Durafourt et al. 2012.

1.2.2.5 Blood brain barrier disruption

The BBB is a continuous and impermeable membrane that prevents the entry of potential harmful substances into the brain. The basic structure of the BBB consists of a capillary network where endothelial cells lack fenestrations and contain tight junction proteins (TJPs) (Lo et al., 2003). TJPs along with adherens junctions form a circumferential zipper-like structure between endothelial cells, limiting hydrophilic molecule passage. The preservation of the TJ is governed by three essential transmembrane proteins: claudins, occludin and junction adhesion molecules which are linked to the actin cytoskeleton through cytoplasmic zona occludens (ZO) proteins: ZO-1, ZO-2 and ZO-3 (Yang and Rosenberg, 2011). At present, it is widely recognised that the BBB is also formed by surrounding pericytes, perivascular astrocytes, neurons, extracellular matrix, microglia and oligodendrocytes and together, these components form the neurovascular unit (NVU) (del Zoppo, 2010).

Following stroke, the NVU becomes disrupted and TJP disassemble, allowing leakage of blood components into the brain parenchyma, a process named vasogenic oedema (Lo et

al., 2003). The effects of vasogenic oedema are overwhelming as it increases ICP, raising the risk of vascular compression, herniation and hemisphere displacement (Dirnagl et al., 1999). One of the initial events that results in damage to the BBB is the marked rise in oxidative stress that occurs resulting in the release of proteases and lipases that damage extracellular matrix and cytoskeletal components (Brouns and De Deyn, 2009). Following reperfusion, BBB breakdown is thought to occur in a biphasic pattern and to be the outcome of inflammation, oxidative stress and angiogenesis (Sandoval and Witt, 2008). Early BBB opening is suggested to occur between 3 to 6 hrs reperfusion and followed by BBB closing at approximately 15 to 24 hrs post reperfusion. After, the secondary phase of BBB breakdown takes place at around 48 to 72 hrs post stroke onset (Belayev et al., 1996; Pillai et al., 2009; Rosenberg et al., 1998; Veltkamp et al., 2005). The final phase of BBB disruption correlates with increased vasogenic oedema and greater tissue damage by allowing free leukocyte flow into the brain parenchyma and extravasation of red blood cells, resulting in haemorrhagic transformation (HT) (Mergenthaler et al., 2004).

1.2.2.6 Cell death after ischaemia

In the ischaemic brain, cell death occurs in a heterogeneous fashion. In the core, cell death occurs through necrosis, a rapid event that takes place within few minutes of stroke onset (Dirnagl et al., 1999). In these cells, the overwhelming Ca^{2+} and H_2O influx induces cytotoxic oedema and nuclear chromatin condensation takes place. Subsequently, nuclear, organelle and plasma membrane become disrupted, releasing intracellular content (Dirnagl et al., 1999). In the penumbra, cell death tends to occur through apoptosis, an organised energy dependent form of cell death that starts hours after injury, lasts for several days and contributes towards infarct expansion (Love, 2003; Mergenthaler et al., 2004). Apoptosis is associated with the upregulation of aspartate-specific cysteine proteases named caspases, particularly through the release of cytochrome C from the mitochondria (Love, 2003). These will cleave structural proteins leading to cytoplasm shrinkage, cell fragmentation, chromatin condensation and cell fragmentation (Love 2003). The main difference between necrosis and apoptosis is that in the former, dying cells will release glutamate and toxins that affect the surrounding cells whereas apoptosis leads to marginal inflammation and genetic content release. Both cell processes may occur in ischaemic cells and are dependent on degree of ischaemia, Ca^{2+} concentration and cellular microenvironment (Brouns and De Deyn, 2009; Unal-Cevik et al., 2004).

1.2.3 Current therapies and challenges

The first goal in ischaemic stroke treatment is to restore blood flow to the ischaemic brain. At the moment, intravenous (IV) alteplase stroke therapy or recombinant tissue plasminogen activator (rt-PA) is the only non-surgical treatment available and it works by lysing the clot obstructing the vessel following IV administration (Roth, 2011). Recanalization and consequent reperfusion of ischaemic brain is associated with reduced neurological deficit and mortality (Rha and Saver, 2007). Nonetheless, IV rt-PA has various limitations, for instance, the efficacy and safety of treatment is restricted to patients assessed within 4.5 hours of symptom onset and is mostly effective when administered within 90 min of symptom start (Emberson et al., 2014). Unfortunately, IV rt-PA may lead to serious complications including symptomatic intracranial haemorrhage, systemic bleeding and orolingual oedema (Tawil and Muir, 2017). Thus, this therapy is clinically challenging since it depends on a short therapeutic time window and balancing the benefit to risk (Figure 1-6). These limitations result in small eligibility numbers, which at the moment comprise 20% of patients (Figure 1-6) (Tawil and Muir, 2017). In addition, IV rt-PA therapy frequently fails to induce successful vessel recanalization, especially in patients with proximal large artery occlusion (Bhatia et al., 2010).

In order to target patients who are not eligible for or did not benefit from IV rt-PA, intra-arterial therapy and mechanical removal of the obstructing clot are a current line of therapy (Tawil and Muir, 2017). In 2015, five separate randomised controlled clinical trials tested the efficacy of stent retrievers for recanalization of proximal vessel occlusion compared to IV rt-PA or standard care. The results in these trials showed that mechanical endovascular thrombectomy significantly improved functional outcome after 90 days follow up (Berkhemer et al., 2015; Campbell et al., 2015; Goyal et al., 2015; Jovin et al., 2015; Saver et al., 2015). In particular, in the MR CLEAN trial, patients subjected to endovascular therapy within 6 hrs of symptom onset displayed improved modified Rankin Scale scores, smaller infarct volumes and lower final National Institutes of Health Stroke Scale (NIHSS) values (Berkhemer et al., 2015). Still, the efficacy of these options is equally time-dependent and relies on the expertise and efficiency of clinical centres (Tawil and Muir, 2017).

Although reperfusion is the main clinical outcome, reperfusion alone may exacerbate tissue salvage through reperfusion injury (Pan et al., 2007). CBF reestablishment leads to exacerbated inflammatory response that promotes hypoperfusion, cerebral oedema, HT and neuronal cell death (Pan et al., 2007). In fact, many patients treated with both thrombolysis

and thrombectomy procedures exhibit a phenomenon termed hyperintense acute reperfusion marker (HARM), characterised by blood vessel permeability in the meninges over the area of the stroke. This phenomenon is associated with worse clinical outcome as well as HT (Kassner et al., 2009; Kidwell et al., 2008; Kohrmann et al., 2012; Renú et al., 2015). Since alteplase administration is the treatment of choice and endovascular therapy is becoming increasingly used (Tawil and Muir, 2017), it is crucial to identify a potential adjuvant therapy with the capacity to limit injury following reperfusion.

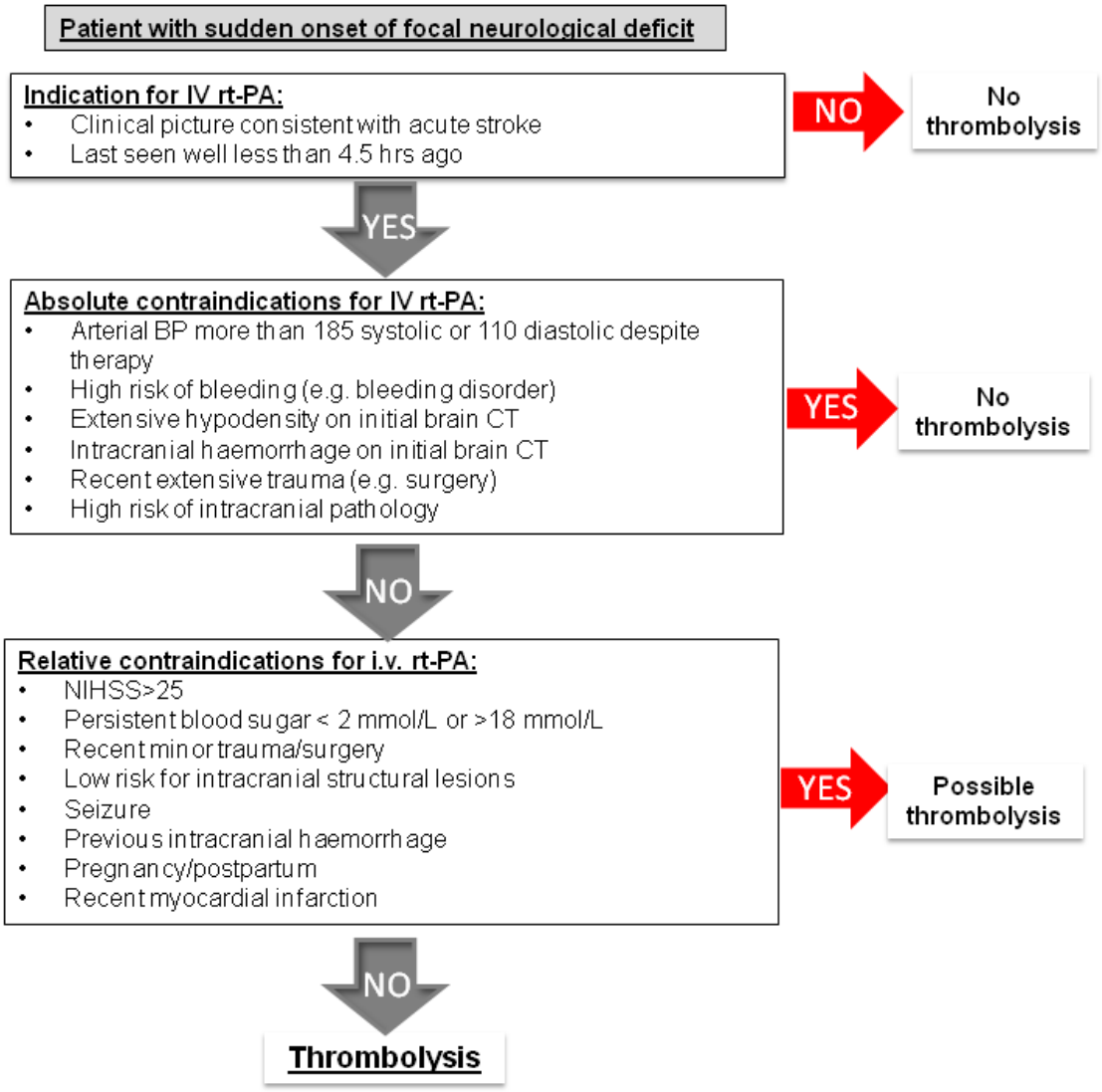

Figure 1-6 Indications and contraindications for thrombolysis (rt-PA) treatment in clinic stroke. BP: blood pressure; CT: computerised tomography; IV: intravenous; NIHSS: National Institutes of Health Stroke Scale. Figure adapted from Tawil & Muir, 2017.

1.2.4 Imaging the ischaemic brain

Imaging has become a critical component of stroke diagnosis with computed tomography (CT) being the most widely used technique clinically and the use of magnetic resonance imaging (MRI) in a research setting being increasingly used. MRI provides a more versatile technique that offers better image quality; however, CT remains the standard tool for initial diagnostics due to its wider availability and cost. These techniques are particularly useful in ruling out IHC and SAH to select patients for thrombolysis therapy (Muir and Macrae, 2016). Plus, these imaging techniques are of extreme relevance to detect alterations in ischaemic lesions and identify patients that will most likely benefit from therapy (Muir and Macrae, 2016). Although CT techniques are still the gold standard in clinic, these show lack of sensitivity in detecting early ischaemic lesions particularly between 6-12 hrs post stroke (Baird and Warach, 1998). On the other hand, MRI offers higher anatomical resolution capable of detecting pathological processes and organ function, arterial occlusion or stenosis in the circle of Willis. Consequently, MRI is a highly useful technique in the stroke context, being widely used in clinical and pre-clinical studies (Muir and Macrae, 2016).

1.2.4.1 Diffusion weighted imaging

Diffusion weighted imaging (DWI) is a sensitive MRI technique for detection of acute ischaemic lesions. The signal is based on the Brownian motion of protons or H_2O in biological tissues (Moseley, Cohen, et al., 1990). Under normal conditions extracellular water molecules diffuse relatively freely; however, following stroke, ATP depletion triggers an influx of extracellular Na^+ and Cl^- into the cell accompanied by H_2O accumulation, causing cytotoxic oedema (Liang et al., 2007). Cytotoxic oedema restricts extracellular H_2O diffusion, increasing the diffusion constant and DWI signal (Moseley, Cohen, et al., 1990). The decrease in H_2O diffusion can be quantified by calculating the apparent diffusion coefficient (ADC), allowing a quantitative measure of diffusion within a voxel. Higher ADC values represent areas of high diffusion whereas a decrease in ADC values is a result of H_2O diffusion restriction (Moseley, Cohen, et al., 1990). The latter is translated into a hyperintense signal on DWI scans and a hypointense signal on the ADC image. DWI can detect early ischaemic damage within minutes of ischaemic stroke onset in both animal models of stroke and in humans (Moseley, Kucharczyk, et al., 1990; Rother et al., 1996; Yoneda et al., 1999). Furthermore, it is reported to consist of a reliable quantification of immediate irreversible ischaemic damage (Baird and Warach, 1998).

DWI is also useful in the context of penumbra volume determination. Along with DWI, Perfusion Weighted imaging (PWI) can be carried out to detect the area of hypoperfusion. Following stroke, if the hypoperfused tissue region is larger than the DWI lesion then this can be used as an approximation of the ischaemic penumbra. Consequently, when overlaying the CBF map and DWI, there is a brain region which is hypoperfused but not irreversibly damaged, named DWI/PWI mismatch and representing the ischaemic penumbra (Schlaug et al., 1999).

1.2.4.2 MRI-T_2 weighted imaging

T_2-weighted imaging can be used to detect vasogenic oedema characterised by accumulation of extracellular fluid due to BBB breakdown. In comparison to normal tissue, infarcted tissue has a longer T_2 relaxation time. As a result, damaged cells will present higher signal intensity on T_2-weighted scans (Baird and Warach, 1998). T_2 fails to detect injury 2-3 hrs after stroke; therefore, it cannot be used to assess early ischaemia severity (Moseley, Kucharczyk, et al., 1990). However, it has been shown to reliably detect infarcted tissue during acute and subacute phases from 7 hrs after stroke (Boisvert et al., 1990; Loubinoux et al., 1997). At 24 hrs following stroke onset, the water content in the parenchyma increases resulting in a hyperintense signal on T_2 weighted imaging and therefore this increases sensitivity for infarct detection by up to 90% (Yuh et al., 1991). During subacute phases, between 24 hrs and 14 days, vasogenic oedema results in better definition of the infarct. As brain swelling and therefore vasogenic oedema begins to resolve around 7 to 10 days post stroke onset, T_2 MRI fogging occurs as a result of inflammatory cell infiltration and lesion resolution, yet, T_2 weighted imaging has been shown to provide adequate infarct detection sensitivity (Ricci et al., 1999).

1.2.5 Animal models of focal cerebral ischaemia

Ischaemic stroke is primarily studied in animal models by permanently or transiently occluding the MCA. Over the decades, several stroke models have been developed with two main purposes: to understand the pathological mechanisms underlying the condition and most importantly, to develop new therapies (Macrae, 2011). Human ischaemic stroke is incredibly diverse in terms of causes and localisation. Conversely, animal models provide a controllable, reproducible and standardised approach to study focal cerebral ischaemia, allowing a greater understanding of the molecular, physiological and biochemical brain alterations that cannot be detected in humans due to its invasive nature

(Fluri et al., 2015; McCabe et al., 2017). In fact, current pharmacological and imaging interventions used in clinic are the outcome of animal model studies. For instance, rt-tPA was first identified as a treatment option in a rabbit model and the usefulness of DWI studied in cats (Moseley, Kucharczyk, et al., 1990; Zivin et al., 1985). Since then, over 1000 agents have been tested in animals of stroke and reported to be neuroprotective (O'Collins et al., 2006); however, the compounds reaching clinical trials failed to show an improved outcome when compared to placebo (Henninger et al., 2010). Potential reasons for this translation failure have been extensively addressed, leading to the formation of The Stroke Therapy Academic Industry Roundtable (STAIR), which provides best practice guidelines to improve preclinical study quality (Fisher et al., 2009).

The majority of stroke studies are performed in rodents, primarily rats, as these are of lower cost, are more ethically accepted compared to larger species and allow access to transgenic techniques. In addition, rodents have a similar cerebral vasculature to that observed in humans and are relatively homogeneous amongst strains (Fluri et al., 2015). In human ischaemic stroke, the most commonly affected vessel is the MCA (Bogousslavsky et al., 1988), thus, a wide range of middle cerebral artery occlusion (MCAO) models have been developed, including the embolic, electrocoagulation, endothelin-1 (ET-1) and filament MCAO models (Longa et al., 1989; Macrae et al., 1993; Sharkey, 1993; Tamura et al., 1981). The choice of animal model is dependent on the drug being studied and its reported mechanism of action, with models of transient focal ischaemia being the most suitable models to examine potential anti-inflammatory agents. The most commonly used are the ET-1 induced and the filament model (Macrae, 2011).

1.2.5.1 Endothelin-1 induced MCAO model

This model was first developed in the rat and is based on the application of the potent vasoconstrictor ET-1 within the MCA territory (Macrae et al., 1993). It can be applied on the cortical surface of the exposed MCA or applied directly on the MCA through intracerebral injection leading to a highly reproducible infarct that covers all cortical layers (Fuxe et al., 1997; Macrae et al., 1993; Sharkey, 1993). Once administered, ET-1 will induce potent dose-dependent vasoconstriction that results in an initial CBF deficit of up to 50% (Biernaskie et al., 2001). After this steep reduction, reperfusion gradually occurs over a number of hours (Macrae, 2011). This model may be an adequate approach to replicate rt-PA administration in the clinic since reperfusion also occurs gradually after therapy (Sutherland et al., 2016). Advantages of this model include the possibility to visually

confirm ischaemia and adjust ET-1 doses accordingly, low mortality and the fact that it is less invasive in terms of surgical preparation (Fluri et al., 2015; Macrae, 2011). Disadvantages include variability in ET-1 potency and stability as well as the fact that ET-1 receptors are present in neurons and astrocytes (Fluri et al., 2015; Macrae, 2011). Once ET-1 receptors are activated, astrocytosis and axonal spouting may take place, impairing result interpretation (Fluri et al., 2015). In addition, ischaemia is reported to develop slowly after ET-1 injection, therefore, this model is considered by some as an unsuitable approach to replicate human stroke (Schirrmacher et al., 2016).

1.2.5.2 Intraluminal filament MCAO model

The intraluminal filament model is the most widely used model in rodents and is characterised by the insertion of a flexible monofilament into the internal carotid artery (ICA) until it occludes the MCA (Macrae, 2011). One of its advantages is that it can be used to study permanent ischaemia by leaving the filament in place or transient ischaemia by removing the filament and allowing reperfusion. In the latter, the most common ischaemic duration periods are 60, 90 and 120 min (Fluri et al., 2015; Garcia et al., 1995). This model allows you to precisely control ischaemia duration, is relatively non-invasive as it does not require craniotomy and it is characterised by large infarcts (Macrae, 2011). Disadvantages include reproducibility and mortality issues. For instance, blocking the MCA should induce both cortical and striatal injuries; however, it is common for some animals to exhibit striatal infarcts only, possibly as a result of inadequate vessel occlusion (Macrae, 2011). Plus, the fact that this is a closed skull model, enhanced cerebral oedema is present between 24-48 hrs post injury and mortality rates can go up to 42% (Macrae, 2011).

Since the majority of thromboembolic strokes occur within the MCA territory, this model is considered suitable to directly replicate the condition; however, in humans, vessel occlusion is often incomplete and partial spontaneous reperfusion usually occurs due to thrombus degradation (Zanette et al., 1995). In the filament model, reperfusion occurs suddenly and for this reason, this model may be deemed unsuitable to test future stroke therapies (Hossmann, 2012). Nonetheless, the success in thrombectomy therapies within the clinic has given new light to the use of this set up. Transient MCAO with the filament model and thrombectomy surgery lead to abrupt reperfusion and induce a similar CBF post-ischaemic profile (Sutherland et al., 2016). Therefore, the filament model is now

considered the most suitable model for studying potential adjunctive therapies that can be given alongside thrombectomy (Sutherland et al., 2016).

1.3 The Renin Angiotensin System: from homeostasis to cardiovascular disease

The Renin Angiotensin System (RAS) is a crucial component of homeostatic control of blood pressure, tissue perfusion, extracellular volume and electrolytes in vertebrates (Skeggs et al., 1976). However, its pathological activation is implicated in the development and progression of cardiovascular disease (CVD) by inducing excessive vasoconstriction, inflammation, oxidative stress, cell growth and hypertrophy (Dzau, 2001). RAS overactivation mediates injury in multiple ischaemic stroke risk factors such as hypertension, myocardial infarction and atherosclerosis (Dzau, 2001). As a result, RAS blockers including angiotensin converting enzyme (ACE) inhibitors and angiotensin II receptor type 1 (AT_1R) blockers (ARBs) have revolutionised the treatment of CVD and shown to decrease stroke incidence in hypertensive patients (Griendling et al., 1996; Thone-Reineke et al., 2006). The impact of RAS overactivation in ischaemic stroke pathology alone is not well understood; however, increasing evidence from animal models suggest that the RAS is not only implicated in injury but may also provide a therapeutic target (Culman et al., 2002; Walther et al., 2002).

1.3.1 Brief historical perspective on the RAS

The RAS was first discovered more than 100 years ago by Tigerstedt & Bergman following the observation that renal cortex extracts, which they named renin, promoted hypertension in a rabbit model (Tigerstedt and Bergman, 1898). The link between these extracts and hypertension was later observed in an ischaemic model of renal injury, in which a pressor substrate was shown to be released following injury (Goldblatt et al., 1934). It was then identified that apart from renin, a short-lived pressor protein, angiotensinogen, was released and served as its substrate. The outcome of this enzymatic reaction was demonstrated to be angiotensin (Ang), initially named as hypertensin and angiotonin by two different research groups (Braun-Menendez et al., 1940; Page and Helmer, 1940). Following the discovery of Ang it was then shown to be expressed in the blood plasma in two distinct isoforms, angiotensin I (Ang I) and angiotensin II (Ang II) (Skeggs et al., 1954). The former was demonstrated to be an inactive decapeptide that is converted to the main effector Ang II through the cleavage activity of ACE at the histidyl-

leucine from the C terminus (Skeggs et al., 1954; Skeggs, Lentz, et al., 1956). Since its initial discovery, new RAS components have been identified and this line of research is ongoing.

1.3.2 The Classical RAS

Under normal physiological conditions, the classical circulating RAS is triggered by multiple stimuli. These include alterations in blood pressure detected at the levels of the renal afferent arteriole, changes in NaCl delivery to the macula densa of the distal tubule and β1 adrenergic receptor nerve stimulation (Reid, 1985). The classical RAS axis is initiated with the release of renin, a single chain aspartyl protein and rate-limiting enzyme, from the juxtaglomerular apparatus of the kidney (Reid, 1985). Renin cleaves the leucine and valine amino acids on angiotensinogen, a α-2 glycoprotein constitutively produced and released from the liver (Deschepper, 1994). The product of this enzymatic activity is Ang I, which is cleaved in plasma and pulmonary circulation by ACE (Corvol et al., 1995; Skeggs, Kahn, et al., 1956). ACE is a carboxypeptidase and the main enzyme responsible for the conversion of Ang I to the potent vasoconstrictor Ang II (Skeggs, Kahn, et al., 1956). Apart from its role in generating Ang II, ACE has the ability to hydrolyse bradykinin, inhibiting its vasodilatory actions (Yang et al., 1970). There are two forms of ACE, somatic and germinal, the former is expressed ubiquitously whereas the latter is predominantly found in testes (Turner and Hooper, 2002). Once generated, Ang II binds to G coupled protein receptors (GPCRs), AT_1R and angiotensin II receptor type II (AT_2R); however, it predominantly exerts its effects through the AT_1R (Mehta and Griendling, 2007). Together these components form the classical arm of RAS defined as the **ACE/Ang II/AT_1R axis** (Figure 1-7).

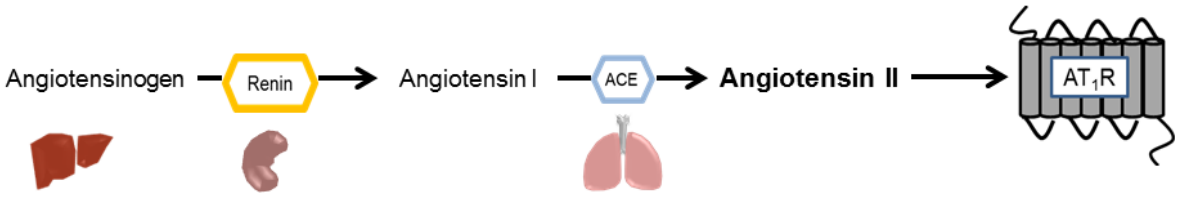

Figure 1-7 The classical RAS. Under physiological conditions, the circulating RAS is triggered and renin released from the juxtaglomerular apparatus. Renin will then cleave angiotensinogen, which is released from liver; to from Ang I. Ang I is converted by ACE in the circulation and lungs to form Ang II, the main effector. Ang II will exert its effects by primarily binding to AT_1R.

1.3.3 The Extended RAS

Advances in the field have demonstrated that the RAS is far more complex than initially thought. Distinct Ang II receptors and signal transduction pathways have been characterised, new biologically active peptides and enzymes identified as well as new pathways for peptide generation (Figure 1-8) (Paul et al., 2006). In addition, it is now accepted that the RAS is ubiquitously expressed and produced as a local/tissue system independent from circulation recruitment and present in several organs, including the brain (Paul et al., 2006).

The discovery of new components and local tissue RAS has changed the conventional conception of the RAS. For instance, it is now understood that renin is released as an inactive pre-prohormone, where the pre-segment acts as signal peptide destined to direct the prohormone for secretion. The prorenin binds to the pro-renin receptor (PRR) present on the cell membrane and the pro-segment is removed to generate active renin (Nguyen et al., 2002; Nguyen and Muller, 2010). This step is crucial in tissue RAS as it provides a mechanism to locally generate renin (Paul et al., 2006). Once Ang II is formed through the classical pathway described above, it will be metabolised by several enzymes such as aminopeptidase A, which converts Ang II to Ang III, the latter stimulating vasopressin release in the brain (Zini et al., 1996). Subsequently Ang III is metabolised by aminopeptidase N to form Ang IV, a ligand for the angiotensin type IV receptor (AT_4R), involved in memory processing (McKinley et al., 2003; Swanson et al., 1992). Most importantly, Ang II can be metabolised by angiotensin converting enzyme 2 (ACE2), a novel zinc metalloproteinase discovered in 2000 (Donoghue et al., 2000). ACE2 is an 805 amino acid sequence type 1 membrane-bound glycoprotein encoded on the X chromosome, presents a molecular weight of 120kDa and shares 42% homology with the catalytic domain ofsomatic ACE (Donoghue et al., 2000; Tipnis et al., 2000). Initially it was shown that ACE2 hydrolysed Ang I to form angiotensin-(1-9) (Ang-(1-9)); however, further studies showed that ACE2 has a 400-fold higher catalytic efficiency for Ang II rather than Ang I (Donoghue et al., 2000; Vickers et al., 2002).

Ang II is the main substrate for ACE2 and the most important product is angiotensin-(1-7) [Ang-(1-7)], a biological active heptapeptide (Santos et al., 2003; Vickers et al., 2002). Ang-(1-7) can be formed through various pathways, for example, Ang (1-9) can be converted by ACE and neprilysin (NEP) forming Ang-(1-7) (Donoghue et al., 2000; Vickers et al., 2002). Moreover, Ang-(1-7) can be formed by the direct actions of NEP,

thimet oligopeptidase (TOP) and prolyl endopeptidases (PEP) on Ang I (Figure 1-8) (Gironacci et al., 2014; Welches et al., 1991; Yamamoto et al., 1992). Ang-(1-7) is also degraded by ACE to produce Ang-(1-5) (Figure 1-8) (Chappell et al., 1998). Further research has identified that Ang-(1-7) specifically activates the Mas receptor (MasR) and its biological effects antagonise the classical ACE/Ang II/AT_1R (Sampaio et al. 2007; Santos et al. 2003). This led to the identification of a new arm of the RAS, the counter-regulatory RAS axis: **ACE2/Ang-(1-7)/MasR axis** (Donoghue et al., 2000; Santos et al., 2003; Vickers et al., 2002).

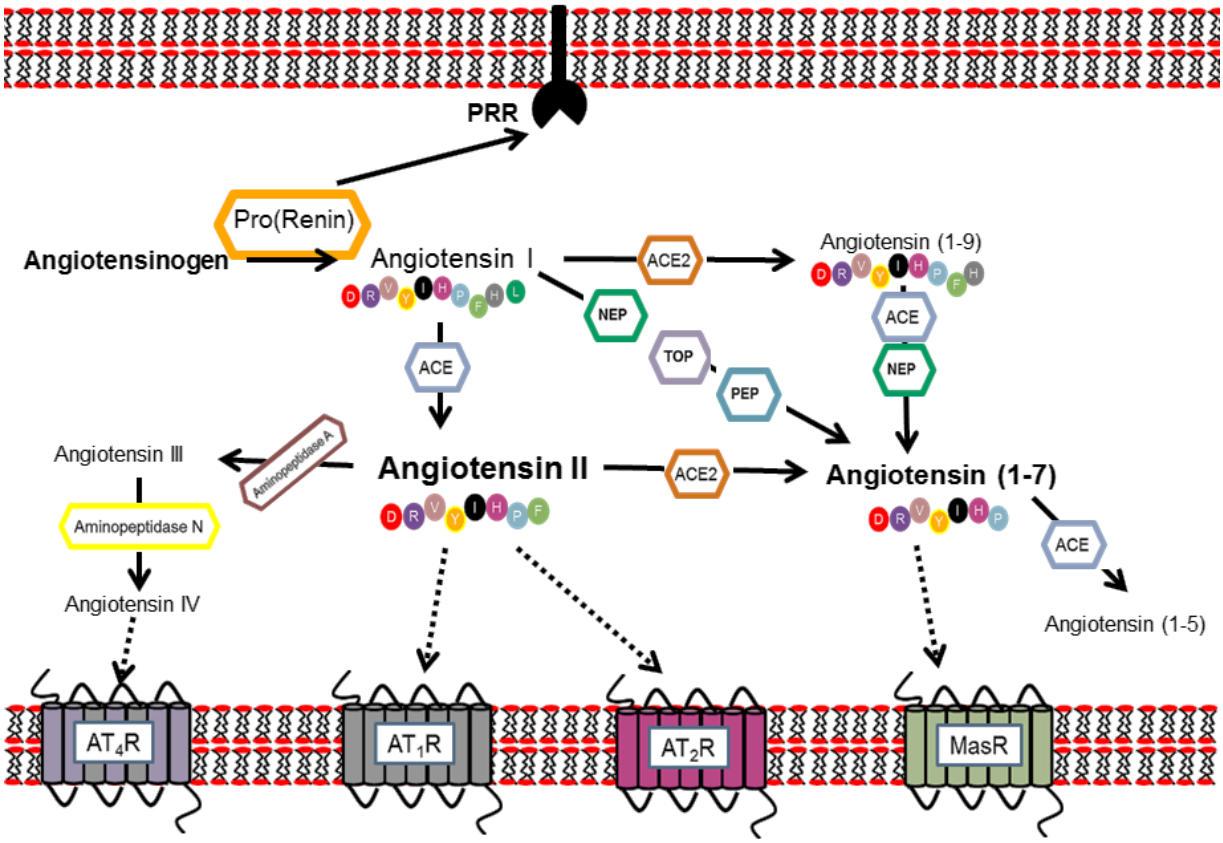

Figure 1-8 The extended RAS. Ang II is generated by the classical pathway and will bind to two receptors, AT_1R and AT_2R. Ang II is cleaved by aminopeptidase A generating Ang III, which is then metabolised by aminopeptidase N forming Ang IV, a ligand for AT_4R. In addition, Ang II is metabolised by ACE2 producing the heptapeptide Ang-(1-7), a ligand for MasR. Other Ang-(1-7) pathways include direct actions of NEP, TOP and PEP on Ang I. Moreover, Ang I can be metabolised by ACE2 generating Ang-(1-9), which is then cleaved by ACE and NEP to produce Ang-(1-7). Once formed, Ang-(1-7) will be degraded by ACE to form Ang-(1-5).

1.3.4 ACE/Ang II/AT_1R: the detrimental axis in cardiovascular disease

Studies conducted in stroke risk factors, primarily hypertension, have provided valuable information regarding the involvement of the RAS in CVD pathology, setting the premise that the RAS may be implicated in ischaemic stroke. As research continues within the stroke field in clarifying this hypothesis, it is plausible to assume that some of the effects induced in peripheral CVDs may overlap with the stroke setting. Therefore, this section will outline findings in peripheral CVDs that support a rationale for RAS targeting in cerebral ischaemia.

Under normal conditions, Ang II is primarily generated by ACE and its plasma levels range between 41.8 – 61.7 pg/mL in healthy humans and 53.0 – 141.6 pg/mL in anaesthetised male rats (Huang et al., 1989; Vilas-Boas et al., 2009). Once formed, Ang II will exhibit a half-life of 30 sec in the circulation and 15 min in tissues (van Kats et al., 1997). Physiologically, Ang II leads to vasoconstriction; aldosterone release from adrenal glands, NaCl reabsorption and K^+ excretion, vasopressin secretion from the pituitary gland and increased sympathetic activity (Reid, 1985). During CVD; however, the RAS is overactive leading to exacerbated formation of Ang II. In turn, Ang II through the AT_1R will mediate the pathophysiology of several conditions including hypertension, atherosclerosis, and myocardial infarction by stimulating vasoconstriction, oxidative stress, inflammation, cellular growth, migration and hypertrophy (Mehta and Griendling, 2007; Touyz and Schiffrin, 2000). For this reason, ACE inhibitors such as ramipril and ARBs, the latter referred to as “sartans” are successfully used to treat hypertension (Menard and Patchett, 2001). Conversely, AT_2R activation is believed to counteract the detrimental effects of the ACE/Ang II/AT_1R axis inducing vasodilation, anti-oxidative, anti-inflammatory and anti-proliferative effects (Schmieder et al., 2007).

1.3.4.1 The Angiotensin II receptor type I

The AT_1R is a GPCR composed of a 359 amino acid protein with approximately 40kDa molecular weight (Mehta and Griendling, 2007). In humans, the AT_1R gene is mapped to chromosome 3 whereas in rodents it is present as two isoforms, AT_{1a} and AT_{1b}, which are mapped on chromosome 17 and 2, respectively (Mehta and Griendling, 2007). These isoforms are not distinguishable pharmacologically; instead, they exhibit different tissue distribution. AT_{1a} is mostly expressed in rat cardiovascular tissues and in the cerebrum and cerebellum whereas AT_{1b} is predominantly found in the adrenal and pituitary glands (Kakar et al., 1992; Kitami et al., 1992). Once activated, AT_1Rs are quickly desensitised (10 min after activation), a process characterised by ligand-receptor uncoupling, receptor endocytosis and total receptor number downregulation (Griendling et al., 1987; Guo et al., 2001). The mechanisms by which AT_1R acts involve multiple G-protein-dependent and G protein-independent signalling pathways and are well characterised in the periphery (Mehta and Griendling, 2007).

The classical GPCR signalling, involves $G\alpha_{q/11}$, $Gq_{12/13}$ and $G_{\beta y}$ coupling to AT_1R, resulting in phospholipase C (PLC), phospholipase A_2 (PLA_2) and phospholipase D (PLD) activation (Ushio-Fukai et al., 1998). PLC quickly triggers the formation of inositol-1,4,5-triphosphate (IP_3) and diacylglycerol (DAG). IP_3 binds to its receptor in the sarcoplasmic reticulum increasing intracellular Ca^{2+} concentration and resulting in vasoconstriction (Kanaide et al., 2003), whereas DAG activates protein kinase C (PKC), leading to vasoconstriction, cell proliferation and oxidative stress by directly activating NOX (Kanaide et al., 2003; Vallega et al., 1988). PLD activation results in the generation of choline and phosphatidic acid, the latter is then converted to DAG (Lassègue et al., 1993). Activation of PLA_2 stimulates the release of arachidonic acid from the phospholipid cell membrane in vascular smooth muscle cells. Arachidonic acid is processed by COX-2 and lipoxygenases to generate prostaglandins (PG) and leukotrienes (LT), which are implicated in vasoconstriction, inflammation and oxidative stress (Figure 1-9) (Griendling et al., 1996).

G-protein independent pathways include NOX, mitogen-activated protein kinases (MAPKs) such as extracellular-signal-related kinase 1/2 (ERK1/2), p38 MAPK and c-Jun NH_2-terminal kinase (JNK) as well as non-receptor tyrosine kinases (NRTKs) including the Src, the Janus kinase/signal transducer and activator of transcription (JAK/STAT) and the focal adhesion kinase (FAK) pathways (Mehta and Griendling, 2007). Furthermore,

Ang II can trigger receptor tyrosine kinase (RTK) activation such as endothelial growth factor receptor (EGFR) and platelet derived growth factor (PDGF), inducing cellular remodelling (Mehta and Griendling, 2007). Ang II activates NOX1 and NOX4 in the vascular cell membrane, generating ROS and potentiating oxidative stress (Lassègue et al., 2001). ROS signalling then activates a series of signalling molecules and transcription factors such as NF-κB and activator protein 1 (AP-1), promoting apoptosis and the expression of inflammatory mediators (Sen and Packer, 1996). Ang II induced activation of p38 MAPK, Src and EGFR is ROS-sensitive and once triggered will mediate cell proliferation, hypertrophy, migration, fibrosis and inflammation (Mehta and Griendling, 2007). Moreover, Ang II induced ERK1/2, JNK and p38 MAPK activation leads to cell proliferation, inflammation and fibrosis (Figure 1-9) (Mehta and Griendling, 2007).

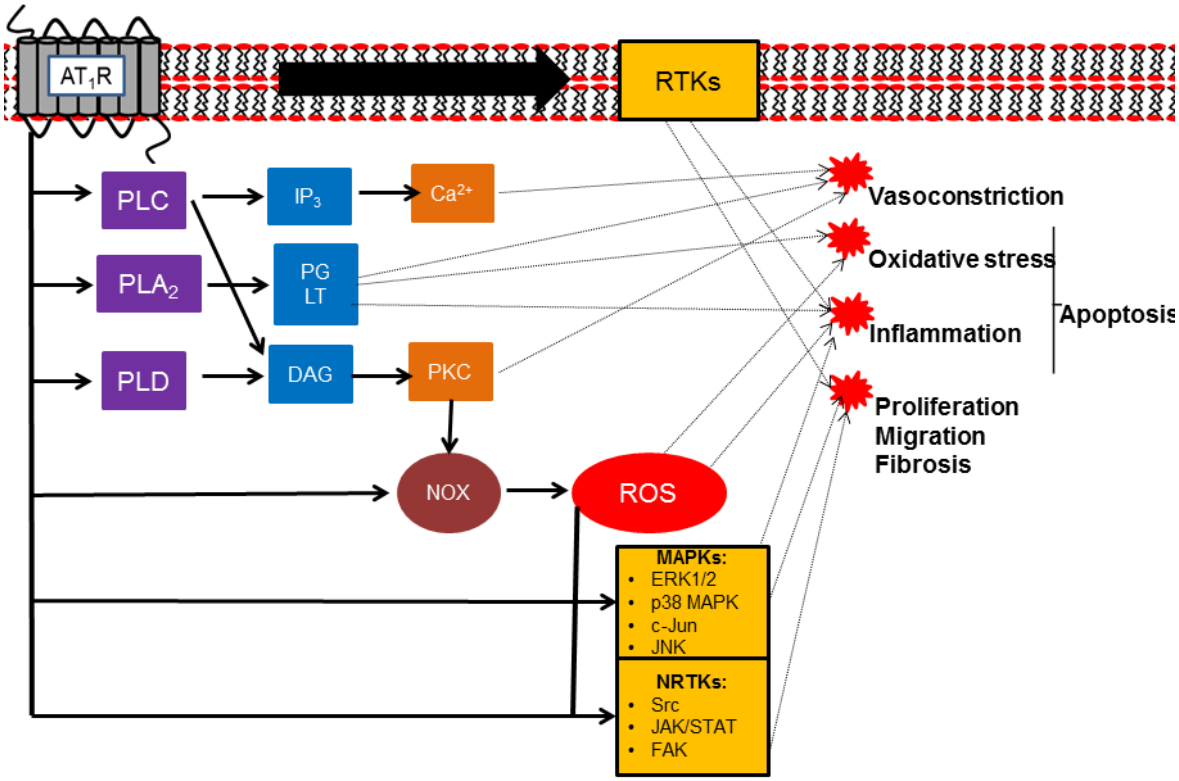

Figure 1-9 The Angiotensin II receptor type I signalling. AT_1R activation through Ang II leads to a wide range of effects including vasoconstriction, oxidative stress, inflammation, proliferation, migration and fibrosis. AT_1R activates PLC, PLA_2 and PLD, receptor tyrosine kinases (RTKs), non-receptor tyrosine kinases (NRTKs) and MAPKs. PLC leads to IP_3 and DAG formation. IP_3 increases intracellular Ca^{2+} whereas DAG activates PKC. PKC and AT_1R activate NOX generating ROS, which will trigger NRTKs and MAPKs. PLA_2 stimulates the production of PG and LT.

1.3.4.2 The Angiotensin II receptor type II

The AT_2R is a GPCR composed of a 363 amino acid peptide with a 41kDa molecular weight. AT_2R is 34% identical to AT_1R and is expressed as one subtype only in both humans and rodents, sharing 92% homology (Griendling et al., 1996). The AT_2R is encoded on the X chromosome and although primarily activated by Ang II, other RAS components have shown to have affinity for this receptor and suggested to pose as possible ligands. The order of affinity is as follows: Ang II>Ang III>Ang IV>Ang-(1-7) (Bosnyak et al., 2011). Moreover, several agonists have been developed such as CGP42112A and Compound 21 (C21), a promising selective non-peptide and orally active AT_2R agonist(Wan et al., 2004). These compounds are currently being tested as possible therapeutic CVD strategies whereas receptor antagonists include PD123319 (Matavelli and Siragy, 2015; Steckelings et al., 2012). AT_2R is predominantly expressed in foetal tissues (Millan et al., 1991; Shanmugam et al., 1996; Tsutsumi and Saavedra, 1991a) and unlike other GPCRs, it does not undergo desensitisation or internalisation (Turu et al., 2006). Instead, receptor activation induces a sustained response whilst possessing constitutive activity independent of ligand binding (Miura et al., 2005).

In CVD, AT_2Rs are suggested to be involved in three main pathways: NO-cyclic guanosine monophosphate (cGMP) system regulation, PLA_2 release stimulation and activation of phosphatases (Nouet and Nahmias, 2000). These effects are G-protein-independent and dependent (Hansen et al., 2000). In endothelial cells, AT_2R activates eNOS stimulating the production of NO, which will then act on guanylyl cyclase to produce cGMP and induce vasorelaxation (Ritter et al., 2002). Similarly, NO induced vasodilation can be triggered through AT_2R interaction with bradykinin receptor 2 (B_2R) by forming AT_2R:B_2R complexes (Abadir et al., 2006). AT_2R activation also leads to PLA_2 stimulation inducing the generation of epoxyeicosatrienoic acids, promoting vasodilation (Arima et al., 1997). Furthermore, AT_2R signalling is implicated in SHR2 domain-containing tyrosine phosphatase (SHP-1), protein phosphatase 2 (PP2A) and MAP kinase phosphatase (MKP-1) activation (Nouet and Nahmias, 2000). PP2A and MKP-1 directly inhibit MAPK (ERK1/2), stimulating apoptotic mechanisms whereas SHP-1 inhibits NOX and ERK1/2, diminishing ROS generation and inflammation (Figure 1-10) (Rompe et al., 2010; Wu et al., 2004).

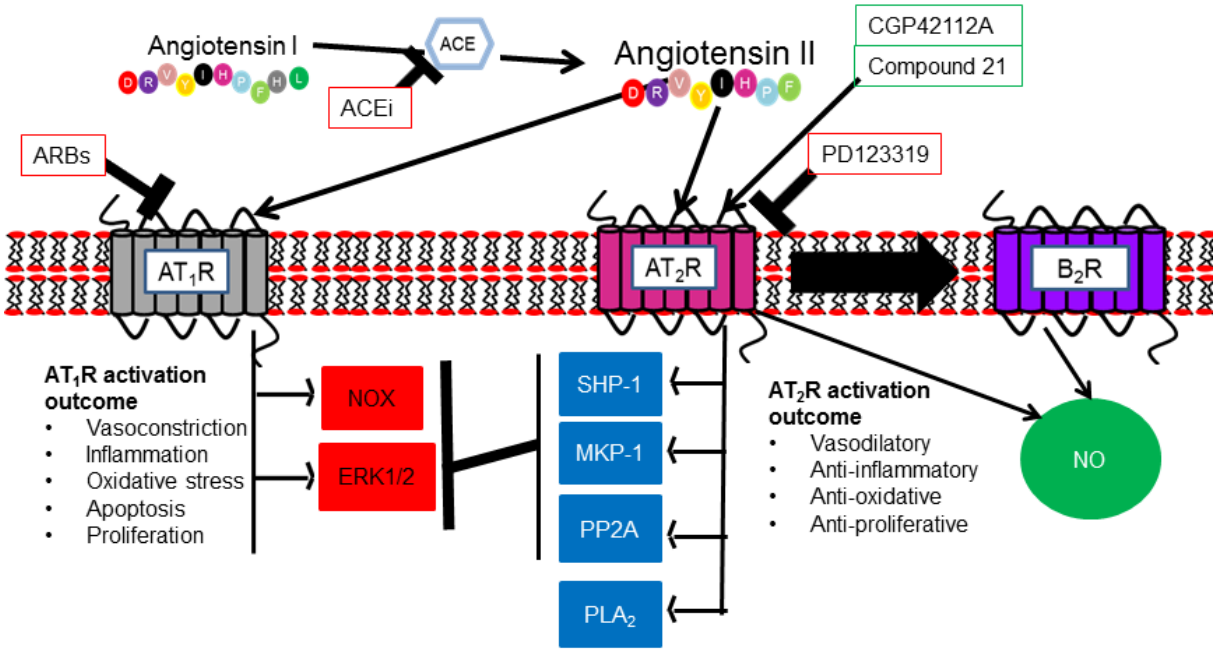

Figure 1-10 The proposed signalling at the Angiotensin II receptor type II. The AT_2R is suggested to counteract the detrimental effects of AT_1R by activating SHP-1, PP2A and MKP-1. These will then inhibit AT_1R induced activation of NOX and ERK1/2. AT_2R is thought to trigger NO formation through eNOS and by interacting with B_2R to enhance NO formation. Additionally, it is suggested to activate PLA_2, possibly inducing vasodilation. Altogether, AT_2R signalling is proposed to induce vasodilatory, anti-inflammatory, anti-oxidative and anti-proliferative effects in CVD. Image also depicts the site of action for ARBs and ACE inhibitors (ACEi) as well as AT_2R agonists, Ang II, CGP42112A & C21, and antagonist, PD123319.

1.3.5 ACE2/Ang-(1-7)/MasR: the counter-regulatory axis

In 1988, Santos and colleagues discovered Ang-(1-7), a biologically active heptapeptide (Santos et al., 1988) generated by the actions of ACE2 on Ang II as well as alternative pathways as described in section 1.3.3. The biological activity of Ang-(1-7) was observed in the rat hypothalamo-neurohypophysial system *in vitro* as it stimulated vasopressin release and in *in vivo* where it triggered a hypotensive and bradycardic response following medulla oblongata stimulation (Campagnole-Santos et al., 1989; Schianove et al., 1988). Under physiological conditions, Ang-(1-7) circulating levels range between 17.1–25.5 pg/mL in humans and are approximately 4 pg/mL in rats (Ocaranza et al., 2006; Vilas-Boas et al., 2009). Ang-(1-7) has a half-life of approximately 30 min following subcutaneous (SC) and IV injections in humans (Kono et al., 1986; Petty et al., 2009). In rodents, the half-life of Ang-(1-7) is very short and reported to be 10 sec following IV administration (Yamada et al., 1998). It is important to note that Ang-(1-7) measurements are often performed using antibody-based immunoassays. As a result, cross-reactivity with

other RAS peptides may occur. Additionally, Ang-(1-7) is quickly degraded by ACE and the detected concentration in tissue samples may not necessarily be accurate.

Ang-(1-7) is suggested to act as the main counter-regulatory mediator of the RAS by inducing vasodilation, anti-proliferative, anti-inflammatory, anti-oxidative effects (Iusuf et al., 2008). For this reason ACE2 activators have been used in preclinical studies such as diminazene aceturate (DIZE) and regarded as a potential antihypertensive drug (Gjymishka et al., 2010). Ang-(1-7) is suggested to directly act as an antagonist on the AT_1R and the AT_{1A} and to mediate part of its effects by activating the AT_2R (Clark et al., 2001; Gironacci et al., 1999; Roks et al., 1999; Walters et al., 2005). Most recently it was discovered that Ang-(1-7) is a selective agonist for the orphan Mas proto-oncogene (K_d =0.83 nmol/L) (Santos et al., 2003).

1.3.5.1 The Mas receptor

The MasR is a GPCR composed of 325 amino acid peptide encoded in the distal half of chromosome 6q (Rabin et al., 1987; Young et al., 1986). It was initially characterised as a proto-oncogene involved in tumorigenesis and inaccurately suggested to be an Ang II and Ang III receptor (Young et al. 1986; Jackson et al. 1988); however, it is now established as a selective receptor for Ang-(1-7) (Santos et al., 2003). The MasR gene is present in humans, rats and mice, sharing a 97% homology between rodents, and it is ubiquitously expressed with highest concentration in the brain (Metzger et al., 1995; Young et al., 1988). Ang-(1-7) promotes MasR internalisation and endocytosis through a clathrin-mediated pathway 10 min post stimuli (Gironacci et al., 2011). Currently, Ang-(1-7) is the main agonist tested in experimental studies whereas A779 is a potent receptor antagonist (Santos et al., 1994). Additionally, specific MasR agonists include AVE 0991 (Santos and Ferreira, 2006).

In CVD, the MasR is suggested to act as an AT_1R antagonist by forming heterodimers and inhibiting Ang II induced vasoconstriction (Kostenis et al., 2005). Nonetheless, MasR activation alone induces vasodilation by stimulating NO production through the protein kinase B (PKB) pathway (Sampaio et al., 2007). Plus, MasR-induced NO production is exacerbated by B_2K interactions, promoting the NO-cGMP signalling pathway (Gironacci et al.,2004). MasR also stimulates PLA_2 and PG generation, contributing towards vasodilation, prevents NOX activation and directly inhibits NF-κB activation (Albrecht, 2007; Meng et al., 2014; Tallant et al., 2005). MasR signalling outcome includes the

enhancement of SH2-containing tyrosine phosphatase (SHP-2), which then inhibits MAPKs (p38 MAPK, ERK1/2 and JNK), diminishing inflammation, oxidative stress, proliferative and cell growth mechanisms (Figure 1-11) (Mercure et al., 2008; Su et al., 2006).

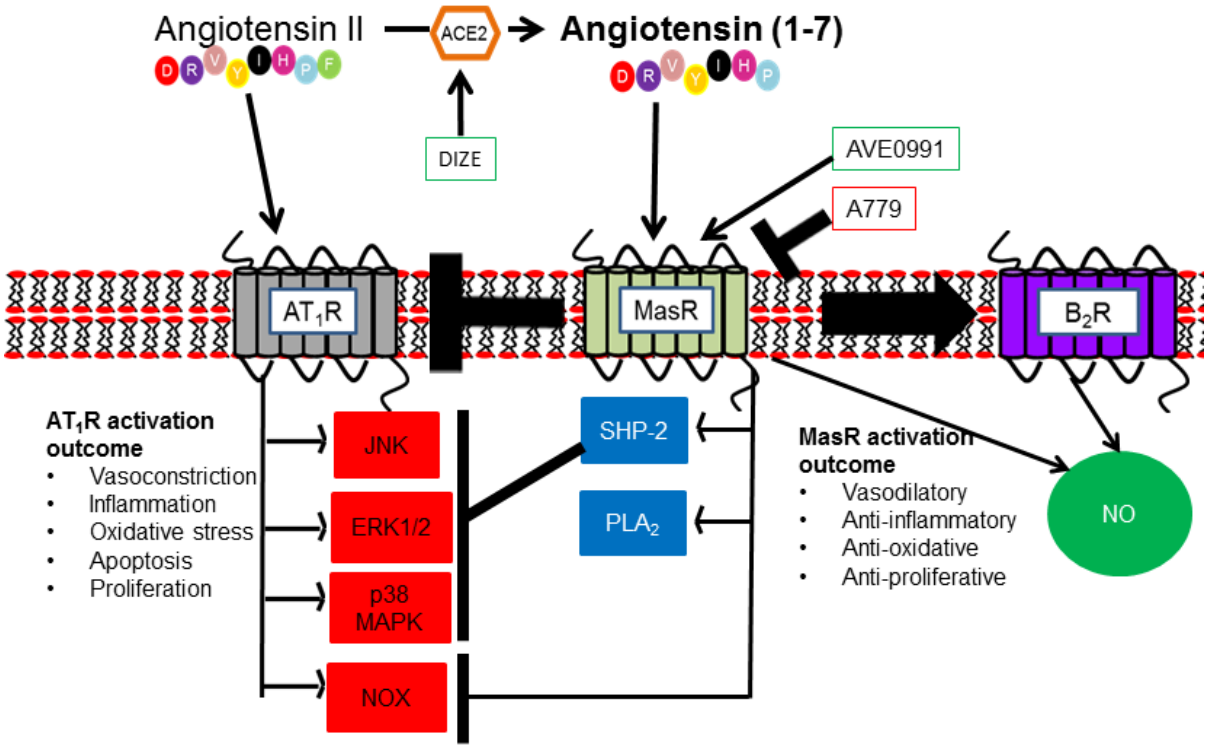

Figure 1-11 The proposed signalling at the Mas receptor. The MasR is suggested to counteract the detrimental effects of AT_1R by activating SHP-2, which will inhibit AT_1R induced activation of ERK1/2, JNK, p38 MAPK. In addition, MasR directly inhibits NOX and AT_1R activation. MasR is suggested to trigger NO formation through eNOS and by interacting with B_2R to enhance NO formation. Moreover, MasR is thought to activate PLA_2, possibly inducing vasodilation. Altogether, MasR signalling is proposed to induce vasodilatory, anti-inflammatory, anti-oxidative and anti-proliferative effects in CVD. Image also depicts the site of action for ACE2 activator, DIZE, as well as MasR agonists, Ang-(1-7) & AVE0991, and antagonist, A779.

1.3.6 Peripheral RAS and stroke incidence

Given that RAS is highly implicated in CVD pathology and antagonising the RAS is the standard care for hypertension, focus has shifted towards its therapeutic effects in ischaemic stroke. For this purpose, several clinical trials have been performed where ARBs and ACE inhibitors were tested as possible stroke preventive therapies in hypertensive patients. The LIFE trial assessed whether losartan reduced cardiovascular disease and mortality (Dahlöf et al., 2002). In this study, patients were either administered losartan or atenolol-based antihypertensive therapy for a minimum period of 4 years where it was

found that losartan treatment resulted in an approximately 25% decrease in fatal or non-fatal stroke risk compared to atenolol (Dahlöf et al., 2002). The ACCESS study was then conducted to examine the safety of blood pressure (BP) reduction as an early therapy for stroke. Although the trial had to be ceased prematurely, the authors identified that hypotension induced by candesartan cilexetil lowered mortality and vascular event incidence compared to placebo (Schrader et al., 2003). Similarly, in the MOSES trial, hypertensive stroke patients treated with eprosartan showed decreased mortality and cerebrovascular events when compared to nitrendipine (calcium channel blocker) (Schrader et al., 2005) while the TRANSCEND trial reported that telmisartan therapy in patients intolerant to ACE inhibitors led to a mild attenuation in stroke incidence compared to placebo (Yusuf et al., 2008a).

Conversely, several studies failed to detect a benefit in preventing stroke incidence with ARBs. Stroke patients randomised to either telmisartan or placebo therapy showed no differences in terms of stroke incidence after 2.5 years follow up (Yusuf et al., 2008b). Moreover, when testing BP lowering in ischaemic or haemorrhagic stroke, candesartan did not induce any beneficial effects (Sandset et al., 2011). Similarly, when testing the ACE inhibitor captopril in hypertensive patients, it was found that the risk of fatal and non-fatal stroke was more common in the captopril-treated group than placebo (Hansson et al., 1999). To date, clinical trials have focused on BP lowering strategies as a means to prevent stroke incidence in hypertensive patients. The clinical trials outlined suggest that the RAS may be implicated in stroke injury; however, there is still limited information regarding the role of the RAS in ischaemic stroke pathology and independently of risk factors.

1.4 Brain RAS and ischaemic stroke

The brain RAS was initially proposed in 1971 upon the discovery that RAS components were present within the brain parenchyma in dogs (Ganten et al., 1971). RAS peptides do not cross the BBB, therefore, RAS activity depends on local synthesis rather than uptake from blood (Schelling et al., 1976). At the same time, the existence of circumventricular organs (CVOs), brain regions that lack BBB and are involved in BP, sodium and water regulation; provide a crossing point between peripheral and central RAS (McKinley et al., 2003; Wright and Harding, 2013). In the past decade, emerging *in vivo* studies have hypothesised that the RAS is implicated in ischaemic stroke independent of BP-induced effects, providing a possible strategy that not only targets risk factors but stroke pathology itself and defining the brain RAS as a therapeutic target.

1.4.1 Brain RAS expression

The existence of a brain RAS depends on locally produced renin and this has been the subject of extensive debate. Renin mRNA is poorly expressed in the brain and its site of production is not clearly defined however, there is evidence that renin mRNA is expressed in astrocytes and neurons (Dzau et al., 1986). On the contrary to the periphery, brain renin expression takes place intracellularly as a non-secreted shorter isoform lacking the signal peptide in its preprorenin sequence (Morimoto et al., 2002). Nevertheless, recent studies postulate that brain renin is actually the outcome of trapped renin and that Ang II is taken from the blood instead of being locally synthesised (van Thiel et al., 2017), contradicting the existence of a local brain RAS.

In addition to renin, other RAS components have been described in the brain. Ang I, Ang II and Ang-(1-7) were detected in plasma, CSF and brain parenchyma using radioimmunoassays (Chappell et al., 1987). Ang-(1-7), in particular, is an endogenous constituent of the brain and its presence is separate from circulating plasma Ang-(1-7) (Chappell et al., 1989). Angiotensinogen is constitutively secreted by astrocytes and also expressed in neurons to a lesser extent (Intebi et al., 1990; Thomas and Sernia, 1988; Yang et al., 1999). ACE is expressed across the brain parenchyma, choroid plexus and it is maximally concentrated within the CVOs (Saavedra & Chevillard 1982; Turner & Hooper 2002). Similarly, ACE2 is widely expressed in the brain and present in arterial and endothelial cells (Hamming et al., 2004), neuronal cell body cytoplasm (Doobay et al., 2007) and cerebellar and medullary astrocytes (Gallagher et al., 2006).

The AT_1R is ubiquitously expressed in the brain and predominantly found within the CVOs (Allen et al., 1998, 1999; Lenkei et al., 1997; McKinley et al., 2003). Likewise, the AT_2R is present in various brain regions including the hypothalamus, cerebellum, subfornical organ, brainstem and thalamus (Allen et al., 1999; Lenkei et al., 1997). Both AT_1R and AT_2R are expressed in dopaminergic neurons, astrocytes and microglia in human, non-human primate, rats and mice as well as in cerebral microvessels and cerebral arteries (Garrido-Gil et al. 2013; Rodriguez-Pallares et al. 2008; Speth & Harik 1985; Tsutsumi & Saavedra 1991b). Regarding MasR expression, this receptor is highly present in the rat's cortex and hippocampus as well as cardiovascular regulatory centres (Becker et al., 2007; Young et al., 1988). It is maximally expressed within neurons and selectively present in brain endothelial cells when compared to peripherally derived endothelial cells

(Becker et al., 2007; Kumar et al., 1996). Furthermore, MasR is present in astrocytes and cultured rat microglia (Guo et al., 2010; Lu et al., 2013; Regenhardt et al., 2013).

1.4.2 Ang II and ischaemic stroke

Until recently, it was unclear whether brain RAS expression was changed after ischaemic stroke; however, it is now established that following injury, the ACE/AngII/AT_1R axis is enhanced. In normotensive rats, Ang II protein expression is increased within the ventral cortex, hypothalamus and rostral ventrolateral medulla (RVLM) compared to non-stroke animals whereas AT_1R protein levels are decreased in the ventral cortex but enhanced in the RVLM, the latter a central nervous system (CNS) centre known to influence peripheral BP (Chang et al., 2014; Kagiyama et al., 2003). In addition, *ACE* mRNA levels were enhanced in the MCA after MCAO, suggesting an exacerbated production of Ang II to promote injury (Stenman and Edvinsson, 2004).

Studies conducted in knockout (KO) mice have helped elucidate the involvement of the classical RAS axis in stroke. AT_1R KO mice subjected to permanent MCAO have a larger penumbra volume and improved CBF within the core and penumbra (Walther et al., 2002). Not surprisingly, mice overexpressing angiotensinogen were shown to have a smaller volume of penumbra volume, enhanced ATP depletion and decreased perfusion within the core and penumbra compared to WT (Walther et al., 2002). Plus, mice carrying human renin and angiotensinogen genes display exacerbated infarcts 24 hrs post MCAO with aggravated neurological deficit (Inaba et al., 2009). The role of Ang II in isolated cerebral vessels following focal cerebral ischaemia has also been investigated. Ang II treatment of isolated MCAs obtained 48 hrs post MCAO, enhances AT_1R induced contractile response when compared to sham animals (Stenman and Edvinsson, 2004). When taken together, these studies suggest that the classical brain RAS plays a role in the pathogenesis of neuronal injury following stroke. In support of this, serum samples obtained 24 hrs after stroke onset in patients indicate that Ang II levels negatively correlates with stroke severity as defined by NIHSS (Mogi et al., 2014).

The AT_2R has also shown to be altered after cerebral ischaemia. After focal cerebral ischaemia, AT_2Rs are upregulated in the rat brain, primarily within the cortical penumbral regions and hippocampus (Makino et al., 1996; Zhu et al., 2000). This indicates a possible role in ischaemic lesion progression; however, it is necessary to clarify whether it is a detrimental or cytoprotective effect. For example, after transient MCAO in normotensive

animals, AT_1R expression either decreases or remains unaltered whereas Ang II and AT_2R mRNA and protein levels are enhanced (Kagiyama et al., 2003; Makino et al., 1996; Zhu et al., 2000). Therefore, it has been suggested that following reperfusion, the AT_2R may mimic actions of the AT_1R instead of providing cytoprotection(Kagiyama et al., 2003; Makino et al., 1996; Zhu et al., 2000). KO studies; however, indicate thatthe AT_2R is in fact cytoprotective since KO mice exhibit larger ischaemic lesions compared to WT after MCAO (Iwai et al., 2004).

1.4.2.1 AT_1R targeting

The mechanisms by which Ang II exerts its detrimental effects have been widely investigated in animal models by testing ARBs (Figure 1-12). The first study conducted in normotensive animals was performed by Dai and colleagues (Dai et al., 1999). There, irbesartan administered 5 days prior to transient MCAO at a non-hypotensive dose improved neurological outcome, an effect associated with a reduction in pro-apoptotic proteins expression, c-Fos and c-Jun, in the ipsilateral cortex (Dai et al., 1999). Disappointingly, the authors did not assess the effect on final infarct volume; however, the results provided a promising line of research with subsequent studies showing that candesartan as an IV bolus after transient MCAO decreased infarct volume and oedema whilst improving neurological deficit (Fagan et al., 2006; Mecca et al., 2009). The underlying neuroprotective effects of ARBs are suggested to be due to an anti-inflammatory and anti-oxidative effect since ARBs attenuate apoptosis TUNEL marker and diminish active microglia/macrophages within the parietal cortex at 3 and 7 days post transient MCAO (Lou et al., 2004). Similarly, in mice, valsartan treatment prior to MCAO was shown to attenuated superoxide production and mRNA expression of *MCP-1* within the ipsilateral hemisphere (Li et al., 2008) whereas candesartan pre-treatment diminished oxidative damage within the ischaemic penumbra (Liu et al., 2008). The impact of Ang II is extended to BBB breakdown exacerbation since olmesartan therapy for a period of 7 days post MCAO reduces Ang II and MMP9 levels within the ipsilateral hemisphere, decreasing cerebral oedema and BBB breakdown (Figure 1-12) (Hosomi et al., 2005).

Other reported ARB induced effects include vasodilation and angiogenesis. In normotensive animals, candesartan IV therapy as a single pre- or post-treatment dose as well as chronic dose following transient MCAO significantly attenuated infarct volume in all groups, an outcome attributed to enhanced CBF (Engelhorn et al., 2004). Similarly, in spontaneously hypertensive rats (SHR), candesartan treatment prior to MCAO decreased

brain AT_1R levels and attenuated the CBF deficit irrespective of BP alterations (Nishimura et al., 2000). The authors proposed that ARBs normalised autoregulation after MCAO, a conclusion subsequently confirmed with chronic SC candesartan administration prior to permanent MCAO and distal MCAO. The authors demonstrated that chronic treatment with candesartan prior to MCAO decreased infarct volume by preventing MCA media thickness remodelling and enhancing CBF within the penumbral areas (Ito et al., 2002). Other possible underlying mechanisms include enhanced neurogenesis and angiogenesis. ARBs increase vascular endothelial growth factor (VEGF), brain derived neurotrophic factor (BDNF) levels within the peri-infarct in both normotensive and SHR animals (Alhusban et al., 2013; Ishrat et al., 2015; Krikov et al., 2008).

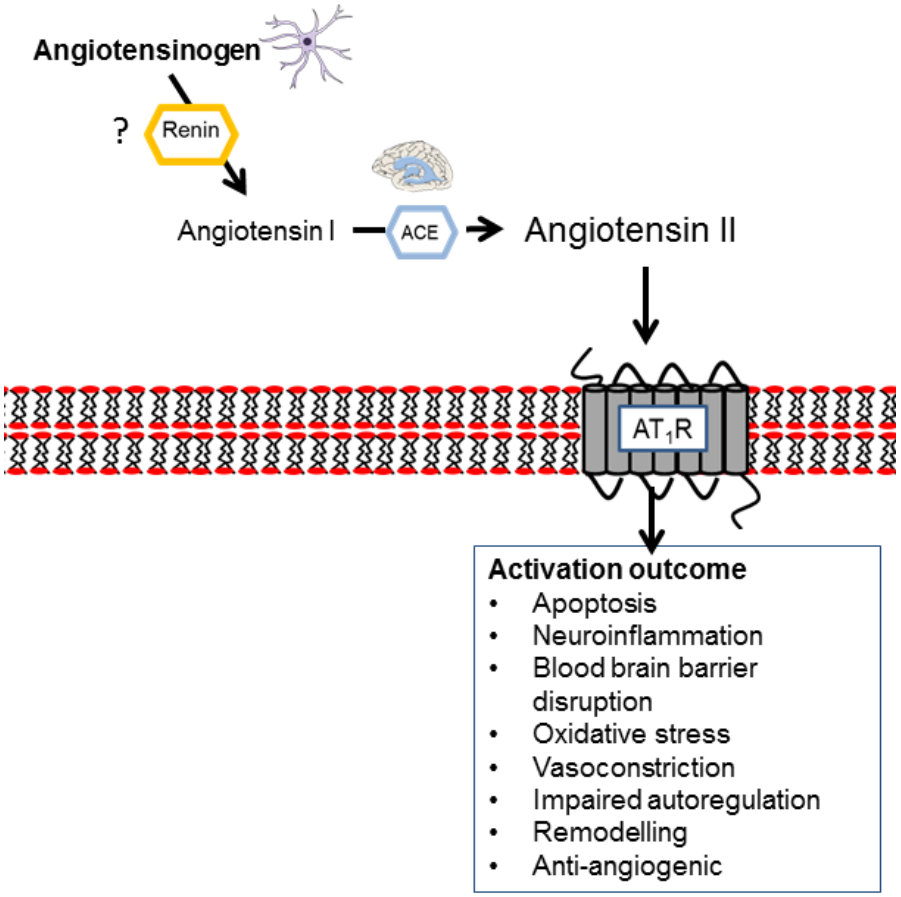

Figure 1-12 The proposed AT_1R induced outcome during ischaemic stroke. In the brain, angiotensinogen is produced by astrocytes whereas the production of renin is unclear. Angiotensinogen will lead to Ang I through renin. Ang I will then be cleaved by ACE possibly in the CVOs or choroid plexus. Ang II will then activate ubiquitous receptor AT_1R leading to apoptosis, neuroinflammation, BBB disruption, oxidative stress, vasoconstriction, impaired autoregulation, remodelling and anti-angiogenic effects during cerebral injury.

1.4.2.2 AT_2R targeting

It is proposed that the neuroprotective mechanisms induced by ARBs might be due to a preferable action of Ang II on the AT_2R (Faure et al., 2008). Plus, the fact that these receptors are upregulated during cerebral ischaemia particularly in the peri-infarct region of the cortex supports this hypothesis (Makino et al., 1996; Zhu et al., 2000).

Initial studies testing AT_2R agonists were conducted in hypertensive animals using the specific AT_2R agonists, GCP42112 or C21 (Table 1-3). In conscious SHR rats, central treatment with CGP42112 before and after ET-1 induced MCAO attenuated lesion volume and improved motor function, independent of BP alterations (McCarthy et al., 2009). The underlying mechanism was suggested to be the result of increased AT_2R expression and decrease of superoxide within the infarcted cortex (McCarthy et al., 2009). Similarly, when CGP42112 was given centrally following MCAO, there was an improved motor function and reduced infarct volume (McCarthy et al., 2012). The improvement in outcome was associated to a reduction in caspase-3 positive apoptotic cells and increase in microglia activity within the peri-infarct area (McCarthy et al., 2012). The authors then conducted a follow up study testing C21 as a pre and post therapy in the same MCAO protocol (McCarthy et al., 2014). C21 attenuated infarct growth and enhanced motor function without BP induced effects 3 days post ET-1 induced MCAO. The underlying mechanism was attributed to increased neuronal survival and microglia activation, reportedly secreting anti-inflammatory mediator BDNF (McCarthy et al., 2014). In addition, myography studies performed in basilar arteries concluded that C21 induced vasodilatory effects could have contributed to enhanced CBF (Table 1-3) (McCarthy et al., 2014). These findings were supported by *in vitro* data where CGP42112 attenuated cell death in primary cortical neurons following oxygen deprivation challenge (OGD) (Lee et al., 2012).

In normotensive rats, C21 was given centrally as both a pre- and post-treatment following ET-1 induced MCAO (Joseph et al., 2014). After 3 days of recovery, C21 decreased infarct volume and improved neurological score, an effect attributed to a decrease in *iNOS* and *CCR2* mRNA expression in the ipsilateral cortex (Joseph et al., 2014). In transient MCAO, intraperitoneal (IP) C21 post treatment for a period of 24 hrs or 7 days was equally neuroprotective (Alhusban et al., 2015). There, C21 upregulated anti-inflammatory cytokine IL-10 whilst decreasing nitrosative markers nitrotyrosine and iNOS within the ipsilateral hemisphere. Moreover, eNOS and AT_2R levels were upregulated whereas AT_1R expression was decreased (Alhusban et al., 2015). Similarly, in a recent study, CGP42112

treatment induced a neuroprotective effect due to decreased IL-1β expression and enhanced IL-10, providing further evidence for an anti-inflammatory mechanism (Ma and Yin, 2016).

The proposed anti-apoptotic, anti-inflammatory and anti-oxidative theory was also detected in mice studies. AT_2R agonism after transient MCAO attenuated infarct lesion possibly due to an enhancement in cell viability (Lee et al., 2012) whereas in permanent MCAO, C21 treatment induced an anti-inflammatory and anti-oxidative effect by diminishing *MCP-1*, *TNF-*α and superoxide expression whilst improving BBB integrity (Min et al., 2014). Most recently, AT_2R agonism was shown to promote neurogenesis and angiogenesis by augmenting VEGF and BDNF in peri-infarct regions in both permanent and transient MCAO models (Alhusban et al., 2015; Mateos et al., 2016; Schwengel et al., 2016). Together, these reports place AT_2R agonism as a potential therapy in ischaemic stroke particularly by preventing oxidative stress and inflammation following reperfusion (Table 1-3). Still, there is a lack of understanding of the effects of C21 in infarct volume following transient MCAO models in normotensive rats.

1.4.3 Ang-(1-7) and ischaemic stroke

Similar to the classical axis, counter-regulatory ACE2/Ang-(1-7)/Mas axis expression is altered after cerebral ischaemia. Lu and colleagues demonstrated that following permanent MCAO, Ang-(1-7) levels in serum and cerebral cortex protein levels are enhanced as early as 6 hrs following injury and remain elevated for at least 48 hrs(Lu et al., 2013). In addition, *MasR* mRNA in the cerebral cortex is upregulated from 6 to 48 hrs reaching a peak at 24 hrs post ischaemic insult (Lu et al., 2013). ACE2 protein and mRNA levels were also shown to be increased at 6 hrs followinginjury, peaking at 12 hrs MCAO and subsequently decreasing to the point where at 48 hrs after MCAO the levels were comparable to sham (Lu et al., 2013). In transient MCAO, MasR protein and mRNA levels are upregulated after 3 days reperfusion and enhanced for at least 7 days whereas Ang-(1-7) protein expression initially decreases at day 1 post-reperfusion and then rises over time in the RVLM (Chang et al., 2014). Similarly, in their study, Chang and colleagues showed that ACE2 levels were equally increased within the RVLM (Chang et al., 2014).

ACE2 expression seems to be important in the clinical setting. Patients who suffered a cardioembolism exhibit higher ACE2 serum levels with its expression correlating with diminished injury severity according to the NIHSS (Mogi et al., 2014). Concomitantly,

transgenic mice overexpressing ACE2 display smaller infarct sizes compared to human renin and angiotensinogen double transgenic mice, an effect that is partially reversed by the MasR antagonist, A779 (Chen et al., 2014). In *in vitro* brain slices obtained from mice overexpressing ACE2 and subjected to OGD, there was reduced cell death and swelling, an effect also inhibited by A779 (J Zheng et al., 2014). Current evidence indicates that similarly to the ACE/Ang II/AT_1R and the alternative receptor AT_2R, the ACE2/Ang-(1-7)/Mas axis expression is altered after stroke. For this reason, it has been hypothesised that when enhancing the endogenous counter-regulatory axis after stroke injury, particularly through Ang-(1-7), neuroprotection may be induced.

1.4.3.1 MasR targeting

The effect of Ang-(1-7) and MasR activation has received recent focus and become a promising target in ischaemic stroke (Table 1-4). In 2011, Mecca and colleagues performed the first experiment examining treatment effects in infarct volume in normotensive rats (Mecca et al., 2011). In their study, Ang-(1-7) was administered centrally as a pre- and post-treatment in an ET-1 induced MCAO model. After 3 days recovery, Ang-(1-7) improved motor function, neurological score and diminished infarct volume by over 50% without impacting BP, an effect reversed by A779 (Mecca et al., 2011). The authors also examined the effect of DIZE, a proposed ACE2 activator, and again demonstrated a reduced infarct volume with the effects of DIZE being abolished with the MasR antagonist, A779 (Mecca et al., 2011). The authors attributed the underlying mechanism to a decrease in iNOS levels within the ipsilateral hemisphere, therefore, providing the first line of evidence for a possible anti-inflammatory and anti-oxidative mechanism (Mecca et al., 2011). Subsequently, other studies confirmed this hypothesis. In Sprague-Dawley rats, central administration of Ang-(1-7) starting 7 days prior to ET-1 induced MCAO decreased infarct volume and led to a reduction in iNOS in ipsilateral cortex at 24 hrs post stroke onset, an effect reversed by A779 (Regenhardt et al., 2013). In addition, treatment reduced mRNA levels for leukocyte chemokine *CXCL12* at 6 hrs post stroke onset and pro-inflammatory mediators *IL-1α*, *IL-6*, *CD11b* at 24 hrs post stroke, confirming an anti-inflammatory role (Regenhardt et al., 2013). These findings were further reinforced in permanent MCAO studies where central Ang-(1-7) infusion through MasR activation, reduced infarct volume and improved neurological function an effect associated with reduced malondialdehyde and superoxide dismutase, NF-κB activity and COX-2 in the peri-infarct as well as TNF-α and IL-1β (Table 1-4) (Jiang et al., 2012).

The anti-inflammatory effect is highly attributed to a direct action on microglia. The MasR is expressed in cultured rat microglia and when subjected to Ang-(1-7) treatment in basal conditions, the cytokine profile shifts from pro-inflammatory to anti-inflammatory by stimulating *IL-10* levels and attenuating *IL-1β*, *TNF-α* and *CD11b* as well as NF-κB activation (Liu et al., 2016). Similarly, in *in vivo* studies, Regenhardt and colleagues support this hypothesis where they observed reduced levels of M1 type markers *iNOS* and *CD11b* within the ipsilateral hemisphere following MCAO (Regenhardt et al., 2013). Furthermore, in stroke prone spontaneously hypertensive rats (SHRSP), Ang-(1-7) administration for 6 weeks increased survival in animals whilst diminishing activated microglia number within the striatum (Regenhardt et al., 2014). More recently, it was shown that older animals overexpressing ACE2 have reduced infarct volume and tissue swelling following MCAO, an outcome prevented by A779. ACE2 led to reduced NOX2 expression in the brain, an effect again ablated by A779 (Zheng et al. 2014). Equally to AT_2R agonism, the anti-inflammatory/anti-oxidative effect of Ang-(1-7) is a fairly well-established mechanism. Yet, these studies have primarily assessed Ang-(1-7)/MasR effects in acute stages of injury as a pre and post-therapy and in ET-1 induced MCAO models.

The vasodilatory effects of Ang-(1-7) in the brain are less well defined; however, there are indications that Ang-(1-7) may enhance NO levels within the brain and possibly enhance CBF after stroke. For instance, central infusion of Ang-(1-7) following MCAO improved neurological score whilst stimulating the expression of NO, bradykinin and its receptors B_2R and B_1R in the core and penumbra (Lu et al., 2008; Zhang et al., 2008). Although infarct volume effects were not assessed in these studies, the outcome observed placed Ang-(1-7) and MasR as possible vasodilators. Furthermore, mice overexpressing ACE2 present enhanced NO within the peri-infarct and diminished NOX, which supports both a MasR induced anti-oxidative and vasodilatory effect (Chen et al., 2014). Recently, Ang-(1-7) infusion for a period of 4 weeks and prior to permanent MCAO was shown to enhance brain capillary density and improve penumbral CBF through a MasR dependently derived eNOS mechanism, thus, placing Ang-(1-7)/MasR signalling as a possible target to enhance CBF following stroke (Jiang et al., 2014). Nonetheless, these effects are controversial since Mecca et al. reported that Ang-(1-7) 7 days prior to stroke did not affect blood flow after ET-1 transient MCAO (Table 1-4) (Mecca et al., 2011).

Table 1-3 Rat studies assessing the therapeutic potential of AT_2R agonists in ischaemic stroke models. BP: blood pressure; CBF: cerebral blood flow; ET-1: endothelin-1; ICV: intracerebroventricular; IP: intraperitoneal; MCAO: middle cerebral artery occlusion; NO: nitric oxide; NS: neurological score; SHR: spontaneously hypertensive rat. Table adapted from Arroja et al., 2016.

Animals	Stroke model	Treatment profile	Treatment outcome	Proposed mechanism	Reference
Male Wistar rats	Transient MCAO 24 hrs or 7 days recovery	**C21** IP bolus Post treatment	Did **not affect** BP **Improved** NS **Improved** functional outcome **Decreased** infarct volume **Decreased** haemorrhage	**Pro-angiogenic and anti-inflammatory**	Alhusban et al., 2015
Male Wistar rats	Permanent MCAO 21 days recovery	**C21** IP bolus Post treatment	**Improved** NS **Decreased** infarct volume	**Pro-angiogenic**	Mateos et al., 2016
Male Sprague Dawley rats	ET-1 induced MCAO 24 hrs recovery	**C21** ICV infusion or IP bolus Pre and post treatment	Did **not affect** BP Did **not affect** CBF **Improved** NS **Decreased** infarct volume	**Anti-inflammatory**	Joseph et al., 2014
Male Sprague Dawley rats	Transient MCAO Up to 7 days recovery	**CGP42112** IP bolus Post treatment	**Decreased** infarct volume	**Anti-inflammatory**	Ma et al., 2016
Male SHR	ET-1 induced MCAO 3 days recovery	**CGP42112** ICV infusion Pre and post treatment	Did **not affect** BP **Improved** motor function **Decreased** infarct volume	**Anti-oxidative**	McCarthy et al., 2009
Male SHR	ET-1 induced MCAO 3 days recovery	**CGP42112** ICV infusion Post treatment	Did **not affect** BP **Improved** motor function **Decreased** infarct volume	**Anti-apoptotic, possibly anti-inflammatory**	McCarthy et al., 2012
Male SHR	ET-1 induced MCAO 3 days recovery	**C21** ICV infusion or IP bolus Pre and post treatment	Did **not affect** BP **Improved** motor function **Decreased** infarct volume	**Anti-apoptotic, anti-inflammatory, vasodilatory**	McCarthy et al., 2014

Table 1-4 Rat studies assessing the therapeutic potential of Ang-(1-7) in ischaemic stroke models. BP: blood pressure; CBF: cerebral blood flow; ET-1: endothelin-1; ICV: intracerebroventricular; MCAO: middle cerebral artery occlusion; NO: nitric oxide; NS: neurological score. Table adapted from Arroja et al., 2016.

Animals	Stroke model	Treatment profile	Treatment outcome	Proposed mechanism	Reference
Male Sprague Dawley rats	Transient MCAO 72 hrs recovery	**Ang-(1-7)** ICV Post treatment	**Improved** NS Infarct volume not assessed	**Possibly vasodilatory through NO expression**	Zhang et al., 2008
Male Sprague Dawley rats	ET-1 induced MCAO 72 hrs recovery	**Ang-(1-7)** ICV Pre and post treatment	Did **not affect** BP Did **not affect** CBF **Improved** NS **Improved** motor function **Decreased** infarct volume	**Anti-inflammatory**	Mecca et al., 2011
Male Sprague Dawley rats	ET-1 induced MCAO 24 hrs recovery	**Ang-(1-7)** ICV Pre and post treatment	Did **not affect** CBF **Improved** NS **Decreased** infarct volume	**Anti-inflammatory and anti-oxidative**	Regenhardt et al., 2013
Male Sprague Dawley rats	Permanent MCAO 24 hrs recovery	**Ang-(1-7)** ICV Pre and post treatment	**Decreased** infarct volume	**Anti-inflammatory**	Jiang et al., 2012
Male Sprague Dawley rats	Permanent MCAO 24 hrs recovery	**Ang-(1-7)** ICV Pre treatment	Did **not affect** BP **Improved** CBF **Improved** NS **Decreased** infarct volume	**Pro-angiogenic and possibly vasodilatory through NO**	Jiang et al., 2014

1.4.4 Summary

Ischaemic stroke is a heterogeneous condition and a major contributor towards mortality and morbidity in the UK. Currently, rt-PA and thrombectomy are the only available therapies and these work by inducing vessel recanalization with the aim to reperfuse the parenchyma. Despite significant efforts from the scientific community, there is a lack of adjuvant neuroprotective agents that could aid the prevention of cerebral damage following rt-PA and/or thrombectomy treatment.

The RAS is widely implicated in CVD and is a major therapeutic target for hypertension, a major stroke risk factor. Studies in CVD have helped elucidate the mechanisms in which RAS induces injury through the ACE/Ang II/AT_1R axis. Additionally, it has allowed the identification of the AT_2R and the counter-regulatory axis ACE2/Ang-(1-7)/MasR, which are thought to serve as an endogenous mechanism to counteract injury. Increasing evidence place the RAS as a locally synthesised system in the brain and a potential mediator in ischaemic stroke injury via the classical axis, independently from risk factors. A few studies have assessed the effects of the ACE2/Ang-(1-7)/MasR axis in normotensive animals and shown to induce vasodilatory, anti-inflammatory, anti-oxidative and pro-angiogenic effects. The main proposed mechanism mediated via the MasR is thought to be anti-inflammatory effects by direct targeting of the microglia; however, these have been mainly assessed by mRNA analysis and in *in vitro* experiments. Moreover, the experiments have been primarily performed in ET-1 MCAO induced models, as a pre- and post-treatment, assessed at acute stages of injury only and by one research group only. Similarly, AT_2R agonism is suggested to induce similar effects to those observed in MasR activation, yet, a potential synergistic effect between these two receptors has not been established. Increasing evidence supports the neuroprotective role of the ACE2/Ang-(1-7)/MasR axis and AT_2R activation following experimental stroke as single therapies. As a result, we aim to study the neuroprotective effect of the counter-regulatory axis following ischaemic stroke as a potential thrombectomy adjuvant therapy using the transient filament MCAO model. In addition, this thesis will examine the underlying mechanisms of the counter-regulatory axis and study a possible synergistic effect with AT_2R agonism.

1.5 Thesis aims

1. To optimise the experimental model of stroke and carry out exploratory therapeutic studies with an ACE2 activator following stroke.

2. To determine the effects of Ang-(1-7) and/or Compound 21 on the extent of tissue salvage following transient focal cerebral ischaemia.

3. To determine the impact of Ang-(1-7) on BBB breakdown and microglia activation following transient focal cerebral ischaemia.

4. To study the effects of Ang-(1-7) on CBF profile following transient focal cerebral ischaemia.

Chapter 2: Methods and Materials

Chapter 2

2.1 Legislation

All studies were carried out under a UK Home Office Project License and in accordance with the Animals (Scientific Procedures) Act, 1986: Project License P643E898D8 and Personal license number 70/22456. Experiments were performed either under protocol number 2 (focal cerebral ischaemia lesions; non-recovery experiments; severity limit: unclassified) or protocol number 3 (focal cerebral ischaemic lesions; recovery experiments; severity limit: substantial). Experiments were reported in accordance with the ARRIVE (Animal Research; Reporting *in vivo* Experiments; https://www.nc3rs.org.uk/arrive-guidelines) and National Centre for the Replacement, Refinement and Reduction of Animals in Research (NC3R's) guidelines. Unless otherwise stated, Mariana Arroja performed all the experimental procedures.

2.2 Animals

Adult male Sprague Dawley or Wistar rats were obtained from Charles River Laboratories (Kent, UK) and housed in the Veterinary Research Facility (VRF), University of Glasgow. Rats were housed in groups of 3 to 4 in a plexiglassbox containing sawdust, nesting material and cardboard tubes. Animals were maintained ina controlled environment with a 12:12 hour light/dark cycle, room temperature maintained between 15-25°C and rat chow food and water were available ad libitum. Upon arrival to VRF, animals were allowed to acclimatise to the new animal facility for 7 days prior to any surgical procedures to allow animals to overcome transportation induced stress (Capdevila et al., 2007). Prior to experimental procedures, all animals were randomly assigned to surgery day and treatment group using an online randomisation generator (www.random.org). In addition, the surgeon (MA) was blinded to treatment allocation, except in Chapter 6.

2.3 Aseptic technique

All surgical procedures were conducted under aseptic techniqueas detailed in our local Project License appendix. Surgical surfaces were disinfected with 70% ethanol (Sigma, UK) and autoclaved drapes positioned on the work area where the sterilised surgical instruments, swabs and cotton buds were placed. During surgery, instruments were further disinfected using chlorhexidine gluconate (Hydrex®, Ecolab, UK) and cleaned with sterile saline (sodium chloride 0.9% w/v, Baxter, UK). Prior to surgery, all animals were

transferred to a separate shaving area within the laboratory where the incision areas were quickly shaved using electric clippers (Wella, Germany) and disinfected with chlorhexidine gluconate. All surgical material used (swabs, cotton buds; etc.) were autoclaved and packaged under sterile conditions and Doccol intraluminal filaments (Doccol Corporation, USA) were disinfected with 70% ethanol and cleaned with sterile saline for a period of 10 min prior to use. The surgeon (MA) was equipped with autoclaved surgical gowns and sterile gloves, which were changed following each surgical procedure.

2.4 Analgesia

Local anaesthetic, ropivacaine (10 mg/mL; Naropin, GSK, UK) was administered SC at surgical incision sites at a dose of 2 mg/kg. For recovery surgery, rats were administered buprenorphine hydrochloride (Vetergesic, Ceva Animal Health Ltd, Amersham, UK) at a dose of 0.03 mg/kg SC prior to anaesthetic recovery. In Chapter 3, where osmotic pumps were implanted prior to stroke surgery, carprofen (Rimadyl, Pfizer, UK) was administered SC at 5 mg/kg at incision site.

When rats are under anaesthesia, they lack corneal reflex, therefore, this may lead to eye damage when performing experiments for long periods of time, particularly during stereotaxic surgery were the microscope light is directly placed above the head. To prevent discomfort upon recovery, Viscotears® liquid gel (Novartis, UK) containing polyacrylic acid as an active ingredient, was applied to the animal's eyes at start of surgery.

2.5 Anaesthetic procedures

2.5.1 Induction

For all experiments, rats were weighted and then transferred to an anaesthetic gas chamber for anaesthesia induction. Induction was carried out with 5% isoflurane (Baxter Healthcare Ltd, UK) delivered in a 30:70% oxygen-nitrous oxide mixture, respectively. To ensure that animals were adequately anaesthetised, breathing rate was closely monitored and the pedal withdrawal reflex assessed by tightly squeezing the hindpaw and observing whether a withdrawal reaction was evoked. Animals were then subjected to either surgical tracheotomy or oral intubation for anaesthesia maintenance throughout surgical experimentation depending on experimental outline.

2.5.2 Maintenance

2.5.2.1 Surgical intubation

In Chapter 3 in non-recovery experiments, rats underwent surgical tracheotomy. Following induction, anaesthesia was maintained with a facemask delivering 2-3% isoflurane in a 30:70% O_2-N_2O mixture. A ventral incision was made through the skin and fascia of the neck using sharp ended scissors (World Precision Instruments, UK) and the underlying sternomastoid and sternohyoid musclessplit by blunt dissection using blunt ended scissors (World Precision Instruments, UK). The sternohyoid muscle was separated by blunt dissection to expose the trachea and the surrounding connective tissue carefully cleared. Two 2-0 sutures (Sofsilk^{TM}, Covidien Ltd, UK) were placed under the trachea at the proximal and distal ends of the trachea and loosely tied. Tension was applied on both threads to maintain the trachea in a straight position andwith the use of microscissors (Braun Medical Ltd, UK) a horizontal incision was made between the tracheal cartilage. A breathing tube (Linton Instrumentation, UK) was carefully inserted into the trachea and advanced towards the bronchi for up to 2 cm, thereby guaranteeing that there was no airway obstruction or damage. The ventilation tube was then quickly connected to the ventilator (Ugo Basile, Linton Instrumentation, UK) where the stroke volume was set to approximately 3 mL at a frequency of 48-50 strokes per minute. To secure the ventilation tube in place, the two sutures were tightly tied around the trachea overlying the breathing tube.

2.5.2.2 Recovery experiments

Endotracheal oral intubation was carried out in all recovery surgeries to ensure better control of anaesthesia and to aid post-surgical recovery. Following induction, a 2-0 silk thread (Sofsilk^{TM}, Covidien Ltd, UK) was placed around the superior incisors and the animal suspended vertically on the corkboard in the supine position. To aid visualisation of the vocal chords, the tongue was retracted to the side of the mouth, any mucous cleared from the oral cavity and a fibre optic light (Schott, USA) was illuminated over the neck. A guide wire (Figure 2-1A) was inserted through the intubation catheter (MillPledge Veterinary, UK) (Figure 2-1B) and advanced into the trachea. After, the guide wire was quickly removed and intubation confirmed by verifying breathing condensation. The ventilator was then connected to the intubation catheter, delivering ~2.5% isoflurane mixture at a 2.5-3 mL stroke volume and 61 strokes per minute frequency. To secure the

intubation tube in place, a stitch using a 4-0 silk suture (Sofsilk^{TM}, Covidien Ltd, UK) was performed around the breathing cannula and upper lip.

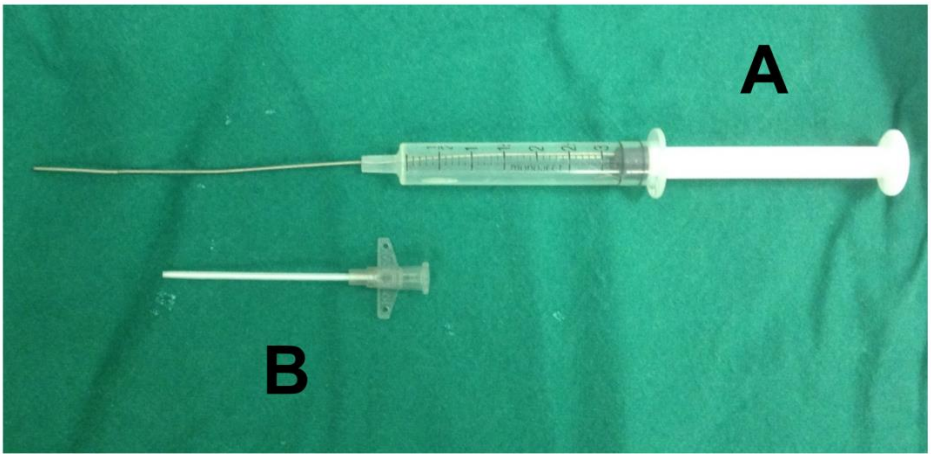

Figure 2-1 Endotracheal oral intubation kit. A) Guide wire consisting of a blunt malleable wire used to guide the intubation tube towards the trachea. **B) Intubation catheter** introduced in the animal' airways consisting of a 45 mm in length guide wire.

2.6 Vessel cannulation

During non-recovery experiments, MABP and blood gases [pH, partial pressure of oxygen ($PaO_{2)}$ & $PaCO_2$] were monitored via the femoral artery. For studies where IV drug administration was carried out, the femoral vein was cannulated. Rats were placed in a supine position and the inner thigh shaved and disinfected with chlorhexidine gluconate. A surgical incision (~1.5 cm) was performed in the inguinal area to expose the femoral artery and vein. Blunt dissection was carried out to clear the connective tissue surrounding the vessels for cannulation. Care was taken to ensure the saphenous nerve that runs along the femoral artery was carefully separated from the vessel.

For each vessel, a folded 4-0 silk thread (Sofsilk^{TM}, Covidien Ltd, UK) was placed under the vessel and cut at the folded region to create two threads. One of the sutures was placed at the distal end near the abductor leg muscle and a tight knot performed. The other suture was placed at the proximal end towards the heart and a loose knot done. Both suture ends were used to apply tension in the vessels by taping them to the corkboard, preventing bleeding at time of cannula insertion. A small incision was made in the vessel with microscissors at the distal end and fine tipped right angled forceps (Braun Medical Ltd, UK) were inserted into the hole to open the vessel and allow insertion of a polythene catheter (external diameter 0.96 mm; internal diameter 0.58 mm) (Smiths Medical

International Ltd, UK) filled with 1% heparinised saline (1000 units/mL) (Wockhardt UK Ltd, UK) and attached to a 1 mL syringe (BD Plastipak^{TM}, UK). The polythene catheter was advanced 1-2 cm into the vessel with the aid of curved micro dissecting watchmaker forceps (Braun Medical Ltd, UK) before obstruction was felt. Blood was withdrawn into the cannula to confirm correct cannula placement before the tension on both proximal and distal ties was removed. The cannula was secured in place by tying each thread around the cannula. Ties were cut short and the incision area sutured using 4-0 sutures. MABP was recorded by connecting the catheter to a pressure transducer, previously flushed with heparinised salineand connected to a monitoring system (Biopac, Acknowledge Software, Biopac Systems, UK).

2.7 Osmotic Pumps

2.7.1 Principle and preparation

In this thesis, ALZET® osmotic pumps (ALZET®, Cupertino, USA) were used as a means for drug delivery in Chapters 3, 4 and 5. ALZET pumps are composed of an impermeable reservoir, osmotic layer, semipermeable membrane and a flow moderator (Figure 2-2). The principle of drug delivery is dependable on pump implantation in the animal. The tissue environment where the pump is implanted will create an osmotic reaction towards the osmotic layer, meaning that the H_2O present in the tissue will flow into the osmotic layer through the semipermeable membrane, causing a compression of the impermeable reservoir. The compression of the reservoir containing the drug will cause drug solution release from the pump to tissue through the flow moderator. ALZET® pumps deliver drugs at different volumes and rates, which are predefined by the manufacturer and dependent upon the permeability of the semipermeable membrane (Theeuwes and Yum, 1976). In this thesis, two different models of osmotic pumps were used.

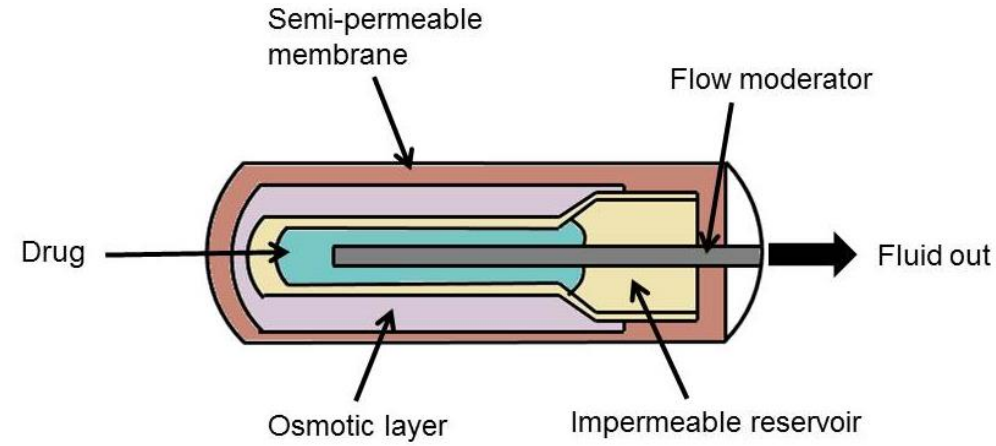

.

Figure 2-2 Osmotic pump drug delivery mechanism. Drug to be delivered is injected into the impermeable reservoir, which is surrounded by an osmotic layer. H_2O present in the tissue will cross into the pump through the semi-permeable membrane creating pressure within the reservoir and causing the release of the drug. Adapted from Theeuwes & Yum, 1976.

In Chapter 3, ALZET® pump Model 2ML1 was used for SC delivery (infusion rate: 10 μL per hour for 7 days, reservoir capacity of 2000 μL) (Figure 2-3A). In Chapters 4 & 5, Model 2001 was used for intracerebroventricular (ICV) delivery (infusion rate: 1.0 μL per hour for 7 days, reservoir volume of 200 μL; Figure 2-3B). For Model 2001, vinyl tubing connected to a magnetic resonance compatible ICV cannula (PlasticsOne®, Virginia, USA) was attached to the flow moderator.

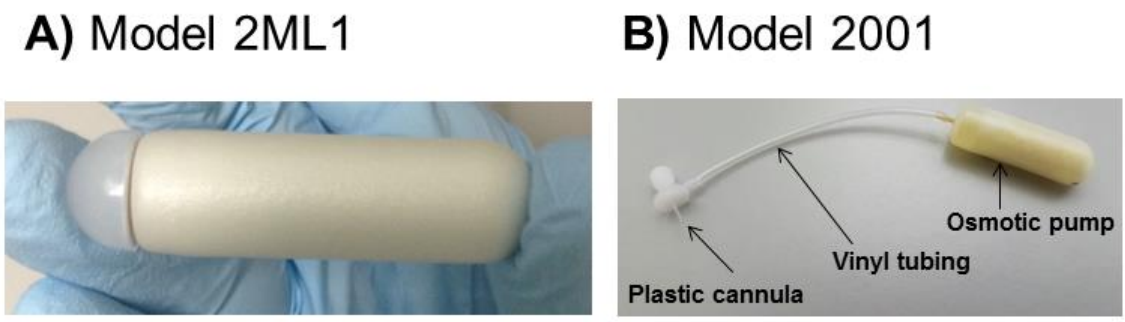

Figure 2-3 Osmotic pumps used in experiments. A) Subcutaneous delivery - Model 2ML1: 10 μL per hour for 7 days, with a reservoir capacity of 2000 μL, length of 5.1 cm and diameter of 1.4 cm **B) Intracerebroventricular delivery** – Model 2001: 1.0 μL per hour for 7 days with a reservoir volume of 200 μL, length of 3.0 cm and diameter of 0.7 cm.

Prior to osmotic pump preparation, the mass of drug infusion was calculated in order to determine drug dilutions to completely fill the pump. The following equation was used:

$$k_0 = Q \times C_d$$

- k_0: mass delivery rate (μg/hr)
- Q: drug volume delivery rate (μL/hr)
- C_d: concentration of the drug in vehicle solution (μg/μL)

Osmotic pumps were filled with a blunt tipped needle to prevent air bubbles and the flow moderator fully inserted in the pump. All osmotic pumps were prepared 24 hrs prior to usage and left in a water bath at 37ºC overnight to prime them for immediate drug delivery. To confirm drug delivery, all pumps were weighed before insertion and again at the end of the experiment after pump removal.

2.7.2 Implantation

2.7.2.1 Subcutaneous

Anaesthesia was induced with 5% isoflurane and rats were then placed on a facemask (2.5-3% isoflurane mixture) for surgical implantation. The fur was shaved in the back area posterior to scapulae and cleaned with chlorehexidine gluconate. A horizontal incision was performed in the mid-scapular area exposing the underlying fat and connective tissue. Blunt dissection was performed in the incision in order to create a SC pocket to place the pump. Once the pocket was of adequate size, the osmotic pump (Model 2ML1) was inserted and lesions sutured with 4-0 silk sutures. The animal was allowed to recover from anaesthesia and returned to its' home cage.

2.7.2.2 Intracerebroventricular

Anaesthesia was induced with 5% isoflurane and rats orally intubated as described in section 1.5.2. Rats were then placed in a stereotaxic frame (Kopft Instruments, CA, USA) and the head was secured in place using ear and tooth bars to prevent movement. After local anaesthetic administration, a midline incision was made on the scalp with a scalpel blade (Swann Morton®, UK) and the underlying fascia cleared to visualise the coronal and

sagittal sutures on the skull surface. Bregma was identified and a stereotaxic needle (Hamilton Company, Nevada, USA) aligned at its level. The right lateral ventricle coordinates for the ICV cannula were 1.6 mm lateral and 0.9 mm posterior according to the Atlas of Paxinos& Watson (Paxinos and Watson, 1997). This position was identified and marked with a pen, this way serving as a guideline to drill the skull in the right lateral ventricle area.

A burr hole was drilled on the skull using a dental drill (NSK Volvere max, Nakanshishi Inc., Japan) until the pial vessels were observed. The stereotaxic needle was used to correctly identify the right lateral ventricle in the brain surface. At this point, a SC pocket was created posteriorly to the scapulae with blunt scissors. The osmotic pump and part of the connecting tubing attached to the ICV cannula were inserted into the SC pocket. After, gel superglue (Superglue power flex gel, Henkel Limited, UK) was placed around the burr hole and with the use of straight forceps, the ICV cannula was inserted into the lateral ventricle and gentle pressure was applied for 3 min to allow the glue to set (Figure 2-4). To prevent cannula displacement during animal movement, the holding top piece of the cannula was removed with the aid of a heated scalpel blade. The incision on the head was then sutured with 4-0 thread and the animal removed from the stereotaxic frame and transferred to the operating board for further procedures.

Figure 2-4 Intracerebroventricular cannula implantation. Rats were placed in a Koft Stereotaxic frame and the head secured with ear and tooth bars. An incision was performed on the scalp to expose the skull and connective tissue cleared. Bregma was identified and used as a guide to define the right lateral ventricle with the coordinates 1.6 mm lateral and 0.9 mm posterior. A burr hole was performed in the right lateral ventricle area, the osmotic pump and vinyl tubing placed in the SC pocket posteriorly to the scapulae and the ICV cannula glued onto the right cerebral ventricle.

2.8 Middle Cerebral Artery Occlusion

The intraluminal filament model was used to induce left MCAO as firstly outlined by Koizumi and colleagues (Koizumi et al., 1986), modified by Longa et al. (Longa et al., 1989) and further altered in-house to minimise vessel damage. Microsurgery was carried out with the aid of a light operating microscope (Zeiss, Germany). A midline incision was performed with sharp scissors between the jaw and the manubrium and the submandibular glands identified. Blunt dissection was carried out in the middle of the glands to expose the sternohyoid muscle overlying the trachea. Blunt dissection was then performed in the intersection between the sternohyoid and sternocleidomastoid muscles to expose the omohyoid muscle overlying the carotid sheath, which was gently dissected. Retractors were placed at the level of the omohyoid and sternohyoid muscles as well as the sternocleidomastoid muscle to clearly visualise the common carotid artery (CCA). The fat and connective tissue surrounding the CCA was carefully dissected with the use of curved and straight forceps to isolate the vessel. The CCA was gently separated from the adjacent vagus nerve through blunt dissection and a folded 4-0 thread placed under it. The thread was cut at the folded zone to originate two different threads, one placed distally and the other proximally towards the heart. After, the vessel was tied off at the proximal side and a loose knot performed at the distal end. Curved and straight forceps were used to carry on with blunt dissection to expose the external carotid artery (ECA), occipital artery (OA), ICA and pterygopalatine artery (PA). A 4-0 thread was placed under the ECA and OA and tension applied by taping the threads to the corkboard. Two 4-0 threads were placed under the ICA in which one was used to tie a loose knot and apply tension at the ICA level and the other advanced to reach the PA/ICA bifurcation. The latter was pulled between the PA/ICA bifurcation and placed around the PA to exert tension, preventing the intraluminal filament from going towards the PA (Figure 2-5A).

Once all the vessels were carefully isolated, an arteriotomy was performed at the CCA level with microscissors, just before the ECA & ICA bifurcation. A Doccol intraluminal filament of 0.39 mm or 0.41 mm tip diameter (403934PK10 or 404134PK10; Doccol Corporation, MA, USA) bent at 22 mm length was inserted through the ICA until it reached the origin of the MCA (Figure 2-5B). The filament was advanced approximately 2 cm and MCAO confirmed once resistance was felt. After the filament was correctly placed, the loose ties around the ICA and CCA were tightly tied to secure the filament in place and the tension applied in the vessels released. To prevent the tissues from drying out, sterile saline was applied in the neck area.

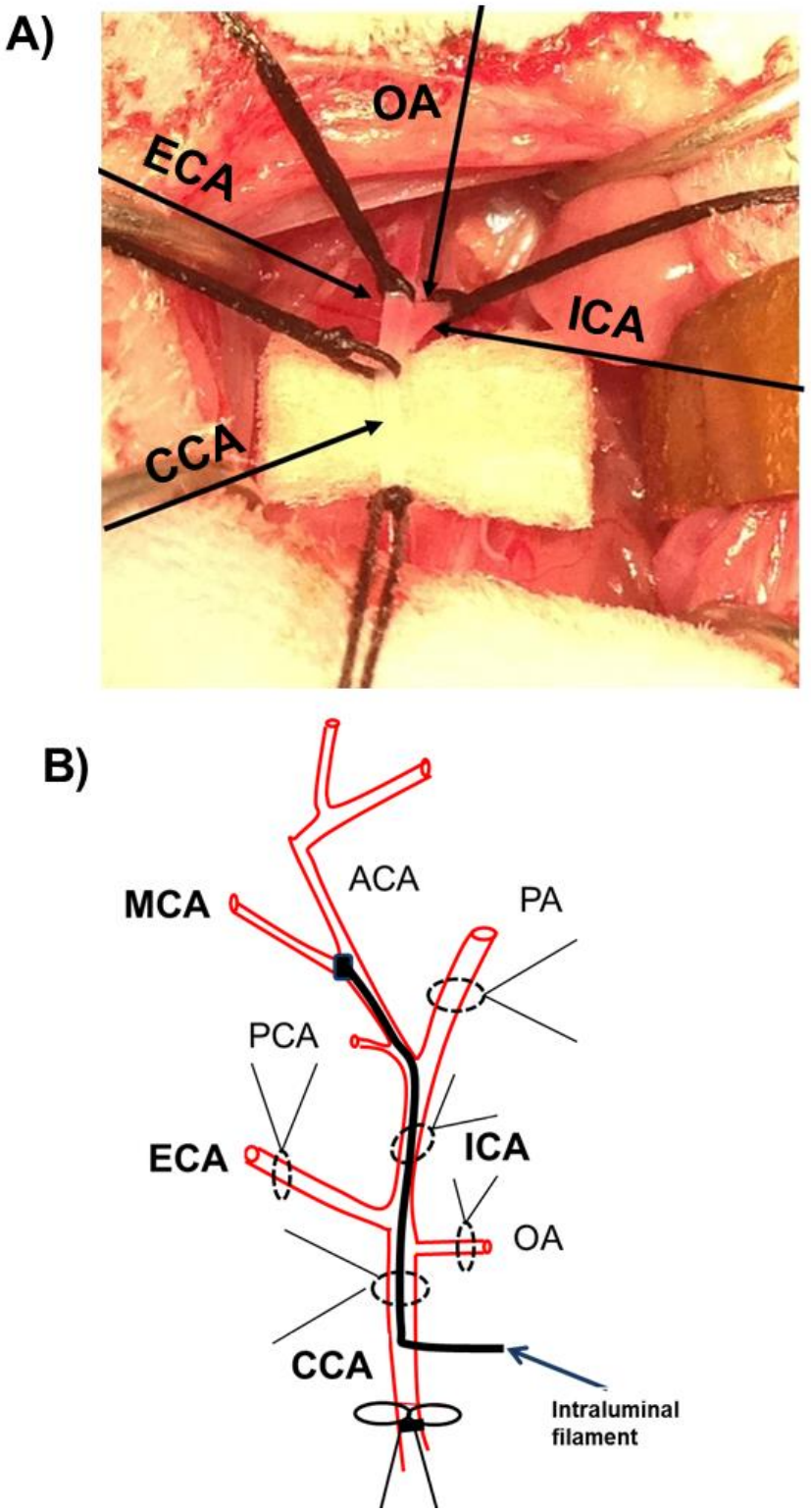

Figure 2-5 Intraluminal filament MCAO model. A) Vessel isolation during surgery; **B) Intraluminal filament occlusion of the MCA.** During surgery 4-0 sutures were placed around the common carotid artery (CCA), external carotid artery (ECA), occipital artery (OA) and internal carotid artery (ICA). Vessels were isolated to facilitate filament insertion. A Doccol filament was inserted through the CCA passing the ICA, the origin of the posterior cerebral artery (PCA) and the PA until it reached the origin of the MCA just before the anterior cerebral artery (ACA). This method of MCAO can be transient or permanent by either removing or leaving the filament in place, respectively. Figure B was adapted from Rami et al. 2008.

2.8.1 Reperfusion

Following 90 min MCAO, tension was applied to the ECA, ICA, OA and PA. The knots performed at the CCA and ICA were untied with the use of thin tipped forceps. The filament was gently pulled back to allow MCA reperfusion and the wound at the CCA sealed with curved diathermy forceps (Eschmann Equipment, Lancing, UK). At this step, care was taken to guarantee that the forceps were moist during electrocoagulation to prevent vessel rupture. After the vessel was adequately sealed, all ties were removed and the thread occluding the CCA at the proximal end untied to allow full reperfusion. The neck area was cleaned with sterile saline, isoflurane levels decreased to 1% and the midline incision sutured with 4-0 sutures.

2.8.2 Post-operative care

Once all incisions were sutured, approximately 1-5 mL of sterile saline were administered SC to aid recovery and prevent dehydration. Buprenorphine, a partial opioid agonist, was also injected SC at a dose of 0.03 mg/kg to alleviate post-operative pain. Isoflurane and NO_2 were switched off and O_2 increased to 100% to maximise recovery from anaesthesia. Once the animals started showing signs of withdrawal reflex, the intubation tube was removed and the rats placed on a face mask at 100% O_2 until fully conscious. Rats were single housed in the recovery room in individual cages lined with absorbent pads until sacrificed. During the recovery period animals were fed food pellets, which were softened in water and supplemented with Complan (Nutricia, UK). Furthermore, water and dry pellets were provided *ad libitum*. Rats were weighed every day and carefully monitored by technical staff and the Named Veterinary Officer (NVO). If the animal's weight dropped below 25% of initial body weight or showed any other issues of concern, the Named Animal Care and Welfare Officer and/or NVO were informed to assess the animal's condition and to make a decision regarding its continuation in the study.

2.9 Magnetic Resonance Imaging

All imaging was performed in a Bruker Pharmascan 7T/30 cm magnet system (Bruker, Ettlingen, Germany) with a gradient coil of 121 mm internal diameter, 400 mT/m and a birdcage resonator of 72 mm. Prior to all imaging sequences, a pilot scan sequence was performed to ensure correct geometry and brain location. MRI scans were conducted at GEMRIC facilities and MRI scans carried out by trained staff: Mr James Mullin, Mrs Lindsay Gallagher, Dr Christopher McCabe and Dr Lisa Roy.

Rats were transferred to the MRI scanner and placed in the prone position in a specialised rat Perspex cradle where the head was restrained by ear and tooth bars and a phased array rat brain surface coil placed above the head. Animals scanned during MCAO were ventilated via oral intubation whereas rats scanned during recovery were ventilated with a face mask during MRI scanning. A rectal probe was inserted and a temperature regulated jacket placed around the animal to maintain and regulate body temperature at a physiological range of 37 ± 0.5ºC.

2.9.1 Diffusion-Weighted Imaging

2.9.1.1 Technical parameters

In Chapter 4, early ischaemic lesion was assessed at 30 and 60 min MCAO by DWI. A 4-shot Spin-Echo planar imaging DWI scan was conducted to generate images across 8 coronal slices with a thickness of 1.5 mm and a resolution of 260 μm. For all DWI scans, the sequence was performed for approximately 3 min under the following parameters: effective echo time (TE) = 22.9 ms, repetition time (TR) = 4,000 ms, matrix size = 96 × 96 and field of view (FOV) = 25 × 25 mm. The gradient strengths, B values, were obtained in three directions of x, y, z and the B values were between 0 and 1,000 sec/mm^2. For all 8 coronal brain sections, ADC maps (mm^2/sec) were generated in Paravision v5 software (Bruker, Ettlingen, Germany). ADC maps were then analysed by following an established imaging protocol with Image J software (https://imagej.nih.gov/ij/).

2.9.1.2 Threshold assessment and analysis

For each ADC map generated, histograms were obtained for all slices in both ipsilateral and contralateral hemispheres. After, the number of pixels for each ADC value ranging from 0 to $2\times10^{-3}mm^2/sec$ at 30 min and 60 min ischaemia following MCAO surgery were calculated. It was previously established in our group that abnormal ADC values following MCAO range between $0.01\text{-}0.58\times10^{-3}mm^2/sec$ (Baskerville et al., 2016; Reid et al., 2012) with the reported threshold being used to outline early ischaemic lesion. The number of pixels per ADC value for 30 min and 60 min MCAO data were plotted, confirming that abnormal ADC values in the ipsilateral hemisphere are within $0.01\text{-}0.58\times10^{-3}mm^2/sec$ (Figure 2-6A&B). Once the reported threshold was validated, it was used for all ADC maps in this thesis. Figure 2-7 displays a processed ADC map prior to the application of the selected threshold (Figure 2-7A) and after the application of the threshold (Figure 2-7B). The brain areas highlighted by the ADC threshold were obtained for each coronal slice, summed and multiplied by slice thickness of 1.5 mm to obtain an early lesion volume for each animal.

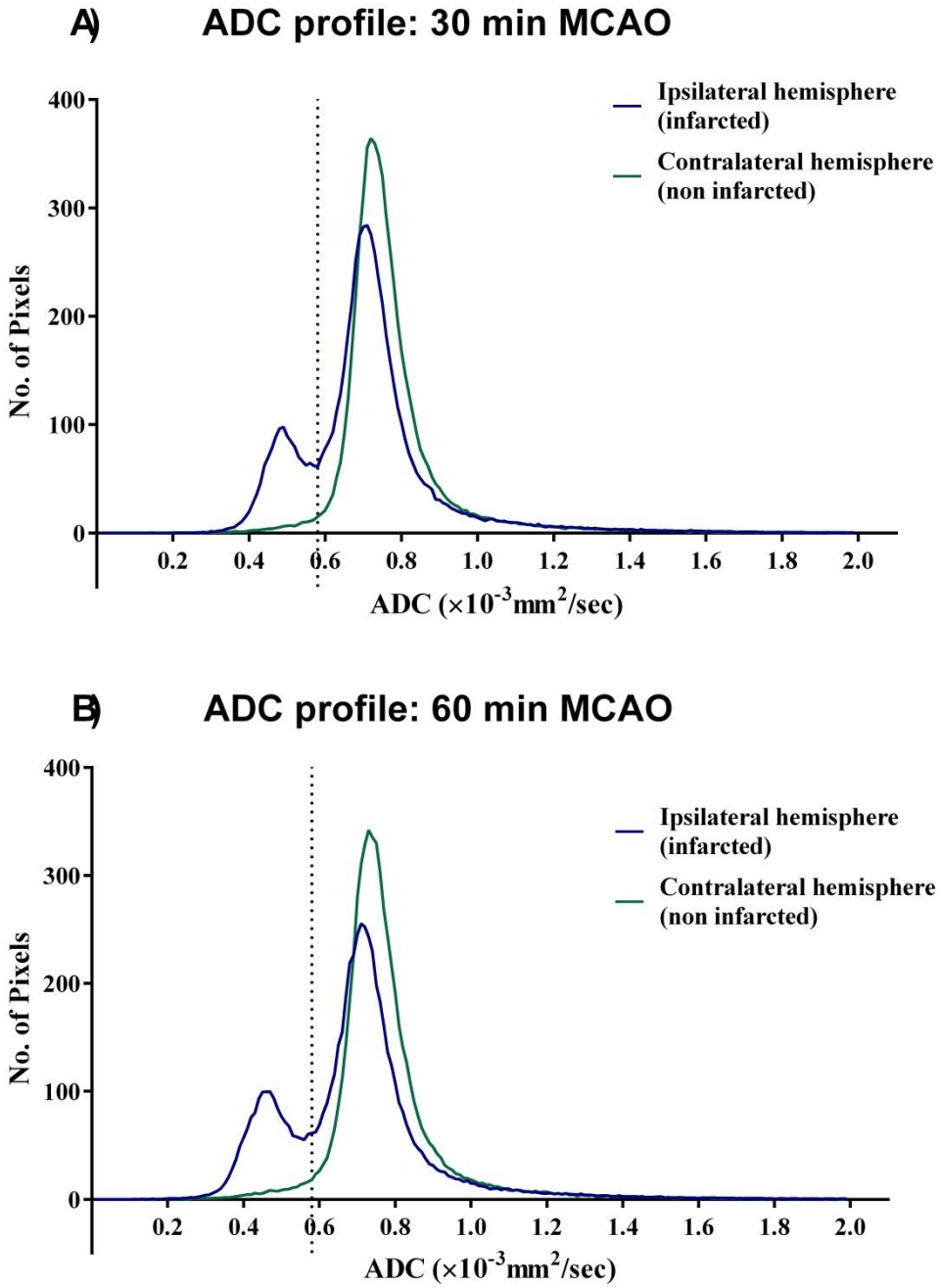

Figure 2-6 ADC value profile at 30 min and 60 min MCAO. A) ADC profile at 30 min MCAO; B) ADC profile at 60 min MCAO. The mean number of image pixels, within a range of ADC values, is expressed as $\times 10^{-3} mm^2/sec$ for 48 rats. The vertical line depicted in each graph is set at the ADC value of $0.58 \times 10^{-3} mm^2/sec$, the suggested threshold to detect abnormal ADC values in the ipsilateral hemisphere. In both 30 min and 60 min MCAO, there is an increase in ADC values in the ipsilateral hemisphere compared to the contralateral hemisphere below and at the threshold defined. Therefore, confirming that to detect ischaemic lesion in ADC maps, a threshold of 0.01 to 0.58 $mm^{-3} mm^2/sec$ should be used.

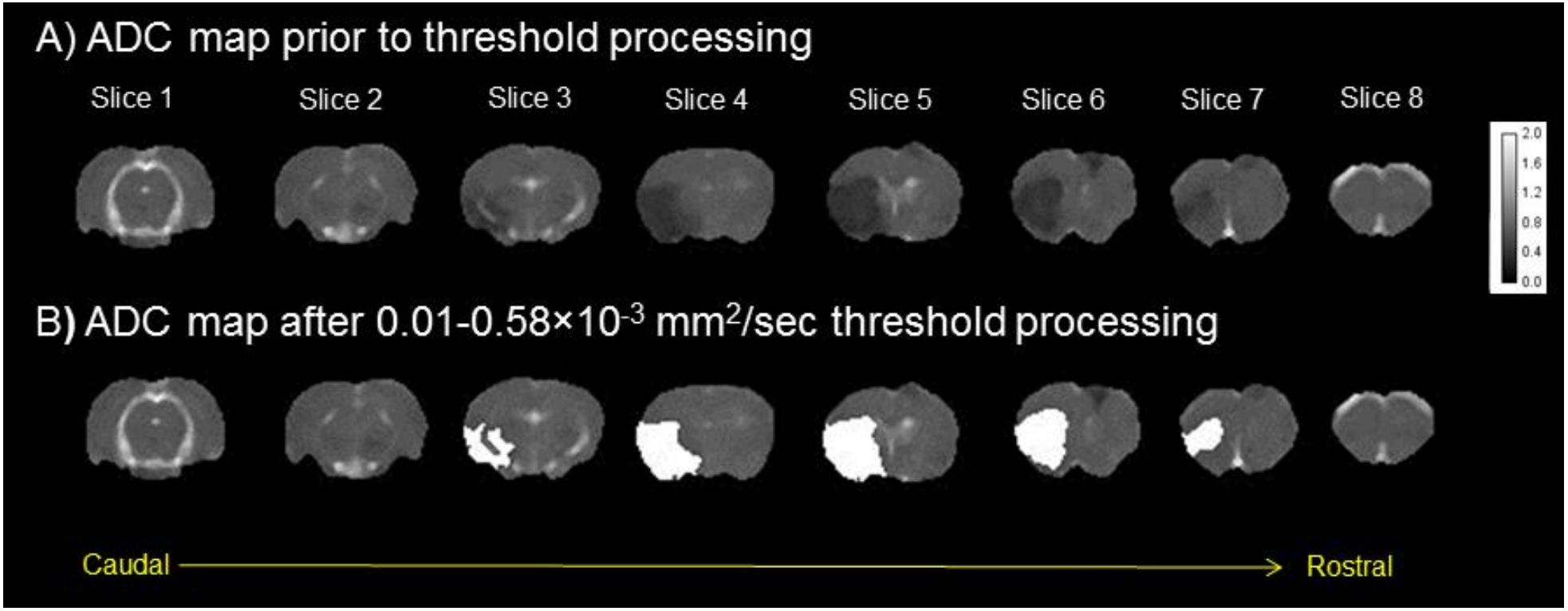

Figure 2-7 ADC map prior to and post threshold processing. A) ADC maps at 60 min MCAO across 8 coronal levels prior to threshold processing. ADC values ranging between 0.0-2.0×10^{-3} mm^2/sec as set by the scale**. B) Respective ADC maps across 8 coronal levels following threshold processing.** Threshold was set at ADC values of 0.01-0.58×10^{-3} mm^2/sec, highlighing early ischaemia lesion depicted in white. ADC values are expressed as ×10^{-3} mm^2/sec.

2.9.2 RARE T_2 weighted Imaging

In Chapters 3, 4 and 5 infarct volume was assessed using a rapid acquisition with refocused echoes (RARE) T_2 weighted sequence at either 24 hrs; 72 hrs or 7 days post MCAO.

2.9.2.1 Technical parameters

T_{2-} weighted imaging was carried out using a RARE sequence with the following paramaters: 16 contiguous coronal slices, slice thickness of 0.75 mm and an in-plane resolution of 98 μm, effective TE: 100 ms, TR: 6,000 ms, matrix size: 256× 256 and FOV: 25 × 25 mm.

2.9.2.2 Image processing and analysis

T_2 weighted images were analysed using ImageJ software. Hyperintense regions, excluding cerebral ventricles, were manually delineated across the 16 slices in mm^2 to define the infarct (Figure 2-8). The infarct areas were summed and multiplied by the slice thickness, 0.75 mm, to obtain the final volume. The ipsilateral and contralateral hemispheres were also delineated and hemipshere volumes calculated. Final infarct volume was corrected to oedema and compression of the contralateral hemisphere using the Gerriets equation (Gerriets et al. 2004) defined by the following formulas:

- **Infarct volume corrected to oedema**

Infarct volume corrected to oedema (mm^3):
Contralateral Hemisphere Volume
–
(Ipsilateral Hemisphere Volume – Lesion Volume)

- **Compression factor**

Compression factor (mm^3):
(Contralateral Hemisphere Volume + Ipsilateral Hemisphere Volume)
÷
(2 × Contralateral Hemisphere Volume)

- **Final infarct volume**

Final infarct volume (mm^3):
Corrected Lesion Volume × Compression Factor

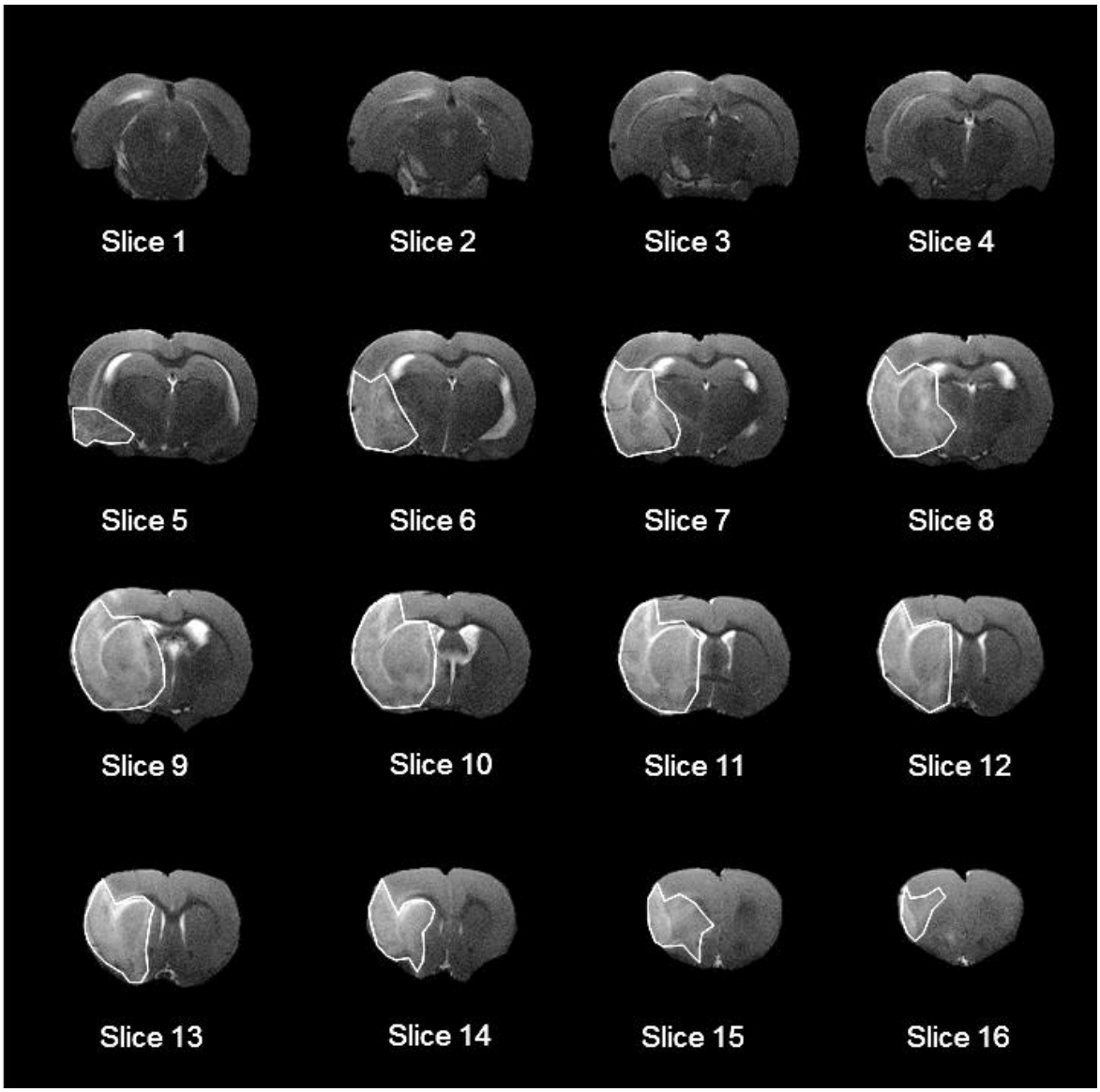

Figure 2-8 Representative RARE T_2 weighted images depicting final infarct volume. Infarct was identified as hyperintense regions across the 16 coronal slices in the ipsilateral hemisphere. Image J was used to delineate the hemisphere volumes and the infarcted tissue, the latter delineated in white. After, infarct volume was corrected for both oedema and contralateral compression using Gerriets equation (Gerriets et al. 2004). The animal represented was subjected to 90 min MCAO and 72 hrs reperfusion at time of assessment.

2.9.3 Magnetic Resonance Angiography

2.9.3.1 Technical parameters

Magnetic resonance angiography (MRA) weighted sequences were carried out to confirm MCAO and/or successful reperfusion. The MRA sequence was a FLASH based sequence with the following parameters: 50 contiguous coronal slices, slice thickness of 0.4 mm, effective TE: 3.8 ms, TR: 15 ms, matrix size: 256×256, FOV: 4×4 mm and a spatial resolution of 156 μm.

2.9.3.2 MCAO and reperfusion assessment

MRA was used as a tool to assess left MCA occlusion and/or reperfusion during and following MCAO. The left and right MCAs were identified as the hyperintense regions running along the coronal sections as indicated in orange (Figure 2-9). Following MCAO, the left MCA was missing due to vessel occlusion whereas flow could clearly be visualised in the right MCA (Figure 2-9A). Upon reperfusion, a clear hyperintense signal can be seen on both MCAs (Figure 2-9B).

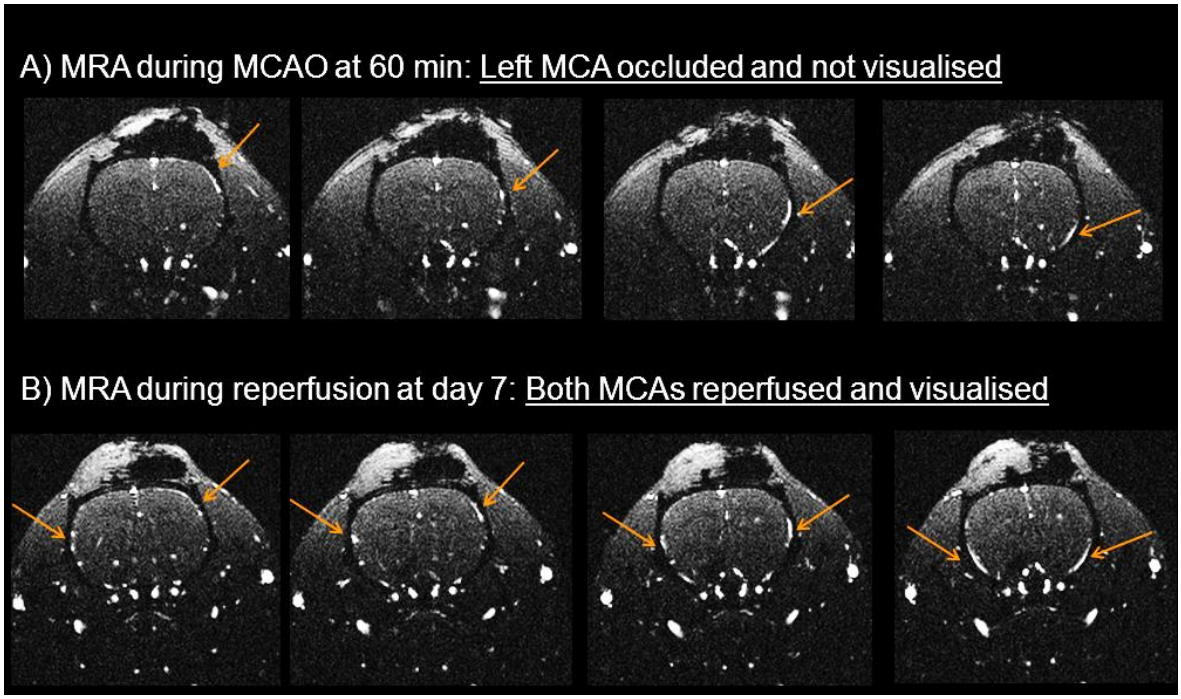

Figure 2-9 MRA across the MCA territory during and post MCAO. A) MRA at 60 min MCAO; B) MRA at 7 days reperfusion. During MCAO, the left MCA is occluded with the intraluminal filament, thus, it is not visualised along the coronal sections on the left side. Conversely, the right MCA is clearly detected and displayed as hyperintense regions in white along the coronal sections. These images indicate successful MCAO. During reperfusion, both left and right MCAs are clearly visualised along the coronal sections, indicating successful reperfusion. Orange arrows outline the location of left and right MCAs depicted in white.

2.10 Plethysmography blood pressure measurement

Conscious tail-cuff BP measurements were carried out in recovery studies (Chapters 3 and 4) to determine the effect of therapy on systolic BP. The method used is a non-invasive technique that enables BP measurement without anaesthetising the animals (Evans et al., 1994).

A week prior to BP measurements, animals were handled and acclimatised to the set up to prevent stress during measurements. On the day of BP assessment, an insulated heat box (dimensions 37 × 35 × 40 cm) was heated with the use of a lamp and a hairdryer (Boots, UK) to 38°C. The animal was then placed in the previously warmed box for a period of 10 min to induce maximal vasodilation of tail arteries and aid BP value detection. Once the animals exhibited little movement and a strong pink colour in their ears, they were deemed sufficiently warm and ready for BP determination. Rats were placed on the bench top and wrapped in a cloth towel, except the tail, and gently held. A tail cuff made of inflatable latex tube was tightly placed at the proximal end of the rat's tail and the piezoceramic transducer introduced on the distal end (Figure 2-10). A few measurements were performed to familiarise the animal with the procedure and once the rat was stable, the latex within the cuff was inflated with an air cylinder until the pressure applied matched the pressure in the tail artery. The signal obtained was recorded by the piezoceramic transducer and converted in the monitoring system, connected to a laptop (Dell, UK), into systolic BP in mmHg. Once the value was obtained, the cuff was deflated to release pressure and the procedure repeated until 10 individual BP measurements were acquired. After, animals were returned to their cages and rewarded with Cheerios (Nestlé®, UK). The mean and standard deviation (S.D.) of the 10 individual values were calculated for each animal and shown as systolic BP.

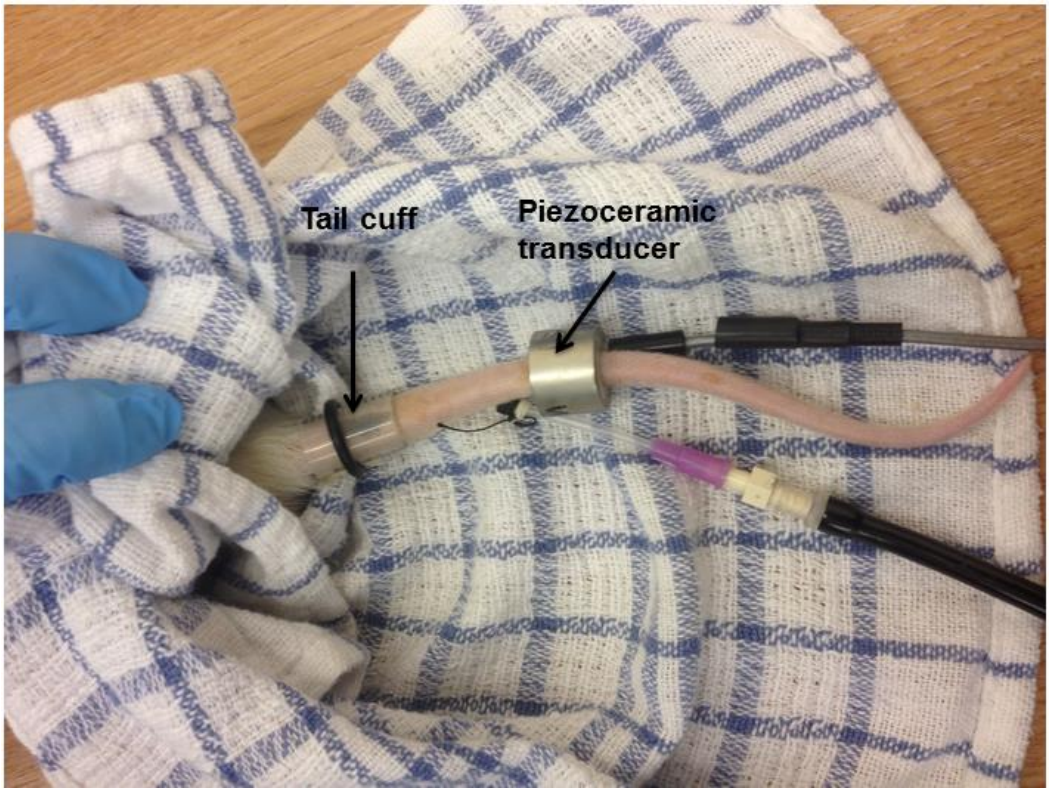

Figure 2-10 Plethysmography systolic BP measurement. A tail cuff containing inflatable latex tubing and a piezoceramic transducer were placed around the rat's tail. The latex within the tail cuff was inflated until the pressure exerted matched the pressure within the tail vessels. This was then detected by the transducer and translated via a monitoring system into systolic BP. The procedure was repeated until 10 individual BP values were obtained for each animal.

2.11 Neurological Score

A neurological score was performed on all animals prior and post-MCAO using an 18 point neurological score as previously described (Garcia et al., 1995). This score has been widely used and shown to successfully correlate with the volume and size of the infarct (Garcia et al., 1995, 2013). The test assesses the rats' performance in 6 distinct and individual assessments with a maximum score of 3 each adding up to 18 points and a total minimum score of 3. The assessments evaluate and score spontaneous activity, symmetry of movement, forelimb symmetry, body proprioception, response to vibrissae touch and climbing. Table 2-1 outlines the protocol followed to evaluate neurological score. The left MCA was occluded in all studies in this thesis and therefore the right side is considered impaired.

Table 2-1 The 18 point neurological Score. The Garcia neurological score is comprised of 6 distinct tests, scored to a maximum of 3 points. The higher the functional outcome, the closer the value is to 18 and vice versa. The table was adapted from Garcia et al., 1995.

Test	Score			
	0	1	2	3
Spontaneous activity (in cage for 5 min)	No movement	Barely moves	Moves but does not approach at least three sides of the cage	Moves and approaches at least three sides of cage
Symmetry of movements (four limbs)	Contralateral side: No movement	Contralateral side: Slight movement	Contralateral side: Moves slower; general movement still forward	Symmetrical outreach
Symmetry of forelimbs (outstretching while held by tail)	Contralateral side: No outreach	Contralateral side: Attempts to outreach but unsuccessfully	Contralateral side: Moves and outreaches less than left side	Symmetrical outreach
Reaction to touch on either side of trunk	N/A	Contralateral side: No response	Contralateral side: Weak response	Symmetrical response
Reaction to vibrissae touch	N/A	Contralateral side: No response	Contralateral side: Weak response	Symmetrical response
Climbing wall of wire cage	N/A	Fails to climb	Contralateral side: Displays weak grip	Normal climbing

2.11.1 Spontaneous activity

Each animal was moved into a clean cage and its behaviour observed for 5 min. A healthy animal will quickly explore the cage and approach all four walls of the cage as well as try to explore beyond the cage walls. Therefore, animals that exhibited this behaviour were given a score of 3. A score of 2 was attributed to animals that were moving in the cage but did not approach at least 3 cage walls. A score of 1 was given to animals that moved in the cage but did not approach any walls nor explored the environment. A score of 0 was attributed to rats that did not move at all during the 5 min inside the cage.

2.11.2 Symmetry of movement in the four limbs

Symmetry of the limbs was evaluated by placing the rat on a bench top or on the floor and observing the animal while walking. Animals showing complete symmetry of the four limbs were given a score of 3. Rats showing that the right limbs were splaying towards the side or moving slower than the left limb, yet exhibiting relatively forward movement, were scored 2. A score of 1 was given to animals that showed slight right limb movement and sideways movement towards the left. A score of 0 was given to animals that showed no right limb movement leading to circling behaviour.

2.11.3 Forelimb symmetry

Rats were held by the tail and placed near the bench top edge. The animals' ability to outreach to the bench top was assessed whilst the hindlimbs were kept in the air. A score of 3 was attributed to rats that showed no preference of the right or left limb to outreach to the edge of the bench, this way, displaying full forelimb symmetry. A score of 2 was attributed to animals showing that the right limb outreached to the bench edge fewer times than the left limb and it often missed touching the bench top when compared to the left side. A score of 1 was given to animals that still attempted to outreach to the bench top with the right limb; however, it was often left hanging. A score of 0 was attributed to rats that showed no movement in the right limb, which assumed a retracted position when compared to the left limb.

2.11.4 Body proprioception

This test was performed once the animals were not moving or exploring and distracted to movement. Without the rat seeing, a pen or pencil was used to touch either side of the trunk and the reaction assessed. A score of 3 was attributed to animals that showed a symmetrical response to trunk touch on either side by turning their heads and showing a startled response upon stimulus. A score of 2 was given to rats exhibiting a weaker response on the right side and a score of 1 if the animal did not respond to stimuli at all.

2.11.5 Response to vibrissae touch

A pencil or pen was used to brush against the rat's vibrissae on both the left and right sides. In healthy animals, brushing a pen on both sides of vibrissae will elicit the animal to turn its head towards the stimuli or try to avoid the pencil, leading to a score of 3. However, animals with neurological deficit will show a weaker reaction to vibrissae touch on the right side and thus, will fall within a score of 2, or not show any response to vibrissae touch at all, which leads to a score of 1.

2.11.6 Climbing

Animals were gripped from the base of the tail and placed onto a wire grid. Animals were given a score of 3 if they successfully climbed to the top of the grid - displaying similar forelimb symmetry and a relatively forward movement. A score of 2 was attributed to animals that attempted to climb but showed a weaker grip of the right side, displaying a sideward movement. A score of 1 was attributed to animals that failed to climb or tried to climb but did not reach halfway of the wire grid.

2.12 Brain tissue processing

2.12.1 Snap freezing

At the end of the experiment, animals were anaesthetised with 5% isoflurane in a 30:70% O_2-NO_2 mixture. Once the animal was deemed as deeply anaesthetised, it was killed by Schedule 1 procedures and the brain carefully removed. The cerebellum and bulbusolfactorus were discarded followed by brain tissue sectioning where the contralateral and ipsilateral hemispheres were separated and further sectioned into core and peri-infarct regions with the aid of RARE T_2 imaging. The tissue sectioned was placed in an individual Eppendorf tubes and quickly snap frozen in liquid nitrogen, to maintain integrity of RNA, and stored at -80^{o}C until further use.

2.12.2 Perfusion fixation

To assess protein levels with immunohistochemistry and perform histological examinations, animals were subjected to transcardial perfusion fixation with 4% paraformaldehyde [(PAM; 4% in 50 mM phosphate buffer; 500 mL), Sigma Aldrich, UK]. Rats were deeply anaesthetised with 5% isoflurane and transferred to a tray containing absorbent pads and anaesthesia continued on a facemask delivering 3% isoflurane. An incision was made in the abdominal wall just underneath the rib cage with the use of large blunt scissors followed by a cut in the diaphragm and rib cage, exposing the pleural cavity. The heart was cleared from connective tissue and the sternum retracted with the aid of a hemostatforcep to clearly visualise the chest cavity. The heart was gripped with hemostat forceps a blunt ended 16-gauge needle, directly connected to a perfusion fixation set up, was inserted at the base of the heart through the left ventricle into the aorta. Once the needle was correctly placed, the needle was clamped to secure in aorta and the right atrium cut with sharp scissors to allow blood drainage. The animal was perfused with 1% heparin (1000 units/mL heparin; 0.9% saline, 1L) dissolved in 250 mL saline at a pressure of ~120 mmHg. Once the blood was completely cleared from the circulation, animals were perfused with 250 mL of 4% PAM at the same pressure as saline infusion. Correct PAM perfusion was confirmed by spontaneous fixation tremors and body stiffness. After, rats were decapitated and the heads immersed in 4% PAM for 24 hrs. Brains were removed from the skull and left in 4% PAM for another 24 hrs and then in 70% ethanol until paraffin embedding processes were performed.

2.12.2.1 Paraffin embedding and sectioning

Tissue was transferred to an automatic processor (Tissue-Tek VIP, Miles Scientific) and subjected to a series of washes in ethanol to dehydrate the tissue and xylene, which acts as a clearing reagent. Brains were placed in paraffin wax for a total of 6 hrs at 60°C to create a paraffin block. The whole process takes 15 hrs to be completed and is described in Table 2-2. For sectioning, paraffin embedded brains were placed on a wooden block and cut at 5 μm sections with the use of a microtome across 8 cerebral coronal levels (Figure 2-11). Two to three 5 μm sections were mounted onto poly-l-lysine coated glass slides, three slides per coronal level. Sections were allowed to dry and stored in a slide storage box until use.

Table 2-2 Paraffin embedding tissue processing. Brains were dehydrated with alcohol for a period of 6 hrs followed by xylene clearing reagent immersion for 3 hrs to then be placed in paraffin for 6 hrs.

Stage	Reagent	Immersion period
1	70% Alcohol	1 hour
2	95% Alcohol	1 hour
3	95% Alcohol	1 hour
4	100% Alcohol	1 hour
5	100% Alcohol	1 hour
6	100% Alcohol	1 hour
7	Xylene	1 hour
8	Xylene	1 hour
9	Xylene	1 hour
10	Paraffin	2 hours
11	Paraffin	2 hours
12	Paraffin	2 hours

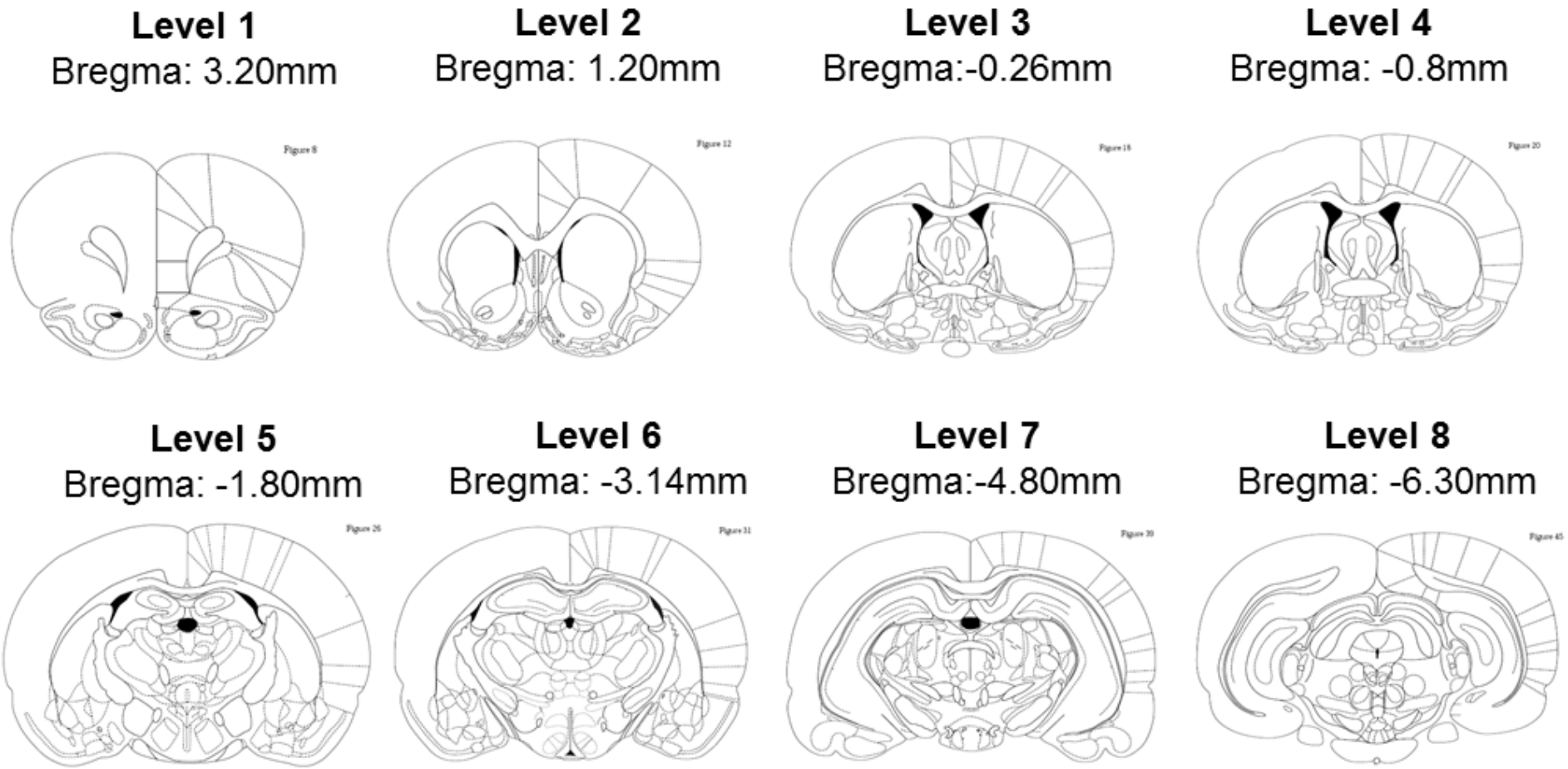

Figure 2-11 The eight coronal levels covering the territory of the MCA. The diagram shows the 8 pre-defined coronal levels and respective distance from bregma, where positive values represent anterior and negative values posterior to bregma. Brain tissue was collected at these levels for histological assessments. The figures were obtained from the stereotaxic atlas of Paxinos & Watson (Paxinos and Watson, 1997).

2.13 Histological analysis

2.13.1 Haematoxylin and Eosin histological staining

Haematoxylin and eosin (H&E) staining technique was used to identify the infarct core and peri-infarct areas to then outline where immunohistochemistry analysis would be performed. Plus, it was used to confirm the quality of the paraffin embedding and sectioning processes.

Brain sections from coronal levels 3 to 5 were selected as these represent the infarct extent across all animals. The sections were stained with H&E (Sugipath, UK) and used to outline infarct core and peri-infarct regions (Table 2-3). Slides were placed in a metal rack and submerged in 100% Histoclear (National Diagnostics, USA, Atlanta) for a period of 15 min with regular agitation. Sections were then rehydrated through a sequence of alcohols: 100% for 6 min, 90% for 3 min and 70% alcohol for 3 min (Sigma Aldrich, UK). After, slides were placed in running water for a period of 4 min and subsequently stained with haematoxylin for 2 min. To remove excess staining and differentiate the slides, sections were submerged in acid alcohol for a few seconds (2-3 dips) and returned to running water for 5 min before being transferred to Scott's Tap Water Substitute (Sigma Aldrich, UK) for 2 min (blueing). Sections were returned to running water for 2 min and dehydrated by being immersed in 70% alcohol for 2 min and 90% alcohol for 2 min. Thereafter, slides were stained with alcoholic eosin (95%) for 2 min. The final steps included three washes in absolute alcohol for 4 min each to then be placed in 100% Histoclear three times for 4 min each. Coverslips were then mounted on the sections with the use of DPX mounting medium (Sigma Aldrich, UK).

Table 2-3 H&E staining procedure for paraffin embedded sections.

Stage	Solution	Time (min)
1	Histoclear 1	5
2	Histoclear 2	5
3	Histoclear 3	5
4	Absolute Alcohol 1	3
5	Absolute Alcohol 2	3
6	90% Alcohol	3
7	70% Alcohol	3
8	Wash in running water	4
9	Haematoxylin	2
10	Wash in running water	5
11	Differentiate in Acid Alcohol	A few dips only
12	Wash in running water	5
13	Scott's Tap Water Substitute	2
14	Wash in running water	2
15	70% Alcohol	2
16	90% Alcohol	2
17	Alcoholic Eosin (95%)	2
18	Absolute Alcohol 1	4
19	Absolute Alcohol 2	4
20	Absolute Alcohol 3	4
21	Histoclear 1	4
22	Histoclear 2	4
23	Histoclear 3	4

2.13.1.1 Identification of the peri-infarct border

H&E sections were analysed under a light microscope at 20x and 40x magnification to outline the core and peri-infarct ipsilateral regions at coronal levels 3, 4 and 5. Once the infarct area was outlined with the help of T_2-weighted imaging, 3 distinct regions of interest (ROIs) were established in the peri-infarct area per coronal level to serve as guidance for immunohistochemical analysis (Figure 2-12).

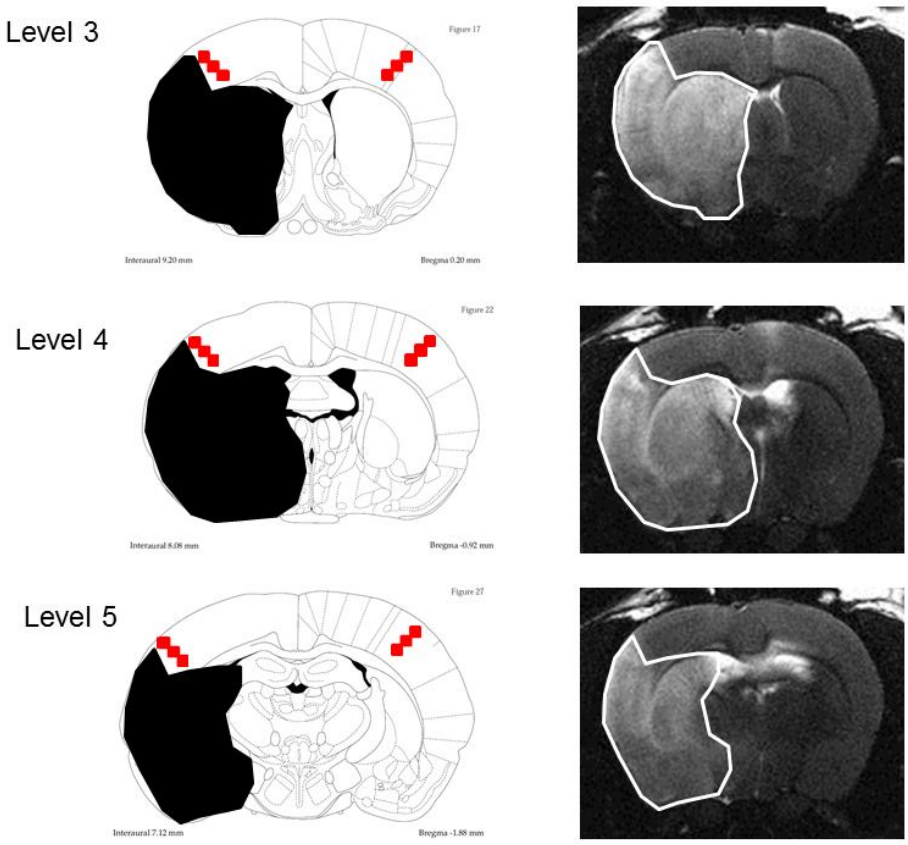

Figure 2-12 Region of interest determination in coronal levels 3, 4 and 5. H&E was used as a tool to identify the infarct (black) across animals in coronal levels 3, 4 and 5 with the help of T_2-wheighed imaging (displayed on the right in white). Once the infarct was identified, the peri-infarct zone and corresponding contralateral areas were evaluated and three independent ROIs (red) determined in each hemisphere to serve as guidance for immunohistochemical analysis.

To accurately determine the peri-infarct region, morphological characteristics of cells were compared. Healthy cells were identified due to the presence of well-defined cytoplasmic structures and large round nuclei (Figure 2-13A). Ischaemic neurons were identified due to the presence of shrunken pyknotic nuclei, an eosinophilic cytoplasm and triangular shape. Moreover, in these cells, surrounding neuropil was disrupted and shown to be unstained (Figure 2-13B). On the other hand, the peri-infarct zone was outlined by identifying regions that showed both cell phenotypes (Figure 2-13C).

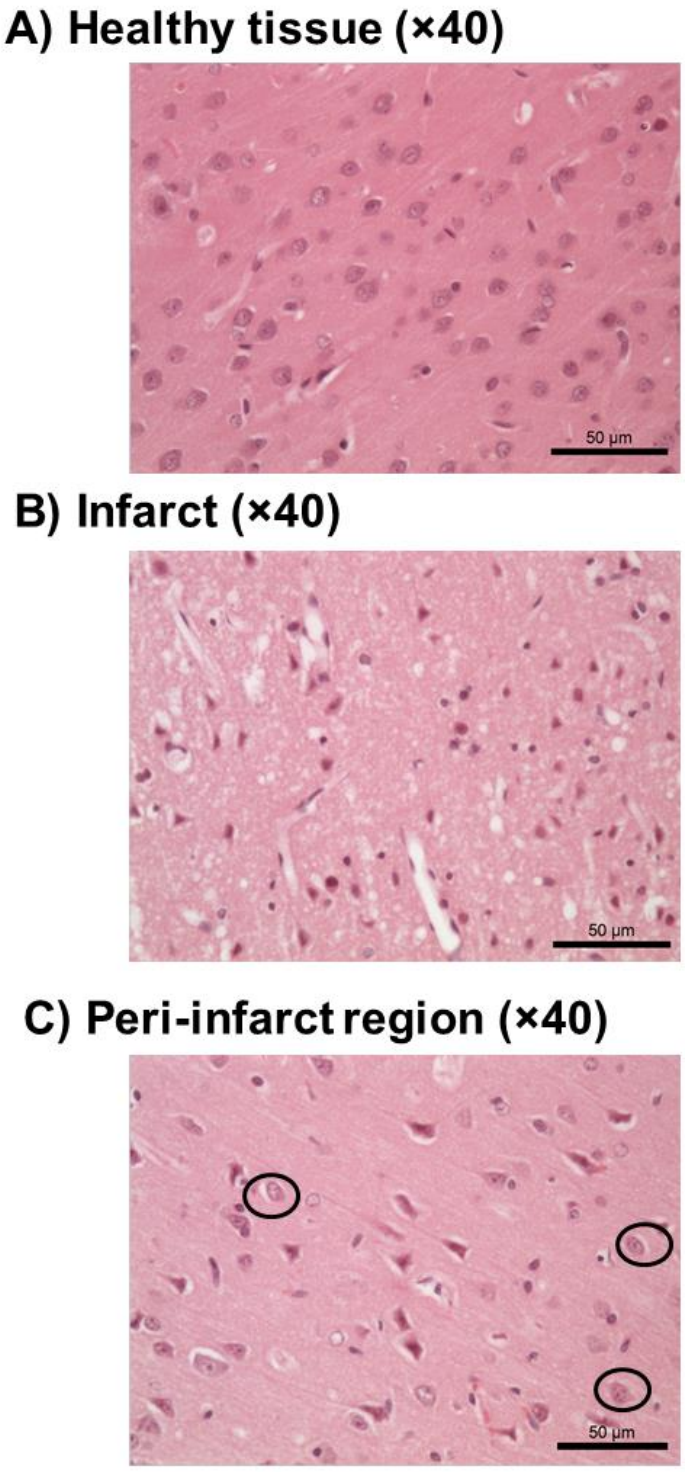

Figure 2-13 H&E peri-infarct region determination. A) Healthy tissue. Cells presenting well-defined cytoplasmic structures and large round nuclei. **B) Ischaemic tissue.** Cells displaying dark stained triangular neurons and pale stained neuropil**. C) Peri-infarct region.** Cells displaying normal morphology characterised by well-defined round nuclei (highlighted in black) as well as ischaemic cells as observed in Figure B. Scale bar represents 50µM.

2.13.2 IBA1 immunohistochemistry labelling

Adjacent sections used for H&E staining were selected to perform immunostaining for ionized calcium-binding adapter molecule 1 (IBA1) positive microglia labelling. To dewax and rehydrate, sections were submerged in 100% histoclear for 15 min and then washed in 100% ethanol for 10 min, 90% ethanol for 5 min, 70% ethanol for 5 min and finally rinsed in cold running tap water for ~5 min. Extreme care was taken to not allow the sections to dry out between washes to prevent non-specific antibody binding. Heat induced antigen retrieval was achieved by placing the sections into a pressure cooker containing an antigen retrieval solution (sodium citrate buffer (pH 6.0)) for 4 min after which slides were left in running cold water for 10 min. After, sections were washed twice in Tris Buffered Saline-T (TBS dissolved in 0.025% Triton x-100; Sigma-Aldrich, UK) for 5 min each. A hydrophobic pen (Dako pen; Agilent, UK) was used to draw a ring around each section on the slide and blocking solution [TBS containing 10% normal goat serum (Vector Laboratories Ltd, UK) and 1% bovine serum albumin (BSA) (Vector Laboratories Ltd, UK)] applied for 2 hrs at room temperature in a humidified chamber. Blocking buffer was then removed and IBA1 primary antibody (Catalog #: ab139590, Abcam, UK) diluted in 1:250 TBS with 1% BSA was applied to the sections and incubated overnight at 4°C. The following day, samples were rinsed in TBS-T twice for 5 min each and the secondary antibody [goat anti-chicken IgY (Catalog #: A-11039; ThermoFisher, UK)] diluted in 1:500 TBS with 1% BSA was added to the sections and incubated at room temperature for 1 hr in a dark room. Slides were rinsed in TBS three times for 5 min each time and mounted using Vectashield medium containing 4’,6-diamidino-2-phenylindole (DAPI) (Vector Laboratories Ltd, UK). The coverslips were applied and secured in place with varnish to seal the slides, which were allowed to dry and stored at 4°C until image analysis.

2.13.2.1 Microglia quantification

The three ROIs previously outlined with H&E in the peri-infarct tissue and corresponding contralateral areas were used as guidance for $IBA1^+$ microglia assessment. Within each coronal section, ROIs were imaged at 40x using a light microscope (Leica Biosystems, UK), attached to a charge-coupled device (CCD) camera and a laptop, and captured using QCapture Pro 6 (QImaging, Surrey, Canada). A negative control (without primary antibody) was run to verify nonspecific secondary antibody binding, confirming specificity (Figure 14A). $IBA1^+$ microglia were then manually counted and summed to provide total

microglia count across each coronal level in the peri-infarct and corresponding contralateral region using Image J Software. In addition, cells in the peri-infarct were classified into resting or activated through morphological assessment. Resting microglia are small cells with little perinuclear cytoplasm and multiple thin ramifying processes branched in various directions. Activated microglia present large soma and thickened and retracted processes (Kettenmann et al., 2011) (Figure 2-14B). In addition, activated microglia can be identified by a giant, amoeboid shape and proposed to be in a phagocytic state (Kettenmann et al., 2011) (Figure 2-15C). Data were expressed as cell number per mm^2 tissue across the 3 coronal levels and activated microglia phenotype expressed as % of total microglia number. Figure 2-15 shows representative images of IBA1 microglia staining in peri-infarct, contralateral and infarct areas.

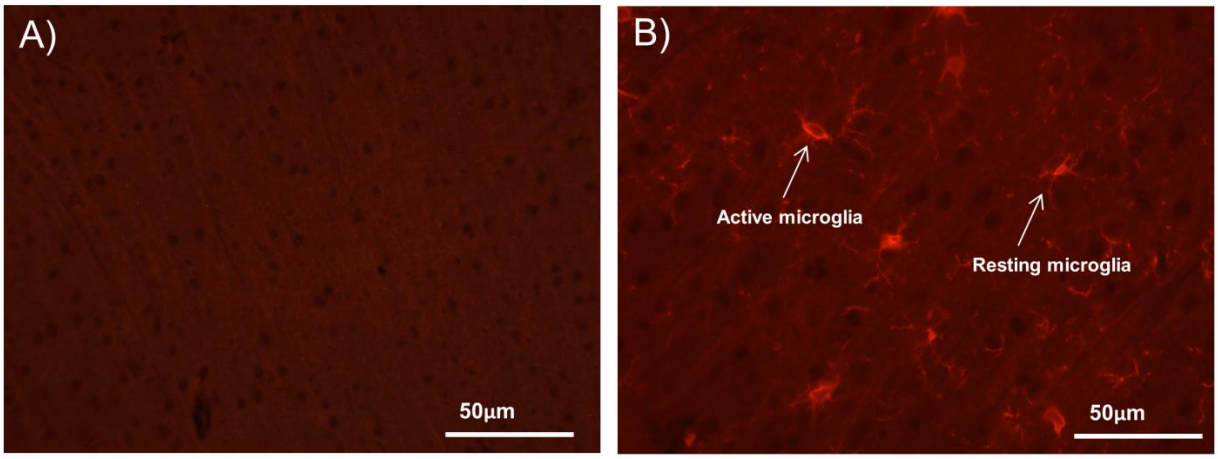

Figure 2-14 Secondary antibody specificity and microglia phenotype. A) Negative control (without primary antibody). Image shows that secondary antibody selected did not induce non-specific binding. **B) Microglia phenotype.** Image shows an example of activated microglia (larger cell body and shorter, thicker processes) and resting microglia (smaller cell bodies and longer, thinner, ramifying processes). Scale bar is set as 50μm.

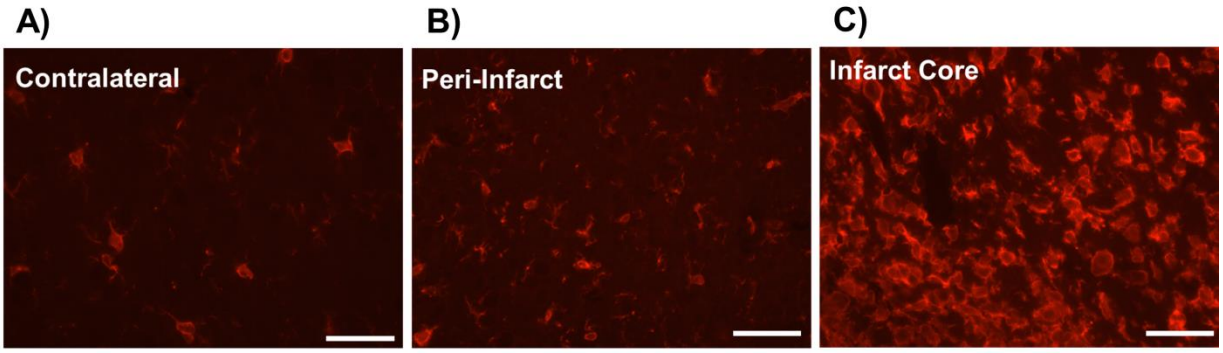

Figure 2-15 Immunohistochemical IBA1$^+$ microglia staining. Representative images of IBA1 microglia staining (red) at 7 days post 90 min MCAO in the contralateral region **(A)**, peri-infarct regions **(B)** and the infarct core **(C)**. Scale bar is set in white and = 50μm.

2.14 RNA extraction

Total RNA was extracted using miRNeasy Mini-kit as outlined by manufacturer (Qiagen, Hilden, Germany). For disruption and homogenisation, 50 mg of brain tissue was placed in sterile polystyrene bijoux (ThermoFisher, UK) and 700 μL of Qiazol (Qiagen, Hilden, Germany) quickly added. The sample was lysed using a tissue homogenizer (Qiagen, UK) programmed at 5000 rpm for 20 secs. Each homogenate was individually transferred to an RNAse free tube and 140 μL of chloroform added to divide the sample into aqueous and organic phases. Samples were left to settle for 5 min at room temperature and centrifuged for a period of 15 min at 12000g at 4°C. The aqueous upper phase containing RNA was carefully collected, this way preventing the pipetting of organic phases, and transferred to new collection tubes where 525 μL of anhydrous ethanol (Sigma-Aldrich, UK) was added and thoroughly mixed. Each sample was transferred into an RNeasy Mini spin column and centrifuged at 8000g at room temperature to bind the RNA to the column membrane. In order to wash away phenol and other contaminants, 350 μL Buffer RWT was added to the column and centrifuged for 15 sec at 8000g, this step was performed twice. Columns were transferred to a new collection tube and then washed with 500 μL of Buffer RPE for 15 sec at 8000g in the first wash and for 2 min at 8000g for the second wash. Before eluting the purified RNA, columns were again transferred to a new collection tube and the samples centrifuged at full speed for 1 min to ensure that the mini column membrane was completely dry. Finally, the columns were transferred to an RNAse free tube and 50 μL of RNase-free H_2O was added to the column and centrifuged at 8000g for 1min to elute the purified RNA.

2.14.1 DNAse I treatment

All samples were subjected to DNAse I treatment to efficiently digest genomic DNA during RNA purification as suggested by the manufacturer (Qiagen, Hilden, Germany). Briefly, between the 350 μL Buffer RWT washes, 80 μL of DNase I (10 μL) dissolved in Buffer RDD (70 μL) was pipetted into the RNeasy Mini column membrane and left to act for 15 min. After this step, 350 μL of Buffer RWT was again added to the column and the protocol proceeded as described above.

2.14.2 RNA purity determination

RNA concentrations [ng/μL] were measured using a NanodropTM ND-1000 Spectrophotometer and v3.1.0 NanoDrop-1000 software (ThermoScientific, Loughborough, UK). The instrument works by applying a light source through a pulsed xenon flash lamp to the sample. The light generated is detected and measured with a spectrometer, which utilises a linear CCD array to analyse the sample. To quantify nucleic acids, the instrument uses a modified Beer-Lambert equation taking into account extinction coefficients with the following calculation:

$$c = (A \times \varepsilon)/b$$

- c: Nucleic acid [ ] (ng/mL)
- A: absorbance (A)
- ε: wavelength dependent extinction coefficient (ng-cm/mL)
- b: path length (cm)

The accepted extinction coefficients were as follows:

- Double stranded DNA: 50 ng-cm//μL
- Single stranded DNA: 33 ng-cm//μL
- RNA: 40 ng-cm//μL

To assess purity, absorbance ratios at 260/280 nm and 260/30 nm were evaluated. Samples with a 260/280 nm ratio ranging between 1.8 and 2.0 were considered pure. Samples with a ratio lower than 1.8 were considered contaminated as it indicates the presence of phenol, protein or genomic DNA. Samples with a 230/260 nm ratio ranging between 1.0 and 2.0 were considered pure. RNA concentrations were obtained as duplicates and averaged for each sample. Purified RNA was stored at -80°C until complementary DNA (cDNA) synthesis.

2.15 Complementary deoxyribonucleic acid synthesis

cDNA was generated from total tissue extracted mRNA by reverse transcription polymerase chain reaction (RT-PCR) using TaqMan® Reverse Transcription Kit as suggested by the manufacturer (Applied Biosystems, UK). This procedure was performedto allow gene expression assessment via qRT-PCR. All procedures were performed on ice and a negative control reaction containing RNAse-free H_2O prepared.

For each sample, 16 μL Mastermix solution was made up containing 1x PCR buffer, 5. mM $MgCl_2$, 2 mM deoxyribonucleotide triphosphate (dNTP) mix (0.5 mM each), 2.5 μM random hexamers, 0.4 U/μL RNAse inhibitor, 1.25 U/μL Multiscribe reverse transcriptase and RNAse-free H_2O (3.7 μL). The Mastermix was added to a 96 well plate (Applied Biosystems, UK) placed on ice. Stock RNA was defrosted and diluted in RNAse-free H_2O to yield 1 μg of RNA in 4 μL. The RNA was then added to the Mastermix to generate a total volume of 20 μL per sample. The 96 well plate was quickly vortexed and centrifuged at 300g for 30 sec before being placed in the PCR block to start RT-PCR under the cycling conditions described in Table 2-4. Once RT-PCR was completed, the cDNA was left in the PCR block at 4°C for up to 60 min and stored at -20°C until use.

Table 2-4 RT-PCR cycling conditions.

Temperature (°C)	Duration (min)	Outcome
25	10	Annealing
48	30	Reverse transcription
95	5	Reverse transcriptase inactivation
4	60	Storage

2.16 Taqman® quantitative real-time polymerase chain reaction

Quantitative real-time polymerase chain reaction (qRT-PCR) is a sensitive technique that allows the amplification and quantification of a specific DNA sequence by using the PCR principle and a thermocycler that captures fluorescence. In qRT-PCR, the 5'-3' exonuclease properties of DNA polymerase are used to cleave target probes and detect the amplification of the gene of interest (Arya et al., 2005). The technique is based on the fluorescence resonance energy transfer (FRET) principle and uses TaqMan probes, non-extendable fluorogenic target sequences, containing a fluorescent reporter dye at the 5'end and a quencher dye at the 3'end. Once the cDNA is denatured, the primer and TaqMan probe anneal to the sequence. During elongation, the probe is cleaved by the DNA polymerase leading to FRET and the fluorescence emitted absorbed by the quenching dye (Figure 2-16A). During amplification processes, dye molecules are further cleaved, increasing fluorescence intensity, which is detected by a thermocycler (Arya et al., 2005) (Figure 2-16B). Gene expression is quantified by assessing the cyclic threshold (Ct) value defined as the fractional PCR cycle number at which the fluorescence is greater than the established threshold defined by the instrument; the greater the Ct value, the lower the gene expression.

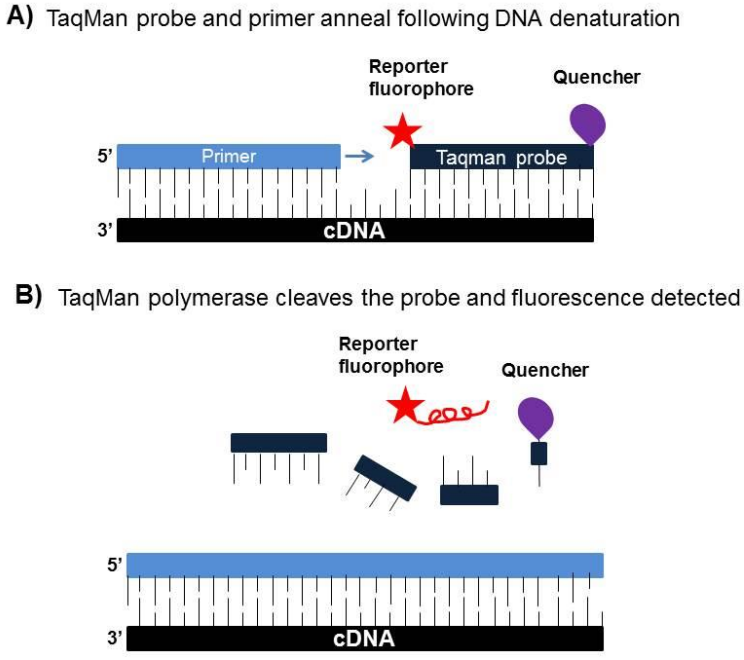

Figure 2-16 The qPCR principle. A) TaqMan probe and primer annealing; **B) Elongation and fluorescence detection.** Following cDNA denaturation, the primer and TaqMan probe will anneal to the sequence. During elongation, the TaqMan probe is cleaved by DNA polymerase leading to the release of a reporter fluorophore, which is absorbed by the quencher dye and detected by the thermocycler. Image adapted from Arya et al., 2005.

2.16.1 Gene expression reaction

Procedures were performed on ice and the reactions carried out according to the manufacturer's instructions in a 384 well plate and in technical duplicates for each gene of interest. qRT-PCR was performed using inventoried FAM labelled fluorescent Taqman® assay probes, which span an exon junction (m1 type) or lie within a single exon (s1 and g1 types) and are described in Table 2-5 and 2-6. Unless otherwise stated, all materials were obtained from ThermoFisher Scientific, UK.

A reaction mixture of 10 μL was prepared for each sample containing 5 μL of Taqman® Universal MasterMix II, 0.5 μL of Taqman probe 20x, 3 μL of RNAse-free H_2O and 1.5 μL of cDNA. For each probe a negative water control was tested. Once the reaction volumes were prepared, samples were centrifuged at maximum speed for 2 min to guarantee that there were no air bubbles that could interfere with qRT-PCR procedures. The 384 well plates were placed in a QuantStudio 12K Flex PCR System and samples incubated in the following cyclic conditions: 95ºC for 10 min to allow enzyme activation, 40 cycles at 95ºC for 15 sec to denature cDNA and 60ºC for 1 min for primer and probe annealing as well as primer extension.

In this thesis, a panel of genes of reference were run for each experiment to assess which gene was most stable between experimental conditions and thus, suitable to use as an internal control (Table 2-5). For mechanistic studies, Taqman® probes were run for Sham and transient MCAO peri-infarct brain samples and tested for RAS components, inflammatory and oxidative stress mediators' gene expression (Table 2-6).

Table 2-5 List of genes of reference examined. FAM labelled Taqman® probe assays used in experimental procedures.

Gene name	Gene symbol	Assay ID	Refseq Gene
Beta-Actin	*Actb*	Rn00667869_m1	NM_031144.3
Beta-2-microglobulin	*B2m*	Rn00560865_m1	NM_012512.2
Glyceraldehyde 3-phosphate dehydrogenase	*Gapdh*	Rn01775763_g1	NM_017008.4
Hypoxanyhine-guanine phosphoribosyltransferase	*Hprt1*	Rn01527840_m1	NM_0012583.2
Ubiquitin C	*Ubc*	Rn01789812_g1	NM_017314.1

Table 2-6 List of genes of interest examined. FAM labelled Taqman® probe assays used in experimental procedures.

Gene name	Gene symbol	Assay ID	Refseq Gene
Angiotensin converting enzyme	*Ace*	Rn00561094_m1	NM_012544.1
Angiotensin converting enzyme 2	*Ace2*	Rn01416293_m1	NM_001012006.1
Arginase 1	*Arg1*	Rn00691090_m1	NM_017134.3
Angiotensin II receptor type 1a	*Atgr1a*	Rn02758772_s1	NM_030985.4
Angiotensin II receptor type 2	*Atgr2r*	Rn00560677_s1	NM_012494.3
C-C motif chemokine 22	*Ccl22*	Rn01536591_m1	NM_057203.1
C-C motif chemokine receptor 2	*Ccr2*	Rn01637698_s1	NM_021866.1
C-C motif chemokine receptor 5	*Ccr5*	Rn00588629_m1	NM_053960.3
C-C motif chemokine receptor 7	*Ccr7*	Rn01465443_m1	NM_199489.4
Cluster differentiation 11b or integrin subunit alpha M	*Itgam*	Rn00709342_m1	NM_012711.1
Cluster differentiation 163	*CD163*	Rn01492519_m1	NM_01107887.1
Cluster differentiation 86	*CD86*	Rn00571654_m1	NM_020081.1
Cyclooxygenase-2 or prostaglandin-endoperoxide synthase 2	*Ptgs2*	Rn01483828_m1	NM_017232.3
Interleukin 10	*Il10*	Rn99999012_m1	NM_012854.2
Interleukin 1β	*Il1b*	Rn00580432_m1	NM_031512.2
Interleukin 6	*Il6*	Rn01410330_m1	NM_012589.2
Nitric oxide synthase 2	*Nos2*	Rn00561646_m1	NM_012611.3
Mas receptor	*Mas1*	Rn00562673_s1	NM_012757.2
Metallopeptidase inhibitor 1	*Timp1*	Rn00587558_m1	NM_053819.1
Matrix metalloproteinase 9	*Mmp9*	Rn00579162_m1	NM_031055.1
Nuclear factor κB p105 subunit	*Nfkb1*	Rn01399572_m1	NM_001276711.1
NADPH oxidase I	*Nox1*	Rn00586652_m1	NM_053683.1
NADPH oxidase 2	*Nox2*	Rn00576710_m1	NM_023965.1
Transforming growth factor β1	*Tgfb1*	Rn00572010_m1	NM_021578.2
Vascular endothelial growth factor A	*Vegfa*	Rn01511602_m1	NM_001110333.2
Vascular endothelial growth factor receptor 2 or kinase insert domain receptor	*Kdr*	Rn00564986_m1	NM_013062.1

2.16.2 Gene of reference optimisation

To guarantee the quality and reliability of the experiments, the expression of a gene of interest is compared to the expression of a gene of reference. The choice of gene of reference is usually based on a gene that is expressed at a constant level in all experimental conditions (Arya et al., 2005). All cDNA samples were run to determine adequate internal control, this way allowing correcting for variability related to starting RNA quantity and quality, cDNA efficiency and PCR amplification. Ct values for hypoxanyhine-guanine phosphoribosyltransferase (*Hrpt1*), glyceraldehyde 3-phosphate dehydrogenase (*Gapdh*), beta-actin (*Actb*), beta-2-microglobulin (*B2m*) and ubiquitin C (*Ubc*) genes were compared between groups. In Chapter 4 the gene of reference *Ubc* was selected whereas in Chapter 5 *Hrpt1* was deemed as suitable.

2.16.2.1 Peri-infarct tissue obtained 7 days post 90 min MCAO

In Chapter 4, *Ubc* was deemed the most suitable reference gene due to comparable Ct values amongst groups and the lowest S.D. [Sham: 27.2±0.59; MCAO-Vehicle (artificial cerebrospinal fluid (aCSF)): 26.55±0.52; MCAO-Ang-(1-7): 26.92±0.49, $P>0.05$] (Figure 2-17A). There were no differences between groups for *Hrpt1*; *Gapdh* and *Actb*; however, these displayed higher S.D. amongst groups compared to *Ubc* (Figure 2-17B:D). *B2m* showed statistically significant Ct values between groups and excluded as a potential internal control (Figure 2-17E).

2.16.2.2 Peri-infarct tissue obtained 24 hrs post 90 min MCAO

In Chapter 5, *Hrpt1* was deemed as the most suitable reference gene due to no significant differences and comparable S.D. between groups [Sham: 27.22 ± 0.3; MCAO-Vehicle (aCSF):26.91 ± 0.47; MCAO-Ang-(1-7): 26.71 ± 0.32; $P>0.05$] (Figure 2-18A). ANOVA's Bartlett's test indicated that S.D. was statistically different between groups for *Gapdh* ($P=0.02$) and therefore, its use was overruled (Figure 2-18B). *Actb*, *B2m* and *Ubc* showed statistical differences amongst groups and were deemed as inadequate reference genes (Figures 2-18C:E).

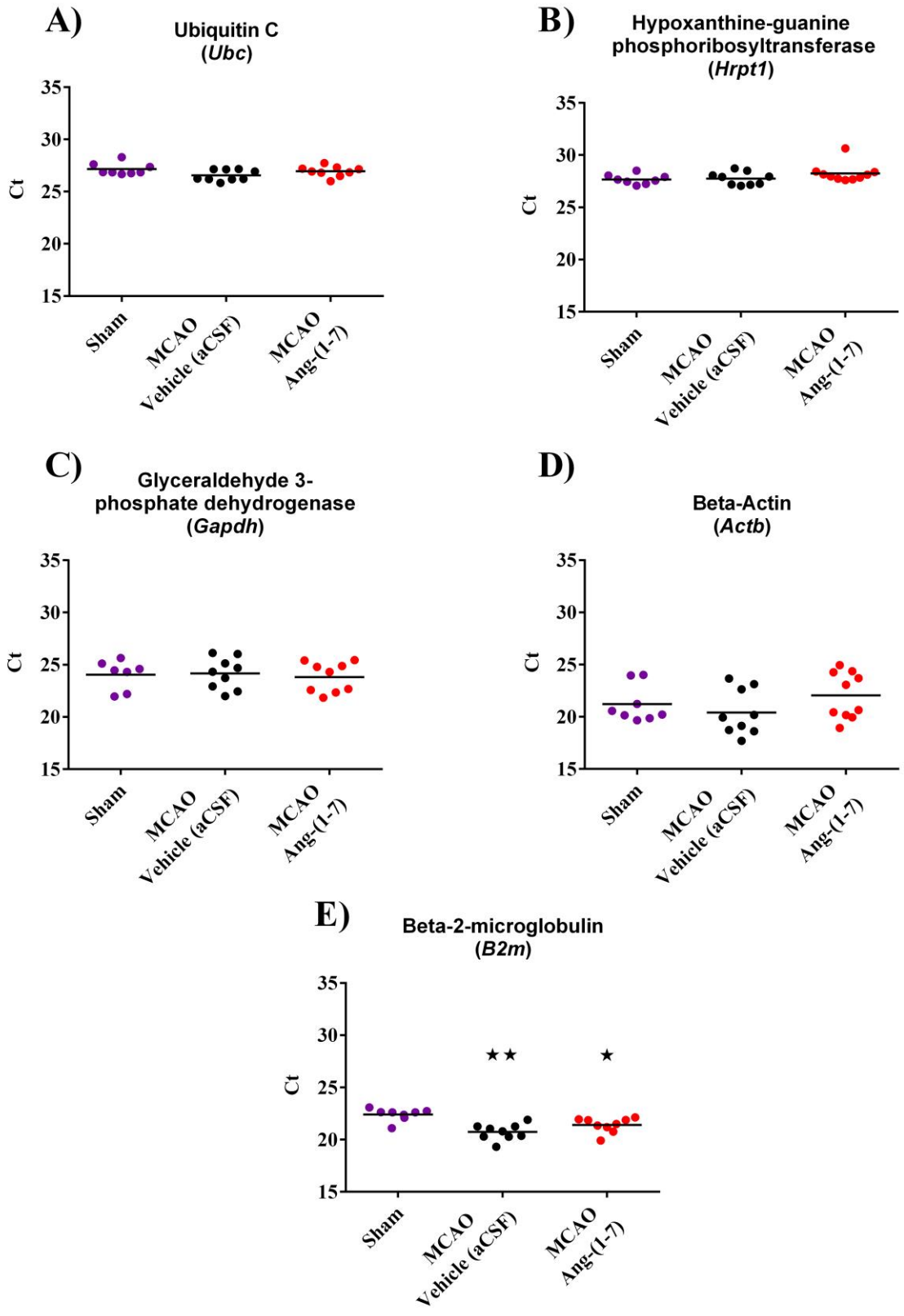

Figure 2-17 Reference gene candidates assessed in peri-infarct regions at 7 days post MCAO. A) *Ubc*; B) *Hrpt1*; C) *Gapdh*; D) *Actb* and E) *B2m*. Data from individual animals are presented as cyclic threshold (Ct) values. Horizontal bar represents mean. Data were analysed using one-way ANOVA with Tukey's post-hoc test, P<0.05 was deemed as significant. *P<0.05 compared to Sham.

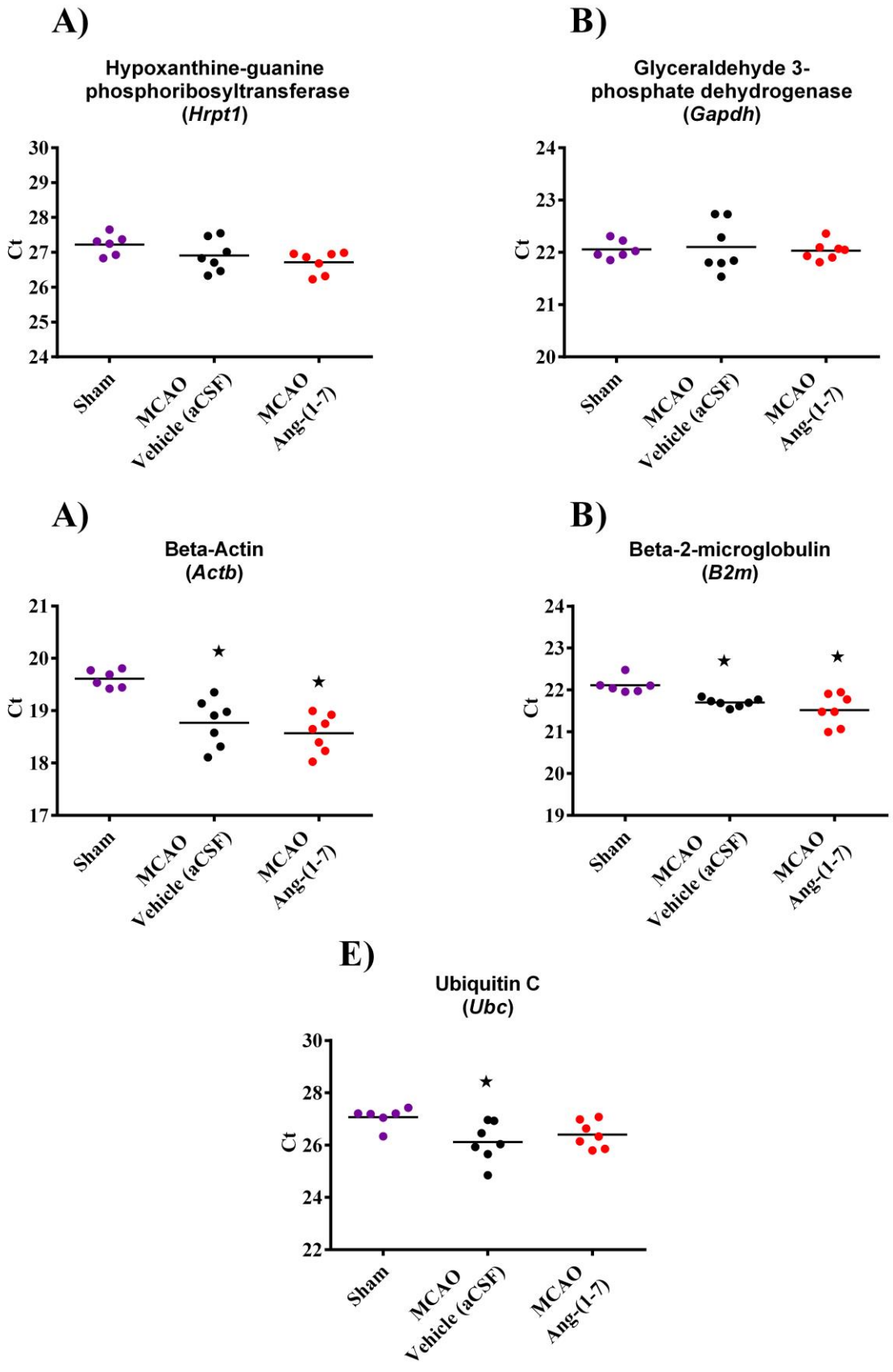

Figure 2-18 Reference gene candidates assessed in peri-infarct regions at 24 hrs post MCAO. A) *Hrpt1*; B) *Gapdh*; C) *Actb*; D) *B2m* and E) *Ubc*. Data from individual animals are presented as cyclic threshold (Ct) values. Horizontal bar represents mean. Data were analysed using one-way ANOVA with Tukey's post-hoc test, P<0.05 was deemed as significant. *P<0.05 compared to Sham.

2.16.3 qRT-PCR analysis

There are two methods to investigate qRT-PCR data, the absolute quantification method and the relative quantification method. The former is a useful analytical method when wanting to determine the starting copy number whereas the latter method is used to compare expression levels to a control sample. The relative quantification method does not require standard curves from serial dilutions of template in each experiment and the most common form of analysis follows the Livak method (Livak and Schmittgen, 2001). The Livak method presents the data in $2^{-\Delta\Delta Ct}$ where ΔCt is the difference between gene of interest and gene of reference and ΔΔCt the difference between the average ΔCt of a treatment group and the average ΔCt for the healthy tissue group, the latter conventionally set as 0 (Schmittgen & Livak, 2008). When expressing the data as $2^{-\Delta\Delta Ct}$, Ct values obtained from the exponential curve are being converted to the linear form. Although there are some reports that indicate the data is normally distributed in the linear form (Livak and Schmittgen, 2001; Schmittgen and Livak, 2008), Ct values measure the number of cycles required to detect the gene of interest. Therefore, the first assumption is that Ct values are normally distributed. In addition, when converting data to the linear form, the results are often skewed presenting exaggerated error bars – an indication of non-normality. All statistics were performed in ΔCt format throughout our studies and presented as such.

Data were presented as a scatter plot in the ΔCt format. Since Ct values indicate opposite expression directions, meaning that the higher the Ct the lower the expression of the gene and vice-versa, data was calculated in -ΔCt so that the values show the correct trend of expression using the following formula:

$$\mathbf{-\Delta Ct} = \text{-Ct (gene of interest)} - \text{Ct (gene of reference)}$$

2.17 Data presentation and statistical analysis

Data are shown as mean ± S.D. or median ± interquartile range (IQR) where applicable. Infarct volume (mm^3), % infarct volume change, systolic BP (mmHg), $IBA1^+$ microglia number/phenotype and qRT-PCR data were compared using unpaired Student's t-test (2 groups). If normality failed, data were compared using non-parametric Mann-Whitney (2 groups) or Kruskal-Wallis (more than 2 groups) test. Data compared within groups were analysed using paired Student's t test. Neurological score was compared using non-parametric Kruskal-Wallis or Mann-Whitney test. Correlations were performed using Pearson correlation coefficient (r) or Spearman correlation where normality failed. For data acquired over time, the summary measure of area under the curve (AUC) was determined for each animal and group means compared with unpaired Student's t-test. It is described by Matthews et al. (1990) that the summary measures of repeated data measurements is an adequate method to statistically analyse serially acquired data as it uses the entire data time to summarise an individual response (Matthews et al., 1990).

In Chapters 4, 5 and 6 a power calculation was performed to determine the minimum required group size for *in vivo* experiments. For all power calculations, a power of 80% and significance level of 5% was used. The means and S.D. selected were based on previous studies. All data was presented as a scatter-plot and analysed using Graphpad Prism 5 software (GraphPad Software, California, UK). $P<0.05$ was deemed as significant.

Chapter 3: Experimental model optimisation and exploratory therapeutic studies with an ACE2 activator following transient MCAO

Chapter 3

3.1 Introduction

In this Chapter, experiments were conducted to optimise the performance of permanent and transient MCAO in rats. The objective was to tackle experimental challenges observed in animal models of stroke as well as optimise drug delivery methods. A first study was performed to assess the most suitable rat strain to use in future therapeutic studies. In addition, a second study was conducted to determine whether systemic therapy delivery is suitable to target the brain RAS following transient MCAO. Simultaneously, Laser Doppler Flowmetry (LDF) was examined as a potential infarct outcome prediction tool to use in subsequent studies.

In humans, 70% of all infarcts occur in the territory of the MCA and its branches (Bogousslavsky et al., 1988). For this reason, MCAO models are widely used to study ischaemic stroke in the preclinical setting. The intraluminal filament model is suitable to performed mechanistic studies and is widely used to assess therapeutic effects on final infarct volume outcome (Macrae, 1992). One of the advantages of this model is that it induces a focal infarction within the MCA territory in rats, mimicking human ischaemic stroke (Garcia et al., 1995). Another advantage is that it allows the studying of permanent MCAO and transient MCAO as the filament may be left in place in the MCA or removed, respectively. In particular, transient MCAO is of clinical relevance since the primary objective of stroke treatment is to recanalise the occluded vessel by administering alteplase or through endovascular thrombectomy procedures. The latter is becoming a widely used method due to its extended therapeutic window and effectiveness in treating proximal occlusions (Tawil and Muir, 2017). Similar to endovascular thrombectomy, the intraluminal filament transient MCAO model induces sudden reperfusion and therefore is a suitable model to investigate adjuvant neuroprotective agents (Sutherland et al., 2016).

Nonetheless, the intraluminal filament model presents some challenges. MCAO leads to high lesion volume variability, which tends to present a bimodal form where animals exhibit either striatal or striato-cortical lesions. This influences how data are interpreted, especially when analysis requires a normal data distribution to test the effect of a neuroprotective agent. This variability accounts for the unsuccessful rates in neuroprotective strategy development. Therefore, contributing factors must be taken into account before conducting neuroprotective studies as outlined by the STAIR guidelines

((STAIR), 1999; Howells et al., 2010). One of the contributing variables is the rat strain selected. There are several rat strains used in experimental stroke with the Sprague-Dawley strain being the most used (Spratt et al., 2006). Sprague-Dawley rats are reported to induce the most variable results as these animals have differing MCA anatomy whereas Wistar rats are suggested to lead to lower variability as a result of smaller vessel diameter (Fox et al., 1993; Kim et al., 2009; Spratt et al., 2006; Ström et al., 2013). Yet, these reports are controversial since other studies suggest the opposite trend (Markgraf et al., 1993; Walberer et al., 2006), thus, further clarification is required.

Infarct volume outcome prediction tools are one way to tackle model derived infarct variability. LDF is extensively used in preclinical stroke to confirm MCAO and ensure adequate reperfusion following filament retrieval (Ansari et al., 2011; Reith et al., 1994). Due to inter- and intra-vascular variability amongst rats and the filament displacement probability during MCAO, LDF use is highly recommended by the STAIR guidelines ((STAIR), 1999). LDF works by measuring the microvascular blood perfusion and determining red blood cell movement within an area of interest (Fredriksson et al., 2007). A single frequency of infrared light is applied over the cortical surface with the use of a probe. The light is scattered by moving cells, resulting in a frequency shift proportional to red cell velocity, providing an arbitrary perfusion unit (AU) of relative cerebral blood flow (rCBF) (Dirnagl et al., 1989; Fredriksson et al., 2007). LDF is also reported to successfully predict final infarct volume when measuring CBF within the MCAO territory (Riva et al., 2012; Soriano et al., 1997). For this reason, LDF will be evaluated as a potential tool to predict final infarct outcome and accurately assess the impact of therapy.

The main outcome of this thesis is to study the therapeutic potential of the counter regulatory RAS axis following ischaemic stroke. MasR, AT_2R agonists and ACE2 activators are suggested to induce a therapeutic effect in animal models of stroke when administered ICV (Joseph et al., 2014; Mecca et al., 2011). Still, ICV administration is highly invasive, may increase the risk of local or systemic infections as well as enhance ICP (Kateb and Heiss, 2013). The brain RAS is separated from the circulating RAS through the BBB, which restricts peripherally derived RAS circulation within the brain (Schelling et al., 1976). Consequently, the brain depends on locally produced RAS mediators to exert its physiological and pharmacological properties. Nonetheless, the existence of CVOs, brain regions lacking BBB, sparked debates on a peripheral RAS interaction with the brain (Deschepper et al., 1986; van Thiel et al., 2017) and the possibility to therapeutically target the brain systemically.

DIZE is a drug safely and widely used to treat animal trypanosomiasis (Kuriakose and Uzonna, 2014). In addition to treating trypanosomiasis, DIZE has ACE2 activating properties, stimulating the conversion of Ang II into counter-regulatory peptide Ang-(1-7) (Gjymishka et al., 2010). DIZE is most effective when administrated SC and shown to be safe at doses of 50 mg/kg/day (Raether et al., 1974). Accordingly, its cytoprotective properties have been tested and confirmed in animal models of cardiac ischaemia, pulmonary hypertension, subtotal nephrectomy and abdominal aortic aneurysms when administered SC at 15 mg/kg/day or 30 mg/kg/day doses (Qi et al., 2013; Rigatto et al., 2013; Thatcher et al., 2014; Velkoska et al., 2015). In an ischaemic stroke model, DIZE ICV therapy starting 4 days prior to ET-1 induced MCAO significantly decreased infarcted grey area and improved neurological outcome at 3 days post injury (Mecca et al., 2011); however, its systemically induced neuroprotection has not yet been tested. On the contrary to Ang-(1-7), which has a half-life of approximately 10 sec, DIZE has a half-life of approximately 5 hrs (Miller et al., 2005; Yamada et al., 1998). Moreover, there is extensive toxicology knowledge regarding DIZE and high SC doses have been shown to be effective and safe in rats. Therefore, this drug was selected to test systemic brain RAS targeting by examining its effects on infarct volume following stroke.

3.1.1 Aims

Study 1**:** To determine variability in infarct volume following permanent MCAO in different rat strains.

Study 2: To determine the effect of systemic administration of the ACE2 activator (DIZE) on infarct volume following transient MCAO.

3.2 Materials and methods

Study 1: To determine variability in infarct volume following permanent MCAO in different strains of rat.

3.2.1 Randomisation, blinding and exclusion

A total of 20 adult male rats weighing between 315-395g were used, 10 Wistar and 10 Sprague Dawley. Animals were randomly assigned to surgery day using an online randomisation generator (www.random.org). Animals that failed to show visual indications of infarct on 2,3,5-Triphenyl-2H-tetrazolium chloride (TTC) stained sections or that died during surgery were excluded. An independent researcher was responsible for collecting the rats on day of surgery and the surgeon was blinded to strain.

3.2.2 Animal preparation and surgical procedures

Wistar (n=9) and Sprague-Dawley (n=8) rats obtained from Charles River were anaesthetised and surgically intubated (Chapter 2.5.2). Throughout the experiment, isoflurane levels were maintained at 2.5% in a 30:70% O_2-N_2O mixture. The femoral artery was cannulated (Chapter 2.6) to record MABP and measure PaO_2, $PaCO_2$ and pH prior to and 1, 2, 3 and 4 hrs post-permanent MCAO. Temperature was monitored through a rectal probe and maintained at 37±0.5ºC. Permanent MCAO was induced as previously described (Chapter 2.8). A silicone coated Doccol filament was advanced along the internal carotid artery until the MCA was blocked. The filament was secured in place and MCAO was carried out for a period of 4 hrs. Animals were then deeply anaesthetised with 5% isoflurane, killed by Schedule 1 procedure and decapitated for whole brain removal.

3.2.3 Infarct volume determination

Whole brain tissue was quickly placed in a container at -20ºC for a period of 20 min prior to coronal section slicing. Brains were then placed in a rat brain matrix (World Precision Instruments, UK) and microtome blades (Feather, Japan) used to obtain 6 sections of 2 mm thickness. TTC was used to stain viable brain tissue and determine the infarct. TTC is a colourless and water-soluble salt that in the presence of functioning mitochondria is oxidised to a lipid soluble bright red formazan by dehydrogenases (Zille et al., 2012). In undamaged tissue, TTC stains a deep red whereas infarcted tissueareas display a white colour (Figure 3-1). TTC (Sigma-Aldrich, Switzerland) was made up to a 2% (w/v)

solution dissolved in phosphate buffered saline pre-warmed to 37ºC. Coronal sections were placed in the 2% TTC solution and left to stain for 15 min until formazan products were visually formed. Fully stained sections were then removed from 2% TTC and placed in 4% PAM to be fixed overnight prior to imaging.

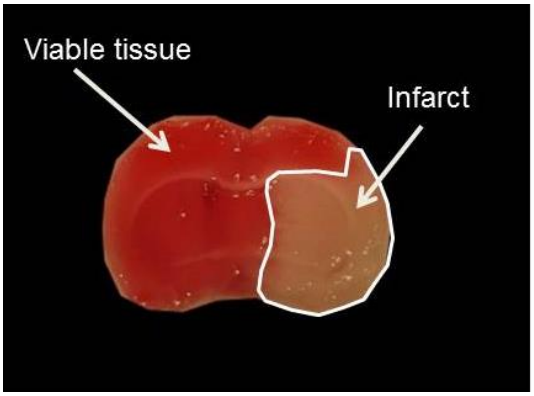

Figure 3-1 Representative image of TTC staining following 4 hrs of permanent MCAO. Image depicts coronal level three with red areas representing viable cerebral tissue and the areas delineated in white depicting the infarcted tissue.

TTC stained sections were imaged with the use of a digital camera (Canon, UK) and a graticule (Imaging Research Inc., Canada) for calibration. Total infarct volume was determined by manually delineating the infarct present on all coronal slices, on both sides, using Image J software. For each coronal slice, the infarct area was measured on both faces of the slice, averaged and summed. Infarct volume was determined by summing the infarct areas and then multiplying by the slice thickness, 2 mm. Infarct volume was not corrected for hemisphere oedema since at the particular time point chosen (4 hrs post permanent MCAO) there was no significant brain oedema present as previously reported (Slivka et al., 1995).

3.2.4 Statistical analysis

Physiological parameters were compared between rat strains using AUC and the means analysed with unpaired Student's t-test or Mann-Whitney test where normality failed. Infarct volume was compared using unpaired Student's t-test. Data were expressed as mean ± S.D. and considered statistically significant when $P<0.05$. Infarct volume data were shown as a scatterplot with the mean indicated in a horizontal bar. All brain images show the median animal for each group.

Study 2: To determine the effect of systemic administration of the ACE2 activator (DIZE) on infarct volume following transient MCAO

3.2.5 Blinding, randomisation and exclusions

Animals were assigned to treatment using a random list generator (www.random.org). Rats were given a number and randomly allocated to receive either Vehicle [distilled water (dH_2O)]; DIZE (15 mg/kg/day) or DIZE (30 mg/kg/day). The randomisation schedule was kept with 2 colleagues not involved with the study. Four days prior to MCAO, drug was prepared by an independent investigator. Thoroughout the experiment, surgeon (MA) was blinded to treatment allocation, with treatment schedule being disclosed following infarct volume analysis. Rats that died before the end of experimental protocol or showed no signs of infarction on MRI-T_2 images were excluded from analysis.

3.2.6 Animals and surgical procedures

A total of 24 male Wistar rats weighing between 295-345g and purchased from Charles River were used in this study; Vehicle (dH_2O) n=9; DIZE (15 mg/kg/day) n=7; or DIZE (30 mg/kg/day) n=8. All animals were subjected to MCAO for a period of 90 min followed by 3 days reperfusion. Rats were treated SC with distilled water (dH_2O) or DIZE (15 mg/kg/day or 30 mg/kg/day) via osmotic pump infusion for a period of 7 days starting 4 days prior to MCAO. Osmotic pumps (ALZET, Model 2ML1) were implanted as described in Chapter 2.7.2. All animals underwent conscious systolic BP measurement and Garcia neurological score prior to therapy and MCAO and at 3 days post MCAO (Chapter 2.7 & Chapter 2.8, respectively). On day of surgery, rats were anaesthetised with 5% isoflurane and orally intubated (Chapter 2.5.2). Once the animal was stable, isoflurane levels were maintained at 2.5% delivering a continuous dose of 30:70% O_2-N_2O mixtures. MCAO was induced for a period of 90 min, as previously described in detail (Chapter 2.8). After 90 min ischaemia, the filament was slowly removed for initiation of reperfusion and rats were recovered for a period of 3 days (Chapter 2.8.1 and Chapter 2.8.2).

3.2.7 Laser Doppler Flowmetry

Laser Doppler Flowmetry (LDF) was used to confirm successful MCAO/reperfusion and investigated as a prediction tool to evaluate final infarct volume. A multi-channel microvascular perfusion monitor OxyFlo 2000^{TM} (Oxford Optronix, Oxford, UK) connected to an OxyFlo probe (needle shaped, 10 mm length and 1 mm diameter) (Figure 3-2A) was used to measure rCBF during MCAO and post reperfusion.

The scalp was shaved using electric hair clippers and the animal quickly placed in the stereotaxic frame to place the LDF probe over the appropriate region of the skull. The rat's head was secured with tooth and ear bars and viscotears applied in the animal's eyes to prevent drying. An incision was performed in the skin overlying the skull with the use of a scalpel and the underlying fascia gently cleared to expose the skull surface and the left ridge. To prevent skull bleeding, pressure was applied with the use of a cotton bud. If excessive bleeding from the scalp continued persistently, 10% perchloric acid dissolved in dH_2O (Sigma Aldrich, UK) was applied with a cotton bud to stop the bleeding and then cleared with sterile saline. CBF was measured within the MCA territory at 1.3 mm posterior and 4.0 mm lateral from bregma (Soriano et al., 1997). Bregma was identified and served as a guide to position the stereotaxic needle over the area of interest, outlined with a marker pen. Next, a burr hole was drilled through the skull to reduce the bone thickness in the area of interest, to maximise the LDF signal. A probe holder of 10 mm diameter (Oxford Optronix Ltd, Oxford, UK) (Figure 3-2B) was glued around the area of interest with extreme care. Conductive electrode gel (Electrode gel, Biopac Systems, UK) was applied with a syringe in the measurement area to aid signal detection. The animal was then removed from the stereotaxic frame and placed on a modified corkboard, with the LDF probe inserted through the corkboard and placed in the probe holder glued to the skull. The laser was then turned on to start measuring CBF in the MCA territory. Following 90 min of MCAO, the filament was removed and successful reperfusion confirmed by an increase in LDF signal for a period of 5 min. The laser was then turned off and the probe and probe holder removed. Figure 3-2C shows a representative image of an animal subjected to LDF imaging.

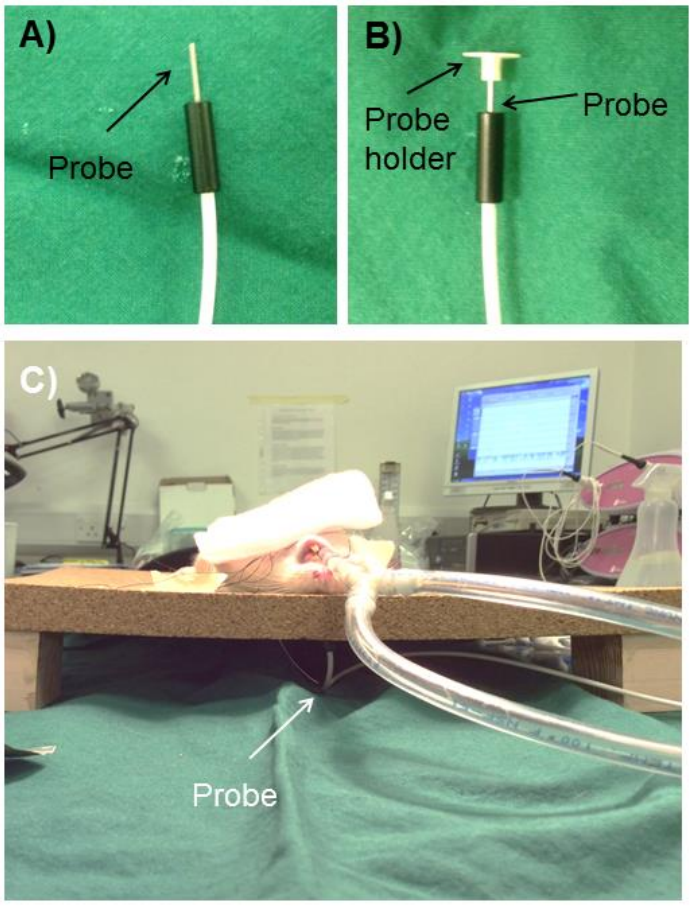

Figure 3-2 The Laser Doppler Flowmetry set up. A) LDF probe needle (10 mm length and 1 mm diameter)**; B) LDF probe connected to the probe holder used to measure CBF in the MCA territory. C) Representative image of an animal subjected to LDF imaging.**

3.2.7.1 LDF analysis

Data were analysed using Acknowledge Biopac software (Biopac Systems Inc, USA). LDF values were obtained for a period of 100 min (6000 sec) and presented as raw data to examine the real time changes in LDF for each individual animal.

To assess mean LDF signal across the treatment groups, data were presented as mean percentage (%) change in LDF compared to the 2 min baseline prior to MCAO. To compare % rCBF decrease at MCAO between groups, data were presented as % signal change at MCAO (filament insertion) - from 1 min baseline to 1 min MCAO - for each individual animal. Similarly, % rCBF change at reperfusion (upon filament removal) - from 90 min MCAO to 1 min reperfusion - was shown for all animals and compared between groups. Changes in rCBF during MCAO were calculated as % signal change from 1 min to 90 min MCAO.

3.2.8 Magnetic Resonance Imaging

Three days post reperfusion, rats were anaesthetised, transferred to the MRI scanner and placed in a rat cradle where the head was restrained with ear and tooth bars. Once a pilot sequence had been obtained to ensure correct geometry, a RARE T_2 weighted sequence was performedas outlined in Chapter 2.9.2. Following MRI scanning, animals were anaesthetised with 5% isoflurane and Schedule 1 procedures performed. Final infarct size was calculated by manually delineating hyperintense regions on T_2-weighted images as described in Chapter 2.9.2 and data corrected for hemispheric swelling.

3.2.9 Statistical analysis

Infarct volume and systolic BP were compared between groups using one-way ANOVA. Neurological score was analysed using Kruskal-Wallis test and presented as median ± IQR. % rCBF change at the time of MCAO and reperfusion as well as during MCAO were analysed between groups using one-way ANOVA or Kruskal-Wallis test where normality failed. Correlations between LDF data and final infarct volume were analysed using Pearson correlation or Spearman non-parametric correlation where normality failed. Data were expressed as mean ± S.D. and considered statistically significant when $P<0.05$. Graphs are presented as a scatterplot with the mean or median indicated as a horizontal bar. All brain images show the median animal for each group.

3.3 Results

Study 1: To determine variability in infarct volume following permanent MCAO in different strains of rat.

3.3.1 Mortality and exclusions

There was no mortality in this experiment. In terms of exclusions, two Sprague-Dawley rats and one Wistar rat were excluded due to lack of infarct on TTC stained sections at 4 hrs post-permanent MCAO.

3.3.2 Wistar rats exhibited significantly larger ischaemic lesions than Sprague-Dawley animals

Wistar rats showed significantly larger lesions when compared to Sprague-Dawley animals [215.9±84.5mm^3 vs 107.9±107.9mm^3 (P=0.04)], (Figure 3-3A). In both groups, infarct volume displayed high variability ranging between 115.4 - 397.9mm^3 in Wistar and 26.7-299.2mm^3 in Sprague-Dawley rats. However, Sprague-Dawley rats exhibited a tendency to generate smaller infarcts as three animals had small subcortical infarcts of 32.5mm^3, 32.7mm^3 and 26.7mm^3. Figure 3-3B illustrates infarct volume spatial distribution in the representative median animal for each group.

3.3.3 No differences in physiological parameters between strains

Physiological parameters were measured and maintained within physiological range across groups (Figure 3-4). There were no differences in MABP between groups during the course of the experiment with a trend for MABP to decrease from 2 hrs post-MCAO until the end of the experiment (P>0.05) (Figure 3-4A). Temperature, pH and $PaCO_2$ were maintained within range for all rats without differences between groups (P>0.05) (Figures 3-4B:D). For all animals, PaO_2 was higher than reference ranges (80-100mmHg), explained by the continuous administration of 30:70 ratio of O_2 and N_2O. Sprague-Dawley animals exhibited slightly higher values than Wistar; however, Mann Whitney analysis of AUC means showed no differences between groups (P>0.05), highlighted by a substantial variability particularly observed in the Sprague-Dawley group (Figure 3-4E).

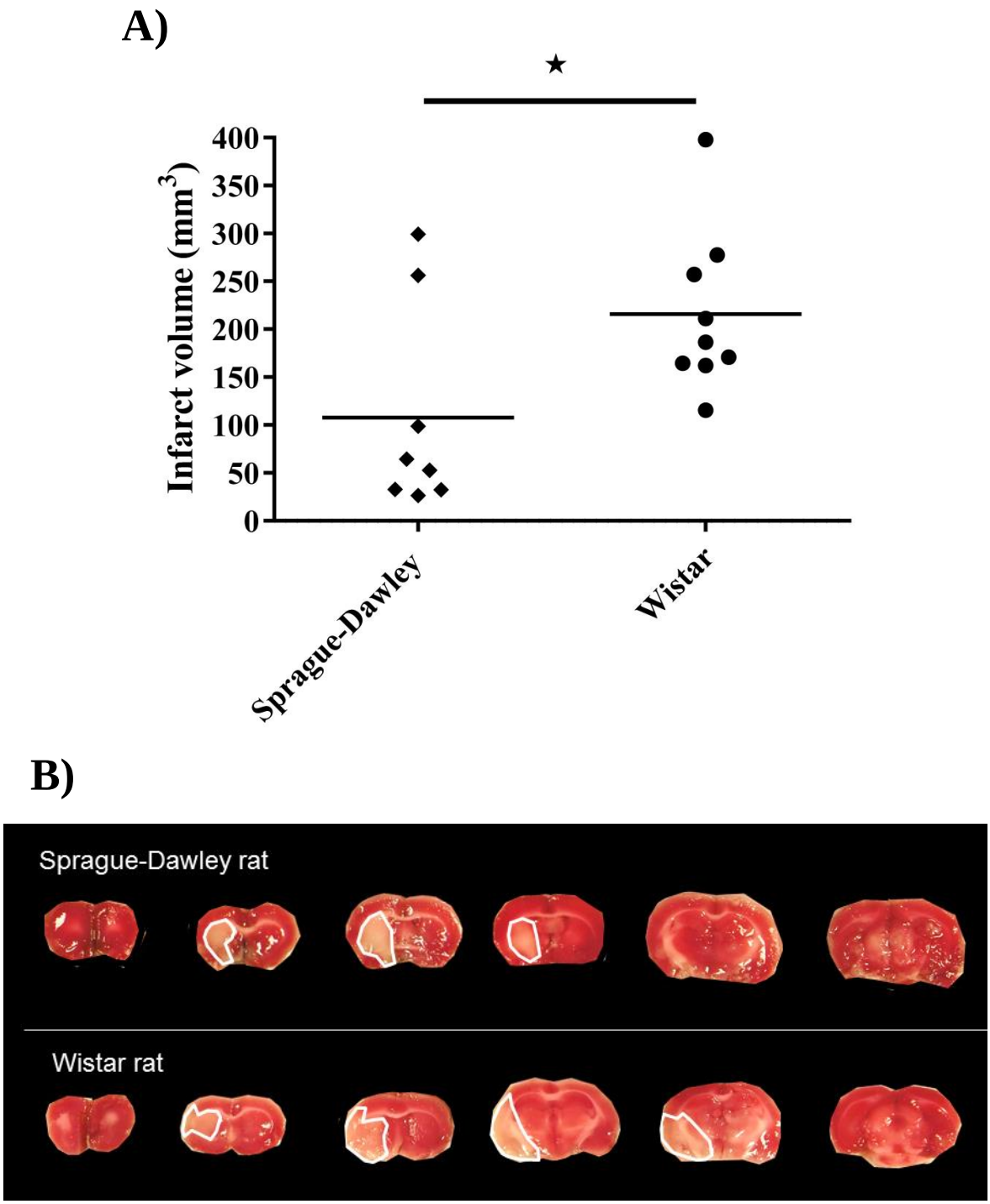

Figure 3-3 Infarct volume data at 4 hrs permanent MCAO. A) Infarct lesion comparison between Sprague-Dawley (n=8) and Wistar rats (n=9). Lesions were significantly smaller in Sprague-Dawley animals when compared to Wistar rats (P=0.04). **B) Spatial distribution of infarct size between groups.** Images depict the median animal in the Sprague-Dawley and Wistar strain groups across 6 coronal sections. For each animal, the infarct is highlighted in white. Data were analysed using unpaired Student's t test, $P<0.05$ was considered statistically significant. Horizontal bar represents the mean.

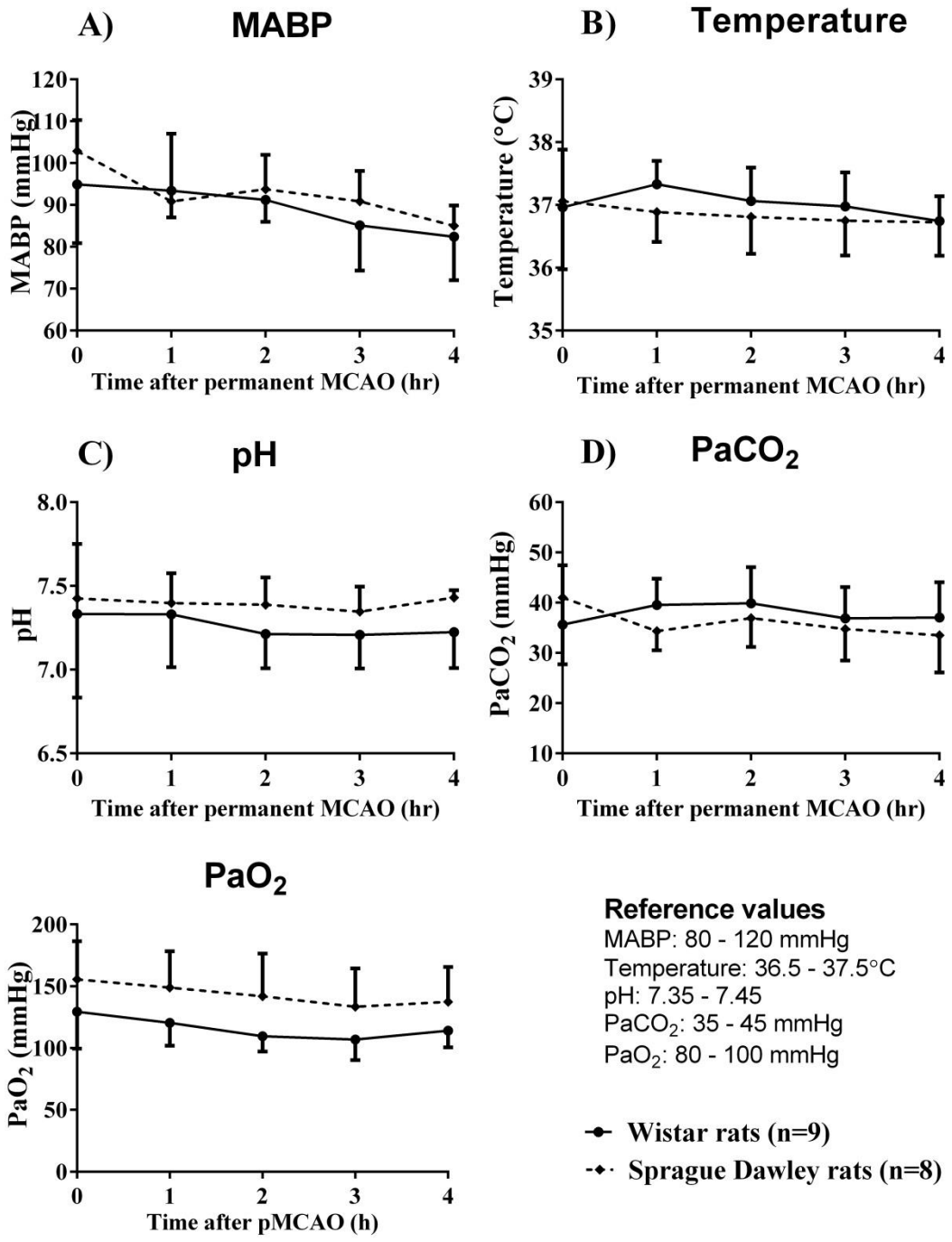

Figure 3-4 Physiological variables during 4 hrs permanent MCAO. A) MABP (mmHg); B) Temperature (ºC); C) pH; D) $PaCO_2$ (mmHg); E) PaO_2 (mmHg). There were no differences between groups for all physiological parameters. Data depict values for Sprague Dawley (n=8) and Wistar rats (n=9). Data were analysed using AUC and means compared using unpaired Student's t test for Figures A-D and non parametric Mann-Whitney test for Figure E, $P<0.05$ was considered statistically significant. Data are expressed as mean ± S.D. Reference values for each physiological parameter are shown in the figure.

Study 2: To determine the effect of systemic administration of the ACE2 activator (DIZE) on infarct volume following transient MCAO

3.3.4 Mortality and exclusions

A total of 24 animals were used in this study of which 4 died during recovery: one DIZE (30 mg/kg/day), one DIZE (15 mg/kg/day) and two Vehicle (dH_2O) treated rats, leading to a 16.6% study mortality. In addition, one animal in DIZE (15 mg/kg/day) died during surgery. A total of 19 animals were included in this study: 7 Vehicle (dH_2O), 5 DIZE (15 mg/kg/day) and 7 DIZE (30 mg/kg/day).

3.3.5 DIZE treatment does not influence systolic BP

There were no differences in conscious systolic BP measurements before and after 90 min MCAO between groups ($P>0.05$) (Figure 3-5A&B). Prior to MCAO and therapy, systolic BP values ranged between 81 mmHg and 194 mmHg, thus, some animals had substantially higher BP than what is expected in normotensive rats (80-120 mmHg). In the Vehicle (dH_2O) group, two animals had a BP of 149 mmHg & 178 mmHg. Similarly, in DIZE (15 mg/kg/day) group, one rat had 160 mmHg while in DIZE (30 mg/kg/day) one animal had a BP of 143 mmHg and another 194 mmHg (Figure 3-5A). At day 3 post transient MCAO, systolic BP was not different between treatment groups ($P>0.05$) with BP values ranging between 92 mmHg to 197 mmHg (Figure 3-5B). The animals exhibiting high BP were visibly stressed during measurements, indicating the need to acclimatise rats to the set up for longer periods of time. In addition, systolic BP change from pre to post MCAO showed that therapy did not influence BP ($P>0.05$) (Figure 3-5C).

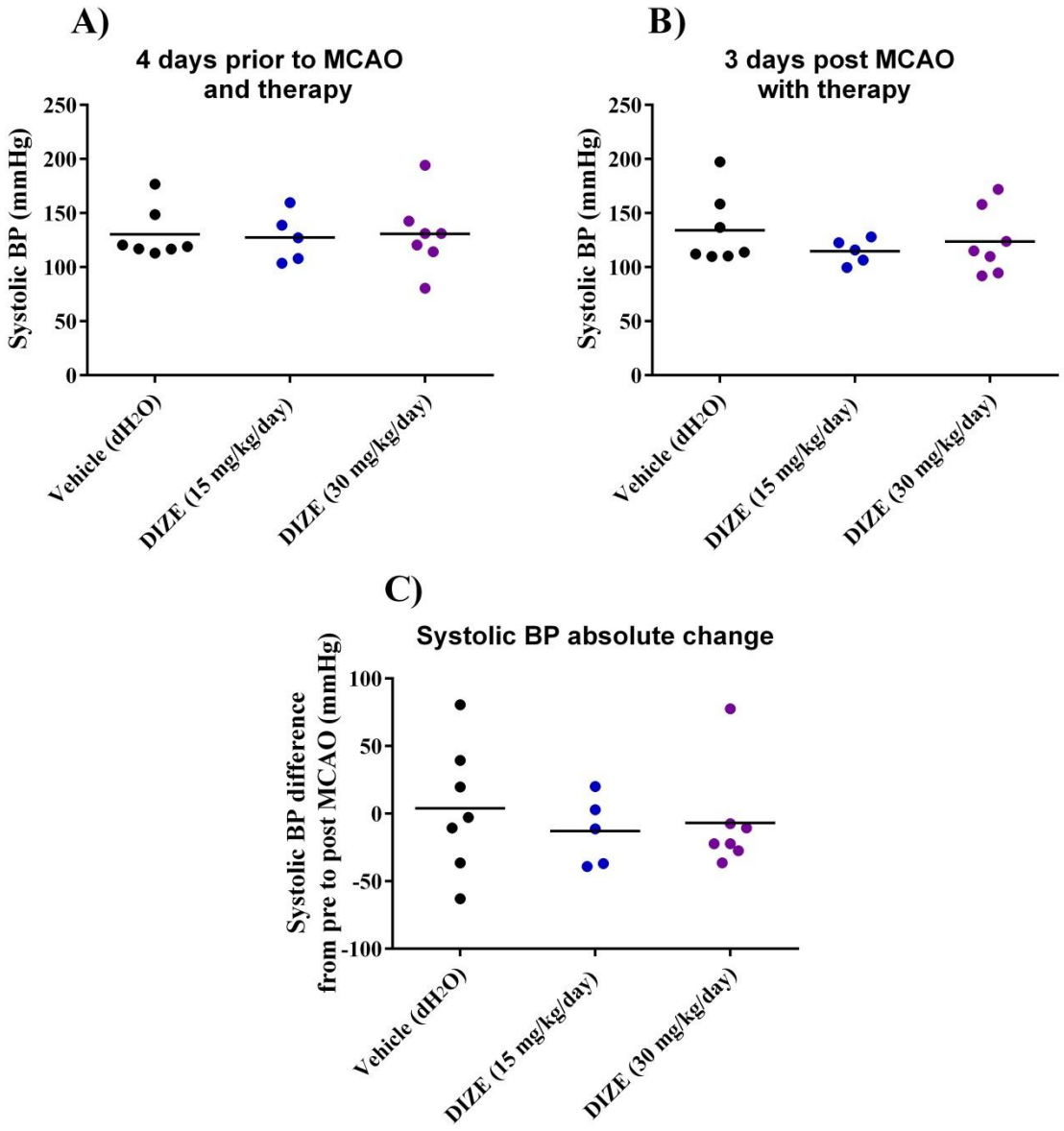

Figure 3-5 Systolic BP. A) 4 days prior to 90 min MCAO and treatment; B) 3 days post 90 min MCAO and 7 days of treatment; C) Systolic BP change between pre to post 90 min MCAO (absolute values). No differences in systolic BP between groups prior to and post 90 min MCAO with therapy (P>0.05). Therapy did not influence systolic BP between pre and post MCAO (P>0.05). Data depicts values for Vehicle (dH_2O; n=7), DIZE (15 mg/kg/day; n=5) and DIZE (30 mg/kg/day; n=7). Data were analysed using one-way ANOVA, P<0.05 was considered statistically significant. Horizontal bar represents the mean.

3.3.6 DIZE treatment does not impact neurological score

An 18-point neurological score was performed 4 days prior to and 3 days post transient MCAO. Before MCAO, all animals scored a maximum 18 points (Figure 3-6A). As expected, MCAO induced a decrease in neurological score in all groups, confirming neurological deficit in all animals included (Figure 3-6B). DIZE treatment did not influence neurological deficit between groups (P>0.05). However, compared to vehicle animals, DIZE treated rats showed a trend to display enhanced neurological deficit.

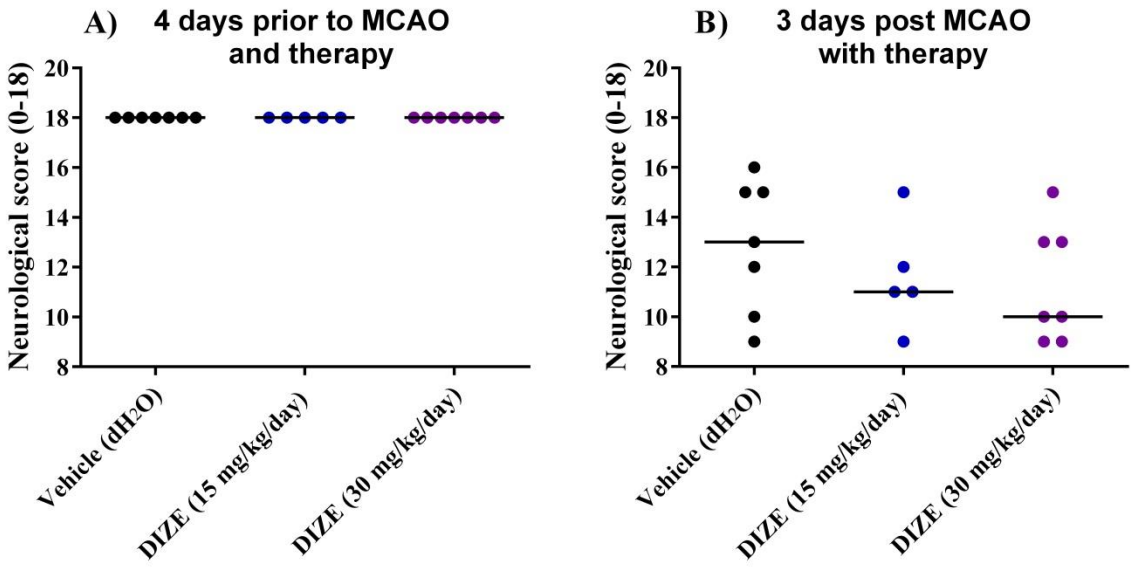

Figure 3-6 Neurological score. A) 4 days prior to 90 min MCAO and treatment; B) 3 days post 90 min MCAO and 7 days of treatment. There were no differences in neurological score between groups prior to and post 90 min MCAO with therapy. Data depict values for Vehicle (dH_2O; n=7), DIZE (15 mg/kg/day; n=5) and DIZE (30 mg/kg/day; n=7). Data were analysed using Kruskal-Wallis test, $P<0.05$ was considered statistically significant. Horizontal bar represents the median.

3.3.7 DIZE treatment has no effect on infarct volume

DIZE SC infusion at 15 mg/kg/day and 30 mg/kg/day doses had not effect on final infarct volume at 3 days post MCAO compared to control animals ($P>0.05$) (Figure 3-7). MCAO induced small lesions particularly in three animals in the Vehicle (dH_2O) group, suggesting that these animals had partial MCA occlusions. Similarly, there was high variability in lesion sizes observed in DIZE treated groups; however, these groups showed a trend to increase final infarct compared to control. Figure 3-8 shows the spatial distribution of final infarct for the median animal in each treatment group.

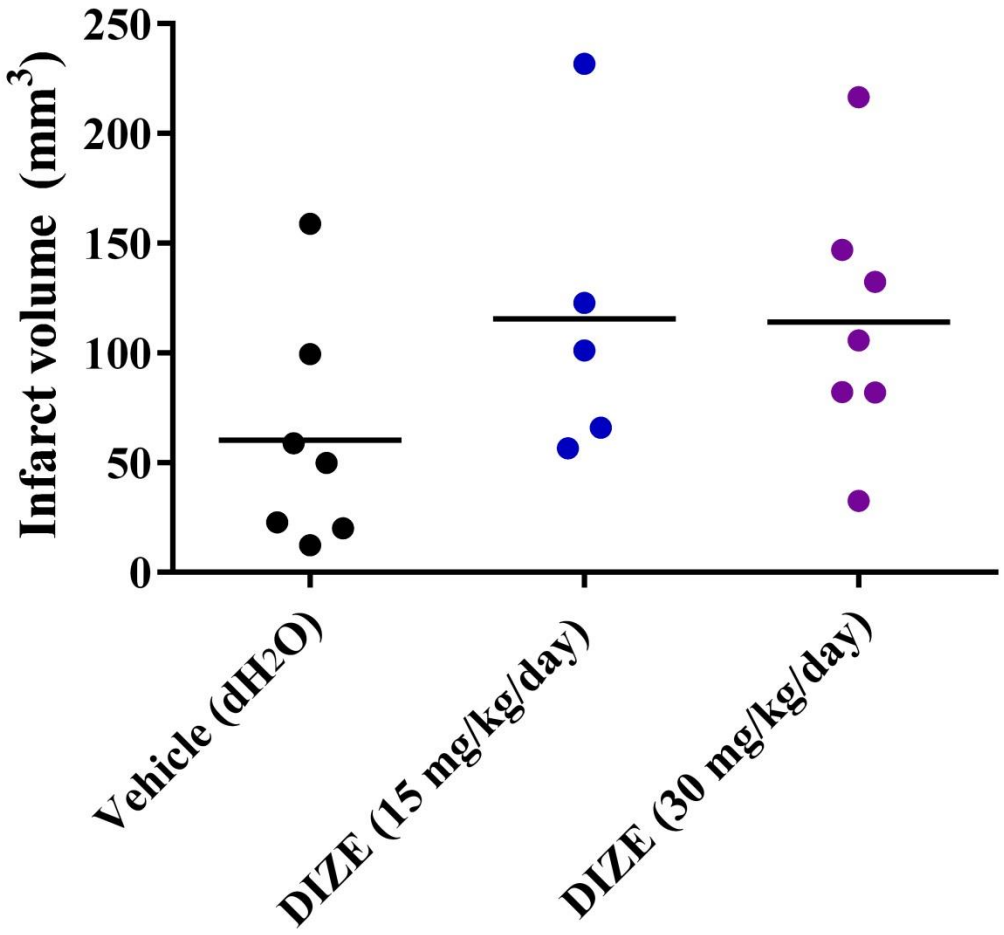

Figure 3-7 Final infarct volume 72 hrs post 90 min MCAO. Infarct lesions at 72 hrs post 90 min MCAO were comparable between groups (P>0.05). Data depict values for Vehicle (dH_2O; n=7), DIZE (15 mg/kg/day; n=5) and DIZE (30 mg/kg/day; n=7). Data were analysed using one-way ANOVA, P<0.05 was considered statistically significant. Horizontal bar represents the mean.

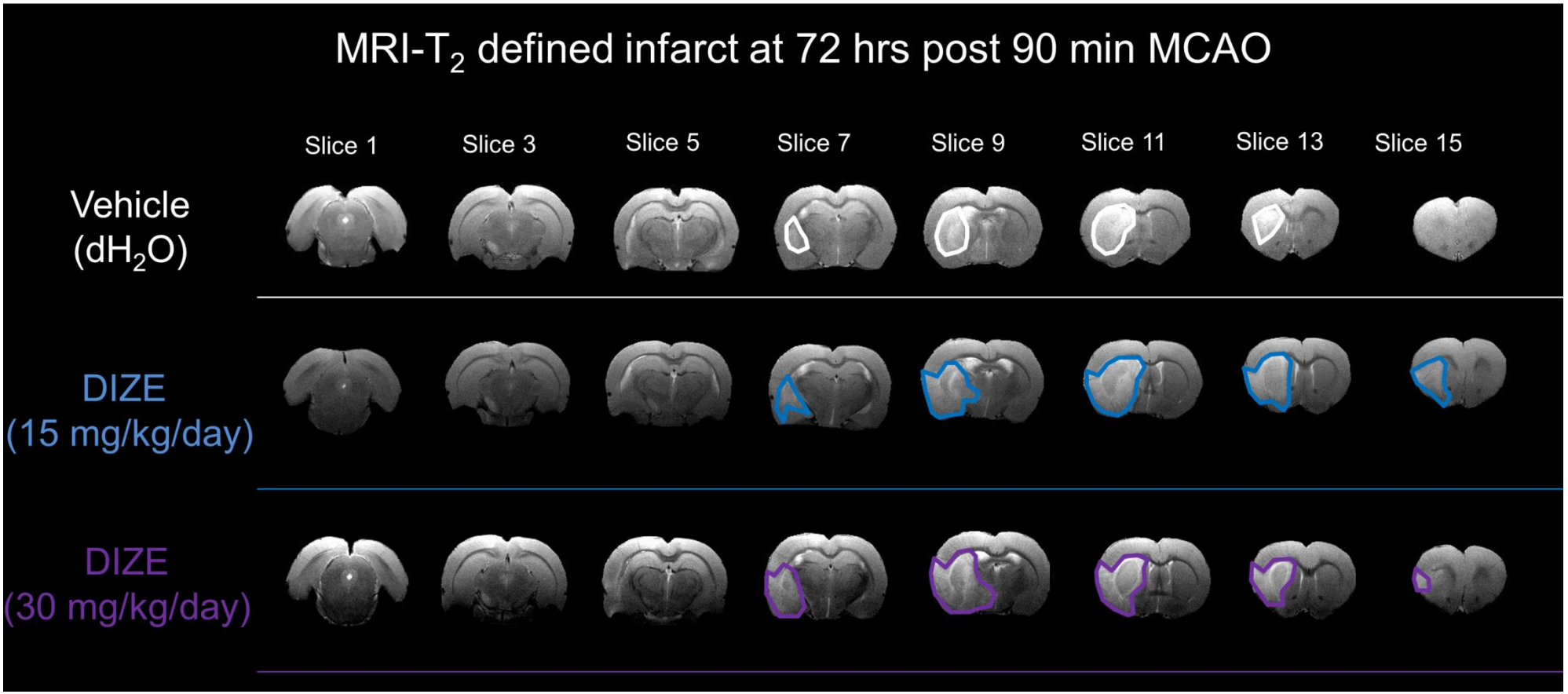

Figure 3-8 Spatial distribution of infarct tissue for Vehicle (dH_2O), DIZE (15 mg/kg/day) and DIZE (30 mg/kg/day) treated animals at 72 hrs post 90 min MCAO. Coronal sections represent the median animal for each treatment group. Infarct is highlighted in white, blue and purple for Vehicle (dH_2O), DIZE (15 mg/kg/day) and DIZE (30 mg/kg/day), respectively.

3.3.8 Laser Doppler Flowmetry

As a result of a technical error, LDF data were not obtained for 3 animals in this study, one in Vehicle (dH_2O) and two in DIZE (30 mg/kg/day) groups. At MCAO, rCBF decreased in all animals, which indicates successful MCAO. Following filament removal (reperfusion), mean rCBF increased for all groups, suggesting successful CBF re-establishment (Figure 3-9). Interestingly, during the course of LDF monitoring, DIZE treated animals showed a slight trend to present exacerbated % rCBF deficit during MCAO when compared to the vehicle group. There was high variability in LDF readings throughout experiments and the extent of rCBF change at time of MCAO and reperfusion amongst animals. Figure 3-10 shows a representative image of successful LDF measurements for Vehicle (dH_2O), DIZE (15 mg/kg/day) and DIZE (30 mg/kg/day) treatment groups.

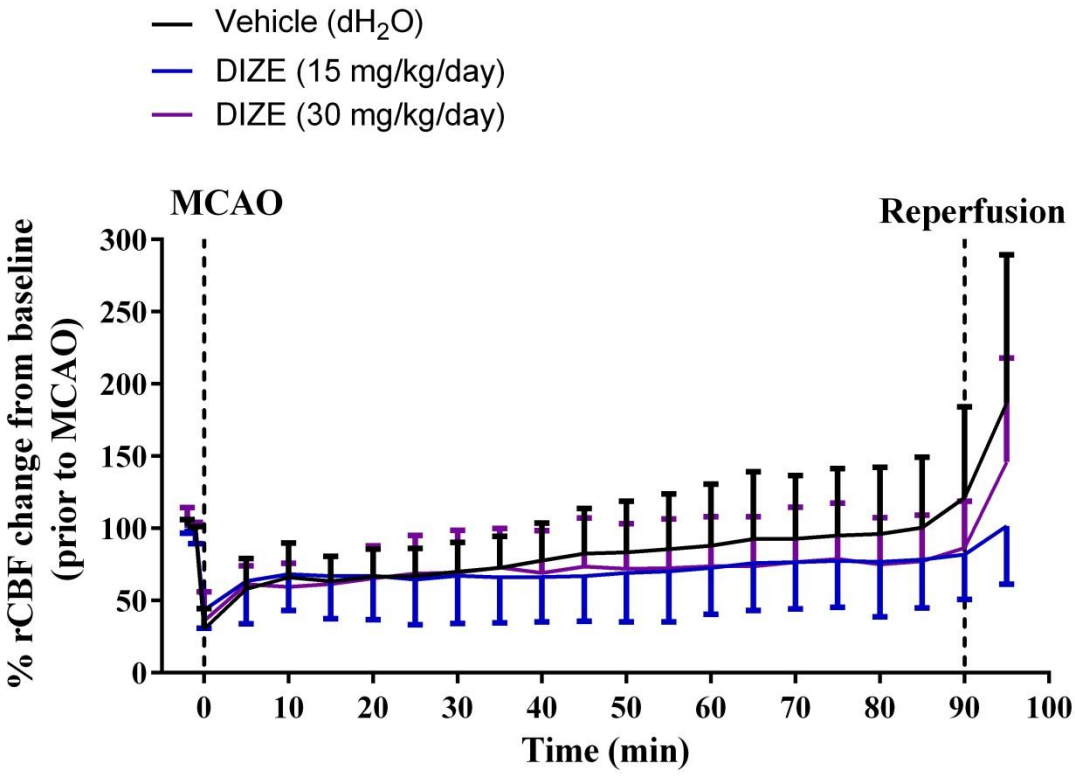

Figure 3-9 % rCBF change during LDF assessments per treatment group. MCAO successfully decreased mean rCBF for all groups and reperfusion increased mean rCBF after filament removal. Data are presented as mean LDF values normalised to 2 min baseline (prior to MCAO, 100%) for Vehicle (dH_2O; n=6), DIZE (15 mg/kg/day; n=5) and DIZE (30 mg/kg/day; n=5). Data are expressed as mean ± S.D. over the course of 100 min.

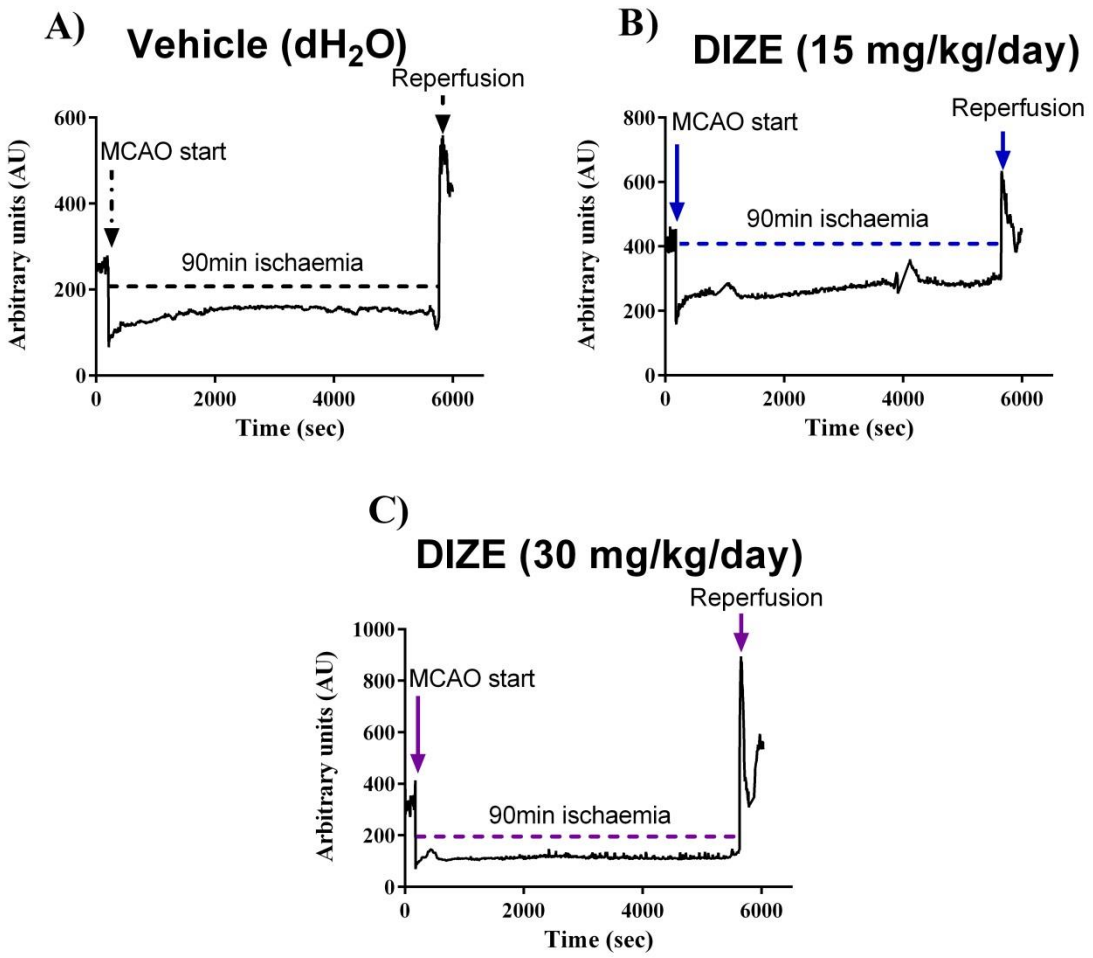

Figure 3-10 Representative image of successful LDF traces. A) Vehicle (dH_2O); B) DIZE (15 mg/kg/day) and C) DIZE (30 mg/kg/day) treated groups. Data are expressed as arbitrary units (AU) over 100 min expressed in seconds (sec). The horizontal dotted line represents 90 min MCAO.

3.3.8.1 LDF reliably detects MCAO but not reperfusion extent

LDF successfully detected a drop in % rCBF at the time of MCAO for all rats included in the study, with no statistical differences amongst groups; Vehicle (dH_2O): -60.9±13.4%, DIZE (15 mg/kg/day): -40.1±18.3%, DIZE (30 mg/kg/day): -56.2±15.5% (Figure 3-11A). Overall, reperfusion increased mean % rCBF for all groups, Vehicle (dH_2O): 185.2±113.3%, DIZE (15 mg/kg/day): 76.5±45.7%, DIZE (30 mg/kg/day): 191.9±225.0%. However, in some animals, rCBF change at reperfusion was relatively small (25.0% in DIZE 15 mg/kg/day or 26.9% in DIZE 30 mg/kg/day groups) (Figure 3-11B). Plus, in the DIZE (30 mg/kg/day) group, one animal displayed a decrease of 14.9% rCBF at time of reperfusion; yet, this rat had a subcortical lesion of 82.2mm^3 and survived the whole

experiment, suggesting successful reperfusion (Figure 3-12). Therefore, these results indicate that LDF does not reliably detect reperfusion extent.

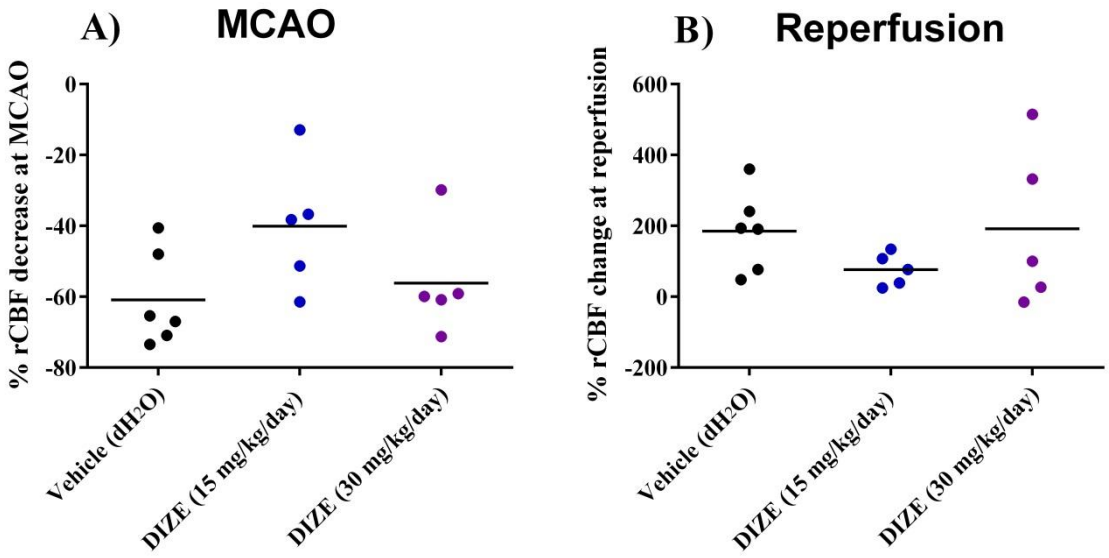

Figure 3-11 % rCBF change at MCAO and at reperfusion.A) % rCBF change at time of MCAO compared to baseline. B) % rCBF change at time of reperfusion compared to 90 min MCAO. LDF successfully detected a decrease in rCBF at time of MCAO for all animals but not at reperfusion. There were no differences between groups in the extent of % rCBF at MCAO and/or reperfusion for Vehicle (dH_2O; n=6), DIZE (15 mg/kg/day; n=5) and DIZE (30 mg/kg/day; n=5). Data were analysed using one-way ANOVA for Figure A and Kruskal-Wallis test for Figure B, $P<0.05$ was considered statistically different. Horizontal bar represents the mean.

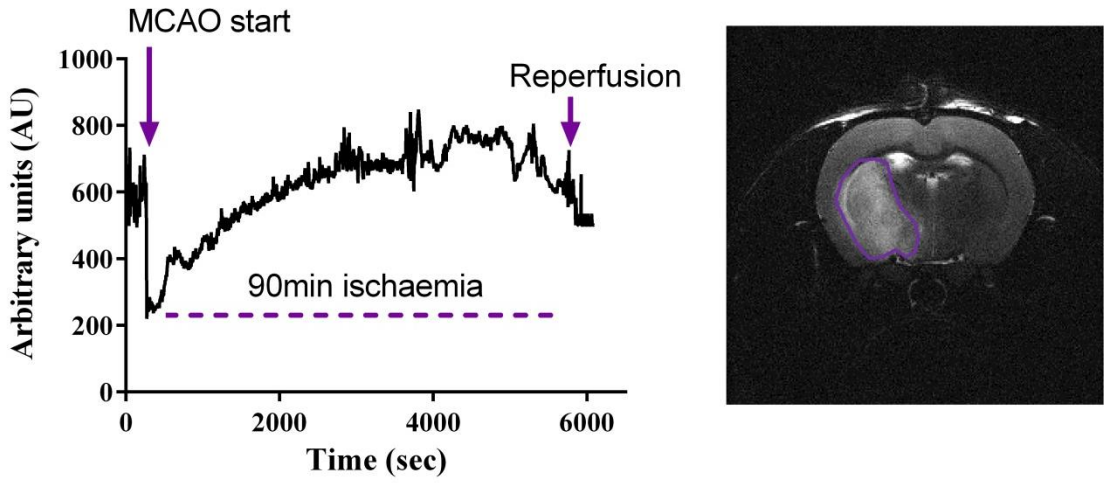

Figure 3-12 Representative LDF trace that detected afailure of reperfusion onset. LDF failed to detect reperfusion onset, exhibiting a 14.9% decrease in rCBF after filament removal in the animal presented. The rat survived the experiment and displayed a final infarct volume of 82.2mm^3. MRI-T_2 image shows a representative figure of the final infarct in coronal level 4 at 3 days post 90 min MCAO. Data are expressed in arbitrary units (AU) over time in seconds (sec). The horizontal dotted line represents 90 min MCAO.

3.3.8.2 % rCBF change at MCAO or at reperfusion does not predict final infarct volume

To study whether the level of ischaemia or reperfusion detected by LDF could predict final infarct outcome, the % change in CBF at MCAO and at reperfusion were correlated with final infarct for each treatment group. LDF change at MCAO did not correlate with final infarct; Vehicle (dH_2O): r=-0.24 (P=0.65), DIZE (15 mg/kg/day): r=-0.63 (P=0.25), DIZE (30 mg/kg/day): r=-0.31 (P=0.61) (Figure 3-13A). Similarly, at reperfusion, the extent of % rCBF increase did not correlate with final infarct volume; Vehicle (dH_2O): r=0.49 (P=0.36), DIZE (15 mg/kg/day): r=0.7 (P=0.23), DIZE (30 mg/kg/day): r=-0.4 (P=0.5), (Figure 3-13B).

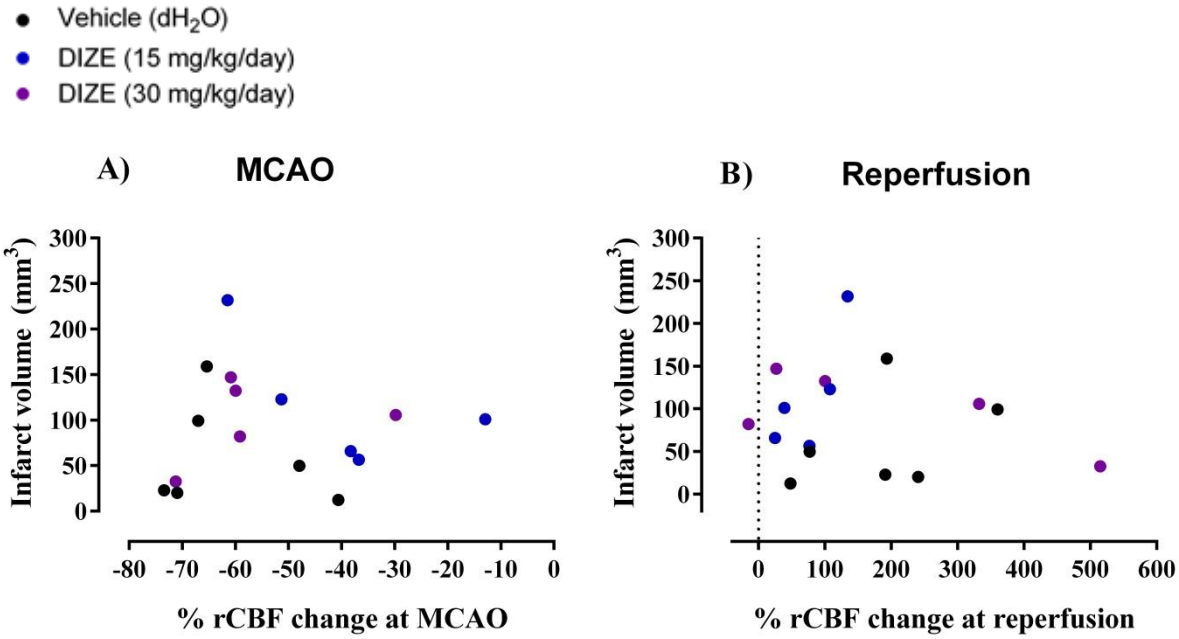

Figure 3-13 Correlation between % rCBF change at MCAO/reperfusion and final infarct volume. A) % rCBF decrease at MCAO vs infarct volume (mm^3) LDF data did not correlate with final infarct for each group (P>0.05)**. B) % rCBF change at reperfusion vs infarct volume (mm^3).** LDF data did not correlate with final infarct for each group (P>0.05). Graphs show values for Vehicle (dH_2O; n=6), DIZE (15 mg/kg/day; n=5) and DIZE (30 mg/kg/day; n=5) treatment groups. The vertical dotted line marks 0% rCBF change. Data were analysing using Pearson parametric correlation for Figure A and Spearman non-parametric correlation for Figure B, P<0.05 was considered statistically significant.

3.3.8.3 % rCBF change during MCAO does not predict infarct volume

Throughout the experiments, it was noticed that there was a recovery in perfusion signal during MCAO for all groups; Vehicle (dH_2O): 147.4±180.4%, DIZE (15 mg/kg/day): 38.2±25.3%, DIZE (30 mg/kg/day): 83.1±76.5% (Figure 3-14A). An increase in rCBF over time could be an indication of early reperfusion or collateral supply recruitment and therefore, smaller lesions. When correlating % rCBF change during MCAO with final infarct volume, improving flow during MCAO did not predict smaller lesions; Vehicle (dH_2O): r=-0.2 (P=0.71), DIZE (15 mg/kg/day): r=-0.4 (P=0.52), DIZE (30 mg/kg/day): r=-0.5 (P=0.45), (Figure 3-14B). Figure 3-15C illustrates the LDF traces for the median animals in the Vehicle (dH_2O), DIZE (15 mg/kg/day) and DIZE (30 mg/kg/day) groups. The animals displayed ischaemic lesions of 20.2mm^3, 122.9mm^{3}and 132.3mm^3, respectively.

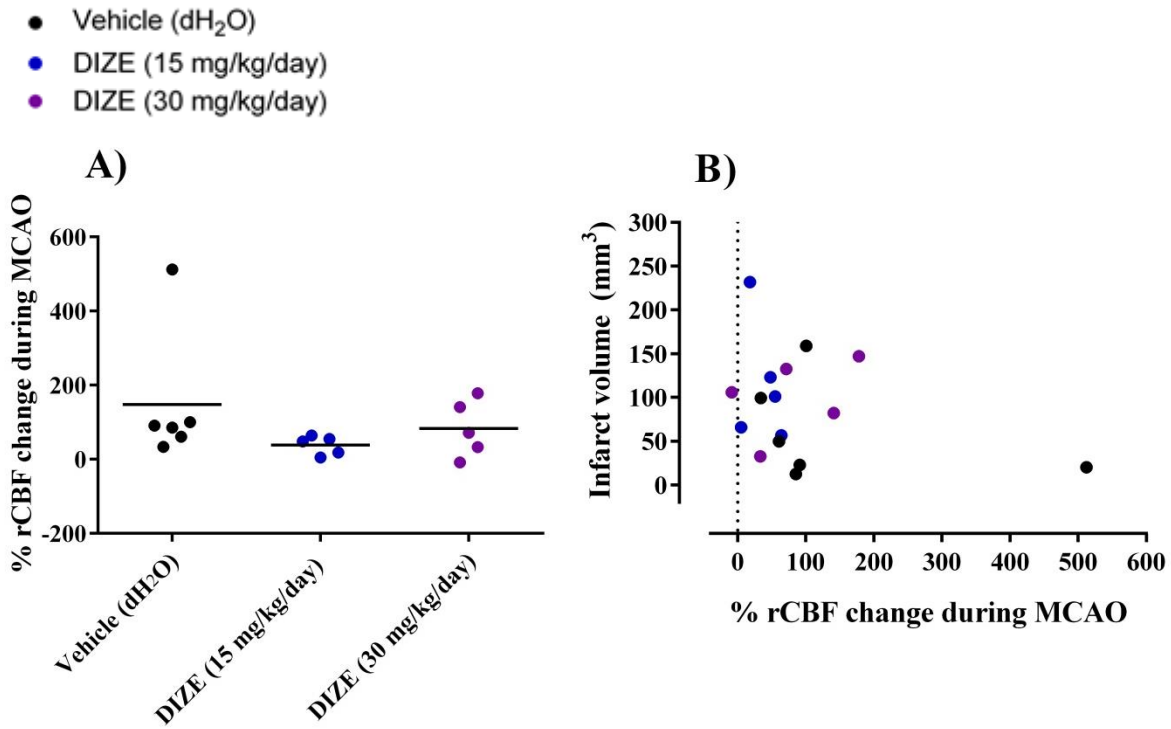

Figure 3-14 % rCBF change during MCAO and correlation with final infarct volume. A) % rCBF change during MCAO; B) Correlation between % rCBF change during MCAO and infarct volume (mm^3). % rCBF increase during MCAO did not differ amongst groups (P>0.05). Additionally, data did not correlate with final infarct for each group (P>0.05). Graphs show values for Vehicle (dH_2O; n=6), DIZE (15 mg/kg/day; n=5) and DIZE (30 mg/kg/day; n=5) treatment groups. The vertical dotted line marks 0% rCBF change. Data were analysed using Kruskal-Wallis non-parametric test for Figure A and non-parametric Spearman correlation for Figure B, P<0.05 was considered statistically significant.

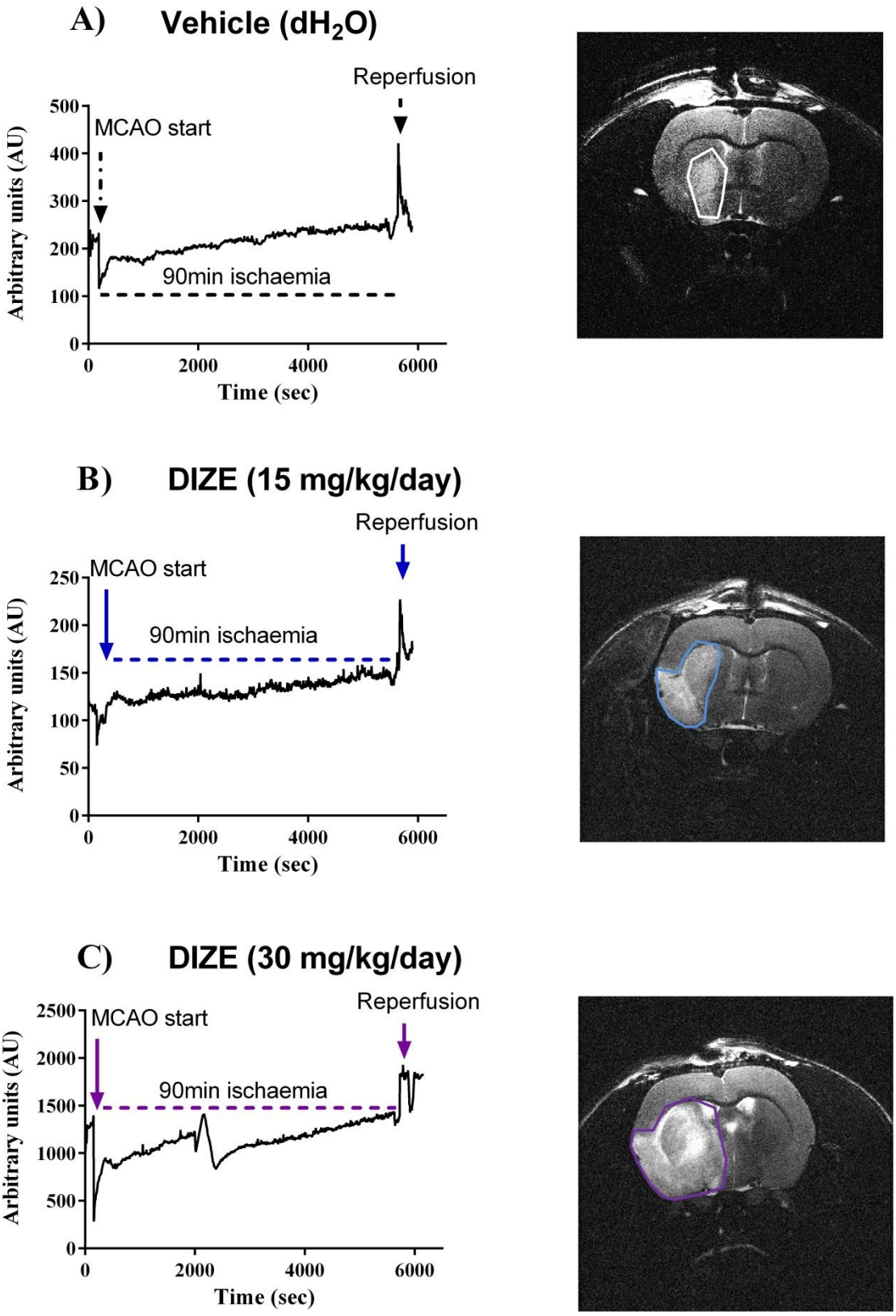

Figure 3-15 Representative LDF traces displaying % rCBF changes during MCAO. A) Vehicle (dH_2O); B) DIZE (15 mg/kg/day) and C) DIZE (30 mg/kg/day). Corresponding MRI-T_2 image represents infarct volume in coronal level 4 for each animal. Data are expressed as arbitrary units (AU) over time in seconds (sec). LDF traces correspond to the median animal in each group. The horizontal dotted line represents 90 min MCAO.

3.3.8.4 LDF predicts haemorrhage following MCAO

In the present study, 3 rats died overnight due to SAH. In these animals, it was noticed that following filament removal to induce reperfusion, there was an abrupt decrease in LDF signal (Figure 3-16). For all animals, the filament was readjusted during MCAO. In two out of the three animals, the filament was readjusted following a steep increase in rCBF during MCAO, a possible indication of partial occlusion (Figure 16A & C). In another rat, the filament was readjusted to ensure correct positioning (Figure 16B), which may have led to accidentally induced SAH. These data show that LDF predicts haemorrhage.

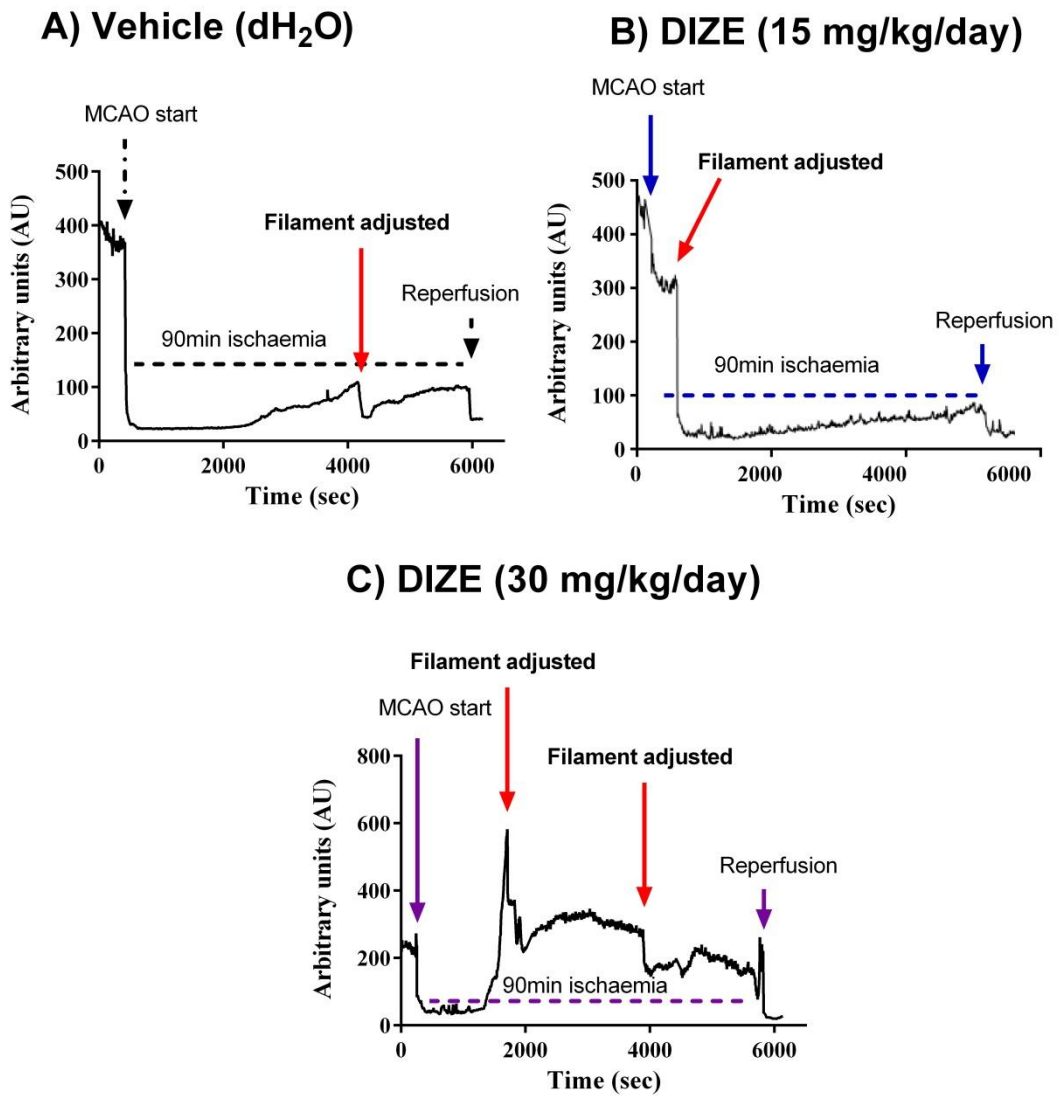

Figure 3-16 Representative LDF traces for SAH mortality cohort. A) Vehicle (dH_2O); B) DIZE (15 mg/kg/day) and C) DIZE (30 mg/kg/day). In all SAH mortality animals, the filament was adjusted during MCAO (highlighted in red) and at time of reperfusion, LDF traces steeply decreased without recovery, an indication of haemorrhage. Data are expressed in arbitrary units (AU) over time in seconds (sec). The horizontal dotted line represents 90 min MCAO.

3.4 Discussion

Infarct size variability is a problem that burdens the entire experimental stroke field as it leads to a higher number of animals needed to obtain a suitable statistical power. The intraluminal filament MCAO is the most widely used animal model. Despite being considered less invasive than other models as it does not require craniotomy, it leads to variable ischaemic lesions. Several factors account for the variability of ischaemic lesions such as rat strain. In our study, lesion volume outcome was compared between Wistar and Sprague-Dawley rats where it was observed that Wistar rats displayed significantly larger and less variable lesions than Sprague-Dawley rats following 4 hrs permanent MCAO. In this thesis, the main outcome is to study the potential of RAS counter-regulatory axis enhancement as an adjuvant therapy along with reperfusion in ischaemic stroke. Following the determination of the most suitable rat strain to be used, Study 2 had the objective to optimise the performance of transient MCAO. Moreover, it investigated the potential of systemic drug delivery to target the brain RAS and the use of LDF as a possible infarct volume prediction method for future experiments. Systemic administration of the ACE2 activator, DIZE, did not significantly alter infarct volume, neurological outcome or systolic BP. In addition, it was determined that LDF is an unreliable and challenging technique unable to predict infarct volume from the severity of the initial ischaemic insult.

3.4.1 Wistar rats showed significantly larger lesions following 4 hrs permanent MCAO than Sprague-Dawley animals

Wistar rats subjected to 4 hrs permanent MCAO displayed significantly larger ischaemic lesions than Sprague-Dawley animals. To guarantee that the infarct volumes obtained were due to MCA occlusion only, MABP and blood gases were assessed prior to and during MCAO as these factors may impact collateral blood vessel vasodilation or constriction (Anderson and Meyer, 2002; Browning et al., 1997; Shin et al., 2008). Temperature was also monitored and maintained to prevent hypothermia, which is neuroprotective in ischaemic stroke (van der Worp et al., 2007). Isoflurane delivered by mechanical ventilation allows the adjustment of anaesthetic levels, providing some control over physiological parameters that could interfere with infarct development (Zausinger et al., 2002). Consequently, MABP, pH, $PaCO_2$ and temperature were maintained stably amongst groups with no significant differences between strains over the course of the experiment. Conversely, for all animals, PaO_2 levels remained higher than the normal range (100 mmHg) due to the continuous administration of 70:30% N_2O-O_2 mixtures. Sprague-

Dawley animals showed a trend to exhibit higher PaO_2 values than Wistar rats; however, there were no significant differences between groups.

Wistar rats are reported to offer larger and less variable ischaemic lesions compared to Sprague-Dawley rats (Kim et al., 2009; Ström et al., 2013). Wistar rats have thinner and underdeveloped posterior communicating arteries when compared to Sprague-Dawley rats, thus, Wistar animals may be more susceptible to injury (Kim et al., 2009). Moreover, Sprague-Dawley rats display at least 6 distinct MCA branching patterns. From a total of 263 Sprague-Dawley rats obtained from the same supplier, 17% presented atypical MCA branching (Fox et al., 1993). This suggests that MCAO extent may be diminished due to atypical provision of CBF to the injured site, justifying enhanced infarct variability in this strain (Fox et al., 1993). One could argue that the choice of animal model may have influenced the results obtained. The permanent model was selected in this study as it does not add an extra variable in terms of reperfusion, which could impact result interpretation. Plus, it was a means to demonstrate that successful MCAO was induced in my hands. Nonetheless, the observations in the study are supported by experiments conducted in transient MCAO. Following 90 min, 2 hrs or 4 hrs MCAO with 24 hrs reperfusion, Wistar rats present greater and less variable cerebral damage as well as lower mortality rates compared to Sprague-Dawley rats (Aspey et al., 2000; Walberer et al., 2006).

Conversely, Walberer and colleagues identified that following 24 hrs permanent MCAO, Sprague-Dawley rats developed significantly larger ischaemic lesion volumes compared to Wistar animals (Walberer et al., 2006). Several factors could be implicated in the differences observed such as stroke severity and infarct volume measurement method. However, the choice of rat vendor is the most likely contributing factor for the discrepancy observed. Animal supplier is a known contributing factor for infarct volume variability amongst strains (Oliff et al., 1995). In our study, animals were obtained from Charles River whereas in Walberer's study rats were purchased from Harlan. When comparing Sprague-Dawley ischaemic injury susceptibility in animals obtained from Harlan or Charles River Laboratories, Harlan animals presented significantly greater CBF reduction and functional deficit following permanent MCAO compared to Charles River rats (Nikolova et al., 2014). Therefore, supporting the decreased severity observed in Sprague-Dawleys in our study. Despite a possible vendor related genetic variability, interstrain differences are equally seen when purchasing rats from the same supplier. Following global cerebral ischaemia in rats obtained from Charles River, Wistar animals were highly predisposed to

severe neuronal damage whereas Sprague-Dawleys exhibited partial damage only (Fuzik et al., 2013), further supporting the findings in our study.

The debate around rat strains led to a meta-analysis conducted in 2013 with the aim to investigate the factors influencing infarct outcome variability. There, 346 articles were examined and it was concluded that the Wistar rat strain and silicone coated intraluminal filament induce the lowest infarct volume variability and mortality (Ström et al., 2013). Most recently, Rewell & Howells concluded that when compared to Wistar Kyoto rats, sample size calculations using Sprague-Dawleys lead to extensively higher cohort numbers due to lesion variability (Rewell and Howells, 2017). Therefore, the authors deemed the Sprague-Dawley rat strain suboptimum for intraluminal filament MCAO model experiments.

3.4.2 DIZE treatment does not influence infarct volume, neurological score or systolic BP following transient MCAO

DIZE administered SC for a period of 7 days, starting 4 days prior to MCAO, had no significant impact on ischaemic lesion volume, neurological score or systolic BP compared to Vehicle (dH_2O). This suggests that systemic administration may not be sufficient to target the brain RAS and induce a neuroprotective effect following MCAO and therefore implies that ICV administration may be the most adequate delivery method as previously observed (Mecca et al., 2011). Our study had various protocol differences compared to Mecca's study. First, the rat strain selected was Wistar opposed to Sprague-Dawley. Second, the animal model used was the intraluminal filament method instead of ET-1-induced MCAO. The pathological mechanisms could differ between models. For instance, the filament model is suitable to replicate thrombectomy strategies whereas the ET-1 induced MCAO may replicate alteplase treatment due to progressive reperfusion induction rather than an abrupt CBF reestablishment (Sutherland et al., 2016). Third, in Mecca's study, final infarct was examined with TTC staining whereas in our studies, MRI-T_2 was selected as the method of infarct determination at 72 hrs. TTC reliably detects infarct areas at 24 hrs post MCAO. After this point, inflammatory cells begin to infiltrate the damaged area with their mitochondria being also stained with TTC (Liszczak et al., 1984). Consequently, aside from differences in the route of administration between the studies, factors such as rat strain and stroke model could be implicated in the discrepancies observed.

DIZE induces a hypotensive effect following systemic and ICV administration in hypertension and ischaemic stroke studies (Gjymishka et al., 2010; Mecca et al., 2011). This outcome is attributed to an increase in ACE2 activity and subsequent Ang-(1-7) generation (Gjymishka et al., 2010; Mecca et al., 2011). However, in our study, treatment did not alter systolic BP compared to control animals. Several animals exhibited a systolic BP above the normal range (80-120 mmHg) before and after MCAO and were visibly stressed during measurements. Concomitantly, a possible hypotensive effect might have been masked, indicating that the acclimatisation period should be extended in future.

DIZE SC therapy at 15 mg/kg/day and 30 mg/kg/day doses for a period of 7 days were selected in these studies. Previously, 15 mg/kg/day SC DIZE attenuated inflammatory responses in rat models of myocardial infarction, subtotal nephrectomy and pulmonary hypertension (Qi et al., 2013; Rigatto et al., 2013; Velkoska et al., 2015). Simultaneously, 30 mg/kg/day dose was safely administered in a Ang II induced mice model of abdominal aortic aneurysms (Thatcher et al., 2014). To examine a dose response effect and to guarantee delivery across the CVOs, higher doses of 15 mg/kg/day and 30 mg/kg/day DIZE were selected. Interestingly, DIZE treatment showed a trend to worsen infarct volume and neurological outcome when compared to control rats. In fact, treated animals were visibly worse during post-operative recovery, exhibiting higher levels of porphyrin and less movement. In female rats, DIZE therapy exerts a negative impact on reproductive performance, possibly inducing a toxic effect (Oguejiofor et al., 2010). Therefore, it is plausible that DIZE might have caused off target effects in our experiments. Nevertheless, the results obtained suggest that systemic brain RAS targeting may not be sufficient to induce drug circulation in the brain and mediate a neuroprotective effect. In addition, DIZE was shown to be unsuitable due to its negative impact in animal wellbeing. In future experiments, the therapeutic potential of the counter-regulatory RAS axis will be studied via an ICV delivery route using a RAS receptor agonist treatment.

Most recently, DIZE was tested as a post stroke therapy administered IP at 4 hrs, 1 day and 2 days after ET-1 induced MCAO in a series of daily doses ranging from 0.75 to 15 mg/kg. Infarct volume was determined 3 days post MCAO and it was concluded that 0.75, 2.5 and 7.5 mg/kg DIZE significantly attenuated infarct volume whereas 15 mg/kg had no effect (Bennion et al., 2015). This follow up experiment emphasises that the dose selected was suboptimal to induce an effect in the brain whilst highlighting that according to the results obtained in this Chapter, ICV administration was a suitable method to be selected.

3.4.3 LDF reliably detects MCAO only but not reperfusion extent

LDF is a reference tool in experimental stroke to confirm proper filament placement. During MCAO, there is no visual control of occlusion, thus, partial occlusions, SAH or the displacement of the filament are often undetected, with the latter leading to early reperfusion (Schmid-Elsaesser et al., 1998). Accordingly, LDF has been indicated as a reliable technique when conducted continuously to confirm occlusion and is recommended by the STAIR guidelines ((STAIR), 1999; Dirnagl et al., 1989).

In our study, LDF successfully detected perfusion deficit in the MCA territory upon filament insertion in all included animals. Although LDF does not allow discernment between full and partial MCAO, it was shown to reliably confirm a reduction in perfusion deficit at MCAO start. A recent study investigated LDF as a standardising method to be conducted during the intraluminal filament model in rats. There, 4 different surgeons with various levels of experience conducted MCAO surgery with or without LDF aid. LDF use decreased the coefficient of variance in terms of infarct size by helping identify the presence or absence of an occlusion (Taninishi et al., 2015), and thus validating the accuracy in MCAO detection at the time of filament placement. In contrast, LDF did not reliably detect reperfusion extent. At time of filament removal, LDF detected a small CBF increase or reperfusion failure in some animals. Yet, these rats presented mid-sized infarcts opposed to large lesions, an indication of successful reperfusion. This could be a reflection of probe movement during the experiment or the presence of a haematoma in the area assessed; possibly caused by the probe tip. Moreover, it could be an indication that reperfusion occurred in brain areas that could not be detected by the LDF probe. Also, these animals could have had a surge in reperfusion during anaesthetic recovery and subsequent increase in BP. Similarly to our study, an experiment conductedin embolic stroke models showed that LDF successfully detected MCAO; however, it did not reliably detect reperfusion following tPA treatment (Henninger et al., 2009). There, it was observed that LDF failed to detect reperfusion in some animals, which developed small infarcts; therefore, supporting our conclusions.

3.4.4 LDF predicts haemorrhage

In our study, 3 animals died overnight due to SAH. It was noticed that in these rats, the filament had been readjusted during MCAO due to CBF increase or to guarantee the filament was adequately secured. SAH occurrence was characterised by a sudden decrease

in rCBF following filament retrieval as previously identified (Hungerhuber et al., 2006; Woitzik and Schilling, 2002). In the MCA filament model, silicone coated filaments cause SAH in 8% of all animals opposed to 30% induced by non-coated filaments (Schmid-Elsaesser et al., 1998). Although Doccol filaments are less likely to induce SAH than non-coated filaments, it was noticed that when adjusting the filament, the likelihood of haemorrhage increases. This shows that following first time insertion, the vessels become sensitive to rupture and one must carefully evaluate whether to readjust the filament or not under the circumstances described above.

3.4.5 LDF does not predict final infarct following transient MCAO

To examine whether LDF changes could predict final infarct volume, rCBF change at MCAO and at reperfusion were correlated with MRI-T_2 data. LDF was shown to be an unsuitable tool to predict final infarct outcome and tackle the lesion variability observed in this animal model. Yet, previous studies contradict our findings where LDF at time of MCAO, successfully predicted infarct volume (Riva et al., 2012; Soriano et al., 1997). In Soriano et al's study, the 3-vessel model was used, which is substantially more severe than the one used in our experiment. By occluding 3 vessels or more, collateral blood supply recruitment becomes impaired, diminishing cortical CBF during ischaemia and offering an enhanced and less variable assessment of perfusion deficit (Soriano et al., 1997). Accordingly, we show that quickly after filament positioning, there was a recovery in CBF during MCAO of various extents amongst animals (Figure 3-14). This gradual increase could signify that the filament was not occluding the vessel completely causing early reperfusion. However, when correlating the extent of rCBF increase during MCAO with final infarct outcome, LDF did not predict smaller lesions. The increase in rCBF is likely due to the recruitment of MCA collaterals through the anterior cerebral artery (ACA) and the leptomeningeal anastomoses (Liebeskind, 2003; Riva et al., 2012; Woitzik and Schilling, 2002).

Collateral vessel recruitment and grade differs amongst individuals in spatial and temporal terms (Liebeskind, 2005). This cannot be reliably detected by LDF as the technique provides a single point measurement only; therefore, collateral recruitment and LDF probe location may have interfered with result interpretation. Moreover, Riva and colleagues showed that following 60 min MCAO in Wistar rats, CBF deficit within the penumbra correlates with final infarct (Riva et al. 2012). There, LDF values were obtained at 2 mm anterior and 2 mm lateral coordinates from bregma (Riva et al., 2012) whereas the

coordinates used in our study were 1.3 mm posterior and 4.0 mm lateral from bregma. It could also be argued that the probe position was not optimal, as it could have been placed within penumbral tissue in some animals yet within the core in others using the same stereotaxic coordinates.

The extent of % rCBF change during MCAO and reperfusion was highly variable amongst animals and technically challenging to perform. For instance, rats have a cortical thickness of approximately 2 mm whilst LDF has a sample volume of approximately 1 mm^3 and 1 mm depth only (Zilles 1985). To ensure adequate signal in this LDF set up, the rats' skull has to be drilled until the pial vessels are visualised; thus, drilling differences amongst animals has the potential to impact LDF signal and result reliability. In addition, absolute flow values are dependent on probe placement and position, with minor changes resulting in significant alterations in CBF recording (Dirnagl et al., 1989). As a result, slight changes in probe holder positioning due to poor probe holder attachment might have influenced the extent of perfusion detection. These variables reflect the technical issues that arise when performing LDF in this set up. Therefore, MRI will be used in future to reliably detect early ischaemic lesion and final infarct volume using DWI and a MRI-T_2 sequence, respectively, and MRA will be used to confirm successful MCAO and MCA reperfusion.

3.4.6 Summary

In this Chapter, Wistar rats were selected as the most suitable strain for the performance of *in vivo* studies due to the generation of mid-large lesions with lower variability compared to Sprague-Dawley rats following permanent MCAO. DIZE SC administration as a pre and post-MCAO therapy failed to induce a neuroprotective effect following transient MCAO. Instead, DIZE treatment showed a trend to exacerbate ischaemic lesion when compared to Vehicle (dH_2O) following 7 days of treatment. The results indicate that systemic DIZE treatment are not optimal to study the therapeutic potential of the counter-regulatory RAS axis following MCAO. LDF successfully detected rCBF reduction at MCAO and predicted haemorrhage; however, it failed to detect reperfusion extent and it did not predict final infarct outcome. LDF proved to be an unreliable method to tackle infarct variability in this animal model. Accordingly, the next Chapters will evaluate the therapeutic potential of the counter-regulatory RAS axis in ischaemic stroke as an ICV therapy with RAS receptor agonists. To tackle infarct volume variability derived from the intraluminal filament model, MRI scanning will be performed to confirm MCAO/reperfusion as well as determine initial and final infarct lesion to study the extent of treatment effects.

Chapter 4: The effects of Ang-(1-7) and/or C21 on the extent of tissue salvage following transient MCAO

Chapter 4

4.1 Introduction

The experiments in this Chapter were designed to assess the therapeutic potential of Ang-(1-7) (MasR agonist) and C21 (AT_2R agonist), either alone or in combination as a potential synergistic therapy following transient MCAO. The primary outcome of this study was to assess the impact of treatment on the extent of cerebral tissue salvage following reperfusion.

Acute ischaemic stroke is a highly disabling condition resulting from the abrupt loss of CBF, leading to neuronal cell death and consequent physical disability (Dirnagl et al., 1999). Currently, the only non-surgical treatment available is alteplase, which acts to lyse the clot/thrombus obstructing the vessel, inducing a transitory reperfusion (Tawil and Muir, 2017). However, alteplase has various limitations, for instance, the efficacy and safety of treatment is restricted to patients within 4.5 hours of symptom onset and it may lead to intracranial haemorrhage (Tawil and Muir, 2017). In addition, it often fails to effectively recanalise large vessel occlusions (Tawil and Muir, 2017). In recent years, mechanical thrombectomy has been shown to be an effective strategy in ischaemic stroke, particularly in large vessel occlusion patients, and with an extended therapeutic window of 6 hrs from symptom onset (Mayank Goyal et al., 2015). This strategy works by mechanically retrieving the obstructing clot/thrombus, inducing an abrupt cerebral reperfusion as opposed to the slower restoration of cerebral perfusion achieved by the thrombolytic action of alteplase. Although reperfusion reestablishment to the occluded vessel is the first line of treatment, it may also exacerbate injury by stimulating leukocyte recruitment, inflammation, oxidative stress and BBB breakdown (Horsch et al., 2015; Pan et al., 2007; Warach and Latour, 2004). Thus, this new line of therapy has reinvigorated the development of neuroprotective adjuvant therapies that could reduce infarct volume progression after reperfusion injury.

The RAS, an endocrine system involved in homeostatic control of blood pressure is linked to the pathology of cardiovascular conditions (e.g. hypertension and myocardial infarction) through an over activation of the ACE/Ang II/AT_1R axis(Dzau, 2001). In ischaemic stroke, the ACE/Ang II/AT_1R is also suggested to be over-activated in the brain and thought to exacerbate cerebral injury by promoting vasoconstriction, oxidative stress and inflammation (Walther et al., 2002). Accordingly, several experiments have tested the neuroprotective properties of ARBs in experimental stroke where these were shown to

reduce the extent of tissue damage and degree of behavioural impairment (Krikov et al., 2008; Liu et al., 2008; Lou et al., 2004), confirming the involvement of the RAS in cerebral pathology. Interestingly, the neuroprotective effects induced by ARBs are proposed to be due to an enhancement of the counter-regulatory RAS axis, ACE2/Ang-(1-7)/MasR, as well as a preferred activation of the Ang II alternative receptor, AT_2R. In the brain, the AT_2R is mainly expressed in foetal tissues; however, following cerebral ischaemia it is upregulated in penumbral regions (Iwai et al., 2004). Similarly, MasR, is upregulated in the brain and serum following MCAO, peaking at 24 hrs post injury and remaining highly expressed at 3 and 7 days post MCAO in rats (Lu et al., 2013). These findings have placed the counter-regulatory axis and the AT_2R as possible therapeutic strategies in cerebral injury.

AT_2R activation in experimental stroke has been shown to reduce infarct volume following transient MCAO in both normotensive and SHRs (Joseph et al., 2014; McCarthy et al., 2009, 2012). In normotensive animals, C21, a highly selective non-peptide AT_2R agonist, reduced infarct volume when administered as a post IP therapy following intraluminal filament transient MCAO. The underlying effect was attributed to an enhanced expression of anti-inflammatory cytokine IL-10 and decreased protein levels of iNOS (Alhusban et al. 2015). The proposed anti-inflammatory effect was further observed in an ET-1 induced MCAO model where C21 administered via ICV infusion as a pre- and post-therapy decreased infarct volume compared to controls at 72 hrs post injury (Joseph et al., 2014). The outcome was attributed to a reduction in cerebral pro-inflammatory markers *iNOS* and *CCR2*, a macrophage chemotaxic receptor (Joseph et al., 2014).

Similarly, Ang-(1-7) induced MasR activation counteracts the ACE/Ang II/AT_1R axis by promoting an anti-inflammatory effect (Jiang et al., 2012; Liu et al., 2016; Mecca et al., 2011; Regenhardt et al., 2013). When administering Ang-(1-7) ICV 3 days prior to and 4 days post ET-1 induced MCAO, Ang-(1-7) attenuated infarct size and neurological deficit, a result suggested to be due to a reduction in *iNOS* (Mecca et al., 2011). Furthermore, in permanent MCAO models, Ang-(1-7) treatment reduced infarct volume due to a NF-κB suppression and subsequent inhibition of pro-inflammatory markers IL-1β, IL-6 and COX-2, therefore, exerting an anti-inflammatory effect (Jiang et al. 2012). It is further hypothesised that Ang-(1-7) exerts its effects by directly acting on MasR present on microglia and modulating microglia/macrophage cytokine profile from an M1 (inflammatory) to an M2 (anti-inflammatory) type (Liu et al., 2016; Regenhardt et al., 2013). For instance, in *in vitro* experiments, Ang-(1-7) treatment on cultured microglia

attenuated NF-κB activation, *IL-1β* and proliferating microglia/macrophage marker *CD11b* expression at basal levels whilst enhancing *IL-10* (Liu et al., 2016). In *in vivo* studies, Ang-(1-7) pre- and post-treatment in ET-1 induced MCAO, downregulated the gene expression of pro-inflammatory M1 markers *IL-6* and *CD11b* in the ipsilateral cortex 24 hrs post injury (Regenhardt et al., 2013), emphasising its potential anti-inflammatory actions.

Given the similarity of activation outcome, increasing evidence postulates that MasR and AT_2R receptors may dimerise and act synergistically. For instance, in ischaemic stroke, PD123319, a AT_2R antagonist, blocked the cerebroprotective effects induced by Ang-(1-7) following transient MCAO whereas C21-induced neuroprotection was reversed when administered in combination with MasR antagonist, A779 (Joseph et al., 2014; Mecca et al., 2011). On the contrary, experiments postulate that MasR and AT_2R could act as two independent protective pathways. In permanent MCAO, Ang-(1-7)-induced infarct size decrease was overturned by MasR antagonist, A779, but not when administered in combination with AT_2R antagonist, PD123319 (Jiang et al., 2012). Additionally, in KO mice, AT_2R agonism generates a vasodilatory effect in aortic rings in MasR-KO (Lemos et al., 2005) whereas in AT_2R-KO mice, Ang-(1-7) exerted an hypotensive effect (Gembardt et al., 2012). Therefore, there is a need to further elucidate the functional implications of simultaneous MasR and AT_2R agonism in the context of ischaemic stroke.

The majority of studies testing the neuroprotective potential of Ang-(1-7) and C21 in transient MCAO have been performed by using the ET-1 induced MCAO model, which induces a gradual reperfusion as opposed to the abrupt reperfusion observed following mechanical thrombectomy procedures (Sutherland et al., 2016). In addition, therapy effects on infarct volume have been primarily assessed as a pre and post stroke treatment, particularly for Ang-(1-7). In the clinic, it is challenging to anticipate when a patient will suffer a stroke. Therefore, there is a need to study the neuroprotective potential of these therapies in models that replicate thrombectomy procedures and as a post-injury therapy administered during subacute/chronic stages of cerebral injury. Importantly, the synergistic neuroprotective potential of MasR and AT_2R agonism as a single or combination therapy following focal cerebral ischaemia in subacute/chronic stages of injury is yet to be determined. Consequently, this study aims to assess the neuroprotective potential of Ang-(1-7) and/or C21 as a post-stroke therapy for a period of 7 days following transient MCAO.

4.1.1 Study Aims

- Primary outcome: To determine the effect of post-stroke central administration of Ang-(1-7) and/or C21 on the extent of tissue salvage following 90 min MCAO with 7 days reperfusion.

- To determine the effects of Ang-(1-7) and/or C21 on blood pressure and functional outcome following 90 min MCAO.

- To dissect potential underlying mechanisms via gene expression assessment of RAS components, leukocyte chemokine receptors, microglia/macrophage phenotype and oxidative stress marker gene expression in ipsilateral peri-infarct regions.

- To qualitatively evaluate microglia total cell count and activated cells in the peri-infarct regions following treatment.

4.2 Methods

4.2.1 Sample size calculation

Sample size was assessed using power analysis programme G*Power (version 4.1, Germany). An "a priori" power analysis was performed for F test ANOVA, fixed effects, one-way. Using data from previous *in house* studies assessing final infarct volume following 90 min MCAO with 7 days reperfusion (mean infarct volume of 170mm^3 and a S.D. of 67mm^3). Ang-(1-7) administered as an ICV infusion was previously demonstrated to induce a 50% reduction in % compared to control (Mecca et al., 2011). Similarly, ICV C21 infusion leads to approximately 50% reduction infarct size compared to vehicle groups (Joseph et al., 2014). Therefore in order to detect an effect size of 50% reduction in infarct volume, a minimum *n* number of 11 for each group with a type I error rate (α) of 0.05 and power of 0.80 was demonstrated to be necessary.

4.2.2 Drug treatment dosage

Ang-(1-7) ICV infusion dose of 1.1 nmol per 1μL/hr dissolved inartificial cerebrospinal fluid(aCSF) was selected based on permanent MCAO and ET-1 induced MCAO studies (Mecca et al., 2011; Jiang et al., 2012; Jiang et al., 2014; Regendhardt et al., 2013). C21 was shown to successfully decrease infarct volume in ET-1 induced MCAO models at a dose of 7.5 ng/hr in normotensive rats (Joseph et al., 2014) and at 50 ng/hr in hypertensive animals (McCarthy et al., 2014). Since higher doses of C21 are suggested to interact with AT_1R; a 7.5 ng/hr dose was selected as recommended by Vicore Pharma®.

All animals were treated ICV for a period of 7 days with treatment starting immediately following reperfusion with the use of ALZET osmotic pumps delivering treatment at a rate of 1μL/hr (ALZET®, Model 2001), dissolved in aCSF (ALZET®, CA, USA). Treatment groups were as follows: **Vehicle** [(aCSF); 1μL/hr; n=13)], **Ang-(1–7)** (1.1 nmol; 1μL/hr; n=13), **C21** (0.0075 μg/hr; 1μL/hr; n=12), **Ang-(1-7) + C21** (1.1 nmol Ang-(1-7) + 0.0075 μg/hr of C21; 1μL/hr; n=11). Ang-(1-7) was purchased from Bachem® (Bachem, Bubendorf, Switzerland) and C21 was kindly supplied by Vicore Pharma®. One day prior to the experiment, osmotic pumps containing allocated treatment were made up and left in a water bath at 37ºC until surgery, in order to prime for drug delivery.

4.2.3 Randomisation and blinding

Rats were assigned a number and randomly allocated to treatment groups through a list randomiser (www.random.org) and prior to study commencement. Investigators, including MA, were blinded to treatment group throughout the experimental study. Treatment schedule was kept by a colleague within the department who was responsible for drug preparation. Systolic BP and neurological score were performed by a blinded independent investigator prior to and post MCAO. Data analysis was performed under a blind fashion by two independent investigators. Once all analysis and assessments were conducted, treatment codes were revealed.

4.2.4 Animals, surgical procedures and recovery

Male Wistar rats (n=102; 300-380g) obtained from Charles River Laboratories were subjected to 90 min MCAO followed by 7 days reperfusion using the intraluminal filament model. One day prior to MCAO, conscious systolic BP was measured (following 7 days acclimatisation period) and neurological score carried out for each rat as previously described (Chapter 2.10 - 11). Neurological score was carried out again at day 3 and 7 reperfusion whereas systolic BP was measured at day 7. On day of surgery, rats were anaesthetised with 5% isoflurane and orally intubated for anaesthesia maintenance at 2-2.5% isoflurane in a 30:70% O_2-NO_2 mixture (Chapter 2.5). Local anaesthetic (Norapin®; 1mg/kg) was administered SC in all incision sites. After, animals were placed in a Kopf stereotaxic frame for ICV osmotic pump cannula implantation in the right cerebral lateral ventricle (Chapter 2.7.2). The animals were then moved to a corkboard and MCAO surgerycarried out (Chapter 2.8). The filament size selected was based on individual animal weight and according to Doccol Corporation guidelines. Following 90 min MCAO, the filament was removed, all the incisions sutured and the animal allowed recovering for a period of 7 days. Recovery and post-operative procedures were carried out as defined in Chapter 2.8.1 and 2.8.2, respectively.

4.2.4.1 Sham procedures

Sham treated animals were anaesthesised as outlined above. A burr hole was drilled in the skull and the cannula inserted into the cerebral ventricle and then quickly removed. MCAO surgery was performed; however, the Doccol filament was introduced into the vessel without occluding the MCA. Anaesthesia was maintained for the same period of time as MCAO animals. Recovery protocol procedeed as described for a period of 7 days.

4.2.5 MRI scanning protocol

At the start of MCAO rats were immediately transferred to the MRI scanner and placed in a rat cradle where the head was restrained with tooth and ear bars and the surface coil placed above the head. The intubation tube was reconnected and a rectal probe along with a homeothermic blanket placed on the animal to maintain anaesthesia and regulate body temperature. Three distinct scans were performed during MCAO: DWI, MRA and RARE T_2 weighted MRI (Chapter 2.9). DWI was performed at 30 and 60 min MCAO and ADC maps generated to detect initial MCAO lesion prior to therapy. MRA was conducted to confirm successful MCAO and correct ICV cannula placement confirmed using RARE T_2 weighted MRI.

The imaging protocol was then repeated following 7 days of reperfusion and recovery. Rats were initially anaesthesised, placed in the scanner and anaesthesia maintained using a facemask. Final infarct volume was determined by a RARE T_2 weighted MRI. MRA was performed to confirm reperfusion of the left MCA. At the end of the MRI scanning, rats were killed and brains removed for either molecular or immunohistochemical assessments (Chapter 2.12:16). Figure 4-1 provides an overview of the experimental protocol conducted.

4.2.5.1 MRI data analysis

Data analysis for DWI and T_2 MRI scanning was performed as described in detail in Chapter 2. Initial ischaemic lesion at 30 and 60 min MCAO was assessed by generating ADC maps (using Paravision v5 software) for each of the 8 coronal slices images obtained following DWI scanning. ADC maps were processed using ImageJ and initial lesion volume was calculated by applying a threshold between 0.01 and $0.58\times10^{-3}mm^2/sec$ (Chapter 2.9.1). RARE T_2 scans were used to determine final infarct volume at 7 days post 90 min MCAO. Image J was used to delineate hypertintense regions across the 16 coronal sections in order to calculate infarct area on each slice. Contralateral and ipsilateral hemisphere volumes were also calculated across the 16 coronal slices (Chapter 2.9.2).

4.2.6 *Post-mortem* assessments

Total RNA was extracted from peri-infarct ipsilateral brain regions for sham (n=7), MCAO-aCSF (n=9) and MCAO-Ang-(1-7) (n=9) treated animals (Chapter 2.14) and cDNA generated from the total extracted RNA by RT-PCR (Chapter 2.15). qRT-PCR was performed and the genes outlined in Chapter 2.16.1 assessed. Results were analysed by taking the means of the technical duplicates and then normalising to theinternal control selected, UBC. Data analysis was conducted as described in Chapter 2.16.3.

Vehicle (aCSF) (n=2), Ang-(1-7) (n=2), C21 (n=2) and Ang-(1-7) + C21 (n=2) treated animals were subjected to perfusion fixation and paraffin embedding/sectioning (Chapter 2.12.2). To identify the peri-infarct, core and contralateral regions, histological analysis was carried out (Chapter 2.13.1). Briefly, brain sections from coronal levels 3 to 5, which correspond to the core of the MCA territory, were selected and stained with H&E and analysed under light microscopy at 40x. Adjacent sections were then selected and immunohistochemistry for microglia marker IBA1 was conducted (Chapter 2.13.2). Three distinct ROIs were defined within the peri-infarct area on each level and a homotopic ROI within the contralateral hemispherewas chosen as a control non-ischaemic area. Sections were imaged at 40x under fluorescent microscopy. $IBA1^{+}$ microglia werecounted using Image J and expressed as number/mm^2 in peri-infarct and contralateral regions across the 3 coronal levels selected. In addition, cells were differentiated into activated and resting, % activated microglia were presented as % from total cell count for each animal.

4.2.7 Exclusion criteria

The exclusion criteria were applied at the end of the study by three independent researchers that were blind to treatment allocation. Before the start of the study exclusion criteria was established and animals excluded if presenting the following characteristics:

- Left MCA not fully occluded at 60 min MCAO or not fully reperfused at day 7 as identified by MRA.

- Cannula for drug delivery not within the cerebral ventricle at day 7 as shown by MRI-T_2.

- ICH of the MCA at day 7 reperfusion as shown by MRI-T_2.

- Animals that died or were sacrificed prior to 7 days recovery.

4.2.8 Statistical analysis

Ischaemic lesion at 30 min, 60 min MCAO and final infarct at 7 days post MCAO were compared between treatment groups using one-way ANOVA. To determine treatment effects, percentage (%) and absolute change in ischaemic lesion from 60 min MCAO and 7 days post MCAO were calculated and compared between groups using one-way ANOVA with Tukey's posthoc test. Systolic BP data were compared using one-way ANOVA. Neurological score data were compared between groups using the non-parametric Kruskal-Wallis test. Absolute ischaemic lesion change from 60 min MCAO to 7 days reperfusion within groups was analysing using paired Student's t test.

Gene expression data were compared between Sham, MCAO-Vehicle (aCSF) and MCAO-Ang-(1-7) groups using one-way ANOVA and shown as -ΔCt normalised to *Ubc*. For immunohistochemistry data, total $IBA1^+$ microglia number and % activated cells were presented for peri-infarct ipsilateral and homotopic contralateral hemisphere regions. Statistical tests were not performed for IBA1 immunohistochemitry data, representing qualitative data.

Data were presented as mean ± S.D or median ± IQR. Data were shown as a scatterplot and a p value of <0.05 was deemed statistically significant.

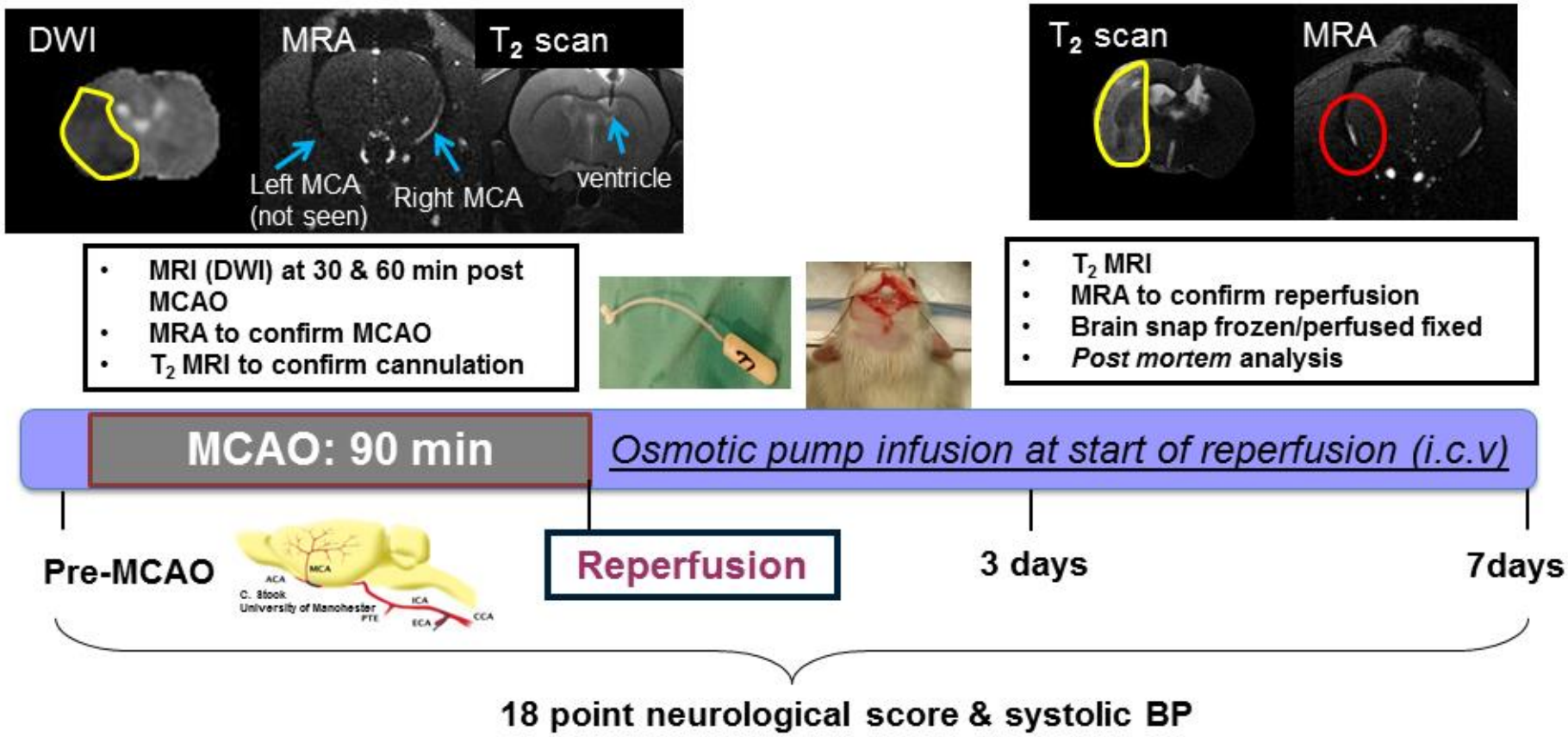

Figure 4-1 Diagram detailing experimental protocol. Prior to MCAO, systolic BP and neurological score were carried out. On day of surgery, MCAO was induced and ICV cannula implanted into the right lateral ventricle. Animal was then placed in the MRI scanner and DWI, MRA and T_2 weighted scans conducted. After 90 min MCAO, reperfusion and treatment started for a period of 7 days. Animals were allowed to recover for 7 days and neurological score and systolic BP assessed. MRI-T_2 weighted and MRA scans were performed at day 7 and brain samples collected for *post mortem* analysis.

4.3 Results

4.3.1 Mortality and surgical death

Out of 102 animals used in this study, a total of 22 rats died or were euthanised during 7 days of recovery (Table 4-1). From these animals, 15 rats died spontaneously: 2 Vehicle (aCSF), 4 Ang-(1-7), 7 C21 and 2 Ang-(1-7) + C21 treated rats. Plus, 7 animals were euthanised due to breathing difficulties or weight loss below 25% of initial body weight: 4 Vehicle (aCSF), 1 C21 and 2 Ang-(1-7) + C21 treated animals (Table 4-1). Overall, this study had a mortality rate of 21.5%, with the C21 group presenting highest mortality within groups (Table 4-1). During surgical procedures, 12 animals died due to experimental error and were not included in mortality rates: 2 Vehicle (aCSF), 3 Ang-(1-7), 2 C21 and 5 Ang-(1-7) + C21 treated rats (Table 4-1).

Table 4-1 Study mortality and surgical death per treatment group.

	Vehicle	**Ang-(1-7)**	**C21**	**C21 + Ang-(1-7)**	**Total *N***
Total animals per group	**25**	**26**	**27**	**24**	**102**
Spontaneous death	2	4	7	2	15
Euthanised	4	0	1	2	7
Mortality	**6**	**4**	**8**	**4**	**22**
Surgical death	**2**	**3**	**2**	**5**	**12**
% mortality per group	**24%**	**15%**	**30%**	**17%**	

4.3.2 Exclusions

In this study, 68 rats survived the experiment of which 49 were included for analysis: 13 Vehicle (aCSF); 13 Ang-(1-7); 12 C21 and 11 Ang-(1-7) + C21 treated animals. Following inspection of the MRI-T_2 scan, 8 rats did not have the ICV cannula placed in the cerebral ventricle and were excluded: 3 Vehicle (aCSF), 3 Ang-(1-7), 1 C21 and 1 combination treated rats (Table 4-2), (Figure 4-2A). In total, 7 rats demonstrated partial MCAO at 60 min MCAO following inspection of the MRA scan: 1 Vehicle (aCSF), 2 Ang-(1-7), 3 C21 and 2 Ang-(1-7) + C21 rats (Table 4-2), (Figure 4-2B). MRA performed at day 7 reperfusion indicated that all animals were reperfused adequately. Moreover, MRI-T_2 revealed that 2 animals had ICH and one animal showed signs of ventricular enlargement

at day 7 reperfusion, indicating infection caused by the presence of the cannula (Table 4-2), (Figure 4-2C).

Table 4-2 Exclusion criteria and excluded animals per treatment group.

	Vehicle	Ang-(1-7)	C21	C21 + Ang-(1-7)	Total N
Surviving animals	**17**	**19**	**17**	**15**	**68**
Cannula not in place	3	3	1	1	8
Partial MCAO	1	2	3	2	7
MCA not reperfused at day 7	0	0	0	0	0
Haemorrhage present at day 7	0	1	0	1	2
Signs of infection at day 7	0	0	1	0	1
Total exclusions	**4**	**6**	**5**	**4**	**19**

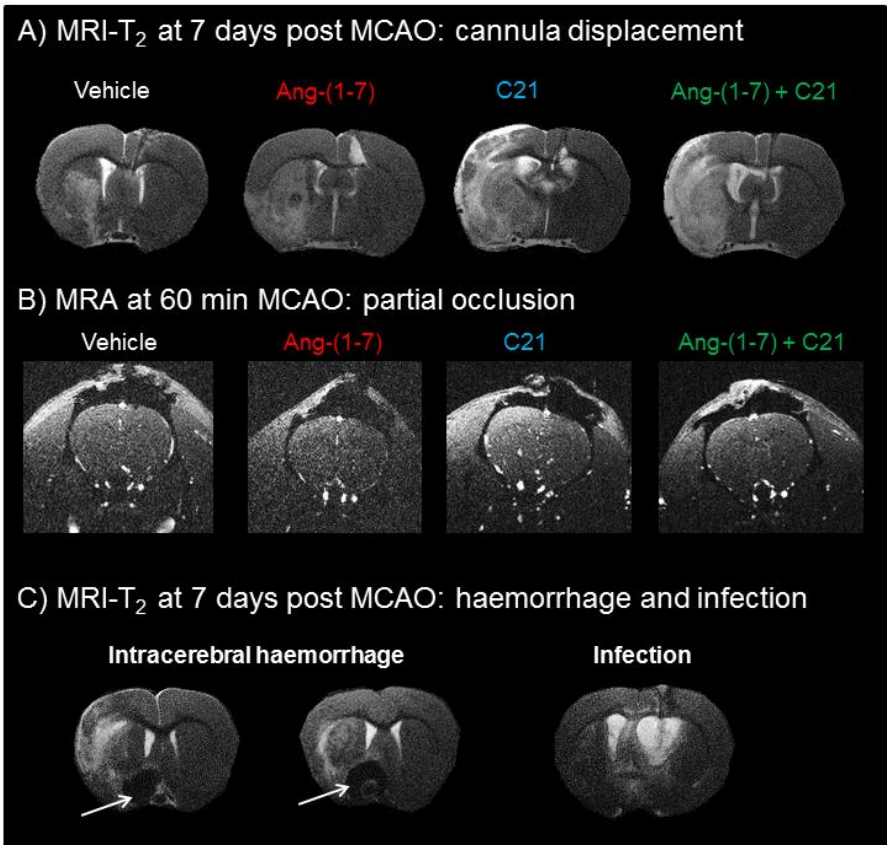

Figure 4-2 Representative images of excluded animals per treatment group. A) Cannula displacement. MRI-T_2 at 7 days post MCAO displaying cannula displacement in the rightlateral cerebral ventricle. **B) Partial occlusions.** MRA at 60 min MCAO showing indications of partial occlusion of the left MCA. **C) ICH and infection.** MRI-T_2 at 7 days post MCAO indicating ICH of the MCA outlined in green and animal with ventricular infection.

4.3.3 Ischaemic lesion evolution during MCAO

4.3.3.1 Variability in baseline lesion volume prior to treatment

MCAO was induced for 90 min and DWI scanning performed at 30 min and 60 min MCAO to examine ischaemic lesion volume evolution prior to treatment. At 30 min MCAO (prior to therapy), all animals exhibited an ischaemic lesion comparable between treatment destined groups; Vehicle (aCSF): 141.8±55.3mm^3; Ang-(1-7): 145.9±57.4mm^3; C21: 106±36.3mm^3 and Ang-(1-7) + C21: 104.3±45.6mm^3 (P>0.05), (Figure 4-3A).

At 60 min MCAO (prior to therapy), lesion volumes were not significantly different between treatment destined groups; however, there was a trend for C21 destined rats to start with smaller lesions compared to the Ang-(1-7) group (P=0.07). Lesion volumes were as follows; Vehicle (aCSF): 171.8±50.8mm^3; Ang-(1-7): 187.1±67.7mm^3; C21: 131.1±41.5mm^3 and Ang-(1-7) + C21: 133.9±63.2mm^3 (P>0.05), (Figure 4-3B). Data indicate that prior to therapy; ADC ischaemic lesions at 30 min and 60 min MCAO are variable within and between groups as indicated by high S.D.

4.3.3.2 MCAO duration increases lesion size

MCAO duration prior to therapy increased ischaemic lesion volume within treatment destined groups for Vehicle (aCSF) (141.8±55.3mm^3 vs 171.8±50.8mm^3); Ang-(1-7) (145.9±57.4mm^3 vs 187.1±67.7mm^3); C21 (106.0±36.3mm^3 vs 131.1±41.5mm^3); Ang-(1-7) + C21 (104.3±45.6mm^3 vs 133.9±63.2mm^3), (Figure 4-4). Figure 4-4 emphasises the variability in ischaemic lesion evolution amongst and between groups prior to therapy.

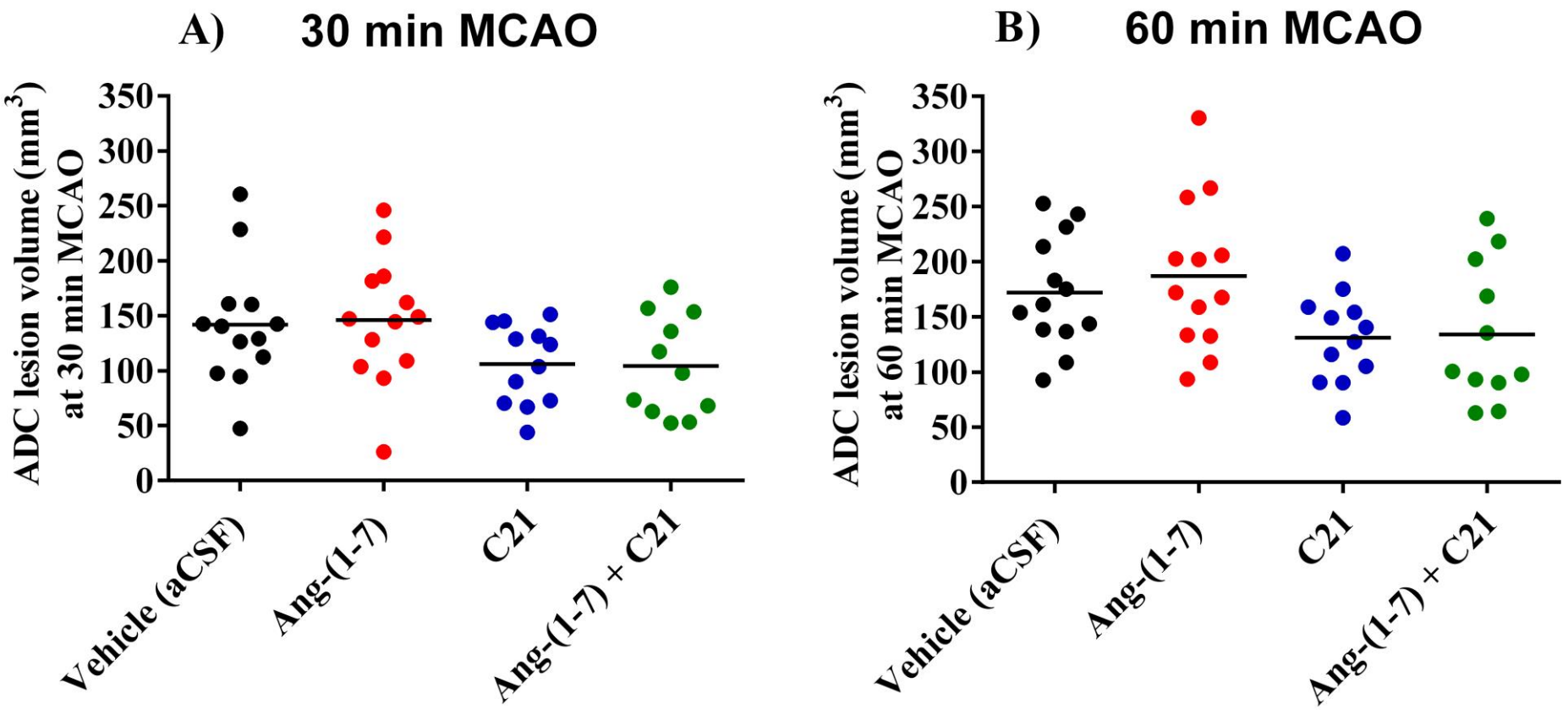

Figure 4-3 Ischaemic lesion during MCAO and prior to therapy. A) 30 min MCAO; B) 60 min MCAO. Lesion volume did not differ between groups at 30 min or 60 min MCAO. Data depicts ADC lesion volume (mm^3) for Vehicle (aCSF) (n=13), Ang-(1-7) (n=13), C21 (n=12) and Ang-(1-7) + C21 (n=11) treatment destined animals. Data were analysed using one-way ANOVA, $P<0.05$ was considered statistically significant. Horizontal bars represent the mean.

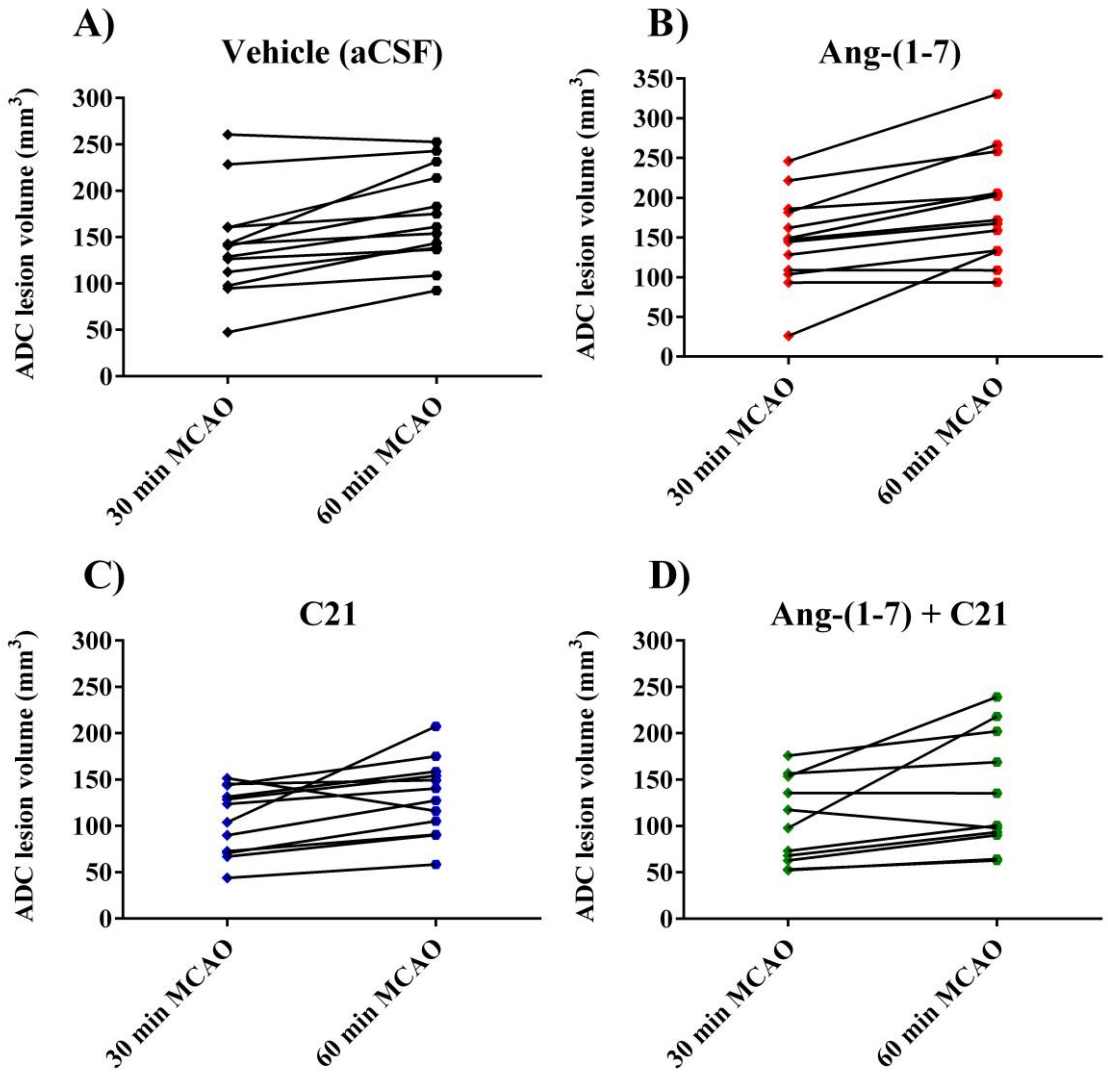

Figure 4-4 Ischaemic lesion evolution within treatment destined groups during MCAO. Data indicate that during ischaemia, ADC lesion increased from 30 min to 60 min MCAO for Vehicle (aCSF) (n=13), Ang-(1-7) (n=13), C21 (n=12) and Ang-(1-7) + C21 (n=11) destined rats. Figure depicts lesion (mm^3) evolution for each individual animal per group, highlighting lesion variability prior to therapy. Data are presented as ADC lesion volume (mm^3) for each individual animal.

4.3.4 Final infarct volume 7 days post MCAO

4.3.4.1 Inter-rater assessment of reproducibility

MRI-T_2 weighted imaging was performed at day 7 to assess final infarct volume and analysed by delineating hyperintense infarct areas. Assessment of reproducibility in delineating infarct volume was carried out by two independent investigators and analysed using parametric Pearson correlation and Bland-Altman plot (Figure 4-5). Data showed that Subject 1 (most experienced) and Subject 2 (least experienced) analyses significantly correlated (r=0.98, P<0.0001), (Figure 4-5A). Moreover, Bland-Altman analysis indicated an acceptable final infarct volume analysis agreement with a bias of 8.3mm^3 (Subject 1 scored a higher infarct volume on an average of 8.3mm^3 than Subject 2) and limits of agreement between -12.3 and 29.0mm^3. Subject 1 consistently scored higher volumes in comparison to Subject 2 as demonstrated by increased values falling on the positive axis (Figure 4-5B). The average of the two analyses was used to determine final infarct volume for each animal.

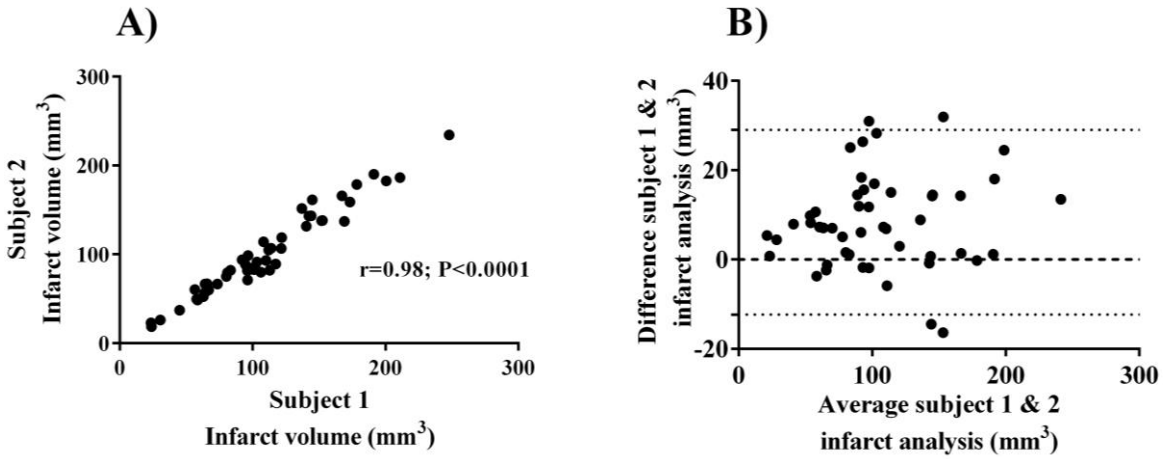

Figure 4-5 Inter-rater variability in infarct volume measurement 7 days post 90 min MCAO. A) Correlation between Subject 1 and Subject 2 analysis. Infarct volume measurements from both Subjects 1 and 2 significantly correlated (r=0.98; P<0.0001). **B) Bland-Altman analysis displaying difference and average in infarct analysis between Subjects**. Analysis agreement had a bias of 8.3mm^3 and limits of agreement were between -12.3 and 29.0mm^3, marked in the figure. Data were analysed using Peason parametric correlation coefficient, P<0.05 was considered statistically significant.

4.3.4.2 Treatment does not impact final infarct volume at 7 days post MCAO

There were no significant differences in final infarct volume at day 7 between treatment groups; Vehicle (aCSF): 130.6±50.7mm^3, Ang-(1-7): 111.3±47.4mm^3; C21: 91.7±40.6mm^3 and Ang-(1-7) + C21: 85.9±48.4mm^3 (P>0.05), (Figure 4-6).

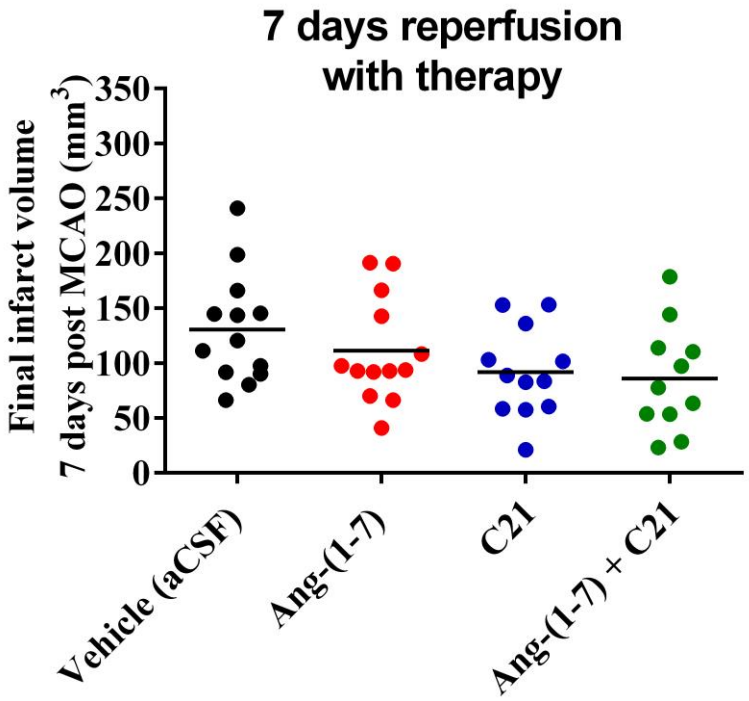

Figure 4-6 Final infarct volume at 7 days post 90 min MCAO. Final infarct was comparable amongst groups following 7 days reperfusion with therapy (P>0.05). Data indicates final infarct (mm^3) for Vehicle (aCSF; n=13), Ang-(1-7) (n=13), C21 (n=12) and Ang-(1-7) + C21 (n=11) treated animals. Data were analysed using one-way ANOVA, P<0.05 was considered statistically significant. Horizontal bars represent the mean.

4.3.5 Impact of treatment on the extent of tissue salvage following reperfusion

4.3.5.1 Reperfusion with and without therapy significantly decreases lesion volume

Reperfusion resulted in a significant decrease in lesion size from 60 min MCAO to 7 days post MCAO with or without therapy in all groups. Vehicle (aCSF): 171.8±50.8mm^3 to 130.6±50.7mm^3 (P<0.0001), (Figure 4-7A); Ang-(1-7): 187.1±67.7mm^3 to 111.3±47.4mm^3 (P<0.0001), (Figure 4-7B); C21: 131.1±41.5mm^3 to 91.7±40.6mm^3 (P<0.0001), (Figure 4-7C), and Ang-(1-7) + C21: 133.9±63.2mm^3 to 85.9±48.4mm^3 (P<0.0001), (Figure 4-7D). To determine therapy effects and account for variability in baseline lesion volume (60 min) prior to treatment, the change in lesion volume was assessed for each individual animal.

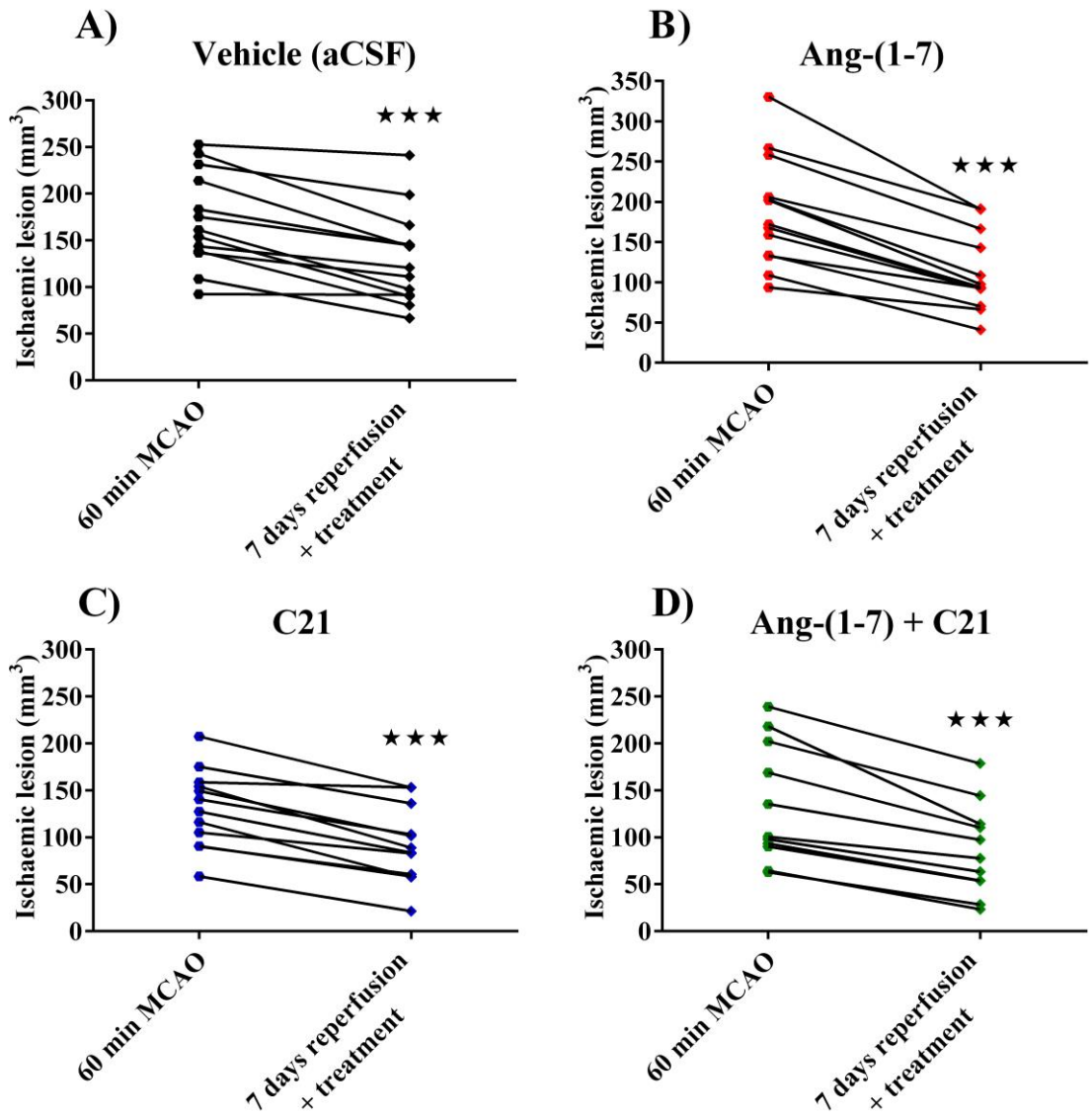

Figure 4-7 Ischaemic lesion evolution from 60 min MCAO to 7 days post 90 min MCAO within treatment groups. A) Vehicle (aCSF); B) Ang-(1-7); C) C21 and D) Ang-(1-7) + C21. Reperfusion with and without treatment significantly attenuated ischaemic lesion volume from 60 min MCAO to 7 days post MCAO for all groups (P<0.0001). Data indicates ischaemic lesion (mm^3) evolution for Vehicle (aCSF; n=13), Ang-(1-7) (n=13), C21 (n=12) and Ang-(1-7) + C21 (n=11) treated animals. Data were analysed using paired Student's t test. ***P<0.0001.

4.3.5.2 Ang-(1-7) with reperfusion increases tissue salvage 7 days post MCAO

When normalising data to lesion size at 60 min MCAO for each animal, Ang-(1-7) infusion with reperfusion for 7 days significantly decreased ischaemic lesion volume to a greater extent than aCSF alone [41.2±10.2% vs 24.5±14.1% reduction, (P=0.01)], (Figure 4-8A). Likewise, Ang-(1-7) + C21 showed a trend to attenuate lesion volume when compared to aCSF alone, however, it did not reach significance [38.5±12.9% vs 24.5±14.1%, (P=0.052)]. On the other hand, C21 showed no difference in ischaemic lesion progression compared to Vehicle (aCSF) [32.6±15.2% vs 24.5±14.1% reduction, (P=0.368)], (Figure 4-8A).

Data were also presented as absolute change in ischaemic lesion from 60 min MCAO to 7 days reperfusion (Figure 4-8B). Results show that Ang-(1-7) infusion with reperfusion significantly decreased absolute ischaemic lesion volume compared to aCSF [41.2±23.6mm^3 vs 75.8±28.4mm^3 reduction, (P=0.0023)], C21 [39.4±16.3mm^3 vs 75.8±28.4mm^3reduction, (P=0.0016)] and Ang-(1-7) + C21 [48.0±22.1mm^3 vs 75.8±28.4mm^3reduction, (P=0.0016)] treated groups. C21 treatment did not differ from combination group (P>0.05). Additionally, C21 and combination groups did not differ from Vehicle (aCSF) group (P>0.05), (Figure 4-8B).

Figures 4-9 to 12 show ADC map at 60 min and corresponding MRI-T_2 scan at 7 days for the median animal in the Vehicle (aCSF), Ang-(1-7), C21 and Ang-(1-7) + C21 treatment groups determined from Figure 4-8A, respectively.

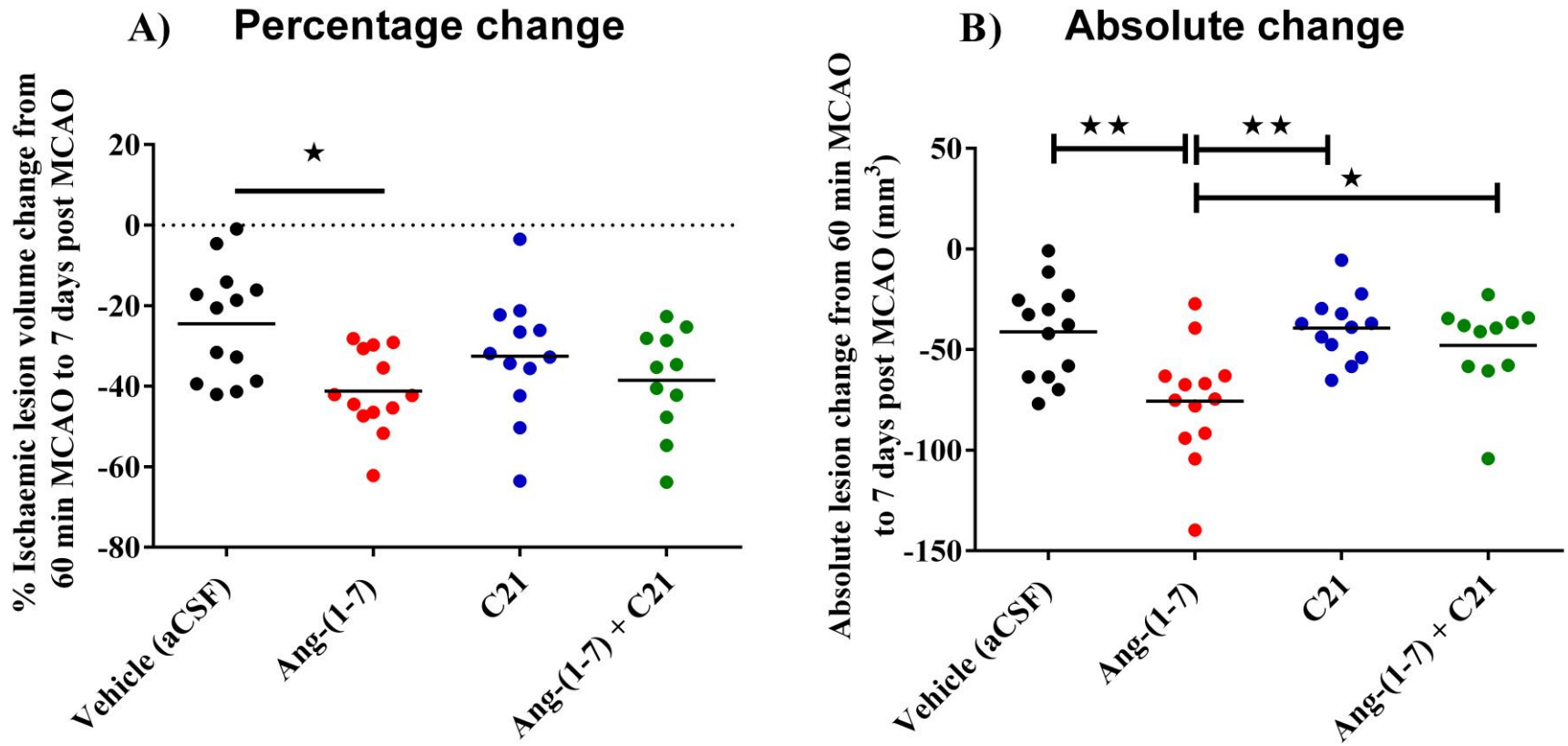

Figure 4-8 Ischaemic lesion evolution from 60 min MCAO to 7 days post 90 min MCAO following therapy. A) % ischaemic lesion change; B) Absolute ischaemic lesion change. Ang-(1-7) treatment along with reperfusion significantly decreased % lesion volume from 60 min MCAO compared to Vehicle (aCSF). In addition, Ang-(1-7) treatment significantly decreased absolute lesion volume (mm^3) from 60 min MCAO compared to Vehicle (aCSF) ($P<0.01$), C21 ($P<0.01$) and Ang-(1-7) + C21 ($P<0.05$). Data depicts % or absolute (mm^3) lesion volume change for Vehicle (aCSF) (n=13), Ang-(1-7) (n=13), C21 (n=12) and Ang-(1-7) + C21 (n=11) treated animals. Data were analysed using one-way ANOVA with Tukey's post hoc analysis, $P<0.05$ was considered statistically significant. Horizontal bars represent the mean. *$P<0.05$; **$P<0.01$.

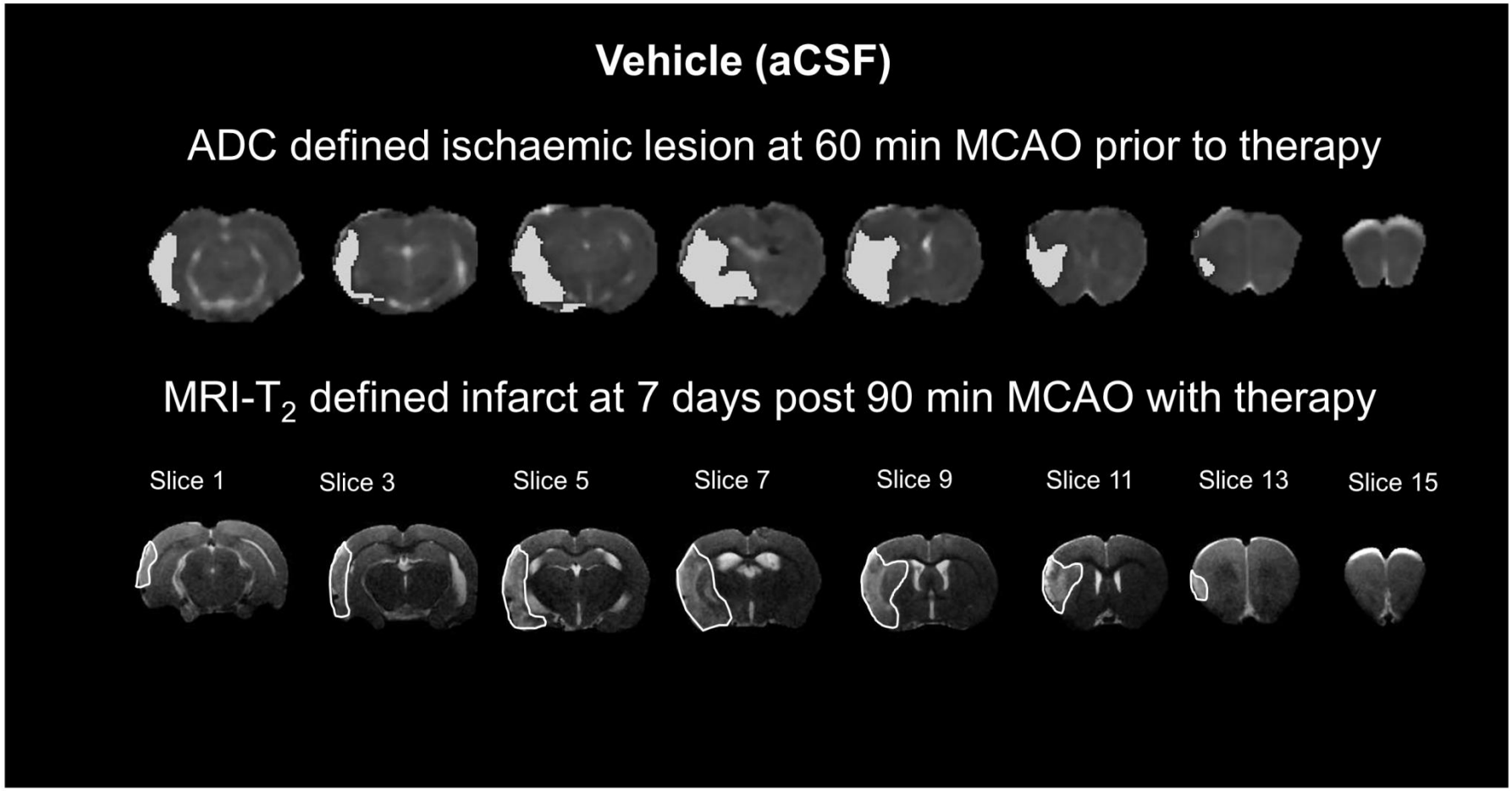

Figure 4-9 Representative image of ischaemic lesion evolution between 60 min MCAO to 7 days post 90 min MCAO for Vehicle (aCSF) treated median animal. Top images depict the ADC ischaemic lesion, highlighted in white, at 60 min MCAO prior to therapy across 8 coronal levels on the top. The bottom images show the corresponding MRI-T_2 final infarct at 7 days post 90 min MCAO, highlighted in white.

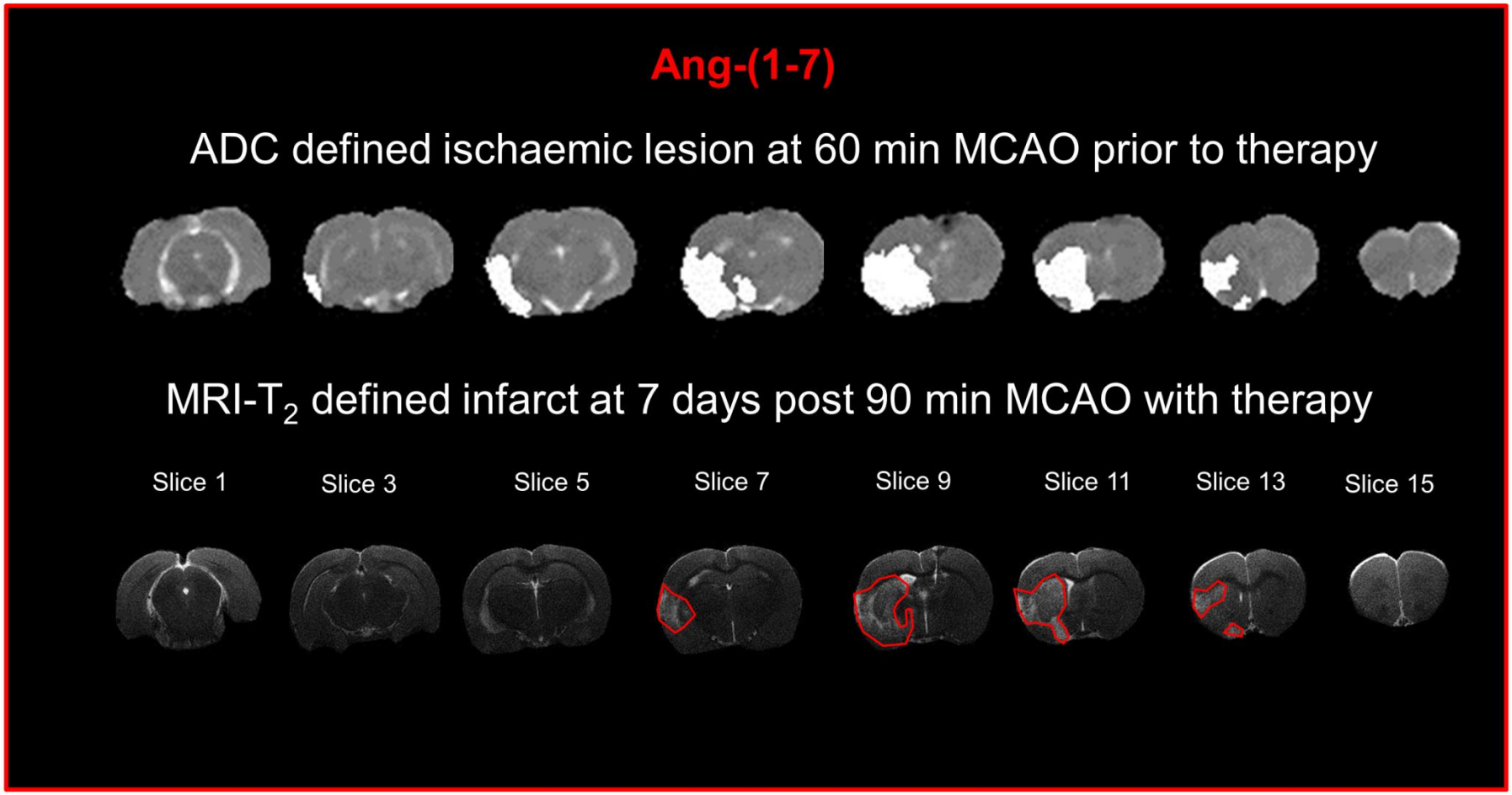

Figure 4-10 Representative image of ischaemic lesion evolution between 60 min MCAO to 7 days post 90 min MCAO for Ang-(1-7) treated median animal. Images show ADC ischaemic lesion, highlighted in white, at 60 min MCAO prior to therapy across 8 coronal levels on the top. The bottom images show the corresponding MRI-T_2 final infarct at 7 days post 90 min MCAO, highlighted in red.

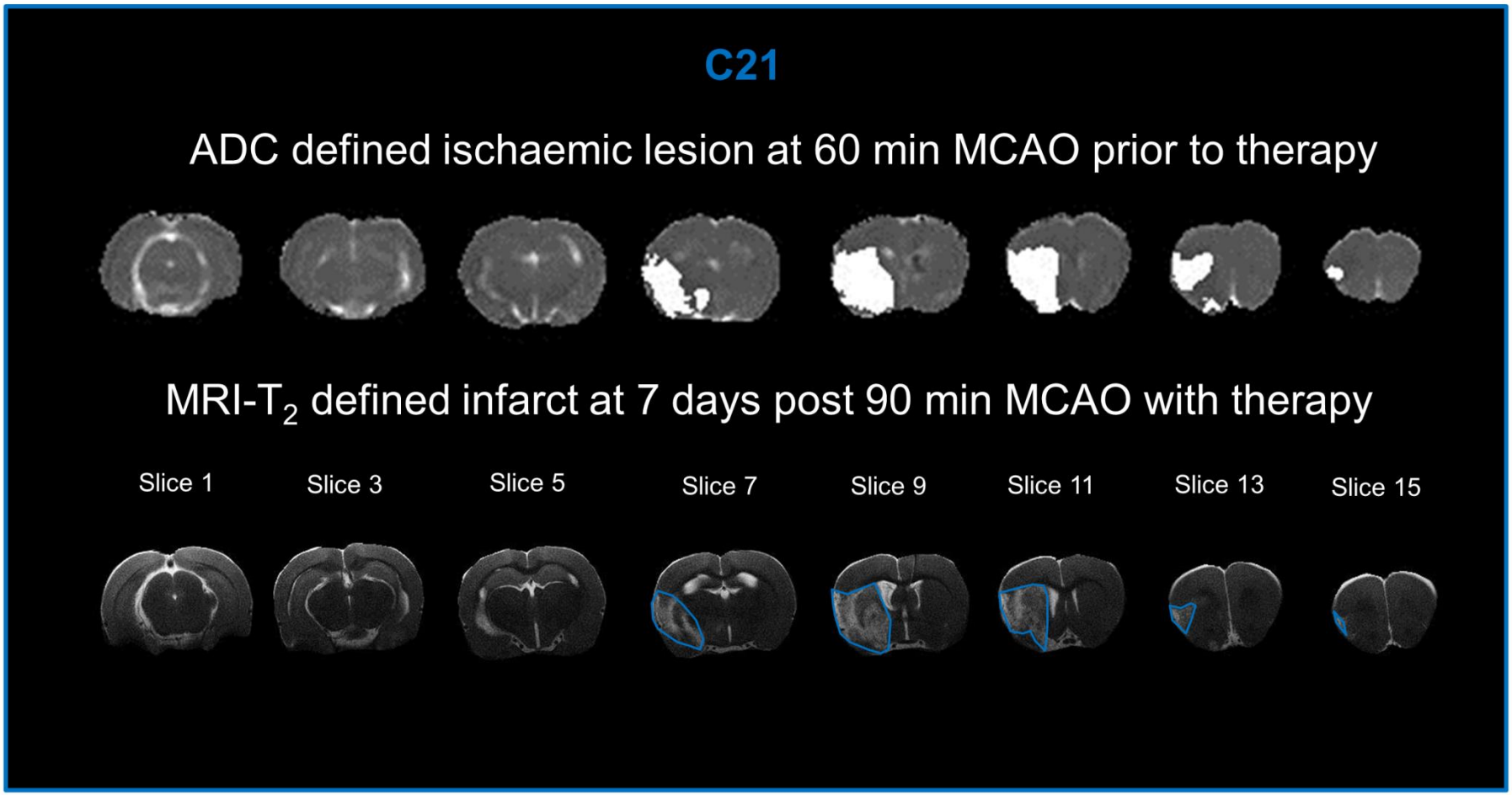

Figure 4-11 Representative image of ischaemic lesion evolution between 60 min MCAO to 7 days post 90 min MCAO for C21 treated median animal. Images show ADC ischaemic lesion, highlighted in white, at 60 min MCAO prior to therapy across 8 coronal levels on the top. The bottom images show the corresponding MRI-T_2 final infarct at 7 days post 90 min MCAO, highlighted in blue.

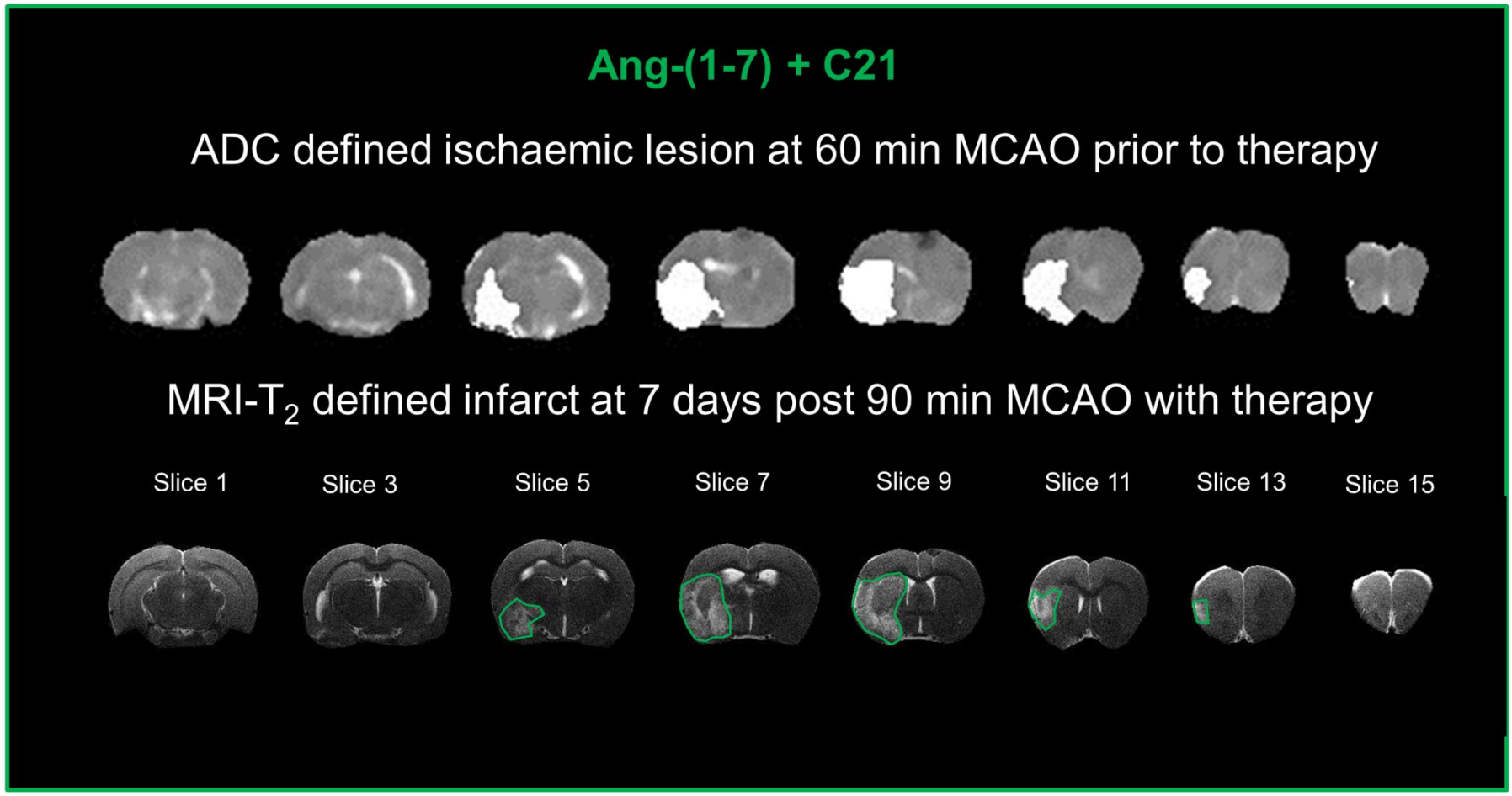

Figure 4-12 Representative image of ischaemic lesion evolution between 60 min MCAO to 7 days post 90 min MCAO for Ang-(1-7) + C21 treated median animal. Images show ADC ischaemic lesion, highlighted in white, at 60 min MCAO prior to therapy across 8 coronal levels on the top. The bottom images show the corresponding MRI-T_2 final infarct at 7 days post 90 min MCAO, highlighted in green.

4.3.6 Treatment does not have any effect on systolic blood pressure.

Prior to MCAO and treatment, systolic BP was comparable amongst groups (P>0.05), (Figure 4-13A). Similarly, at day 7 post MCAO with treatment, BP was not significantly different between groups; Vehicle (aCSF): 129±23mmHg; Ang-(1-7): 118±21mmHg, C21: 114±27mmHg, Ang-(1-7) + C21: 125±27mmHg (P>0.05), (Figure 4-13B). BP change from pre to post MCAO did not differ amongst groups; Vehicle (aCSF): 15.20±25mmHg, Ang-(1-7): 15.58±25mmHg, C21: 8.427±22mmHg, Ang-(1-7) + C21: 12.13±33mmHg (P>0.05), Figure 4-13C). At day 7, BP could not be obtained for two animals, one in Vehicle (aCSF) and one in C21 treated groups due to the rats being highly stressed during measurements.

4.3.7 Treatment does not improve neurological function

Neurological score was assessed prior to MCAO and at 3 and 7 days post-MCAO. Prior to MCAO, all animals scored a maximum of 18 points and were therefore, included in the study (Figure 4-14A). Day 3 post MCAO, neurological score decreased for all rats, indicating a neurological deficit induced by MCAO; however, data were not significantly different between groups: Vehicle (aCSF), 11.0 (IQR: 10.0; 12.5); Ang-(1-7), 12.0 (IQR: 10.5; 12.5); C21, 11.0 (IQR: 10.3; 12.0); Ang-(1-7) + C21, 11.0 (IQR: 10.0; 11.0); (P>0.05), (Figure 4-14B). At day 7 post MCAO, there was an improvement in neurological score for all groups but no statistically differences observed between groups: Vehicle (aCSF), 14.00 (IQR: 11; 15); Ang-(1-7), 15 (IQR: 14; 15); C21, 14 (IQR: 12.3; 15.8); Ang-(1-7) + C21, 14 (IQR: 12; 15); (P>0.05), (Figure 4-14C).

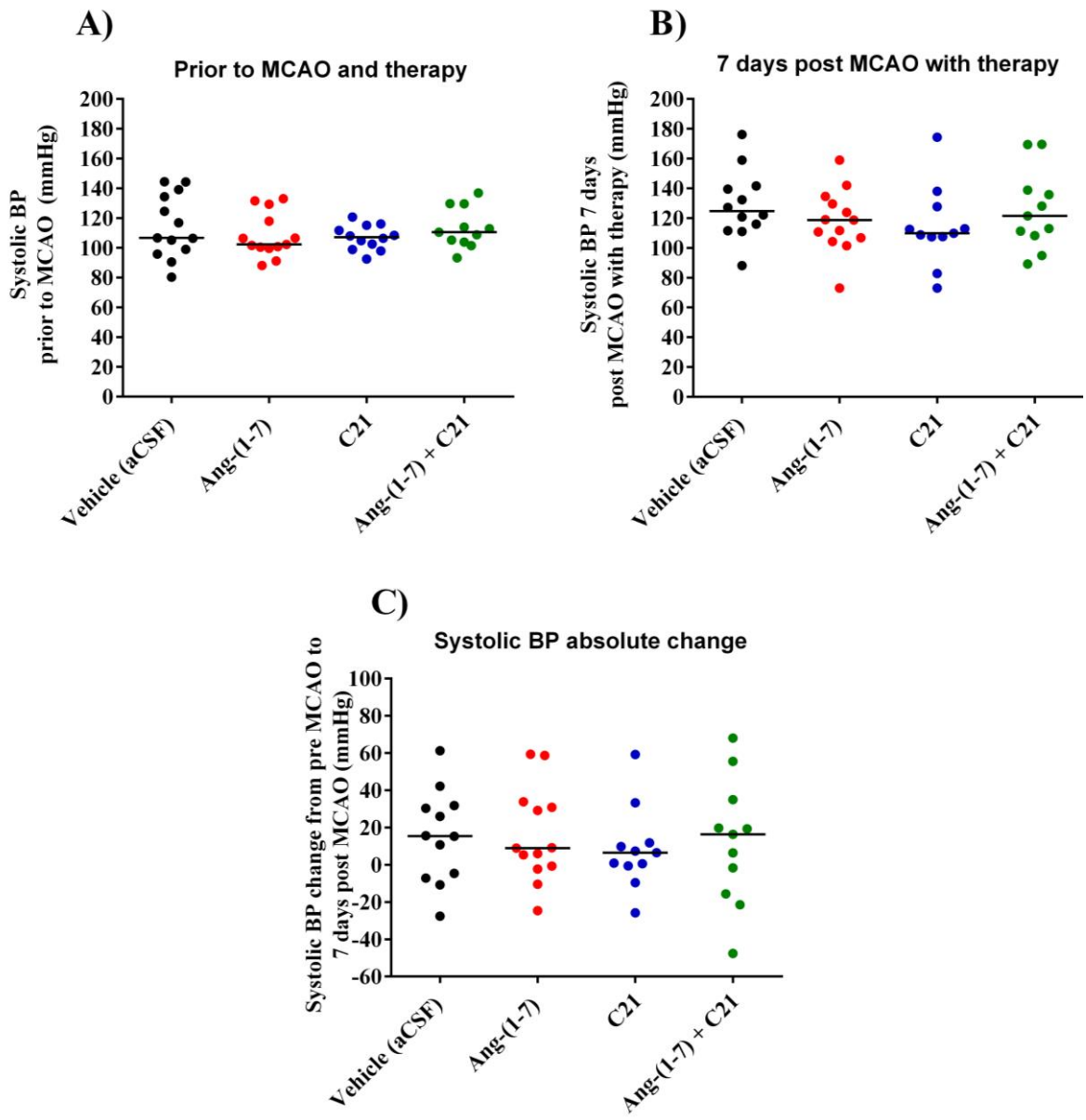

Figure 4-13 Systolic BP. A) Systolic BP prior to MCAO and therapy; B) Systolic BP 7 days post MCAO with therapy; C) Systolic BP absolute change from pre MCAO to 7 days post MCAO with therapy. There were no differences in systolic BP prior to MCAO or post MCAO with therapy between groups (P>0.05). In addition, BP change over time was comparable amongst treatment groups (P>0.05). Data depicts BP values for Vehicle (aCSF; n=13-12), Ang-(1-7) (n=13), C21 (n=12-11) and Ang-(1-7) + C21 (n=11) treated animals. Data were analysed using one-way ANOVA, P<0.05 was considered statistically significant. Horizontal bars represent the mean.

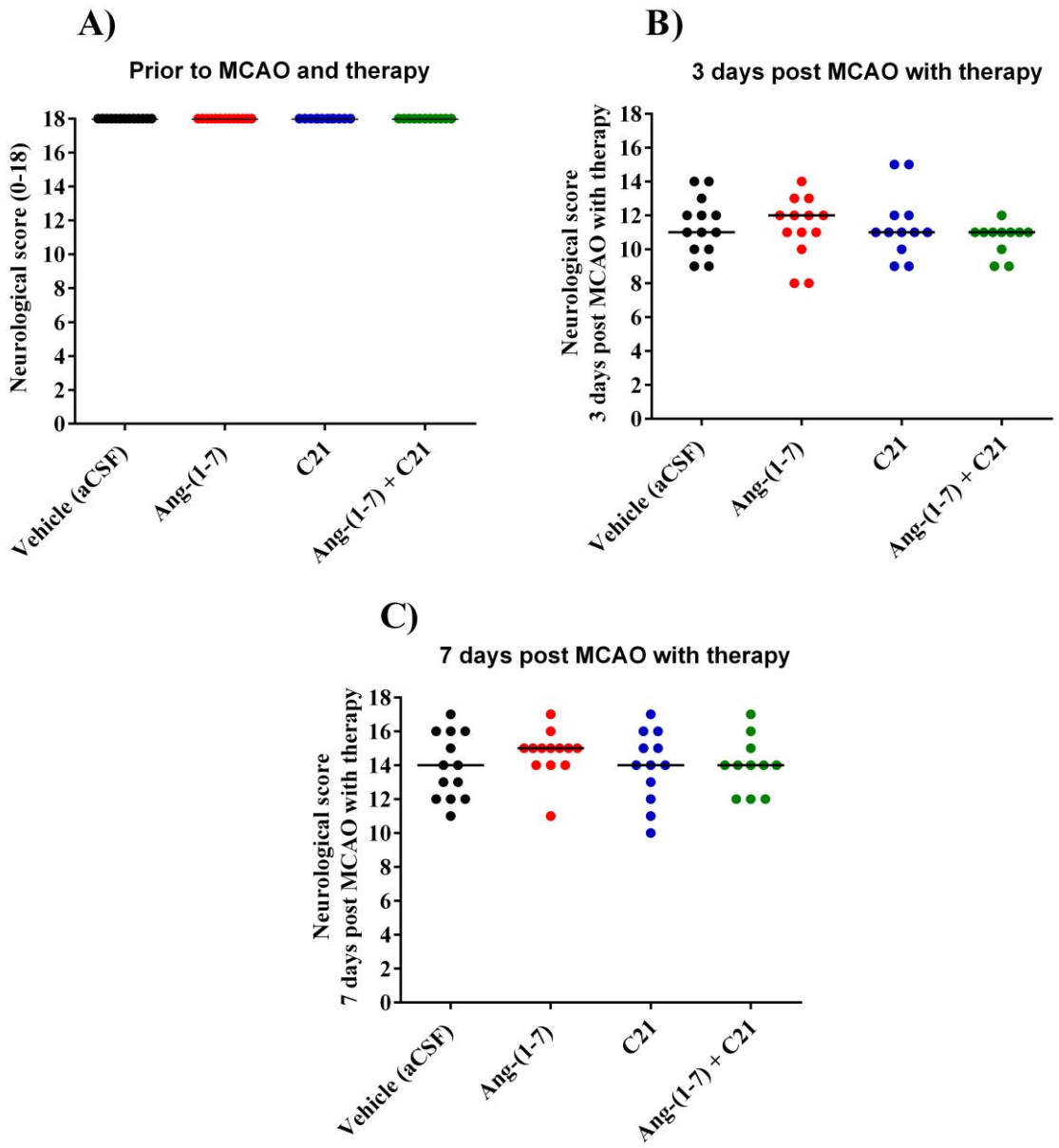

Figure 4-14 Neurological score. A) Prior to MCAO and therapy; B) 3 days post MCAO with therapy; C) 7 days post MCAO with therapy. All animals scored a maximum of 18 prior to MCAO and therapy**.** There were no significant differences in neurological between groups at 3 and 7 days post MCAO with therapy (P>0.05). Data depicts values forVehicle (aCSF; n=13), Ang-(1-7) (n=13), C21 (n=12) and Ang-(1-7) + C21 (n=11) treated animals. Data were analysed using non-parametric Kruskal-Wallis test, P<0.05 was considered statistically significant. Horizontal bars represent the mean.

4.4 Quantitative Real Time PCR

At day 7 following 90 min MCAO brain tissue from the peri-infarct region from Sham (n=7), MCAO-aCSF (n=9) and MCAO-Ang-(1-7) (n=9) treated animals were analysed for gene expression. *Ubc* was the most stable reference gene and selected for data normalisation (Chapter 2.16.2).

4.4.1 MCAO significantly decreases *Mas1* expression at 7 days reperfusion

To investigate potential alterations in classical and counter-regulatory axis components, gene expression for RAS receptors AT_{1A} (*Agtr1a*), AT_2R (*Atgr2*) *MasR* (*Mas1*) and enzymes *ACE* (*Ace*) and *ACE2* (*Ace2*) were assessed. Moreover, B_2R (*Bdkrb2*) gene expression was evaluated due to reports that Ang-(1-7)'s effects may be partly mediated by B_2R signalling (Lu et al., 2008).

Following 90 min MCAO and 7 days reperfusion, the expression of *Atgr1a* was comparable to sham treatment and not significantly different between vehicle and Ang-(1-7) treated rats (Figure 4-15A), (P>0.05). Conversely, *Atgr2* levels were significantly increased in control treated rats following MCAO when compared to Sham [-4.5±1.6 vs -8.0±1.4 (P=0.002)], (Figure 4-15B) while Ang-(1-7) showed a trend to attenuate this increase (-6.4±2.1), (Figure 4-15B). Interestingly, *Mas1* significantly decreased following MCAO in both Vehicle (aCSF) and Ang-(1-7) treated groups compared to Sham [-4.4±1.0 vs -2.7±0.8 (P=0.02); -4.2±1.5 vs -2.7±0.8 (P=0.046); respectively], (Figure 4-15C).

Ace and *Ace2* expression was similar to Sham levels following MCAO in both Vehicle and Ang-(1-7) treated groups (P>0.05), (Figure 4-15D&E). Similarly, *Bdkrb2* expression was comparable to Sham animals following MCAO (P>0.05), (Figure 4-15F).

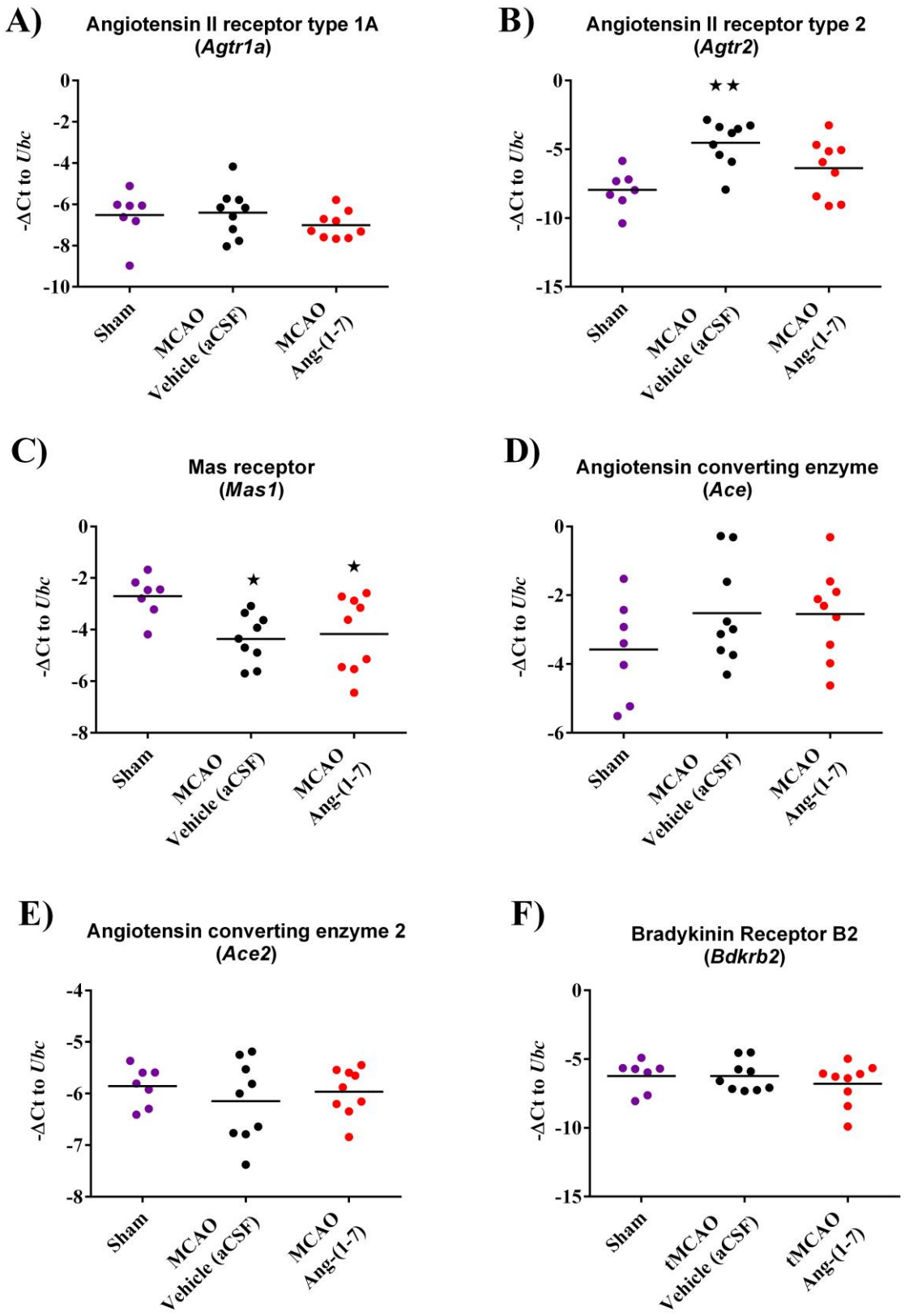

Figure 4-15 RAS components and *B$_2$R* gene expression 7 days post 90 min MCAO. A) *Atgr1a*; B) *Atgr2r*; C) *Mas1*; D) *Ace*; E) *Ace2* and F) *Bdkrb2*. MCAO significantly upregulates *Atgr2r* in Vehicle (aCSF) treated animals only compared to Sham (P>0.05). *Mas1* is significantly downregulated following MCAO in both Vehicle (aCSF) and Ang-(1-7) treated animals compared to Sham (P>0.05). There were no differences between groups for *Atgr1a*, *Ace*, *Ace2* and *Bdkrb2*levels. Data were presented as -ΔCt normalised to *Ubc* for Sham (n=7); Vehicle (aCSF) (n=9) and Ang-(1-7) (n=9) treated animals in peri-infarct regions. Data were analysed using one-way ANOVA with Tukey's post-hoc test, P<0.05 was considered statistically significant. Horizontal bars represent the mean. *P<0.05; **P<0.01 compared to Sham.

4.4.2 *Ptgs2* and *Nfkb1* levels are unchanged following treatment

COX-2 (*Ptgs2*) was comparable to Sham levels following MCAO (P>0.05), (Figure 4-16A). Moreover, there were no differences between treatment groups for *NF-κB* (*Nfkb 1*) following MCAO (P>0.05), (Figure 4-16B).

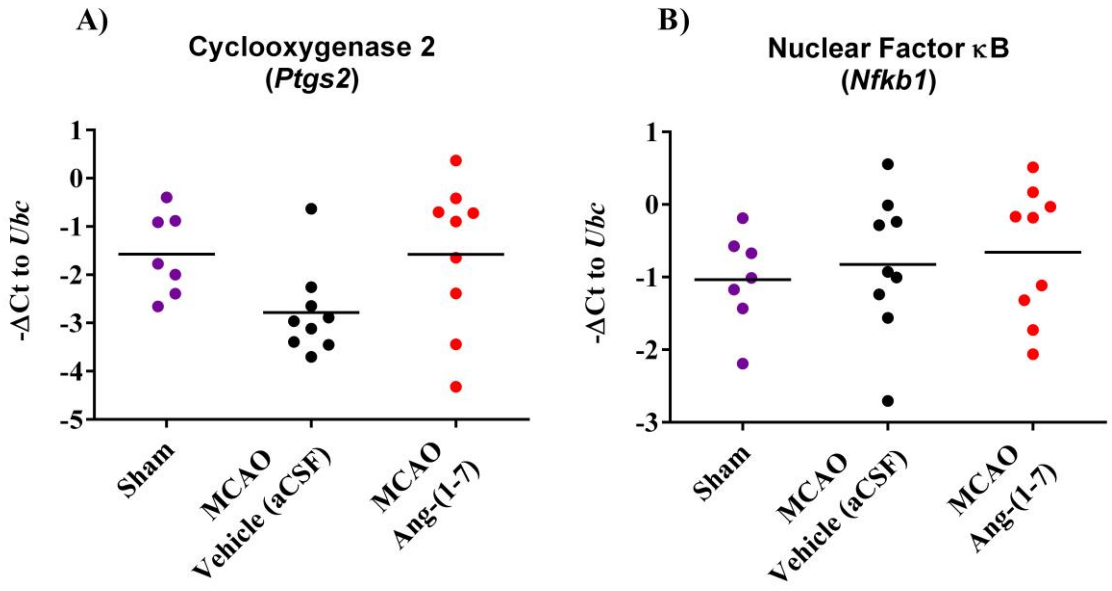

Figure 4-16 *COX-2* and *NF-κB* gene expression 7 days post 90 min MCAO. A) *Ptgs2*; B) *Nfkb1*. MCAO does not impact *Ptgs2* or *Nfkb1* expression at 7 days post MCAO in peri-infarct regions compared to Sham. Data were presented as -ΔCt normalised to *Ubc* for Sham (n=7); Vehicle (aCSF) (n=9) and Ang-(1-7) (n=9) treated animals in peri-infarct regions. Data were analysed using one-way ANOVA, P<0.05 was considered statistically significant. Horizontal bars represent the mean.

4.4.3 Ang-(1-7) significantly attenuates *Nox1* expression when compared to Vehicle (aCSF) treated animals

Nox1 expression was significantly decreased in Vehicle (aCSF) treated animals following MCAO when compared to Sham group [-7.8±1.0 vs -6.5±0.6 (P=0.04)]. In contrast, Ang-(1-7) treatment attenuated this decrease with levels similar to that observed in sham rats [-6.6±1.2 vs -7.8±1.0 (P=0.04)], (Figure 4-17A). *Nox2* levels were unchanged between groups (P>0.05), (Figure 4-17B).

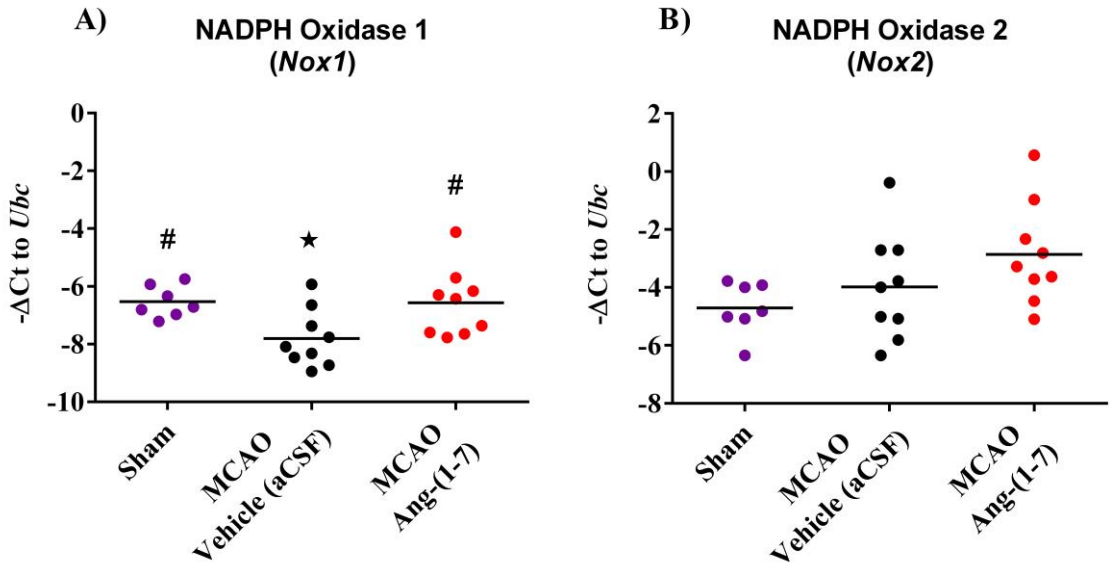

Figure 4-17 *NOX* type 1 and 2 gene expression 7 days post 90 min MCAO. A) *Nox1*; B) *Nox2*. MCAO-Vehicle (aCSF) significantly downregulated *Nox1* expression compared Sham (P<0.05) whereas MCAO-Ang-(1-7) treatment significantly upregulated *Nox1* expression compared to MCAO-Vehicle therapy (P<0.05). MCAO did not alter *Nox2* expression compared to Sham (P>0.05). Data were presented as -ΔCt normalised to *Ubc* for Sham (n=7); Vehicle (aCSF; n=9) and Ang-(1-7) (n=9) treated animals in peri-infarct regions. Data were analysed using one-way ANOVA with Tukey's post-hoc test, P<0.05 was considered statistically significant. Horizontal bars represent the mean. *P<0.05 compared to Sham; #P<0.05 compared to MCAO-Vehicle (aCSF).

4.4.4 *Ccr5* expression is increased following transient MCAO

The expression of *Cxcr2* and *Ccr2* were unchanged in both vehicle and Ang-(1-7) treated rats following transient MCAO when compared to sham rats (P>0.05), (Figures 4-18A&B). In contrast, *Ccr5*, was shown to be significantly increased following MCAO in both Vehicle (aCSF) and Ang-(1-7) treatment groups when compared to Sham [-0.6±0.9 vs -2.3±0.8 (P=0.0009); -0.7±0.7 vs -2.3±0.8 (P=0.001), respectively], (Figure 4-18C).

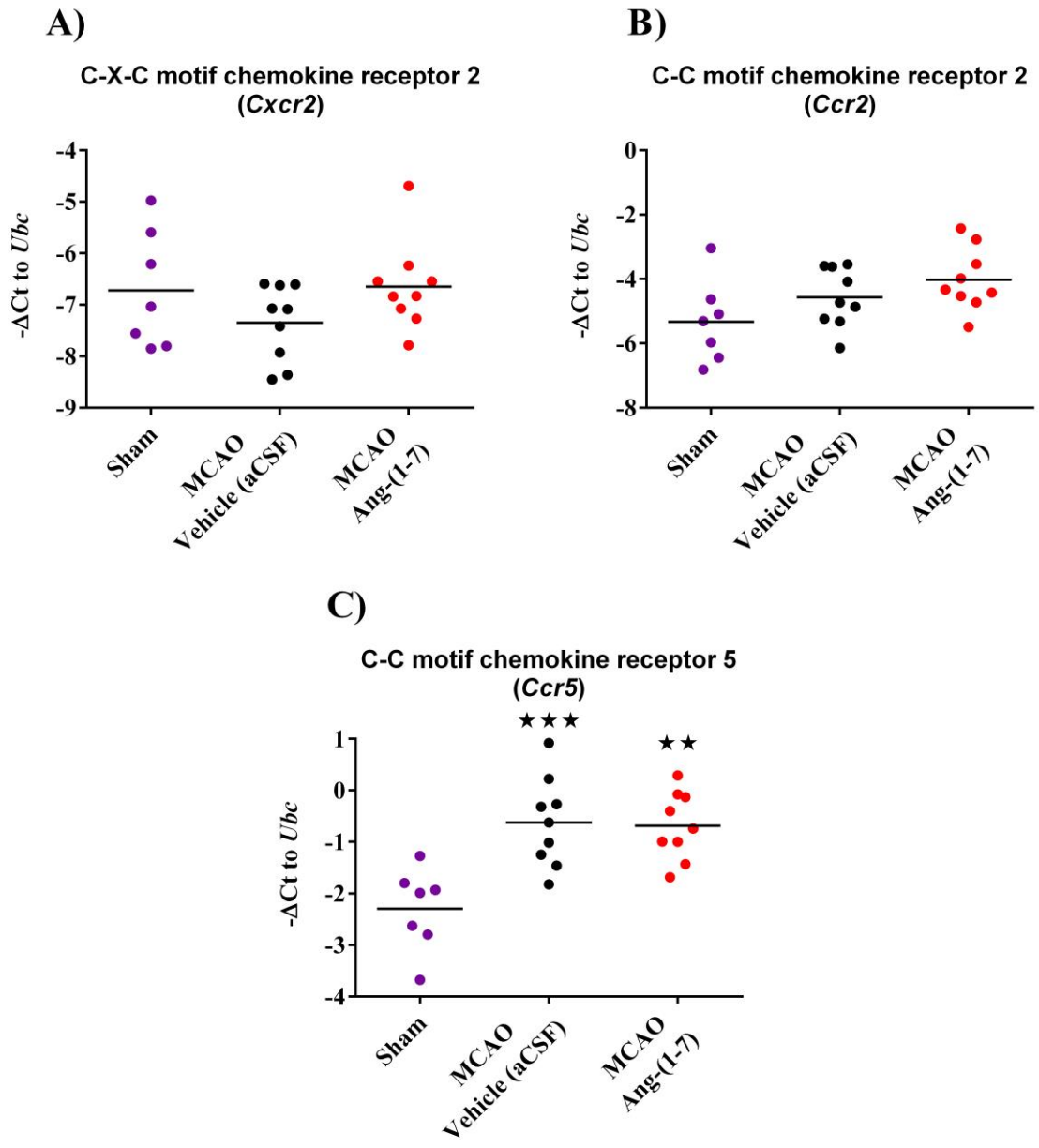

Figure 4-18 Chemokine receptor gene expression 7 days post 90 min MCAO. A) *Cxcr2*; B) *Ccr2*; C) *Ccr5*. MCAO did not alter *Cxcr2* or *Ccr2* expression compared to Sham animals (P>0.05). On the other hand, MCAO significantly upregulated *Ccr5* in both Vehicle (aCSF) and Ang-(1-7) treated animals compared to Sham (P<0.01). Data were presented as -ΔCt normalised to *Ubc* for Sham (n=7); Vehicle (aCSF; n=9) and Ang-(1-7) (n=9) treated animals in peri-infarct regions. Data were analysed using one-way ANOVA with Tukey's post-hoc test, P<0.05 was considered statistically significant. Horizontal bars represent the mean. **P<0.01, ***P<0.001 compared to Sham.

4.4.5 Treatment does not impact M1 type profile marker mRNA expression

Gene expression for M1 type markers *CD86* (*CD86*), *CD11b* (*Itgam*), *IL-1β (Il1b*), *IL-6* (*Il6*), *CCR7* (*Ccr7*) and *iNOS* (*Nos2*) were examined in peri-infarct regions in all samples. *CD86* levels was significantly increased following 90 min MCAO in both vehicle and Ang-(1-7) treated rats compared to Sham animals [-1.7±1.2 vs -5.1±1.1 ($P<0.001$); -2.1±1.4 vs -5.1±1.1 ($P<0.001$); respectively] (Figure 1-19A). Similarly, *Itgam* was upregulated following MCAO in both vehicle and Ang-(1-7) treated groups when compared to Sham rats [-0.6±1.3 vs -4.1±0.8 ($P<0.01$); -1.3±1.3 vs -4.1±0.8 ($P<0.01$); respectively], (Figure 4-19B). *Ccr7*, *Il6* and *Il1b* were unchanged following MCAO and Ang-(1-7) treatment had no effect ($P>0.05$), (Figure 4-19C, D, E). In contrast, *Nos2* expression was undetected in both Sham and MCAO peri-infarct brain tissue.

4.4.6 Treatment does not impact M2 type profile marker mRNA expression

Gene expression for M2 type markers *Arg1* (*Arg1*), *CD163* (*CD163*), *CCL22* (*Ccl22*), *TGF-β1* (*Tgfb1*) and *IL-10* (*Il10*) were examined in peri-infarct regions in all samples. *Arg1*, *CD163* and *Ccl22* levels were unchanged following MCAO in both vehicle and Ang-(1-7) treated rats when compared to sham treated rats ($P>0.05$), (Figure 4-20A, B, C) whereas *Il10* was not detected in peri-infarct regions in all rats. *Tgfb1* expression was significantly increased in Vehicle (aCSF) treated rats following 90 min MCAO compared to Sham [1.7±1.3 vs -0.3±0.6 ($P<0.05$)], (Figure 4-20D). In contrast, there was a trend for Ang-(1-7) treated group to attenuate *Tgfb1* levels (Figure 4-20D).

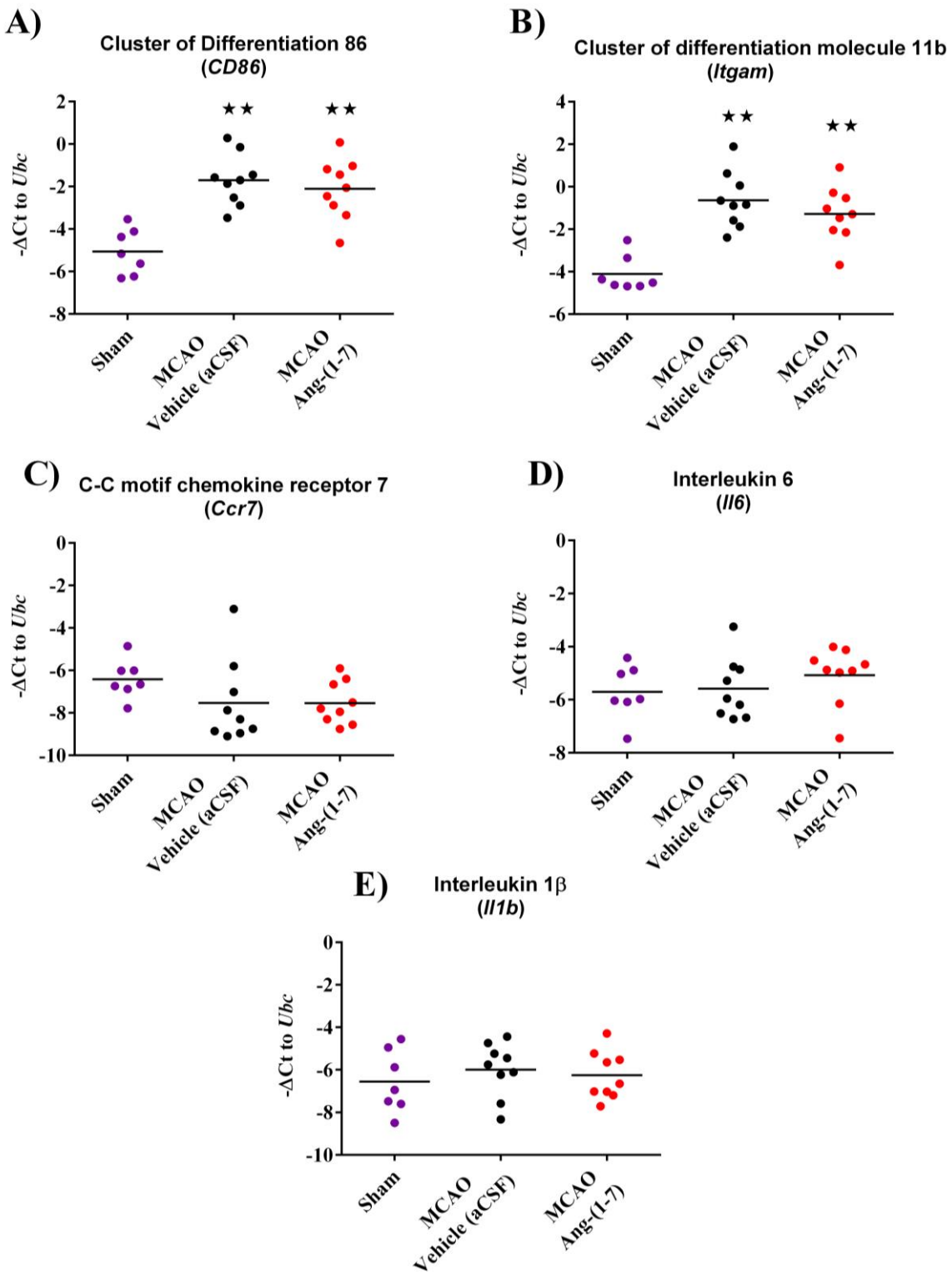

Figure 4-19 M1 type microglia/macrophage markers 7 days post 90 min MCAO. A) *CD86*; B) *Itgam*; B) *Ccr7*; C) *Il6* and D) *Il1b*. MCAO significantly upregulates *CD86* and *Itgam* compared to Sham treated animals (P<0.01). MCAO does not alter *Ccr7*, *Il6* or *Il1b* compared to Sham animals. Data were presented as -ΔCt normalised to *Ubc* for Sham (n=7); Vehicle (aCSF; n=9) and Ang-(1-7) (n=9) treated animals in peri-infarct regions. Data were analysed using one-way ANOVA with Tukey's post-hoc test, P<0.05 was considered statistically significant. Horizontal bars represent the mean. **P<0.01 compared to Sham.

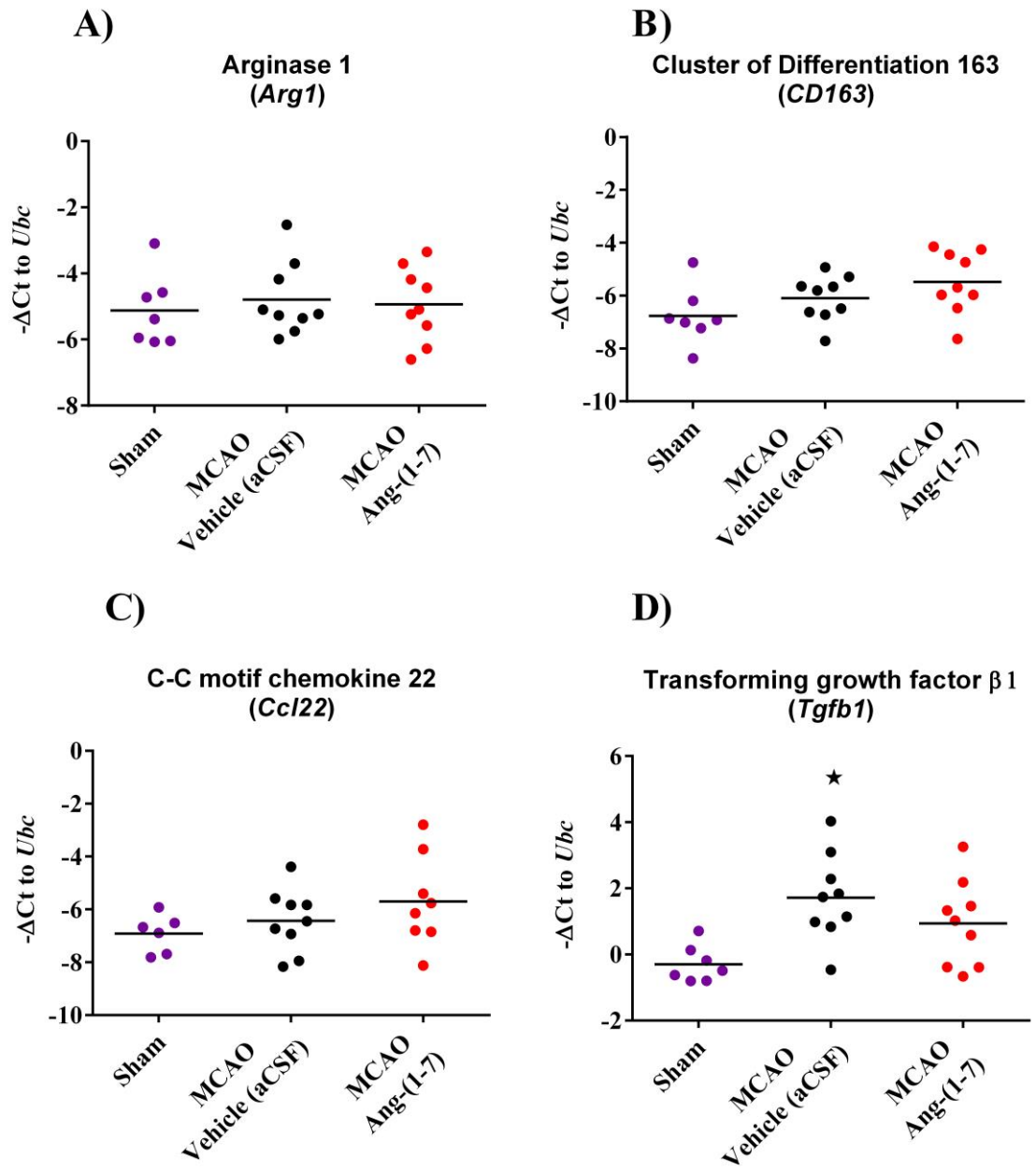

Figure 4-20 M2 type microglia/macrophage markers 7 days post 90 min MCAO. A) *Arg1*; B) *CD163*; C) *Ccl22* and D) *Tgfb1*. MCAO-Vehicle (aCSF) group significantly upregulated *Tgfb1* compared to Sham treated animals (P<0.01). MCAO did not alter *Arg1*, *CD163* or *Ccl22* compared to Sham animals. Data were presented as -ΔCt normalised to *Ubc* for Sham (n=7); Vehicle (aCSF; n=9) and Ang-(1-7) (n=9) treated animals in peri-infarct regions. Data were analysed using one-way ANOVA with Tukey's post-hoc test, P<0.05 was considered statistically significant. Horizontal bars represent the mean. *P<0.05 compared to Sham.

4.4.7 Assessment of IBA1$^+$ microglia

Immunohistochemistry was performed across coronal levels 3, 4 and 5 for Vehicle (aCSF) n=2), Ang-(1-7) (n=2), C21 (n=2) and Ang-(1-7) + C21 (n=2) treated groups. This data set provides a qualitative assessment of total IBA1$^+$ microglia per group.

Mean total IBA1$^+$ microglia number did not show an indication of Ang-(1-7) induced effects compared to other groups; Vehicle (aCSF): 259.0±1.5 n°/mm^2, Ang-(1-7): 260.0±79.4 n°/mm^2, C21: 260.0±79.4 n°/mm^{2}and Ang-(1-7) + C21: 225.7±33.8 n°/mm^2 treated animals (Figure 4-21A). Similarly, mean total IBA1$^+$ microglia number in the homotopic region of the contralateral hemisphere did not indicate a trend for an Ang-(1-7) induced effect compared to other groups; Vehicle (aCSF): 141.4±29.4 n°/mm^2, Ang-(1-7): 163.3±4.4 n°/mm^2, C21: 132.1±7.4 n°/mm^2, Ang-(1-7) + C21: 151.8±64.7 n°/mm^2 (Figure 4-21B). Results indicate higher numbers of total stained cells in the peri-infarct area compared to the homotopic contralateral region.

When assessing % activated IBA1$^+$ microglia from total numbers, values were comparable amongst groups in the peri-infarct area; Vehicle (aCSF): 95.2±1.1%, Ang-(1-7): 96.5±2.2%, C21: 99.2±0.4%, Ang-(1-7) + C21: 99.2±1.2% (Figure 4-22A). Similarly, % activated IBA1$^+$ in the homotopic contralateral region did not suggest an Ang-(1-7) induced effect compared to other groups; Vehicle (aCSF): 82.4±6.8%, Ang-(1-7): 77.2±8.4%, C21: 85.4±11.4%, Ang-(1-7) + C21: 78.3±5.4% (Figure 4-22B). Moreover, immunohistochemistry showed that at 7 days reperfusion, IBA1$^+$ microglia are mainly present within the ischaemic core and exhibiting an amoeboid/active phenotype (Figures 4-23 to 24).

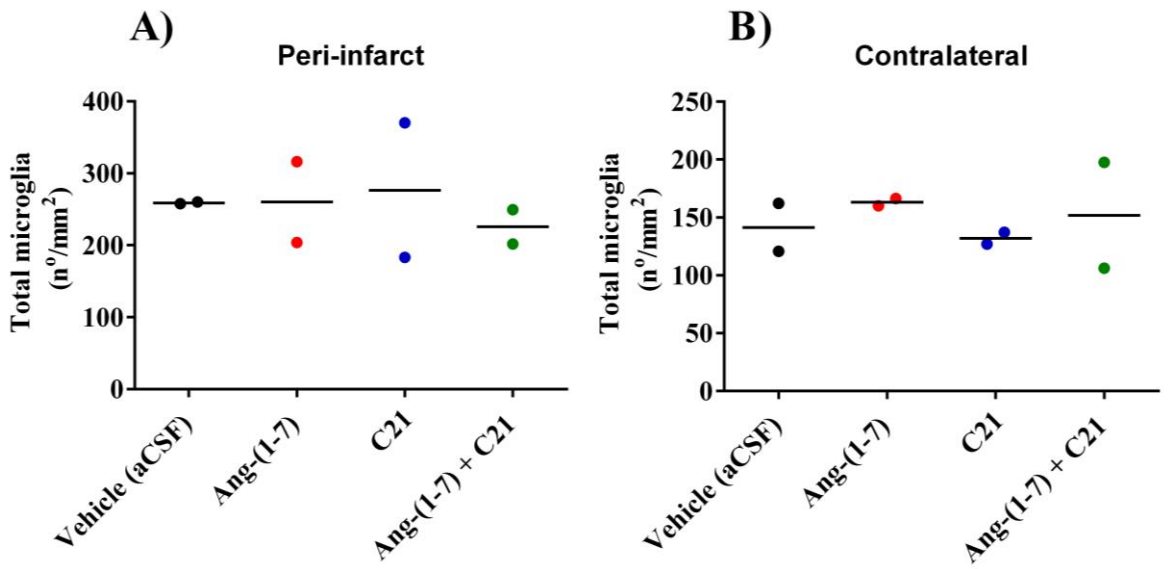

Figure 4-21 Total IBA1$^+$ microglia number in peri-infarct and contralateral regions 7 days post 90 min MCAO. A) Peri-infarct region; B) Homotopic contralateral region. Data shows total microglia number per mm^2 brain area for Vehicle (aCSF; n=2), Ang-(1-7) (n=2), C21 (n=2) and Ang-(1-7) + C21 (n=2) treated animals. Horizontal bar represents the mean.

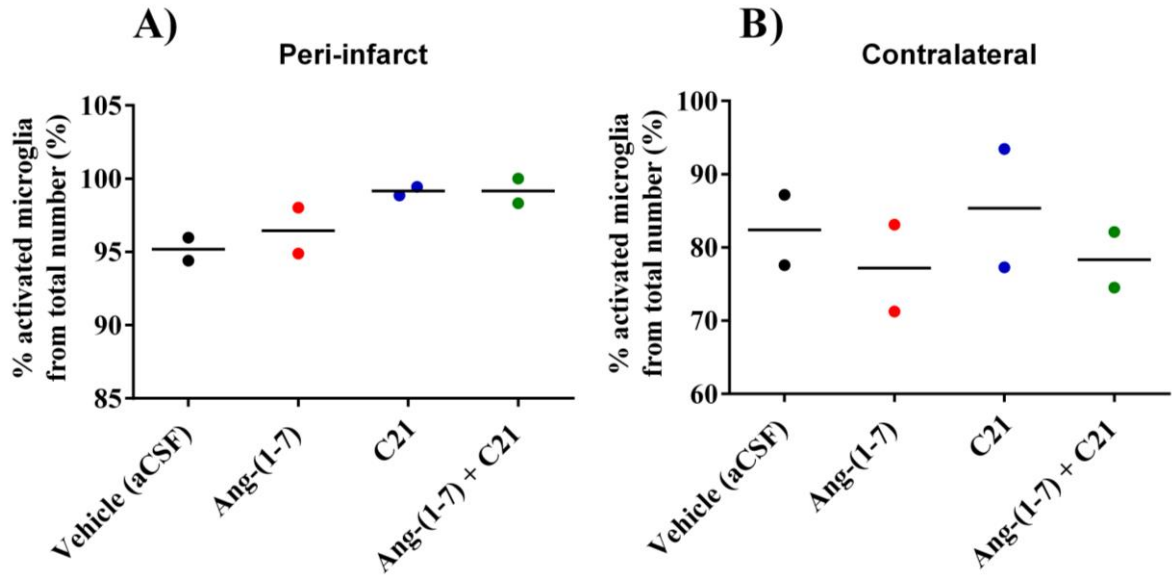

Figure 4-22 % activated microglia in peri-infarct and contralateral regions 7 days post 90 min MCAO. A) Peri-infarct region; B) Homotopic contralateral regions. % activated cells from total number for Vehicle (aCSF; n=2), Ang-(1-7) (n=2), C21 (n=2), Ang-(1-7) (n=2) treated animals. Horizontal bar represents the mean.

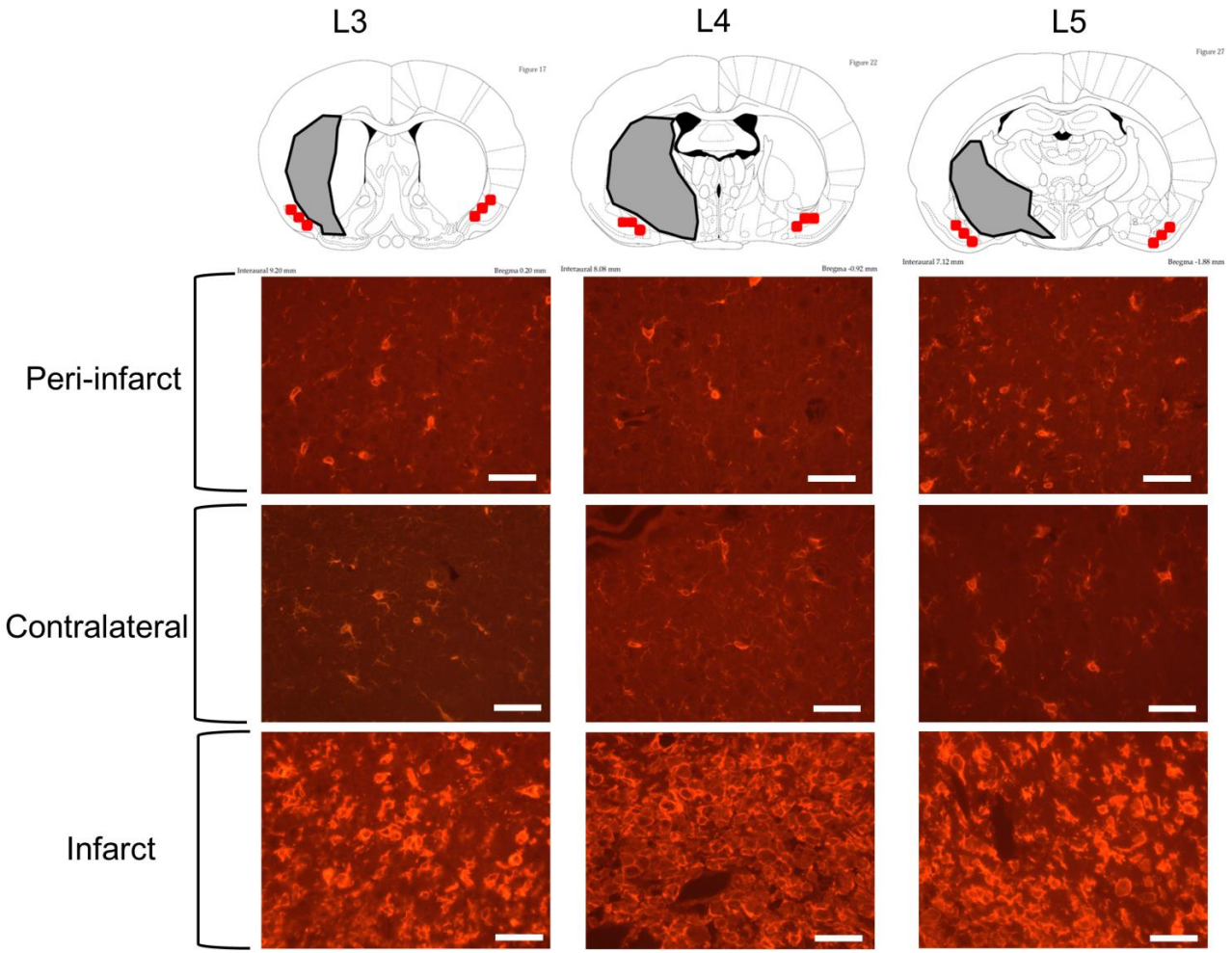

Figure 4-23 IBA1⁺ microglia staining in peri-infarct, contralateral and infarct regions for Vehicle (aCSF) treated animal. Peri-infarct regions were defined with the aid of histology analysis as defined in Paxinos and Watson coronal levels. Infarct was outlined (grey) and three ROIs were defined for imaging and IBA1⁺ cell count in peri-infarct and homotopic contralateral areas (red squares). IBA1⁺ microglia staining (highlighed in red) across coronal levels 3, 4 and 5 indicate that active microglia are mainly concentrated in infarct areas. Scale is set at 50μM per white bar.

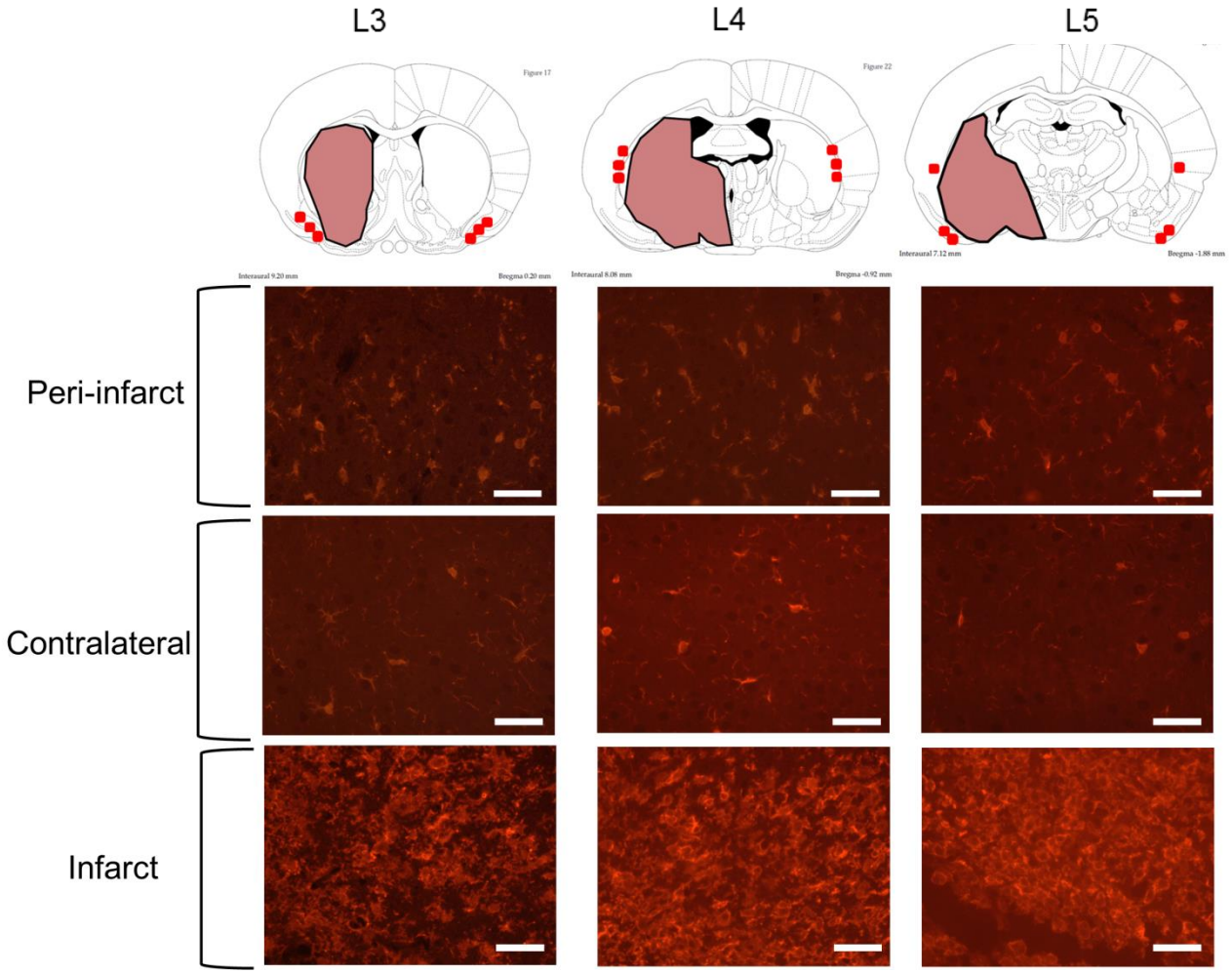

Figure 4-24 IBA1$^+$ microglia staining in peri-infarct, contralateral and infarct regions for Ang-(1-7) treated animal. Peri-infarct regions were defined with the aid of histology analysis as defined in Paxinos and Watson coronal levels. Infarct was outlined (higlighted in pink) and three ROIs were defined for imaging and IBA1$^+$ cell count in peri-infarct and homotopic contralateral areas (red squares). IBA1$^+$ microglia staining (highlighed in red) across coronal levels 3, 4 and 5 indicate that active microglia are mainly concentrated in infarct areas. Scale is set at 50μM per white bar.

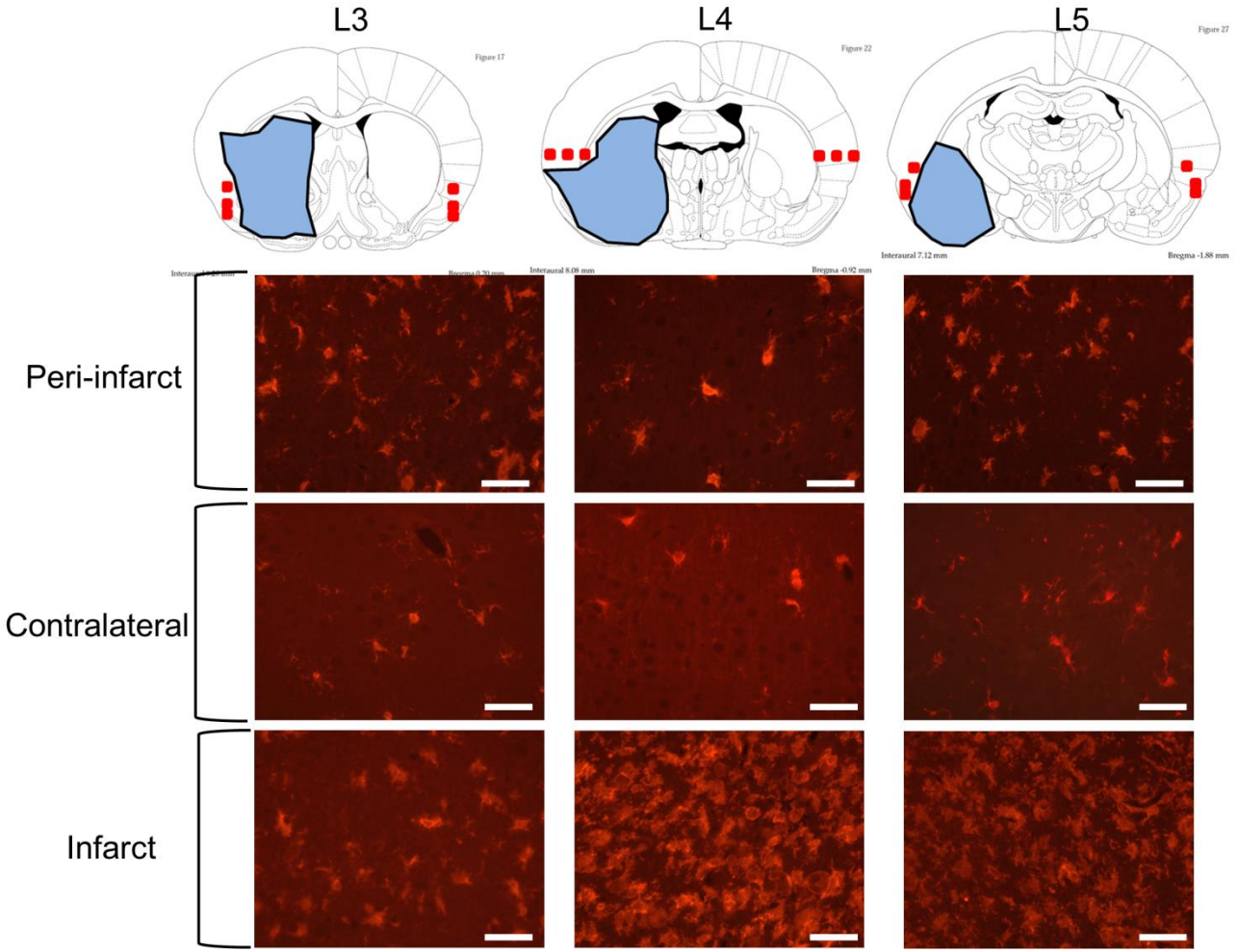

Figure 4-25 IBA1^{+} microglia staining in peri-infarct, contralateral and infarct regions for C21 treated animal. Peri-infarct regions were defined with the aid of histology analysis as defined in Paxinos and Watson coronal levels. Infarct was outlined (higlighted in blue) and three ROIs were defined for imaging and IBA1^{+}cell count in peri-infarct and homotopic contralateral areas (red squares). IBA1^{+} microglia staining (highlighed in red) across coronal levels 3, 4 and 5 indicate that active microglia are mainly concentrated in infarct areas. Scale is set at 50μM per white bar.

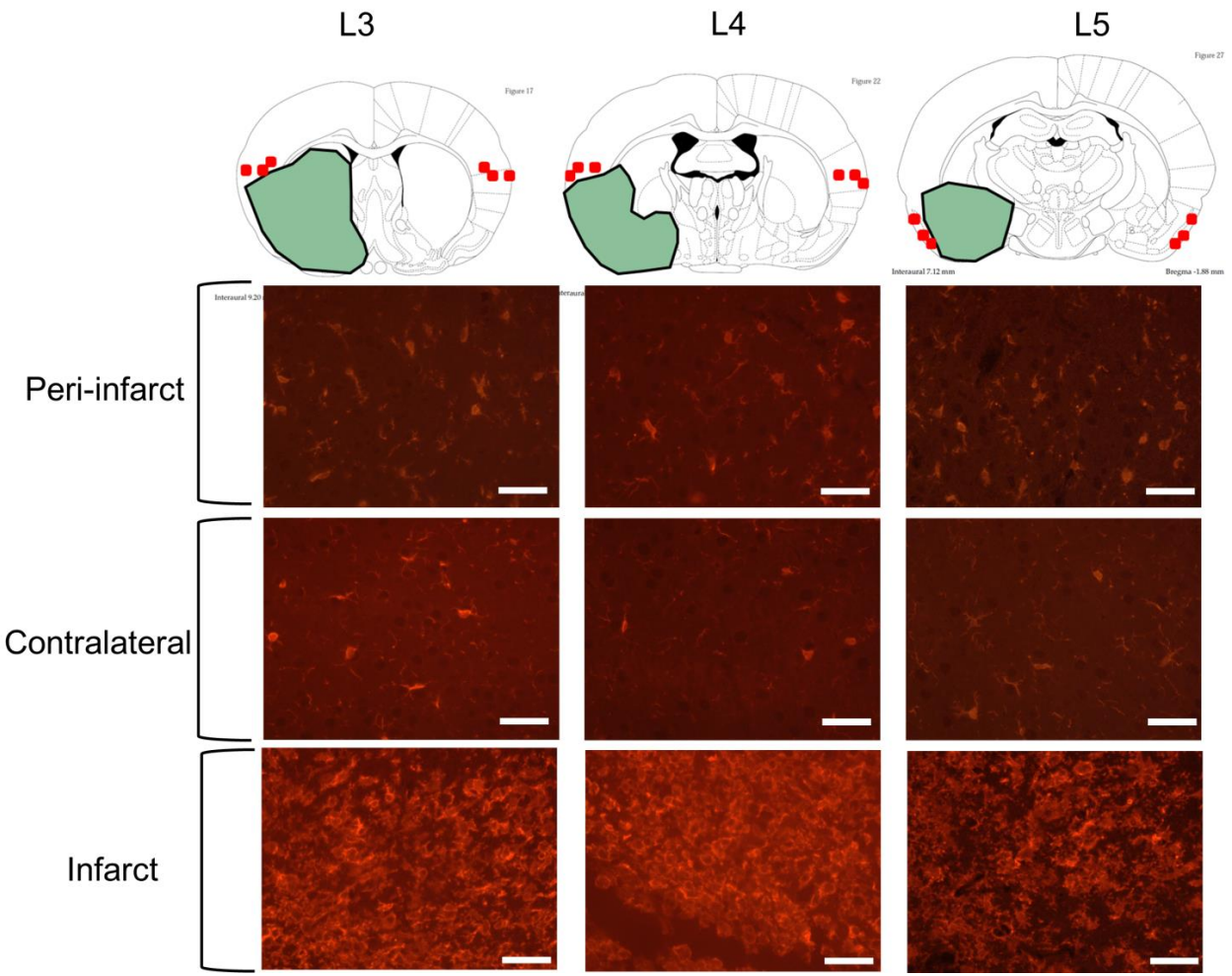

Figure 4-26 IBA1$^+$ microglia staining in peri-infarct, contralateral and infarct regions for Ang-(1-7) + C21 treated animal. Peri-infarct regions were defined with the aid of histology analysis as defined in Paxinos and Watson coronal levels. Infarct was outlined (higlighted in green) and three ROIs were defined for imaging and IBA1$^+$cell count in peri-infarct and homotopic contralateral areas (red squares). IBA1$^+$ microglia staining (highlighed in red) across coronal levels 3, 4 and 5 indicate that active microglia are mainly concentrated in infarct areas. Scale is set at 50μM per white bar.

4.5 Discussion

This is the first study to investigate the impact of Ang-(1-7) and/or C21 on the extent of tissue salvage following 90 min MCAO and 7 days reperfusion with treatment. We have demonstrated that Ang-(1-7) treatment increases tissue salvage following transient MCAO when compared to vehicle treatment; however, C21 or combination therapy had no effect. This effect was not a result of changes in BP over the time course. These experiments had strict exclusion criteria and with the help of MRI, it was possible to confirm that all animals had correct ICV cannula placement and that the MCA was successfully occluded during ischaemia with complete MCA reperfusion following filament removal.

4.5.1 Ischaemic lesions are variable during MCAO and prior to therapy

The use of DWI-MRI immediately following MCAO allowed us to determine the initial ischaemic lesion during MCAO and prior to reperfusion and treatment in all groups. As expected, the acute ADC lesion volume increased between 30 and 60 min MCAO prior to reperfusion and treatment. Although MRA confirmed successful MCAO, considerable variability in the baseline lesion volume prior to reperfusion and treatment was observed, an outcome widely detected within experimental stroke. This variability is likely due to inter-animal variability in collateral vessel supply. Specifically, leptomeningeal anastomoses variances between MCA and ACA or posterior cerebral artery collateral anastomoses may lead to enhanced or diminished collateral blood supply to the ischaemic brain by providing retrograde blood flow to the MCA territory – distal from occlusion (Cuccione et al. 2016). In support of this, differences in the extent of collateral supply in humans have been shown to influence ischaemic stroke outcome (Liebeskind, 2014). For instance, poor collateral grade leads to exacerbated stroke severity at 3 to 5 days post recanalization in stroke patients (Bang et al., 2007). In addition, in the Solitaire flow restoration device versus the Merci Retriever (SWIFT) trial, patients with enhanced collateral supply were associated with reduced ischaemic damage prior to therapy (Saver et al., 2012).

In our study, anaesthetic levels and ventilator stroke volume and rate were the same for all animals during MCAO. However, for the purpose of animal welfare during recovery, the femoral artery was not cannulated, which meant that MABP, $PaCO_2$, PaO_2 and pH levels were not monitored during MCAO surgery. This is relevant since mild rises in BP enhance cerebral tissue oxygenation and collateral blood flow in the core and penumbral areas

during MCAO whereas low $PaCO_2$ levels and pH promote infarction (Anderson and Meyer, 2002; Browning et al., 1997; Shin et al., 2008). Importantly, in the present study, animals were moved between the MRI scanner and surgical bench, and vice versa, which altered body temperature. Animals were maintained within the 37±0.5ºC range by performing the transfer as quickly as possible; however, cooling in small animals is neuroprotective and this may have been a contributing factor to lesion variability (van der Worp et al., 2007). By carrying out acute imaging during MCAO, it allowed us to overcome this variability and to assess the change in lesion volume following reperfusion with or without treatment in individual animals.

4.5.2 Reperfusion results in tissue salvage

MRI-T_2 analysis of infarct requires manual delineation of the hyperintense signal, thus, introducing an element of variability due to the subjective nature of delineating the infarct. As a result, two blinded independent investigators assessed final infarct volume. Inter-rater assessments showed successful reproducibility and the mean infarct volume for the two analyses was used for study outcome evaluation.

For all groups, reperfusion with and without treatment significantly decreased lesion volume by day 7 compared to 60 min MCAO. These findings are in agreement with thrombectomy trials in which, early initiation of reperfusion alone or in combination with IV alteplase improves functional outcome in ischaemic stroke patients (Berkhemer et al., 2015; Campbell et al., 2015; M Goyal et al., 2015; Jovin et al., 2015; Saver et al., 2015). One of the concerns of abrupt reperfusion restoration is that a rise in ipsilateral CBF above metabolic demand might lead to reperfusion injury or “cerebral hyperperfusion syndrome”. This syndrome is characterised by exacerbated brain injury caused by BBB breakdown, impaired autoregulation and enhanced inflammatory responses (Ogasawara et al., 2003). One other concern is the development of HT, which is thought to be caused by enhanced reperfusion in areas of pronounced perfusion deficit (Fiehler et al., 2005). Our data, however, depicts that following transient MCAO in Wistar rats; reperfusion alone does not exacerbate injury or cerebral haemorrhage at 7 days post MCAO, since from all surviving animals; ICH was only present in two animals, confirming the protective nature of reperfusion alone.

The extent of tissue salvage following reperfusion differed amongst animals. In vehicle treated animals, lesion volume decrease ranged from 42% to 1% from initial lesion and, as

mentioned above, differences in collateral grade amongst animals are a probable contributing factor. In the clinic, robust collateral supply is associated with successful recanalization, greater reperfusion and better clinical outcome (Liebeskind et al., 2014; Saver et al., 2012). Therefore, the extent of collateral grade is likely to influence the degree of reperfusion and subsequent infarct volume outcome. In addition, secondary injury mechanisms are another possible contributor. Rats subjected to 90 min MCAO display maximal injury from 48 to 72 hrs reperfusion that then reduces at 7 and 14 days post stroke onset (Neumann-Haefelin et al., 2000; Rewell et al., 2017). These findings are further confirmed with our neurological score data, which show that at 3 days post MCAO rats had substantial neurological impairment that then improved at 7 days post MCAO for all groups. Although reperfusion is beneficial in the longer term, secondary injury mechanisms such as BBB disruption may impact infarct outcome amongst animals (Pillai et al., 2013).

Interestingly, when comparing data at day 7 only, there were no differences in final infarct volume between treatment groups. Previous studies in the ET-1 induced MCAO model showed that Ang-(1-7) and C21 administered ICV as a pre and post stroke onset therapy led to a 50% reduction in final infarct when assessed at end-points (Joseph et al., 2014; Mecca et al., 2011; Regenhardt et al., 2013). Our experiment; however, suggests that any potential action induced by drug therapy is of mild to moderate effect and likely masked by the variability in initial lesion sizes. In turn, this may lead to false positive results by an overestimation of effect sizes or treatment effects could also be undetected (Leithner et al., 2015). Therefore, early ADC imaging has been considered a crucial tool to avoid type I and type II errors in neuroprotective studies and experimental stroke study quality (Leithner et al., 2015). Accordingly, the treatment effects on final infarct volume were examined by normalising the data to each animals own respective baseline lesion volume at 60 min MCAO.

4.5.3 Ang-(1-7) treatment with reperfusion increases tissue salvage possibly through NOX1 expression

When normalising data to initial lesion, Ang-(1-7) treatment along with reperfusion significantly attenuated lesion progression at day 7 when compared to Vehicle (aCSF). Similarly, absolute change in infarct volume between 60 min MCAO and 7 days recovery showed that Ang-(1-7) treatment alone significantly decreased ischaemic lesion compared to all other groups. This study shows for the first time that Ang-(1-7) treatment for a period

of 7 days during reperfusion has the potential to attenuate ischaemic lesion progression without impacting systolic BP. These results go in accordance with ET-1 induced MCAO studies where Ang-(1-7) treatment as a pre and/or post therapy was shown to be neuroprotective (Regenhardt et al. 2013; Mecca et al. 2011). One of the objectives of this study was to assess potential mechanistic effects underlying the outcome observed. In particular, this study focused on the Ang-(1-7) induced anti-inflammatory/anti-oxidative mechanism hypothesis which is widely reported in the literature (Jiang et al., 2012, 2013; Mecca et al., 2011; Regenhardt et al., 2013). Our study indicates that *COX-2* or *NF-κB* mRNA levels were not significantly altered by Ang-(1-7) as previously reported (Jiang et al., 2012; Liu et al., 2016). Similarly, when assessing leukocyte chemokine receptors and microglia/macrophage markers, Ang-(1-7) did not significantly affect gene expression levels at day 7 compared to Vehicle (aCSF).

In the brain, the RAS classical axis activates NOX1 and NOX2 isoforms, which are involved in the pathology of cerebral ischaemia (Garrido and Griendling, 2009; Zhang et al., 2016). Specifically, Ang II induces an inward Ca^{2+} current in neurons due to NOX2-derived ROS and stimulates superoxide in cerebral arteries through NOX1 (Wang et al. 2006; Sun et al. 2005; Jackman et al. 2009; Kahles et al. 2010). Our data shows that phagocytic *NOX2*, the main mediator in neuroinflammation-derived superoxide production (Girouard et al. 2009), was expressed at Sham levels without Ang-(1-7) treatment effects observed. Interestingly, gene expression results indicate that Ang-(1-7) treatment might exert its mechanisms by targeting NOX1. In peri-infarct brain regions, *NOX1* mRNA levels were decreased in Vehicle (aCSF) treated rats when compared to sham brain tissue; however, this decrease was significantly attenuated in Ang-(1-7) treated rats. NOXs are the major source of ROS and important mediators in oxidative stress, a known mechanism of injury following stroke (Lipton 1999; Gursoy-Ozdemir et al. 2004). Yet, aside from its involvement in cellular injury, reports suggest that ROS might have a role in CNS cellular maintenance, particularly in cellular growth and neurological synaptic plasticity (Knapp and Klann, 2002; Suzukawa et al., 2000; Tsatmali et al., 2005). Therefore, by preventing NOX downregulation post-stroke, Ang-(1-7) could mediate therapeutic effects. Still, the cellular locus at which Ang-(1-7) may be acting is yet to be defined.

KO studies have investigated the impact of NOX1 following MCAO, in which it was observed that NOX1-KO mice have larger infarcts compared to wild type (WT) animals (Choi et al., 2015). Additionally, NOX1-KO mice subjected to MCAO and treated with Ang II, displayed lower levels of ROS yet extensively larger infarct volumes when

compared to WT mice (Jackman et al., 2009). As a result, NOX1 might be neuroprotective in the context of cerebral injury. The mechanism behind this protective effect is not well understood; however, research indicates that it may be a ROS derived neurogenesis effect. In embryonic rat cortical cells, ROS intracellular accumulation is associated with cellular differentiation into neurons (Tsatmali et al., 2005) whereas in PC12, an immortalised neuronal cell line, neuronal differentiation through nerve growth factor is dependent on ROS concentration (Suzukawa et al., 2000). One could postulate that Ang-(1-7) enhances neurogenesis and homeostatic maintenance through NOX1 derived ROS and thus, improved ischaemic lesion by day 7.

A caveat in the present study is the lack of protein assessments and the small number of samples collected for immunohistochemical analysis. Therefore, it is not possible to conclude whether Ang-(1-7) might be promoting neurogenesis by targeting NOX1. Immunohistochemical co-localisation analysis of NOX1 and proliferating cell nuclear antigen antibodies in the peri-infarct region would have been a suitable approach to test the neurogenesis hypothesis (Sierra et al., 2011).

4.5.3.1 Central Ang-(1-7) infusion does not modify brain RAS components

AT_{1A} receptor mRNA expression was not altered at day 7 following MCAO in peri-infarct brain tissue. The same outcome was verified in ET-1 induced MCAO, where *AT_1R* gene expression was comparable to Sham rats following 72 hrs reperfusion (Mecca et al., 2011). Similarly, *ACE* gene expression did not change following MCAO in peri-infarct regions. These results propose that at day 7 following 90 min MCAO, the classical axis within the brain is not altered and that its detrimental effects might be temporally dependent. For instance, a recent study showed that following permanent MCAO, *AT_{1A}* gene expression was upregulated at 24 hrs injury only (Wakayama et al., 2017). Therefore, it is plausible that in normotensive animals, Ang II and AT_1R may exert its detrimental effects in MCAO injury at an earlier stage (e.g. 24 hrs) rather than at subacute/chronic phases. However, to confirm ACE/Ang II/AT_1R over activation at the time point evaluated, brain Ang II and AT_1R protein levels would have to be assessed following MCAO and compared to Sham in the model used.

AT_2R mRNA levels were significantly increased following MCAO in the present study. Previous reports have shown that following MCAO, *AT_2R* mRNA levels increase at 24 hrs and 72 hrs with our data indicating that at day 7 this upregulation persists (Kagiyama et al.,

2003; Makino et al., 1996; Zhu et al., 2000). Interestingly, *ACE2* was compared to Sham as reported in ET-1 induced MCAO models at 72 hrs post stroke onset (Mecca et al. 2011) whereas MCAO significantly decreased *MasR* expression in peri-infarct regions. It has been previously suggested that both ACE2 and MasR (mRNA and protein levels) are upregulated following 120 min MCAO at day 7 in the RVLM (Chang et al. 2014). In our studies, brain tissue obtained for mRNA analysis was excised from the cortical region corresponding to the peri-infarct; thus, counter-regulatory RAS expression in other CNS areas such as the medulla was not assessed. Nonetheless, our results indicate that in the model used, AT_2R and MasR have a time-dependent role following cerebral ischaemia within the peri-infarct areas. Therefore, MasR agonism possibly exerts its maximal cytoprotective effects at acute/subacute whilst AT_2R agonism may provide neuroprotection at a subacute/chronic phase of injury. This could justify why neuroprotection was observed for MasR agonism but not with AT_2R agonism in our study.

In addition, a preceding study postulated that Ang-(1-7)'s protective effects may be partly mediated by B_2R signalling, thereby enhancing a vasodilatory effect (Lu et al., 2008). Following transient MCAO, Ang-(1-7) ICV post treatment enhances the expression of B_2R and up to 72 hrs post stroke onset (Lu et al., 2008). However, in the present study, B_2R mRNA levels were expressed to Sham levels without Ang-(1-7) treatment effects, thus, the effect observed is unlikely due to bradykinin signalling exacerbation.

4.5.3.2 Ang-(1-7) does not alter microglia/macrophage and leukocyte infiltration markers following MCAO

Following 7 days reperfusion with treatment, Ang-(1-7) did not alter pro-inflammatory mediators or microglia/macrophage M1/M2 mRNA profile. The brain tissue samples used to examine gene expression do not discern cell specific cytokine profile; still, these results provide an indication that at this time point, Ang-(1-7) does not exert a microglia/macrophage induced anti-inflammatory effect. Ang-(1-7) reaches its maximum cerebral tissue concentration at 24 hrs post-transient MCAO (Lu et al. 2013), thus, possibly exerting a microglia-derived anti-inflammatory effect at an earlier time point in injury as previously reported (Regenhardt et al., 2013). Simultaneously, inflammatory gene expression for *COX-2*, *NF-κB*, *NOX2*, *IL-6*, *IL-1β* were expressed at Sham levels in MCAO groups while *IL-10* and *iNOS* were undetected in all samples.

The balance between M1/M2 microglia/macrophage phenotype is dynamic after ischaemic stroke and the underlying mechanisms are not well understood (Cotrina et al., 2017; Ritzel

et al., 2015). It is proposed that following transient MCAO and at day 7, these cells express a M1 phenotype (Hu et al., 2012). Our data supports this hypothesis since M1 type markers *CD86* and *CD11b* were upregulated following MCAO. This indicates that in the peri-infarct, microglia/macrophages are active and involved in antigen presenting to T cells as suggested by CD11b and CD86, respectively (Taylor and Sansing, 2013). M2 phenotype is reported to occur up to 5 days post MCAO and then shift towards a M1 phenotype (Hu et al., 2012). From all the M2 markers studied, *TGF-β1* only was upregulated 7 days following MCAO, without Ang-(1-7) induced effects. Microglia are major sources of TGF-β1 in the brain (Welser-Alves and Milner, 2013) and once released it will contribute towards tissue regeneration as well as T regulatory (Treg) cell development, hence cellular repair (Iadecola and Anrather, 2011; Liesz et al., 2009). Together, the data obtained indicates that Ang-(1-7) therapy did not influence microglia/macrophage cytokine profile.

To obtain a qualitative assessment of treatment effects on microglia numbers and phenotype within the peri-infarct, $IBA1^+$ microglia were evaluated. Following 90 min MCAO with 7 days reperfusion, AT_1R blockers decrease infarct volume due to a decrease in microglia activation in the ipsilateral hemisphere (Lou et al., 2004). In the present study, $IBA1^+$ immunostaining indicated that MasR agonism through Ang-(1-7) therapy did not influence microglia activation or total number in the peri-infarct region. This emphasises that Ang-(1-7) does not act at the microglia level at this time point. It was also observed that $IBA1^+$ cells numbers were enhanced in ipsilateral peri-infarct regions compared to the contralateral side and mostly concentrated within the infarct core for all groups. In the infarct region, all $IBA1^+$ cells exhibited an amoeboid/active form; suggesting that repair mechanisms are taking place by clearing cellular debris (Denes et al., 2007).

Ang-(1-7) does not mediate its effects via leukocyte recruitment at day 7. Neutrophils peak between 1 and 3 days post MCAO with numbers subsequently declining by day 7, whereas macrophages levels peak between day 3 and 7 (Grønberg et al., 2013). Our data shows that *CXCR2* and *CCR2*, neutrophil and macrophage chemokine receptors, were unchanged following MCAO when compared to Sham without treatment effects. Conversely, *CCR5* was significantly upregulated following MCAO without Ang-(1-7) induced effects. CCR5 is expressed in T cells, astrocytes, microglia and neurons (Westmoreland et al., 2002). T cells are reported to infiltrate infarcted brain 3 to 7 days post injury and peak no earlier than 5 days post MCAO (Grønberg et al., 2013), which justifies the increase in *CCR5* gene expression. The role of this receptor in ischaemic stroke is not well understood; however, KO studies indicate that 7 days following MCAO, CCR5-KO mice have larger infarcts

than WT mice (Sorce et al., 2010), proposing a role in cellular repair possibly through Treg cell recruitment and activation (Li et al., 2017).

4.5.4 AT_2R receptor agonism and combined AT_2R/MasR agonism has no effect on tissue salvage

AT_2R agonism did not attenuate ischaemic lesion progression following 7 days MCAO. One possibility for the effect observed is that the dose selected might not have been at a therapeutic level. C21 elicits AT_1R specific effects at higher doses (Gao, Zhang et al. 2011), thus, the dose used in our study, 7.5 ng/hr, was selected as recommended by Vicore Pharma®. Supportively, Joseph et al. used the same C21 dose as this study; yet, in their experiment, the effects on infarct volume were assessed in a single 2 mm coronal brain section from each rat by TTC staining whereas in the present study we assessed the entire rostral-caudal extent of damage. Conversely, McCarthy et al., observed a neuroprotective effect when testing 50 ng/hr C21 dose ICV in SHRs following MCAO but not at lower doses (McCarthy et al., 2014), highlighting that higher doses might be needed in future studies.

Similarly to our study, C21 treatment for 4 days post-MCAO did not impact infarct volume when compared to control groups (Schwengel et al., 2016). Instead, C21 treatment decreased mortality between groups (Schwengel et al., 2016) whereas in the present study, C21 treated rats exhibited the highest mortality out of all groups. Furthermore, in Schwengel's experiment, neurological score was significantly improved at 1, 2 and 4 days post transient MCAO, an effect not observed in our experiment. The improvement in NS was associated with an upregulation of BDNF gene and protein expression within the ipsilateral hemisphere, which possibly led to an anti-apoptotic effect in penumbral regions (Schwengel et al., 2016). The authors did not perform acute MRI to assess the baseline lesion volume; therefore, it could be possible that in the model used, C21 might have induced a mild effect on infarct progression at 4 days reperfusion. It is important to note that in Schwengel's experiment, studies were conducted in mice and C21 administered IP (Schwengel et al., 2016); therefore, this method of administration may be more suitable and effective than the one used in our study.

AT_2R activation could have a neuroprotective effect at later stages of injury as evidenced by an upregulation of AT_2R gene expression in peri-infarct regions following 7 days reperfusion. A recent study examined the neuroprotective potential of C21 treatment

following transient MCAO for a period of 3 weeks (Bennion et al., 2017). There, it was shown that C21 therapy attenuated infarct volume when compared to control animals (Bennion et al., 2017), thus, confirming this hypothesis. It is suggested that C21 post stroke treatment IP might impact infarct volume by enhancing angiogenesis via the eNOS/NO pathway following 90 min MCAO (Alhusban et al., 2015). The angiogenic hypothesis was further examined in a chronic intraluminal permanent MCAO model in which C21 was administered as a post therapy for 21 days and shown to improve neurological function, an outcome associated with an upregulation of VEGF protein and gene expression levels in the ipsilateral hemisphere (Mateos et al., 2016).

Interestingly, a combination of C21 and Ang-(1-7) had no effect on tissue salvage or neurological outcome in the present study. When examining % ischaemic lesion change between 60 min MCAO and 7 days recovery, the combination group showed a trend to improve infarct evolution; however, absolute lesion change suggested that combination therapy did not impact infarct progression. This indicates that at 7 days post 90 min MCAO, simultaneous AT_2R and MasR receptor agonism does not act synergistically to enhance neuroprotection as initially hypothesised. One of the limitations of Ang-(1-7) treatment is that it is a short 7 amino acid peptide and once in circulation it has a half-life of approximately 10 sec (Yamada et al., 1998). Although Ang-(1-7) has high selectivity for MasR (Santos et al., 2003), its short half-life impacts its actions, which might justify why only a mild to moderate effect was observed. Conversely, C21 has a K(i) value of 0.4 nmol/L for the AT_2R, displaying high selectivity, and an estimated half-life of 4 hrs in rats (Wan et al., 2004), therefore, suggesting that its actions were prolonged in the combination group compared to Ang-(1-7). MasR agonists are being developed and these include AVE 0991, a non-peptide compound, high selective for the MasR and orally active(Santos and Ferreira, 2006). AVE 0991 is thought to have higher efficacy and a longer half-life than Ang-(1-7) (Santos and Ferreira, 2006); nevertheless, its effects only recently started being tested in the context of ischaemic stroke and so far were unsuccessful (Lee et al., 2015).

4.5.4.1 Treatment did not impact neurological score

In this study, there were no differences in neurological score at 3 and 7 days post 90 min MCAO between groups. Ang-(1-7) induced a mild effect on tissue salvage at day 7, which was detected when normalising data to initial lesion at 60 min MCAO. When assessing infarct volume at day 7, treatment effects were not detected due to infarct volume variability, therefore, it would be unlikely to see any functional improvement between groups. At the same time, the Garcia score might have not been a sensitive test to detect subtle changes induced by therapy. The 18 point score is an easy and simple test to detect function but is of a highly subjective nature (Schaar et al., 2010). Instead, behavioural assessments could have been a better approach.

Sensorimotor tests such as the adhesive removal test are reported to detect functional impairments up to 11 weeks following cerebral ischaemia, displaying high sensitivity to sensory neglect in small cerebral lesions (Zarruk et al., 2011). Other tests include the passive avoidance test which is a highly sensitive cognitive test, detecting impairment up to 7 weeks following MCAO by examining avoidance learning and shown to successfully correlate with size of lesion. Moreover, the beam walking test, which assesses motor coordination provides good sensitivity after MCAO (Zarruk et al., 2011). In future, these tests could be selected to study functional outcome.

4.5.5 Summary

Ang-(1-7) ICV treatment along with reperfusion for 7 days post MCAO significantly increased tissue salvage when normalising data to initial lesion without impacting BP. Ang-(1-7) has a short half-life which might have contributed to a mild to moderate effect that was not detected when assessing data at day 7. The results obtained suggest that selective MasR agonists may provide neuroprotection along with reperfusion following thrombectomy. On the other hand, C21 alone and in combination with Ang-(1-7) did not show a significant impact in lesion growth at 7 days reperfusion.

Following MCAO, neurological score was shown to decrease for all animals at day 3 and subsequently improve by day 7. As predicted, and as a result of comparable infarct lesions at day 7, there were no differences in neurological score between groups. However, it must be noted that the score used for functional assessment was not sensitive enough to detect potential Ang-(1-7)-induced alterations. Instead, it provided an overall indication of animal condition. In future, behavioural examinations such as the adhesive removal test should be used as these provide a more sensitive evaluation of deficit.

The mechanism of action underlying the actions of Ang-(1-7) was assessed via gene expression assays. Although a conclusion could not be drawn from mRNA level only, Ang-(1-7) may have a role in oxidative stress by attenuating the decrease in NOX1 levels seen with vehicle treatment and possibly impacting neurogenesis. In normotensive rats, MCAO does not induce an imbalance in AT_{1A} gene expression; however, AT_2R was upregulated and *MasR* gene expression significantly decreased following injury. MasR activation possibly exerts its neuroprotective effects at an earlier stage in injury whereas AT_2R agonism might act at a subacute/chronic level. In terms of treatment effects induced by Ang-(1-7) in gene expression, there were no differences in RAS components, chemokine leukocyte receptors, pro-inflammatory and anti-inflammatory markers compared to Vehicle (aCSF).

In conclusion, Ang-(1-7) treatment along with reperfusion following MCAO for a period of 7 days attenuates cerebral infarct progression possibly by acting on oxidative stress levels or inflammatory responses at an earlier time point. To elucidate potential underlying mechanisms that could explain the neuroprotection observed, Ang-(1-7) treatment will be examined at an acute stage of injury in the subsequent study.

Chapter 5: The effects of Ang-(1-7) on BBB breakdown and microglia activation following transient MCAO

Chapter 5

In Chapter 4, Ang-(1-7) significantly increased tissue salvage following reperfusion, a mechanism independent of inflammatory responses. Literature reports often attribute Ang-(1-7)'s neuroprotective effect to a direct anti-inflammatory mechanism on microglia/macrophages (Liu et al., 2016; Regenhardt et al., 2013). In turn, microglia activation is implicated in BBB disruption by generating ROS and pro-inflammatory cytokine release (Yenari et al., 2006). Therefore, Ang-(1-7) may act to maintain integrity of the BBB via an inhibition of microglia activation. This study was designed to determine the effects of Ang-(1-7) post stroke therapy on BBB breakdown, infarct volume, microglia/macrophage activation and pro- and anti-inflammatory gene expression following 90 min MCAO and 24 hrs reperfusion.

5.1 Introduction

The BBB is a specialised structurethat separates the CNS from the periphery and consists of endothelial cells anastomosed to one another through TJPs. The endothelial cells in the BBB are surrounded by astrocytes, pericytes, neurons and basement membranes, ultimately forming the NVU, and providing functional and structural support to the BBB (Yang & Rosenberg 2011; Zlokovic 2008). After ischaemic stroke, the BBB becomes disrupted, allowing intravascular proteins to enter the brain parenchyma as well as inflammatory cells. In turn, this causes brain vasogenic oedema, increases the risk of HT and contributes towards morbidity and mortality (Chapouly et al., 2015; Haley and Lawrence, 2017).

In the clinic, many patients exhibit a phenomenon termed HARM, characterised by blood vessel permeability in the meninges over the area of the stroke and associated with worse clinical outcome (Kohrmann et al. 2012). This is of extreme importance as thrombolysis treatment is reported to induce BBB breakdown and lead towards the development of HARM and HT (Kassner et al., 2009; Kidwell et al., 2008; Lakhan et al., 2013). Likewise, patients subjected to thrombectomy and presenting signs of BBB leakage, are equally associated with poorer clinical outcomeand HT (Renú et al., 2015). Since alteplase administration is the treatment of choice and endovascular therapy is becoming increasingly used, it is crucial to identify a potential adjuvant therapy with the capacity to limit BBB breakdown injury.

In rodents, BBB breakdown is proposed to occur in a biphasic manner following reperfusion onset; yet, there is no agreement on when the BBB opens and closes. Evidence from experimental studies suggests that the early opening of the BBB occurs between 3 to 6 hrs following reperfusion. Following this, the barrier closes again at approximately 15 to 24 hrs post reperfusion and by 48 to 72 hrs post reperfusion BBB breakdown is maximal (Belayev et al., 1996; Pillai et al., 2009; Rosenberg et al., 1998; Veltkamp et al., 2005). Nevertheless, the biphasic pattern of BBB opening is controversial as MRI studies indicate that BBB breakdown is a continuous, long-lasting mechanism and evident for at least 5 weeks post injury (Strbian et al. 2008; Nagel et al. 2008; Lin et al. 2008). For this reason, the dynamics of BBB breakdown require further understanding as it could help determine optimal time points for neuroprotective therapy administration.

BBB breakdown derives from an interplay of mechanisms such as inflammation, oxidative stress and angiogenesis within the NVU (Sandoval and Witt, 2008). In particular, metalloproteinases (MMPs) are widely implicated in BBB breakdown by degrading components of the extracellular matrix and TJPs. For instance, metalloproteinase 2 (MMP2) is involved in the initial disruption at 3 hrs post MCAO whereas MMP9 promotes BBB breakdown between 24-72 hrs post stroke onset (Rosell et al., 2006; Rosenberg et al., 1998; Sandoval and Witt, 2008; Yang et al., 2007). At later stages, BBB disruption is also mediated by ROS, leukocyte extravasation and pro-inflammatory mediators including COX-2 and iNOS(da Fonseca et al., 2014). In addition, at this stage, the angiogenic mediator, vascular endothelial growth factor A (VEGFA) is thought to enhance BBB leakage by activating vascular endothelial growth factor receptor 2 (VEGFR-2) present on endothelial cells (Valable et al., 2005; Zhang et al., 2000). Together, these reports highlight the complexity of the mechanisms underlying BBB breakdown following stroke.

In recent years, the role of microglia in contributing towards the integrity of the NVU has received particular focus. Following stroke onset, these cells are quickly activated, recruited into the injured site and thought to exacerbate injury (da Fonseca et al., 2014). Supporting evidence suggest that following LPS-induced rat microglia activation, activated cells disrupt TJPs by stimulating NOX and subsequently ROS in a BBB disruption model (Sumi et al., 2010). Similarly, *in vitro,* studies have shown that microglia enhance barrier leakage by producing pro-inflammatory cytokines and ROS, an outcome reversed by minocycline and apocycin therapy (Yenari et al., 2006). In *in vivo* models, rats subjected to MCAO and minocycline treatment showed reduced BBB breakdown, a result suggested to be due to microglia phenotype modulation, promoting M2 profile (Yang et al., 2015).

Conversely, a recent study demonstrated that microglial cells rapidly aggregate around injured capillaries and mediate prompt resealing of the leaked barrier (Lou et al., 2016), proposing a protective role.

Ang-(1-7) is widely reported to modulate microglia/macrophage phenotype at 24 hrs and 72 hrs post stroke onset in normotensive rats as well as in *in vitro* models (Liu et al., 2016; Mecca et al., 2011; Regenhardt et al., 2013). In microglial cell cultures, Ang-(1-7) treatment prevented the upregulation of *IL-6*, *IL-1β* and NF-κB activation whilst stimulating the generation of anti-inflammatory cytokine, *IL-10* (Liu et al., 2016). Furthermore, Ang-(1-7) treatment attenuated *iNOS* and *CD11b* gene expression in normotensive rats following stroke, indicating that treatment inhibits microglia/macrophage activation and modulates M1/M2 phenotype (Regenhardt et al., 2013). Accordingly, these reports place Ang-(1-7) as a possible neuroprotective drug by potentially modulating microglia phenotype and indirectly targeting the BBB.

In experimental stroke, literature points towards a detrimental role of the classical RAS in BBB breakdown. In rat brain capillary endothelial cells subjected to 6 hrs oxygen glucose deprivation and 24 hrs reoxygenation, candesartan therapy reversed BBB disruption without impacting TJP expression or oxidative stress (So et al., 2015). The pre-treatment effects of candesartan were then tested in normotensive rats subjected to 60 min MCAO followed by 24 hrs reperfusion. The authors showed that at this time point, MCAO led to an exacerbated BBB breakdown with candesartan preventing disruption (Panahpour, Nekooeian, et al., 2014). A follow up experiment was then conducted testing the ACE inhibitor, enalapril as a post-stroke therapy. There, enalapril decreased BBB permeability due to an antioxidant effectin the same MCAO protocol (Panahpour, Dehghani, et al., 2014). Moreover, in embolic MCAO, Wistar rats subjected to candesartan and t-PA combination therapy displayed reduced HT, an outcome associated to decreased NF-κB activity (Ishrat et al., 2013). These findings implicate the classical axis in BBB injury; highlighting a potential therapeutic effect of the counter-regulatory axis.

Recently, the effect of Ang-(1-7) on BBB breakdown was tested in an animal model of stroke. A dose response curve for Ang-(1-7) was carried out in rats at 24 hrs following transient MCAO and the authors demonstrated a reduction in BBB breakdown at a dose of 0.5 pmol/hr and 5 pmol/hr (Wu et al., 2015). The outcome observed was attributed to drug induced TJP preservation through MMP9 expression downregulation and enhancement of metallopeptidase inhibitor 1 (TIMP1) levels (Wu et al., 2015). In neuroprotective studies,

Ang-(1-7) has been shown to attenuate infarct progression when administered ICV at a dose of 1.1 nmol/hr following 24 hrs, 48 hrs, 72 hrs post MCAO onset as well as 7 days as seen in Chapter 4 (Jiang et al., 2012, 2014; Mecca et al., 2011; Regenhardt et al., 2013). One could hypothesise that the underlying mechanism involves BBB preservation. Yet, the effect of Ang-(1-7) in BBB disruption at a dose of 1.1 nmol/hr has not been tested as a post-stroke therapy following 90 min MCAO and examined with MRI.

In Chapter 4, Ang-(1-7) along with reperfusion increased tissue salvage compared to vehicle treated rats. Mechanistic data showed that Ang-(1-7) did not influence RAS, pro- and anti-inflammatory or microglia/macrophage M1/M2 phenotype marker gene expression and qualitative IBA1 positive microglia cell count at day 7 post reperfusion. Currently, there is evidence that implicates the involvement of the RAS in BBB damage, inflammation and microglia/macrophage activation at acute stages of cerebral injury. As a result, this study hypothesised that Ang-(1-7) exerts its neuroprotective effects by attenuating BBB disruption at 24 hrs post MCAO via a direct anti-inflammatory effect on microglia in the peri-infarct.

5.1.1 Study aims:

- Primary outcome: To evaluate the effects of post stroke Ang-(1-7) treatment on BBB breakdown following transient focal cerebral ischaemia.

- To investigate the effects of Ang-(1-7) on infarct volume following transient focal cerebral ischaemia.

- To determine the impact of Ang-(1-7) treatment on inflammatory gene expression and microglia activation in peri-infarct regions.

5.2 Methods

5.2.1 Sample size calculation

Sample size was assessed using power analysis programme G*Power (version 4.1, Germany). An "a priori" power analysis was performed for a t test between two independent means. Using data from the previous study, MCAO with reperfusion induces an infarct volume of 130.6mm^3 with a S.D. (σ) of 50.7mm^3. Ang-(1-7) administered as an ICV infusion was reported to induce approximately 50% reduction in infarcted tissue at 24 hrs post stroke onset (Regenhardt et al., 2013). To detect an effect size of 50% reduction in infarct volume, a minimum *n* number of 9 for each group with a type I error rate (α) of 0.05 and power of 0.80 was obtained.

5.2.2 Randomisation and blinding

Prior to study commencement, rats were assigned a number and randomly allocated to either Vehicle (aCSF; 1 μL/hr) or Ang-(1-7) (1.1 nmol; 1μL/hr) treatment groups via a list randomiser (www.random.org). Investigators were blinded to treatment group throughout the experimental study. Treatment schedule was kept by a colleague within the department who was responsible for drug preparation one day prior to the experiment. One day prior to 90 min MCAO and at 24 hrs post MCAO, an 18 point neurological score was performed for each rat as previously described (Chapter 2.11). Data analysis was performed by the investigator blinded to treatment group. Once all analysis and assessments were performed, the treatment codes were revealed.

5.2.3 Animals and surgical procedures

Male Wistar rats (n=33; 311-342g) were subjected to 90 min cerebral ischaemia and ICV treatment via osmotic pump (ALZET®, Model 2001) of Vehicle (aCSF) or Ang-(1-7) at start of reperfusion for 24 hrs. Experimental procedures and recovery were carried out as outlined in Chapter 2 and 4. In this study, 4-0 nylon silicone coated tip monofilament (403934PK10 or 404134PK10; Doccol Corporation, MA, USA) were used to occlude the MCA. For sham animals, surgery was performed as outlined; however, the filament was not introduced into the vessel to occlude the MCA.

5.2.3.1 Tail vein cannulation

After 24 hrs reperfusion, rats were subjected to MRI imaging and gadolinium-diethylenetriamine penta-acetic acid (Gd-DTPA, Magnevist®, Bayer, UK) contrast agent IV injection for BBB breakdown assessment. Animals were anaesthetised in an induction chamber with 5% isoflurane and then placed on a facemask at 3% isoflurane in a 70:30% N_2O/O_2 mixture. The tail vein was heated with a heating lamp to vasodilate the vessels, this way aiding vessel visualisation. Once the veins were easily identified, a 26 gauge × 19 mm cannula (MillPledge Veterinary, UK) was used to cannulate the dorsal vein starting at the distal end. Successful cannulation was confirmed by blood sample withdrawal through the cannula. The cannula was then secured in place using super glue to prevent cannula displacement when transferring to the MRI scanner. The cannula was attached to an MR compatible syringe connected to tubing to allow contrast agent administration to be carried out while the rat is in the MRI scanner and during scanning.

5.2.4 MRI scanning protocol

The rat was placed in the cradle and the head restrained with ear and tooth bars and the surface coil placed above the head. Anaesthesia set at 3% isoflurane mixture was administered via facemask. Temperature was monitored with a rectal probe and controlled with an homeothermic blanket.

MRA was carried out to confirm left MCA reperfusion and MRI-T_2 performed to then assess infarct outcome. For these two scans, data was analysed and corrected to oedema and hemispheric compression as described in detail in Chapter 2. To quantify BBB breakdown, MRI-T_1 weighted imaging was carried out prior to and post Gd-DTPA tail vein injection at 5, 10, 15, 20, 25 and 30 min from injection start. The sequence used was a RARE T_1 with the following parameters: 8 coronal slices with a slice thickness of 1.5 mm, effective TE=13.5 ms, TR=800 ms and matrix size=256 × 256 with a FOV= 30 × 30 mm resulting in a plane resolution of 117μM.

5.2.4.1 MRI-T_1 image analysis

RARE-T_1 imaging analysis was conducted using Matlab (MathWorks Ltd, UK). MRI data was exported in DICOM format to be processed by an in-house developed Matlab code written by Dr Antoine Vallatos.

Gd-DTPA uptake was determined in % signal change contrast-enhanced images for each time point post Gd-DTPA injection. % signal change maps were generated by subtracting MRI-T_1 images before and after Gd-DTPA injection and normalising to pre-contrast MRI-T_1 scan. The following equation was carried out, where M represents image:

$$\left(M_{postGd} - M_{preGd}\right) \times 100/M_{preGd}$$

To calculate Gd-DTPA brain volume uptake in signal change maps, a series of ROIs were manually selected on the dataset to generate a range of masks:

1. A "noise" region situated outside the animal position was selected to calculate signal-to-noise ratio (SNR), therefore, removing variability that may have been caused by movement or scanning conditions (Figure 5-1A).

2. The "whole brain" region was outlined on the MRI-T_1 data prior to Gd-DTPA injection to remove background noise (Figure 5-1B).

3. To avoid false positives from Gd-DTPA leakage outside the brain or in the surgery site where the ICV cannula was inserted, a "half brain/ipsilateral" region of interest was also selected on the T_1 data prior to Gd-DTPA injection. In this experiment, a MRI phantom scan was not applied, thus, when selecting the half brain region, extreme care was taken to not include the base of the brain regions, which are usually detected in signal change maps caused by signal decay (Figure 5-1C).

4. Cerebral ventricles were outlined with the guidance of MRI-T_2 images (Figure 5-1D) and excluded from analysis.

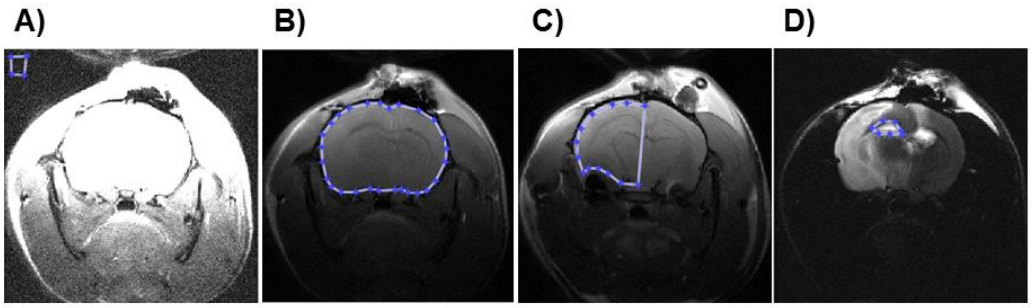

Figure 5-1 MRI-T_1 image analysis protocol. A) Noise mask outline B) Whole brain ROI C) Half brain/ipsilateral ROI. Images A, B, C were performed on MRI-T_1 data prior to Gd-DTPA injection**. D) Cerebral ventricle ROI.** MRI-T_2 scans were used to outline the cerebral ventricles.

Once all the ROIs had been performed, the "half brain/ipsilateral" masks were applied on the post Gd-DTPA scans and pixels intercepting the cerebral ventricles removed from the image. The SNR and % noise were calculated by carrying out the following formulas, where σ_M is defined as noise standard deviation of the magnitude image as previously described (Gudbjartsson and Patz, 1995):

$$SNR = \frac{(M_{postGd} - M_{preGd})}{\sigma_M}\sqrt{2 - \frac{\pi}{2}}$$

$$\%Noise = \frac{\sigma_M}{M_{postGd} - M_{preGd}} \times 100$$

After, % noise to signal change maps were generated and investigated to identify noise contribution within all images. It was observed that for all rats, noise contribution was approximately above 2% and below 5% for all image pixels within the brain (Figure 5-2A). As a result, % signal change maps were generated for each time point post Gd-DTPA injection (Figure 5-2B) and a 25% threshold, five times higher than noise contribution (<5%), was arbitrarily set to quantify Gd-DPTA volume uptake in all post injection scans.

To determine Gd-DTPA uptake volume (mm^3) within the ipsilateral hemisphere, a binary mask was generated. Values below the established threshold were set as 0 and values above the threshold set as 1 (Figure 5-2C). The voxels defined as 1 were counted and multiplied by the voxel dimensions to obtain the overall Gd-DTPA uptake brain volume (mm^3) for each of the 6-time point scans. After, a final Gd-DTPA uptake volume was obtained by averaging the volumes determined in each 6-time point % signal change map.

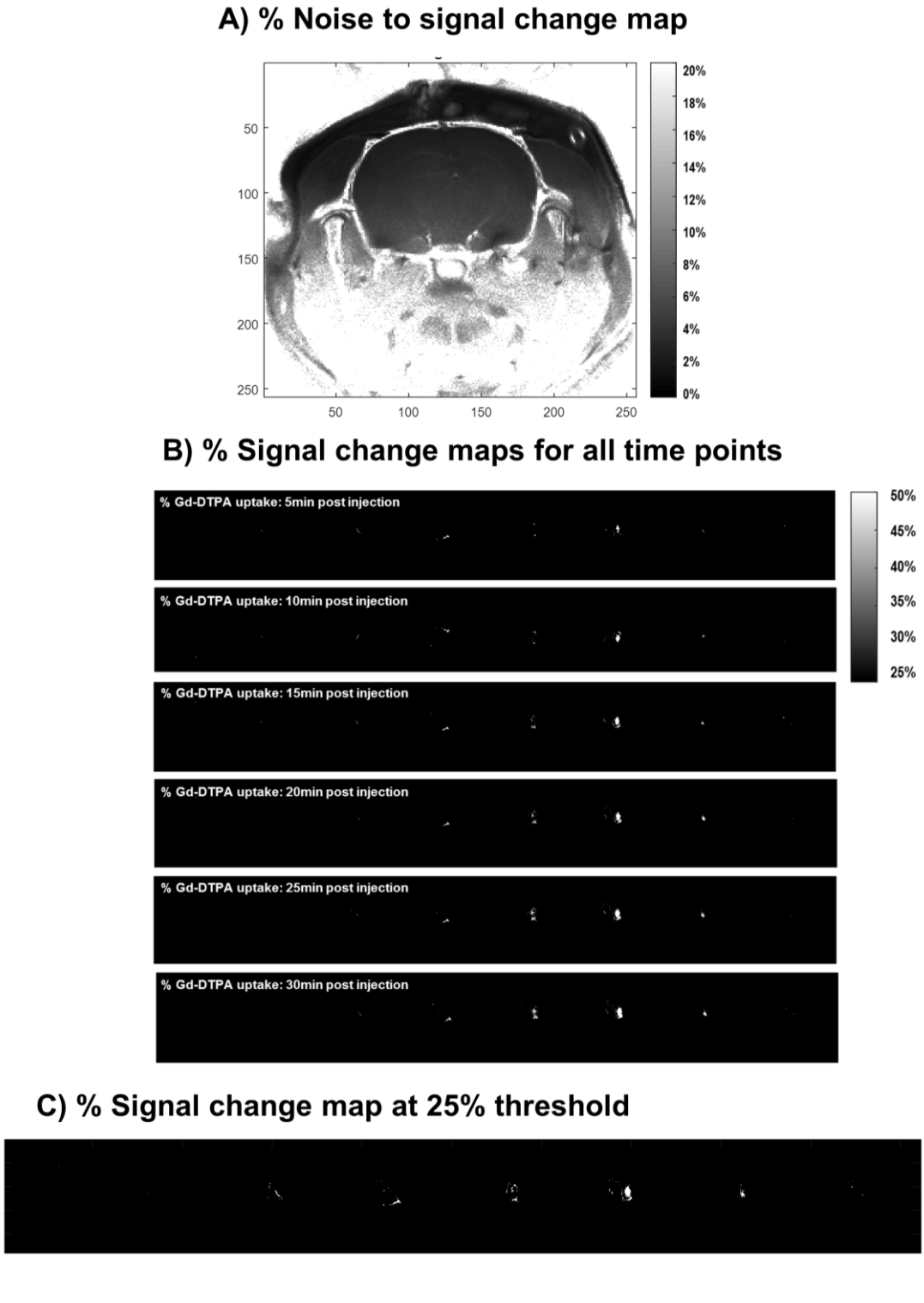

Figure 5-2 MRI-T_1 % signal change map assessment. A) % noise to signal change map. Image shows the noise contribution in signal change in a representative brain scan slice. It was observed that for all scanning images, noise was above 2% and below 5% for the majority of pixels. A threshold of 25%, five times higher the noise contribution (<5%) was defined to determine Gd-DTPA uptake in ipsilateral hemisphere across. **B) % Signal change map prior to threshold assessment.** Gd-DTPA uptake in the ipsilateral hemisphere at 5 min, 10 min, 15 min, 20 min, 25 min and 30 min post Gd-DTPA injection across 8 coronal levels. **C) % Signal change map at 25% threshold.** Representative image of Gd-DTPA uptake signal change in ipsilateral hemisphere defined at 25% threshold and at 20 min post Gd-DTPA injection across 8 coronal levels. Scale is defined from 0 to 1, where 0 represents voxels below threshold and 1 represents voxel values above the threshold (identified in white) and used to calculate Gd-DTPA uptake brain volume (mm^3).

5.2.5 Brain tissue processing

At the end of the MRI scanning, animals were removed from the MRI cradle and deeply anaesthetised for brain removal. For 14 rats (7 animals in each group), cerebral tissue was quickly sectioned into contralateral and ipsilateral sides and further divided into core and penumbra, snap frozen in liquid nitrogen and placed in -80^{o}C for gene expression. The remaining 10 animals (5 in each group) were perfusion fixed for histological assessment and IBA1^{+} microglia analysis carried out as defined in Chapter 2.

5.2.6 Exclusion criteria

The exclusion criteria were applied at the end of the study by two independent researchers that were blind to treatment allocation. Animals were excluded if presenting the following characteristics:

- Cannula not adequately placed in the cerebral ventricle at 24 hrs reperfusion as identified by MRI-T_2.
- MCA not adequately reperfused at 24 hrs reperfusion as shown by MRA
- ICH at the MCA origin at 24 hrs reperfusion as shown by MRI-T_2.
- Animals that died or were sacrificed prior to study completion.

5.2.7 Statistical analysis

Hemisphere volumes were compared within groups using paired Student's t-test. Infarct volume and Gd-DTPA uptake were compared across treatment groups using unpaired Student's t-test. Infarct volume intra-rater variability was assessed using parametric Pearson correlation and Bland-Altman analysis. Neurological score was compared using non parametric Mann-Whitney test.

Gene expression data were compared between Sham, MCAO-Vehicle(aCSF) and MCAO-Ang-(1-7) groups using one-way ANOVA with Tukey's post hoc test andshown as -ΔCt normalised to *Hrpt1*.

Total $IBA1^+$ microglia expressed as $n°/mm^2$ and % activated microglia from total cell number were compared between MCAO-Vehicle(aCSF) and MCAO-Ang-(1-7) treated groups in peri-infarct and homotopic contralateral regions using unpaired Student's t-test. Total microglia count and % activated microglia were compared within groups using paired Student's t-test.

Data are presented as mean ± S.D or median ± IQR. A p value of <0.05 was deemed statistically significant.

5.3 Results

5.3.1 Mortality and exclusions

A total of 33 animals were used in these experiments, where two in the Vehicle (aCSF) group died overnight, leading to a study mortality of 6.1%.

MRI-T_2 showed that 3 animals did not have the ICV cannula correctly placed [1 in the Vehicle (aCSF) and 2 in the Ang-(1-7) treated groups] and were therefore, excluded from this study. All animals demonstrated reperfusion of the MCA at 24 hrs post 90 min MCAO as determined by MRA and a total of 28 animals were included for infarct volume and neurological score analysis, 13 in the Vehicle (aCSF) and 15 in the Ang-(1-7) treated groups. For BBB breakdown assessment, 5 animals were excluded from analysis, 1 in the Vehicle (aCSF) and 4 in the Ang-(1-7) treated groups, as contrast agent injection was unsuccessful during tail vein injections. As a result, Gd-DTPA uptake was assessed in 12 rats in the Vehicle (aCSF) and 11 in the Ang-(1-7) groups.

5.3.2 Neurological Score

In this study, DWI or MRA were not conducted during MCAO. Consequently, investigators were blinded to initial lesion size and whether MCA was fully occluded. All animals with indications of neurological deficit at 24 hrs were included in this study. Garcia score shows that all animals had neurological impairment in both Vehicle (aCSF) and Ang-(1-7) treatment groups (Figure 5-3).

5.3.2.1 Ang-(1-7) does not affect neurological score

Data did not statistically differ between treatment groups, with Ang-(1-7) not influencing neurological outcome when compared to Vehicle (aCSF) treated animals ($P>0.05$). The median score for the Ang-(1-7) treated group was 11 (IQR: 10.0; 15.0). Similarly, Vehicle (aCSF) animals scored a median value of 13 (IQR: 10.50; 14.50), (Figure 5-3).

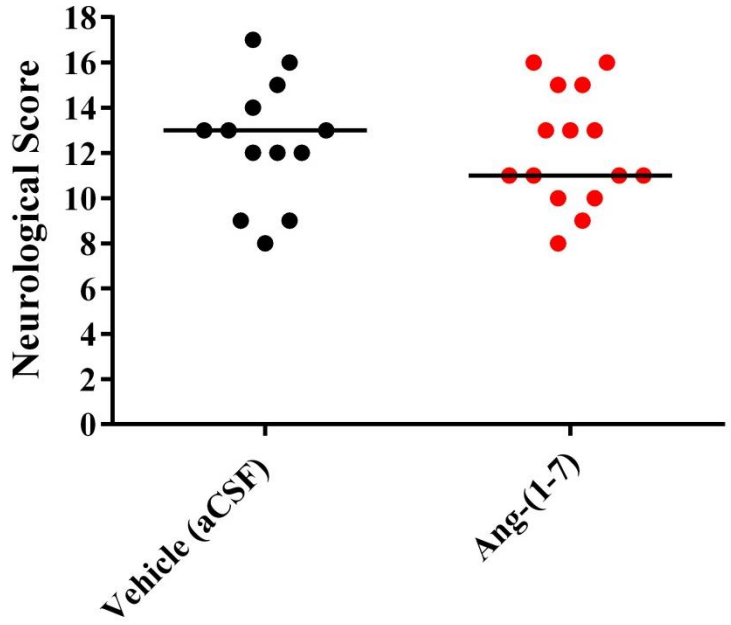

Figure 5-3 Neurological Score 24 hrs post 90 min MCAO. Neurological score at 24 hrs for Vehicle (aCSF) (n=13) and Ang-(1-7) (n=15) treated animals. There were no significant differences in neurological score between groups (P>0.05). Data were analysed with non-parametric Mann-Whitney test; P<0.05 was deemed as significant. Horizontal bar represents the median.

5.3.3 Hemisphere swelling

MRI-T_2 image analysis indicated that at 24 hrs post MCAO, ipsilateral hemisphere volume was significantly larger than contralateral hemisphere for both Vehicle (aCSF) [720.4±40.6mm^3 vs 653.7±35.8mm^3 (P<0.001)] and Ang-(1-7) [745.3±54.9mm^3 vs 665.4±39.1mm^3 (P<0.001)] treated groups (Figure 5-4A&B). These results indicate significant brain oedema at this time point following transient MCAO.

5.3.3.1 Ang-(1-7) does not affect % hemispheric swelling

The % of ipsilateral hemisphere swelling was calculated as a measure of vasogenic oedema. When assessing % hemisphere swelling between groups, Ang-(1-7) treatment did not impact % hemisphere swelling with values being comparable to Vehicle (aCSF) group [12.2±7.7% vs 10.6±10.1% (P>0.05)], (Figure 5-4C).

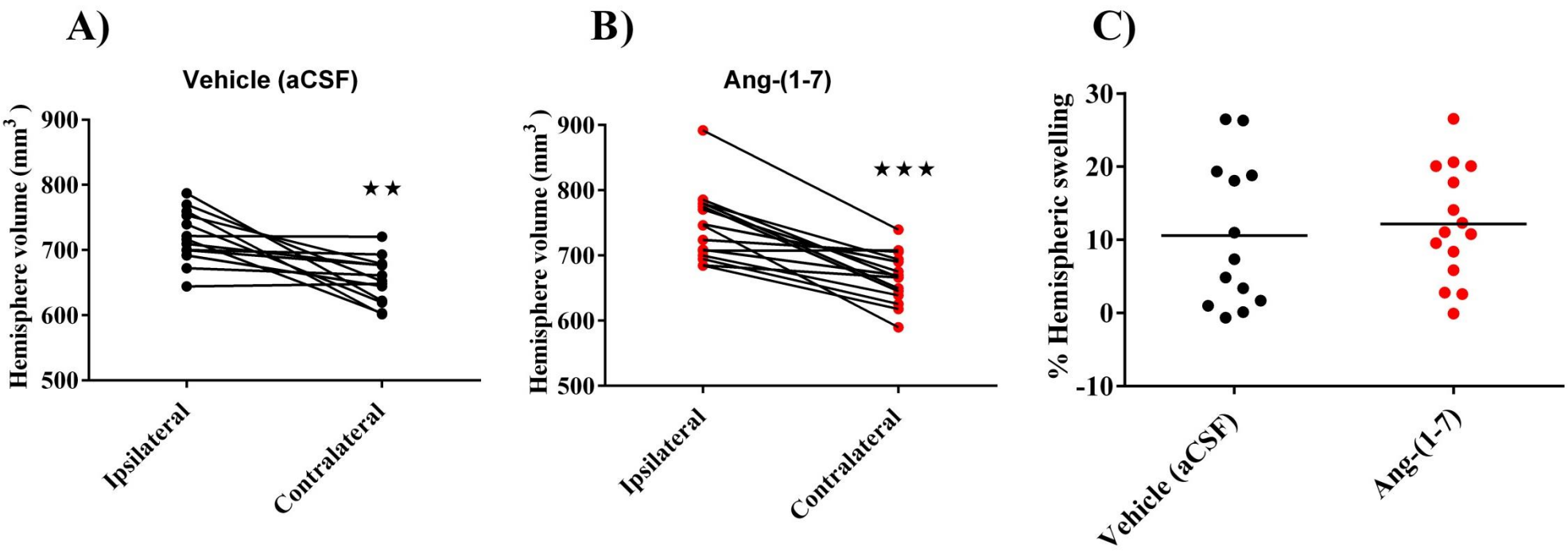

Figure 5-4 Hemispheric swelling 24 hrs post 90 min MCAO. A) Hemispheric volume for Vehicle (aCSF) treated animals; B) Hemispheric volume for Ang-(1-7) treated animals and C) % hemispheric swelling between groups. At 24 hrs post MCAO, ipsilateral hemisphere was significantly larger than the contralateral hemisphere for both Vehicle (aCSF) (P=0.002) and Ang-(1-7) (P<0.001) treated animals. Data indicates that there were no differences between Vehicle (aCSF) and Ang-(1-7) treated animals regarding % hemisphere swelling at 24 hrs post MCAO (P>0.05). Data depicts values for Vehicle (aCSF) (n=13) and Ang-(1-7) (n=15) treated animals. Figures A & B were analysed using paired Student's t test and Figure C analysed with unpaired Student's t test; *P<0.05 was deemed as significant. Horizontal bar represents the mean. **P<0.01; ***P<0.001.

5.3.4 Infarct volume

5.3.4.1 Ang-(1-7) does not change infarct outcome at 24 hrs reperfusion

Infarct volume was analysed blind to treatment groups and independently analysed on two separate occasions to assess intra-rater reproducibility (r= 0.99; P<0.0001), (Figure 5-5A). Bland-Altman assessments indicated that both analyses had a bias of -2.8mm^3 and a S.D of 15.5mm^3 with limits of agreement at -33.1mm^3 and 27.6mm^3 ranges (Figure 5-5B). The average of both analyses was taken as the final volume for each animal and corrected to hemisphere volume.

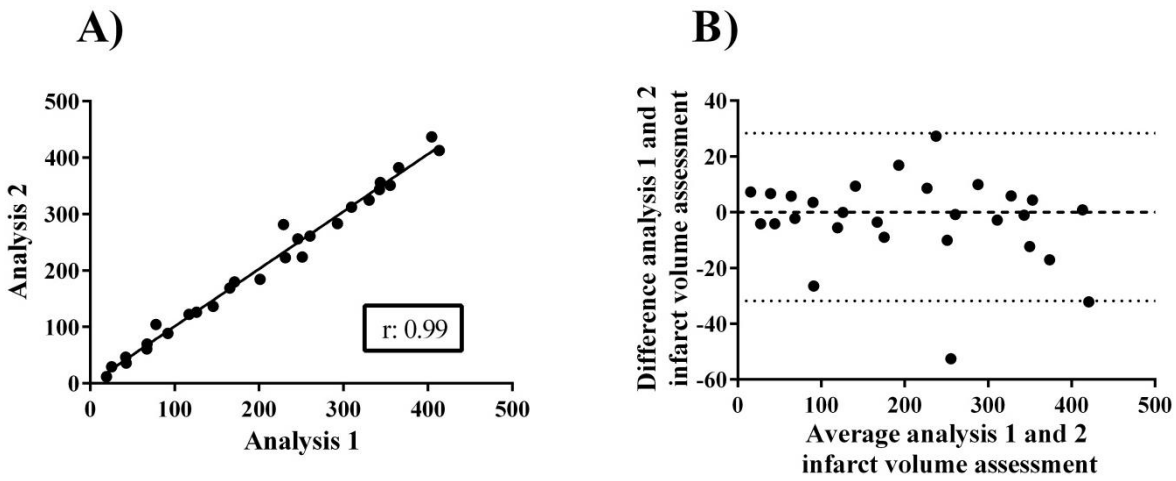

Figure 5-5 Intra-rater variability in infarct volume measurement 24 hrs post 90 min MCAO. A) Correlation between infarct volume analyses. Infarct volume was blindly assessed two independent times for each animal. Pearson correlation indicates that both analyses significantly correlate with a Pearson r of 0.99 (P<0.0001). **B) Bland-Altman analysis displaying difference and average in infarct analyses.** Both infarct volume analyses had a bias of -2.8mm^3 and a S.D. of 15.5mm^3 with limits of agreement at -33.1mm^{3}and 27.6mm^3 ranges. Horizontal lines represent limits of agreements and the intersection of x and yaxis at 0,0 coordinates.

At 24 hrs post 90 min MCAO, Ang-(1-7) treatment did not change infarct volume when compared to the control group. Infarct volume was 136.4±91.4mm^3 for Vehicle (aCSF) and 147.6±92.7mm^3 for Ang-(1-7) treated groups (P>0.05), (Figure 5-6). Two animals in both groups exhibited extremely small lesions, below 33mm^3, and this could be an indication that these animals had partial occlusions. Figure 5-7 illustrates the median animal for each treatment group.

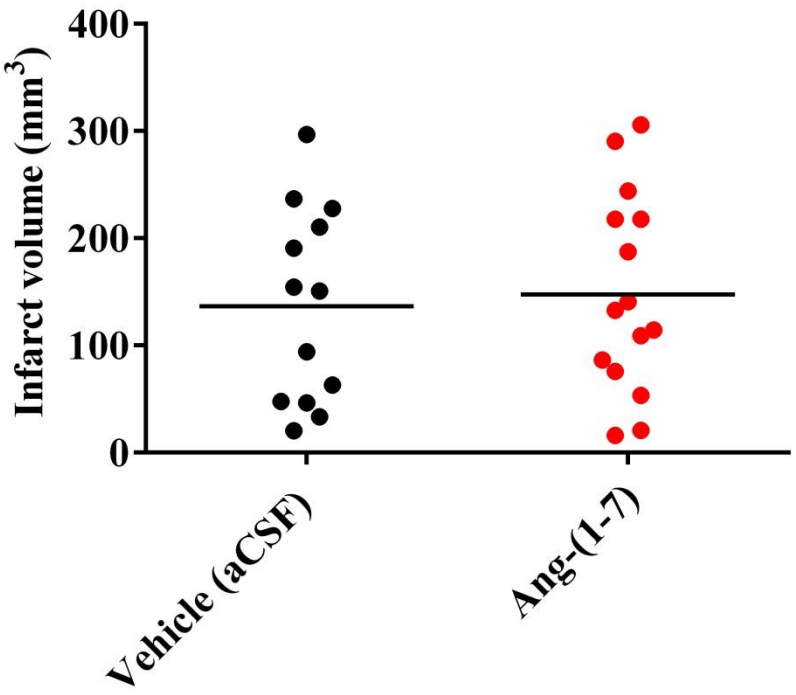

Figure 5-6 Infarct volume 24 hrs post 90 min MCAO. Infarct volume was not significantly different between groups (P>0.05). Data indicates infarct volume (mm^3) for Vehicle (aCSF; n=13), Ang-(1-7) (n=15) treated animals. Data were analysed using unpaired Student's t test; *P<0.05 was deemed as significant. Horizontal bar represents the mean.

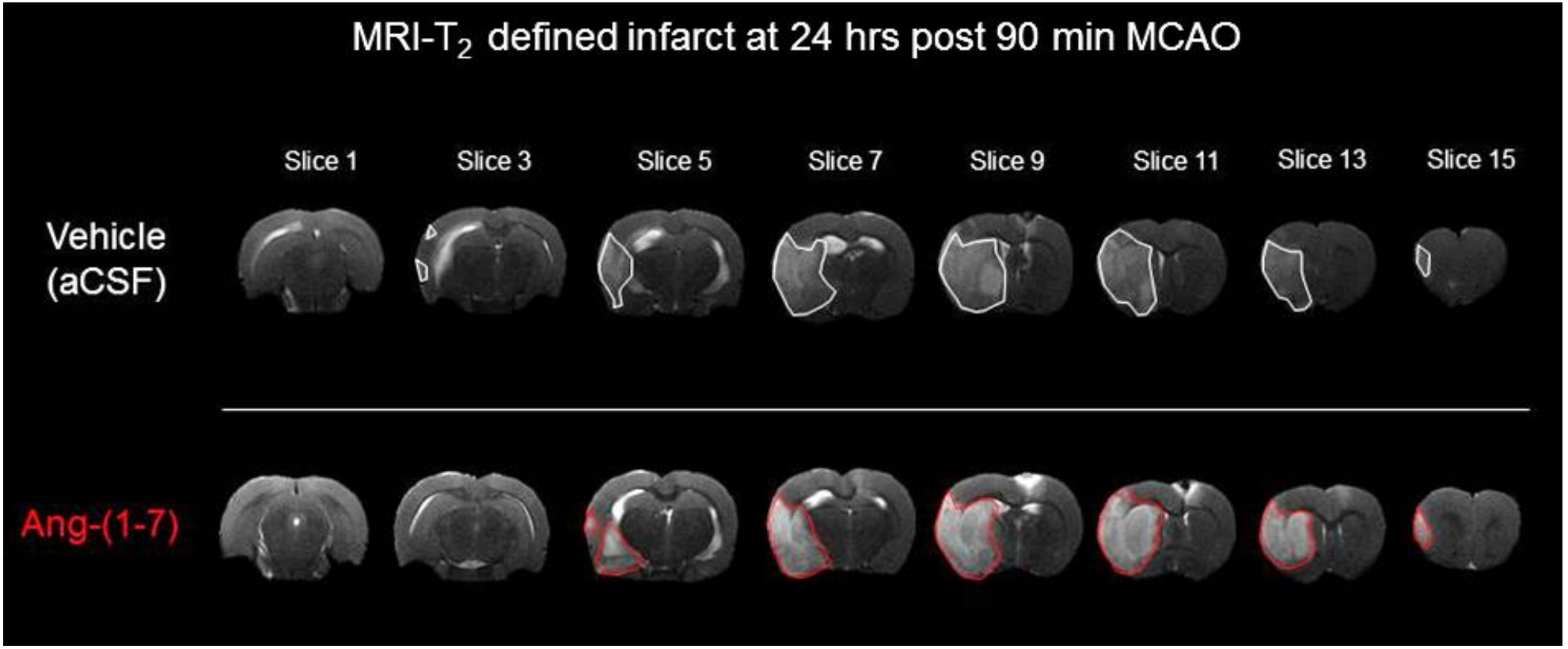

Figure 5-7 Infarct volume distribution for Vehicle (aCSF) and Ang-(1-7) treated median animals. Images show MRI-T_2 delineated infarct at 24 hrs post 90 min MCAO highlighted across 8 coronal levels. The top sequence illustrates the median animal in the Vehicle (aCSF) treated group highlighted in white whereas the bottom sequence shows the infarct size in the median animal in the Ang-(1-7) treated group highlighted in red.

5.3.5 Blood brain barrier breakdown assessment

The impact of Ang-(1-7) treatment on the extent of BBB breakdown at 24 hrs post 90 min MCAO was assessed by carrying out MRI-T_1-weighted sequences prior to and post- Gd-DTPA contrast agent IV injection at 5, 10, 15, 20, 25 and 30 min from injection start. The Gd-DTPA uptake volume determined at the 6 time points post injection was averaged to establish final Gd-DTPA cerebral uptake volume within the ipsilateral hemisphere.

5.3.5.1 Ang-(1-7) does not affect Gd-DTPA enhancement 24 hrs post tMCAO

Ang-(1-7) did not alter total Gd-DTPA uptake volume in the ipsilateral hemisphere when compared to Vehicle (aCSF) [19.7±8.7mm^3 vs 19.4±7.7mm^3 (P>0.05)], (Figure 5-8A). Total Gd-DTPA uptake volume was more variable in the Vehicle group, where 3 rats had very little uptake while 1 animal had an uptake of approximately 66mm^3, highlighting that at 24 hrs reperfusion there is considerable variability in the extent of BBB breakdown.

The extent of Gd-DTPA uptake was expressed as a % of the respective infarct areas. Similarly, Ang-(1-7) treatment did not influence Gd-DTPA enhancement in infarct areas compared to Vehicle (aCSF) treatment [16.8±23.0% vs 19.0±22.3% (P>0.05)], (Figure 5-8B). Together, these results suggest that Ang-(1-7) has no effect on BBB breakdown 24 hrs post MCAO. Figure 5-9 and 5-10 show a representative image of Gd-DTPA enhancement in infarct areas for the median animal in Vehicle (aCSF) and Ang-(1-7) groups, respectively.

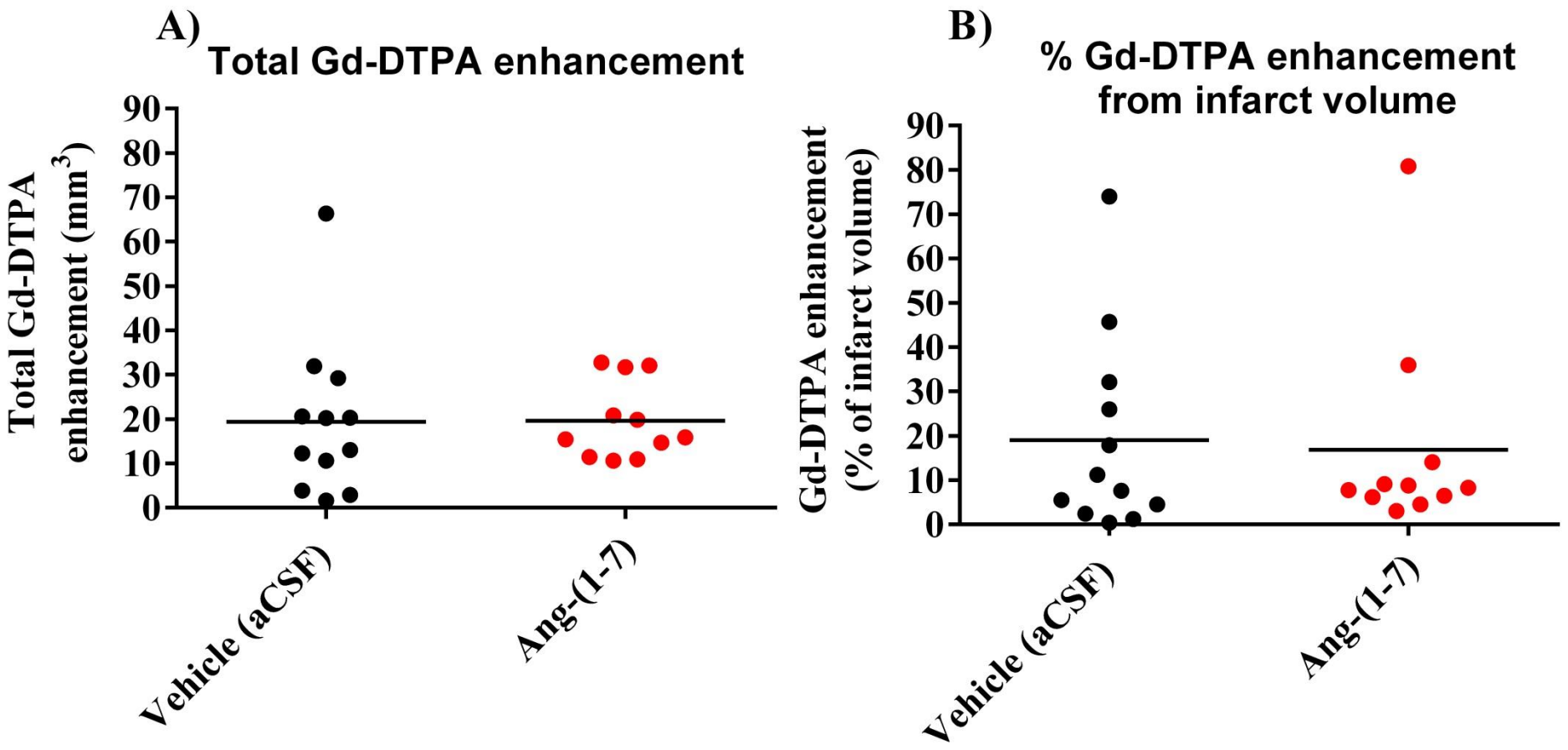

Figure 5-8 Gd-DTPA enhancement 24 hrs post 90 min MCAO. A) Total ipsilateral hemisphere Gd-DTPA volume uptake (mm^3) and B) Gd-DTPA volume uptake expressed as % of infarct volume (%). Ang-(1-7) treatment does not influence total Gd-DTPA volume or % uptake in infarct areas at 24 hrs post 90 min MCAO ($P>0.05$). Data depicts values for Vehicle (aCSF) (n=12) and Ang-(1-7) (n=11) treated animals. Data were analysed using unpaired Student's t test; $P<0.05$ was deemed as significant. Horizontal bar represents the mean.

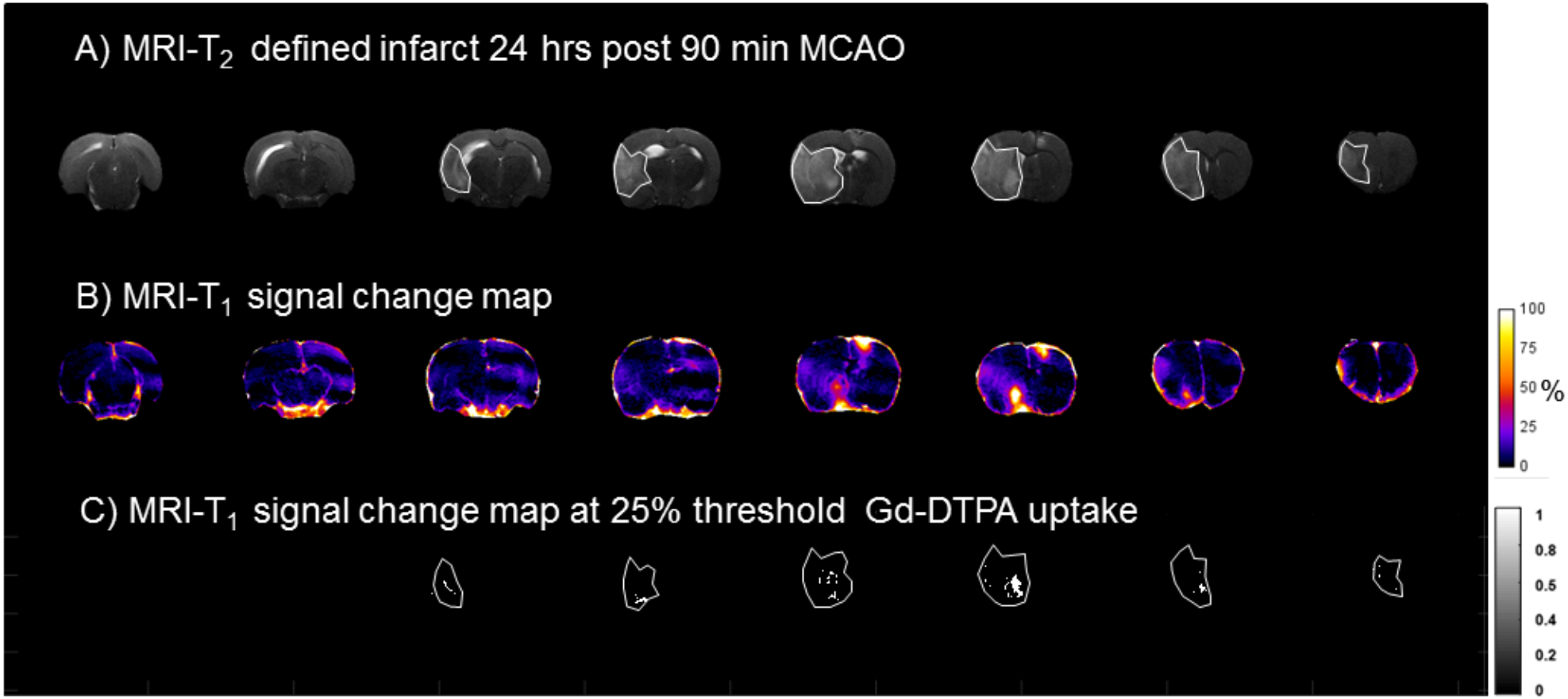

Figure 5-9 Gd-DTPA enhancement in Vehicle (aCSF) treated median animal. A) MRI-T_2 delineated infarct at 24 hrs post 90 min MCAO. Images show infarct volume across 8 coronal levels, highlighted in white. **B) MRI-T_1 signal change map.** % signal change map from pre to 30 min post Gd-DTPA injection. Images show Gd-DTPA enhancement across 8 coronal levels and the scale is set from 0 to 100% of Gd-DTPA enhancement. The Gd-DTPA enhancement observed in the contralateral hemisphere is due to ICV cannula placement. **C) MRI-T_1 signal change map at 25% threshold assessment.** Gd-DTPA enhancement at 25% threshold within the infarct areas as determined by MRI-T_2. Gd-DTPA uptake is highlighted in white and the scale bar defined from 0 to 1, where the voxels defined as 1 were counted and multiplied by the voxel dimensions to obtain the overall Gd-DTPA uptake brain volume.

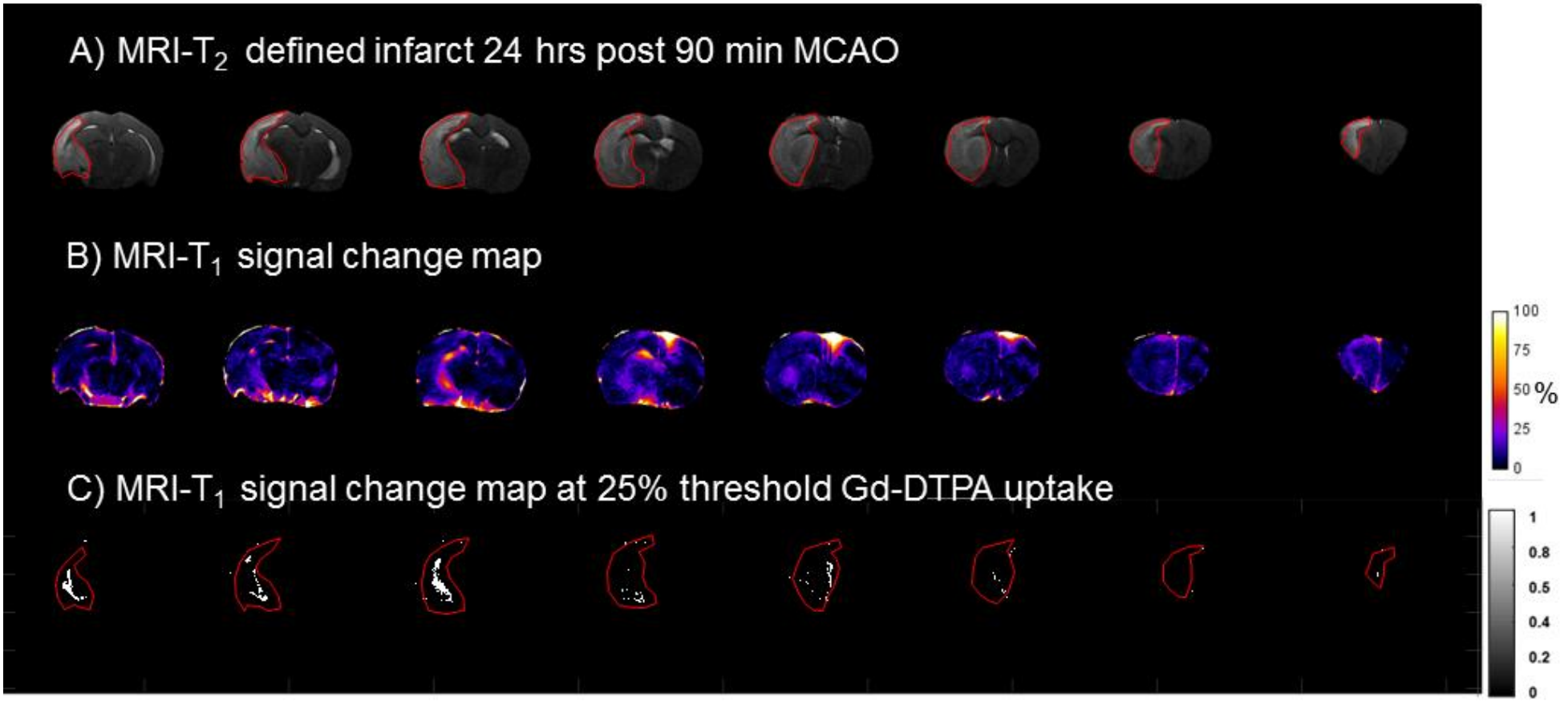

Figure 5-10 Gd-DTPA enhancement in Ang-(1-7) treated median animal. A) MRI-T_2 delineated infarct at 24 hrs post 90 min MCAO. Images show infarct volume across 8 coronal levels, highlighted in red. **B) MRI-T_1 signal change map.** Figures show % signal change map from pre to 30 min post Gd-DTPA injection prior to image processing as defined in the methods. Images show Gd-DTPA enhancement across 8 coronal levels andthe scale is set from 0 to 100% Gd-DTPA enhancement. The Gd-DTPA enhancement observed in the contralateral hemisphere is due to ICV cannula placement. **C) MRI-T_1 signal change map at 25% threshold assessment.** Gd-DTPA enhancement at 25% threshold within the infarct areas as determined by MRI-T_2. Gd-DTPA uptake is highlighted in white and scale bar is defined from 0 to 1, where the voxels defined as 1 were counted and multiplied by the voxel dimensions to obtain the overall Gd-DTPA uptake brain volume.

5.4 IBA1$^+$ microglia assessment

Immunohistochemistry was performed across coronal levels 3, 4 and 5 for Vehicle (aCSF, n=5) and Ang-(1-7) (n=5) treated groups as defined in Chapter 2. Peri-infarct regions and ischaemic area were defined with the aid of H&E staining where 3 ROIs were outlined in the peri-infarct area in ipsilateral and homotopic contralateral hemispheres. IBA1$^+$ microglia were counted in each of the 3 ROIs per coronal section and averaged. Data were expressed in n°/mm^2 taking into account cell count within each coronal level. In addition, cells were differentiated into resting or activated (Chapter 2) and presented as % activated microglia from total cell count.

5.4.1 Ang-(1-7) does not influence microglia levels in peri-infarct and contralateral regions compared to Vehicle (aCSF)

Total microglial numbers were similar between Ang-(1-7) and Vehicle (aCSF) treated groups in peri infarct regions [106.1±36.3 n°/mm^2 vs 111.1±45.4 n°/mm^2 (P>0.05)], (Figure 5-11A). Similarly, in the homotopic contralateral region, Ang-(1-7) treatment did not influence total microglia count when compared to Vehicle (aCSF) [129.0±20.3 n°/mm^2 vs 130.6±29.3 n°/mm^2 (P>0.05)], (Figure 5-11B).

Treatment did not alter % activated microglia in the peri-infarct region when compared to the Vehicle (aCSF) group [86.2±30.8% vs 93.0±11.7% (P>0.05)], (Figure 5-12A). Similarly, % activated microglia was comparable between groups in the homotopic contralateral hemisphere [62.2±2.9% vs 68.3±24.1% (P>0.05)], (Figure 5-12B). Together, this data suggests that Ang-(1-7) does not alter total microglia count or cell activation at 24 hrs post MCAO.

Data also indicates that cell numbers were similar in the peri-infarct and homotopic contralateral hemisphere within groups. Although microglia were not counted in the infarct, it was observed that IBA1$^+$ cells were rarely observed in this area. Figure 5-13 and 5-14 show a representative image of IBA1$^+$ microglia staining within the peri-infarct, contralateral and ischaemic core. Images represent IBA1$^+$ positive staining across the three assessed coronal levels for the median animal in the Vehicle (aCSF) and Ang-(1-7) treated group, respectively.

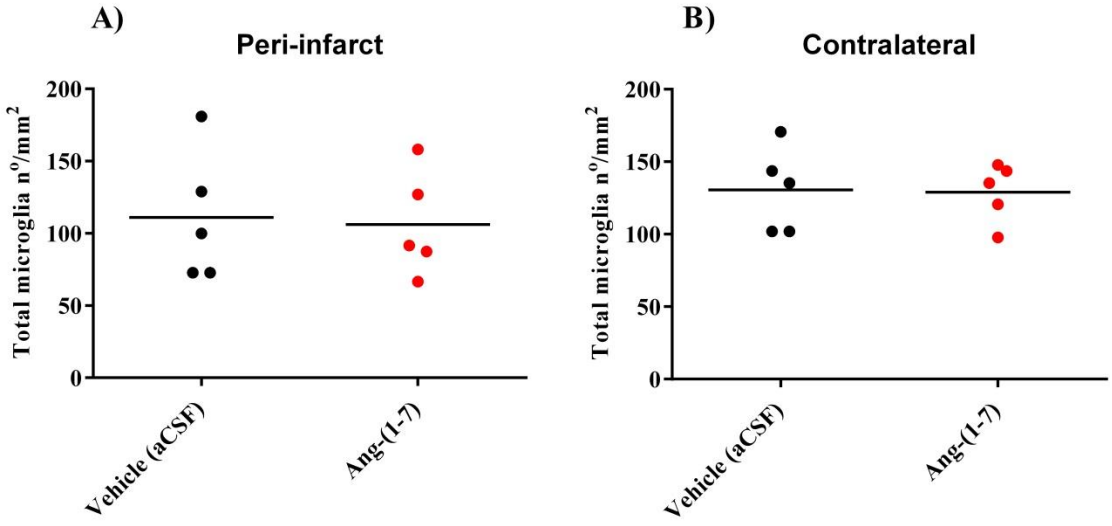

Figure 5-11 Total microglia in peri-infarct and contralateral regions 24 hrs post 90 min MCAO. A) Peri-infarct region; B) Homotopic contralateral region. Total microglia n°/mm^2 were comparable between Vehicle (aCSF) and Ang-(1-7) treated groups (P>0.05) in both peri-infarct and homotopic contralateral regions. Data shows total cell number per mm^2 brain area for Vehicle (aCSF; n=5) and Ang-(1-7) (n=5) treated animals. Data were analysed with unpaired Student's t test; P<0.05 was deemed as significant. Horizontal bar represents the mean.

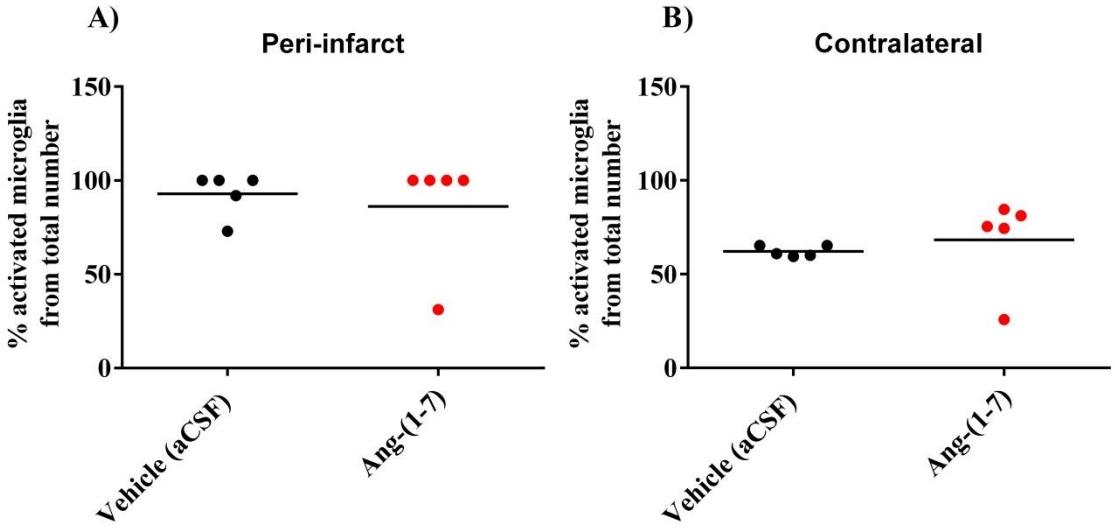

Figure 5-12 % activated microglia in peri-infarct and contralateral regions 24 hrs post 90 min MCAO. A) Peri-infarct region; B) Homotopic contralateral region. % activated cells from total number were comparable between treatment groups in both peri-infarct and homotopic contralateral regions (P>0.05). Data shows % activated microglia from total number for Vehicle (aCSF; n=5) and Ang-(1-7) (n=5) treated animals. Data were analysed with unpaired Student's t test; P<0.05 was deemed as significant. Horizontal bar represents the mean.

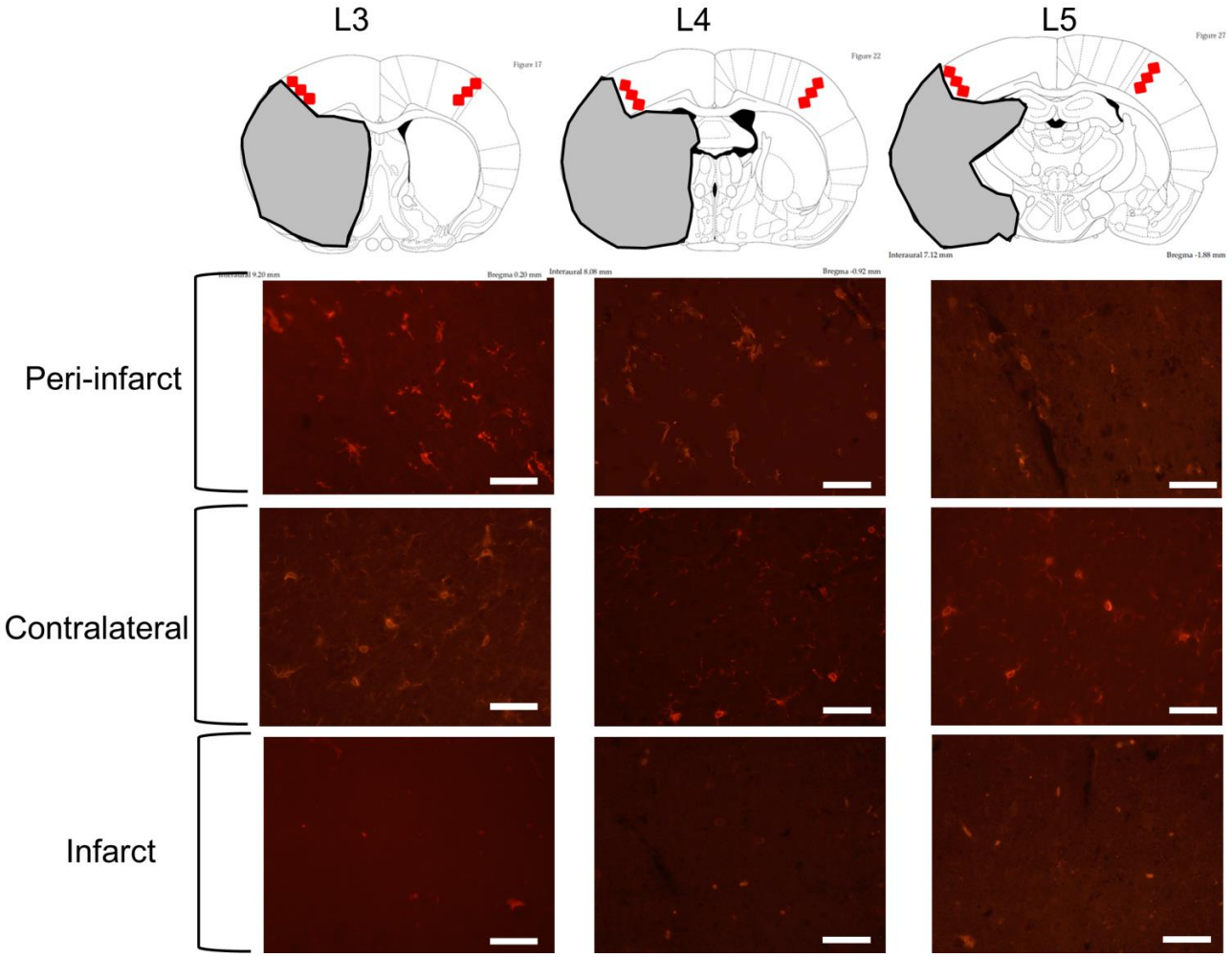

Figure 5-13 IBA1$^+$ microglia staining in peri-infarct, contralateral and infarct regions for Vehicle (aCSF) treated animal. Peri-infarct regions were defined with the aid of histology analysis as defined in Paxinos and Watson coronal levels. Infarct was outlined (grey) and three ROIs were defined for imaging and IBA1$^+$ cell count in peri-infarct and homotopic contralateral areas (red squares). IBA1$^+$ microglia immunohistochemistry staining (highlighed in red) across coronal levels 3, 4 and 5. Scale is set at 50μM per white bar.

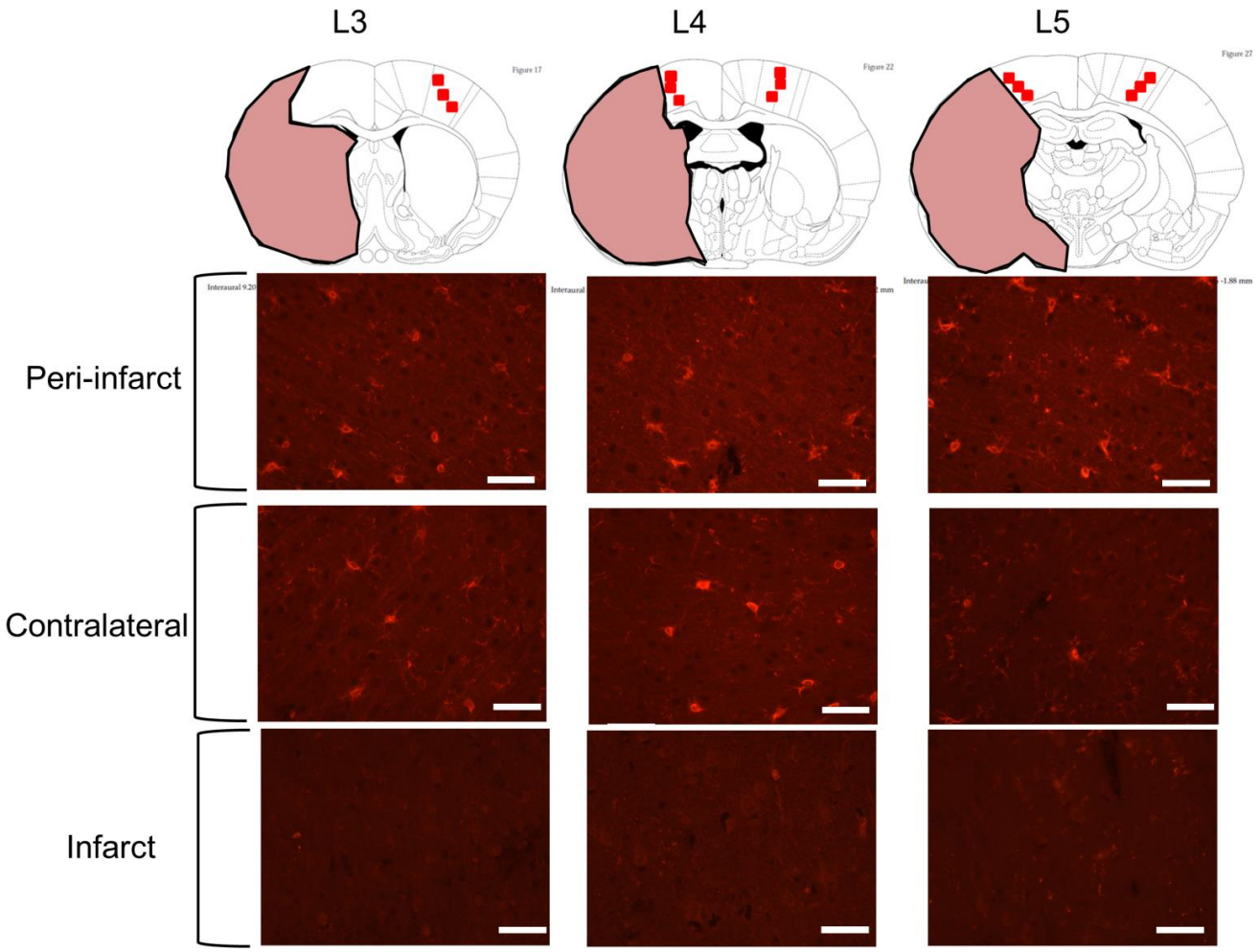

Figure 5-14 IBA1$^+$ microglia staining in peri-infarct, contralateral and infarct regions for Ang-(1-7) treated animal. Peri-infarct regions were defined with the aid of histology analysis as defined in Paxinos and Watson coronal levels. Infarct was outlined (pink) and three ROIs were defined for imaging and IBA1$^+$ cell count in peri-infarct and homotopic contralateral areas (red squares). IBA1$^+$ microglia immunohistochemistry staining (highlighed in red) across coronal levels 3, 4 and 5. Scale is set at 50μM per white bar.

5.4.2 Total microglia count is comparable between peri infarct and contralateral regions within groups at 24 hrs

In the prior section, it was observed that microglia numbers were similar between peri-infarct and contralateral regions. To confirm that the model successfully increased activated microglia within the peri-infarct in comparison to the homotopic contralateral region, values were compared within each group.

In the Vehicle (aCSF) animals, total microglia cell count was comparable between peri-infarct and homotopic contralateral regions [111.1±45.44 n°/mm^2 vs 130.6±29.28 n°/mm^2 ($P>0.05$), respectively], (Figure 5-15A). The peri-infarct region exhibited significantly higher % of activated microglia [92.97±11.74% vs 62.20±2.89% ($P<0.01$), respectively] (Figure 5-15B). Similarly, in the Ang-(1-7) group, total microglia count were comparable between regions [106.1±36.27 n°/mm^2 vs 129.0±20.27 n°/mm^2 ($P>0.05$)], (Figure 5-16A). The peri-infarct exhibited significantly higher levels of % activated microglia compared to the contralateral region [86.23±30.79% vs 68.28±24.07%; ($P<0.01$)], (Figure 5-16B). These results indicate that although total cell count was comparable within peri-infarct and homotopic regions, MCAO successfully led to an increase in % of activated cells within the peri-infarct compared to homotopic contralateral regions for both groups.

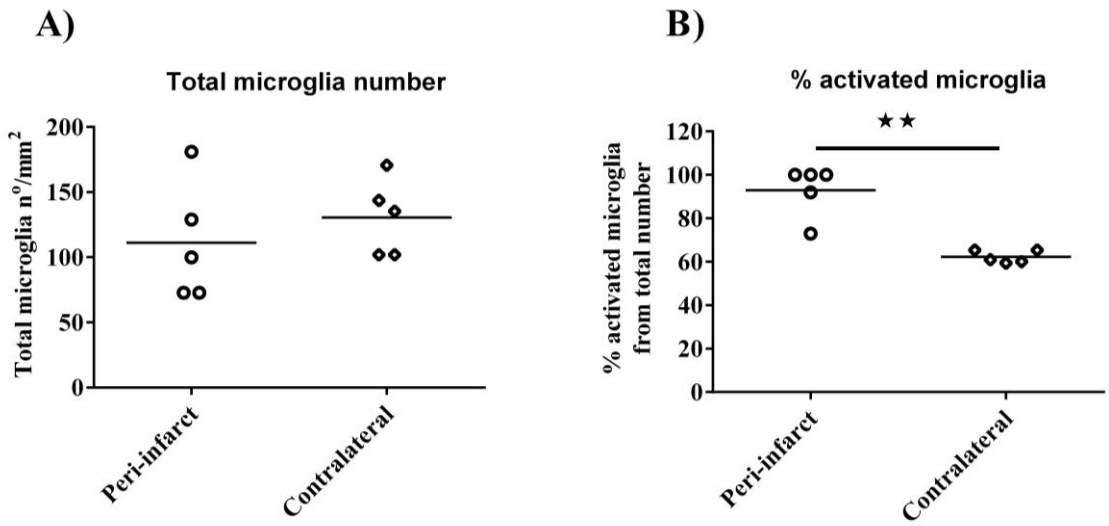

Figure 5-15 IBA1⁺ microglia assessment within Vehicle (aCSF) treated group. A) Total cell count; B) % activated cells. Total microglia n°/mm² was comparable in peri-infarct and contralateral regions (P>0.05). % activated cells were significantly higher in the peri-infarct region compared to the contralateral side (P<0.01)**.** Data were expressed as total nº/mm² or % of total cell count. Data were analysed with paired Student's t test; P<0.05 was deemed as significant. Horizontal bar represents the mean.

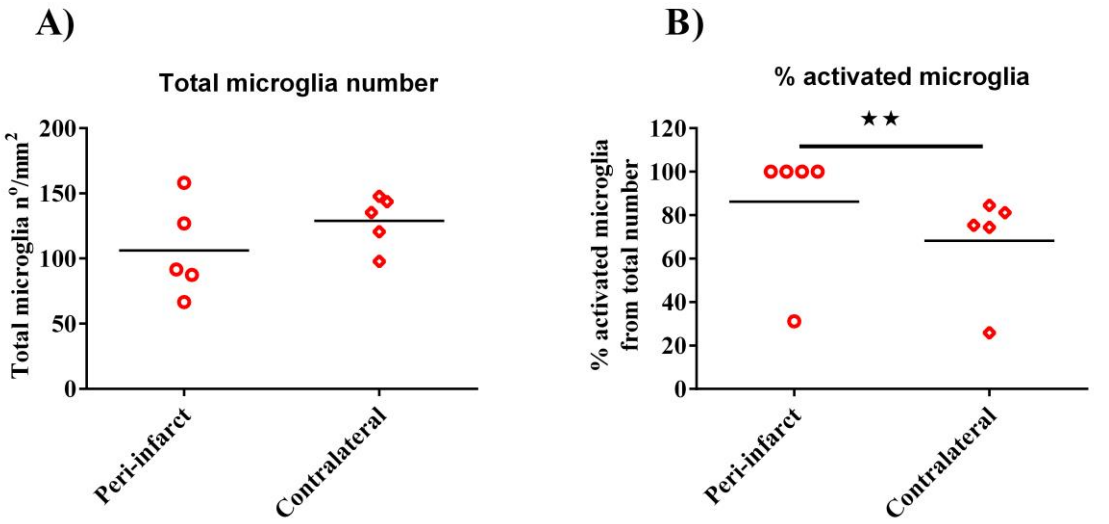

Figure 5-16 IBA1⁺ microglia assessment within Ang-(1-7) treated group. A) Total cell count; B) % activated cells. Total microglia n°/mm² were comparable in peri-infarct and contralateral regions (P>0.05). % activated cells were significantly higher in the peri-infarct region compared to the contralateral side (P<0.01)**.** Data were expressed as total nº/mm² or % of total cell count. Data were analysed with paired Student's t test; P<0.05 was deemed as significant. Horizontal bar represents the mean.

5.5 Quantitative Real Time PCR

Following 24 hrs reperfusion, peri-infarct ipsilateral brain regions for Sham (n=6), MCAO-aCSF (n=7) and MCAO-Ang-(1-7) (n=7) treated animals were assessed for gene expression. *Hrpt1* was selected as internal control for data normalisation as described in detail in Chapter 2.

5.5.1 MCAO did not affect RAS or *Bdkrb2* expression

Following 24 hrs post 90 min MCAO, *Atgr1a*, *Atgr2r*, *Mas1*, *Ace*, *Ace2* and *Bdkrb2* levels were comparable to Sham tissue, P>0.05 (Figure 6-17A:F).

5.5.2 MCAO significantly increased *Mmp9* and *Timp1* expression

Mmp9 expression was significantly higher in MCAO-aCSF group when compared to Sham tissue [-3.1±1.6 vs -5.8±2.0 (P<0.05)], (Figure 5-18A). MCAO-Ang-(1-7) showed a trend to significantly upregulate *Mmp9* expression when compared to Sham, however, this was not statistically significant [-3.3±1.9 vs -5.8±2.0 (P=0.056)], (Figure 5-18A). Treatment did not change *Mmp9* expression following MCAO.

Timp1 was significantly upregulated following MCAO in both Vehicle (aCSF) and Ang-(1-7) treated animals compared to Sham; 2.1±2.5 vs -3.3±0.6 (P<0.001) and 3.1±1.9 vs -3.3±0.6 (P<0.001), respectively (Figure 5-18B). The relative expression of *Timp1* was higher than *Mmp9* at this time point, perhaps explaining the low levels of brain Gd-DTPA uptake after 90 min MCAO. Supportively, the average Ct values for *Timp1* were 25.0 and 23.6 for Vehicle and Ang-(1-7) treated groups whereas *Mmp9* Ct values were 30.2 and 30.0, respectively.

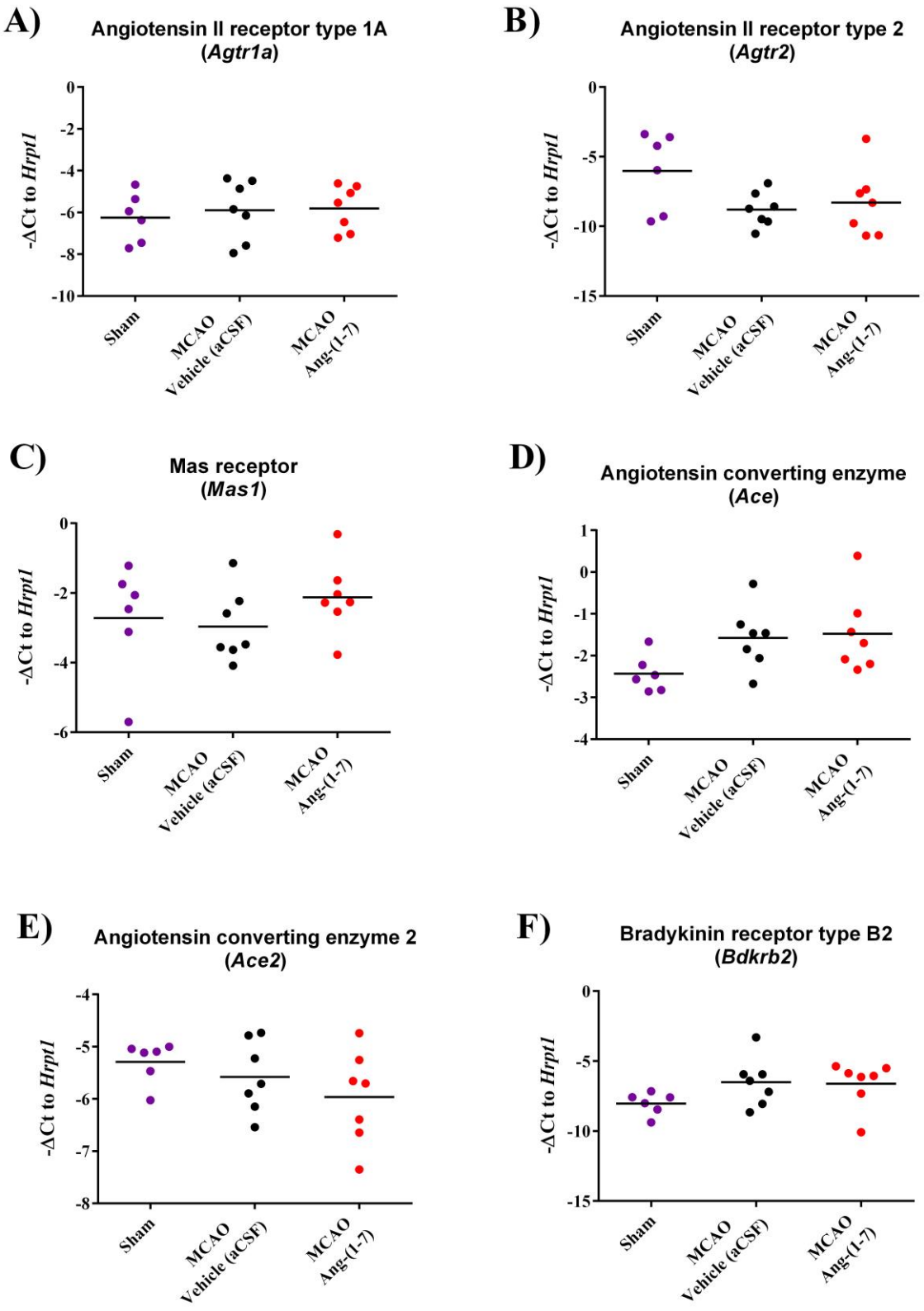

Figure 5-17 RAS components and B_2R gene expression 24 hrs post 90 min MCAO. A) *Atgr1a*; B) *Atgr2*; C) *Mas1*; D) *Ace*; E) *Ace2* and F) *Bdkrb2*. MCAO did not alter RAS mediators or B_2R gene expression in both Vehicle (aCSF) and Ang-(1-7) treated animals compared to Sham ($P>0.05$). Data were presented as -ΔCt normalised to *Hrpt1* for Sham (n=6); MCAO-Vehicle (aCSF;n=7) and MCAO-Ang-(1-7) (n=7) treated animals in peri-infarct regions. Data were analysed with one-way ANOVA; $P<0.05$ was deemed as significant. Horizontal bar represents the mean.

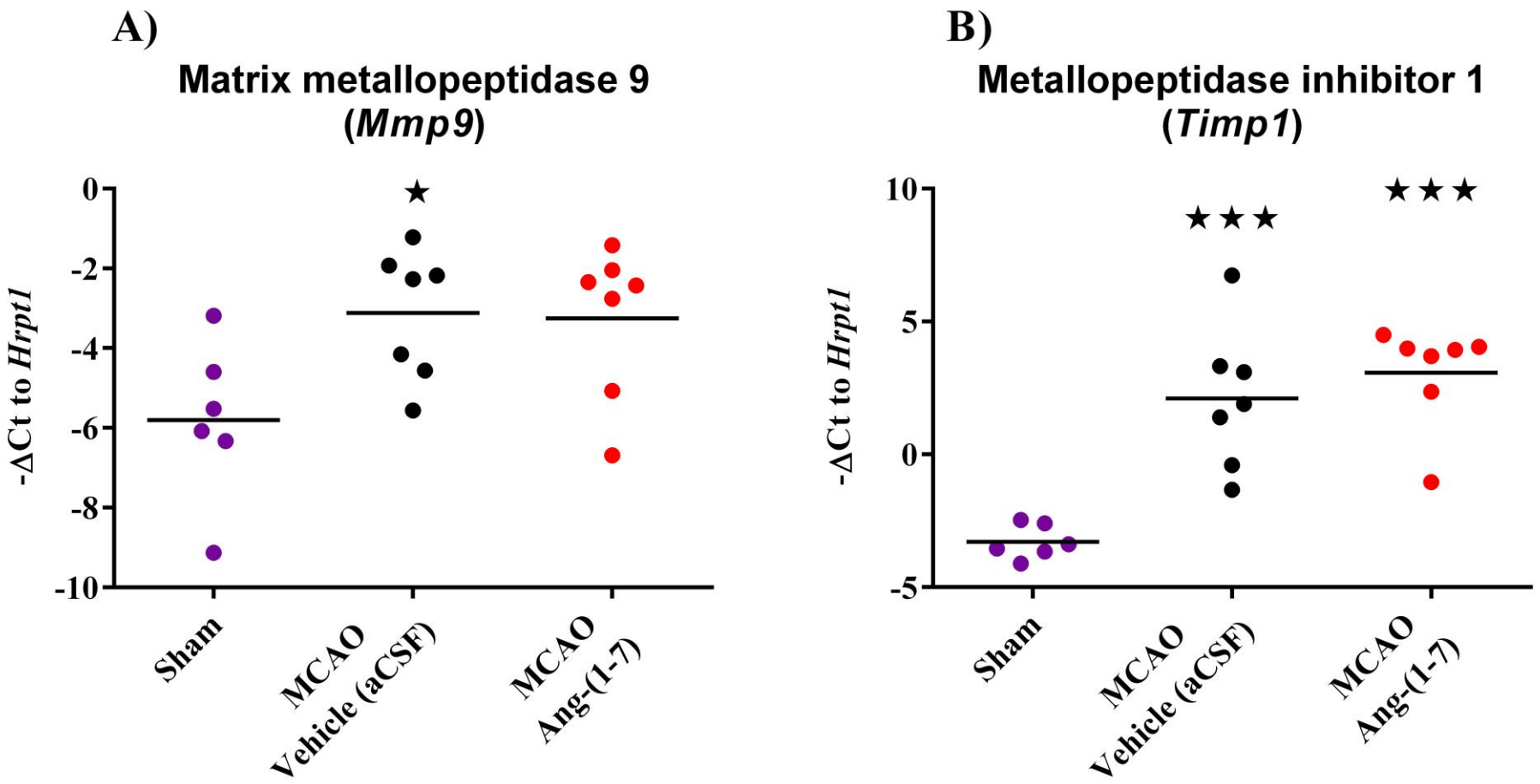

Figure 5-18 *MMP9* and *TIMP1* gene expression 24 hrs post 90 min MCAO. A) *Mmp9* and B) *Timp1*. MCAO significantly upregulated *Mmp9* in MCAO-aCSF group compared to Sham (P<0.01). MCAO-Ang-(1-7) animals showed a trend to significantly upregulate *Mmp9* compared to Sham (P=0.056). There were no statistical differences between MCAO-Vehicle and MCAO-Ang-(1-7) groups. MCAO significantly upregulated *Timp1* expression compared to Sham in both Vehicle (aCSF) (P<0.001) and Ang-(1-7) (P<0.001) treated groups. Data were presented as -ΔCt normalised to *Hrpt1* for Sham (n=6); MCAO-Vehicle (aCSF;n=7) and MCAO-Ang-(1-7) (n=7) treated animals in peri-infarct regions. Data were analysed with one-way ANOVA with Tukey's post-hoc test; P<0.05 was deemed as significant. *P<0.05; ***P<0.001 compared to Sham. Horizontal bar represents the mean.

5.5.2.1 Ang-(1-7) treatment did not impact *Vegfa* or *Kdr* expression

VEGFA (*Vegfa*) and VEGFR-2 (*Kdr*) levels were comparable between groups, P>0.05 (Figure 5-19A&B).

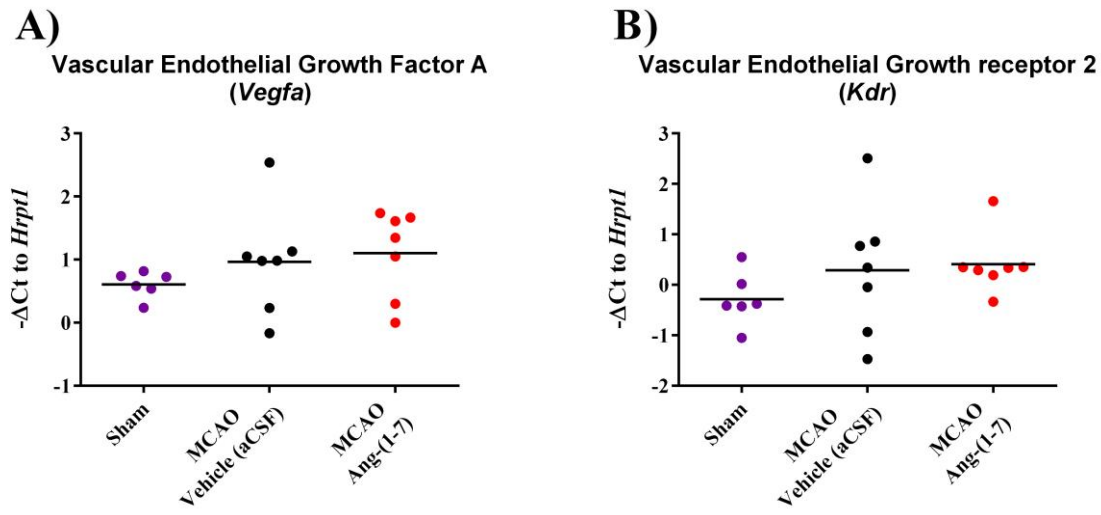

Figure 5-19 *VEGFA* and *VEGFR-2* gene expression 24 hrs post 90 min MCAO. A) *Vegfa* and B) *Kdr*. MCAO did not alter *Vegfa* or *Kdr* expression when compared to Sham (P>0.05). Data were presented as -ΔCt normalised to *Hrpt1* for Sham (n=6); MCAO-Vehicle (aCSF; n=7) and MCAO-Ang-(1-7) (n=7) treated animals in peri-infarct regions. Data were analysed with one-way ANOVA; P<0.05 was deemed as significant. Horizontal bar represents the mean.

5.5.3 MCAO significantly increased *Ptgs2* but not *Nfkb1*

MCAO in Vehicle (aCSF) and Ang-(1-7) treated groups significantly upregulated *Ptgs2* expression compared to Sham tissue; 0.7±1.7 vs -1.8±1.1 (P<0.05) and 1.4±1.8 vs -1.8±1.1 (P<0.05), respectively (Figure 5-20A). Conversely, *Nfkb1* levels ware comparable to Sham levels between groups (P>0.05), (Figure 5-20B).

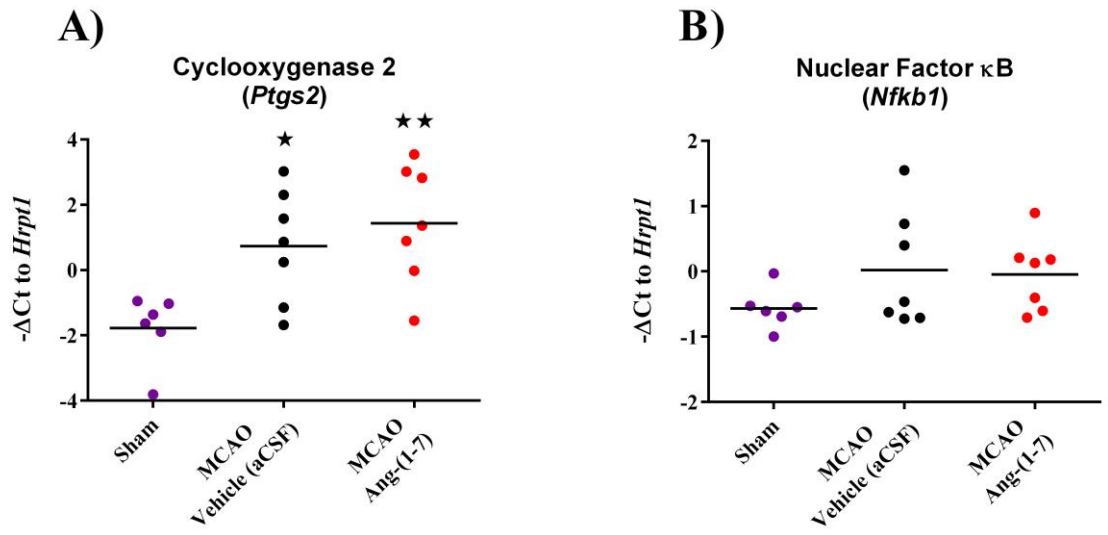

Figure 5-20 *COX-2* and *NF-κB* gene expression 24 hrs post 90 min MCAO. A) *Ptgs2* and B) *Nfkb1*. MCAO significantly upregulated *Ptgs2* expression when compared to Sham (P<0.05). Conversely, *Nfkb1* levels were comparable amongst groups (P>0.05). Data were presented as -ΔCt normalised to *Hrpt1* for Sham (n=6); MCAO-Vehicle (aCSF; n=7) and MCAO-Ang-(1-7) (n=7) treated animals in peri-infarct regions. Data were analysed with one-way ANOVA with Tukey's post-hoc test; P<0.05 was deemed as significant. Horizontal bar represents the mean. *P<0.05; **P<0.01 compared to Sham.

5.5.4 MCAO significantly upregulated *Cxcr2*, *Ccr2* and *Ccr5*

Cxcr2 was significantly upregulated in MCAO-Vehicle (aCSF) and MCAO-Ang-(1-7) when compared to Sham animals in peri-infarct regions: -5.0±2.3 vs -8.8±1.2 (P=0.002) and -6.0±1.6 vs -8.8±1.2 (P=0.02), respectively (Figure 5-21A). Similarly, MCAO significantly upregulated *Ccr2* in Vehicle and Ang-(1-7) treated groups compared to Sham: -3.2±2.2 vs -6.2±0.8 (P=0.01) and -3.0±1.8 vs -6.3±0.8 (P=0.009), respectively (Figure 5-21B). *Ccr5* levels significantly increased following MCAO-Vehicle (aCSF) compared to Sham, -1.24±0.50 vs -2.12±0.76 (P=0.04). MCAO-Ang-(1-7) treated rats showed a trend to prevent the increase in *Ccr5* expression as seen in MCAO-Vehicle animals. MCAO-Ang-(1-7) *Ccr5* values were not significantly different from Sham (P=0.64) or MCAO-Vehicle rats (P=0.17), (Figure 5-21C).

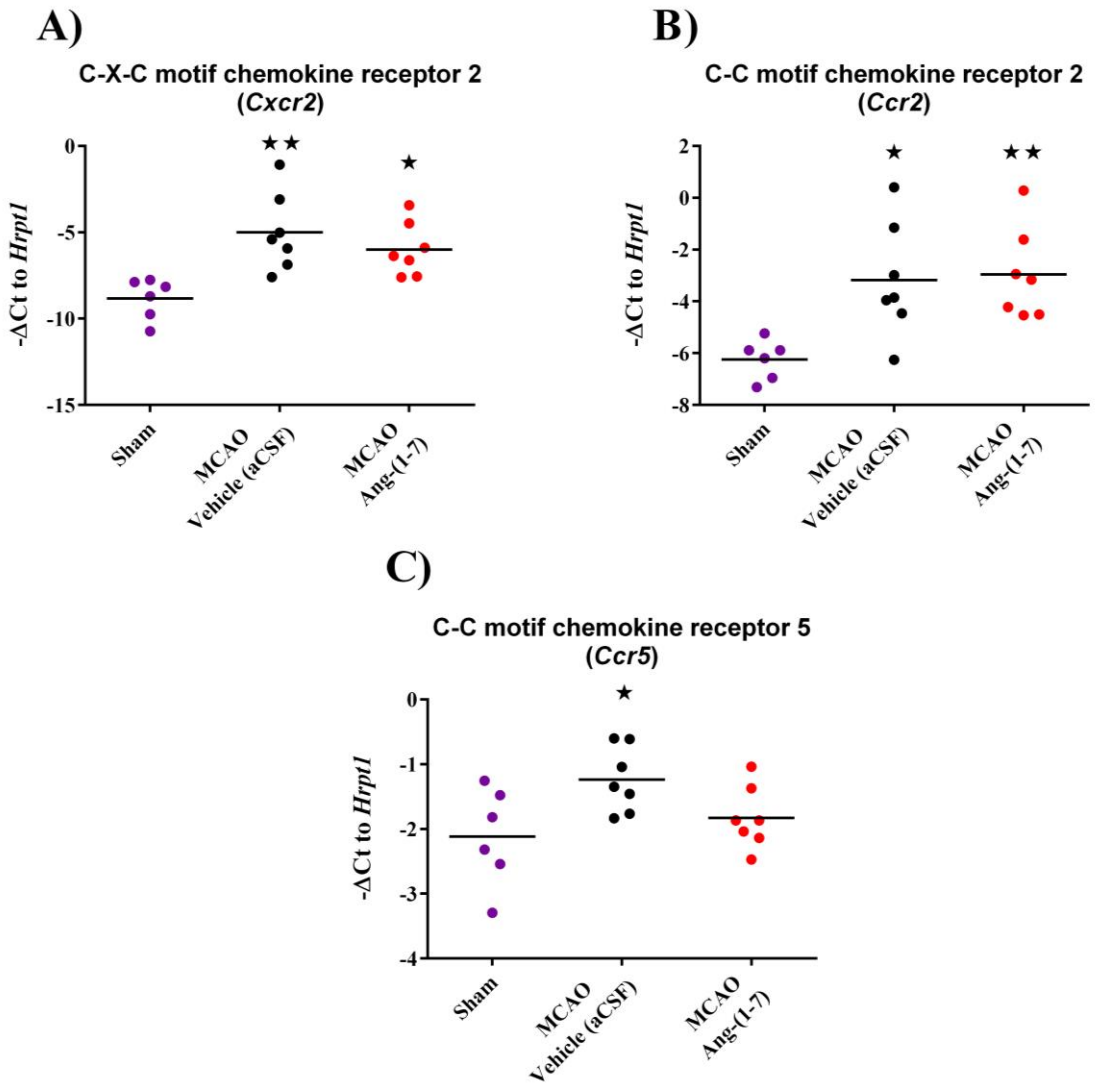

Figure 5-21 Chemokine receptor expression 24 hrs post 90 min MCAO. A) *Cxcr2*; B) C*cr2* and C) Ccr5. MCAO significantly upregulated *Cxcr2* and *Ccr2* expression compared to Sham animals (P<0.05). MCAO significantly upregulated *Ccr5* in MCAO-aCSF group compared to sham (P<0.05) whereas MCAO-Ang-(1-7) was not significantly different from Sham or MCAO-Vehicle (aCSF) (P>0.05). Data were presented as -ΔCt normalised to *Hrpt1* for Sham (n=6); MCAO-Vehicle (aCSF; n=7) and MCAO-Ang-(1-7) (n=7) treated animals in peri-infarct regions. Data were analysed with one-way ANOVA with Tukey's post-hoc test; P<0.05 was deemed as significant. Horizontal bar represents the mean. *P<0.05 compared to Sham.

5.5.5 MCAO does not impact *Nox1* or *Nox2* expression

Nox1 and *Nox2* gene expression were comparable to Sham levels between groups (P>0.05), (Figure 5-22A&B).

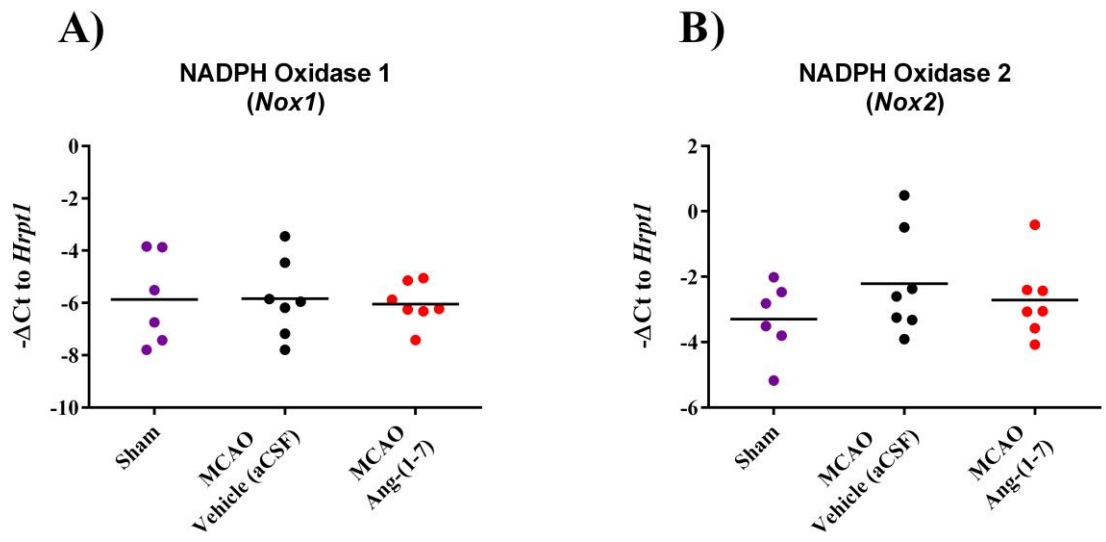

Figure 5-22 *NOX* type 1 and type 2 gene expression 24 hrs post 90 min MCAO. A) *Nox1*; B) *Nox2*. Data shows that MCAO did not alter *Nox1* or *Nox2* compared to Sham (P>0.05). Data were presented as -ΔCt normalised to *Hrpt1* for Sham (n=6); MCAO-Vehicle (aCSF; n=7) and MCAO-Ang-(1-7) (n=7) treated animals in peri-infarct regions. Horizontal bar represents the mean. Data were analysed with one-way ANOVA; P<0.05 was deemed as significant.

5.5.6 MCAO increased M1 type microglia/macrophage profile expression

MCAO significantly upregulated *CD86* levels compared to Sham; -3.2±1.5 vs -5.6±0.8 and -3.3±1.6 vs -5.6±0.8 (P<0.001) in Vehicle and Ang-(1-7) treated rats, respectively (Figure 5-23A). Similarly, MCAO significantly increased *Itgam* [-0.3±0.8 vs -3.2±0.7 and -0.8±0.7 vs -3.2±0.7 (P<0.001)] (Figure 5-23B), *Il6* [-3.8±2.6 vs -8.7±0.9 and -3.2±1.7 vs -8.7±0.9 (P<0.001)] (Figure 5-23C), *Il1b* [-4.89±1.95 vs -7.62±0.60 (P=0.002) and -4.91±1.82 vs -7.62±0.60 (P<0.001)] (Figure 5-23D), *Nos2* [-4.9±2.8 vs -10.4±1.1 and -4.8±1.8 vs -10.4±1.1 (P<0.001)] (Figure 5-23E), in both vehicle and Ang-(1-7) treated groups compared to sham, respectively. Ang-(1-7) did not change the gene expression of M1 type markers compared to MCAO-aCSF (Figures 5-23A:E).

Ccr7 showed a trend to increase following MCAO, however, it was most predominant in Ang-(1-7) treated animals being statistically different when compared to Sham [-5.2±1.9 vs -7.7±1.0 (P<0.05)], (Figure 5-23F). MCAO-Vehicle values did not differ from Sham or Ang-(1-7) treated groups (P>0.05).

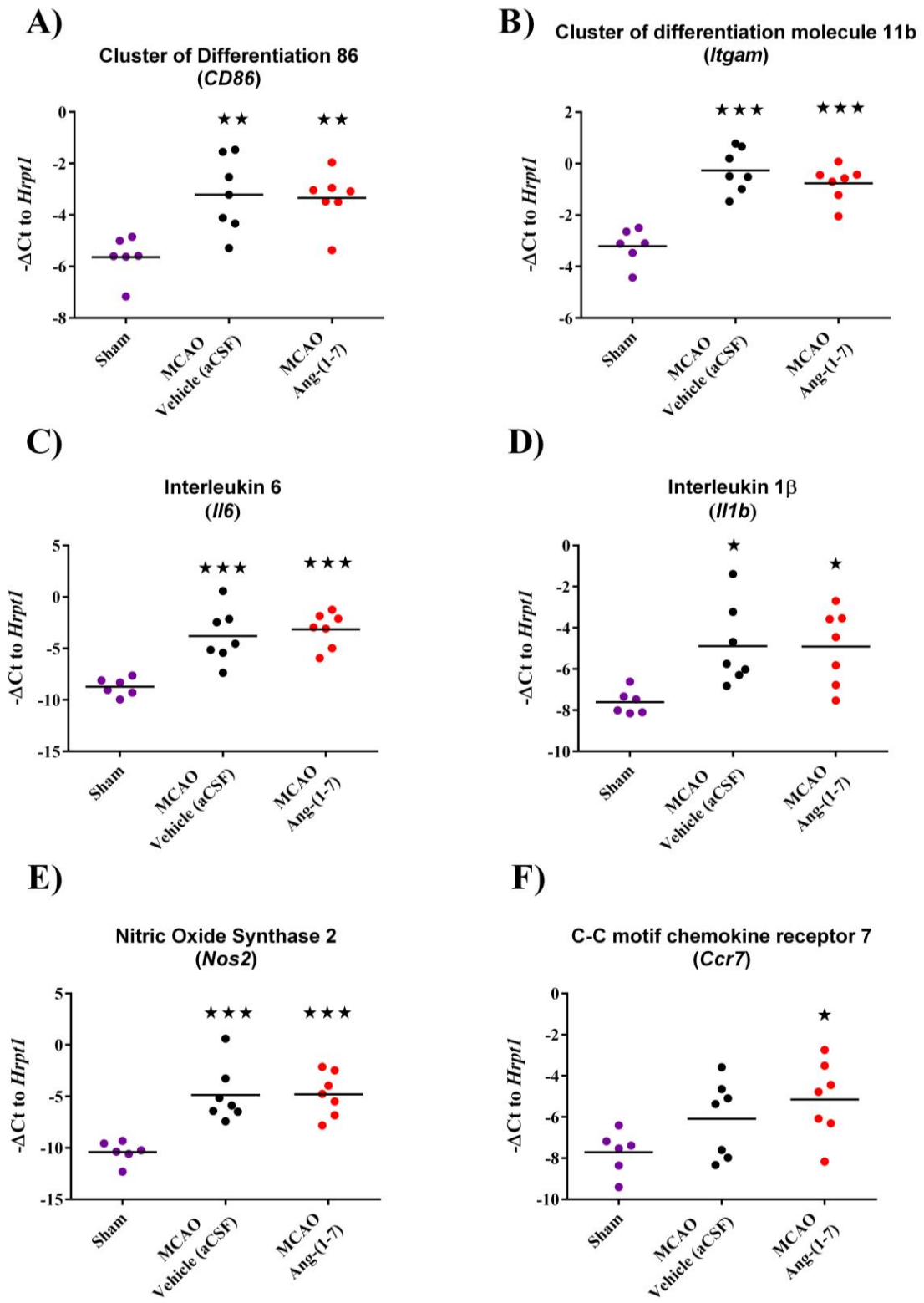

Figure 5-23 M1 type microglia/macrophage markers 24 hrs post 90 min MCAO. A) *CD86*; B) *Itgam*; C) *Il6*; D) *Il1b*; E) *Nos2* and F) *Ccr7*. MCAO significantly upregulated the expression of *CD86*, *Itgam, Il6*, *Il1b* and *Nos2* compared to Sham (P<0.05) with no differences between MCAO treatment groups (P>0.05). *Ccr7* was significantly upregulated in MCAO-Ang-(1-7) treatment group compared to Sham. MCAO-Vehicle (aCSF) *Ccr7* values did not significantly differ from Sham or MCAO-Ang-(1-7) groups (P>0.05). Data were presented as -ΔCt normalised to *Hrpt1* for Sham (n=6); MCAO-Vehicle (aCSF;n=7) and MCAO-Ang-(1-7) (n=7) treated animals in peri-infarct regions. Data were analysed with one-way ANOVA with Tukey's post-hoc test; P<0.05 was deemed as significant. Horizontal bar represents the mean. *P<0.05; **P<0.01; ***P<0.001 compared to Sham.

5.5.7 MCAO increased M2 microglia/macrophage markers, *Ccl22* and *Tgfb1* but not *Arg1* or *CD163*

M2 surface markers *Arg1* and *CD163* were comparable to Sham following MCAO (Figure 5-24A&B). Conversely, MCAO significantly increased the expression of *Ccl22* [-5.3±1.9 vs -8.3±0.7 and -5.5±2.1 vs -8.3±0.7 (P<0.05)] and *Tgfb1* [1.5±1.2 vs -0.2±0.8 (P<0.05) and 1.8±1.0 vs -0.2±0.8, (P<0.001)] when compared to Sham animals in control and Ang-(1-7) animals, respectively (Figure 5-24C&D). *Il10* was not detected in peri-infarct samples.

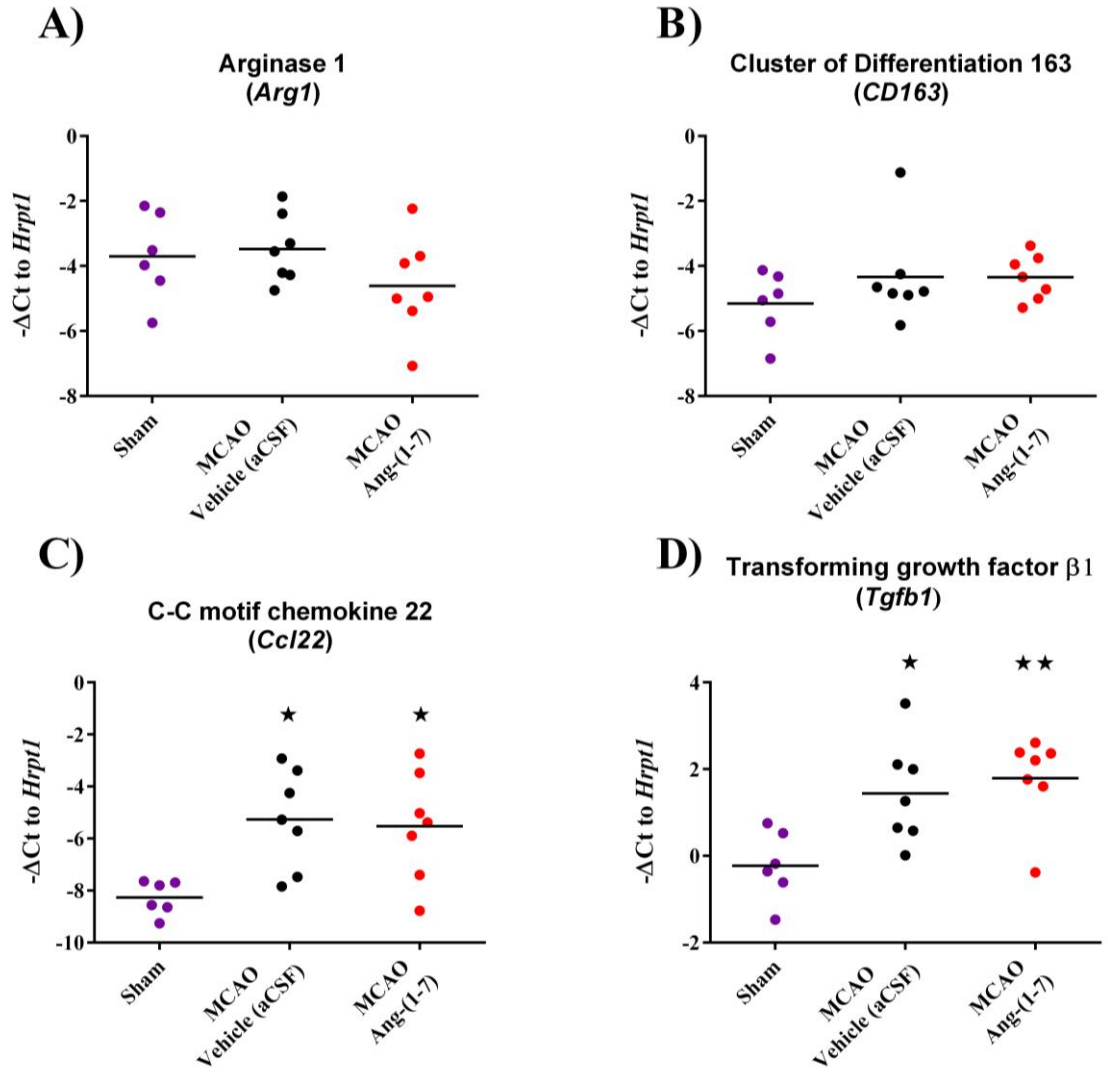

Figure 5-24 M2 type microglia/macrophage markers 24 hrs post 90 min MCAO. A) *Arg1*; B) *Cd163*; C) *Ccl22* and D) *Tgfb1*. MCAO significantly upregulated the expression of *Ccl22* and *Tgfb1* compared to Sham (P<0.05). Conversely, *Arg1* and *CD163* levels were comparable between groups (P>0.05). Data were presented as -ΔCt normalised to *Hrpt1* for Sham (n=6); MCAO-Vehicle (aCSF;n=7) and MCAO-Ang-(1-7) (n=7) treated animals in peri-infarct regions. Data were analysed with one-way ANOVA with Tukey's post-hoc test; P<0.05 was deemed as significant. Horizontal bar represents the mean. *P<0.05; **P<0.01; ***P<0.001 compared to Sham.

5.6 Discussion

This study was designed to examine the potential impact of Ang-(1-7) on BBB breakdown, infarct volume; microglia number/activation and gene expression at 24 hrs post 90 min MCAO. The time point selected represents a stage where the BBB is transitioning from a closed to open state and the final infarct has not yet matured (Pillai et al. 2013; Neumann-Haefelin et al. 2000). Results indicate that at 24 hrs post MCAO, Ang-(1-7) treatment does not improve BBB breakdown, infarct volume, microglia number, activation or pro and anti-inflammatory gene expression markers when compared to Vehicle (aCSF) treated animals.

5.6.1 Ang-(1-7) does not affect BBB breakdown and vasogenic oedema 24 hrs post MCAO

For the first time, the effects of Ang-(1-7) on BBB breakdown at 24 hrs post MCAO were evaluated with contrast enhanced MRI. Moreover, MRI-T_2 and MRA were used to confirm that the ICV cannula was adequately placed in the ventricle and that all animals were reperfused at 24 hrs. Results show that at 24 hrs following transient focal cerebral ischaemia, central Ang-(1-7) treatment does not influence total Gd-DTPA enhancement volume across the ipsilateral hemisphere. Similarly, % Gd-DTPA extravasation per infarct volume was comparable to the Vehicle (aCSF) group, indicating that treatment had no effect on BBB breakdown at this time point. MRI-T_2 analysis successfully identified that at the time point assessed; vasogenic oedema is present within the ipsilateral hemisphere as hemispheric volume was significantly higher when compared to contralateral side. Still, when comparing hemispheric swelling between groups, data showed no differences induced by therapy. These results highlight that Ang-(1-7) does not act by preventing BBB disruption or vasogenic oedema in our hands.

The “classical axis” of the RAS has been implicated in BBB disruption pathology following stroke in *in vitro* models as well as *in vivo* assessments following MCAO in normotensive rats (Panahpour, Nekooeian, et al. 2014; So et al. 2015; Panahpour, Dehghani, et al. 2014); therefore, setting the premise that the counter-regulatory axis might offer a protective effect. Ang-(1-7) was previously tested in a normotensive MCAO rat model where it was shown that treatment decreased Evans Blue (EB) extravasation 24 hrs post 90 min MCAO. The outcome observed was attributed to a reduction of MMP9 and enhancement of TIMP1 gene and protein expression, which promoted claudin-5 and ZO-1

preservation (Wu et al., 2015). In Wu's study, Ang-(1-7) was tested at 5 different doses (0.005 pmol/hr; 0.005 pmol/hr; 0.05 pmol/hr; 0.5 pmol/hr; 5 pmol/hr) with the authors identifying that Ang-(1-7) prevented BBB disruption at higher doses only (0.5 pmol/hr and 5 pmol/hr) and subsequently proposing a dose dependent effect on BBB preservation (Wu et al., 2015). In our study, Ang-(1-7) was administered at a dose of 1.1 nmol/hr, which is substantially higher than the doses used beforehand. Therefore, in future, lower doses might be more effective. Additionally, Wu's study did not evaluate the extent of infarct volume damage; thus, the results obtained could not be associated with a treatment-induced effect in the ischaemic damage, contrarily to our experiment.

MRI was chosen as the method of assessing BBB breakdown as it is the most commonly used technique to study BBB disruption in both preclinical and clinical studies (Wunder et al., 2012). Alternatively, Wu et al. selected EB extravasation as a method of assessing integrity of the BBB (Wu et al., 2015). Although EB extravasation is a simple and widely used method, it has the disadvantage of potentially overestimating BBB breakdown as it presents reversible binding kinetics to serum albumin and also binds to other plasma proteins and tissues (Connelly et al. 2015). Conversely, Gd-DTPA does not bind to albumin and induces a differential extravasation pattern to that observed in EB staining, perhaps explaining the contradicting results. Yet, studies using Gadofluorine M, a new contrast agent formulation with strong binding properties to albumin, identified that following stroke; Gadofluorine M leads to highly sensitive signal enhancement within 24 hrs and an extravasation pattern similar to that observed in EB assessment (Stoll et al., 2009). One could postulate that the absence of Gd-DTPA signal enhancement does not necessarily mean that BBB breakdown is not occurring but rather that Gd-DTPA might not be sensitive enough to detect subtle changes.

Gd-DTPA contrast enhancement technique was shown to be quite challenging as contrast administration failed in 5 rats, which meant that more animals were required to have a sufficient sample size. Furthermore, several factors influence Gd-DTPA distribution amongst rats including vessel permeability, surface area, blood flow as well as intravascular and extracellular-extravascular volume fractions (Kassner and Merali, 2015). Physiological parameters were not assessed during imaging or included in BBB breakdown analysis; therefore, one could assume that these variables might have influenced Gd-DTPA extravasation amongst rats. Alternatively, dynamic contrast enhanced MRI (DCE-MRI) takes into account these factors and provides a sensitive method to detect subtle MRI-T_1 contrast enhancement changes when compared to contrast-enhanced T_1 alone (Heye et al.,

2014). In DCE-MRI, multiple sampling times are obtained characterising the enhancement over time, this way, allowing mapping of spatial BBB breakdown throughout the brain. To do so, compartmental models are used to define the contrast exchange between blood plasma and tissue extracellular compartment (Heye et al., 2014; Kassner and Merali, 2015)**.** This type of assessment has been shown to consistently detect BBB breakdown in a sensitive manner in both preclinical and clinical studies 24 hrs post MCAO (Lin et al., 2002; Merali et al., 2017), providing a suitable alternative method to use in future.

It is important to note that this proof of principle study was conducted in young, healthy male rats. As mRNA data indicates, RAS components were expressed to Sham levels, suggesting that the RAS may not be implicated in cerebral injury at 24 hrs and justifying the results obtained. It is possible, however, that in co-morbidity animal models, counter-regulatory axis targeting may be beneficial in preventing BBB injury. For instance, SHRSPs subjected to salt loading or Ang II with candesartan treatment, showed that treatment prevented BBB impairment and superoxide generation (Kim-Mitsuyama et al., 2005). Additionally, in Dahl salt-sensitive rats, olmesartan therapy reduced BBB breakdown in the hippocampus by attenuating Ang II levels and preserving TJPs (Pelisch et al., 2011). As a result, in comorbid models, counter-regulatory targeting therapies may provide an enhanced benefit rather than what is seen in normotensive models.

5.6.1.1 BBB breakdown displays a variable pattern at 24 hrs reperfusion

Gd-DTPA uptake at 24 hrs displayed a variable pattern amongst animals. In some rats, contrast enhancement was remotely present in areas of infarct whereas in others, it was identified in over 70% of the ischaemic area. These results imply that at this time point, the BBB is at a transient point of disruption. This suggests a biphasic BBB pattern rather than a continuous disruption as previously hypothesised (Belayev et al., 1996; Pillai et al., 2009; Rosenberg et al., 1998; Veltkamp et al., 2005). The transient pattern of BBB disruption at 24 hrs post stroke is not well characterised. However, it is postulated that this mechanism is an outcome of claudin-5 and occludin protein expression decrease in the endothelial cells yet present in astrocytes surrounding the vasculature, justifying this temporary closure (Yang et al., 2007). In addition, TJPs are suggested to reassemble due to a reversal in ROS mediated injury (Meyer et al., 2001). Supportively, qPCR results showed that in peri-infarct regions, *NOX1* and *NOX2* mRNA levels were comparable to Sham levels. There is no consensus regarding the time point at which the BBB is at its maximum disruption, with literature proposing that it might occur between 48 hrs and 72 hrs reperfusion (Belayev et

al., 1996; Pillai et al., 2009; Rosenberg et al., 1998; Veltkamp et al., 2005). Since at 24 hrs BBB opening was shown to vary amongst animals, the time point selected may not have been optimal to examine the treatment effect of Ang-(1-7) on BBB breakdown. Longitudinal experiments investigating the impact of Ang-(1-7) on BBB disruption should be performed to identify the appropriate time at which maximal barrier disruption occurs and whether this is influenced by treatment.

Although our findings indicate that BBB disruption is variable at the point assessed, vasogenic oedema was present and detected by differences in hemispheric volumes. It could be argued that oedema is the outcome of the first phase of BBB opening (Rosenberg et al., 1998). At the same time, following 90 min MCAO, the expression of TJPs in Fluorescein Isothiocyanate (FITC)-albumin leakage regions are unaltered at 24 hrs reperfusion, yet, structural alterations take place in the vascular endothelium causing swelling and oedema (Krueger et al., 2017). Therefore, in some animals, it is likely that structural endothelial cell changes are occurring and allowing free flow of water molecules into the brain; however, the TJP integrity might not allow the extravasation of Gd-DTPA.

5.6.1.2 MCAO upregulates *MMP9* and *TIMP1* gene expression with no Ang-(1-7) induced effects

To dissect potential undetected effects, the expression for markers involved in BBB disruption were assessed with qPCR. *MMP9* mRNA levels were upregulated following MCAO compared to Sham whereas MCAO-Ang-(1-7) rats indicated a trend to increase *MMP9*, nearly reaching significance. In turn, MMP9 may be acting to disrupt the BBB, explaining why disruption was observed in all animals even if at low levels in some. Indeed, MMP9 is of special relevance in BBB disruption since stroke patients with increased serum MMP9 levels demonstrate exacerbated DWI lesion growth and higher risk of developing HT (Inzitari et al., 2013; Rosell et al., 2005), highlighting its involvement in BBB breakdown in preclinical and clinical studies. Ang-(1-7) was previously suggested to decrease MMP9 mRNA and protein expression following 90 min MCAO with 24 hrs reperfusion (Wu et al., 2015). Our data, however, contradicts previous findings and further emphasises that therapy does not alter BBB breakdown at the time point examined.

MMP9 is regulated by TIMP1 by non-covalent binding in the MMP catalytic domains (Turner and Sharp, 2016). In our study, *TIMP1* mRNA expression was significantly increased following MCAO and contrarily to Wu's study (Wu et al., 2015); we demonstrate no Ang-(1-7) therapy induced effects. Interestingly, the relative expression of

TIMP1 was substantially higher than *MMP9* in brain samples, perhaps explaining the decrease in BBB breakdown at this time point. In fact, MMP9/TIMP1 ratio, favouring MMP9 expression, positively correlates with brain damage following cerebral ischaemia in preclinical and clinical assessments (Li et al., 2013; Piccardi et al., 2015), thus, increases in TIMP1 could protect MMP9-derived ECM and TJP degradation. The protective role of TIMP1 in BBB breakdown has been extensively studied. TIMP1-KO mice display enhanced MMP9 protein expression compared to WT, which was associated with BBB disruption (Fujimoto et al., 2008). On the contrary, mice overexpressing TIMP1 had reduced MMP9 levels, an effect linked to attenuated infarct volume and ameliorated BBB leakage (Tejima et al., 2009). These results place MMP9 as a main mediator in barrier disruption that is possibly being reversed by TIMP1. To confirm these effects, MMP9 and TIMP1 protein levels through Western Blot or immunohistochemistry should be assessed within the peri-infarct regions as well as TJP protein levels to confirm preservation/degradation. At the same time, complementary experiments such as gelatinzymography could be performed to study MMP9/TIMP1 induced ECM and TJP degrading activity in cultured brain cells (Toth et al., 2012).

Other BBB breakdown markers studied were VEGFA and VEGFR-2. VEGFA is a potent growth factor involved in BBB breakdown in the early phases of injury through VEGFR-2 activation (Bates et al., 2002). The role of VEGFA in mediating stroke injury is well described, with its inhibition at 24 hrs reperfusion attenuating BBB disruption following stroke (Zhang et al., 2017). In permanent MCAO, Ang-(1-7) therapy was shown to alter VEGF expression at 24 hrs post stroke onset (Jiang et al., 2014); however, in the present study, *VEGFA* and *VEGFR-2* mRNA expression levels were comparable to Sham animals in MCAO groups. VEGFA and VEGFR-2 proteins are highly present 3 days post injury in the lesion site (Lennmyr et al., 1998), thus, VEGFA could be mainly involved in the subsequent BBB opening between 48-72 hrs, where there is a dramatic increase in permeability (Pillai et al., 2013).

5.6.1.3 Ang-(1-7) does not alter inflammation, oxidative stress or leukocyte infiltration markers

In ET-induced MCAO models, Ang-(1-7) therapy is suggested to induce an anti-inflammatory effect at 24 hrs and 72 hrs post stroke onset by attenuating *iNOS* mRNA and protein expression in the ipsilateral hemisphere (Mecca et al., 2011; Regenhardt et al., 2013). In addition, in permanent MCAO, Ang-(1-7) treatment decreased COX-2 protein levels in peri-infarct tissue at 24 hrs post injury start (Jiang et al., 2012). iNOS and COX-2

enzymes are thought to interact with one another as COX-2-positive neurons are present in close proximity to iNOS positive neutrophils (Nogawa et al., 1998). This in turn, stimulates an increase in ROS and toxic prostanoids promoting BBB breakdown (Nogawa et al., 1998). The mRNA levels for both these mediators were upregulated following MCAO in peri-infarct regions, highlighting its involvement in injury. However, compared to vehicle treated group, Ang-(1-7) treatment did not change *iNOS* and *COX-2* gene expression at 24 hrs post stroke onset.

Ang-(1-7) is also suggested to decrease phosphorylated IκB-α and NF-κB p65 protein levels as well as attenuate NF-κB mRNA and protein levels in microglia cultures (Jiang et al., 2012; Liu et al., 2016). Following MCAO, *NF-κB* mRNA levels were comparable to Sham animals. Yet, the expression of *iNOS*, *COX-2*, *IL-6*, and *MMP9* were upregulated following MCAO and these are dependent on NF-κB activation (Harari and Liao, 2010). Ang-(1-7) did not alter *NF-κB*, *IL-6*, *MMP9*, *COX-2* or *iNOS*; therefore, suggesting that Ang-(1-7) does not induce an anti-inflammatory effect in the animal model used and as a post-stroke onset therapy. Simultaneously, the method used to study therapy effects on NF-κB levels may not have been appropriate. In future studies, Western Blot or immunohistochemistry analysis of NF-κB components such as p50, p52 and RelB subunits should be assessed as well as protein signalling pathway components.

We then assessed *NOX1* and *NOX2* mRNA levels since Ang II is suggested to enhance oxidative stress in the brain through these mediators (Wang et al. 2006; Sun et al. 2005; Jackman et al. 2009; Kahles et al. 2010). NOX1 and NOX2 enzymes are main mediators of vascular damage and shown to contribute towards BBB breakdown (Chen et al., 2011; Gray and Jandeleit-Dahm, 2015). Specifically, when inhibiting NOX with apocynin or by genetic ablation, the severity of BBB disruption is reduced (Chen et al., 2009). In the present study, *NOX1* and *NOX2* were expressed at Sham levels at 24 hrs following transient MCAO, possibly an indication of reduced oxidative stress and thereby explaining the biphasic BBB pattern at 24 hrs (Meyer et al., 2001). Interestingly, Ang-(1-7) did not change *NOX1* or *NOX2* mRNA expression, contrarily to what was observed at day 7 post transient MCAO in Chapter 4. These results further emphasise that at 24 hrs reperfusion, Ang-(1-7) post stroke therapy does not alter inflammatory or oxidative stress markers.

The effects of Ang-(1-7) on leukocyte chemokine receptors *CXCR2*, *CCR2* and *CCR5* were also studied. CXCR2 mediates neutrophil extravasation and is implicated in BBB

breakdown by increasing the permeability of endothelial cell monolayers cells (Gelderblom et al., 2012). CCR2 regulates the mobilisation of monocytes from bone marrow to inflammatory sites and its expression in astrocytes and endothelial cells is directly implicated in BBB breakdown by inducing TJP phosphorylation (Chu et al., 2014; Dimitrijevic et al., 2006). Moreover, CCR5 was recently suggested to stimulate Treg cell chemotaxis following stroke leading to Treg-induced BBB preservation (Li et al., 2017). In the present study, MCAO significantly increased the expression of *CCR2*, *CXCR2* and *CCR5* at 24 hrs post injury. Ang-(1-7) treatment did not significantly alter leukocyte chemokine receptor mRNA expression compared to vehicle treated animals; however, it showed a trend to prevent the increase in *CCR5* expression as seen in the control group. The role of CCR5 in BBB breakdown is currently not well understood and a potential Ang-(1-7) effect on this receptor should be studied. Nonetheless, these results postulate that Ang-(1-7) does not influence leukocyte infiltration.

5.6.2 Ang-(1-7) does not impact infarct volume, neurological score or RAS mediators

In normotensive rats, the ischaemic lesion following reperfusion has been shown to peak at 2 days and subsequently decrease by day 7 (Neumann-Haefelin et al., 2000); therefore, at 24 hrs post MCAO, the infarct volume may not have fully matured. Ang-(1-7) is proposed to act at this stage of injury by decreasing infarct volume following ET-1 induced MCAO (Regenhardt et al., 2013). Our results, however, contradict previous findings as infarct volume and neurological score were comparable to Vehicle (aCSF). DWI-MRI was not performed during MCAO; thus, it was not possible to normalise final ischaemic lesion to initial lesion as we did in the previous Chapter. Ang-(1-7) could be exerting a mild neuroprotective effect that is not detected due to lesion variability during MCAO, similar to what was seen in Chapter 4. Furthermore, MRA was not performed during MCAO and therefore variability due to partial occlusions may play a role in the present study. Neurological score was used as a tool to examine whether rats should be included in this experiment and indeed, all animals exhibited neurological deficit at 24 hrs. However, Ang-(1-7) failed to induce a therapeutic effect in neurological score similar to what was observed in Chapter 4.

Interestingly, at 24 hrs post injury onset, MCAO alone did not induce any alterations in RAS components' gene expression, emphasising that the RAS may not be implicated in cerebral injury at this time point. Consequently, it is plausible that the RAS might be

implicated in injury at 48-72 hrs post stroke onset once injury reaches its hiatus. Contrary to our findings, *MasR* and *ACE2* mRNA levels were previously shown to be upregulated 24 hrs following stroke onset in a permanent MCAO model (Lu et al., 2013). One could postulate that MasR and ACE2 are implicated in models of persistent hypoxia at 24 hrs but not in reperfusion injury. In addition, *B_2R* mRNA levels were similar to Sham, indicating that at 24 hrs post MCAO, Ang-(1-7) does not stimulate B_2R expression and subsequent vasodilation, as previously suggested (Lu et al., 2008).

5.6.3 Ang-(1-7) does not affect IBA1$^+$ microglia or M1/M2 microglia/macrophage mRNA profile

Ang-(1-7) is reported to act on microglia/macrophages in experimental stroke models (Liu et al., 2016; Mecca et al., 2011; Regenhardt et al., 2013, 2014). Firstly, MasR is expressed in microglia and secondly, Ang-(1-7) treatment is thought to modulate microglia/macrophage inflammatory gene and protein expression (Liu et al. 2016; Regenhardt et al. 2013). Equally, Ang-(1-7) therapy prevented LPS-induced NO induction in primary glial cultures (Regenhardt et al., 2013), supporting this hypothesis. In the present study, IBA1$^+$ microglia total numbers did not differ between Ang-(1-7) and Vehicle (aCSF) treatment in peri-infarct and the homotopic contralateral regions. Similarly, the % of activated microglia in both peri-infarct and contralateral regions were comparable between groups.

To confirm the validity of the model used, IBA1$^+$ microglia numbers/activation were compared within groups. Total IBA1$^+$ cell numbers were similar in peri-infarct and contralateral regions in both groups; however, MCAO increased % activated microglia in the peri-infarct region compared to the homotopic contralateral side. Therefore, confirming that transient focal cerebral ischaemia alone resulted in a significant activation of microglia within the peri-infarct region. Previous studies have shown that following 90 min MCAO, IBA1$^+$ microglia appear in the peri-infarct regions as early as 3.5 hrs hours post-reperfusion and peak at 7 days (Ito et al., 2001). Thus, indicating that microglia numbers are not maximal at 24 hrs. In addition, in the ischaemic core, IBA1$^+$ microglia were scarcely present. Microglia degenerate 12 hrs after reperfusion with active IBA1$^+$ cells then infiltrating the core after 24 hrs and peaking at 4 and 7 days post-reperfusion (Ito et al., 2001). We show that at early stages of microglia infiltration Ang-(1-7) does not alter IBA1$^+$ cell number or activation. Similarly, at day 7 when microglia levels reach its hiatus, there were no indications of Ang-(1-7) induced effects (Chapter 4).

Microglia/macrophage M1 and M2 type mRNA markers were similar between MCAO groups. Previous findings demonstrated that Ang-(1-7) attenuated *CD11b* and iNOS mRNA at 24 hrs following ET-1 induced MCAO (Regenhardt et al., 2013). Our results show that all M1 type markers *CD11b*, *CD86*, *IL-1β*, *IL-6*, *CCR7* and *iNOS* mRNA levels were upregulated following MCAO with Ang-(1-7) having no effect on expression. In Regenhardt's study, Ang-(1-7) was administered as a pre and post therapy for a total of 7 days in the ET-1 induced MCAO model, whereas in our protocol, Ang-(1-7) was administered for 24 hrs only and tested in the intraluminal filament MCAO model. Once could postulate that due to its short half-life, Ang-(1-7) might act in a cumulative manner at the MasR level and that 24 hr treatment duration might not have been sufficient to observe an effect in our model. Furthermore, in *in vitro* assessments, Ang-(1-7) administration on microglia cultures for either 6 or 12 hrs at 100 nM decreased microglial expression of *IL-1β* and *TNF-α* whilst upregulating *IL-10* levels (Liu et al., 2016). However, in our study, *IL-10* mRNA expression was undetected in all groups whereas *IL-1β* and *IL-6* were upregulated in both Vehicle and Ang-(1-7) treated rats following MCAO.

M2 specific cell surface markers, *Arg1* and *CD163* (Cherry et al., 2014), were comparable to Sham levels following MCAO with no Ang-(1-7) induced effects. Interestingly, M2 markers *TGF-β1* and *CCL22* were upregulated following MCAO in the peri-infarct regions and again with Ang-(1-7) treatment having no effect on mRNA levels. The TGF-β signalling pathway is implicated in the regulation of BBB functional integrity and TJP expression by decreasing endothelial cell permeability (Dohgu et al., 2004; Ronaldson et al., 2009). Conversely, the role of CCL22 in BBB disruption and ischaemic injury is not well understood; however, it might be involved in repair. For instance, in human ischaemic brains, CCL22 protein levels were shown to be decreased in the infarcted tissue vasculature and this reduction was associated with enhanced neurological severity (García-Berrocoso et al., 2014). Together these results strongly suggest that Ang-(1-7) post stroke therapy for 24 hrs does not interfere with microglia number, phenotype or inflammatory profile whilst highlighting a complex interplay of injury/repair mechanisms.

5.7 Summary

This study shows for the first time that Ang-(1-7) treatment as a post stroke therapy for 24 hrs does not influence BBB breakdown, final infarct volume, microglia number and activation and pro- or anti-inflammatory mRNA gene expression. BBB breakdown was quantified following Gd-DTPA contrast agent administration with MRI-T_1. Here, some animals presented high levels of Gd-DTPA enhancement within the infarct regions whereas others showed scarce Gd-DTPA leakage. These findings suggest that at 24 hrs, the BBB is in a transient phase of opening, implying that BBB breakdown follows a biphasic pattern in rats. Ang-(1-7) did not alter BBB breakdown following 24 hrs reperfusion or the expression of BBB breakdown markers *MMP9*, *TIMP1*, *VEGFA* or *VEGFR-2*. Moreover, infarct volume was comparable between Ang-(1-7) and Vehicle (aCSF) treated groups, an outcome further evidenced by neurological score. Ang-(1-7) did not alter gene expression for leukocyte extravasation or pro-inflammatory mechanisms, although these were upregulated following injury. Ang-(1-7) did not influence $IBA1^+$ microglia total cell count or influence cellular phenotype in peri-infarct and contralateral regions. Interestingly, RAS mediator mRNA levels were comparable to Sham, indicating that RAS may not be implicated in injury at this stage in normotensive rats and possibly explaining the results obtained.

In conclusion, this study provides robust evidence that Ang-(1-7) does not attenuate BBB breakdown, infarct volume, and microglia phenotype nor pro- anti-inflammatory gene expression at 24 hrs in normotensive rats. At the same time, our results highlight a complex interplay of mediators potentially acting to simultaneously promote and reverse injury following stroke and at the time point selected.

Chapter 6: The effects of Ang-(1-7) on cortical CBF following transient MCAO

Chapter 6

6.1 Introduction

In Chapter 4, Ang-(1-7) significantly increased tissue salvage following reperfusion when compared to vehicle treatment. In Chapter 5, Ang-(1-7) had noeffect on BBB breakdown, infarct volume or microglia number/activation at 24hrs post stroke onset. To further elucidate a possible underlying mechanism, this study was designed to determine whether Ang-(1-7) treatment has any direct effect on the cerebrovasculature following transient MCAO.

The CNS is dependent on appropriate delivery of glucose and oxygen, which relies on CBF being maintained at critical levels, approximately 55-60 mL/100g/min in healthy humans (Ellenbogen et al., 2012). Following MCAO, cerebral perfusion is severely reduced within the ischaemic core resulting in irreversible cell death within minutes. The ischaemic core is surrounded by the ischaemic penumbra, a region of reduced blood flow where electrical activity is impaired yet ion homeostasis and metabolic activity maintaineddue to collateral vessel supply (Heiss, 2000). In humans, it was determined that the CBF threshold for the ischaemic penumbra is between 12-22 mL/100g/min whereas values below represent the ischaemic core. On the other hand, when CBF is above 22 mL/100g/min but less than 55-60 mL/100g/min the brain is placed in a state of benign oligaemia, which is in a less severe hypoperfused state and not at risk of infarction (Heiss, 2000).

Once reperfusion is established after cerebral ischaemia, damaged tissue undergoes post-ischaemic hyperperfusion which is then quickly followed by post-ischaemic hypoperfusion, possibly due to capillary narrowing, plugging and loss of arteriolar reactivity (Attwell et al., 2010; Hauck et al., 2004; Leffler et al., 1989). Therapeutic strategies with the ability to reverse ongoing hypoperfusion following reperfusion therefore have the potential to be protective in stroke (Sutherland et al., 2011). This assumption is further supported by clinical studies where better functioning collaterals are associated with greater reperfusion following thrombectomy and subsequent reduction in ischaemic lesions (Liebeskind, 2014).

One other important mechanism thought to be implicated in ischaemic injury is CSD (Hartings et al., 2003; Mies et al., 1993). This phenomenon is associated with a loss of

electrical and ionic homeostasis in neurons and astrocytes, resulting in cortical excitatory mechanisms (Kramer et al., 2016). In healthy tissue, CSD is compensated by a neuronal hyperaemic response; however, following focal cerebral ischaemia this effect cannot be achieved promoting further ischaemia, a phenomenon termed PID (Lauritzen et al., 1990; Windmuller et al., 2005). PIDs have been mostly studied during MCAO; with frequency and duration within peri-infarct areas being associated with exacerbated infarct size (Hartings et al., 2003; Mies et al., 1993). Similarly, following reperfusion, PIDs have been shown to occur particularly after 2 hrs of reperfusion onset, potentiating injury (Hartings et al., 2006).

Vasodilation is one of the most widely reported effects induced by Ang-(1-7) in the vasculature and has been observed in canine coronary arteries (Brosnihan et al., 1996; Feterik et al., 2000), porcine coronary endothelium (Gorelik et al., 1998), rabbit arterioles (Ren et al., 2002), rat MCAs (Durand et al., 2010) and vascular coronary beds (Moraes et al., 2017). In addition, Ang-(1-7) is suggested to modulate systemic and regional blood flow in rats, improving regional haemodynamics within the brain (Sampaio et al., 2003). Following ischaemic stroke, there are few studies assessing the direct cerebrovascular effects of Ang-(1-7) and these contain contradicting results. A study conducted in 2011 showed that in ET-1-induced MCAO, Ang-(1-7) ICV administration as a pre and post treatment did not improve cerebral perfusion during MCAO when compared to Vehicle treated rats (Mecca et al., 2011). Conversely, in Wistar rats, 4 weeks of Ang-(1-7) ICV pre-treatment followed by permanent MCAO improved perfusion in peri-infarct regions 1 hr and 24 hrs post stroke onset (Jiang et al., 2014). Accordingly, there is a need to evaluate the acute impact of Ang-(1-7) administration on cerebral perfusion.

Laser Speckle Contrast Imaging (LSCI) has become a widely used tool to study cortical CBF after focal cerebral ischaemia (Armitage et al., 2010; Liu et al., 2017; Strong et al., 2006; Winship et al., 2014). LSCI is used to monitor perfusion within the cortical surface and with a high temporal and spatial resolution (Dunn, 2012). The technique uses the speckle phenomenon, consisting of an interference pattern generated by light scattered/reflected from an area of interest. In this method, a laser is applied onto the cerebral cortex and as it comes into contact with moving particles such as red blood cells, the speckle pattern becomes blurred (Dunn, 2012; Wood et al., 2016). The patterns within each image pixel are detected by a CCD camera attached to the laser, allowing to map temporal and spatial cortical CBF alterations (Dunn, 2012; Dunn et al., 2001; Strong et al.,

2006). Due to its ability to detect CBF alteration in near-real time, LSCI is also a useful method to reliably study PIDs during and following MCAO (Paul et al., 2005).

Reports have emphasised the need to assess the effects of potential neuroprotective strategies on CBF within the preclinical setting before proceeding to clinical trials (Sutherland et al., 2011). Accordingly, this study aims to examine the impact of acute administration of Ang-(1-7) on the dynamic changes in cortical perfusion following reperfusion after MCAO.

6.1.1 Aims:

- To determine the effect of acute systemic infusion of Ang-(1-7)/Vehicle on cortical perfusion immediately following initiation of reperfusion after MCAO.

- To determine whether Ang-(1-7) treatment influences the occurrence of PIDs during reperfusion.

6.2 Methods and materials

6.2.1 Sample size calculation

Power calculations were performed using the power analysis programme G*Power (version 4.1, Germany). An "a priori" power analysis was performed for t test: difference between two independent means (unpaired Student's t test) to assess Ang-(1-7) treatment impact and Vehicle (dH_2O) on cortical perfusion. Ang-(1-7) ICV infusion was shown to induce a 10% improvement in perfusion when compared to Vehicle treated animals in the peri-infarct region 1 hr after MCAO (Jiang et al., 2014). We have conducted pilot experiments using LSCI where we have analysed the perfusion in different ROIs. Within the hypoperfused territory (CBF between 43-75% of normal) at 1 hr following MCAO, perfusion mean values were 68.6 and S.D. was 4 in perfusion units (PU). Using these data, a p value of 0.05 and setting power at 80%, a total sample size of 10 was determined (*n* of 5 per group) to detect changes in perfusion of at least 10% between groups.

6.2.2 Animals and surgical procedures

In this study, 18 male Wistar rats (310-353g) were used and subjected to 90 min MCAO and 90 min reperfusion. Rats were initially anaesthetised with 5% isoflurane delivered in a 30:70% O_2-NO_2 mixture ratio as described in Chapter 2.5.1 and aseptic technique carried out as outlined in Chapter 2.3. Rats were then orally intubated and mechanically ventilated at 3-4 mL stroke volume and 56-58 strokes per min delivering 2.5% isoflurane. To reduce tracheal secretions that could obstruct the intubation tube during the experiment, atropine sulphatewas administered SC (0.05 mg/kg; Martindale Pharmaceuticals, UK) prior to surgery and local anaesthetic, ropivacaine (Norapin®), administered SC at incision sites.

6.2.2.1 Physiological monitoring and drug delivery

All animals were subjected to physiological monitoring of MABP and blood gases (pH, PaO_2 and $PaCO_2$) through a cannula inserted in the left femoral artery. Drug delivery and α-chloralose administration were performed in the left and right femoral veins, respectively. The left femoral artery, left femoral vein and right femoral vein were cannulated as described in Chapter 2.6. Rectal temperature was monitored and regulated with the aid of an electric blanket.

6.2.2.2 Skull Thinning

Following blood vessel cannulation, rats were transferred to a stereotaxic frame for skull thinning procedures. The head was secured in place with the use of ear and tooth bars tightly adjusted to prevent movement. A midline incision was performed in the skull with a scalpel and the underlying connective tissue cleared to visualise the skull surface. To enhance the FOV and prevent drilling obstruction, four 4.0 threads were sutured onto each side of the incision and tension applied to prevent the skin from interfering with the drilling. A dental drill (NSK Volvere max, Nakanshishi Inc., Japan) was then used to thin the skull surface by applying continuous vertical strokes across the scalp surface. The procedure was carried out until the pial vessels were visualised and the skull surface uniformly thinned. Throughout the procedure, dH_2O was regularly used to regulate the skull temperature, preventing vessel damage due to heat, and to clean the bone dust produced. Scalp and muscle bleeding was ceased by applying pressure with a sterilised cotton bud. In cases where bleeding was persistent, 10% perchloric acid (Sigma Aldrich, UK) was applied to the scalp with a cotton bud and then thoroughly cleaned with dH_2O.

6.2.2.3 MCAO and reperfusion

Following skull thinning procedures, rats were removed from the stereotaxic frame and placed onto the corkboard for MCAO procedures as described in Chapter 2.8. A modified 4-0 nylon silicone coated tip monofilament (404134PK10; Doccol Corporation, MA, USA) was used to occlude the MCA for a period of 90 min. To allow reperfusion to be induced whilst the animal was subjected to LSCI, a small 5.0 suture was tied and glued at the end of the Doccol filament and gently placed outside the incision site just before the forelimbs. After 90 min MCAO, the 5.0 suture attached to the monofilament occluding the MCA, was gently pulled back with the aid of clamping forceps. Animals were allowed to reperfuse for 90 min and then sacrificed via Schedule 1 procedures.

6.2.3 α-chloralose

Isoflurane was selected as the anaesthetic of choice to perform surgical procedures as it provides adequate anaesthetic levels, which are easily controllable. Although isoflurane has been deemed by some researchers as a suitable anaesthetic to be used in cerebrovascular studies (Franceschini et al., 2010; Masamoto et al., 2006), it is suggested to dose dependently induce cerebral vasodilation, enhance vascular reactivity and alter autoregulation (Iida et al., 1998; Sicard et al., 2003). On the other hand, α -chloralose is

not a suitable anaesthetic to induce anaesthesia; however, it has been found to preserve cerebral autoregulation and decrease arterial CO_2 sensitivity and is, therefore, the anaesthetic of choice to study CBF dynamics (Masamoto and Kanno, 2012; Ueki et al., 1992). Accordingly, at MCAO start and prior to LSCI, anaesthesia was switched from isoflurane to α-chloralose and animals allowed to stabilise prior to imaging. α-chloralose was prepared fresh by dissolving 250 mg of α-chloralose (Sigma-Aldrich, UK) in 25 mL of dH_2O. The solution was stirred and heated to 75ºC to dissolve. Once fully dissolved, the solution was kept at 58ºC in a water bath until administration.

α-chloralose dose was selected based on previous reports (Haensel et al., 2015). An initial IV α-chloralose bolus of 80 mg/kg at near body temperature was administered with the use of a 5 mL syringe (2.8 mL in a 350g rat) and slowly injected into the right femoral vein to prevent a steep drop in MABP. Once MABP started decreasing, isoflurane concentration levels were reduced to 1.5%. Immediately after the IV bolus, α-chloralose was administered as a 40 mg/kg/hr infusion (1.4 mL/hr in a 350g rat). MABP was closely monitored as well as the response to hindlimb pinch to ensure adequate anaesthesia and to determine at what point isoflurane levels should be turned off. Once MABP started to decrease, isoflurane was gradually switched off. Animals were allowed to stabilise for a period of 60 min prior to CBF assessments. During the full duration of the LSCI protocol, animals were ventilated with 30:70% an O_2-NO_2 mixture and anaesthesia maintained at a continuous infusion of 40 mg/kg/hr α-chloralose.

6.2.4 Ang-(1-7) dose selection

In this experiment, treatment could not be infused ICV as it would compromise LSCI. For this reason, IV administration was selected as the treatment method. Ang-(1-7) has a short half-life and to guarantee treatment delivery in cerebral vessels, a dose 5 times higher than the one used in ICV studies was selected: 5 nmol/hr Ang-(1-7) infusion dissolved in dH_2O. Treatment was administered IV as a continuous infusion at near body temperature in the left femoral vein for 90 min beginning immediately following reperfusion. The Ang-(1-7)/Vehicle IV delivery rate was the same as the infusion rate set for α-chloralose IV infusion according to animal weight (1.4 mL/hr in a 350g rat). Control animals were subjected to dH_2O infusion only.

6.2.5 Laser speckle contrast imaging

6.2.5.1 System

LSCI was carried out using a PeriCam PSI System (Perimed, Sweden) with a solid-state laser diode of 785 nm for blood perfusion measurements and at a FOV of 1.4 cm width and 1.4 cm height. The laser beam was spread over a rectangular surface by a diffuser and placed 10 cm distance from the skull surface providing a measurement area of 5.9 × 5.9 cm (Figure 6-1A). Speckle patterns were generated from the backscattered light from the laser beam illumination and recorded through a 1388 × 1038 pixel CCD camera inside the PeriCam PSI head at a frame rate of 10 images per second (50 Hz mains frequency). Dynamic changes in CBF speckle patterns were acquired at 1 image per 5 seconds (average of 50 images) at a spatial resolution of 0.02 mm (Figure 6-1B). In addition, a monochrome intensity image was generated from the total amount of reflected light (Figure 6-1C).

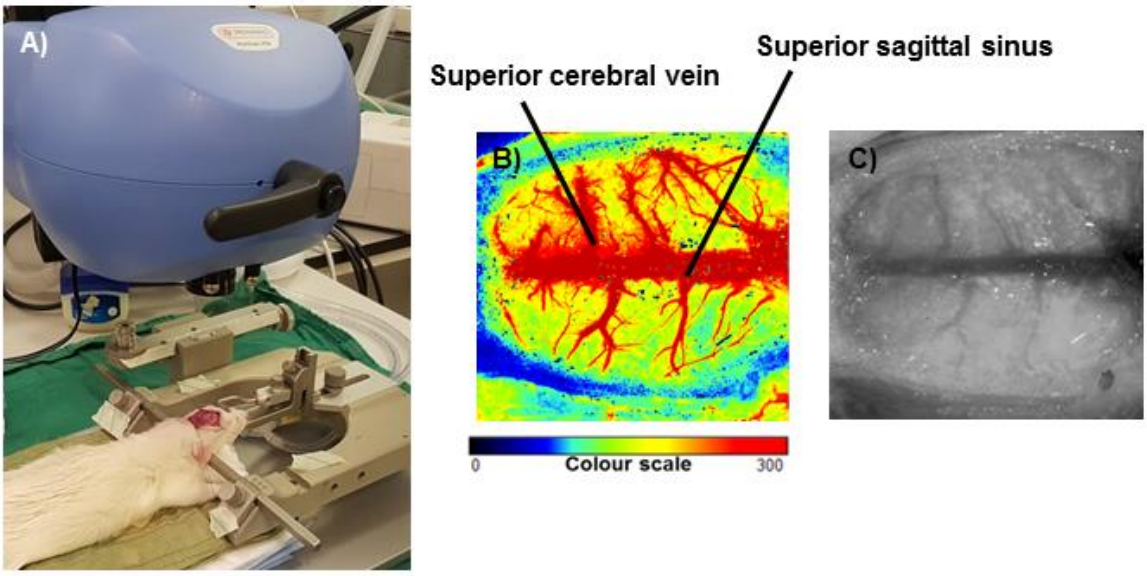

Figure 6-1 The LSCI system. A) Animal subjected to LSCI. Rats were placed in a stereotaxic frame and head secured with tooth and ear bars. The skull previously thinned is exposed by retracting overlying skin with the aid of 4.0 sutures sutured onto incision edges and taped onto the frame. The LSCI camera was placed 10 cm from the skull surface, Johnson & Johnson oil applied on the brain surface and imaging started. **B) Representative image of dynamic change in CBF speckle patterns**. Cortical perfusion map prior to MCAO displaying the superior sagittal sinus. Colour scale is set from 0 to 300 PU, where red represents increased perfusion**. C) Monochrome intensity image**. Cortical surface image displaying the amount of reflected light in the scalp.

6.2.5.2 Imaging protocol

Following skull thinning and MCAO onset, animals were placed on a stereotaxic frame and the head secured in place with the use of ear and tooth bars. The skull was exposed with the aid of four separate 4-0 threads sutured onto the edges of the skin incision and taped onto the stereotaxic frame to enhance FOV. To prevent skull drying, which could impact reliability of results, Johnson & Johnson oil (Johnson & Johnson, USA) was applied on the skull surface and left in place during the whole experiment. Imaging started at 60 min MCAO and was carried out for 2 hrs. Following 90 min MCAO, the filament was retracted in order to induce reperfusion of the MCA and IV Ang-(1-7)/Vehicle treatment started for a period of 90 min.

6.2.5.3 Imaging analysis

Once the imaging protocol was completed, raw speckle images were obtained for each rat and processed in PU using PIMSoft, a PeriCam PSI dedicated Software (Perimed, Sweden). In this study, we were interested in assessing the impact of Ang-(1-7) on perfusion in the contralateral hemisphere as well as the ischaemic core, ischaemic penumbra and oligaemic/perfused areas in the ipsilateral hemisphere during reperfusion. The first step in image analysis consisted in the determination of the ipsilateral ROIs and to do so, thresholds were establishedon mean perfusion values within the contralateral hemisphereduring MCAO. A ROI was outlined on the contralateral hemisphere and a mean perfusion value (PU) was calculated from the images recorded during MCAO for a period of 15 min. From this mean perfusion value, a set of thresholds were applied to define the ischaemic core (<43% of contralateral perfusion), ischaemic penumbra (43-75% of contralateral perfusion) and oligaemic/perfused tissue (76%-100%) during MCAO (McLeod et al., 2015; Shen et al., 2003). These ROIs were then used to assess changes in perfusion over time. Figure 6-2 shows a representative image of the ROIs outlined in each rat. The superior sagittal sinus was excluded from analysis.

The second step in image analysis consisted in the determination of a baseline mean perfusion value for each individual ROI by averaging the images recorded during MCAO for a period of 15 min. The perfusion signal was then normalised to the mean signal during MCAO within the respective ROI’s allowing us to calculate the % change in perfusion following reperfusion with or without treatment.

To identify PID occurrence during reperfusion for each animal, the cerebral perfusion videos obtained during LSCI were analysed and fast hyperaemic responses in the peri-infarct region were counted.

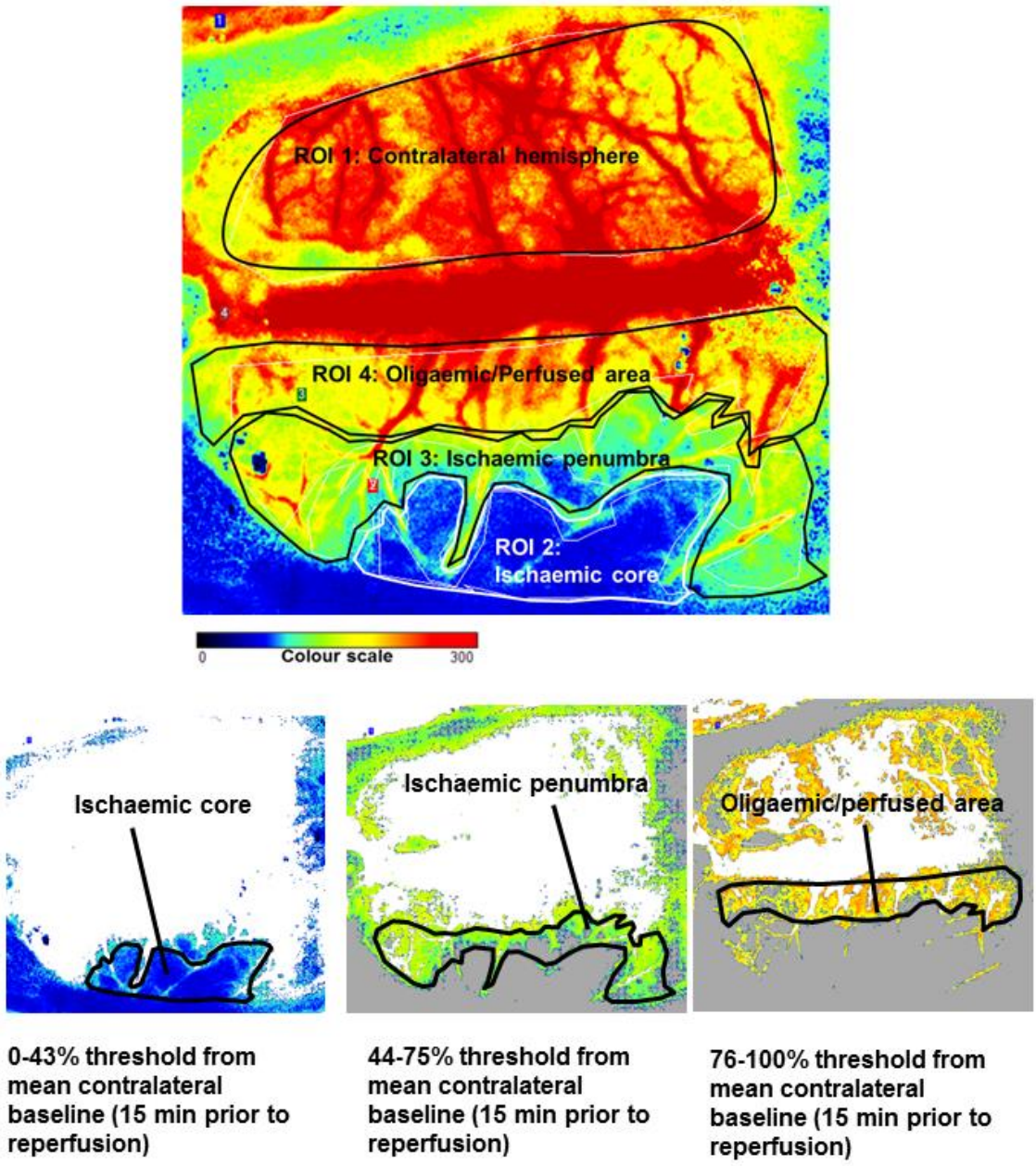

Figure 6-2 Determination of ROIs for cortical perfusion analysis. Mean PU values obtained in the contralateral hemisphere between 75-90 min MCAOwere used to apply thresholds across the ipsilateral hemisphere. **Ischaemic core** was set as 0-43% of mean PU in contralateral hemisphere during MCAO. **Ischaemic penumbra** was set as 44-75% of mean PU in contralateral hemisphere during MCAO. **Oligaemic/perfused region** was set as 76-100% of mean PU in contralateral hemisphere during MCAO. Colour scale is set as 0 to 300 PU for the top image.

6.2.6 Randomisation, blinding and exclusions

Animals were randomly assigned to surgery day using an online randomisation plan generator (www.random.org). Surgeon (MA) was not blinded to treatment assignment.

Rats displaying the following characteristics were excluded:

- Failure to completely reperfuse the entire cortical surfaceupon filament retrieval.
- SAH
- Animals that did not exhibit evidence of cortical perfusion deficit.
- Persistent muscle, skin and scalp bleeding impairing cortical cerebral perfusion measurement.

6.2.7 Statistics

Physiological parameters pH, PaO_2, $PaCO_2$, temperature were analysed using repeated measures two-way ANOVA followed by Sidak's test to correct for multiple comparisons with time and treatment as factors.

MABP and cerebral perfusion within the contralateral hemisphere, ischaemic core, ischaemic penumbra and oligaemic/perfused areas in the ipsilateral hemisphere were presented as a time course, starting at baseline (MCAO) and finishing at 90 min reperfusion. Differences between treatment groups in MABP and perfusion dynamics were analysed by assessing the summary measure of AUC during reperfusion and the means compared using unpaired Student t-test. PIDs were counted during the reperfusion period and analysed between groups using unpaired Student t-test. Data were presented as mean ± S.D. and $p<0.05$ deemed as statistically significant.

Descriptive perfusion alterations for all ROIs within groups were shown as mean PU ± S.D. Statistics were not conducted for this data set.

6.3 Results

6.3.1 Exclusions

A total of 18 male Wistar rats were used in this study and 7 were excluded: 4 in Vehicle (dH_2O) and 3 in the Ang-(1-7) treatment groups. Two animals in the Ang-(1-7) and three in the Vehicle (dH_2O) treatment groups failed to completely reperfuse the entire cortical surface upon filament removal. From these animals, one in each group showed signs of haemorrhage seen as darker patches in the perfusion map within the ipsilateral hemisphere. In addition, one rat in Ang-(1-7) group showed signs of partial occlusion due to lack of cortical perfusion deficit during MCAO. One Vehicle (dH_2O) treated rat had to be excluded due to excessive bleeding originating from the skull and adjacent muscles/skin, which caused frequent imaging obstruction and influenced the reliability of the values obtained. Overall, 11 animals were included, 5 in Vehicle (dH_2O) and 6 in Ang-(1-7). Figure 6-3 shows all excluded animals in Vehicle (dH_2O) and Ang-(1-7) treated groups.

6.3.2 Physiological parameters

Physiological parameters pH, $PaCO_2$, PaO_2 were measured and recorded during isoflurane and α-chloralose anaesthesia. Parameteres were maintained within physiological range with the exception of PaO_2, which was higher throughout experimental procedures due to mechanical ventilation with 30% O_2. Prior to stroke surgery, all physiological parameters were maintained stable between groups with no statistical differences at this time point ($P>0.05$), (Table 6-1).

At MCAO baseline and just prior to reperfusion, blood pH and arterial $PaCO_2$ were maintained within range. Rectal temperature was slightly lower for both treatment groups and the most challenging parameter to maintain stable as rats had to be frequently moved between surgical corkboard and stereotaxic frame for surgical procedures. There were no statistical differences between physiological parameters between groups during MCAO ($P>0.05$), (Table 6-1). During reperfusion, all physiological values were set within range between groups, to the exception of PaO_2, with no statistical differences ($P>0.05$), (Table 6-1).

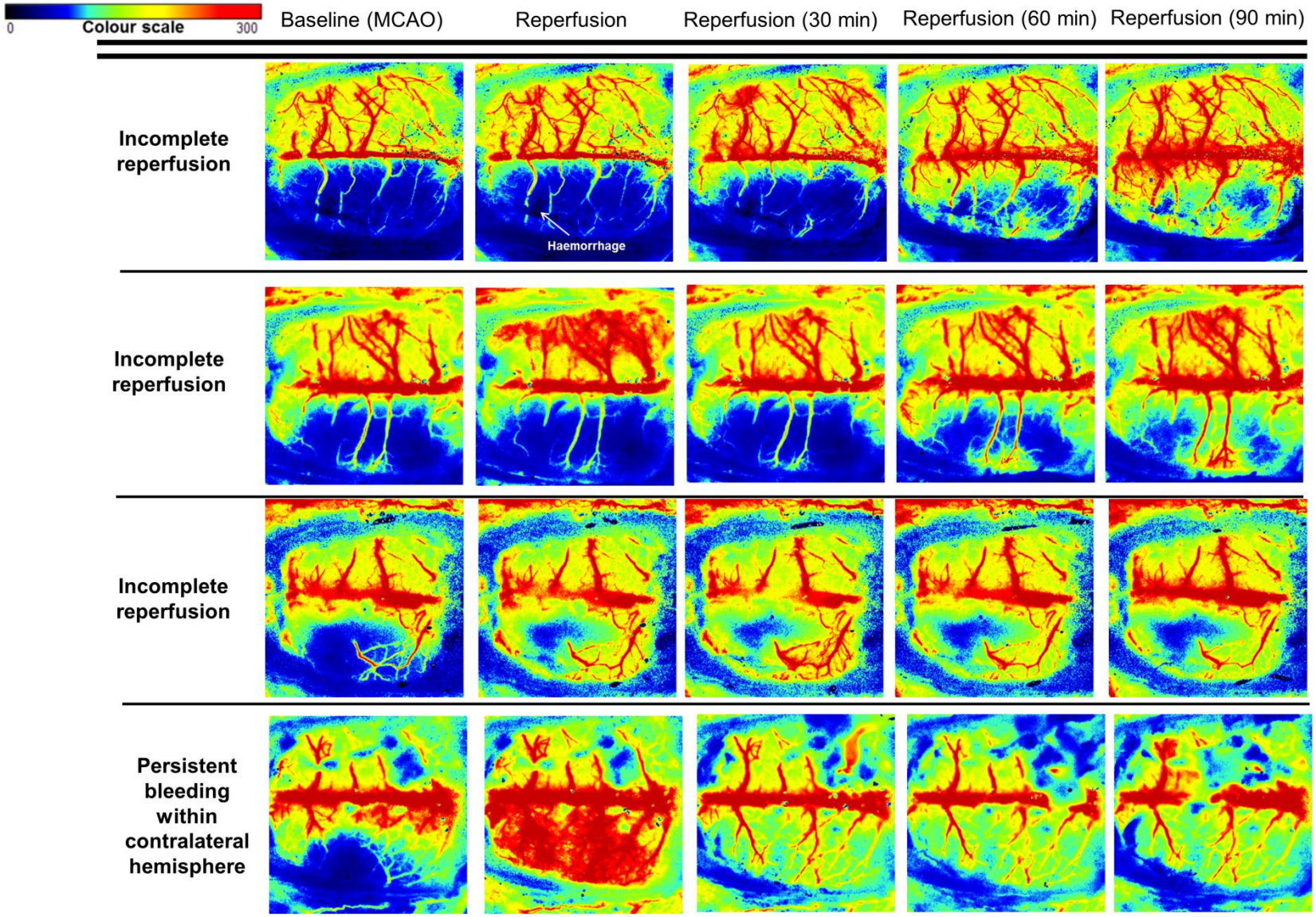

A)

Vehicle(dH_2O)

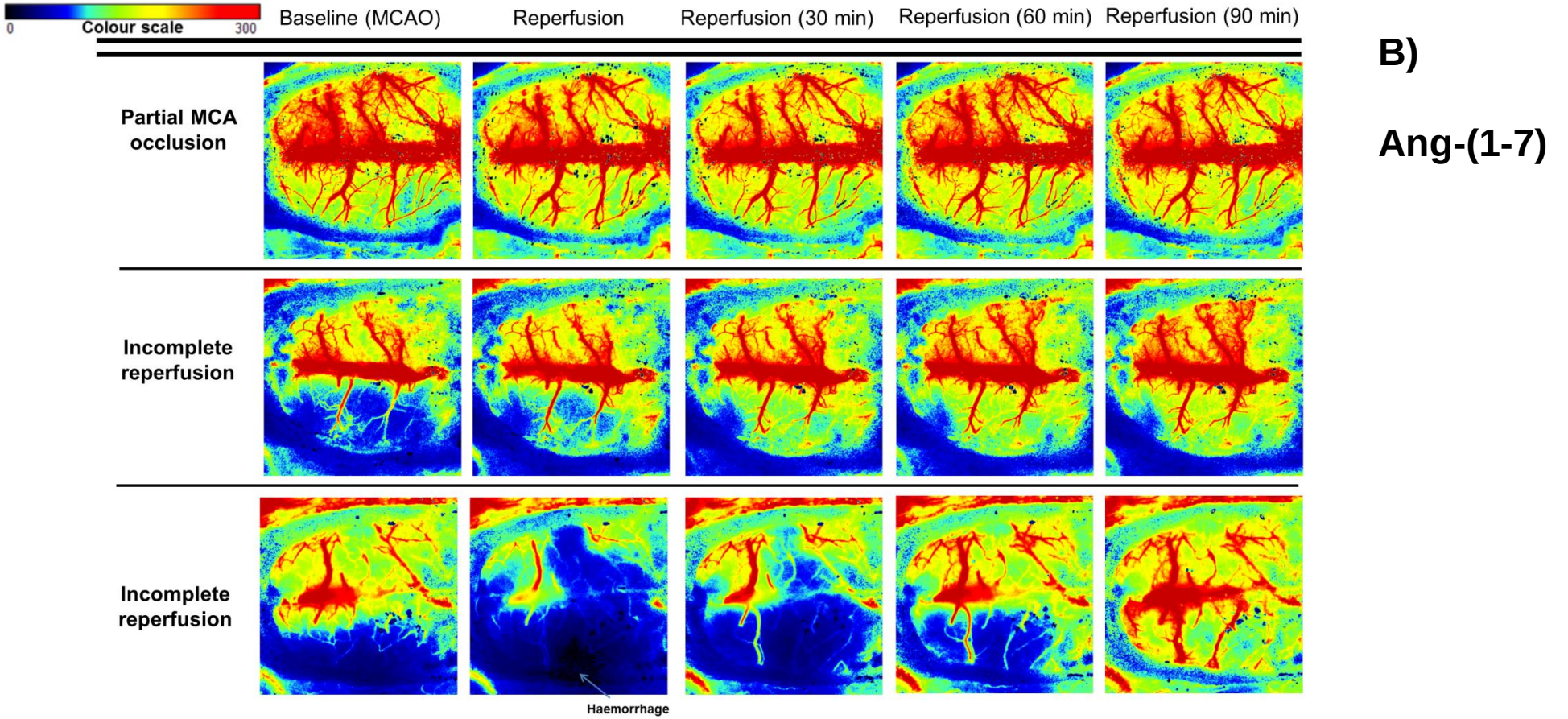

Figure 6-3 Excluded animals. A) Vehicle (dH_2O) group. Three animals failed to complelety reperfuse the entire cortical surface upon filament retrieval. One other rat was excluded due to persistent bleeding originating from the skull and adjacent muscles and skin, often interfering with imaging particularly in the contralateral hemisphere. **B) Ang-(1-7) group.** Two animals failed to completely reperfuse the entire cortical surface upon filament retrieval. One other rat was excluded due to partial MCAO, indicated by lack of perfusion deficit in the ipsilateral hemisphere during MCAO. Arrows indicate haemorrhage in animals within Vehicle (dH_2O) and Ang-(1-7) treated groups. Colour scale is set from 0 to 300 PU. A representative image of cerebral perfusion dynamics at baseline, reperfusion and every 30 min post reperfusion is shown for each animal.

Table 6-1 Physiological parameteres: pH, PaO_2, $PaCO_2$ and temperature prior to MCAO, at baseline and 1 hr reperfusion. Blood pH and $PaCO_2$ were maintained within the normal physiological range for Vehicle (dH_2O) and Ang-(1-7) treated groups thoroughout the experiment. PaO_2 was above range in all experiments due to mechanical ventilation. Temperature was slightly below range 36.5°C for both groups at baseline due to animal movement between frames. There were no statistical differences between groups at all-time points. Data were analysed using repeated measures two-way ANOVA; $P<0.05$ was deemed as significant. Data are expressed as mean ± S.D.

		Vehicle (dH_2O)	Ang-(1-7)
Prior to MCAO surgery	Blood pH	7.4±0.1	7.4±0.03
	Arterial PaO_2 (mmHg)	136.8±36.5	120.0±19.0
	Arterial $PaCO_2$ (mmHg)	43.5±7.2	41.8±2.9
	Temperature (°C)	36.6±0.6	36.7±0.4
MCAO (Baseline prior to therapy)	Blood pH	7.4±0.1	7.4±0.1
	Arterial PaO_2 (mmHg)	147.1±17.6	169.3±36.2
	Arterial $PaCO_2$ (mmHg)	36.6±6.0	42.3±5.5
	Temperature (°C)	36.2±0.6	36.3±1.0
Reperfusion (1 hr)	Blood pH	7.4±0.01	7.4±0.1
	Arterial PaO_2 (mmHg)	135.8±29.6	151.4±57.8
	Arterial $PaCO_2$ (mmHg)	42.2±3.9	44.4±5.0
	Temperature (°C)	36.8±0.2	37.1±0.7

6.3.2.1 Mean arterial blood pressure

MABP values (mmHg) during MCAO and following reperfusion with MABP maintained within normal levels throughout (80-120mmHg) (Figure 6-4). Prior to reperfusion, MABP was 101.2±10.8 mmHg in Vehicle (dH_2O) and 100.7±16.9 mmHg in Ang-(1-7) treated groups. Comparison of mean group AUC values showed that there were no differences between groups in MABP during MCAO (P>0.05) and reperfusion with treatment (P>0.05).

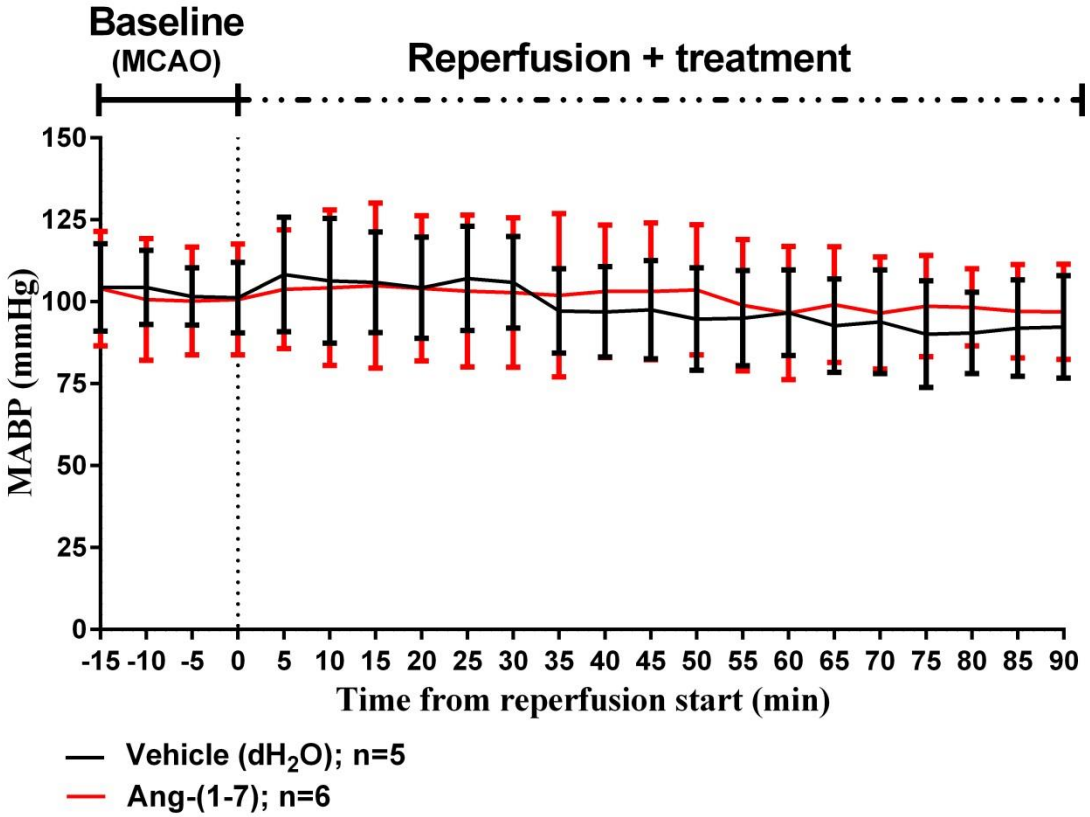

Figure 6-4 Mean arterial blood pressure. During baseline (MCAO), MABP was stable between groups with values being maintained within healthy ranges (80-120 mmHg). Following reperfusion and treatment, MABP values were maintained within range for all rats with no significant differences between treatment groups (P>0.05). Data displays values for Vehicle (dH_2O; n=5) and Ang-(1-7) (n=6). Data were analysed with mean AUC comparisons followed by unpaired Student's t test; *P<0.05 was deemed as significant. Data are expressed as mean ± S.D.

6.3.3 Cerebral perfusion following stroke

MCAO successfully decreased perfusion in the ipsilateral hemisphere when compared to contralateral hemisphere. Results are presented as mean PU obtained for Vehicle (dH_2O) (Figure 6-5A) and Ang-(1-7) (Figure 6-5B) treated animals for all ROIs.

Following 90 min MCAO, the filament was removed from the MCA to start reperfusion. In Vehicle rats, there was a trend for perfusion to increase in the contralateral hemisphere over the course of 90 min reperfusion by 15.3±13.5 PU. Conversely, the Ang-(1-7) treated group, perfusion values showed fluctuations, with a small indication to decrease overtime by 13.4±14.8 PU. Reperfusion start caused an increase in perfusion in both treatment groups in the ipsilateral hemisphere. In Vehicle treated animals, reperfusion induced a 97.5±25.6 PU increase inperfusion within the ischaemic core, 72.6±34.0 PU increase within the ischaemic penumbra and 15.4±34.7 PU rise in oligaemic/perfused ROI. In Ang-(1-7) treated animals, reperfusion resulted in a 110.2±34.6 PU increase within the ischaemic core, 40.9±26.6 PU in the ischaemic penumbra and 4.8±15.9 PU in oligaemic/perfused region. Reperfusion resulted in a marked increase in perfusion within the ischaemic core, penumbra and oligaemic/perfused ROIs in both groups, particularly within the first 15 min after reperfusion. After 20 min of reperfusion there was a general trend for perfusion to decrease over time in both groups. Figure 6-6 shows a representative image of an animal within each group at baseline, reperfusion and every 30 min post reperfusion. Images display the decrease in perfusion in ipsilateral hemisphere compared to the contralateral side over time.

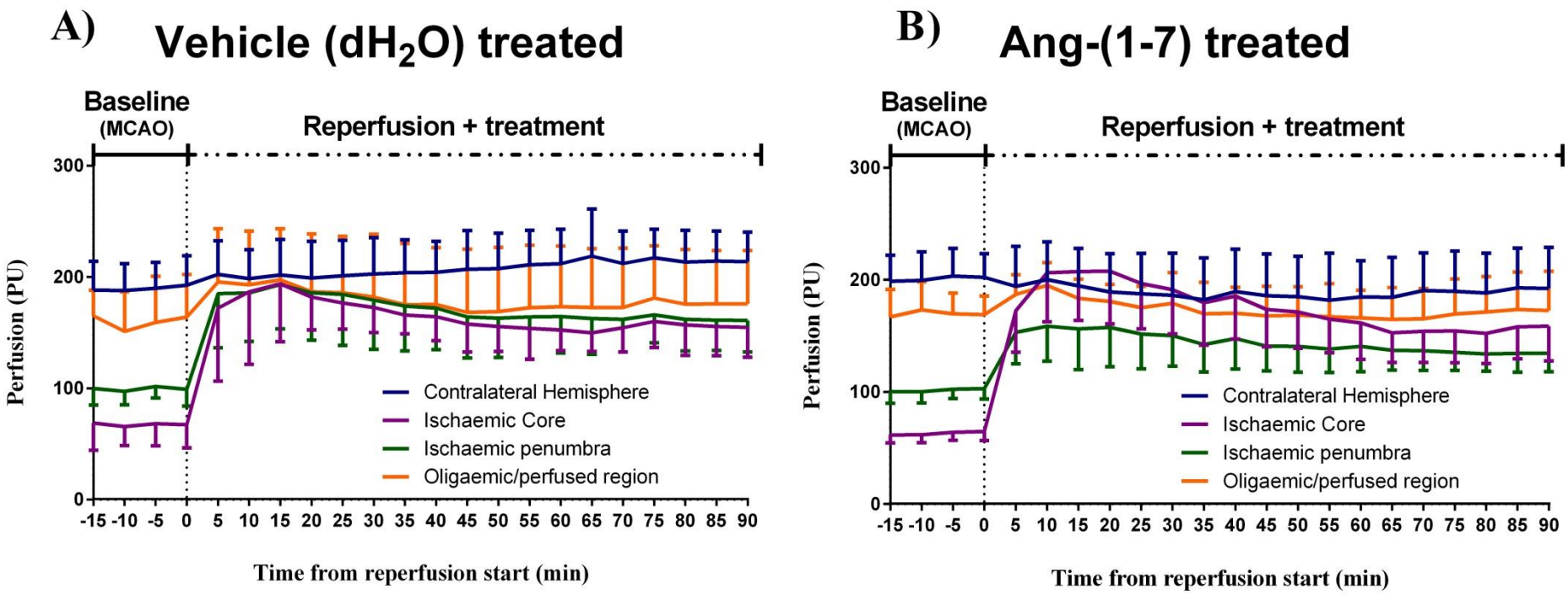

Figure 6-5 Cerebral perfusion change during the experimental protocol. A) Vehicle (dH_2O) treated animals. During baseline (MCAO) perfusion was higher in the contralateral hemisphere compared to the ipsilateral hemisphere. Following reperfusion, there was a trend for perfusion to increase over time in the contralateral hemisphere. Reperfusion start induced a steep increase in perfusion within the ischaemic core, ischaemic penumbra and oligaemic/perfused region peaking at 15 min post reperfusion and subsequently decreasing for the following 75 min of imaging. **B) Ang-(1-7) treated animals**. During baseline, perfusion values were higher in the contralateral hemisphere compared to the ipsilateral hemisphere. Following reperfusion, perfusion valuesfluctuated in the contralateral hemisphere and showed a trend to decrease. Reperfusion start induced a steep increase in perfusion within the ischaemic core, hypoperfused area and oligemic region with values peaking at 20 min post reperfusion in the ischaemic core and ischaemic penumbra. Perfusion subsequently decreased for the following 70 min of imaging in these two areas. In the oligaemic/perfused region, perfusion values peaked at 10 min post reperfusion and thendecreased over time. Data are expressed as mean± S.D.in PU for Vehicle (dH_2O; n=5) and Ang-(1-7) (n=6) treated rats.

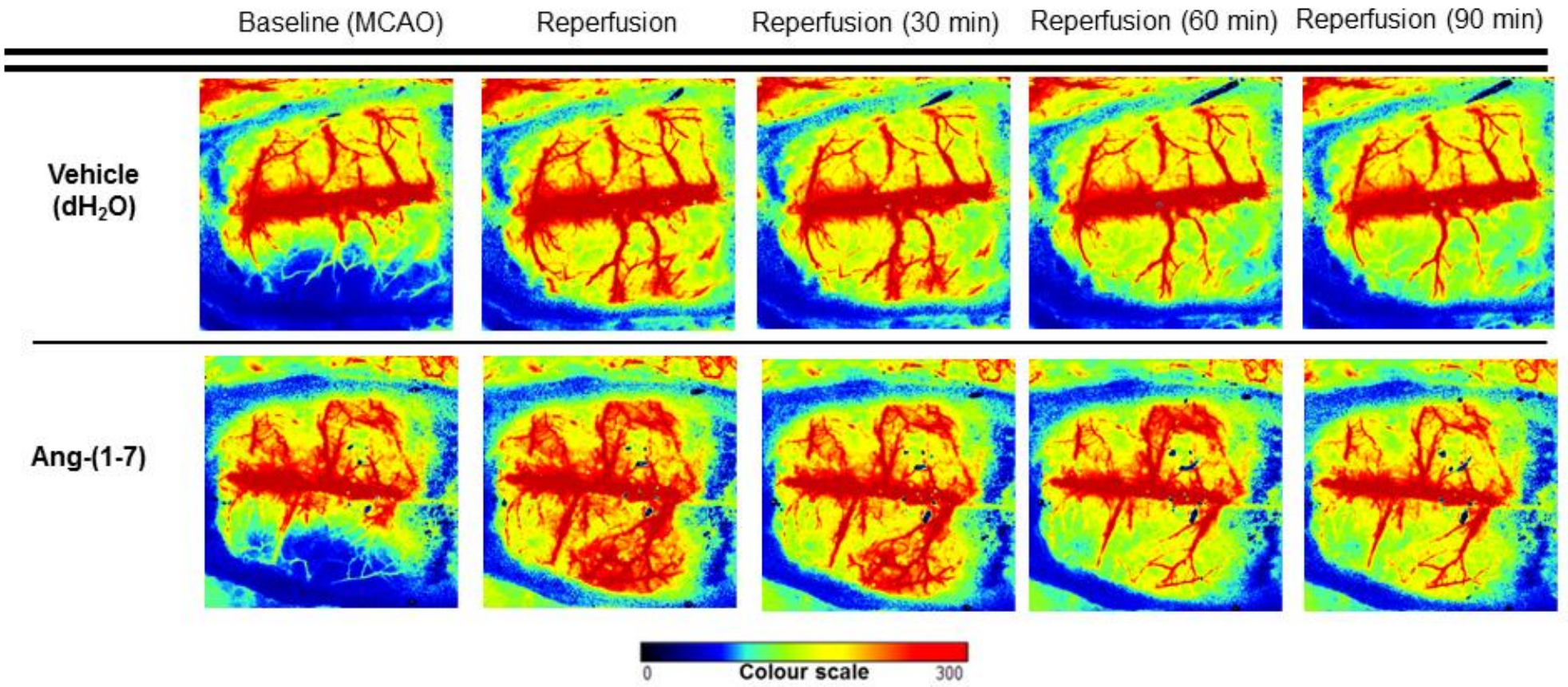

Figure 6-6 Representative images of cortical cerebral perfusion dynamics over time per treatment group. Top and bottom figures display cerebral perfusion dynamics for Vehicle (dH_2O) and Ang-(1-7) treated groups at MCAO, reperfusion and every 30 min post reperfusion start, respectively. For each animal, there was a gradual decrease in cortical perfusion within the ipsilateral side when compared to the contralateral hemisphere after reperfusion onset.

6.3.4 Ang-(1-7) treatment significantly decreases perfusion in the contralateral hemisphere

Following reperfusion there was a trend for perfusion to increase in the contralateral hemisphere over the 90 min time course, whereas Ang-(1-7) treated rats showed a trend to decrease contralateral perfusion. In Vehicle treated rats, perfusion increased by 11.7±8.1% whereas Ang-(1-7) treatment induced a 4.5±10.4% reduction between 0-90 min reperfusion. Comparison of mean group AUC values showed that Ang-(1-7) treatment significantly decreased cortical perfusion compared to Vehicle (P=0.02), (Figure 6-7). Figure 6-8 displays a representative image of perfusion dynamics in the contralateral hemisphere for the median rat in each treatment group. Since data were evaluated as perfusion change from baseline for all animals, baseline images were subtracted from the whole data set to confirm the trend observed (Figure 6-8).

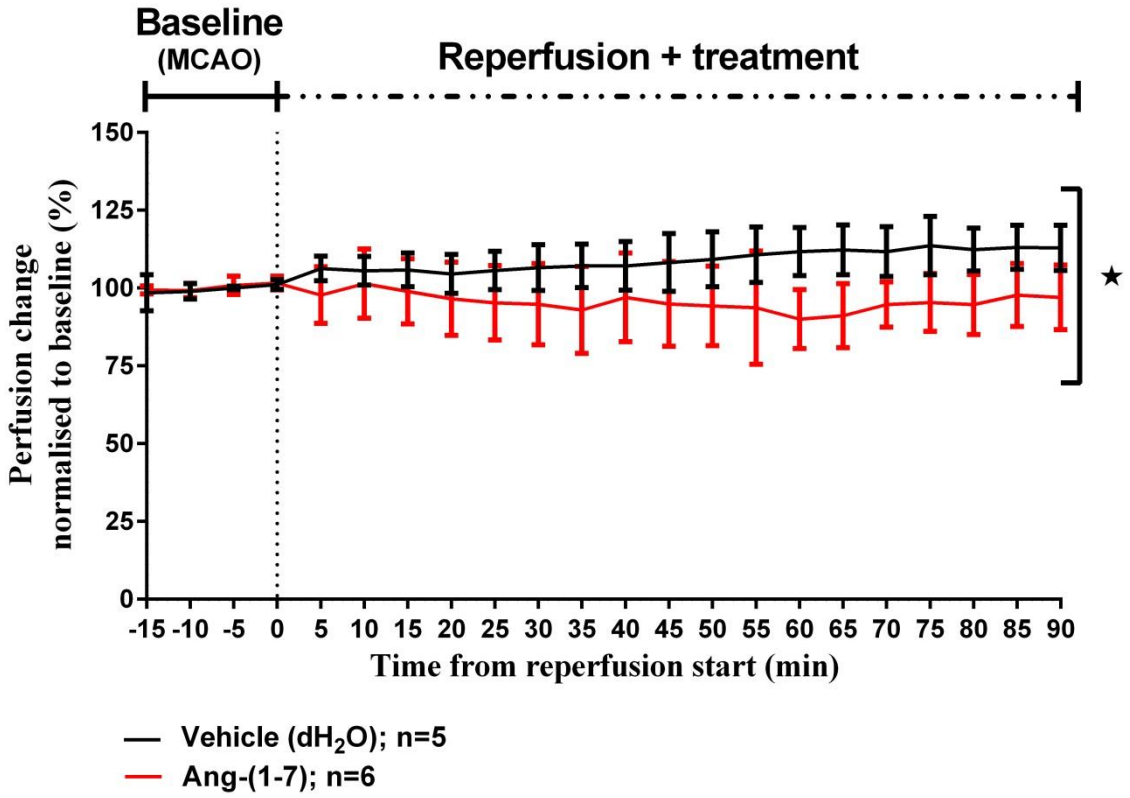

Figure 6-7 Contralateral hemisphere perfusion % change from baseline. Following reperfusion, Vehicle (dH_2O) animals showed a trend to increase perfusion during 90 min reperfusion whereas Ang-(1-7) treated animals showed a trend to attenuate it. Ang-(1-7) treatment induced a significant change in contralateral hemisphere perfusion compared to Vehicle (dH_2O) (P=0.02). Data displays values for Vehicle (dH_2O; n=5) and Ang-(1-7) (n=6) treated animals. Data were analysed with mean AUC comparisons followed by unpaired Student's t test; *P<0.05 was deemed as significant. Data are expressed as mean ± S.D. % from baseline.

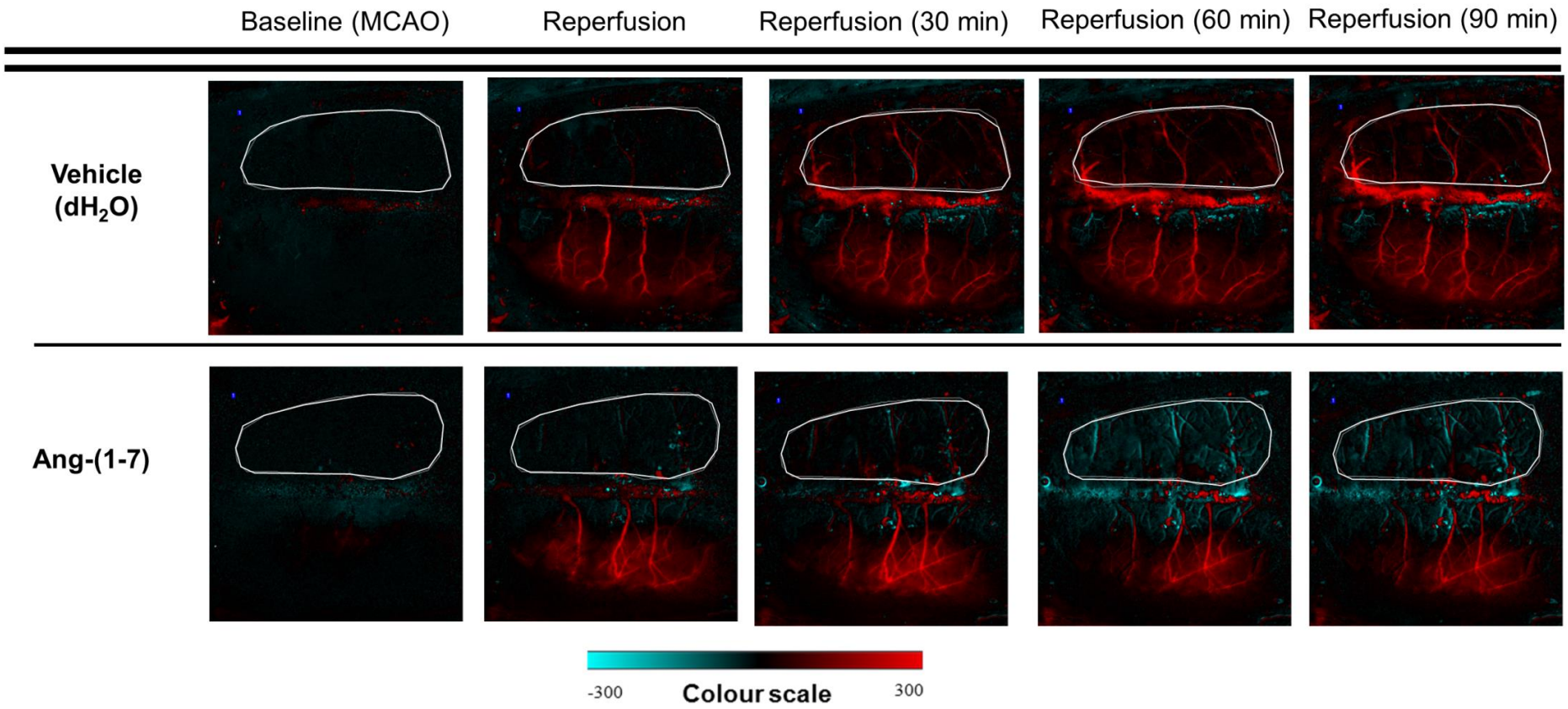

Figure 6-8 Contralateral hemisphere perfusion dynamics normalised to baseline. Top and bottom figures display contralateral perfusion dynamics for the median animals in the Vehicle (dH_2O) and Ang-(1-7) treated groups at MCAO, reperfusion and every 30 min post reperfusion start, respectively. Image pixels within baseline (MCAO) were subtracted from all images obtained during reperfusion. Vehicle (dH_2O) treated rat displays an increase in perfusion in the contralateral hemisphere during 90 min reperfusion (contralateral ROI outlined in white). On the other hand, Ang-(1-7) treated animal displays a decrease in perfusion within contralateral hemisphere when normalised to MCAO. Colour scale ranges from -300 to 300 PU, where red represents increased perfusion and blue represents decreased perfusion from baseline (MCAO).

6.3.5 Ang-(1-7) treatment does not influence perfusion in the ipsilateral hemisphere

In the ischaemic core, reperfusion led to a steep increase in perfusion in Vehicle (dH_2O) and Ang-(1-7) treated groups, 157.2±62.4% and 174.1±62.4% from start to 5 min reperfusion, respectively (Figure 6-9). Ang-(1-7) treatment showed a trend to enhance perfusion compared to the control group, however, comparison of mean group AUC values indicated that differences were not significant when compared to the Vehicle group ($P>0.05$), (Figure 6-9). Both groups displayed high variability in perfusion extent. For the Ang-(1-7) group, 3 rats showed higher perfusion changes than the remaining group cohort whereas in the Vehicle group, values were fairly consistent with the exception of one animal.

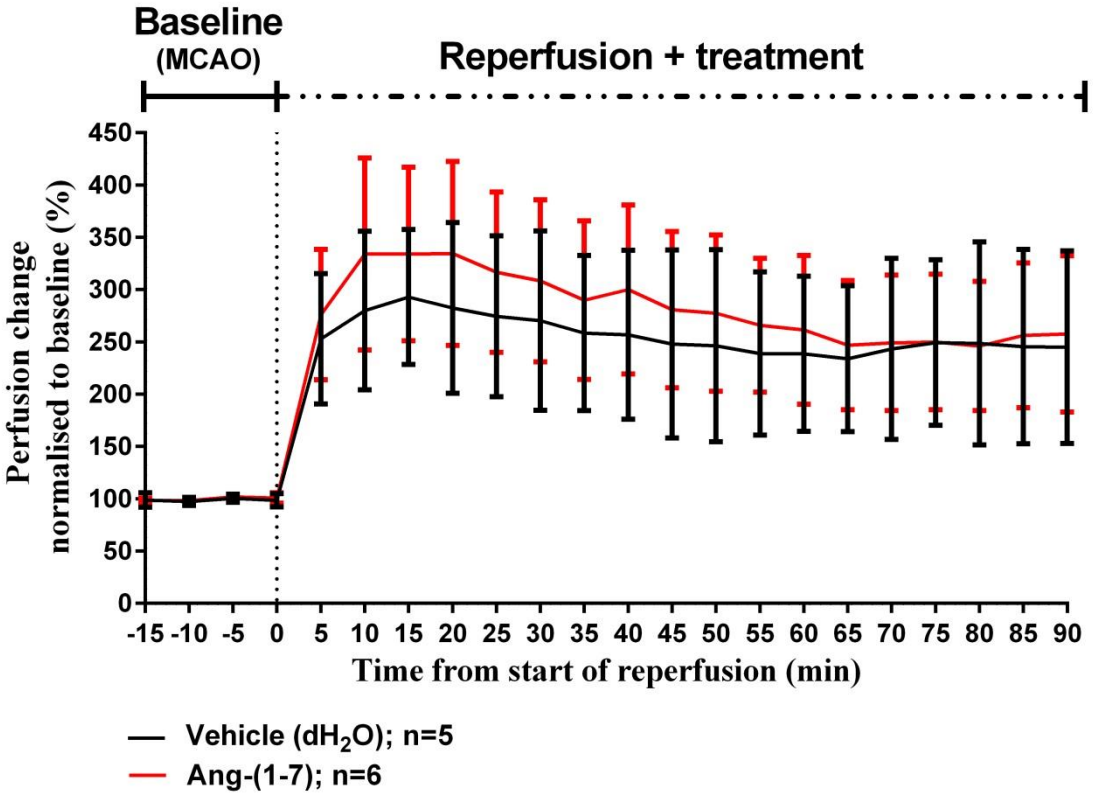

Figure 6-9 Ischaemic core perfusion % change from baseline. Following reperfusion, there was a steep increase in perfusion within Vehicle (dH_2O) and Ang-(1-7) treated animals and followed by perfusion attenuation overtime. Ang-(1-7) did not significantly alter perfusion within the ischaemic core compared to control group ($P>0.05$). Data displays values for Vehicle (dH_2O; n=5) and Ang-(1-7) (n=6) treated animals. Data were analysed with mean AUC comparisons followed by unpaired Student's t test; *$P<0.05$ was deemed as significant. Data are expressed as mean ± S.D. % from baseline.

In the ischaemic penumbra, reperfusion led to a cerebral perfusion increase in Vehicle and Ang-(1-7) treated groups, 87.8±47.7% and 62.5±17.5% from start to 5 min reperfusion, respectively (Figure 6-10). During the course of reperfusion, Ang-(1-7) did not influence perfusion when compared to Vehicle as determined by comparison of mean group AUC values (P>0.05), (Figure 6-10).

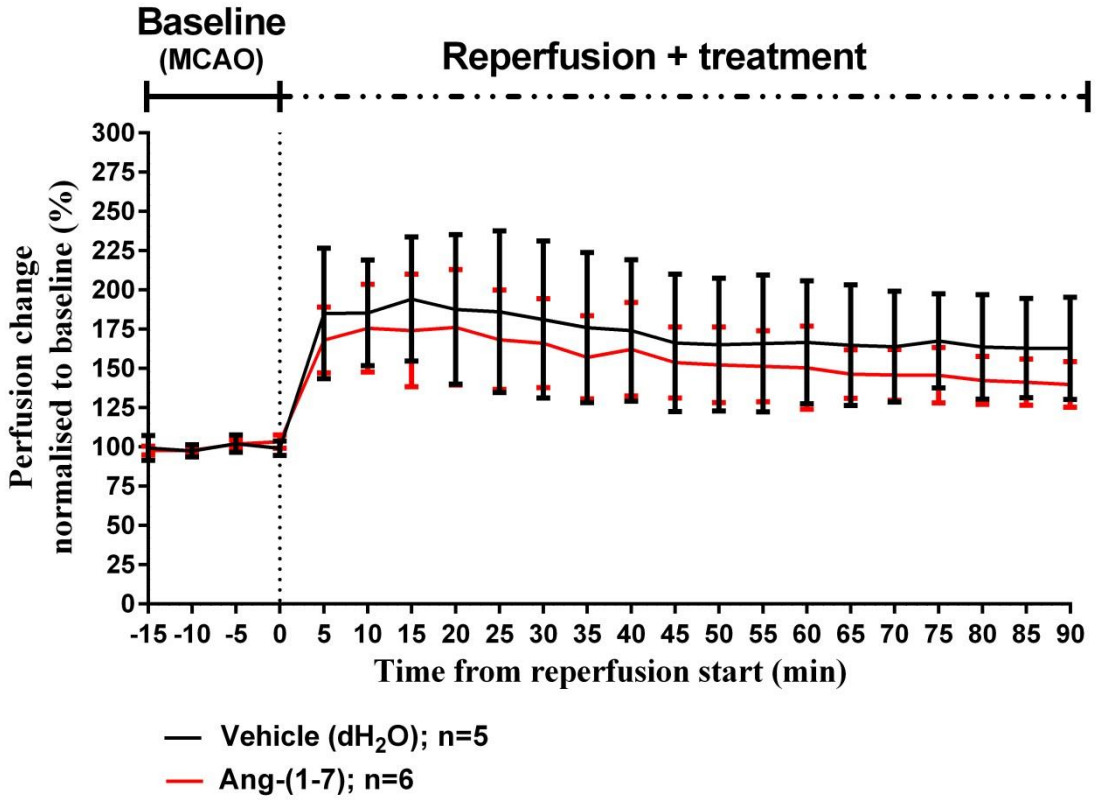

Figure 6-10 Ischaemic penumbra perfusion % change from baseline. Following reperfusion, there was an increase in perfusion within Vehicle (dH_2O) and Ang-(1-7) treated animals and followed by perfusion attenuation over time. Treatment had no impact in perfusion within the ischaemic penumbra compared to control animals (P>0.05). Data displays values for Vehicle (dH_2O; n=5) and Ang-(1-7) (n=6) treated animals. Data were analysed with mean AUC comparisons followed by unpaired Student's t test; *P<0.05 was deemed as significant. Data are expressed as mean ± S.D. % from baseline.

In the oligaemic/perfused region, reperfusion led to a slight increase in perfusion in Vehicle (dH_2O) and Ang-(1-7) treated groups, 19.9±19.9% and 15.0±8.4% from start to 5 min reperfusion, respectively (Figure 6-11). Comparison of mean group AUC values showed that Ang-(1-7) treatment did not differ from vehicle treated animals over 90 min reperfusion (P>0.05), (Figure 6-11), further confirming that Ang-(1-7) does not enhance perfusion within the ipsilateral hemisphere.

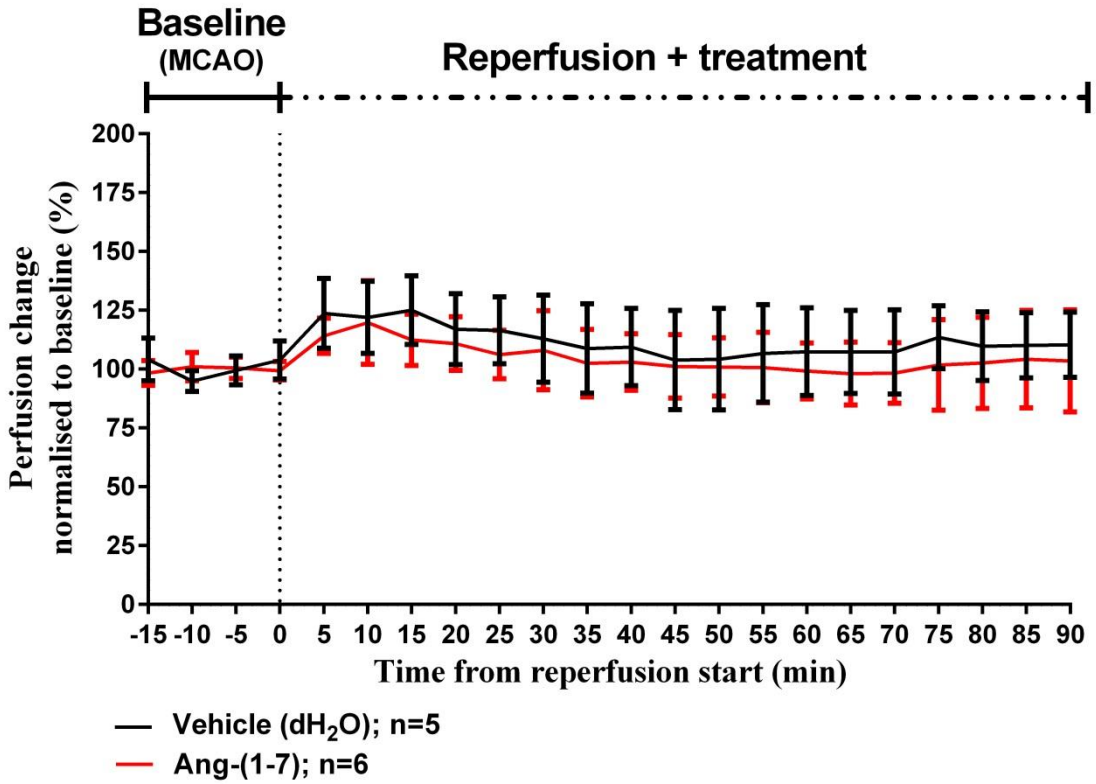

Figure 6-11 Oligaemic/perfused area perfusion % change from baseline. Following reperfusion, there was a slight increase in perfusion within Vehicle (dH_2O) and Ang-(1-7) treated animals, peaking at 15 min and 10 min, respectively. Treatment did not influence cerebral perfusion within the oligaemic/perfused area during reperfusion (P>0.05). Data displays values for Vehicle (dH_2O; n=5) and Ang-(1-7) (n=6) treated animals. Data were analysed with mean AUC comparisons followed by unpaired Student's t test; *P<0.05 was deemed as significant. Data are expressed as mean ± S.D. % from baseline.

6.3.6 Peri-infarct depolarisations

PIDs were quantified across ipsilateral and contralateral hemispheres. PIDs were detected in 1 out of 5 rats for Vehicle group and 3 out of 6 rats for Ang-1-7. There were no significant differences in the frequency of PIDs between groups [0.5±0.55 vs 0.2±0.5 (P>0.05)], (Figure 6-12). PIDs occurred a few seconds after reperfusion onset and were not evident afterwards.

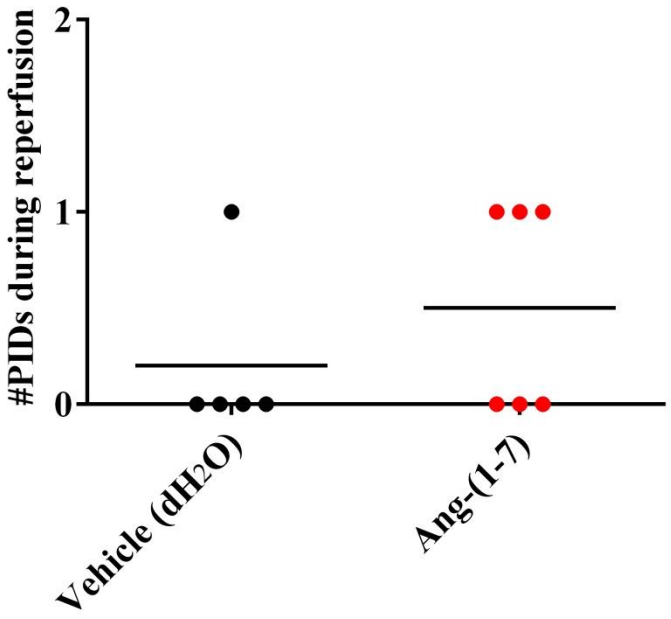

Figure 6-12 Peri-infarct depolarisation frequency during reperfusion. PIDs were detected in four animals just after reperfusion onset, one in control group and three in Ang-(1-7) treated rats. Treatment did not influence PIDs occurrence during reperfusion ($P>0.05$). Data were analysed using unpaired Student t test; *$P<0.05$ was deemed as significant. Horizontal bar represents the mean.

6.4 Discussion

This study was designed to examine the potential impact of Ang-(1-7) in improving cortical perfusion in ipsilateral and contralateral hemispheres during 90 min reperfusion following MCAO. Ang-(1-7) therapy at 5 nmol/hr IV infusion had no significant effect on cerebral perfusion within the ischaemic core, ischaemic penumbra and oligaemic/perfused tissue. In contrast, within the contralateral hemisphere, there was a significant decrease in cerebral perfusion in Ang-(1-7) treated animals. Moreover, treatment did not diminish PID frequency during reperfusion or impact MABP during the course of the experiment. To our knowledge, this experiment shows for the first time cortical surface perfusion dynamics during MCAO and following reperfusion with LSCI technique whilst testing Ang-(1-7) therapy.

For several years MRI and CT have been conducted aiming to identify thresholds to successfully defined core from penumbra in both clinical and preclinical settings (Albers et al., 2006; An et al., 2015; Davis et al., 2008; Reid et al., 2012). However, these have proven to be a challenge due to inconsistencies regarding choice of imaging techniques and selection of perfusion and mismatch parameters (Davis et al., 2008). In MRI-DWI assessments, ADC abnormal thresholds comprising the ischaemic core represent ADC

pixels <43% of mean contralateral CBF at 1 hr, 3 hrs and 4 hrs MCAO (Meng et al., 2004; Robertson et al., 2015; Shen et al., 2003). On the other hand, following MCAO in male Wistar rats, perfusion CT performed at 90 min ischaemia identified that the ischaemic core represented <55% of mean contralateral CBF whereas the penumbra was accurately predicted at a <75% threshold (McLeod et al., 2015). To study the impact of Ang-(1-7) in ischaemic core, penumbra and oligaemic/perfused regions, the ischaemic core threshold <43% of contralateral CBF was selected as it was consistently observed in 3 studies. The penumbra was defined between 44-75% of perfusion as defined by McLeod et al whereas oligaemic/perfused areas were arbitrarily set as 76-100%.

In this study, 5 out of 7 rats were excluded due to incomplete cortical surface reperfusion upon filament retrieval. Several factors could be implicated in this event such as poor collateral blood supply or "no-reflow" mechanisms, the latter characterised by inflammatory cell recruitment and microvessel lumen obstruction (Burrows et al., 2015; Liebeskind et al., 2014; Saver et al., 2012). In turn, delays in cortical perfusion lead to prolonged ischaemia and likely contribute towards lesion evolution. This observation supports Chapter 4 findings, where it was seen that reperfusion alone exerts differential levels on infarct volume progression. Furthermore, it explains why LDF could not detect reperfusion in all animals in Chapter 3. Although inhomogeneous reperfusion is an interesting phenomenon in itself, reperfusion onset took place at different rates in these animals and to account for this variability, animals were excluded from analysis.

For all included animals, cortical cerebral perfusion was successfully measured with no significant alterations in pH, $PaCO_2$, PaO_2 or temperature between treatment groups with changes in physiological parameters being quickly corrected to the advised range. Body temperature was difficult to maintain stably amongst animals due to frequent movement between corkboard and stereotaxic frame to perform surgical procedures and imaging. A drop in temperature is suggested to decrease perfusion in pigs (Ehrlich et al., 2002) and it is possible that temperature alterations might have affected cerebral perfusion measurements in our study.

6.4.1 Ang-(1-7) does not alter MABP

MABP was continuously measured and maintained at stable levels throughout imaging, without treatment effects. Moreover, MABP fluctuations did not influence cerebral haemodynamics during reperfusion, thereby indicating that α-chloralose was an adequate anaesthetic for CBF experiments, as previously indicated (Haensel, 2015). A caveat with the use of α-chloralose is that this compound cannot be dissolved in small volumes otherwise it precipitates; therefore, larger volumes had to be administered in the animals. The recommended IV volumes to be administered in rats are typically 5 mL/kg bolus (1.75 mL in a 350g rat) and 4 mL/kg/hr infusion (1.4 mL/hr in a 350g rat) (Diehl et al., 2001). However, in our study, an IV bolus of 2.8 mL and infusion volume of 2.8 mL/hr (α-chloralose and therapy) was administered to a 350g rat. Nonetheless, animal welfare guidelines also suggest that a 12 mL/hr IV infusion is well tolerated in rats, consisting of a substantially larger volume than the one administered in our studies (Workman et al., 2010). Plus, in the present study, the animals were continuously monitored during the experiment and at no point were there indications of negative physiological consequences as highlighted by the stable MABP values.

In this study, Ang-(1-7) IV infusion therapy did not influence MABP. Yet, Ang-(1-7) might have vasodepressor or vasoconstrictive properties depending on the animal model and dose studied. For example, Ang-(1-7) infusion increased MABP when administered SC at a dose of 24 μg/kg/hr in a model of subtotal nephrectomy (Velkoska et al., 2015) whereas Ang-(1-7) IV infusion at 0.3 nmol/hr did not influence MABP in conscious rats (Walters et al., 2005). Similarly, direct Ang-(1-7) stimulation in the dorsal medulla caused a hypotensive response (Campagnole-Santos et al., 1989), a mechanism further supported in Mas-KO mouse studies, which exhibited elevated BP when compared to WT animals (Xu et al., 2008). However, in a more recent study, Mas-KO mice showed comparable MABP to WT (Botelho-Santos et al., 2012).

It is fair to deduct that the effect of Ang-(1-7) on MABP is controversial and possibly due to the use of different anaesthetics between studies. The majority of anaesthetics induce MABP fluctuations that could influence result interpretation with isoflurane and chloralose-urethane being considered the most suitable anaesthetics for cardiovascular studies (Bencze et al., 2013; Fitzner Toft et al., 2006). Moreover, to account for the short half-life and the differing route of administration from previous Chapters, the Ang-(1-7) dose used in the present study: 5 nmol/hr, was arbitrarily selected as 5 times higher than

the one used in ICV experiments. Therefore, Ang-(1-7) may modulate MABP at higher doses as seen in Velkoska's experiment (Velkoska et al., 2015) but not at smaller doses as observed in our study. This goes in agreement with the results observed in conscious systolic BP measurements in Chapter 4 and previous reports in stroke studies in both normotensive and SHR animals (Jiang et al., 2013; Mecca et al., 2011; Regenhardt et al., 2013).

6.4.2 Contralateral hemisphere perfusion is significantly lower in Ang-(1-7) treated animals

A surprising feature in the results was that contralateral perfusion increased over time in the Vehicle (dH_2O) group and showed a slight trend to decrease in Ang-(1-7) treated animals, displaying a statistical difference between groups. In the contralateral hemisphere one would expect perfusion values to remain fairly stable over time following stroke (Harston et al., 2017; Hartmann, 2010). Therefore, the possibility that the effect observed might be a false positive or a reflection of alterations in $PaCO_2$ over time that failed to be detected, cannot be excluded.

Increasing reports claim and demonstrate that the vast majority of conclusions within biomedical research are false, likely due to the small *n* numbers used (Button et al., 2013; Ioannidis, 2005). Although both groups met the *n* number criteria set in the power calculation; the lower the power in a study, the less likely a statistical effect actually reflects a real effect (Ioannidis, 2005). Conversely, when an experiment with small *n* numbers identifies a true effect, it is probable that the effect provided is exaggerated, an effect inflation referred to as "winner's curse" (Ioannidis, 2008; Ioannidis et al., 2011). The statistical observation must be examined with caution and follow up studies should be performed to confirm the reproducibility of these results.

If the effect is indeed physiological, it could be the outcome of "steal phenomena" reversal. The "steal phenomena" is characterised by a shift in blood flow to non-ischaemic areas and is associated with worsened neurological outcome in patients (Alexandrov et al., 2007). A CBF shift towards the contralateral hemisphere via the anterior communicating artery could diminish perfusion within the ipsilateral hemisphere and promote injury. Concomitantly, revascularisation in cervical carotid stenosis patients leads to perfusion enhancement in the contralateral hemisphere with the degree of perfusion correlating with the grade of stenosis (Sadato et al., 2017). As a result, Ang-(1-7) could be acting to prevent

contralateral CBF shifting and, as a consequence, ipsilateral injury in the longer term. To confirm this hypothesis, further studies need to be performed to understand the physiological impact and underlying mechanisms.

6.4.3 Ang-(1-7) does not alter ipsilateral hemisphere perfusion

Throughout the imaging period, Ang-(1-7) did not improve perfusion within the ischaemic core, ischaemic penumbra or oligaemic/perfused area. The role of Ang-(1-7) in improving ipsilateral cerebral perfusion is somewhat controversial with these results strengthening the hypothesis that at lower doses, Ang-(1-7) has no effect. In stroke, Ang-(1-7)'s effects have been studied as an ICV delivery and with the use of LDF techniques; which allow a measure of perfusion in a limited area within the MCA territory (Jiang et al., 2014; Mecca et al., 2011). In our study, LSCI provided a sensitive near real-time mapping of cortical surface vasculature during reperfusion and was therefore, a reliable semi-quantitative measure of cerebral perfusion across the cortical surface. Importantly, the animal models, drug administration method and time of CBF dynamics assessment used in previous studies were substantially different from the methodology used in our study (Jiang et al., 2014; Mecca et al., 2011). For instance, in Mecca's study, Ang-(1-7) was administered as a 3 day pre-therapy in the ET-1 induced MCAO model and the impact of treatment on CBF was evaluated prior to and 1 hr post ET-1 injection (Mecca et al. 2011). In Jiang's study, studies were performed in the permanent MCAO model, Ang-(1-7) therapy administered for 4 weeks prior to injury and CBF dynamics were studied at MCAO onset as well as 1 hr and 24 hrs post stroke onset (Jiang et al. 2014). Consequently, the present study is the first experiment to evaluate the effects of Ang-(1-7) on CBF as a post stroke therapy, in a transient MCAO model, at reperfusion and with LSCI.

In the ischaemic core there was a trend for Ang-(1-7) to improve perfusion in comparison to Vehicle (dH_2O); however, the differences were not statistically different. Out of 6 animals in the Ang-(1-7) group, 3 showed higher levels of perfusion upon filament retrieval whereas in the control group, only 1 animal displayed perfusion increase to a similar extent. This variability in perfusion within the ischaemic core might reflect differences in reperfusion alone, possibly due to larger ischaemic lesions. For instance, patients that develop post-ischaemic hyperperfusion in infarcted areas display increased bioenergetic depletion, confirmed by greater ADC coefficients (Kidwell et al., 2001). Accordingly, it is plausible that animals with increased perfusion in this region developed exacerbated ischaemic lesions. Contrarily, the results could be an indication that these

particular animals had better functioning collateral supply than the remaining cohort as seen in the clinic and thus, enhanced tissue salvage (Bhaskar et al., 2017). To confirm this, lesion volumes would have to be assessed; however, this was not performed in our study, representing a study limitation.

The impact of Ang-(1-7) in human brain CBF has not yet been evaluated, however, experiments conducted in human brain vascular smooth muscle cell cultures suggest that 0.1 μM Ang-(1-7) treatment inhibits cell migration, proliferation and apoptosis (Bihl et al., 2015). Furthermore, Ang-(1-7) administration in isolated canine MCA and femoral arteries induced vascular relaxation in arterial rings with intact endothelium, an outcome observed at higher doses only (Feterik et al., 2000). Similarly, topical application of Ang-(1-7) in pial arterioles in anaesthetised pigs induced a modest vasodilation at high doses (Meng and Busija, 1993). Although the studies described were conducted in normoxic conditions, the results set the premise that Ang-(1-7) treatment could have the potential to enhance CBF following cerebral injury.

There are several factors that could have contributed towards the neutral effect seen within the ipsilateral hemisphere in the present study. Firstly, the experiments conducted by Meng & Busija and Feterik et al suggest that Ang-(1-7) treatment leads to a cerebral vasodilatory effect when administered directly and at higher doses only (Feterik et al., 2000; Meng and Busija, 1993). Consequently, a 5 nmol/hr IV infusion dose through the femoral vein may not have been sufficient to enhance CBF in the compromised ipsilateral hemisphere.

Secondly, the animal model used and treatment schedule may present contributing factors. In *in vivo* models, Ang-(1-7) pre-treatment for 48 hrs (1.1 nmol/hr ICV) did not influence ipsilateral perfusion at MCAO and at 24 hrs permanent MCAO when compared to vehicle (Jiang et al., 2012). However, in a follow up study, Ang-(1-7) pre-treatment for 4 weeks increased CBF in the peripheral region at 1 hr and 24 hrs permanent MCAO, an effect attributed to an improvement in NO production and VEGF protein levels (Jiang et al., 2014). The results observed suggest that Ang-(1-7) acts in a cumulative manner and longer treatment schedules are necessary to observe a cerebrovascular effect in the penumbral region. Additionally, Ang-(1-7) possibly enhances perfusion in permanent models; however, in transient MCAO models, reperfusion alone may transcend an Ang-(1-7) induced vascular outcome. In accordance, following ET-1 induced MCAO, CBF was shown to transiently increase over 60 min in the ipsilateral hemisphere; however, Ang-(1-7) 1.1 nmol/hr ICV treatment did not influence haemodynamics or vessel diameter

compared to vehicle therapy in normotensive rats (Mecca et al., 2011), supporting this hypothesis.

Finally, Ang-(1-7) could produce a cerebrovascular effect at later stages of injury. Following transient MCAO, Ang-(1-7) ICV post stroke therapy upregulated bradykinin expression in ischaemic tissue at 6 hrs and 48 hrs after reperfusion at moderate and higher doses (100 pmol/hr and 10 nmol/hr) (Lu et al., 2008). Plus, Ang-(1-7) at 10 nmol/hr ICV treatment stimulated NO levels from 3 to 72 hrs reperfusion (Zhang et al., 2008). Both bradykinin and NO are potent vasodilatory mediators; therefore, Ang-(1-7) could incite vasodilation from 3 hrs post reperfusion start. Overall, Ang-(1-7) did not influence cortical cerebral perfusion in the ipsilateral hemisphere following 90 min MCAO, yet, it is plausible that Ang-(1-7) might enhance ipsilateral CBF when administered locally, at high doses and at later stages of injury. It is also important to note that, in the present study, perfusion assessments represent an outcome of both arterial and venous flow. Therefore, the impact of therapy in influencing cerebral vascular dynamics within individual vessels and in the subcortical vasculature was not addressed. In future, myography experiments in cerebral vessels (e.g MCA) following MCAO, could be a suitable experiment to confirm the results obtained.

6.4.3.1 Ipsilateral perfusion does not recover to contralateral levels

Reperfusion following 90 min MCAO resulted in an initial period of hyperperfusion, lasting for 15 min in Vehicle and 20 min in Ang-(1-7) treated animals within the ischaemic core and the ischaemic penumbra. Conversely, in the oligaemic/perfused region, hyperperfusion was evident for 10 min in the Ang-(1-7) group and for 15 min in control animals. This initial period of hyperperfusion was then followed by hypoperfusion across the ipsilateral hemisphere until the end of the experiment. Perfusion values in the ipsilateral side remained below contralateral values during the hypoperfusion phase, suggesting that during 90 min reperfusion, the brain is still at risk of further hypoxic injury.

The underlying mechanism behind hyperperfusion is not well understood; however, accumulation of acid metabolites, ROS and CO_2 during MCAO are thought to lead to abnormal vasodilation in the ischaemic area (Jackman & Iadecola 2015). Although this mechanism is a hallmark of efficient reperfusion after MCAO and confirmation that MCA reperfusion was successful, it could also be a contributor towards stroke progression (Pan et al., 2007; Sage et al., 1984). For example, in rats, post-ischaemic hyperperfusion was

associated with larger cortical infarcts and shown to mediate MCA remodelling due to vascular oxidative stress and inflammation (Onetti et al., 2015; Pérez-Asensio et al., 2010), hence its possible role in infarct progression.

Similarly, the causes underlying hypoperfusion require further evaluation. One hypothesis includes vessel obstruction and increase in vascular resistance mediated by endothelial and glial cell swelling (Hossmann and Lechtape-Grüter, 1971). Other studies indicate that hypoperfusion is caused by vessel constriction, vasospasm, oedema and the "no reflow" phenomena (Kunz & Iadecola 2009; Ames et al. 1968). Other possible causes include pericyte constriction during and following MCAO (Hall et al., 2014) as well as MCA myogenic tone and reactivity impairment, thus, promoting vessel resistance (Ahnstedt et al., 2016; Cipolla et al., 1997, 2014).

Ang-(1-7) did not influence cerebral perfusion during hyper- or hypoperfusion phases. However, the findings in this study highlight the neuroprotective potential of CBF enhancing therapies when administered at acute stages of reperfusion onset and during the hypoperfusion phase.

6.4.4 Ang-(1-7) does not interfere with PID frequency

Until now, the study of therapy impact on PIDs has been compromised by the lack of methods that provided sufficient spatial and temporal sampling(Strong et al., 2006). LSCI is a suitable technique to tackle these changes and was shown to successfully identify PIDs frequency across the cortical surface during MCAO and reperfusion. In this study, Ang-(1-7) at the dose selected did not interfere with PID number during reperfusion.

PIDs follow a biphasic pattern and are reported to occur during MCAO and between 2 to 12 hrs after reperfusion (Hartings et al., 2003). PIDs were shown to initiate no earlier than 2 hrs after reperfusion and to induce a detrimental effect that correlated with final infarct at 24 hrs (Hartings et al., 2006). In our study, PIDs occurred in 4 out of 11 animals, 1 in control and 3 in Ang-(1-7) treated rats and these took place just after reperfusion reestablishment. Our study implies that during 90 min reperfusion, the biphasic pattern of PID has not yet started as previously suggested (Hartings et al., 2006).

6.4.5 Summary

This study assessed for the first time the impact of Ang-(1-7) 5 nmol/hr IV infusion in cortical perfusion after stroke with LSCI. Ang-(1-7) therapy delivered on reperfusion did not improve perfusion within the ischaemic core, ischaemic penumbra and oligaemic/perfusion regions across the ipsilateral hemisphere. Treatment did not alter MABP, $PaCO_2$, PaO_2, pH and temperature compared to control with α-chloralose showing to be a suitable anaesthetic for CBF imaging. Moreover, Ang-(1-7) did not influence the occurrence of PIDs, which tended to occur just after reperfusion onset.

Interestingly, Ang-(1-7) prevented perfusion increase in the contralateral hemisphere compared to control animals. It could be hypothesised that these results are the outcome of $PaCO_2$ variations that were not detected at later stages of reperfusion and represent a false positive. However, if the mechanism in indeed physiological, it is an indication that Ang-(1-7) may prevent "steal phenomena" towards the contralateral hemisphere. Conversely, Ang-(1-7) did not alter cerebral haemodynamics in the ipsilateral hemisphere. It is possible that 90 min treatment at the dose selected was not sufficient to induce an effect, with literature suggesting that Ang-(1-7) induces vasodilatory effects when administered locally, at high doses, for extensive therapeutic schedules and when studied in permanent MCAO models (Jiang et al., 2014; Feterik, 2000).

In conclusion, this study provides robust evidence that Ang-(1-7) IV treatment at 5 nmol/hr dose does not influence ipsilateral cortical cerebral perfusion, PID frequency or MABP at the dose selected for 90 min reperfusion following MCAO. At the same time, Ang-(1-7) may be acting to prevent "steal phenomena" towards the contralateral hemisphere. Follow up studies need to be performed to confirm the reproducibility of the effect observed.

Chapter 7: General Discussion

Chapter 7

In this Chapter, an overall summary of study findings will be provided where study limitations will be addressed and possible future studies outlined. Firstly, the restraints and directions of preclinical neuroprotective studies in normotensive animal models will be discussed.

7.1 Animal models of ischaemic stroke

In preclinical stroke, over 1000 compounds have been reported to provide neuroprotection in animal models; however, apart from alteplase, all the interventions reaching clinical trials have failed to be effective (Henninger et al., 2010; O'Collins et al., 2006). The major translational roadblocks are attributed to experimental design as well as animal model limitations (Macleod et al., 2008; Rewell and Howells, 2017). In an attempt to minimise cofounding variables from interfering with study interpretation, we ensured that appropriate experimental design was carried out for instance the use of randomisation and blinding and acute imaging as recommended within the STAIR guidelines ((STAIR), 1999). In addition, ensuring good animal welfare during and after stroke surgery was taken into account according to the recommendations in the recently published IMPROVE (Ischaemia Models: Procedural Refinements of in Vivo Experiments) guidelines (Percie du Sert et al., 2017).

For neuroprotective studies (Chapters 4-6), sample size calculations were performed to determine adequate animal numbers to detect a therapeutic effect. Sample size calculations were not conducted in Chapter 3 since these experiments consisted of pilot studies to assess methodologies to use in subsequent neuroprotective assessments. All studies were randomised according to a random list generator (www.random.org) and an independent investigator kept the allocation schedule. Blinding was carried out for all drug studies where an independent investigator not involved in the study was responsible for preparing the appropriate drug or vehicle according to the allocation schedule. Data analysis was also conducted in a blinded manner by ensuring that experiments were coded in an unbiased manner. In Chapter 6, the author was responsible for drug infusion calculations, which had to be corrected for animal weight on day of surgery, and was not blinded to therapy. To account to this potential source of bias, treatment was disclosed and prepared at the time of reperfusion and administered by an independent investigator. In addition, blood gases were closely monitored and data analysed twice by the author and a blinded researcher.

It is important to note that experiments carried out in rodents cannot directly replicate clinical stroke. Rats have a lissencephalic brain with different neuroanatomical and functional structure to that observed in humans, which have a large gyrencephalic brain (Figure 7-1) (Sommer, 2017). White matter represents 60% of brain tissue in humans whereas in rats only 15% (Krafft et al., 2012). Since white matter damage is an important factor implicated in stroke prognosis in all major stroke subtypes; rodents experiments pose a challenge in terms of accurate modelling (Ahmad et al., 2015). Additionally, rodents have the ability to rapidly recover from ischaemic insult on the contrary to humans, limiting behavioural and neurological deficit assessments (Sommer, 2017). Nevertheless, rodents present a similar cerebrovascular anatomy to that observed in humans with both species having a circle of Willis. In addition, rodents provide a cheap, standardised and reproducible approach to study the pathophysiological mechanisms of ischaemic damage and the impact of potential therapeutic interventions (Fluri et al., 2015; McCabe et al., 2017).

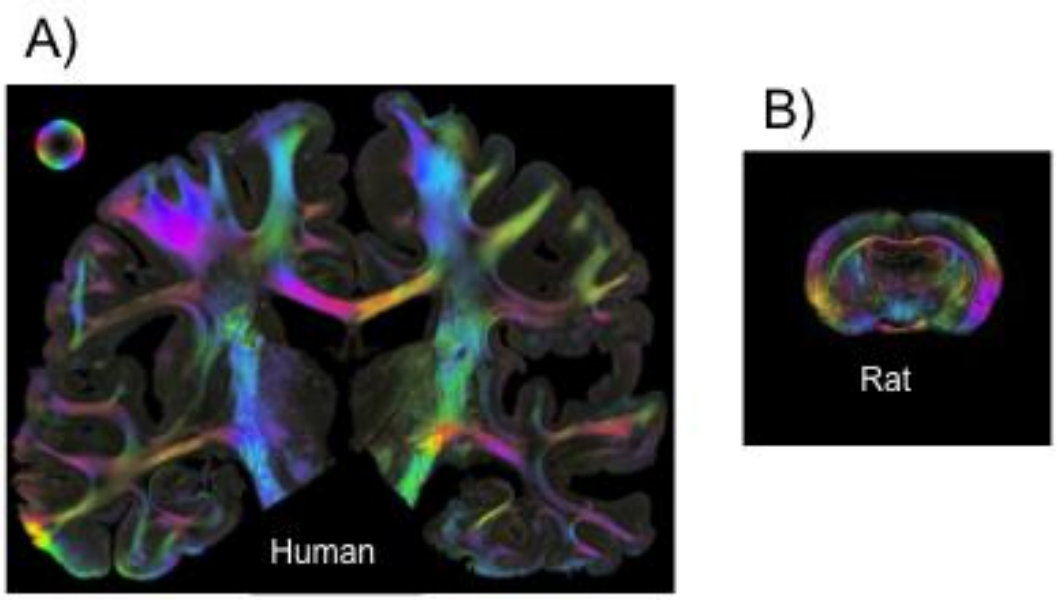

Figure 7-1 Structural and anatomical differences between human (A) and rat (B) brains. 3D-polarised light imaging illustrating connectivity, colour sphere represents the direction of fibers. Figure adapted and obtained from Sommers et al, 2017.

One important consideration in preclinical stroke is the selection of the most adequate model of focal cerebral ischaemia. In this thesis the intraluminal filament model was selected as it mimics human stroke localisation and allows to investigate the impact of reperfusion on outcome (Garcia et al., 1995; Kumar et al., 2016). In the clinic, spontaneous reperfusion occurs up to 17% of stroke patients in the first hours after stroke onset whereas the intraluminal filament model induces an abrupt reperfusion (Kassem-Moussa and Graffagnino, 2002). Although the animal model selected does not accurately represent the entire stroke population, it induces sudden and abrupt reperfusion that closely mimics mechanical thrombectomy procedures (Sutherland et al., 2016), which are primarily performed in patients with proximal large vessel occlusion of the anterior circulation and/or non-responsive to alteplase (Tawil and Muir, 2017). The validity of the model used was further confirmed in Chapter 4 where reperfusion alone improved outcome, a result equally observed in the clinic in large artery occlusion patients subjected to thrombectomy (Dargazanli et al., 2017).

The studies presented within this dissertation highlight the importance of selecting the most adequate rat strain and study methods for neuroprotective studies. A major drawback of the intraluminal filament model and the use of normotensive animals is infarct volume variability. In Chapter 3 we showed that in comparison to Wistar rats, Sprague-Dawley rats exhibited enhanced variability, thereby limiting the validity of using this strain for neuroprotective studies (Figure 3-3) (Rewell and Howells, 2017; Ström et al., 2013). STAIR guidelines recommend the use of LDF to confirm successful MCAO and suggest a minimum of 60% CBF reduction for inclusion criteria ((STAIR), 1999). In addition, several groups use LDF as a means to predict infarct volume variability or study CBF (Soriano et al. 1997; McCabe et al. 2017). We have demonstrated that LDF is a challenging method that does not correlate with final infarct volume nor adequately detect the extent of reperfusion (Figure 3-13). The use of LDF provided evidence of accidental SAH with the filament model, however; in general, the technique adds an extra variable and negatively impacts animal recovery while providing limited information. Instead, MRI techniques provided an accurate and reliable tool of outcome assessment and allowed the establishment of strict exclusion criteria. DWI during MCAO was useful to determine the starting lesion and allowed us to use each animal as its own control in order to examine the impact of therapy on infarct volume (McCabe et al., 2017). MRI-T_2 allowed us to confirm successful ICV placement of cannula and MRA confirmed adequate MCAO and MCA reperfusion.

Although a strict methodological and design criterion was employed in the studies outlined in this thesis, DWI data during MCAO emphasised the variability in ischaemic lesion volume in Wistar rats prior to therapy and reperfusion (Figure 4-4). Additionally, LSCI showed that several animals exhibited variability in the extent of cortical reperfusion following removal of the filament, which improved over time at different rates (Figure 7-3). This brings attention to the extent of MCAO and subsequent variability in reperfusion in normotensive rats and its impact on data interpretation, especially when assessing therapeutic interventions. With respect to reperfusion, it is challenging to determine which animals display inhomogeneous cortical reperfusion and the reasons for this are still poorly understood. This means that these rats are usually included in study cohorts introducing a variable that may greatly impact outcome interpretation. Contrary to normotensive animals, hypertensive rats exhibit larger infarcts and smaller collaterals with diminished vasodilator capacity, which limits infarct variability (McCabe et al. 2009; Reid et al. 2012). However, hypertensive rats present significantly less penumbral volumes that influence the chance to detect a drug effect (Rewell and Howells, 2017). For this reason, proof of principle studies are recommended to be conducted in normotensive rats prior to the addition of a co-morbidity such as hypertension ((STAIR), 1999). This thesis demonstrates that in order to accurately determine efficacy of therapeutic interventions, the use of acute imaging to confirm baseline lesion volume and confirmation of successful MCAO and/or MCA reperfusion greatly enhances the statistical power of studies and avoids type II errors. In turn, this emphasises the need for robust collaborations amongst the stroke field for improved experimental reproducibility.

7.2 Counter-regulatory axis as an ischaemic stroke target

This thesis aimed to examine the therapeutic potential of the counter regulatory axis of the RAS, ACE2/Ang-(1-7)/MasR, in ischaemic stroke. Due to the reported beneficial effects induced by MasR and AT_2R agonism following cerebral ischaemia (Chapter 1), this first therapeutic study examined the effects of MasR, AT_2R and combined MasR and AT_2R agonism in a model of transient focal cerebral ischaemia. We showed that reperfusion along with Ang-(1-7) ICV infusion further prevented lesion growth expansion at 7 days when compared to baseline lesion volume (60 min MCAO) whereas C21 (AT_2R agonist) or combination therapy did not induce any additional therapeutic effects when compared to vehicle treatment. In addition, therapy did not influence systolic BP or neurological outcome at days 3 and 7 for any group. This study establishes that at day 7 following reperfusion, MasR and AT_2R agonism do not act synergistically to prevent ischaemic

lesion growth at the doses administered; however, MasR agonism alone may confer some additional protection in combination with reperfusion.

Interestingly, the neuroprotective effect of Ang-(1-7) could only be detected when taking into account the initial baseline lesion since there were no differences between groups at day 7. This suggests that following abrupt reperfusion, central infusion of Ang-(1-7) treatment leads to a mild to moderate effect at the dose selected, in contrast to the large effect sizes observed in previous published studies at 24 hrs and 72 hrs, albeit using different models of focal cerebral ischaemia (Mecca et al., 2011; Regenhardt et al., 2013). Our experiments also confirm that the RAS is imbalanced after cerebral injury since *AT_2R* mRNA was upregulated and *MasR* downregulated at 7 days post MCAO. Interestingly, the classical RAS axis mediators *ACE* and *AT_1R* were not altered, confirming that transient MCAO enhances *AT_2R* expression only (Kagiyama et al., 2003; Zhu et al., 2000). Whilst Ang-(1-7) is reported to act at the microglial level by influencing its phenotype or diminishing NF-κB and COX-2 activity (Liu et al., 2016; Regenhardt et al., 2013); our mRNA data implies that Ang-(1-7) does not induce an anti-inflammatory effect. Instead, Ang-(1-7) could exert its effect by promoting neurogenesis through NOX1 expression.

A drawback in this study was the lack of protein assessment. Brains were collected for immunohistochemistry assessment at the end of the study, which meant that *n* numbers were low for a quantitative assessment of protein levels for microglia activation. Plus, NOX1 was not examined in terms of protein and for this reason it was not possible to conclude whether Ang-(1-7) might be inducing its effects by enhancing NOX1. It is common practice to use mRNA levels as a way to correlate with protein levels; however, relative abundance of protein may not be proportional to relative mRNA expression. In mammals, mRNAs are produced at lower rates than protein with mRNAs displaying a half-life of up to 7 hrs compared to 46 hrs for proteins (Vogel and Marcotte, 2012). To confirm the proposed mechanism, NOX1 protein levels would have to be examined and colocalised with a proliferation marker such as proliferating cell nuclear antigen, which is reported to label neuroprogenitor cells (Sierra et al., 2011).

Next, we hypothesised that MasR targeting induces its therapeutic effect in a biphasic pattern and at earlier stages of injury. Ang-(1-7) was administered as central infusion immediately following stroke for 24 hrs and its effects on BBB breakdown and infarct volume evaluated. Although vasogenic oedema was present, an indication of BBB breakdown, the BBB at this time point was at a transient state with some animals

presenting high Gd-DTPA extravasation and others minimal uptake. Not surprisingly, Ang-(1-7) did not alter hemispheric swelling or BBB breakdown. In addition, final infarct volume was comparable to vehicle animals and no differences in neurological outcome were observed at this time point. This reinforces the suggestion that Ang-(1-7) induces a mild effect that cannot be detected when analysing data at end points only. Mechanistic data performed at 24 hrs confirmed that Ang-(1-7) does not influence microglia number or activation nor affect gene expression levels for the markers assessed. However, an interesting finding was that at 24 hrs, RAS mediator gene expression was comparable to sham following MCAO, emphasising the biphasic nature of the RAS in cerebral injury and implying that the RAS may not be implicated in injury at this time point.

Overall, Chapters 4 & 5 demonstrate that Ang-(1-7) does not induce an anti-inflammatory effects, contrary to previous reports (Jiang et al., 2012; Mecca et al., 2011; Regenhardt et al., 2013). In an attempt to study the effects of Ang-(1-7) on microglia/macrophage phenotype, M1 and M2 type markers were selected and gene expression examined. The presence of multiple activation phenotypes for microglia is a relatively recent concept and there is no consensus regarding specific mediators for both M1 and M2 profiling (Ransohoff, 2016). Plus, as described above, gene expression may not provide an accurate measurement for microglia phenotype. Methods that are more accurate include flow cytometry where peri-infarct homogenates are subjected to M1/M2 marker antibody staining and protein levels quantified. Furthermore, *NF-κB* mRNA levels in the peri-infarct tissue was shown to be comparable to sham in both Chapter 4 & 5; to confirm NF-κB activation and expression as well as therapy impact, nuclear translocation assays and signalling pathway investigation at protein levels would have to be assessed.

Finally, in Chapter 6, the effects of Ang-(1-7) on CBF at a hyperacute stage of injury were assessed with LSCI. The role of Ang-(1-7) on the cerebrovasculature is controversial and until now examined with LDF, which provides a limited spatial assessment of CBF (Jiang et al., 2014; Mecca et al., 2011). We examined CBF across the entire cortical surface and demonstrated that IV infusion of Ang-(1-7) immediately following reperfusion did not influence CBF within the ipsilateral hemisphere; however, it prevented CBF enhancement in the contralateral hemisphere without influencing MABP or PIDs. This effect could be the outcome of "steal phenomena" reversal by Ang-(1-7), thus, preventing CBF shift from the ipsilateral side. There was a large variability in the results obtained, particularly in the ipsilateral hemisphere. Subsequent power calculations indicate that to detect a drug effect of at least 10% in the ischaemic penumbra and in the model used an n=11 per group would

be required. Consequently, follow up experiments should be performed to confirm study reproducibility.

One of the major limitations in the studies performed was that drugs had to be administered ICV. This method is not a recommended route of administration in the clinic as it impairs the ability to administer sustainable long-term therapies. Additionally, central treatment was technically challenging and resulted in cannula misplacement in several animals, which had to be excluded. C21 is a highly selective AT_2R agonist with a 4 hr half-life and shown to induce therapeutic effects when administered IP (Alhusban et al., 2015; Wan et al., 2004). Conversely, Ang-(1-7) has a half-life of 10 sec in the circulation and is hydrophilic (Iusuf et al., 2008; Trask and Ferrario, 2007), thus, to maximise Ang-(1-7)'s therapeutic potential, drugs were administered centrally. Furthermore, Chapter 3 studies provided an indication that RAS targeting via peripheral administration may not be suitable to perform proof of principle experiments in ischaemic stroke, hence the method selected.

It has been reported that RAS mediators do not cross the BBB, thus, the brain relies on locally produced peptides (Schelling et al., 1976). Interestingly, recent evidence now proposes that the brain RAS does not exist and the presence of RAS peptides is actually the outcome of trapped mediators from the circulation (Sigmund et al., 2017), setting the premise of new peripheral routes to target the brain RAS after stroke. A study conducted this year verified that an Ang II vaccine administered SC, reduced infarct volume after permanent MCAO (Wakayama et al., 2017), highlighting the neuroprotective potential of systemic RAS targeting. In Chapter 6, Ang-(1-7) was administered as an IV infusion to allow successful LSCI whilst maximising the activation of MasR present on cerebral endothelial cells (Becker et al., 2007; Kumar et al., 1996). The fact that Ang-(1-7) induced an effect on CBF supports the hypothesis that in future, Ang-(1-7) systemic therapy may also be adequate in ischaemic stroke. In the clinic, Ang-(1-7) was recently tested SC at 20 mg/kg/day in phase II metastatic sarcoma trials and proven to be well tolerated (Savage et al., 2016). Plus, a phase I clinical trial is being conducted testing the effects of IV Ang-(1-7) infusion of up to 20 ng/kg/min in human hypertension and expected to be completed in 2018 (clinicaltrials.gov). These scientific advances may help direct future steps in stroke studies; still, the peptide's short half-life poses a therapeutic challenge that must be taken into account. To tackle this limitation, an alternative includes novel cyclic Ang-(1-7) analogues, which are resistant to human ACE and consist in a stable, long-lasting and possibly suitable approach to use in future (Wester et al., 2017).

7.3 Future studies

Despite the efforts to elucidate the underlying mechanisms responsible for the neuroprotection observed in Chapter 4, these remain mostly elusive. Since Ang-(1-7) induced a mild to moderate neuroprotective effect in this thesis, it is crucial to perform IV dose response experiments to confirm the effect observed and test treatment feasibility in the stroke setting. Once the neuroprotective effect has been demonstrated through alternative methods of administration and at a more efficient extent, further studies should then be conducted.

In Chapter 4, we showed that Ang-(1-7) alone decreased infarct volume progression from 60 min MCAO to 7 days reperfusion. However, C21 and combination therapy did not exert a neuroprotective effect, suggesting that both MasR and AT_2R agonism does not synergistically decrease infarct volume. To understand the implications of receptor antagonism in infarct volume outcome in the model used, MasR antagonist, A779, and AT_2R antagonist, PD123319, cohorts should be studied in future. In addition, to examine whether Ang-(1-7)-mediated neuroprotection is dependent on both MasR and AT_2R activation in the model used, receptor antagonists should be administered along with Ang-(1-7) in subsequent experiments.

The experiments in Chapter 6 propose that Ang-(1-7) IV administration influences CBF profile to some extent, therefore, it could hypothetically preserve the penumbra. An important study to be conducted is the effect of Ang-(1-7) on the extent of penumbra salvage using DWI/PWI mismatch. In the clinic, penumbra determination with DWI/PWI mismatch has proven to be effective in determining patients who most likely benefit from alteplase and thrombectomy procedures (Albers et al., 2006; Wheeler et al., 2013), therefore, it is likely that in future, DWI/PWI mismatch will become part of standard eligibility criteria. Consequently, mismatch studies are crucial to evaluate the efficacy of a neuroprotective agent and its translation from preclinical to clinical studies (Fisher et al., 2009).

The results in this thesis emphasise that the effects of Ang-(1-7) may be time dependent and of various aetiologies. A logical study to perform would be the effect of Ang-(1-7) on BBB breakdown at 72 hrs post stroke when the BBB is maximally permeable and inflammatory mechanisms at its hiatus (Sandoval and Witt, 2008). In addition, Ang-(1-7) is thought to prevent lesion growth in permanent MCAO by stimulating angiogenesis via

the eNOS/NO and VEGF pathways (Jiang et al., 2014), thus, its role in angiogenesis at later stages of injury could be assessed in transient models. Interestingly, central treatment with C21 failed to induce a neuroprotective effect, yet, this compound is implicated in neuroprotection following ischaemic stroke when administered IP (Alhusban et al., 2015; Joseph et al., 2014; Lee et al., 2012; Schwengel et al., 2016). Our mRNA data implies that the AT_2R may be involved in injury at 7 days post reperfusion; therefore, AT_2R targeting may be potentially beneficial at later stages of injury. Accordingly, in permanent MCAO studies, C21 induces an angiogenic effect following 21 days therapy whereas in transient MCAO, 3 week C21 treatment diminishes infarct volume (Bennion et al., 2017; Mateos et al., 2016), supporting this hypothesis. By performing time course experiments, one would be able to evaluate at what time points MasR and/or AT_2R targeting following stroke could be most beneficial.

In vivo experiments should be supported with *in vitro* examinations. As mentioned in Chapter 1, AT_1R signalling is detrimental through a variety of processes involving the activation of G-protein dependent and independent pathways. While these signalling pathways are well described in peripheral CVD, there is limited information in neuronal cells. Similarly, the signalling pathways underlying AT_2R or MasR activation are scarcely known in ischaemic stroke. Previous studies conducted by our lab have demonstrated that in smooth muscle cells, MasR inhibits ERK1/2 (McKinney et al., 2015); however, it is yet to be established whether in neuronal cells, MasR leads to SHP-2 activation and effectively inhibits MAPKs or NOX as outlined in Chapter 1. Equally, whether AT_2R agonism leads to MPK-1, SHP-1 and PP2A activation should be assessed. To do so, primary neuronal cells would be subjected to OGD challenge and treatment upon reoxygenation. After, signalling pathways would be assessed in cell lysates using protein arrays such as PathScan Antibody Array from Cell Signalling Technology, which allows a simultaneously and quantitative measurement of at least 30 phosphorylated proteins (Kopf et al., 2005).

Finally, the use of normotensive young male animals is relevant in the context of proof of principle studies; however, these do not reflect the stroke population in clinic, which often exhibit a spectrum of co-morbidities (Fisher et al., 2009). The author of this thesis (MA) collaborated in a follow up study where Ang-(1-7) and A779 (MasR antagonist) were tested in the same experimental protocol in SHRSPs (unpublished data). Ang-(1-7) failed to induce a neuroprotective effect; however, MasR antagonism exacerbated injury. This further emphasises that Ang-(1-7) at the dose administered may not be optimal whilst stressing the therapeutic potential of specific MasR agonists in both normotensive and

hypertensive settings. Nonetheless, the effects of Ang-(1-7) in females, diabetic and older rats are yet to be studied. In particular, sex is thought to highly influence RAS expression. Testosterone is suggested to stimulate the “classical axis” whilst oestrogen promotes AT_2R expression and counter-regulatory RAS axis activity (Sullivan 2008; Silva-Antonialli et al. 2004; Sampson et al. 2008; Sullivan et al. 2015). Plus, female rats subjected to ovariectomy display enhanced AT_1R brain expression and diminished AT_2R levels, hence, a possible involvement in the elderly population (Rodriguez-Perez et al., 2010). The therapeutic potential of the counter-regulatory RAS axis should be evaluated in these settings before proceeding to larger animals.

7.4 Conclusions

This thesis conducted novel studies examining the therapeutic potential of the counter-regulatory axis of the RAS following transient MCAO using acute imaging techniques. We demonstrated that the RAS is implicated in cerebral injury in a biphasic pattern with MasR agonism as a post stroke therapy inducing a mild to moderate neuroprotective effect at 7 days reperfusion. Our studies indicate that Ang-(1-7) did not exert its effect via an anti-inflammatory mechanism nor prevented BBB breakdown at 24 hrs reperfusion. Instead, we hypothesise that Ang-(1-7) may exert its effects by enhancing neurogenesis through NOX1 enhancement and/or CBF modulation after stroke onset. Although this thesis provides encouraging findings, the underlying mechanism is still elusive and further investigations should be conducted. In particular, the therapeutic potential of selective MasR agonists as adjuvant systemic therapies should be assessed. This thesis strongly emphasises the importance of adequate methodologies when performing neuroprotective studies, which should be closely considered in future experiments.

List of References

(STAIR), S.T.A.I.R., 1999. Recommendations for standards regarding preclinical neuroprotective and restorative drug development. In *Stroke*. pp. 2752–2758.

Abadir, P.M. et al., 2006. Angiotensin II Type 2 Receptor-Bradykinin B2 Receptor Functional Heterodimerization. *Hypertension*, 48(2), pp.316–322.

Adams, H. & Biller, J., 2015. Classification of Subtypes of Ischemic Stroke. *Stroke*, 46(5), pp.e114–e117.

Adamson, J., Beswick, A. & Ebrahim, S., 2004. Is stroke the most common cause of disability? *Journal of Stroke and Cerebrovascular Diseases*, 13(4), pp.171–177.

Ahmad, A. et al., 2015. Considerations for the Optimization of Induced White Matter Injury Preclinical Models. *Frontiers in Neurology*, 6, p.172.

Ahnstedt, H. et al., 2016. Effects of Early Post-Ischemic Reperfusion and tPA on Cerebrovascular Function and Nitrosative Stress in Female Rats. *Translational Stroke Research*, 7(3), pp.228–238.

Albers, G.W. et al., 2006. Magnetic resonance imaging profiles predict clinical response to early reperfusion: The diffusion and perfusion imaging evaluation for understanding stroke evolution (DEFUSE) study. *Annals of Neurology*, 60(5), pp.508–517.

Albrecht, D., 2007. Angiotensin-(1-7)-induced plasticity changes in the lateral amygdala are mediated by COX-2 and NO. *Learning & Memory*, 14(3), pp.177–184.

Alexandrov, A. V et al., 2007. Reversed Robin Hood Syndrome in Acute Ischemic Stroke Patients Subjects and Methods. *Stroke*, 38(11), pp.3045–8.

Alhusban, A. et al., 2013. AT1 receptor antagonism is proangiogenic in the brain: BDNF a novel mediator. *The Journal of Pharmacology and Experimental Therapeutics*, 344(2), pp.348–59.

Alhusban, A. et al., 2015. Compound 21 is pro-angiogenic in the brain and results in sustained recovery after ischemic stroke. *Journal of Hypertension*, 33(1), pp.170–180.

Allen, A.M. et al., 1999. Angiotensin II receptors in the human brain. *Regulatory peptides*, 79(1), pp.1–7.

Allen, A.M. et al., 1998. Angiotensin receptors in the nervous system. *Brain research bulletin*, 47(1), pp.17–28.

Ames, A. et al., 1968. Cerebral ischemia. II. The no-reflow phenomenon. *The American journal of pathology*, 52(2), pp.437–53.

An, H. et al., 2015. Defining the Ischemic Penumbra Using Magnetic Resonance Oxygen Metabolic Index. *Stroke*, 46(4).

Anderson, R.E. & Meyer, F.B., 2002. Protection of focal cerebral ischemia by alkalinization of systemic pH. *Neurosurgery*, 51(5), pp.1256-65–6.

Ankarcrona, M. et al., 1995. Glutamate-induced neuronal death: A succession of necrosis or apoptosis depending on mitochondrial function. *Neuron*, 15(4), pp.961–973.

Ansari, S. et al., 2011. Intraluminal Middle Cerebral Artery Occlusion (MCAO) Model for Ischemic Stroke with Laser Doppler Flowmetry Guidance in Mice. *Journal of Visualized Experiments*, (51), p.2879.

Appelros, P., Stegmayr, B. & Terént, A., 2009. Sex differences in stroke epidemiology: a systematic review. *Stroke*, 40(4), pp.1082–90.

Arboix, A., 2015. Cardiovascular risk factors for acute stroke: Risk profiles in the different subtypes of ischemic stroke. *World journal of clinical cases*, 3(5), pp.418–29.

Arboix, A. et al., 2005. Clinical study of 39 patients with atypical lacunar syndrome. *Journal of Neurology, Neurosurgery & Psychiatry*, 77(3), pp.381–384.

Arboix, A. & Martí-Vilalta, J.L., 2009. Lacunar stroke. *Expert Review of Neurotherapeutics*, 9(2), pp.179–196.

Arima, S. et al., 1997. Possible role of P-450 metabolite of arachidonic acid in vasodilator mechanism of angiotensin II type 2 receptor in the isolated microperfused rabbit afferent arteriole. *The Journal of clinical investigation*, 100(11), pp.2816–23.

Armitage, G.A. et al., 2010. Laser Speckle Contrast Imaging of Collateral Blood Flow during Acute Ischemic Stroke. *Journal of Cerebral Blood Flow & Metabolism*, 30(8), pp.1432–1436.

Arroja, M.M.C., Reid, E. & McCabe, C., 2016. Therapeutic potential of the renin angiotensin system in ischaemic stroke. *Experimental & translational stroke medicine*, 8, p.8.

Arya, M. et al., 2005. Basic principles of real-time quantitative PCR. *Expert Rev. Mol. Diagn*, 5(2), pp.209–19.

Aspey, B.S. et al., 2000. Temporary middle cerebral artery occlusion in the rat: consistent protocol for a model of stroke and reperfusion. *Neuropathology and applied neurobiology*, 26(3), pp.232–42.

Astrup, J. et al., 1977. Cortical Evoked Potential and Extracellular K + and H + at Critical Levels of Brain Ischemia. *Stroke*, 8(1), pp.51–57.

Astrup, J., 1982. Energy-requiring cell functions in the ischemic brain Their critical supply and possible inhibition in protective therapy. *J Neurosurg*, 56(56), pp.482–497.

Astrup, J., Siesjö, B.K. & Symon, L., 1981. Thresholds in cerebral ischemia - the ischemic penumbra. *Stroke*, 12(6), pp.723–5.

Attwell, D. et al., 2010. Glial and neuronal control of brain blood flow. *Nature*, 468(7321), pp.232–243.

Ayata, C. & Lauritzen, M., 2015. ESpreading Depression, Spreading Depolarizations, and the Cerebral Vasculature. *Physiological reviews*, 95(3), pp.953–993.

Back, T. et al., 1996. Induction of Spreading Depression in the Ischemic Hemisphere following Experimental Middle Cerebral Artery Occlusion: Effect on Infarct Morphology. *Journal of Cerebral Blood Flow & Metabolism*, 16(2), pp.202–213.

Baird, A.E. & Warach, S., 1998. Magnetic Resonance Imaging of Acute Stroke. *Journal of Cerebral Blood Flow & Metabolism*, 18(6), pp.583–609.

Bang, O.Y. et al., 2007. Impact of collateral flow on tissue fate in acute ischaemic stroke. *Journal of Neurology, Neurosurgery & Psychiatry*, 79(6), pp.625–629.

Baron, J.C. et al., 2008. Noninvasive Tomographic Study of Cerebral Blood Flow and Oxygen Metabolism in vivo. *European Neurology*, 20(3), pp.273–284.

Baskerville, T.A. et al., 2016. The influence of gender on “tissue at risk” in acute stroke: A diffusion-weighted magnetic resonance imaging study in a rat model of focal cerebral ischaemia. *Journal of Cerebral Blood Flow & Metabolism*, 36(2), pp.381–386.

Bates, D.O. et al., 2002. Regulation of microvascular permeability by vascular endothelial growth factors. *Journal of anatomy*, 200(6), pp.581–97.

Becker, L.K. et al., 2007. Immunofluorescence localization of the receptor Mas in cardiovascular-related areas of the rat brain. *AJP: Heart and Circulatory Physiology*, 293(3), pp.H1416–H1424.

Belayev, L. et al., 1996. Quantitative evaluation of blood-brain barrier permeability following middle cerebral artery occlusion in rats. *Brain Research*, 739(1–2), pp.88–96.

Benakis, C. et al., 2015. The role of microglia and myeloid immune cells in acute cerebral ischemia. *Frontiers in Cellular Neuroscience*, 8. Available at: http://journal.frontiersin.org/article/10.3389/fncel.2014.00461/abstract.

Bencze, M., Behuliak, M. & Zicha, J., 2013. The impact of four different classes of anesthetics on the mechanisms of blood pressure regulation in normotensive and spontaneously hypertensive rats. *Physiological research*, 62(5), pp.471–8.

Bennion, D.M. et al., 2015. Activation of the Neuroprotective Angiotensin-Converting Enzyme 2 in Rat Ischemic Stroke. *Hypertension (Dallas, Tex. : 1979)*, 66(1), pp.141–8.

Bennion, D.M. et al., 2017. Post-stroke angiotensin II type 2 receptor activation provides long-term neuroprotection in aged rats. *PLOS ONE*, 12(7), p.e0180738.

Berkhemer, O.A. et al., 2015. A Randomized Trial of Intraarterial Treatment for Acute Ischemic Stroke. *New England Journal of Medicine*, 372(1), pp.11–20.

Bhaskar, S. et al., 2017. Baseline collateral status and infarct topography in post-ischaemic perilesional hyperperfusion: An arterial spin labelling study. *Journal of Cerebral Blood Flow & Metabolism*, 37(3), pp.1148–1162.

Bhatia, R. et al., 2010. Low Rates of Acute Recanalization With Intravenous Recombinant Tissue Plasminogen Activator in Ischemic Stroke. *Stroke*, 41(10).

Biernaskie, J. et al., 2001. A serial MR study of cerebral blood flow changes and lesion development following endothelin-1-induced ischemia in rats. *Magnetic resonance in medicine*, 46(4), pp.827–30.

Bihl, J.C. et al., 2015. Angiotensin-(1–7) counteracts the effects of Ang II on vascular smooth muscle cells, vascular remodeling and hemorrhagic stroke: Role of the NFκB inflammatory pathway. *Vascular Pharmacology*, 73, pp.115–123.

Bogousslavsky, J., Van Melle, G. & Regli, F., 1988. The Lausanne Stroke Registry: analysis of 1,000 consecutive patients with first stroke. *Stroke*, 19(9), pp.1083–92.

Boisvert, D.P., Handa, Y. & Allen, P.S., 1990. Proton relaxation in acute and subacute ischemic brain edema. *Advances in neurology*, 52, pp.407–13.

Bosnyak, S. et al., 2011. Relative affinity of angiotensin peptides and novel ligands at AT 1 and AT 2 receptors. *Clinical Science*, 121(7), pp.297–303.

Botelho-Santos, G.A. et al., 2012. Altered regional blood flow distribution in Mas-deficient mice. *Therapeutic Advances in Cardiovascular Disease*, 6(5), pp.201–211.

Branston, N.M. et al., 1974. Relationship between the cortical evoked potential and local cortical blood flow following acute middle cerebral artery occlusion in the baboon. *Experimental neurology*, 45(2), pp.195–208.

Braun-Menendez, E. et al., 1940. The substance causing renal hypertension. *J. Physiol.*, 98(3), pp.283–298.

Brosnihan, K.B., Li, P. & Ferrario, C.M., 1996. Angiotensin-(1-7) dilates canine coronary arteries through kinins and nitric oxide. *Hypertension (Dallas, Tex. : 1979)*, 27(3 Pt 2), pp.523–8.

Brouns, R. & De Deyn, P., 2009. The complexity of neurobiological processes in acute ischemic stroke. *Clinical Neurology and Neurosurgery*, 111(6), pp.483–495.

Browning, J.L. et al., 1997. Effects of halothane, alpha-chloralose, and pCO2 on injury volume and CSF beta-endorphin levels in focal cerebral ischemia. *Molecular and chemical neuropathology*, 31(1), pp.29–42.

Burrows, F.E. et al., 2015. Delayed reperfusion deficits after experimental stroke

account for increased pathophysiology. *Journal of cerebral blood flow and metabolism : official journal of the International Society of Cerebral Blood Flow and Metabolism*, 35(2), pp.277–84.

Button, K.S. et al., 2013. Power failure: why small sample size undermines the reliability of neuroscience. *Nature Reviews Neuroscience*, 14(5), pp.365–376.

Campagne, M. van L. et al., 1999. Secondary Reduction in the Apparent Diffusion Coefficient of Water, Increase in Cerebral Blood Volume, and Delayed Neuronal Death after Middle Cerebral Artery Occlusion and Early Reperfusion in the Rat. *Journal of Cerebral Blood Flow & Metabolism*, 19(12), pp.1354–1364.

Campagnole-Santos, M.J. et al., 1989. Cardiovascular effects of angiotensin-(1-7) injected into the dorsal medulla of rats. *The American journal of physiology*, 257(1 Pt 2), pp.H324-9.

Campbell, B.C.V. et al., 2015. Endovascular Therapy for Ischemic Stroke with Perfusion-Imaging Selection. *New England Journal of Medicine*, 372(11), pp.1009–1018.

Capdevila, S. et al., 2007. Acclimatization of rats after ground transportation to a new animal facility. *Laboratory Animals*, 41(2), pp.255–261.

Chalmers, J. et al., 2003. International Society of Hypertension (ISH): statement on blood pressure lowering and stroke prevention. *Journal of hypertension*, 21(4), pp.651–63.

Chang, A.Y.W. et al., 2014. Interplay between brain stem angiotensins and monocyte chemoattractant protein-1 as a novel mechanism for pressor response after ischemic stroke. *Neurobiology of Disease*, 71, pp.292–304.

Chapouly, C. et al., 2015. Astrocytic TYMP and VEGFA drive blood–brain barrier opening in inflammatory central nervous system lesions. *Brain*, 138(6), pp.1548–1567.

Chappell, M.C. et al., 1987. Characterization by high performance liquid chromatography of angiotensin peptides in the plasma and cerebrospinal fluid of the dog. *Peptides*, 8(5), pp.939–42.

Chappell, M.C. et al., 1989. Identification of angiotensin-(1-7) in rat brain. Evidence for differential processing of angiotensin peptides. *The Journal of biological chemistry*, 264(28), pp.16518–23.

Chappell, M.C. et al., 1998. Metabolism of angiotensin-(1-7) by angiotensin-converting enzyme. *Hypertension*, 31(1 Pt 2), pp.362–7.

Chen, H. et al., 2011. NADPH oxidase is involved in post-ischemic brain inflammation. *Neurobiology of Disease*, 42(3), pp.341–348.

Chen, H., Song, Y.S. & Chan, P.H., 2009. Inhibition of NADPH Oxidase is Neuroprotective after Ischemia—Reperfusion. *Journal of Cerebral Blood Flow & Metabolism*, 29(7), pp.1262–1272.

Chen, J. et al., 2014. Neuronal over-expression of ACE2 protects brain from ischemia-induced damage. *Neuropharmacology*, 79, pp.550–558.

Chen, P.-H. et al., 2012. Classifying Ischemic Stroke, from TOAST to CISS. *CNS Neuroscience & Therapeutics*, 18(6), pp.452–456.

Cheret, C. et al., 2008. Neurotoxic Activation of Microglia Is Promoted by a Nox1-Dependent NADPH Oxidase. *Journal of Neuroscience*, 28(46), pp.12039–12051.

Cherry, J.D., Olschowka, J.A. & O'Banion, M.K., 2014. Neuroinflammation and M2 microglia: the good, the bad, and the inflamed. *Journal of neuroinflammation*, 11, p.98.

Choi, D.-H. et al., 2015. Role of Neuronal NADPH Oxidase 1 in the Peri-Infarct Regions after Stroke. *PloS one*, 10(1), p.e0116814.

Chu, H.X. et al., 2014. Role of CCR2 in Inflammatory Conditions of the Central

Nervous System. *Journal of Cerebral Blood Flow & Metabolism*, 34(9), pp.1425–1429.

Cipolla, M.J. et al., 2014. Postischemic Reperfusion Causes Smooth Muscle Calcium Sensitization and Vasoconstriction of Parenchymal Arterioles. *Stroke*, 45(8), pp.2425–2430.

Cipolla, M.J. et al., 1997. Reperfusion decreases myogenic reactivity and alters middle cerebral artery function after focal cerebral ischemia in rats. *Stroke*, 28(1), pp.176–80.

Clark, M.A., Tallant, E.A. & Diz, D.I., 2001. Downregulation of the AT1A receptor by pharmacologic concentrations of Angiotensin-(1-7). *Journal of cardiovascular pharmacology*, 37(4), pp.437–48.

Connelly, J.J. et al., 2015. Markers for blood-brain barrier integrity: how appropriate is Evans blue in the twenty-first century and what are the alternatives? *Frontiers in neuroscience*, 9, p.385.

Corraini, P. et al., 2017. Long-Term Risk of Dementia Among Survivors of Ischemic or Hemorrhagic Stroke. *Stroke*, 48(1), pp.180–186.

Corrigan, M.L., Escuro, A.A. & Kirby, D., 2013. *Handbook of clinical nutrition and stroke*, Humana Press.

Corvol, P. et al., 1995. Recent advances in knowledge of the structure and function of the angiotensin I converting enzyme. *Journal of hypertension. Supplement : official journal of the International Society of Hypertension*, 13(3), pp.S3-10.

Cotrina, M.L. et al., 2017. Direct comparison of microglial dynamics and inflammatory profile in photothrombotic and arterial occlusion evoked stroke. *Neuroscience*, 343, pp.483–494.

Crack, P.J. & Taylor, J.M., 2005. Reactive oxygen species and the modulation of stroke. *Free Radical Biology and Medicine*, 38(11), pp.1433–1444.

Cuccione, E. et al., 2016. Cerebral collateral circulation in experimental ischemic stroke. *Experimental & translational stroke medicine*, 8, p.2.

Culman, J. et al., 2002. The renin-angiotensin system in the brain: possible therapeutic implications for AT(1)-receptor blockers. *Journal of human hypertension*, 16 Suppl 3(September 2002), pp.S64–S70.

Dahlöf, B. et al., 2002. Cardiovascular morbidity and mortality in the Losartan Intervention For Endpoint reduction in hypertension study (LIFE): a randomised trial against atenolol. *The Lancet*, 359(9311), pp.995–1003.

Dai, W.J. et al., 1999. Blockade of central angiotensin AT(1) receptors improves neurological outcome and reduces expression of AP-1 transcription factors after focal brain ischemia in rats. *Stroke; a journal of cerebral circulation*.

Dargazanli, C. et al., 2017. Is Reperfusion Useful in Ischaemic Stroke Patients Presenting with a Low National Institutes of Health Stroke Scale and a Proximal Large Vessel Occlusion of the Anterior Circulation? *Cerebrovascular Diseases*, 43(5–6), pp.305–312.

Davis, S.M. et al., 2008. Effects of alteplase beyond 3 h after stroke in the Echoplanar Imaging Thrombolytic Evaluation Trial (EPITHET): a placebo-controlled randomised trial. *The Lancet Neurology*, 7(4), pp.299–309.

Deb, P. et al., 2010. Pathophysiologic mechanisms of acute ischemic stroke: An overview with emphasis on therapeutic significance beyond thrombolysis. *Pathophysiology : the official journal of the International Society for Pathophysiology*, 17(3), pp.197–218.

Denes, A. et al., 2007. Proliferating Resident Microglia after Focal Cerebral Ischaemia in Mice. *Journal of Cerebral Blood Flow & Metabolism*, 27(12), pp.1941–1953.

Derdeyn, C.P., 2007. Mechanisms of Ischemic Stroke Secondary to Large Artery

Atherosclerotic Disease. *Neuroimaging Clinics of North America*, 17(3), pp.303–311.

Deschepper, C.F., 1994. Angiotensinogen: hormonal regulation and relative importance in the generation of angiotensin II. *Kidney international*, 46(6), pp.1561–3.

Deschepper, C.F., Bouhnik, J. & Ganong, W.F., 1986. Colocalization of angiotensinogen and glial fibrillary acidic protein in astrocytes in rat brain. *Brain research*, 374(1), pp.195–8.

Diehl, K.H. et al., 2001. A good practice guide to the administration of substances and removal of blood, including routes and volumes. *Journal of applied toxicology : JAT*, 21(1), pp.15–23.

Dimitrijevic, O.B. et al., 2007. Absence of the Chemokine Receptor CCR2 Protects Against Cerebral Ischemia/Reperfusion Injury in Mice. *Stroke*, 38(4), pp.1345–53.

Dimitrijevic, O.B. et al., 2006. Effects of the Chemokine CCL2 on Blood–Brain Barrier Permeability during Ischemia–Reperfusion Injury. *Journal of Cerebral Blood Flow & Metabolism*, 26(6), pp.797–810.

Dirnagl, U. et al., 1989. Continuous Measurement of Cerebral Cortical Blood Flow by Laser-Doppler Flowmetry in a Rat Stroke Model. *Journal Cerebral Blood Flow Metabolism*, 9(5), pp.589–96.

Dirnagl, U., Iadecola, C. & Moskowitz, M.A., 1999. Pathobiology of ischaemic stroke: an integrated view. *Trends in Neurosciences*, 22(9), pp.391–397.

Dirnagl, U. & Pulsinelli, W., 1990. Autoregulation of Cerebral Blood Flow in Experimental Focal Brain Ischemia. *Journal of Cerebral Blood Flow & Metabolism*, 10(3), pp.327–336.

Dohgu, S. et al., 2004. Transforming growth factor-beta1 upregulates the tight junction and P-glycoprotein of brain microvascular endothelial cells. *Cellular and molecular neurobiology*, 24(3), pp.491–7.

Dohmen, C. et al., 2007. Cortical spreading depression and peri-infarct depolarisation in human ischemic stroke. *Journal of Cerebral Blood Flow and Metabolism*, 27(SUPPL. 1), p.BO04-03.

Donoghue, M. et al., 2000. A novel angiotensin-converting enzyme-related carboxypeptidase (ACE2) converts angiotensin I to angiotensin 1-9. *Circulation research*, 87(5), pp.E1-9.

Doobay, M.F. et al., 2007. Differential expression of neuronal ACE2 in transgenic mice with overexpression of the brain renin-angiotensin system. *American journal of physiology. Regulatory, integrative and comparative physiology*, 292(1), pp.R373-81.

Dunn, A.K. et al., 2001. Dynamic Imaging of Cerebral Blood Flow Using Laser Speckle. *Journal of Cerebral Blood Flow & Metabolism*, 21(3), pp.195–201.

Dunn, A.K., 2012. Laser Speckle Contrast Imaging of Cerebral Blood Flow. *Annals of Biomedical Engineering*, 40(2), pp.367–377.

Dupont, S. et al., 2010. Aneurysmal Subarachnoid Hemorrhage: An Overview for the Practicing Neurologist. *Seminars in Neurology*, 30(5), pp.545–554.

Durafourt, B.A. et al., 2012. Comparison of polarization properties of human adult microglia and blood-derived macrophages. *Glia*, 60(5), pp.717–727.

Durand, M.J. et al., 2010. Angiotensin-(1-7) and low-dose angiotensin II infusion reverse salt-induced endothelial dysfunction via different mechanisms in rat middle cerebral arteries. *American journal of physiology. Heart and circulatory physiology*, 299, pp.H1024–H1033.

Dzau, V.J. et al., 1986. Identification of renin and angiotensinogen messenger RNA sequences in mouse and rat brains. *Hypertension (Dallas, Tex. : 1979)*, 8(6), pp.544–8.

Dzau, V.J., 2001. Theodore Cooper Lecture: Tissue angiotensin and pathobiology of vascular disease: a unifying hypothesis. *Hypertension*, 37(4), pp.1047–52.

Ehrlich, M.P. et al., 2002. Effect of hypothermia on cerebral blood flow and metabolism in the pig. *The Annals of thoracic surgery*, 73(1), pp.191–7.

Ellenbogen, R.G., Abdulrauf, S.I. & Sekhar, L.N., 2012. *Principles of neurological surgery* R. G. Ellenbogen, ed., Saunders/Elsevier.

Elliott, J. & Smith, M., 2010. The Acute Management of Intracerebral Hemorrhage. *Anesthesia & Analgesia*, 110(5), pp.1419–1427.

Emberson, J. et al., 2014. Effect of treatment delay, age, and stroke severity on the effects of intravenous thrombolysis with alteplase for acute ischaemic stroke: a meta-analysis of individual patient data from randomised trials. *The Lancet*, 384(9958), pp.1929–1935.

Engelhorn, T. et al., 2004. The Angiotensin II Type 1 – Receptor Blocker Candesartan Increases Cerebral Blood Flow , Reduces Infarct Size , and Improves Neurologic Outcome After Transient Cerebral Ischemia in Rats. , pp.467–474.

Engelter, S.T. et al., 2006. Epidemiology of Aphasia Attributable to First Ischemic Stroke: Incidence, Severity, Fluency, Etiology, and Thrombolysis. *Stroke*, 37(6), pp.1379–1384.

Evans, A.L. et al., 1994. Improved system for measuring systolic blood pressure in the conscious rat. *Medical & biological engineering & computing*, 32(1), pp.101–2.

Fabricius, M. et al., 2006. Cortical spreading depression and peri-infarct depolarization in acutely injured human cerebral cortex. *Brain*, 129(3), pp.778–790.

Fagan, S.C. et al., 2006. Hypertension after experimental cerebral ischemia: candesartan provides neurovascular protection. *Journal of hypertension*, 24(3), pp.535–9.

Faure, S. et al., 2008. Protective effect of candesartan in experimental ischemic stroke in the rat mediated by AT2 and AT4 receptors. *Journal of hypertension*, 26(10), pp.2008–2015.

Feigin, V.L. et al., 2014. Global and regional burden of stroke during 1990-2010: findings from the Global Burden of Disease Study 2010. *The Lancet*, 383(9913), pp.245–54.

Ferro, J.M., Massaro, A.R. & Mas, J.-L., 2010. Aetiological diagnosis of ischaemic stroke in young adults. *The Lancet Neurology*, 9(11), pp.1085–1096.

Feterik, K., Smith, L. & Katusic, Z.S., 2000. Angiotensin-(1-7) causes endothelium-dependent relaxation in canine middle cerebral artery. *Brain Research*, 873(1), pp.75–82.

Fiehler, J. et al., 2005. Reperfusion after severe local perfusion deficit precedes hemorrhagic transformation: an MRI study in acute stroke patients. *Cerebrovascular diseases (Basel, Switzerland)*, 19(2), pp.117–24.

Fisher, M. et al., 2009. Update of the Stroke Therapy Academic Industry Roundtable Preclinical Recommendations. *Stroke*, 40(6), pp.2244–2250.

Fitzner Toft, M. et al., 2006. The impact of different blood sampling methods on laboratory rats under different types of anaesthesia. *Laboratory Animals*, 40(3), pp.261–74.

Fluri, F., Schuhmann, M.K. & Kleinschnitz, C., 2015. Animal models of ischemic stroke and their application in clinical research. *Drug design, development and therapy*, 9, pp.3445–54.

da Fonseca, A.C.C. et al., 2014. The impact of microglial activation on blood-brain barrier in brain diseases. *Frontiers in cellular neuroscience*, 8, p.362.

Ford, A.L. et al., 2012. Defining the ischemic penumbra using hyperacute

neuroimaging: deriving quantitative ischemic thresholds. *Translational stroke research*, 3(2), pp.198–204.

Fox, G. et al., 1993. Anatomic variation of the middle cerebral artery in the Sprague-Dawley rat. *Stroke*, 24(12), pp.2087-92–3.

Franceschini, M.A. et al., 2010. The effect of different anesthetics on neurovascular coupling. *NeuroImage*, 51(4), pp.1367–1377.

Fredriksson, I., Fors, C. & Johansson, J., 2007. Laser Doppler Flowmetry -a Theoretical Framework. *Department of Biomedical Engineering, Linköping University*, www.imt.li. Available at: www.imt.liu.se/bit/ldf/ldfmain.html.

Fujimoto, M. et al., 2008. Tissue Inhibitor of Metalloproteinases Protect Blood—Brain Barrier Disruption in Focal Cerebral Ischemia. *Journal of Cerebral Blood Flow & Metabolism*, 28(10), pp.1674–1685.

Furukawa, K. et al., 1997. The actin-severing protein gelsolin modulates calcium channel and NMDA receptor activities and vulnerability to excitotoxicity in hippocampal neurons. *The Journal of neuroscience*, 17(21), pp.8178–86.

Fuxe, K. et al., 1997. Endothelin-1 induced lesions of the frontoparietal cortex of the rat. A possible model of focal cortical ischemia. *Neuroreport*, 8(11), pp.2623–9.

Fuzik, J. et al., 2013. Fundamental interstrain differences in cortical activity between Wistar and Sprague–Dawley rats during global ischemia. *Neuroscience*, 228, pp.371–381.

Gallagher, P.E. et al., 2006. Distinct roles for ANG II and ANG- (1 – 7) in the regulation of angiotensin-converting enzyme 2 in rat astrocytes. *Am J Physiol Cell Physiol*, 1032, pp.420–426.

Ganten, D. et al., 1971. Renin in dog brain. *The American journal of physiology*, 221(6), pp.1733–7.

García-Berrocoso, T. et al., 2014. Chemokines after human ischemic stroke: From neurovascular unit to blood using protein arrays. *Translational Proteomics*, 3, pp.1–9.

Garcia, J. et al., 2013. Comparison of infarct volume and behavioral deficit in Wistar Kyoto and spontaneously hypertensive rat after transient occlusion of the middle cerebral artery. *Springerplus*, 2, p.414.

Garcia, J.H., Wagner, S., et al., 1995. Neurological deficit and extent of neuronal necrosis attributable to middle cerebral artery occlusion in rats. Statistical validation. *Stroke*, 26(4), p.627–34; discussion 635.

Garcia, J.H., Liu, K.F. & Ho, K.L., 1995. Neuronal necrosis after middle cerebral artery occlusion in Wistar rats progresses at different time intervals in the caudoputamen and the cortex. *Stroke*, 26(4), p.636–42; discussion 643.

Garrido-Gil, P. et al., 2013. Expression of angiotensinogen and receptors for angiotensin and prorenin in the monkey and human substantia nigra: An intracellular renin-angiotensin system in the nigra. *Brain Structure and Function*, 218(2), pp.373–388.

Garrido, A.M. & Griendling, K.K., 2009. NADPH oxidases and angiotensin II receptor signaling. *Molecular and cellular endocrinology*, 302(2), pp.148–58.

Gelderblom, M. et al., 2012. Neutralization of the IL-17 axis diminishes neutrophil invasion and protects from ischemic stroke. *Blood*, 120(18), pp.3793–3802.

Gembardt, F. et al., 2012. Hemodynamic effects of vasorelaxant compounds in mice lacking one, two or all three angiotensin II receptors. *Hypertension Research*, 35(5), pp.547–551.

George, P.M. & Steinberg, G.K., 2015. Novel Stroke Therapeutics: Unraveling Stroke Pathophysiology and Its Impact on Clinical Treatments. *Neuron*, 87(2), pp.297–309.

Gerriets, T. et al., 2004. Noninvasive Quantification of Brain Edema and the

Space-Occupying Effect in Rat Stroke Models Using Magnetic Resonance Imaging. *Stroke*, 35(2), pp.566–571.
Gironacci, M.M. et al., 2004. Angiotensin-(1–7) Inhibitory Mechanism of Norepinephrine Release in Hypertensive Rats. *Hypertension*, 44, pp.783–787.
Gironacci, M.M. et al., 2011. Angiotensin (1-7) induces mas receptor internalization. *Hypertension*, 58(2), pp.176–181.
Gironacci, M.M. et al., 2014. Protective axis of the renin–angiotensin system in the brain. *Clinical Science*, 127(5).
Gironacci, M.M., Coba, M.P. & Peña, C., 1999. Angiotensin-(1-7) binds at the type 1 angiotensin II receptors in rat renal cortex. *Regulatory peptides*, 84(1–3), pp.51–4.
Girouard, H. et al., 2009. NMDA Receptor Activation Increases Free Radical Production through Nitric Oxide and NOX2. *Journal of Neuroscience*, 29(8), pp.2545–2552.
Gjymishka, A. et al., 2010. Diminazene Aceturate Is an ACE2 Activator and a Novel Antihypertensive Drug. *The FASEB Journal*, 24(1 Supplement), p.1032.3-1032.3.
Go, A.S. et al., 2014. Heart Disease and Stroke Statistics--2014 Update: A Report From the American Heart Association. *Circulation*, 129(3), pp.e28–e292.
Goldblatt, H. et al., 1934. Studies on experimental hypertension: I. The production of persistent elevation of systolic blood pressure by means of renal ischemia. *The Journal of experimental medicine*, 59(3), pp.347–79.
Goldstein, L.B. et al., 2006. Primary Prevention of Ischemic Stroke. *Stroke*, 37(6), pp.1583–1633.
Gorelik, G., Carbini, L.A. & Scicli, A.G., 1998. Angiotensin 1-7 induces bradykinin-mediated relaxation in porcine coronary artery. *The Journal of pharmacology and experimental therapeutics*, 286(1), pp.403–10.
Goyal, M. et al., 2015. Randomized assessment of rapid endovascular treatment of ischemic stroke. *N Engl J Med*, 372(11), pp.1019–1030.
Gray, S.P. & Jandeleit-Dahm, K.A., 2015. The role of NADPH Oxidase in Vascular Disease – Hypertension, Atherosclerosis & Stroke. *Current Pharmaceutical Design*, 21(41), pp.5933–44.
Griendling, K.K. et al., 1987. Correlation of receptor sequestration with sustained diacylglycerol accumulation in angiotensin II-stimulated cultured vascular smooth muscle cells. *The Journal of biological chemistry*, 262(30), pp.14555–62.
Griendling, K.K., Lasskgue, B. & Alexander, R.W., 1996. Angiotensin receptors and their therapeutic implications. *Annu Rev. Pharmacol. Toxicol.*, 36, pp.281–306.
Grønberg, N.V. et al., 2013. Leukocyte infiltration in experimental stroke. *Journal of neuroinflammation*, 10, p.115.
Gudbjartsson, H. & Patz, S., 1995. The Rician distribution of noisy MRI data. *Magnetic resonance in medicine*, 34(6), pp.910–4.
Guo, D. et al., 2001. The angiotensin II type 1 receptor and receptor-associated proteins. *Cell Research*, 11(3), pp.165–180.
Guo, F. et al., 2010. Astroglia are a possible cellular substrate of angiotensin(1-7) effects in the rostral ventrolateral medulla. *Cardiovascular Research*, 87(3), pp.578–584.
Gursoy-Ozdemir, Y., Can, A. & Dalkara, T., 2004. Reperfusion-Induced Oxidative/Nitrative Injury to Neurovascular Unit After Focal Cerebral Ischemia. *Stroke*, 35(6), pp.1449–1453.
Haensel, J.X., Spain, A. & Martin, C., 2015. A systematic review of physiological methods in rodent pharmacological MRI studies. *Psychopharmacology*,

232(3), pp.489–99.
Haley, M.J. & Lawrence, C.B., 2017. The blood–brain barrier after stroke: Structural studies and the role of transcytotic vesicles. *Journal of Cerebral Blood Flow & Metabolism*, 37(2), pp.456–470.
Hall, C.N. et al., 2014. Capillary pericytes regulate cerebral blood flow in health and disease. *Nature*, 508(7494), pp.55–60.
Hansen, J.L. et al., 2000. Functional reconstitution of the angiotensin II type 2 receptor and G(i) activation. *Circulation research*, 87(9), pp.753–9.
Hansson, L. et al., 1999. Effect of angiotensin-converting-enzyme inhibition compared with conventional therapy on cardiovascular morbidity and mortality in hypertension: the Captopril Prevention Project (CAPPP) randomised trial. *Lancet*, 353(9153), pp.611–6.
Harari, O.A. & Liao, J.K., 2010. NF-κB and innate immunity in ischemic stroke. *Annals of the New York Academy of Sciences*, 1207, pp.32–40.
Harston, G.W.J. et al., 2017. Quantification of serial cerebral blood flow in acute stroke using arterial spin labeling. *Stroke*, 48(1), pp.123–130.
Hartings, J.A. et al., 2003. Delayed secondary phase of peri-infarct depolarizations after focal cerebral ischemia: relation to infarct growth and neuroprotection. *The Journal of neuroscience*, 23(37), pp.11602–10.
Hartings, J.A., Tortella, F.C. & Rolli, M.L., 2006. AC Electrocorticographic Correlates of Peri-Infarct Depolarizations during Transient Focal Ischemia and Reperfusion. *Journal of Cerebral Blood Flow & Metabolism*, 26(5), pp.696–707.
Hartmann, a, 2010. Prolonged disturbances of regional cerebral blood flow in transient ischemic attacks. *Stroke*, 16(6), pp.932–9.
Hauck, E.F. et al., 2004. Capillary Flow and Diameter Changes during Reperfusion after Global Cerebral Ischemia Studied by Intravital Video Microscopy. *Journal of Cerebral Blood Flow & Metabolism*, 24(4), pp.383–391.
Heiss, W.-D., 2000. Ischemic Penumbra: Evidence From Functional Imaging in Man. *Journal of Cerebral Blood Flow & Metabolism*, 20(9), pp.1276–1293.
Heiss, W.-D. & Rosner, G., 1983. Functional recovery of cortical neurons as related to degree and duration of ischemia. *Annals of Neurology*, 14(3), pp.294–301.
Heiss, W.., 1983. Flow Thresholds of Functional and Morphological Damage of Brain Tissue. *Stroke*, 14(3), pp.329–31.
Henninger, N. et al., 2009. Laser Doppler flowmetry predicts occlusion but not tPA-mediated reperfusion success after rat embolic stroke. *Experimental Neurology*, 215(2), pp.290–297.
Henninger, N., Kumar, R. & Fisher, M., 2010. Acute ischemic stroke therapy. *Expert Review of Cardiovascular Therapy*, 8(10), pp.1389–1398.
Heye, A.K. et al., 2014. Assessment of blood-brain barrier disruption using dynamic contrast-enhanced MRI. A systematic review. *NeuroImage. Clinical*, 6, pp.262–74.
Hoehn, M. et al., 2001. Application of magnetic resonance to animal models of cerebral ischemia. *Journal of Magnetic Resonance Imaging*, 14(5), pp.491–509.
Horsch, A.D. et al., 2015. Relation between reperfusion and hemorrhagic transformation in acute ischemic stroke. *Neuroradiology*, 57(12), pp.1219–25.
Hosomi, N. et al., 2005. Angiotensin type 1 receptor blockage improves ischemic injury following transient focal cerebral ischemia. *Neuroscience*, 134(1), pp.225–231.
Hossmann, K.-A., 2012. The two pathophysiologies of focal brain ischemia: implications for translational stroke research. *Journal of cerebral blood flow*

and metabolism : official journal of the International Society of Cerebral Blood Flow and Metabolism, 32(7), pp.1310–6.

Hossmann, K.-A. & Lechtape-Grüter, H., 1971. Blood Flow and Recovery of the Cat Brain after Complete Ischemia for 1 Hour. *European Neurology*, 6(1–6), pp.318–322.

Hossmann, K.A., 1996. Periinfarct depolarizations. *Cerebrovascular and brain metabolism reviews*, 8(3), pp.195–208.

Hossmann, K. & Traystman, R.J., 2008. Chapter 4 Cerebral blood flow and the ischemic penumbra. In pp. 67–92.

Howells, D.W. et al., 2010. Different Strokes for Different Folks: The Rich Diversity of Animal Models of Focal Cerebral Ischemia. *Journal of Cerebral Blood Flow & Metabolism*, 30(8), pp.1412–1431.

Hu, X. et al., 2012. Microglia/Macrophage Polarization Dynamics Reveal Novel Mechanism of Injury Expansion After Focal Cerebral Ischemia. *Stroke*, 43(11), pp.3063–3070.

Huang, H. et al., 1989. Measurement of angiotensin II concentration in rat plasma: pathophysiological applications. *Clinical and experimental hypertension. Part A, Theory and practice*, 11(8), pp.1535–48.

Huang, J., Upadhyay, U.M. & Tamargo, R.J., 2006. Inflammation in stroke and focal cerebral ischemia. *Surgical Neurology*, 66(3), pp.232–245.

Hungerhuber, E. et al., 2006. Simultaneous bilateral laser Doppler fluxmetry and electrophysiological recording during middle cerebral artery occlusion in rats. *Journal of Neuroscience Methods*, 154(1–2), pp.109–115.

Iadecola, C., 1997. Bright and dark sides of nitric oxide in ischemic brain injury. *Trends in Neurosciences*, 20(3), pp.132–139.

Iadecola, C. & Anrather, J., 2011. The immunology of stroke: from mechanisms to translation. *Nature Medicine*, 17(7), pp.796–808.

Iida, H. et al., 1998. Isoflurane and sevoflurane induce vasodilation of cerebral vessels via ATP-sensitive K+ channel activation. *Anesthesiology*, 89(4), pp.954–60.

Infanger, D.W., Sharma, R. V. & Davisson, R.L., 2006. NADPH Oxidases of the Brain: Distribution, Regulation, and Function. *Antioxidants & Redox Signaling*, 8(9–10), pp.1583–1596.

Intebi, A.D. et al., 1990. Angiotensinogen production by rat astroglial cells in vitro and in vivo. *Neuroscience*, 34(3), pp.545–54.

Inzitari, D. et al., 2013. MMP9 Variation After Thrombolysis Is Associated With Hemorrhagic Transformation of Lesion and Death. *Stroke*, 44(10), pp.2901–2903.

Ioannidis, J.P.A., 2008. Why Most Discovered True Associations Are Inflated. *Epidemiology*, 19(5), pp.640–648.

Ioannidis, J.P.A., 2005. Why Most Published Research Findings Are False. *PLoS Medicine*, 2(8), p.e124.

Ioannidis, J.P.A., Tarone, R. & McLaughlin, J.K., 2011. The False-positive to False-negative Ratio in Epidemiologic Studies. *Epidemiology*, 22(4), pp.450–456.

Ishrat, T. et al., 2013. Candesartan Reduces the Hemorrhage Associated with Delayed Tissue Plasminogen Activator Treatment in Rat Embolic Stroke. *Neurochemical Research*, 38(12), pp.2668–2677.

Ishrat, T. et al., 2015. Low-Dose Candesartan Enhances Molecular Mediators of Neuroplasticity and Subsequent Functional Recovery After Ischemic Stroke in Rats. *Molecular Neurobiology*, 51(3), pp.1542–1553.

Ito, D. et al., 2001. Enhanced Expression of Iba1, Ionized Calcium-Binding Adapter Molecule 1, After Transient Focal Cerebral Ischemia In Rat Brain.

Stroke, 32(5), pp.1208–15.
Ito, T. et al., 2002. Protection against ischemia and improvement of cerebral blood flow in genetically hypertensive rats by chronic pretreatment with an angiotensin II AT1 antagonist. *Stroke*, 33(9), pp.2297–2303.
Iusuf, D. et al., 2008. Angiotensin-(1-7): Pharmacological properties and pharmacotherapeutic perspectives. *European Journal of Pharmacology*, 585(2–3), pp.303–312.
Iwai, M. et al., 2004. Possible inhibition of focal cerebral ischemia by angiotensin II type 2 receptor stimulation. *Circulation*, 110(7), pp.843–848.
Jackman, K.A. et al., 2009. Importance of NOX1 for angiotensin II-induced cerebrovascular superoxide production and cortical infarct volume following ischemic stroke. *Brain Research*, 1286, pp.215–220.
Jackman, K. & Iadecola, C., 2015. Neurovascular Regulation in the Ischemic Brain. *Antioxidants & Redox Signaling*, 22(2), pp.149–160.
Jackson, T.R. et al., 1988. The mas oncogene encodes an angiotensin receptor. *Nature*, 335(6189), pp.437–440.
Jiang, T. et al., 2014. Angiotensin-(1-7) induces cerebral ischaemic tolerance by promoting brain angiogenesis in a Mas/eNOS-dependent pathway. *British journal of pharmacology*, 171(18), pp.4222–4232.
Jiang, T. et al., 2013. Angiotensin-(1-7) modulates renin–angiotensin system associated with reducing oxidative stress and attenuating neuronal apoptosis in the brain of hypertensive rats. *Pharmacological Research*, 67(1), pp.84–93.
Jiang, T. et al., 2012. Suppressing inflammation by inhibiting the NF-κB pathway contributes to the neuroprotective effect of angiotensin-(1-7) in rats with permanent cerebral ischaemia. *British Journal of Pharmacology*, 167(7), pp.1520–1532.
Jickling, G.C. et al., 2015. Targeting neutrophils in ischemic stroke: translational insights from experimental studies. *Journal of cerebral blood flow and metabolism : official journal of the International Society of Cerebral Blood Flow and Metabolism*, 35(6), pp.888–901.
Joglar, B. et al., 2009. The inflammatory response in the MPTP model of Parkinson's disease is mediated by brain angiotensin: relevance to progression of the disease. *Journal of Neurochemistry*, 109(2), pp.656–669.
Jones, T.H. et al., 1981. Thresholds of focal cerebral ischemia in awake monkeys. *Journal of Neurosurgery*, 54(6), pp.773–782.
Joseph, J.P. et al., 2014. The angiotensin type 2 receptor agonist Compound 21 elicits cerebroprotection in endothelin-1 induced ischemic stroke. *Neuropharmacology*, 81, pp.134–141.
Jovin, T.G. et al., 2015. Thrombectomy within 8 Hours after Symptom Onset in Ischemic Stroke. *New England Journal of Medicine*, 372(24), pp.2296–2306.
Kagiyama, T., Kagiyama, S. & Phillips, I., 2003. Expression of angiotensin type 1 and 2 receptors in brain after transient middle cerebral artery occlusion in rats. *Regulatory Peptides*, 110(3), pp.241–247.
Kahles, T. et al., 2010. NADPH oxidase Nox1 contributes to ischemic injury in experimental stroke in mice. *Neurobiology of Disease*, 40(1), pp.185–192.
Kakar, S.S. et al., 1992. Angiotensin II type-1 receptor subtype cDNAs: differential tissue expression and hormonal regulation. *Biochemical and biophysical research communications*, 183(3), pp.1090–6.
Kanaide, H. et al., 2003. Cellular Mechanism of Vasoconstriction Induced by Angiotensin II: It Remains to Be Determined. *Circulation Research*, 93(11), pp.1015–1017.
Kassem-Moussa, H. & Graffagnino, C., 2002. Nonocclusion and spontaneous recanalization rates in acute ischemic stroke: a review of cerebral

angiography studies. *Archives of neurology*, 59(12), pp.1870–3.
Kassner, A. et al., 2009. Recombinant Tissue Plasminogen Activator Increases Blood-Brain Barrier Disruption in Acute Ischemic Stroke: An MR Imaging Permeability Study. *American Journal of Neuroradiology*, 30(10), pp.1864–1869.
Kassner, A. & Merali, Z., 2015. Assessment of Blood–Brain Barrier Disruption in Stroke. *Stroke*, 46, pp.3310–3315.
Kateb, B. & Heiss, J.D., 2013. *The Textbook of nanoneuroscience and nanoneurosurgery*, CRC Press/Taylor & Francis.
van Kats, J.P. et al., 1997. Angiotensin II type 1 (AT1) receptor-mediated accumulation of angiotensin II in tissues and its intracellular half-life in vivo. *Hypertension*, 30(1 Pt 1), pp.42–9.
Kettenmann, H. et al., 2011. Physiology of microglia. *Physiological reviews*, 91(2), pp.461–553.
Khare, S., 2016. Risk factors of transient ischemic attack: An overview. *Journal of mid-life health*, 7(1), pp.2–7.
Kidwell, C.S. et al., 2001. Diffusion-perfusion MRI characterization of post-recanalization hyperperfusion in humans. *Neurology*, 57(11), pp.2015–21.
Kidwell, C.S. et al., 2008. Thrombolytic Toxicity: Blood Brain Barrier Disruption in Human Ischemic Stroke. *Cerebrovascular Diseases*, 25(4), pp.338–343.
Kim-Mitsuyama, S. et al., 2005. Critical Role of Angiotensin II in Excess Salt-Induced Brain Oxidative Stress of Stroke-Prone Spontaneously Hypertensive Rats. *Stroke*, 36(5), pp.1083–8.
Kim, S.-K., Cho, K.-O. & Kim, S.Y., 2009. The plasticity of posterior communicating artery influences on the outcome of white matter injury induced by chronic cerebral hypoperfusion in rats. *Neurological Research*, 31(3), pp.245–250.
Kitami, Y. et al., 1992. Differential gene expression and regulation of type-1 angiotensin II receptor subtypes in the rat. *Biochemical and biophysical research communications*, 188(1), pp.446–52.
Knapp, L.T. & Klann, E., 2002. Potentiation of hippocampal synaptic transmission by superoxide requires the oxidative activation of protein kinase C. *The Journal of neuroscience : the official journal of the Society for Neuroscience*, 22(3), pp.674–83.
Kohrmann, M. et al., 2012. The Hyperintense Acute Reperfusion Marker on Fluid-Attenuated Inversion Recovery Magnetic Resonance Imaging Is Caused by Gadolinium in the Cerebrospinal Fluid. *Stroke*, 43(1), pp.259–261.
Koizumi, J. et al., 1986. Experimental studies of ischemic brain edema. I. A new experimental model of cerebral embolism in rats in which recirculation can be introduced in the ischemic area. *Jpn J Stroke*, 8, pp.1–8.
Kono, T. et al., 1986. Biological activities of angiotensin II-(1-6)-hexapeptide and angiotensin II-(1-7)-heptapeptide in man. *Life sciences*, 38(16), pp.1515–9.
Kopf, E., Shnitzer, D. & Zharhary, D., 2005. Panorama™ Ab Microarray Cell Signaling kit: A unique tool for protein expression analysis. *PROTEOMICS*, 5(9), pp.2412–2416.
Kostenis, E. et al., 2005. G-protein-coupled receptor Mas is a physiological antagonist of the angiotensin II type 1 receptor. *Circulation*, 111(14), pp.1806–13.
Kostulas, N. et al., 1999. Increased IL-1beta, IL-8, and IL-17 mRNA expression in blood mononuclear cells observed in a prospective ischemic stroke study. *Stroke*, 30(10), pp.2174–9.
Krafft, P.R. et al., 2012. Etiology of Stroke and Choice of Models. *International Journal of Stroke*, 7(5), pp.398–406.

Kramer, D.R. et al., 2016. Cortical spreading depolarization: Pathophysiology, implications, and future directions. *Journal of Clinical Neuroscience*, 24, pp.22–27.

Krikov, M. et al., 2008. Candesartan but not ramipril pretreatment improves outcome after stroke and stimulates neurotrophin BNDF/TrkB system in rats. *Journal of hypertension*, 26(3), pp.544–552.

Kristián, T. & Siesjö, B.K., 1998. Calcium in ischemic cell death. *Stroke*, 29(3), pp.705–18.

Krueger, M. et al., 2017. Stroke-induced blood–brain barrier breakdown along the vascular tree – No preferential affection of arteries in different animal models and in humans. *Journal of Cerebral Blood Flow & Metabolism*, 37(7), pp.2539–2554.

Kumar, A., Aakriti & Gupta, V., 2016. A review on animal models of stroke: An update. *Brain Research Bulletin*, 122, pp.35–44.

Kumar, M. et al., 1996. Selective expression of c-mas proto-oncogene in rat cerebral endothelial cells. *Neuroreport*, 8(1), pp.93–6.

Kunz, A. & Iadecola, C., 2009. Cerebral vascular dysregulation in the ischemic brain. *Handbook of clinical neurology*, 92, pp.283–305.

Kuriakose, S. & Uzonna, J.E., 2014. Diminazene aceturate (Berenil), a new use for an old compound? *International Immunopharmacology*, 21(2), pp.342–345.

Lakhan, S.E. et al., 2013. Matrix Metalloproteinases and Blood-Brain Barrier Disruption in Acute Ischemic Stroke. *Frontiers in Neurology*, 4, p.32.

Lakhan, S.E., Kirchgessner, A. & Hofer, M., 2009. Inflammatory mechanisms in ischemic stroke: therapeutic approaches. *Journal of translational medicine*, 7, p.97.

Lassègue, B. et al., 2001. Novel gp91(phox) homologues in vascular smooth muscle cells : nox1 mediates angiotensin II-induced superoxide formation and redox-sensitive signaling pathways. *Circulation research*, 88(9), pp.888–94.

Lassègue, B. et al., 1993. Phosphatidylcholine is a major source of phosphatidic acid and diacylglycerol in angiotensin II-stimulated vascular smooth-muscle cells. *The Biochemical journal*, 292 (Pt 2, pp.509–17.

Lauritzen, M. et al., 1990. Cortical Spreading Depression is Associated with Arachidonic Acid Accumulation and Preservation of Energy Charge. *Journal of Cerebral Blood Flow & Metabolism*, 10(1), pp.115–122.

Lawrence, E.S. et al., 2001. Estimates of the prevalence of acute stroke impairments and disability in a multiethnic population. *Stroke*, 32(6), pp.1279–84.

Leão, A.A.P., 1944. Spreading depression of activity in the cerebral cortex. *Journal of physiology*, 7(6), pp.359–390.

Lee, D.H. et al., 2005. Imaging of the ischemic penumbra in acute stroke. *Korean journal of radiology*, 6(2), pp.64–74.

Lee, S. et al., 2015. Effect of a Selective Mas Receptor Agonist in Cerebral Ischemia In Vitro and In Vivo. *Plos One*, 10(11), p.e0142087.

Lee, S. et al., 2012. Neuroprotective effect of an angiotensin receptor type 2 agonist following cerebral ischemia in vitro and in vivo. *Experimental & Translational Stroke Medicine*, 4(1), p.16.

Leffler, C.W. et al., 1989. Effects of ischemia on brain blood flow and oxygen consumption of newborn pigs. *The American journal of physiology*, 257(6 Pt 2), pp.H1917-26.

Leithner, C. et al., 2015. Infarct Volume Prediction by Early Magnetic Resonance Imaging in a Murine Stroke Model Depends on Ischemia Duration and Time of Imaging. *Stroke*, 46(11).

Lemos, V.S. et al., 2005. The Endothelium-dependent Vasodilator Effect of the

Nonpeptide Ang(1-7) Mimic Ave 0991 Is Abolished in the Aorta of mas-knockout mice. *Journal of Cardiovascular Pharmacology*, 46(3), pp.274–279.

Lenkei, Z. et al., 1997. Expression of Angiotensin Type-1 (AT1) and Type-2 (AT2) Receptor mRNAs in the Adult Rat Brain: A Functional Neuroanatomical Review. *Frontiers in Neuroendocrinology*, 18(4), pp.383–439.

Lennmyr, F. et al., 1998. Expression of vascular endothelial growth factor (VEGF) and its receptors (Flt-1 and Flk-1) following permanent and transient occlusion of the middle cerebral artery in the rat. *Journal of neuropathology and experimental neurology*, 57(9), pp.874–82.

Li, D.-D. et al., 2013. The roles of MMP-9/TIMP-1 in cerebral edema following experimental acute cerebral infarction in rats. *Neuroscience Letters*, 550, pp.168–172.

Li, J.M. et al., 2008. Temporary pretreatment with the angiotensin II type 1 receptor blocker, valsartan, prevents ischemic brain damage through an increase in capillary density. *Stroke*, 39(7), pp.2029–2036.

Li, P. et al., 2017. C-C Chemokine Receptor Type 5 (CCR5) Mediated Docking of Transferred Tregs Protects Against Early Blood Brain Barrier Disruption After Stroke. *Journal of the American Heart Association*, 6(8), p.e006387.

Liang, D. et al., 2007. Cytotoxic edema: mechanisms of pathological cell swelling. *Neurosurgical focus*, 22(5), p.E2.

Liebeskind, D.S., 2003. Collateral Circulation. *Stroke*, 34(2279–2284).

Liebeskind, D.S., 2014. Collateral lessons from recent acute ischemic stroke trials. *Neurological research*, 36(5), pp.397–402.

Liebeskind, D.S. et al., 2014. Collaterals at angiography and outcomes in the interventional management of stroke (IMS) III trial. *Stroke*, 45(3), pp.759–764.

Liebeskind, D.S., 2005. Collaterals in Acute Stroke: Beyond the Clot. *Neuroimaging Clinics of North America*, 15(3), pp.553–573.

Liesz, A. et al., 2009. Regulatory T cells are key cerebroprotective immunomodulators in acute experimental stroke. *Nature Medicine*, 15(2), pp.192–199.

Lin, C.-Y. et al., 2008. Dynamic Changes in Vascular Permeability, Cerebral Blood Volume, Vascular Density, and Size after Transient Focal Cerebral Ischemia in Rats: Evaluation with Contrast-Enhanced Magnetic Resonance Imaging. *Journal of Cerebral Blood Flow & Metabolism*, 28(8), pp.1491–1501.

Lin, T.-N. et al., 2002. Dynamic changes in cerebral blood flow and angiogenesis after transient focal cerebral ischemia in rats. Evaluation with serial magnetic resonance imaging. *Stroke*, 33(12), pp.2985–91.

Lipton, P., 1999. Ischemic Cell Death in Brain Neurons. *Physiological Reviews*, 79(4), pp.1431–568.

Liszczak, T.M. et al., 1984. Limitations of tetrazolium salts in delineating infarcted brain. *Acta neuropathologica*, 65(2), pp.150–7.

Liu, H. et al., 2008. Protective mechanisms of the angiotensin II type 1 receptor blocker candesartan against cerebral ischemia: in-vivo and in-vitro studies. *Journal of hypertension*, 26(7), pp.1435–45.

Liu, M., Shi, P. & Sumners, C., 2016. Direct anti-inflammatory effects of angiotensin-(1-7) on microglia. *Journal of Neurochemistry*, 136(1), pp.163–171.

Liu, Q. et al., 2017. Monitoring acute stroke in mouse model using laser speckle imaging-guided visible-light optical coherence tomography. *IEEE Transactions on Biomedical Engineering*, pp.1–1.

Liu, T. et al., 1994. Tumor necrosis factor-alpha expression in ischemic neurons. *Stroke*, 25(7), pp.1481–8.

Livak, K.J. & Schmittgen, T.D., 2001. Analysis of Relative Gene Expression Data

Using Real-Time Quantitative PCR and the 2−ΔΔCT Method. *Methods*, 25(4), pp.402–408.

Lo, E.H., Dalkara, T. & Moskowitz, M.A., 2003. Neurological diseases: Mechanisms, challenges and opportunities in stroke. *Nature Reviews Neuroscience*, 4(5), pp.399–414.

Longa, E.Z. et al., 1989. Reversible middle cerebral artery occlusion without craniectomy in rats. *Stroke*, 20(1), pp.84–91.

Lou, M. et al., 2004. Sustained Blockade of Brain AT1 Receptors Before and After Focal Cerebral Ischemia Alleviates Neurologic Deficits and Reduces Neuronal Injury, Apoptosis, and Inflammatory Responses in the Rat. *Journal Cerebral Blood Flow Metabolism*, 24(5), pp.536–47.

Lou, N. et al., 2016. Purinergic receptor P2RY12-dependent microglial closure of the injured blood-brain barrier. *Proceedings of the National Academy of Sciences of the United States of America*, 113(4), pp.1074–9.

Loubinoux, I. et al., 1997. Spreading of Vasogenic Edema and Cytotoxic Edema Assessed by Quantitative Diffusion and T2 Magnetic Resonance Imaging. *Stroke*, 28(2), pp.419–26.

Love, S., 2003. Apoptosis and brain ischaemia. *Progress in Neuro-Psychopharmacology and Biological Psychiatry*, 27(2), pp.267–282.

Lu, J. et al., 2013. The expression of angiotensin-converting enzyme 2-angiotensin-(1-7)-Mas receptor axis are upregulated after acute cerebral ischemic stroke in rats. *Neuropeptides*, 47(5), pp.289–295.

Lu, J., Zhang, Y. & Shi, J., 2008a. Effects of intracerebroventricular infusion of angiotensin-(1-7) on bradykinin formation and the kinin receptor expression after focal cerebral ischemia-reperfusion in rats. *Brain Research*, 1219, pp.127–135.

Lu, J., Zhang, Y. & Shi, J., 2008b. Effects of intracerebroventricular infusion of angiotensin-(1–7) on bradykinin formation and the kinin receptor expression after focal cerebral ischemia–reperfusion in rats. *Brain Research*, 1219, pp.127–135.

Luitse, M.J. et al., 2012. Diabetes, hyperglycaemia, and acute ischaemic stroke. *The Lancet Neurology*, 11(3), pp.261–271.

Ma, C.-Y. & Yin, L., 2016. Neuroprotective effect of angiotensin II type 2 receptor during cerebral ischemia/reperfusion. *Neural regeneration research*, 11(7), pp.1102–7.

Macleod, M.R. et al., 2008. Evidence for the Efficacy of NXY-059 in Experimental Focal Cerebral Ischaemia Is Confounded by Study Quality. *Stroke*, 39(10), pp.2824–2829.

Macrae, I., 2011. Preclinical stroke research - advantages and disadvantages of the most common rodent models of focal ischaemia. *British Journal of Pharmacology*, 164(4), pp.1062–1078.

Macrae, I.M. et al., 1993. Endothelin-1-Induced Reductions in Cerebral Blood Flow: Dose Dependency, Time Course, and Neuropathological Consequences. *Journal of Cerebral Blood Flow & Metabolism*, 13(2), pp.276–284.

Macrae, I.M., 1992. New models of focal cerebral ischaemia. *Br. J. clin. Pharmac*, 34, pp.302–308.

Makino, I. et al., 1996. Transient upregulation of the AT2 receptor mRNA level after global ischemia in the rat brain. *Neuropeptides*, 30(6), pp.596–601.

Markgraf, C.G. et al., 1993. Comparative Histopathologic Consequences of Photothrombotic Occlusion of the Distal Middle Cerebral Artery in Sprague-Dawley and Wistar Rats. *Stroke*, 24(2), pp.286–292.

Masamoto, K. et al., 2006. Relationship between Neural, Vascular, and BOLD

Signals in Isoflurane-Anesthetized Rat Somatosensory Cortex. *Cerebral Cortex*, 17(4), pp.942–950.

Masamoto, K. & Kanno, I., 2012. Anesthesia and the quantitative evaluation of neurovascular coupling. *Journal of cerebral blood flow and metabolism : official journal of the International Society of Cerebral Blood Flow and Metabolism*, 32(7), pp.1233–47.

Matavelli, L.C. & Siragy, H.M., 2015. AT2 receptor activities and pathophysiological implications. *Journal of cardiovascular pharmacology*, 65(3), pp.226–32.

Mateos, L., Perez-Alvarez, M.J. & Wandosell, F., 2016. Angiotensin II type-2 receptor stimulation induces neuronal VEGF synthesis after cerebral ischemia. *Biochimica et Biophysica Acta (BBA) - Molecular Basis of Disease*, 1862(7), pp.1297–1308.

Matsuura, T. & Bureš, J., 1971. The minimum volume of depolarized neural tissue required for triggering cortical spreading depression in rat. *Experimental Brain Research*, 12(3), pp.238–249.

Matthews, J.N. et al., 1990. Analysis of serial measurements in medical research. *BMJ (Clinical research ed.)*, 300(6719), pp.230–5.

McCabe, C. et al., 2017. Animal models of ischaemic stroke and characterisation of the ischaemic penumbra. *Neuropharmacology*, S0028-3908(17), pp.30439–2.

McCabe, C. et al., 2009. Differences in the evolution of the ischemic penumbra in stroke-prone spontaneously hypertensive and wistar-kyoto rats. *Stroke*, 40(12), pp.3864–3868.

McCarthy, C.A. et al., 2009. Angiotensin AT2 receptor stimulation causes neuroprotection in a conscious rat model of stroke. *Stroke*, 40(4), pp.1482–1489.

McCarthy, C.A. et al., 2012. Angiotensin II Type 2 receptor stimulation initiated after stroke causes neuroprotection in conscious rats. *Hypertension*, 60(6), pp.1531–1537.

McCarthy, C.A. et al., 2014. Direct angiotensin AT2 receptor stimulation using a novel AT2 receptor agonist, compound 21, evokes neuroprotection in conscious hypertensive rats. *PLoS ONE*, 9(4), p.e95762.

McKinley, M.J. et al., 2003. The brain renin-angiotensin system: Location and physiological roles. *International Journal of Biochemistry and Cell Biology*, 35(6), pp.901–918.

McKinney, C.A. et al., 2015. Angiotensin-(1-7) and angiotensin-(1-9) inhibit vascular smooth muscle cell growth and migration in vitro and vascular remodelling in vivo. *Atherosclerosis*, 241(1), p.e44.

McLeod, D.D. et al., 2015. Perfusion Computed Tomography Thresholds Defining Ischemic Penumbra and Infarct Core: Studies in a Rat Stroke Model. *International Journal of Stroke*, 10(4), pp.553–559.

Mecca, A.P. et al., 2009. Candesartan pretreatment in cerebroprotective in a rat model of endothelin-1-induced middle cerebral artery occlusion. *Experimental Physiology*, 94(8), pp.937–946.

Mecca, A.P. et al., 2011. Cerebroprotection by angiotensin-(1-7) in endothelin-1-induced ischaemic stroke. *Experimental physiology*, 96(10), pp.1084–96.

Mehta, P.K. & Griendling, K.K., 2007. Angiotensin II cell signaling: physiological and pathological effects in the cardiovascular system. *American Journal of Physiology Cell Physiology*, 292(1), pp.C82-97.

Menard, J. & Patchett, A.A., 2001. Angiotensin-converting enzyme inhibitors. *Advances in protein chemistry*, 56, pp.13–75.

Meng, W. & Busija, D.W., 1993. Comparative effects of angiotensin-(1-7) and

angiotensin II on piglet pial arterioles. *Stroke*, 24(12), p.2041–4; discussion 2045.

Meng, X. et al., 2004. Characterizing the diffusion/perfusion mismatch in experimental focal cerebral ischemia. *Annals of neurology*, 55(2), pp.207–12.

Meng, Y. et al., 2014. Angiotensin-Converting Enzyme 2/Angiotensin-(1-7)/Mas Axis Protects against Lung Fibrosis by Inhibiting the MAPK/NF-κB Pathway. *American Journal of Respiratory Cell and Molecular Biology*, 50(4), pp.723–736.

Merali, Z. et al., 2017. Evolution of blood-brain-barrier permeability after acute ischemic stroke. *PLOS ONE*, 12(2), p.e0171558.

Mercure, C. et al., 2008. Angiotensin(1-7) blunts hypertensive cardiac remodeling by a direct effect on the heart. *Circulation Research*, 103(11), pp.1319–1326.

Mergenthaler, P., Dirnagl, U. & Meisel, A., 2004. Pathophysiology of Stroke: Lessons from Animal Models. *Metabolic Brain Disease*, 19(3/4), pp.151–167.

Metzger, R. et al., 1995. Expression of the mouse and rat mas proto-oncogene in the brain and peripheral tissues. *FEBS letters*, 357(1), pp.27–32.

Meyer, T.N. et al., 2001. Reassembly of the tight junction after oxidative stress depends on tyrosine kinase activity. *The Journal of biological chemistry*, 276(25), pp.22048–55.

Mies, G., Iijima, T. & Hossmann, K.A., 1993. Correlation between peri-infarct DC shifts and ischaemic neuronal damage in rat. *Neuroreport*, 4(6), pp.709–11.

Millan, M.A. et al., 1991. Differential distribution of AT1 and AT2 angiotensin II receptor subtypes in the rat brain during development. *Proceedings of the National Academy of Sciences of the United States of America*, 88(24), pp.11440–4.

Miller, A.A., Drummond, G.R. & Sobey, C.G., 2006. Novel isoforms of NADPH-oxidase in cerebral vascular control. *Pharmacology & Therapeutics*, 111(3), pp.928–948.

Miller, D.B. et al., 2005. The pharmacokinetics of diminazene aceturate after intramuscular administration in healthy dogs. *J S Afr Vet Assoc.*, 76(3), pp.146–50.

Min, L.J. et al., 2014. Direct stimulation of angiotensin II type 2 receptor initiated after stroke ameliorates ischemic brain damage. *American Journal of Hypertension,* 27(8), pp.1036-1044.

Miura, S., Karnik, S.S. & Saku, K., 2005. Constitutively Active Homo-oligomeric Angiotensin II Type 2 Receptor Induces Cell Signaling Independent of Receptor Conformation and Ligand Stimulation. *Journal of Biological Chemistry*, 280(18), pp.18237–18244.

Mogi, M. et al., 2014. Serum levels of renin-angiotensin system components in acute stroke patients. *Geriatrics & Gerontology International*, 14(4), pp.793–798.

Moraes, P.L. et al., 2017. Vasodilator effect of Angiotensin- (1-7) on vascular coronary bed of rats: Role of Mas, ACE and ACE2. *Protein & Peptide Letters*, 24.

Morimoto, S., Cassell, M.D. & Sigmund, C.D., 2002. The brain renin-angiotensin system in transgenic mice carrying a highly regulated human renin transgene. *Circulation research*, 90(1), pp.80–6.

Moseley, M.E., Kucharczyk, J., et al., 1990. Diffusion-weighted MR imaging of acute stroke: correlation with T2-weighted and magnetic susceptibility-enhanced MR imaging in cats. *AJNR. American journal of neuroradiology*, 11(3), pp.423–9.

Moseley, M.E., Cohen, Y., et al., 1990. Diffusion-weighted MR imaging of anisotropic water diffusion in cat central nervous system. *Radiology*, 176(2),

pp.439–445.
Moskowitz, M.A., Lo, E.H. & Iadecola, C., 2010. The science of stroke: mechanisms in search of treatments. *Neuron*, 67(2), pp.181–98.
Muir, K.W. & Macrae, I.M., 2016. Neuroimaging as a Selection Tool and Endpoint in Clinical and Pre-clinical Trials. *Translational stroke research*, 7(5), pp.368–77.
Nagel, S. et al., 2008. Minocycline and hypothermia for reperfusion injury after focal cerebral ischemia in the rat—Effects on BBB breakdown and MMP expression in the acute and subacute phase. *Brain Research*, 1188, pp.198–206.
Nedergaard, M. & Hansen, A.J., 1988. Spreading depression is not associated with neuronal injury in the normal brain. *Brain Research*, 449(1–2), pp.395–398.
Neumann-Haefelin, T. et al., 2000. Serial MRI After Transient Focal Cerebral Ischemia in Rats. *Stroke*, 31(8).
Nguyen, G. et al., 2002. Pivotal role of the renin/prorenin receptor in angiotensin II production and cellular responses to renin. *The Journal of clinical investigation*, 109(11), pp.1417–27.
Nguyen, G. & Muller, D.N., 2010. The biology of the (pro)renin receptor. *Journal of the American Society of Nephrology : JASN*, 21(1), pp.18–23.
Nikolova, S., Lee, T.-Y. & Bartha, R., 2014. The Severity of Ischemia Varies in Sprague-Dawley Rats from Different Vendors. *ISRN Stroke*, 2014, pp.1–9.
Nishimura, Y., Ito, T. & Saavedra, J.M., 2000. Angiotensin II AT1 Blockade Normalizes Cerebrovascular Autoregulation and Reduces Cerebral Ischemia in Spontaneously Hypertensive Rats. *Stroke*, 31(10).
Nogawa, S. et al., 1998. Interaction between inducible nitric oxide synthase and cyclooxygenase-2 after cerebral ischemia. *Pharmacology*, 95(18), pp.10966–10971.
Nouet, S. & Nahmias, C., 2000. Signal transduction from the angiotensin II AT2 receptor. *Trends in endocrinology and metabolism: TEM*, 11(1), pp.1–6.
O'Collins, V.E. et al., 2006. 1,026 Experimental treatments in acute stroke. *Annals of Neurology*, 59(3), pp.467–477.
O'Donnell, M.J. et al., 2010. Risk factors for ischaemic and intracerebral haemorrhagic stroke in 22 countries (the INTERSTROKE study): a case-control study. *The Lancet*, 376(9735), pp.112–123.
Ocaranza, M.P. et al., 2006. Effect of hypertension on angiotensin-(1–7) levels in rats with different angiotensin-I converting enzyme polymorphism. *Life Sciences*, 78(14), pp.1535–1542.
Ogasawara, K. et al., 2003. Prediction and monitoring of cerebral hyperperfusion after carotid endarterectomy by using single-photon emission computerized tomography scanning. *Journal of Neurosurgery*, 99(3), pp.504–510.
Oguejiofor, C., Ochiogu, I. & Umeoduagu, C., 2010. Increasing doses of diminazene aceturate: adverse reproductive effects in female Wistar rats. *Asian Pacific Journal of Tropical Medicine*, 3(11), pp.887–889.
Oliff, H.S. et al., 1995. The role of strain/vendor differences on the outcome of focal ischemia induced by intraluminal middle cerebral artery occlusion in the rat. *Brain Research*, 675(1), pp.20–26.
Oliff, H.S., Coyle, P. & Weber, E., 1997. Rat Strain and Vendor Differences in Collateral Anastomoses. *Journal of Cerebral Blood Flow & Metabolism*, 17(5), pp.571–576.
Olsson, S.B. & Halperin, J.L., 2005. Prevention of Stroke in Patients with Atrial Fibrillation. *Seminars in Vascular Medicine*, 5(3), pp.285–292.
Onetti, Y. et al., 2015. Middle cerebral artery remodeling following transient brain

ischemia is linked to early postischemic hyperemia: A target of uric acid treatment. *American Journal of Physiology - Heart and Circulatory Physiology*, 308(8).

Page, I.H. & Helmer, O.M., 1940. A crystalline pressor substance (angiotonin) resulting from the reaction between renin and renin-activator. *The Journal of experimental medicine*, 71(1), pp.29–42.

Pan, J. et al., 2007. Reperfusion injury following cerebral ischemia: pathophysiology, MR imaging, and potential therapies. *Neuroradiology*, 49(2), pp.93–102.

Panahpour, H., Dehghani, G.A. & Bohlooli, S., 2014. Enalapril attenuates ischaemic brain oedema and protects the blood–brain barrier in rats via an antioxidant action. *Clinical and Experimental Pharmacology and Physiology*, 41(3), pp.220–226.

Panahpour, H., Nekooeian, A.A. & Dehghani, G.A., 2014. Candesartan attenuates ischemic brain edema and protects the blood-brain barrier integrity from ischemia/reperfusion injury in rats. *Iranian biomedical journal*, 18(4), pp.232–8.

Paul, J.S. et al., 2005. Imaging the development of an ischemic core following photochemically induced cortical infarction in rats using Laser Speckle Contrast Analysis (LASCA).

Paul, M. et al., 2006. Physiology of local renin-angiotensin systems. *Physiological reviews*, 86(3), pp.747–803.

Paxinos, G. & Watson, C., 1997. The Rat Brain in Stereotaxic Coordinates. *Academic Press, San Diego*, 3rd.

Pelisch, N. et al., 2011. Blockade of AT1 Receptors Protects the Blood-Brain Barrier and Improves Cognition in Dahl Salt-Sensitive Hypertensive Rats. *American Journal of Hypertension*, 24(3), pp.362–368.

Percie du Sert, N. et al., 2017. The IMPROVE Guidelines (Ischaemia Models: Procedural Refinements Of in Vivo Experiments). *Journal of Cerebral Blood Flow & Metabolism*, 37(11), pp.3488–3517.

Pérez-Asensio, F.J. et al., 2010. Antioxidant CR-6 protects against reperfusion injury after a transient episode of focal brain ischemia in rats. *Journal of cerebral blood flow and metabolism : official journal of the International Society of Cerebral Blood Flow and Metabolism*, 30(3), pp.638–52.

Piccardi, B. et al., 2015. Unbalanced Metalloproteinase-9 and Tissue Inhibitors of Metalloproteinases Ratios Predict Hemorrhagic Transformation of Lesion in Ischemic Stroke Patients Treated with Thrombolysis: Results from the MAGIC Study. *Frontiers in neurology*, 6, p.121.

Pillai, D.R. et al., 2009. Cerebral Ischemia–Reperfusion Injury in Rats—A 3 T MRI Study on Biphasic Blood–Brain Barrier Opening and the Dynamics of Edema Formation. *Journal of Cerebral Blood Flow & Metabolism*, 29(11), pp.1846–1855.

Pillai, D.R. et al., 2013. Neurovascular protection by targeting early blood–brain barrier disruption with neurotrophic factors after ischemia–reperfusion in rats*. *Journal of Cerebral Blood Flow & Metabolism*, 33(10), pp.557–566.

Qi, Y. et al., 2013. Diminazene Aceturate Enhances Angiotensin-Converting Enzyme 2 Activity and Attenuates Ischemia-Induced Cardiac Pathophysiology. *Hypertension*, 62(4), pp.746–752.

Rabin, M. et al., 1987. Human ros1 and mas1 oncogenes located in regions of chromosome 6 associated with tumor-specific rearrangements. *Oncogene research*, 1(2), pp.169–78.

Raether, W. et al., 1974. Pharmacokinetic and chemoprophylactic studies on Berenil in Wistar rats. *Z Tropenmed Parasitol.*, 23(4), pp.418–27.

Ramakrishnan, G., A., G. & R., I., 2012. Understanding and Augmenting Collateral Blood Flow During Ischemic Stroke. In *Acute Ischemic Stroke*. InTech.

Rami, A., Bechmann, I. & Stehle, J., 2008. Exploiting endogenous anti-apoptotic proteins for novel therapeutic strategies in cerebral ischemia. *Progress in Neurobiology*, 85(3), pp.273–296.

Ransohoff, R.M., 2016. A polarizing question: do M1 and M2 microglia exist? *Nature Neuroscience*, 19(8), pp.987–991.

Rapp, J.H. et al., 2003. Cerebral Ischemia and Infarction From Atheroemboli <100 microm in Size. *Stroke*, 34(8), pp.1976–1980.

Regenhardt, R.W. et al., 2013. Anti-inflammatory effects of angiotensin-(1-7) in ischemic stroke. *Neuropharmacology*, 71, pp.154–163.

Regenhardt, R.W. et al., 2014. Centrally administered angiotensin-(1-7) increases the survival of stroke-prone spontaneously hypertensive rats. *Experimental Physiology*, 99(2), pp.442–453.

Reid, E. et al., 2012. Penumbra detection using PWI/DWI mismatch MRI in a rat stroke model with and without comorbidity: comparison of methods. *Journal of cerebral blood flow and metabolism : official journal of the International Society of Cerebral Blood Flow and Metabolism*, 32(9), pp.1765–77.

Reid, I.A., 1985. The Renin-Angiotensin System and Body Function. *Archives of Internal Medicine*, 145(8), p.1475.

Reith, W. et al., 1994. Laser Doppler flowmetry of focal ischaemia and reperfusion in deep brain structures in rats. *Acta Neurochirurgica*, 131(1–2), pp.151–156.

Ren, Y., Garvin, J.L. & Carretero, O.A., 2002. Vasodilator action of angiotensin-(1-7) on isolated rabbit afferent arterioles. *Hypertension (Dallas, Tex. : 1979)*, 39(3), pp.799–802.

Renú, A. et al., 2015. Relevance of Blood–Brain Barrier Disruption After Endovascular Treatment of Ischemic Stroke. *Stroke*, 46(3), pp.673–679.

Rewell, S. & Howells, D.W., 2017. The Right Rodent for the Job: Infarct Variability Between Strains and Its Impact on Logistics of Experimental Animal Studies. In Springer, Cham, pp. 667–687.

Rewell, S.S.J. et al., 2017. Evolution of ischemic damage and behavioural deficit over 6 months after MCAo in the rat: Selecting the optimal outcomes and statistical power for multi-centre preclinical trials. *PloS one*, 12(2), p.e0171688.

Rha, J.-H. & Saver, J.L., 2007. The Impact of Recanalization on Ischemic Stroke Outcome. *Stroke*, 38(3), pp.967–73.

Ricci, P.E. et al., 1999. A comparison of fast spin-echo, fluid-attenuated inversion-recovery, and diffusion-weighted MR imaging in the first 10 days after cerebral infarction. *AJNR. American journal of neuroradiology*, 20(8), pp.1535–42.

Rigatto, K. et al., 2013. Diminazene aceturate improves autonomic modulation in pulmonary hypertension. *European Journal of Pharmacology*, 713(1–3), pp.89–93.

Ritter, O. et al., 2002. AT2-Receptor activation regulates myocardial eNOS expression via the calcineurin-NF-AT pathway. *The FASEB Journal*, 17(2), pp.283–5.

Ritzel, R.M. et al., 2015. Functional differences between microglia and monocytes after ischemic stroke. *Journal of neuroinflammation*, 12, p.106.

Riva, M. et al., 2012. Hemodynamic monitoring of intracranial collateral flow predicts tissue and functional outcome in experimental ischemic stroke. *Experimental Neurology*, 233(2), pp.815–820.

Robertson, C.A. et al., 2015. Detection of ischemic penumbra using combined perfusion and T2* oxygen challenge imaging. *International journal of stroke : official journal of the International Stroke Society*, 10(1), pp.42–50.

Rodriguez-Pallares, J. et al., 2008. Brain angiotensin enhances dopaminergic cell death via microglial activation and NADPH-derived ROS. *Neurobiology of Disease*, 31(1), pp.58–73.

Rodriguez-Perez, A.I. et al., 2010. Estrogen and angiotensin interaction in the substantia nigra. Relevance to postmenopausal Parkinson's disease. *Experimental Neurology*, 224(2), pp.517–526.

Roks, A.J. et al., 1999. Angiotensin-(1-7) is a modulator of the human renin-angiotensin system. *Hypertension (Dallas, Tex. : 1979)*, 34(2), pp.296–301.

Rompe, F. et al., 2010. Direct Angiotensin II Type 2 Receptor Stimulation Acts Anti-Inflammatory Through Epoxyeicosatrienoic Acid and Inhibition of Nuclear Factor B. *Hypertension*, 55(4), pp.924–931.

Ronaldson, P.T. et al., 2009. Transforming growth factor-beta signaling alters substrate permeability and tight junction protein expression at the blood-brain barrier during inflammatory pain. *Journal of cerebral blood flow and metabolism*, 29(6), pp.1084–98.

Rosell, A. et al., 2005. A Matrix Metalloproteinase Protein Array Reveals a Strong Relation Between MMP-9 and MMP-13 With Diffusion-Weighted Image Lesion Increase in Human Stroke. *Stroke*, 36(7), pp.1415–1420.

Rosell, A. et al., 2006. Increased Brain Expression of Matrix Metalloproteinase-9 After Ischemic and Hemorrhagic Human Stroke. *Stroke*, 37(6), pp.1399–1406.

Rosenberg, G.A., Estrada, E.Y. & Dencoff, J.E., 1998. Matrix Metalloproteinases and TIMPs Are Associated With Blood-Brain Barrier Opening After Reperfusion in Rat Brain. *Stroke*, 29(10), pp.2189–95.

Roth, J.M., 2011. Recombinant tissue plasminogen activator for the treatment of acute ischemic stroke. *Proceedings (Baylor University. Medical Center)*, 24(3), pp.257–9.

Rother, J. et al., 1996. MR Detection of Cortical Spreading Depression Immediately After Focal Ischemia in the Rat. *Journal of Cerebral Blood Flow and Metabolism*, 16, pp.214–220.

Rothwell, N., Allan, S. & Toulmond, S., 1997. The role of interleukin 1 in acute neurodegeneration and stroke: pathophysiological and therapeutic implications. *Journal of Clinical Investigation*, 100(11), pp.2648–2652.

Rovira, A. et al., 2005. Distribution territories and causative mechanisms of ischemic stroke. *European Radiology*, 15(3), pp.416–426.

Saavedra, J.M. & Chevillard, C., 1982. Angiotensin-converting enzyme is present in the subfornical organ and other circumventricular organs of the rat. *Neuroscience letters*, 29(2), pp.123–7.

Sacco, R.L. et al., 2013. An Updated Definition of Stroke for the 21st Century. *Stroke*, 44(7), pp.2064–2089.

Sacco, R.L. et al., 1997. Risk Factors. *Stroke*, 28(7), pp.1507–17.

Sadato, A. et al., 2017. Carotid stenting for unilateral stenosis can increase contralateral hemispheric cerebral blood flow. *Journal of NeuroInterventional Surgery*, 10(4): 351-354.

Sage, J.I., Van Uitert, R.L. & Duffy, T.E., 1984. Early changes in blood brain barrier permeability to small molecules after transient cerebral ischemia. *Stroke*, 15(1), pp.46–50.

Saka, Ö., Mcguire, A. & Wolfe, C., 2009. Cost of stroke in the United Kingdom. *Age and Ageing*, 38(1), pp.27–32.

Sampaio, W.O. et al., 2007. Angiotensin-(1-7) through receptor Mas mediates endothelial nitric oxide synthase activation via Akt-dependent pathways. *Hypertension (Dallas, Tex. : 1979)*, 49(1), pp.185–92.

Sampaio, W.O., Nascimento, A.A.S. & Santos, R.A.S., 2003. Systemic and regional hemodynamic effects of angiotensin-(1–7) in rats. *American Journal*

of Physiology - Heart and Circulatory Physiology, 284(6), pp.H1985-94.
Sampson, A.K. et al., 2008. Enhanced angiotensin II type 2 receptor mechanisms mediate decreases in arterial pressure attributable to chronic low-dose angiotensin II in female rats. *Hypertension*, 52(4), pp.666–671.
Sanderson, T.H. et al., 2013. Molecular mechanisms of ischemia-reperfusion injury in brain: pivotal role of the mitochondrial membrane potential in reactive oxygen species generation. *Molecular neurobiology*, 47(1), pp.9–23.
Sandoval, K.E. & Witt, K.A., 2008. Blood-brain barrier tight junction permeability and ischemic stroke. *Neurobiology of Disease*, 32(2), pp.200–219.
Sandset, E.C. et al., 2011. The angiotensin-receptor blocker candesartan for treatment of acute stroke (SCAST): A randomised, placebo-controlled, double-blind trial. *The Lancet*, 377(9767), pp.741–750.
Santos, R.A. et al., 1994. Characterization of a new angiotensin antagonist selective for angiotensin-(1-7): evidence that the actions of angiotensin-(1-7) are mediated by specific angiotensin receptors. *Brain research bulletin*, 35(4), pp.293–8.
Santos, R.A. et al., 1988. Converting enzyme activity and angiotensin metabolism in the dog brainstem. *Hypertension (Dallas, Tex. : 1979)*, 11(2 Pt 2), pp.I153-7.
Santos, R.A.S. et al., 2003. Angiotensin-(1-7) is an endogenous ligand for the G protein-coupled receptor Mas. *Proceedings of the National Academy of Sciences of the United States of America*, 100(14), pp.8258–63.
Santos, R.A.S. & Ferreira, A.J., 2006. Pharmacological Effects of AVE 0991, a Nonpeptide Angiotensin-(1-7) Receptor Agonist. *Cardiovascular Drug Reviews*, 24(3–4), pp.239–246.
Savage, P.D. et al., 2016. Phase II Trial of Angiotensin-(1-7) for the Treatment of Patients with Metastatic Sarcoma. *Sarcoma*, 2016, pp.1–7.
Saver, J.L., Proposal for a Universal Definition of Cerebral Infarction Recent Developments in the Definition of Myocardial Infarction.
Saver, J.L. et al., 2012. Solitaire flow restoration device versus the Merci Retriever in patients with acute ischaemic stroke (SWIFT): a randomised, parallel-group, non-inferiority trial. *The Lancet*, 380(9849), pp.1241–1249.
Saver, J.L. et al., 2015. Stent-Retriever Thrombectomy after Intravenous t-PA vs. t-PA Alone in Stroke. *New England Journal of Medicine*, 372(24), pp.2285–2295.
Schaar, K.L., Brenneman, M.M. & Savitz, S.I., 2010. Functional assessments in the rodent stroke model. *Experimental & Translational Stroke Medicine*, 2(1), p.13.
Schelling, P. et al., 1976. Impermeability of the Blood—Cerebrospinal Fluid Barrier for Angiotensin II in Rats. *Clinical Science*, 51(s3), p.399s–402s.
Schianove, M. et al., 1988. Release of vasopressin from the rat hypothalamo-neurohypophysial system by angiotensin-(1-7) heptapeptide. *Neurobiology*, 85, pp.4095–4098.
Schilling, M. et al., 2009. Effects of monocyte chemoattractant protein 1 on blood-borne cell recruitment after transient focal cerebral ischemia in mice. *Neuroscience*, 161(3), pp.806–812.
Schirrmacher, R. et al., 2016. Which Aspects of Stroke Do Animal Models Capture? A Multitracer Micro-PET Study of Focal Ischemia with Endothelin-1. *Cerebrovascular diseases (Basel, Switzerland)*, 41(3–4), pp.139–47.
Schlaug, G. et al., 1999. The ischemic penumbra Operationally defined by diffusion and perfusion MRI. *Neurology*, 53(7), pp.1528–1537.
Schmid-Elsaesser, R. et al., 1998. A critical reevaluation of the intraluminal thread model of focal cerebral ischemia: evidence of inadvertent premature

reperfusion and subarachnoid hemorrhage in rats by laser-Doppler flowmetry. *Stroke*, 29(10), pp.2162–2170.

Schmieder, R.E. et al., 2007. Renin-angiotensin system and cardiovascular risk. *Lancet*, 369(9568), pp.1208–1219.

Schmittgen, T.D. & Livak, K.J., 2008. Analyzing real-time PCR data by the comparative CT method. *Nature Protocols*, 3(6), pp.1101–1108.

Schrader, J. et al., 2005. Morbidity and mortality after stroke, eprosartan compared with nitrendipine for secondary prevention: Principal results of a prospective randomized controlled study (MOSES). *Stroke*, 36(6), pp.1218–1224.

Schrader, J. et al., 2003. The ACCESS study: Evaluation of Acute Candesartan Cilexetil Therapy in Stroke Survivors. *Stroke*, 34(7), pp.1699–1703.

Schulz, A. et al., 2014. Absolute quantification of endogenous angiotensin II levels in human plasma using ESI-LC-MS/MS. *Clinical Proteomics*, 11(1), p.37.

Schwengel, K. et al., 2016. Angiotensin AT2-receptor stimulation improves survival and neurological outcome after experimental stroke in mice. *Journal of Molecular Medicine*, 94(8), pp.957–966.

Sen, C.K. & Packer, L., 1996. Antioxidant and redox regulation of gene transcription. *FASEB journal : official publication of the Federation of American Societies for Experimental Biology*, 10(7), pp.709–20.

Shanmugam, S., Corvol, P. & Gasc, J.M., 1996. Angiotensin II type 2 receptor mRNA expression in the developing cardiopulmonary system of the rat. *Hypertension*, 28(1), pp.91–7.

Shardlow, E. & Jackson, A., 2008. Cerebral blood flow and intracranial pressure. *Anaesthesia & Intensive Care Medicine*, 9(5), pp.222–225.

Sharkey, J., 1993. Perivascular Microapplication of Endothelin-1: A New Model of Focal Cerebral Ischaemia in the Rat. *Journal of Cerebral Blood Flow & Metabolism*, 13(5), pp.865–871.

Shen, Q. et al., 2003. Pixel-by-pixel spatiotemporal progression of focal ischemia derived using quantitative perfusion and diffusion imaging. *Journal of cerebral blood flow and metabolism : official journal of the International Society of Cerebral Blood Flow and Metabolism*, 23(12), pp.1479–88.

Shin, H.K. et al., 2008. Mild Induced Hypertension Improves Blood Flow and Oxygen Metabolism in Transient Focal Cerebral Ischemia. *Stroke*, 39, pp.1548–55.

Shin, H.K. et al., 2006. Vasoconstrictive Neurovascular Coupling during Focal Ischemic Depolarizations. *Journal of Cerebral Blood Flow & Metabolism*, 26(8), pp.1018–1030.

Sicard, K. et al., 2003. Regional Cerebral Blood Flow and BOLD Responses in Conscious and Anesthetized Rats under Basal and Hypercapnic Conditions: Implications for Functional MRI Studies. *Journal of Cerebral Blood Flow & Metabolism*, 23(4), pp.472–481.

Sierra, A., Encinas, J.M. & Maletic-Savatic, M., 2011. Adult human neurogenesis: from microscopy to magnetic resonance imaging. *Frontiers in neuroscience*, 5, p.47.

Sigmund, C.D., Diz, D.I. & Chappell, M.C., 2017. No Brain Renin–Angiotensin System. *Hypertension*, 69(6).

Silva-Antonialli, M.M. et al., 2004. A lower ratio of AT1/AT2 receptors of angiotensin II is found in female than in male spontaneously hypertensive rats. *Cardiovascular Research*, 62(3), pp.587–593.

Skeggs, L., Lentz, K., et al., 1956. The amino acid sequence of hypertensin. II. *The Journal of experimental medicine*, 104(2), pp.193–7.

Skeggs, L. et al., 1954. The existence of two forms of hypertensin. *The Journal of experimental medicine*, 99(3), pp.275–82.

Skeggs, L., Kahn, J. & Shumway, N., 1956. The preparation and function of the hypertensin-converting enzyme. *The Journal of experimental medicine*, 103(3), pp.295–9.

Skeggs, L.T. et al., 1976. The biochemistry of the renin-angiotensin system and its role in hypertension. *The American journal of medicine*, 60(6), pp.737–48.

Slivka, A., Murphy, E. & Horrocks, L., 1995. Cerebral edema after temporary and permanent middle cerebral artery occlusion in the rat. *Stroke*, 26(6), pp.1061-5-6.

So, G. et al., 2015. Candesartan Improves Ischemia-Induced Impairment of the Blood–Brain Barrier In Vitro. *Cellular and Molecular Neurobiology*, 35(4), pp.563–572.

Sommer, C.J., 2017. Ischemic stroke: experimental models and reality. *Acta neuropathologica*, 133(2), pp.245–261.

Sorce, S. et al., 2010. Increased brain damage after ischaemic stroke in mice lacking the chemokine receptor CCR5. *British journal of pharmacology*, 160(2), pp.311–21.

Soriano, M.A. et al., 1997. Cortical infarct volume is dependent on the ischemic reduction of perifocal cerebral blood flow in a three-vessel intraluminal MCA occlusion/reperfusion model in the rat. *Brain Research*, 747(2), pp.273–278.

Speth, R.C. & Harik, S.I., 1985. Angiotensin II receptor binding sites in brain microvessels. *Proceedings of the National Academy of Sciences of the United States of America*, 82(18), pp.6340–3.

Spratt, N.J. et al., 2006. Modification of the method of thread manufacture improves stroke induction rate and reduces mortality after thread-occlusion of the middle cerebral artery in young or aged rats. *Journal of Neuroscience Methods*, 155(2), pp.285–290.

Staals, J. et al., 2014. Stroke subtype, vascular risk factors, and total MRI brain small-vessel disease burden. *Neurology*, 83(14), pp.1228–34.

Steckelings, U.M. et al., 2012. AT2 receptor agonists. *Current Opinion in Nephrology and Hypertension*, 21(2), pp.142–146.

Stenman, E. & Edvinsson, L., 2004. Cerebral Ischemia Enhances Vascular Angiotensin AT1 Receptor-Mediated Contraction in Rats. *Stroke*, 35(4), pp.970–974.

Stoll, G. et al., 2009. Transient Widespread Blood—Brain Barrier Alterations after Cerebral Photothrombosis as Revealed by Gadofluorine M-Enhanced Magnetic Resonance Imaging. *Journal of Cerebral Blood Flow & Metabolism*, 29(2), pp.331–341.

Strbian, D. et al., 2008. The blood–brain barrier is continuously open for several weeks following transient focal cerebral ischemia. *Neuroscience*, 153(1), pp.175–181.

Stroke Association, 2017. State of the nation. Available at: https://www.stroke.org.uk/sites/default/files/state_of_the_nation_2017_final_1.pdf.

Ström, J.O. et al., 2013. Method parameters' impact on mortality and variability in rat stroke experiments: a meta-analysis. *BMC Neuroscience*, 14(1), p.41.

Strong, A.J. et al., 2006. Evaluation of Laser Speckle Flowmetry for Imaging Cortical Perfusion in Experimental Stroke Studies: Quantitation of Perfusion and Detection of Peri-Infarct Depolarisations. *Journal of Cerebral Blood Flow & Metabolism*, 26(5), pp.645–653.

Su, Z., Zimpelmann, J. & Burns, K.D., 2006. Angiotensin-(1–7) inhibits angiotensin II-stimulated phosphorylation of MAP kinases in proximal tubular cells. *Kidney International*, 69(12), pp.2212–2218.

Sullivan, J.C., 2008. Sex and the renin-angiotensin system: inequality between the

sexes in response to RAS stimulation and inhibition. *American journal of physiology. Regulatory, integrative and comparative physiology*, 294(4), pp.R1220-6.

Sumi, N. et al., 2010. Lipopolysaccharide-Activated Microglia Induce Dysfunction of the Blood–Brain Barrier in Rat Microvascular Endothelial Cells Co-Cultured with Microglia. *Cellular and Molecular Neurobiology*, 30(2), pp.247–253.

Sun, C. et al., 2005. NAD(P)H Oxidase Inhibition Attenuates Neuronal Chronotropic Actions of Angiotensin II. *Circulation Research*, 96(6), pp.659–666.

Sutherland, B.A. et al., 2011. Cerebral blood flow alteration in neuroprotection following cerebral ischaemia. *The Journal of Physiology*, 589(17), pp.4105–4114.

Sutherland, B.A. et al., 2016. The transient intraluminal filament middle cerebral artery occlusion model as a model of endovascular thrombectomy in stroke. *Journal Cerebral Blood Flow Metabolism*, 36(2), pp.363–369.

Suzukawa, K. et al., 2000. Nerve growth factor-induced neuronal differentiation requires generation of Rac1-regulated reactive oxygen species. *The Journal of biological chemistry*, 275(18), pp.13175–8.

Suzuki, S. et al., 1999. Temporal Profile and Cellular Localization of Interleukin-6 Protein after Focal Cerebral Ischemia in Rats. *Journal of Cerebral Blood Flow & Metabolism*, 19(11), pp.1256–1262.

Swanson, G.N. et al., 1992. Discovery of a distinct binding site for angiotensin II (3-8), a putative angiotensin IV receptor. *Regulatory Peptides*, 40(3), pp.409–419.

Swanson, R.A. et al., 1990. A Semiautomated Method for Measuring Brain Infarct Volume. *Journal of Cerebral Blood Flow & Metabolism*, 10(2), pp.290–293.

Symon, L., Pasztor, E. & Branston, N.M., 1974. The distribution and density of reduced cerebral blood flow following acute middle cerebral artery occlusion: an experimental study by the technique of hydrogen clearance in baboons. *Stroke*, 5(3), pp.355–64.

Tallant, E.A., Ferrario, C.M. & Gallagher, P.E., 2005. Angiotensin-(1-7) inhibits growth of cardiac myocytes through activation of the mas receptor. *American journal of physiology. Heart and circulatory physiology*, 289(4), pp.H1560-6.

Tamura, A. et al., 1981. Focal Cerebral Ischaemia in the Rat: 1. Description of Technique and Early Neuropathological Consequences following Middle Cerebral Artery Occlusion. *Journal of Cerebral Blood Flow & Metabolism*, 1(1), pp.53–60.

Taninishi, H. et al., 2015. A blinded randomized assessment of laser Doppler flowmetry efficacy in standardizing outcome from intraluminal filament MCAO in the rat. *Journal of Neuroscience Methods*, 241, pp.111–120.

Tawil, S. El & Muir, K.W., 2017. Thrombolysis and thrombectomy for acute ischaemic stroke. *Clinical Medicine*, 17(2), pp.161–165.

Taylor, R.A. & Sansing, L.H., 2013. Microglial responses after ischemic stroke and intracerebral hemorrhage. *Clinical & developmental immunology*, 2013, p.746068.

Tejima, E. et al., 2009. Neuroprotective effects of overexpressing tissue inhibitor of metalloproteinase TIMP-1. *Journal of neurotrauma*, 26(11), pp.1935–41.

Terao, S. et al., 2008. Blood cell-derived RANTES mediates cerebral microvascular dysfunction, inflammation, and tissue injury after focal ischemia-reperfusion. *Stroke*, 39(9), pp.2560–70.

Thatcher, S.E. et al., 2014. Angiotensin-converting enzyme 2 decreases formation and severity of angiotensin II-induced abdominal aortic aneurysms. *Arteriosclerosis, thrombosis, and vascular biology*, 34(12), pp.2617–23.

Theeuwes, F. & Yum, S.I., 1976. Principles of the design and operation of generic osmotic pumps for the delivery of semisolid or liquid drug formulations. *Annals of Biomedical Engineering*, 4(4), pp.343–53.

van Thiel, B.S. et al., 2017. Brain Renin–Angiotensin System: Does it Exist? *Hypertension*, 69(6), pp.1136–1144.

Thomas, W.G. & Sernia, C., 1988. Immunocytochemical localization of angiotensinogen in the rat brain. *Neuroscience*, 25(1), pp.319–41.

Thone-Reineke, C., Steckelings, U.M. & Unger, T., 2006. Angiotensin receptor blockers and cerebral protection in stroke. *J.Hypertens.Suppl*, 24(0952–1178 (Print)), pp.S115--S121.

Tigerstedt, R. & Bergman, P.Q., 1898. Niere und Kreislauf 1. *Skandinavisches Archiv Für Physiologie*, 8(1), pp.223–271.

Tipnis, S.R. et al., 2000. A human homolog of angiotensin-converting enzyme. Cloning and functional expression as a captopril-insensitive carboxypeptidase. *The Journal of biological chemistry*, 275(43), pp.33238–43.

Toth, M., Sohail, A. & Fridman, R., 2012. Assessment of Gelatinases (MMP-2 and MMP-9) by Gelatin Zymography. *Methods Mol Biol*, 878, pp.121–135.

Touyz, R.M. & Schiffrin, E.L., 2000. Signal transduction mechanisms mediating the physiological and pathophysiological actions of angiotensin II in vascular smooth muscle cells. *Pharmacological reviews*, 52(4), pp.639–72.

Trask, A.J. & Ferrario, C.M., 2007. Angiotensin-(1-7): Pharmacology and New Perspectives in Cardiovascular Treatments. *Cardiovascular Drug Reviews*, 25(2), pp.162–174.

Tsatmali, M., Walcott, E.C. & Crossin, K.L., 2005. Newborn neurons acquire high levels of reactive oxygen species and increased mitochondrial proteins upon differentiation from progenitors. *Brain Research*, 1040(1–2), pp.137–150.

Tsutsumi, K. & Saavedra, J.M., 1991a. Characterization and development of angiotensin II receptor subtypes (AT1 and AT2) in rat brain. *The American journal of physiology*, 261(1 Pt 2), pp.R209-16.

Tsutsumi, K. & Saavedra, J.M., 1991b. Characterization of AT2 angiotensin II receptors in rat anterior cerebral arteries. *The American journal of physiology*, 261(3 Pt 2), pp.H667-70.

Turner, A.J. & Hooper, N.M., 2002. The angiotensin-converting enzyme gene family: genomics and pharmacology. *Trends in Pharmacological Sciences*, 23(4).

Turner, R.J. & Sharp, F.R., 2016. Implications of MMP9 for Blood Brain Barrier Disruption and Hemorrhagic Transformation Following Ischemic Stroke. *Frontiers in cellular neuroscience*, 10, p.56.

Turu, G. et al., 2006. Differential β-arrestin binding of AT 1 and AT 2 angiotensin receptors. *FEBS Letters*, 580(1), pp.41–45.

Ueki, M., Mies, G. & Hossmann, K.A., 1992. Effect of alpha-chloralose, halothane, pentobarbital and nitrous oxide anesthesia on metabolic coupling in somatosensory cortex of rat. *Acta anaesthesiologica Scandinavica*, 36(4), pp.318–22.

Unal-Cevik, I. et al., 2004. Apoptotic and Necrotic Death Mechanisms Are Concomitantly Activated in the Same Cell After Cerebral Ischemia. *Stroke*, 35(9), pp.2189–2194.

Ushio-Fukai, M. et al., 1998. Temporal dispersion of activation of phospholipase C-beta1 and -gamma isoforms by angiotensin II in vascular smooth muscle cells. Role of alphaq/11, alpha12, and beta gamma G protein subunits. *The Journal of biological chemistry*, 273(31), pp.19772–7.

Valable, S. et al., 2005. VEGF-Induced BBB Permeability is Associated with an MMP-9 Activity Increase in Cerebral ischemia: Both Effects Decreased by

ANG-1. *Journal of Cerebral Blood Flow & Metabolism*, 25(11), pp.1491–1504.
Vallega, G.A. et al., 1988. Vascular smooth muscle Na+-H+ exchanger kinetics and its activation by angiotensin II. *The American journal of physiology*, 254(6 Pt 1), pp.C751-8.
Vallet, P. et al., 2005. Neuronal expression of the NADPH oxidase NOX4, and its regulation in mouse experimental brain ischemia. *Neuroscience*, 132(2), pp.233–238.
Velkoska, E. et al., 2015. Short-Term Treatment with Diminazene Aceturate Ameliorates the Reduction in Kidney ACE2 Activity in Rats with Subtotal Nephrectomy. *PLOS ONE*, 10(3), p.e0118758.
Veltkamp, R. et al., 2005. Hyperbaric Oxygen Reduces Blood–Brain Barrier Damage and Edema After Transient Focal Cerebral Ischemia. *Stroke*, 36(8), pp.1679–83.
Vickers, C. et al., 2002. Hydrolysis of biological peptides by human angiotensin-converting enzyme-related carboxypeptidase. *Journal of Biological Chemistry*, 277(17), pp.14838–14843.
Vilas-Boas, W.W. et al., 2009. Relationship between angiotensin-(1-7) and angiotensin II correlates with hemodynamic changes in human liver cirrhosis. *World journal of gastroenterology*, 15(20), pp.2512–9.
Vogel, C. & Marcotte, E.M., 2012. Insights into the regulation of protein abundance from proteomic and transcriptomic analyses. *Nature Reviews Genetics*, 13(4), pp.227–32.
Wakayama, K. et al., 2017. Angiotensin II Peptide Vaccine Protects Ischemic Brain Through Reducing Oxidative Stress. *Stroke*, 48(5), pp.1362–1368.
Walberer, M. et al., 2006. Experimental stroke: ischaemic lesion volume and oedema formation differ among rat strains (a comparison between Wistar and Sprague-Dawley rats using MRI). *Laboratory Animals*, 40(1), pp.1–8.
Walters, P.E., Gaspari, T.A. & Widdop, R.E., 2005. Angiotensin-(1-7) Acts as a Vasodepressor Agent Via Angiotensin II Type 2 Receptors in Conscious Rats. *Hypertension*, 45(5), pp.960–966.
Walther, T. et al., 2002. Ischemic injury in experimental stroke depends on angiotensin II. *The FASEB journal : official publication of the Federation of American Societies for Experimental Biology*, 16(2), pp.169–176.
Wan, Y. et al., 2004. Design, Synthesis, and Biological Evaluation of the First Selective Nonpeptide AT 2 Receptor Agonist. *Journal of Medicinal Chemistry*, 47(24), pp.5995–6008.
Wang, G. et al., 2006. Nox2, Ca2+, and Protein Kinase C Play a Role in Angiotensin II-Induced Free Radical Production in Nucleus Tractus Solitarius. *Hypertension*, 48(3), pp.482–489.
Warach, S. & Latour, L.L., 2004. Evidence of Reperfusion Injury, Exacerbated by Thrombolytic Therapy, in Human Focal Brain Ischemia Using a Novel Imaging Marker of Early Blood-Brain Barrier Disruption. *Stroke*, 35(11_suppl_1), pp.2659–2661.
Welches, W.R. et al., 1991. Evidence that prolyl endopeptidase participates in the processing of brain angiotensin. *Journal of hypertension*, 9(7), pp.631–8.
Welser-Alves, J. V & Milner, R., 2013. Microglia are the major source of TNF-α and TGF-β1 in postnatal glial cultures; regulation by cytokines, lipopolysaccharide, and vitronectin. *Neurochemistry international*, 63(1), pp.47–53.
Wester, A. et al., 2017. Stabilization of Angiotensin-(1–7) by key substitution with a cyclic non-natural amino acid. *Amino Acids*, 49(10), pp.1733–1742.
Westmoreland, S. V et al., 2002. Developmental expression patterns of CCR5 and CXCR4 in the rhesus macaque brain. *Journal of neuroimmunology*, 122(1–2),

pp.146–58.
Wheeler, H.M. et al., 2013. Early Diffusion-Weighted Imaging and Perfusion-Weighted Imaging Lesion Volumes Forecast Final Infarct Size in DEFUSE 2. *Stroke*, 44(3), pp.681–685.
Windmuller, O. et al., 2005. Ion changes in spreading ischaemia induce rat middle cerebral artery constriction in the absence of NO. *Brain*, 128(9), pp.2042–2051.
Winship, I.R. et al., 2014. Augmenting collateral blood flow during ischemic stroke via transient aortic occlusion. *Journal of cerebral blood flow and metabolism : official journal of the International Society of Cerebral Blood Flow and Metabolism*, 34(1), pp.61–71.
Woitzik, J. & Schilling, L., 2002. Control of completeness and immediate detection of bleeding by a single laser-Doppler flow probe during intravascular middle cerebral artery occlusion in rats. *Journal of Neuroscience Methods*, 122(1), pp.75–78.
Wood, T. et al., 2016. Monitoring of cerebral blood flow during hypoxia-ischemia and resuscitation in the neonatal rat using laser speckle imaging. *Physiological reports*, 4(7), p.e12749.
Woodruff, T.M. et al., 2011. Pathophysiology, treatment, and animal and cellular models of human ischemic stroke. *Molecular neurodegeneration*, 6(1), p.11.
Workman, P. et al., 2010. Guidelines for the welfare and use of animals in cancer research. *British journal of cancer*, 102(11), pp.1555–77.
van der Worp, H.B. et al., 2007. Hypothermia in animal models of acute ischaemic stroke: a systematic review and meta-analysis. *Brain*, 130(12), pp.3063–3074.
Wright, J.W. & Harding, J.W., 2013. The brain renin-angiotensin system: A diversity of functions and implications for CNS diseases. *Pflugers Archiv European Journal of Physiology*, 465(1), pp.133–151.
Wu, J. et al., 2015. Ang-(1–7) exerts protective role in blood–brain barrier damage by the balance of TIMP-1/MMP-9. *European Journal of Pharmacology*, 748, pp.30–36.
Wu, L. et al., 2004. Regulation of Inhibitory Protein-κB and Monocyte Chemoattractant Protein-1 by Angiotensin II Type 2 Receptor-Activated Src Homology Protein Tyrosine Phosphatase-1 in Fetal Vascular Smooth Muscle Cells. *Molecular Endocrinology*, 18(3), pp.666–678.
Wunder, A. et al., 2012. Imaging blood-brain barrier dysfunction in animal disease models. *Epilepsia*, 53(s6), pp.14–21.
Xu, P. et al., 2008. Endothelial Dysfunction and Elevated Blood Pressure in Mas Gene-Deleted Mice. *Hypertension*, 51(2), pp.574–580.
Yamada, K. et al., 1998. Converting enzyme determines plasma clearance of angiotensin-(1-7). *Hypertension (Dallas, Tex. : 1979)*, 32(3), pp.496–502.
Yamamoto, K. et al., 1992. In vivo metabolism of angiotensin I by neutral endopeptidase (EC 3.4.24.11) in spontaneously hypertensive rats. *Hypertension*, 19(6 Pt 2), pp.692–6.
Yang, G. et al., 1999. The angiotensinogen gene is expressed in both astrocytes and neurons in murine central nervous system. *Brain research*, 817(1–2), pp.123–31.
Yang, H.Y., Erdös, E.G. & Levin, Y., 1970. A dipeptidyl carboxypeptidase that converts angiotensin I and inactivates bradykinin. *Biochimica et biophysica acta*, 214(2), pp.374–6.
Yang, Y. et al., 2015. Attenuation of acute stroke injury in rat brain by minocycline promotes blood–brain barrier remodeling and alternative microglia/macrophage activation during recovery. *Journal of Neuroinflammation*, 12(1), p.26.

Yang, Y. et al., 2007. Matrix metalloproteinase-mediated disruption of tight junction proteins in cerebral vessels is reversed by synthetic matrix metalloproteinase inhibitor in focal ischemia in rat. *Journal of Cerebral Blood Flow & Metabolism*, 27(4), pp.697–709.

Yang, Y. & Rosenberg, G.A., 2011. Blood–Brain Barrier Breakdown in Acute and Chronic Cerebrovascular Disease. *Stroke*, 42(11), pp.3323–8.

Yenari, M.A. et al., 2006. Microglia Potentiate Damage to Blood–Brain Barrier Constituents. *Stroke*, 37(4), pp.1087–93.

Yoneda, Y. et al., 1999. Diffusion-weighted magnetic resonance imaging: detection of ischemic injury 39 minutes after onset in a stroke patient. *Annals of neurology*, 45(6), pp.794–7.

Young, D. et al., 1988. Characterization of the rat mas oncogene and its high-level expression in the hippocampus and cerebral cortex of rat brain. *Proceedings of the National Academy of Sciences of the United States of America*, 85(14), pp.5339–42.

Young, D. et al., 1986. Isolation and characterization of a new cellular oncogene encoding a protein with multiple potential transmembrane domains. *Cell*, 45(5), pp.711–9.

Yuh, W.T. et al., 1991. MR imaging of cerebral ischemia: findings in the first 24 hours. *American Journal of Neuroradiology*, 12(4), pp.621–629.

Yusuf, S. et al., 2008a. Effects of the angiotensin-receptor blocker telmisartan on cardiovascular events in high-risk patients intolerant to angiotensin-converting enzyme inhibitors: a randomised controlled trial. *The Lancet*, 372(9644), pp.1174–1183.

Yusuf, S. et al., 2008b. Telmisartan to Prevent Recurrent Stroke and Cardiovascular Events. *New England Journal of Medicine*, 359(12), pp.1225–1237.

Zanette, E.M. et al., 1995. Spontaneous middle cerebral artery reperfusion in ischemic stroke. A follow-up study with transcranial Doppler. *Stroke*, 26(3), pp.430–3.

Zarruk, J.G. et al., 2011. Neurological tests for functional outcome assessment in rodent models of ischaemic stroke. *Revista de neurologia*, 53(10), pp.607–18.

Zausinger, S., Baethmann, A. & Schmid-Elsaesser, R., 2002. Anesthetic methods in rats determine outcome after experimental focal cerebral ischemia: mechanical ventilation is required to obtain controlled experimental conditions. *Brain Research Protocols*, 9(2), pp.112–121.

Zhang, H.-T. et al., 2017. Early VEGF inhibition attenuates blood-brain barrier disruption in ischemic rat brains by regulating the expression of MMPs. *Molecular medicine reports*, 15(1), pp.57–64.

Zhang, L. et al., 2016. NADPH Oxidase: A Potential Target for Treatment of Stroke. *Oxidative medicine and cellular longevity*, 2016, p.5026984.

Zhang, Y. et al., 2008. Central administration of angiotensin-(1-7) stimulates nitric oxide release and upregulates the endothelial nitric oxide synthase expression following focal cerebral ischemia/reperfusion in rats. *Neuropeptides*, 42(5–6), pp.593–600.

Zhang, Z.G. et al., 2000. VEGF enhances angiogenesis and promotes blood-brain barrier leakage in the ischemic brain. *Journal of Clinical Investigation*, 106(7), pp.829–838.

Zheng, J. et al., 2014. Activation of the ACE2/Ang-(1–7)/Mas pathway reduces oxygen–glucose deprivation-induced tissue swelling, ROS production, and cell death in mouse brain with angiotensin II overproduction. *Neuroscience*, 273, pp.39–51.

Zheng, J.-L. et al., 2014. Angiotensin Converting Enzyme 2/Ang-(1-7)/Mas Axis

Protects Brain from Ischemic Injury with a Tendency of Age-dependence. *CNS Neuroscience & Therapeutics*, 20(5), pp.452–459.

Zhu, Y.Z. et al., 2000. Expression of angiotensin II AT2 receptor in the acute phase of stroke in rats. *Neuroreport*, 11(6), pp.1191–1194.

Zille, M. et al., 2012. Visualizing cell death in experimental focal cerebral ischemia: promises, problems, and perspectives Promises and Problems in Visualizing Cell Death in Stroke. *Journal of Cerebral Blood Flow & Metabolism*, 32150(10), pp.213–231.

Zilles, K., 1985. *The Cortex of the Rat*, Berlin, Heidelberg: Springer Berlin Heidelberg.

Zimmerman, M.C. et al., 2004. Requirement for Rac1-Dependent NADPH Oxidase in the Cardiovascular and Dipsogenic Actions of Angiotensin II in the Brain. *Circulation Research*, 95(5), pp.532–539.

Zini, S. et al., 1996. Identification of metabolic pathways of brain angiotensin II and III using specific aminopeptidase inhibitors: predominant role of angiotensin III in the control of vasopressin release. *Proceedings of the National Academy of Sciences of the United States of America*, 93(21), pp.11968–73.

Zivin, J.A. et al., 1985. Tissue plasminogen activator reduces neurological damage after cerebral embolism. *Science (New York, N.Y.)*, 230(4731), pp.1289–92.

Zlokovic, B. V., 2008. The Blood-Brain Barrier in Health and Chronic Neurodegenerative Disorders. *Neuron*, 57(2), pp.178–201.

del Zoppo, G.J., 2010. The neurovascular unit in the setting of stroke. *Journal of internal medicine*, 267(2), pp.156–71.